A Brain-Computer Interface Integrated with Virtual Reality and Robotic Exoskeletons for Enhanced Visual and Kinaesthetic Stimuli

Paul Dominick Emor Baniqued

Submitted in accordance with the requirements

for the degree of Doctor of Philosophy

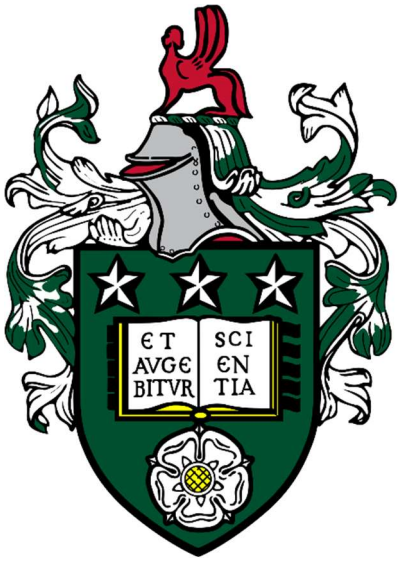

The University of Leeds

School of Mechanical Engineering

and School of Psychology

February 2022

Intellectual Property

The candidate confirms that the work submitted is his own, except where work that has formed part of a jointly authored publication has been included. The contribution of the candidate and the other authors to this work has been explicitly indicated below. The candidate confirms that appropriate credit has been given within the thesis where reference has been made to the work of others.

Some parts of the work presented in this thesis have been published in the following article:

Baniqued, P. D. E., Stanyer, E. C., Awais, M., Alazmani, A., Jackson, A. E., Mon-Williams, M. A., Mushtaq, F., and Holt, R. J. "Brain-computer interface robotics for hand rehabilitation after stroke: a systematic review".

In: Journal of NeuroEngineering and Rehabilitation (JNER), 2021.

The above publication is primarily the work of the candidate.

Abstract

Brain-computer interfaces (BCI) allow the direct control of robotic devices for neurorehabilitation and measure brain activity patterns following the user's intent. In the past two decades, the use of non-invasive techniques such as electroencephalography and motor imagery in BCI has gained traction. However, many of the mechanisms that drive the proficiency of humans in eliciting discernible signals for BCI remains unestablished. The main objective of this thesis is to explore and assess what improvements can be made for an integrated BCI-robotic system for hand rehabilitation.

Chapter 2 presents a systematic review of BCI-hand robot systems developed from 2010 to late 2019 in terms of their technical and clinical reports. Around 30 studies were identified as eligible for review and among these, 19 were still in their prototype or pre-clinical stages of development. A degree of inferiority was observed from these systems in providing the necessary visual and kinaesthetic stimuli during motor imagery BCI training. Chapter 3 discusses the theoretical background to arrive at a hypothesis that an enhanced visual and kinaesthetic stimulus, through a virtual reality (VR) game environment and a robotic hand exoskeleton, will improve motor imagery BCI performance in terms of online classification accuracy, class prediction probabilities, and electroencephalography signals. Chapters 4 and 5 focus on designing, developing, integrating, and testing a BCI-VR-robot prototype to address the research aims. Chapter 6 tests the hypothesis by performing a motor imagery BCI paradigm self-experiment with an enhanced visual and kinaesthetic stimulus against a control.

A significant increase ($p = 0.0422$) in classification accuracies is reported among groups with enhanced visual stimulus through VR versus those without. Six out of eight sessions among the VR groups have a median of class probability values exceeding a pre-set threshold value of 0.6. Finally, the thesis concludes in Chapter 7 with a general discussion on how these findings could suggest the role of new and emerging technologies such as VR and robotics in advancing BCI-robotic systems and how the contributions of this work may help improve the usability and accessibility of such systems, not only in rehabilitation but also in skills learning and education.

Buod (Abstract in Filipino)

Ang mga brain-computer interface (BCI) ay may kakayahang mag kontrol ng robot para sa rehabilitasyon ng mga sakit at pinsala na may kinalaman sa utak. Ito ay batay sa pagsukat ng aktibidad ng utak kasunod sa hangarin ng gumagamit. Isang paraan upang magamit ang mga ito ay ang pagkuha ng electroencephalography habang nag-iimahe ng paggalaw. Sa mahigit na dalawang dekada ng pagsusuri, karamihan ng kaalaman sa mga mekanismo na nagtutulak sa kahusayan ng mga tao na gumawa ng signal para sa BCI ay nananatiling mababaw. Ang pangunahing layunin ng tesis na ito ay upang tuklasin at suriin kung anong pagbubuti ang maaaring gawin para sa mga BCI at robot upang mapagaling ang paggalaw ng kamay ng isang pasiyente.

Inilalahad sa Kabanata 2 ang isang sistematikong pagsusuri na ginawa upang surbeyin ang mga sistema ng BCI-robot na binuo noong 2010 hanggang sa 2019 para sa mga kamay base sa mga tuntunin ng kanilang mga teknolohikal at klinikal na ulat. Sa 30 na mga sistema na nakuha, 19 dito ang nasa kanilang prototype o pre-klinikal na yugto ng pag-unlad. Ang nakitang kakulangan sa mga sistemang ito ay ang antas ng pagbibigay ng kinakailangang biswal at kinestetik na stimuli habang nag-iimahe ng paggalaw. Sa Kabanata 3, mas pinalawak pa ang diskusyong ito upang makarating sa teorya na kayang pahusayin ang paggamit ng BCI sa pamamagitan ng virtual reality (VR) at isang uri ng robot na nasusuot sa kamay. Sa mga Kabanatang 4 at 5, itinutuon ang talakayan sa pagdisenyo, pag-unlad, pagsasama, at pagsubok ng ng isang BCI-VR-robot prototype upang matuguran ang mga hangarin sa pagsasaliksik. Sa Kabanata 6, sinusubukan naman ang mga teoryang nabanggit sa pamamagitan ng pagsasagawa ng eksperimento sa sarili gamit ang prototype.

Inuulat ng kasulatan na ito ang isang makabuluhang pagtaas ($p = 0.0422$) ng mga puntos sa mga sesyon na may larong ginawa habang may suot na VR kumpara sa mga sesyon na wala. Anim sa walong mga sesyon sa grupo na may kasamang VR ang nakapasa sa aming pamantayan na 0.6 para sa posibilidad na makatama ang kompyuter sa kanyang prediksyon. At sa panghuling kabanata, Kabanata 7, tinatapos ang tesis na ito sa pamamagitan ng pagbibigay ng isang pangkalahatang talakayan tungkol sa mga kontribusyon para mapaunlad ang mga naturing na sistema, hindi lamang para sa rehabilitasyon, kundi pati na rin sa pag-aaral ng kasanayan at edukasyon.

Acknowledgements

I would like to thank several people and organisations who have helped me produce this work. This thesis would not be possible without your contributions.

First and foremost, my most sincere thanks to my supervision team at the University of Leeds, composed of Dr Raymond Holt, Dr Ali Alazmani, Dr Faisal Mushtaq, Dr Ryan Morehead, and Professor Mark Mon-Williams. Thank you for being patient with me and allowing me to explore and develop my research agenda.

Thanks to my sponsor, the British Council Philippines, and the Newton Fund Programme for funding my research and doctoral studies.

Thanks to my colleagues in the Immersive Cognition Laboratory, Jack, Matthew, Mshari, Hassan, Max, Zeynep, JP, Emily, Emily, Awais, and Awais. I am very grateful for all the lessons and memories that I have acquired during our times.

To the students and interns who have worked with me in this research, Qasim, Michal, Amy, Claudie, and Katie, thank you for all your help. I hope you have learned a lot in our time together as much as I have learned from you. I wish you all success in your future endeavours.

Thanks to all the people in the Institute of Design, Robotics, and Optimisation, the 3D Printing and Additive Manufacturing Laboratory, and the Prototyping Laboratory.

Finally, thanks to my parents, Elpidio Roy Baniqued and Carmencita Ojacastro Emor Baniqued, who have worked so hard to raise a son with a curious mind. I developed my early interest in science and engineering because of your efforts. Thanks to my brother and game buddy Emmanuel Emor Baniqued. You have all been a source of encouragement and inspiration.

Thank you very much!

Abbreviations

ADL	Activities of Daily Living
ANOVA	Analysis of Variance
AO	Action Observation
AR	Augmented Reality
ARAT	Action Research Arm Test
BCI	Brain-Computer Interface
CNN	Convolutional Neural Network
CSP	Common Spatial Patterns
CSV	Comma Separated Values
DIP	Distal Interphalangeal
DOF	Degrees of Freedom
EEG	Electroencephalography
EMG	Electromyography
EOG	Electrooculography
ERD	Event-Related Desynchronisation
ERS	Event-Related Synchronisation
FIR	Finite Impulse Response
FMA	Fugl-Meyer Motor Assessment
GS	Grip Strength
HMD	Head Mounted Device
IADL	Instrumental ADL
LCD	Liquid Crystal Display
LDA	Linear Discriminant Analysis
LED	Light-Emitting Diode
LR	Logistic Regression
LSL	Labstreaminglayer
MCP	Metacarpophalangeal
ME	Motor Execution
MI	Motor Imagery
MIQ	Movement Imagery Questionnaire
NN	Neural Network
PIP	Proximal Interphalangeal
PLA	Polylactic Acid
RCT	Randomised Controlled Trial
RNN	Recurrent Neural Network
ROM	Range of Motion
SVM	Support Vector Machine
TFR	Time-Frequency Analysis
TRL	Technology Readiness Level
UK	United Kingdom
USA	United States of America
VEP	Visually-Evoked Potential
VR	Virtual Reality
Wi-Fi	Wireless Fidelity
XDF	Extensible Data Format

Table of Contents

List of Figures

List of Tables

List of Equations

Chapter 1
Introduction

In 1924, Hans Berger, a German neurologist, first devised a method to amplify a brain's electrophysiological signals using a radio amplifier and thin silver foils that are in contact with a human's scalp. He later coined the term *electroencephalogram (EEG)* to describe recordings based on this technique (Teplan, 2002). Almost a hundred years later, in 2021, EEG has been the method of choice for clinicians to perform non-invasive, portable, and reliable imaging of brain activity for diagnosing certain diseases and for neuroscientists to record electrophysiological responses during experiments that involve human cognition, action, and planning. Berger's innovations also led researchers in developing the technology behind what would be known as *brain-computer interfaces (BCI)* – an emerging and rapidly advancing group of systems that use brain activity signals to control devices (Graimann et al., 2010). A BCI is an artificial system composed of hardware and software that provides direct communication between the brain and a device based on its user's intent. The resulting flow of information (e.g., modulation of the sensorimotor rhythm) bypasses the normal efferent pathways of the body's peripheral nervous system[1]. Instead, a BCI recognises a user's intent by measuring event-related brain activity and translating it into executable commands usually done by a computer, hence the term: brain-computer interface. Although far from what the popular media and science-fiction depict what these technologies can do (i.e., command military equipment like Yuri in the videogame Command & Conquer: Red Alert or using the *Cerebro*, a device that can amplify brainwaves to locate certain beings in Marvel Comics' The X-Men), the current technology for BCI allows us to control or trigger simpler devices and processes such as computer cursors, videogames, and even robotic systems (Vidal, 1973; Wolpaw et al., 2002; Wolpaw and Wolpaw, 2012; Bozinovski, 2013).

[1] The term "efferent" refers to the neural pathway that carries signals away from the brain and spinal cord (Central Nervous System) towards an effector such as motor neurons (Peripheral Nervous System)

One specific application of brain-computer interfaces, which excites research scientists and medical device developers alike, is the neurorehabilitation of brain injuries such as stroke. Stroke, also known as a cerebrovascular accident, is a widespread medical condition that affects the lives of many individuals. The 2019 global data for stroke shows a prevalence of above 101 million (101,474,558.48), where 12% are first-time incidents (University of Washington Institute for Health Metrics and Evaluation, 2021). Strokes occur when there is a failure to supply blood to the brain caused by ischaemic (clotting) or haemorrhagic (bleeding) mechanisms. The sudden deficiency of oxygen damages the brain tissues leading to death or, if survived, a life with neurological impairment. Because of this, the World Health Organization (WHO) has also regarded stroke as one of the top causes of disability (World Health Organization, 2011). According to some studies, stroke is perceived to have a higher burden among low and middle-income countries (World Health Organization, 2011; Mukherjee and Patil, 2011; Benjamin et al., 2018) and may be due to the lack of access to well-established therapy programmes and other healthcare options.

Of the many neurological deficiencies after stroke, motor weakness, especially in the extremities, are the most obvious symptom to a patient or an outside observer (O'Dell et al., 2009). Motor weakness, as well as other cognitive and sensory deficiencies in stroke, is hemiparetic (i.e., "Hemi-" half/one-sided "paresis" motor weakness) and depends on the severity of the neurological damage (O'Dell et al., 2009). Despite the symptoms affecting typical motor and cognitive functions, recovery after stroke is possible via natural and induced mechanisms (Krakauer, 2005; Fregni and Pascual-Leone, 2006; O'Dell et al., 2009). Cortical neuroplasticity, the ability of the motor cortex to reorganise and thus relearn motor skills, is the underlying principle behind standard interventional therapy and relies on both intensive and repetitive stimuli (Hallett, 2001; Fregni and Pascual-Leone, 2006). This type of plasticity is use-dependent which means it is induced by the repeated experience of initiating and achieving a specified target; making the active participation of the patient in performing the therapy exercises an integral part of the motor re-learning process (Zeiler and Krakauer, 2013; Mawase et al., 2017). With the use of a brain-computer interface, a stroke rehabilitation regimen is improved in promoting active participation by allowing the intent-based control of systems such as robotic devices (Marchal-Crespo and Reinkensmeyer, 2009) and computer-based video games

(Vanbellingen et al., 2017). The primary motivation for developing such technologies is rooted in providing better and more accessible treatment options with lesser economic costs.

The main objective of this thesis is to look deep into the field of brain-computer interfaces and robotics to assess what can be done to improve neurorehabilitation and provide a cost-effective solution to its current accessibility problem. This research focuses on the motor rehabilitation of the hands as a case for BCI-robot systems. An emerging interest in hand and wrist therapy, through prehension exercises, is observed as it directly promotes the independence of a patient in performing activities of daily living (ADL) or instrumental activities of daily living (IADL) (Taylor and Schwarz, 1955). ADL involves using bare hands or individual fingers to perform tasks requiring dexterity, such as picking or placing objects, dressing up (i.e., buttoning one's shirt), and maintaining personal hygiene. IADL, as the term implies, makes use of an instrument to aid the hands, such as cutlery (e.g., spoons, forks, knives, etc.) during eating or a pen/pencil for writing (Krakauer, 2006). While this research focuses on the rehabilitation of the hands, the concepts that will be discussed in succeeding chapters can also be applied in other rehabilitation regimes such as whole upper extremity therapy, lower extremity therapy, and mobility therapy using a brain-computer interface.

The specific objectives of this thesis are:

- to look into the scientific literature for existing BCI-hand robot systems by performing a thorough and systematic review of existing research work. In this way, the current gaps in the body of knowledge for BCI-hand robot systems can be laid out, leading to the development of a new and suitable research question
- to propose the use of scientific and engineering methods in hypothesising and prototyping a solution that can address these questions
- to experiment and analyse the gathered data and then relate to the bigger picture of improving brain-computer interfaces and robotic systems for rehabilitation

Figure 1.1 presents a map of the thesis with a short description of the succeeding chapters.

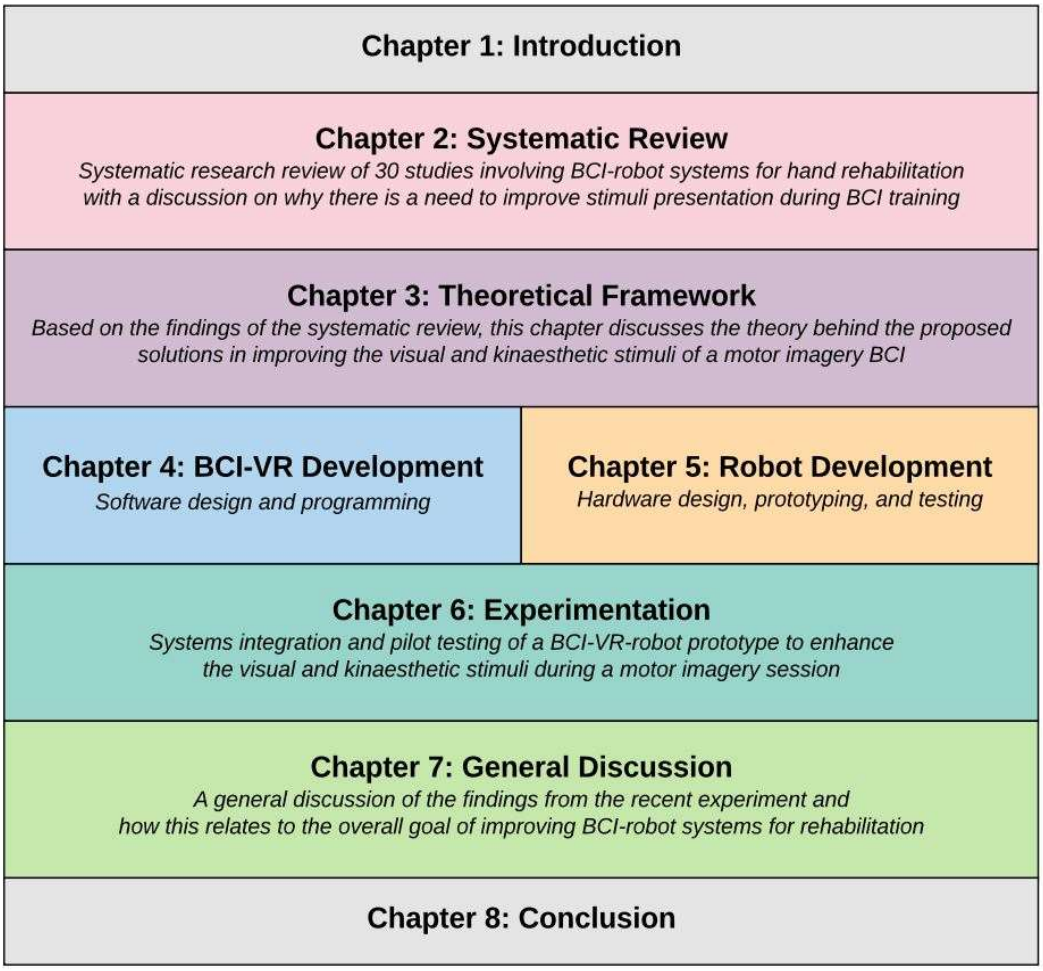

Figure 1.1: A map of the thesis with a short description of succeeding chapters

Chapter 2 presents a systematic review of integrated brain-computer interfaces and wearable hand robot systems for rehabilitation after stroke. As a summary of my findings from the 30 BCI-hand robot systems that passed my screening criteria, I report the need to improve the way stimuli, through cue and feedback, is presented to a user during BCI training. In Chapter 3, I further expand this by discussing the theory of BCI use, focusing on sensorimotor rhythm modulation by motor imagery as a viable mode, and laying out a potential solution for improving motor imagery BCI classification accuracy based on two factors: visual stimuli and kinaesthetic stimuli. Here, I discuss that by improving on these factors, we can promote neuroplasticity and significantly impact the time and resources needed for neurophysiological recovery (Nojima et al., 2012; Liu et al., 2014; Chowdhury, Meena, et al., 2018). In Chapters 4 and 5, I present

engineering solutions to the two aforementioned factors. Chapter 4 focuses on the software design and programming of a motor imagery BCI paradigm with enhanced visual stimuli through a virtual reality environment, while Chapter 5 focuses on the hardware design, prototyping, and testing of a low-cost robotic hand exoskeleton to provide kinaesthetic stimuli as part of the cue component (i.e., instructing and guiding the users to perform the tasks).

Chapter 6 presents the integration of these systems into a BCI-VR-robot prototype and the methods, results, and discussion of a self-experiment performed to test my hypothesis. The ongoing coronavirus disease (COVID) pandemic in the United Kingdom at the time of this study (2020) restricted most physical/in-person research activities, including experiments involving healthy human participants – the initially intended method to test my hypothesis. With careful consideration of the probable outcomes and quality of research, we (i.e., myself and my doctoral supervision team) have decided to progress this study with a self-experiment. I discuss the implications of my recent findings to the main objective of this thesis through a general discussion in Chapter 7. Finally, this chapter also summarises and concludes the contributions of this thesis to the current body of scientific knowledge with recommendations for future work.

Chapter 2

Systematic Review of Wearable Robots and Brain-Computer Interfaces for Hand Rehabilitation After Stroke

2.1. Introduction

The growing interest in robot-assisted rehabilitation is driven by the increasing number of people requiring therapy and the global phenomenon of insufficient numbers of therapists to deliver rehabilitation exercises to patients (McHugh and Swain, 2014; Ntsiea, 2019). Robotic systems allow a therapist to prescribe exercises that can then be guided by the robot rather than the therapist. An essential principle within such systems is that the robots assist the patient in actively undertaking a prescribed movement rather than the patient's limb being moved passively. This means that the system must sense when the patient is trying to generate the required movement (given that, by definition, the patient struggles typically with the action). One potential solution to this issue is to use force sensors that can detect when the patient is starting to generate movement (at which point the robot's motors can provide assistive forces). It is also possible to use measures of muscle activation (i.e., *electromyographic or EMG* signals) to detect the intent to move (Manguerra et al., 2018). In the last two decades, there has been a concerted effort by groups of clinicians, neuroscientists and engineers to integrate robotic systems with brain activity signals correlated with a patient trying to generate a movement actively, or imagine a motor action, to enhance the efficacy and effectiveness of stroke rehabilitation – these systems fall under the definition of brain-computer interfaces or BCI (Wolpaw and Wolpaw, 2012). Figure 2.1 shows a typical BCI setup for robot-assisted rehabilitation.

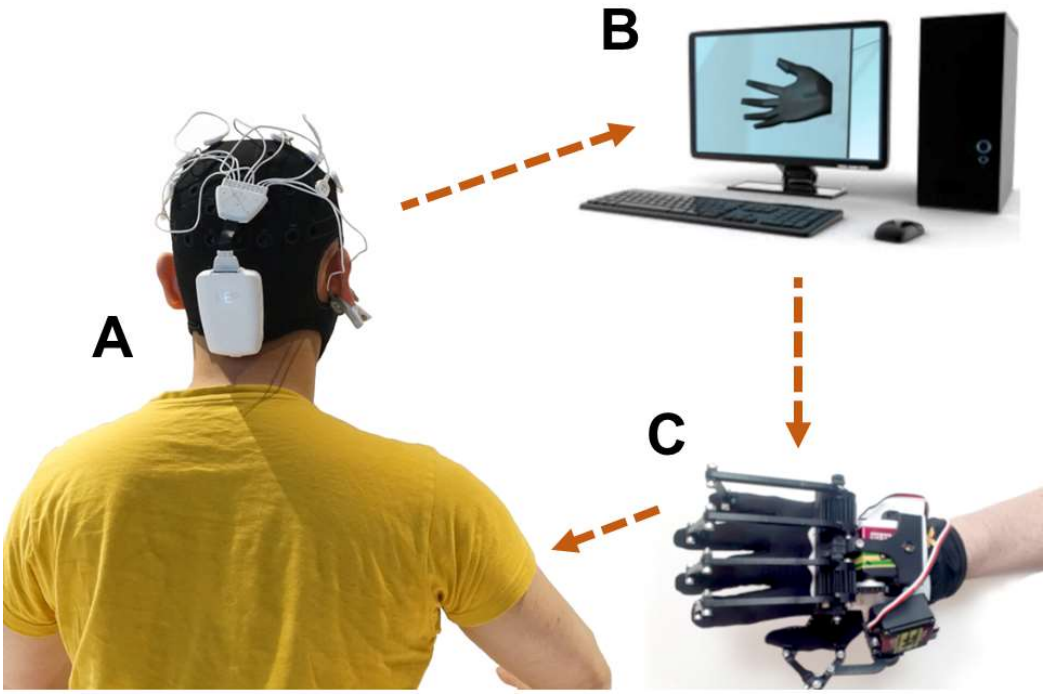

Figure 2.1: Typical brain-computer interface setup for robot-assisted rehabilitation. The main components of this BCI are: (A) an EEG acquisition device that can transmit data to a computer, (B) a computer unit for data processing and visual display, and (C) a robotic device that assists the user to perform a particular task

BCIs allow brain state-dependent control of robotic devices to aid stroke patients during upper limb therapy. While BCIs in their general form has been in development for almost 50 years (Vidal, 1973) and were theoretically made possible since the discovery of the scalp-recorded human electroencephalogram in the 1920s (Berger, 1929), their application to rehabilitation is more recent (Birbaumer et al., 1999; Hochberg et al., 2006; Silvoni et al., 2011). The use of a BCI follows a cue-feedback process. A cue, which may come in various combinations of sensory stimuli, is an instruction to the user to perform a mental task. Feedback is the result of the processing of physiological signals (usually based on the predicted outcome of a pre-trained classifier) recorded during the mental task and is provided back to the user to inform them of the outcome of that cue-feedback cycle (i.e., a trial). I discuss the processes involved in BCI use in Chapter 3 (Section 3.4 – Brain-Computer Interfaces based on Motor Imagery).

Most robotic devices used in upper limb rehabilitation exist as exoskeletons or end-effectors. Robotic exoskeletons (i.e., powered orthoses, braces) are wearable devices where the actuators are biomechanically aligned with the wearer's joints and linkages, allowing the additional torque to provide assistance, augmentation and even resistance during training (Molteni et al., 2018). In comparison, end-effector systems generate movement by applying forces to the most distal extremity segment via handles and attachments (Molteni et al., 2018). Rehabilitation robots are classified as Class II-B medical devices (i.e., a therapeutic device that administers the exchange of energy, mechanical in the case of robots, to a patient). In this class, safety considerations are essential during development (Guiochet et al., 2012; European Commission, 2016). Most commercial robots focus on arms and legs, each offering a unique therapy methodology. There is also a category of devices that target the hands and fingers. While often less studied than the proximal areas of the upper limb, hand and finger rehabilitation are core components in regaining daily living activities (ADL) (Yue et al., 2017). Many ADLs require dexterous and fine motor movements (e.g. grasping and pinching), and there is evidence that even patients with minimal proximal shoulder and elbow control can regain some hand capacity long-term following stroke (Houwink et al., 2013).

The strategy of BCI-robot systems (i.e., systems that integrate BCI and robots into one unified system) in rehabilitation is to recognise the patient's intention to move or perform a task via a neural or physiological signal and then use a robotic device to provide assistive forces in a manner that mimics the actions of a therapist during standard therapy sessions (Takahashi et al., 2016). The resulting feedback is patient-driven and is designed to aid in closing the neural loop from intention to execution. This process is said to promote use-dependent neuroplasticity within intact brain regions and relies on the repeated experience of initiation, execution, and feedback (Hallett, 2001; Fregni and Pascual-Leone, 2006).

At the robot end of the system, the device can be operated continuously or by a trigger to perform a predefined motion. A continuous control strategy increases the temporal volitional control over the robot instead of triggered assistance where a threshold is applied, and the robot finishes the movement for the participant. The choice of using one control strategy over the other relies on two major factors: (1) the ability of a patient to produce an intent signal and (2)

the capability of the system to extract and map out an intent signal successfully. The patient's recovery stage reflects the first factor. For example, a trigger strategy might be ideal for severely impaired patients who cannot produce a stable signal for robotic control. In contrast, a continuous strategy can be implemented for those who can provide enough stability in their movement intent but are still not fully recovered and be considered independent. The second factor is based on knowing the state-of-the-art of BCI-robots in rehabilitation and is one of the main questions targeted for this study.

The BCI end of the system mainly focuses on developing the optimum strategy for brain signal data acquisition. The aforementioned scalp-recorded EEG signal is a commonly used instrument for data acquisition in BCI systems because it is non-invasive, easy to use, and can detect relevant brain activity with high temporal resolution (Teplan, 2002; Cohen, 2014). In principle, the recognition of motor imagery, the imagination of movement without execution, via EEG can control a device independent of muscle activity (Graimann et al., 2010). It has been reported that motor imagery-based BCI can discriminate motor intent by detecting event-related spectral perturbations (Pfurtscheller and Lopes da Silva, 1999; Li et al., 2018). These can be decomposed as event-related desynchronisation/synchronisation (ERD/S) patterns in the μ (9-11 Hz) and β (14-30 Hz) sensorimotor rhythm of EEG signals (Pfurtscheller and Lopes da Silva, 1999). However, EEG also brings with it some challenges. Various artefacts often conceal these neural markers and may be difficult to recognise through the raw EEG signal alone. Thus, signal processing (including feature extraction and classification) is vital for obtaining a good motor imagery signal for robotic control. A general pipeline for EEG data processing involves several steps. First, the data undergo a series of pre-processing routines (e.g., filtering and artefact removal) before feature extraction and classification as a control signal for the robotic hand. Feature extraction involves recognising useful information (e.g., spectral power, time epochs, spatial filtering) for better discriminability among mental states. For example, the common spatial patterns (CSP) algorithm is a type of spatial filter that maximises the variance of band pass-filtered EEG from one class to discriminate it from another (Lotte and Guan, 2011). Finally, classification (which can range from linear and simple algorithms such as Linear Discriminant Analysis (LDA), Linear Support Vector Machine (L-SVM) up to more complex techniques in deep learning such as Convolutional Neural Networks (CNN) and Recurrent Neural Networks

(RNN) (Schirrmeister et al., 2017; Roy et al., 2019) involves the translation of these signals of intent to an action that provides the user feedback and closes the loop of the motor intent-to-action circuit.

The potential of motor imagery-based BCIs has gained considerable attention because the neural activity involved in the control of the robotic device may be a key component in the rehabilitation itself. For example, motor imagery of movement is thought to activate some neural networks involved in movement execution (Hardwick et al., 2018; Xu et al., 2014; Sharma and Baron, 2013; Jeannerod, 2001). The resulting rationale is that encouraging the use of motor imagery could increase the capacity of the motor cortex to control major muscle movements and decrease the necessity to use neural circuits damaged post-stroke. The scientific justification for this approach was first provided by Jeannerod (Jeannerod, 2001), who suggested that the neural substrates of motor imagery are part of a shared network that is also activated during the simulation of action by the observation of action (Jeannerod, 2001). These 'mirror neuron' systems are thought to be an essential component of motor control and learning (Jeannerod, 2001) – hence the belief that activating these systems could aid rehabilitation. The use of a motor imagery-BCI to control a robot compared to traditional motor imagery and physical practice provides several benefits to its user and the practitioner. These advantages include the fact that the former can provide a more streamlined approach such as sensing physiological states, automating visual and kinaesthetic feedback, enriching the task, and increasing user motivation through gamification. There are also general concerns around the utility of motor imagery without physical movement (and the corresponding muscle development that comes from these), and it is possible that these issues could be overcome through a control strategy that progressively reduces the amount of support provided by the motor imagery-BCI system and encourages active motor control (Marchal-Crespo and Reinkensmeyer, 2009; Brookes et al., 2020).

A recent meta-analysis of the neural correlates of action (motor imagery, action observation and motor execution) quantified 'conjunct' and 'contrast' networks in the cortical and subcortical regions (Hardwick et al., 2018). This analysis, which took advantage of open-source historical data from functional magnetic resonance imaging studies, reported consistent

activation in the premotor, parietal, and somatosensory areas for motor imagery, observation, and execution. Predicated on such data, researchers have reasoned that performing motor imagery should cause activation of the neural substrates that are also involved in controlling movement. Furthermore, there have been several research projects that have used action observation in combination with motor imagery in neurorehabilitation (Mulder, 2007; Vogt et al., 2013; Friesen et al., 2017) and motor learning studies (Eaves et al., 2016; T. Kim et al., 2017) over the last decade.

One implication of using motor imagery and action observation to justify the use of BCI approaches is that great care must be taken about the quality of the environment in which the rehabilitation takes place. While people can learn to modulate their brain rhythms without using motor imagery, and there is variability across individuals in their ability to imagine motor actions, motor imagery-driven BCI systems require (by design at least) the patient to imagine a movement. Likewise, action observation requires the patients to see the action clearly. This suggests that the richness and vividness of the visual cues provided are essential for an effective BCI system. It is also reasonable to assume that feedback is vital within these processes, and thus the quality of feedback should also be considered essential. After all, motor imagery and action observation are just tools to modulate brain states (Vogt et al., 2013), and the effectiveness of these tools vary from one stroke patient to another (Nakano and Kodama, 2017). Finally, motivation is important in promoting active participation during therapy (Mawase et al., 2017; Laver et al., 2017). Thus, a good BCI system should incorporate an approach (such as gaming and positive reward) that increases motivation. In addition, recent advances in technology make it far easier to create a rehabilitation environment that provides rich vivid cues, gives salient feedback, and motivates. For example, the rise of immersive technologies, including virtual reality (VR) and augmented reality (AR) platforms (Brookes et al., 2019; Laver et al., 2017; Vourvopoulos et al., 2015), allows for the creation of engaging visual experiences that have the potential to improve a patient's self-efficacy (Johnston et al., 2007) and thereby encourage the patient to maintain the rehabilitation regime. One specific example of this is visually amplifying the movement made by a patient when the movement is of a limited extent so that the patient can see their efforts are producing results (Hülsmann et al., 2019).

In this review, I set out to examine the literature to achieve a better understanding of the current value and potential of BCI-based robotic therapy with three specific objectives:

1. Identify how BCI technologies are being utilised in controlling robotic devices for hand rehabilitation. My focus is on the study design and the tasks employed to set up a BCI-hand robot therapy protocol.

2. Document the readiness of BCI systems. Because BCI for rehabilitation is still an emerging field of research, I expect that most studies would be in their proof-of-concept or clinical testing stages of development. My purpose is to determine the limits of this technology in terms of (a) resolution of hand motor imagery detection (i.e., from gross to fine motor tasks) and (b) the degree of robotic control.

3. Evaluate the clinical significance of BCI-hand robot systems by looking at the outcome measures in motor recovery and determine if a standard protocol exists for these interventions.

It is important to note that there have been several recent reviews exploring BCI for stroke rehabilitation. For example, Monge-Pereira et al. (Monge-Pereira et al., 2017) compiled EEG-based BCI studies for upper limb stroke rehabilitation. Their systematic review (involving 13 clinical studies on stroke and hemiplegic patients) reported on research methodological quality and improvements in the motor abilities of stroke patients. Cervera et al. (Cervera et al., 2017) performed a meta-analysis on the clinical effectiveness of BCI-based stroke therapy in 9 randomised clinical trials (RCT). McConnell et al. (McConnell et al., 2017) undertook a narrative review of 110 robotic devices with brain-machine interfaces for hand rehabilitation post-stroke. These reviews, in general, have reported that such systems provide improvements in both functional and clinical outcomes in pilot studies or trials involving small sample sizes. Thus, the literature indicates that EEG-based BCI is a promising general rehabilitation approach post-stroke. The current work complements these previous reports by providing the first systematic examination of BCI-robot systems for the rehabilitation of fine motor skills associated with hand movement and profiling these systems from a technical and clinical perspective.

2.2. Methodology

2.2.1. Protocol Registration

Details of the protocol for this systematic review were registered on the International Prospective Register of Systematic Reviews (PROSPERO) and can be accessed at www.crd.york.ac.uk/PROSPERO (ID: CRD42018112107).

2.2.2. Search Strategy and Eligibility

An in-depth search of articles from January 2010 to October 2019 was performed on Ovid MEDLINE, Embase, PEDro, PsycINFO, IEEE Xplore and Cochrane Library. Only full-text articles published in English were selected for this review. Table 2.1 shows the combination of keywords used in the literature searching.

Table 2.1: Literature search keyword combinations

Set 1 (OR)		**Set 2 (OR)**		**Set 3 (OR)**
Brain-computer interface/BCI Electroencephalography/EEG Brain-machine interface/BMI Neural control interface Mind-machine interface	AND	Stroke (rehabilitation/ therapy/treatment/recovery) Motor (rehabilitation, therapy/treatment/recovery) Neurorehabilitation Neurotherapy Hand (rehabilitation/therapy/ recovery/exercises/movement)	AND	Robotic (exoskeleton/ orthosis) Powered (exoskeleton/ orthosis) Robot Device

The inclusion criteria for the articles were: (1) publications that reported the development of an EEG-based BCI; (2) studies targeted toward the rehabilitation of the hand after stroke; (3) studies that involved the use of BCI and a robotic device (e.g., exoskeleton, end-effector type, platform-types, etc.); (4) studies that performed a pilot test on healthy participants or a clinical trial with people who have had a stroke. The articles were also screened for the following exclusion criteria: (1) studies that targeted neurological diseases other than stroke; (2) studies that used other intention sensing mechanisms (electromyography/EMG, electrooculography/EOG, non-paretic hand, other body parts, etc.).

Two reviewers (i.e., myself and a colleague) performed independent screenings of titles and abstracts based on the inclusion and exclusion criteria. The use of a third reviewer was planned a priori in cases where a lack of consensus existed around eligibility. However, consensus was achieved from the first two reviewers during this stage. Full-text articles were then obtained, and a second screening was performed until a final list of studies was agreed to be included for data extraction.

2.2.3. Data Extraction

The general characteristics of the study and their corresponding results were extracted from the full-text articles by the reviewers following the Preferred Reporting Items for Systematic Reviews and Meta-Analysis (PRISMA) checklist. The data fields were extracted and categorised as follows:

- Participant characteristics: sample population, healthy or stroke patients, handedness, age, sex, and the duration post-stroke: acute (<2 weeks), subacute (3-11 weeks), early chronic (12-24 weeks), and chronic (>24 weeks). The mean duration since stroke was also accounted for if reported.
- Study design: a general description of study design, experimental and control groups
- Task design: description of the task instructed and stimuli presentation (cue and feedback modalities, i.e., visual, kinaesthetic, auditory, etc.)
- Technical specifications of the system: EEG system used (including the number of channels), robot device used (e.g. hand exoskeleton, end-effector, etc.), actuation mode, and control strategy
- Main outcomes of the study: clinical outcomes (for studies involving stroke patients), classification accuracies based on correct predictions over the total number of trials (participant, group, and study levels; with consideration of the algorithm used and the number of trials set to train the classifier), and other significant findings

This data extraction strategy allowed me to evaluate further the technology and clinical use of the BCI-robot systems used in this study.

2.2.4. Technology Evaluation

EEG Acquisition

The signal acquisition element of an EEG-based BCI is critical to its success in recognising task-related intent. To better understand current practice, I gathered the type of electrode used (i.e., standard saline-soaked, gel or dry electrodes), the number of channels and its corresponding placement in the EEG cap. To illustrate where signals are recorded, I plotted the frequency with which electrodes were used across studies on a topographical map using the 10-20 international electrode placement system.

Signal Processing

I evaluated each study's signal processing strategies, looking specifically at the feature extraction and classification techniques within their respective data pipelines. In addition, for the studies that reported classification accuracy (i.e., comparing the predicted class against the ground truth), I compared their results to the current state-of-the-art classification accuracy published in the literature.

Robot-Assisted Rehabilitation

As the receiving end of the BCI pipeline and the provider of kinaesthetic feedback to the user, the robot-assisted device for hand rehabilitation plays a crucial role in providing the intervention in this therapy regimen. Therefore, I evaluated the robot components based on their actuation type, targeted body part (i.e., single-finger, multi-finger, whole hand), and control strategy. I also reported on commercially available systems, which has passed a series of regulatory processes, making them fit for commercial use, were classified as gold standard devices.

Technological Readiness

I assessed the development stages of the system as a whole by performing a Technological Readiness Assessment. Using this strategy, I was able to determine the maturity of the systems through a Technology Readiness Level (TRL) scale of 1-9 and quantify its implementation in a research or clinical setting (Office of the Director of Defense Research and Engineering Washington DC, 2009). Since a BCI-robot for rehabilitation can be categorised as a Class II-B medical device, I have adapted a customised TRL scale to account for these requirements (Office of the Director of Defense Research and Engineering Washington DC, 2009). The customised TRL accounts for prototype development and pilot testing in human participants (TRL 3), safety testing (TRL 4-5), and small scale (TRL 6) to large scale (TRL 7-8) clinical trials. Performing a technology readiness assessment on each device should allow us to map out the technology's adoption and perceived usefulness. For example, if most of the studies have used devices that have a TRL below the clinical trials stage (TRL 6-8), then I can confidently say that the BCI-robot system is not yet widely accepted in the clinical community. In this way, I can focus on questions that improve my understanding of the factors that impede its use as a viable therapy option for stroke survivors.

2.2.5. Clinical Use

Clinical Outcomes Measures

For studies involving stroke patients, clinical outcomes were obtained based on muscle improvement measures such as Fugl-Meyer Motor Assessment Upper Extremity (FMA-UE) scores (Fugl-Meyer et al., 1975), Action Research Arm Test (ARAT) scores (Lyle, 1981), United Kingdom Medical Research Council (UK-MRC) muscle grade (Matthews, 1977), Grip Strength (GS) Test and Pinch Strength (PS) Test scores (i.e., kilogram force collected using an electronic hand dynamometer) among others.

Physiotherapy Evidence Database (PEDro) Scale for Methodological Quality

A methodological quality assessment was also performed for clinical studies based on the PEDro Scale (Maher et al., 2003). This scale evaluates studies with a checklist of 11 items based on experts' consensus criteria in physiotherapy practice. The complete details of the criteria can be found online (PEDro Scale, 1999). A higher score on the scale (6 and above) implied better methodological quality but are not used as a measure of validity in terms of clinical outcomes. Pre-defined scores from this scale were already present in studies appearing in the PEDro search. However, studies without PEDro scores or those not present in the PEDro database had to be manually evaluated by myself against the 11-item checklist (five of seven studies).

2.3. Results

2.3.1. Search Results

Figure 2.2 shows the study selection process and the number of articles obtained at each stage.

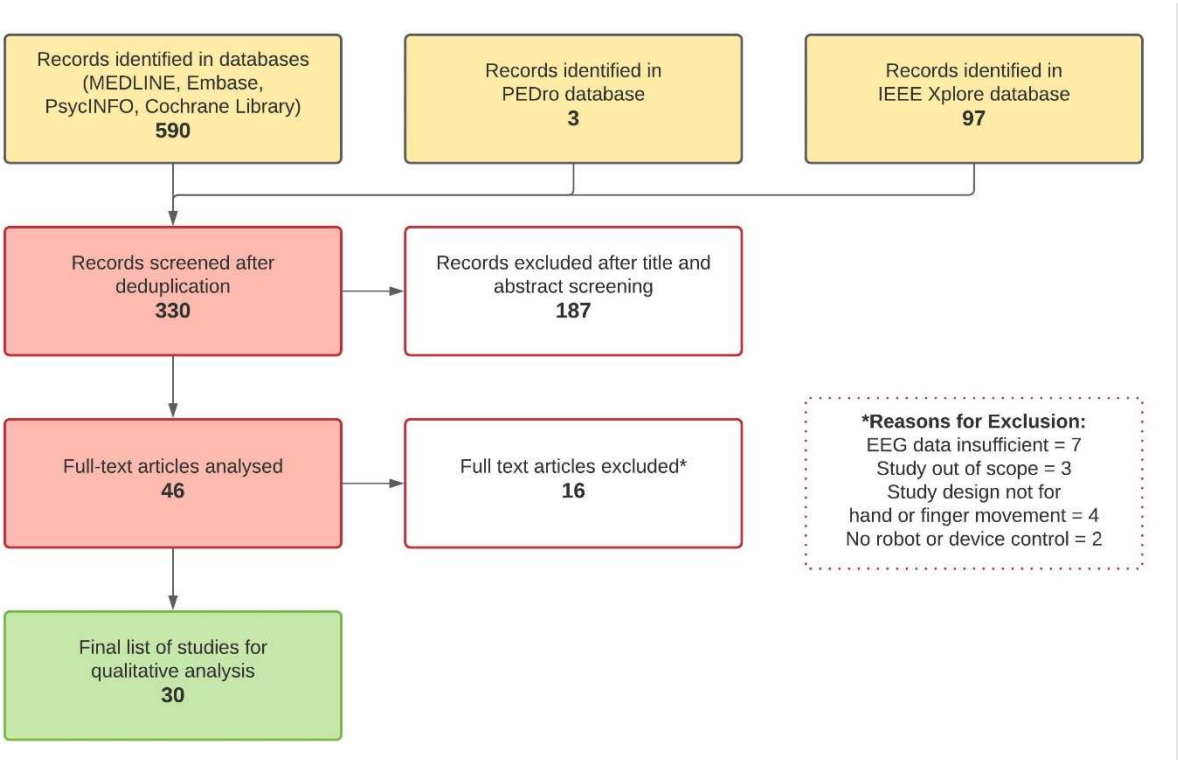

Figure 2.2: Study selection flowchart

A total of 590 studies were initially identified. After deduplication, 330 studies underwent title and abstract screening. Forty-six studies passed this stage, and among these, 16 were removed after full-text screening due to the following reasons: insufficient EEG and robotic data (Broetz et al., 2010; Bergamasco et al., 2011; Cincotti et al., 2012; Ushiba et al., 2014; George et al., 2014; Belardinelli et al., 2017; Rathee et al., 2019) – these studies were either short papers that did not specify the required data fields specified in Section 2.3.3 or there was a lack of detail in the information provided for it to be included in the final table, the study was out of scope (Pellegrino et al., 2012; Norman, 2017; Naros and Gharabaghi, 2017), the study design was not for hand/finger movement (Formaggio et al., 2013; Shiman et al., 2015; Sarasola-Sanz et al., 2017; Bousseta et al., 2018), no robot or mechatronic device was involved in the study (Muralidharan et al., 2011; Ono et al., 2013). A final sample of 30 studies were included in the qualitative review. Among the 30 studies, 11 (Ang et al., 2014; Barsotti et al., 2015; Ono et al., 2016; Bundy et al., 2017; Frolov et al., 2017; Chowdhury, Raza, et al., 2018; Wang et al., 2018; Norman et al., 2018; Chowdhury, Meena, et al., 2018; Carino-Escobar et al., 2019; Tsuchimoto et al., 2019) were involved in testing the BCI-hand robot system on chronic and subacute stroke patients ((Ang et al., 2014; Frolov et al., 2017; Wang et al., 2018; Tsuchimoto et al., 2019) were RCTs) while the rest involved testing on healthy participants (Fok et al., 2011; King et al., 2011; Holmes et al., 2012; Ramos-Murguialday et al., 2012; Coffey et al., 2014; Witkowski et al., 2014; Bauer et al., 2015; Cantillo-Negrete et al., 2015; Vukelic and Gharabaghi, 2015; Ramos-Murguialday and Birbaumer, 2015; Chowdhury et al., 2015; Stan et al., 2015; Naros et al., 2016; Diab et al., 2016; Tacchino et al., 2017; Randazzo et al., 2018; Ono et al., 2018; Li et al., 2019; Zhang et al., 2019). Appendix A shows the full data table for this study.

Studies with Healthy Participants (Prototype Group)

The studies which involved pilot testing on healthy human participants had a combined total of 207 individuals (sample size ranging from 1-32) who had no history of stroke or other neurological diseases. Right-handed individuals made up 44.24% of the combined population, while 55.76% were unreported. These studies aimed to report the successful implementation of a BCI-robot system for hand rehabilitation and were more heterogeneous in study and task designs than

those involving clinical testing. The most common approach was to design and implement a hand orthosis controlled by MI which accounted for 9 out of the 19 studies and were measured based on classification accuracy during the calibration/training period and online testing. Li et al. (Li et al., 2019) and Stan et al. (Stan et al., 2015) also aimed to trigger a hand orthosis, but instead of MI, the triggers used by Li et al. is based on an attention threshold, while Stan et al. used a vision-based P300 speller BCI. Bauer et al. (Bauer et al., 2015) compared MI against ME using a BCI-device while Ono et al. (Ono et al., 2018) studied the implementation of an action observation strategy with a combined visual and kinaesthetic feedback or auditory feedback. Five more studies (Ramos-Murguialday et al., 2012; Vukelic and Gharabaghi, 2015; Ramos-Murguialday and Birbaumer, 2015; Naros et al., 2016; Tacchino et al., 2017) focused on varying the feedback while two more (Witkowski et al., 2014; Zhang et al., 2019) assessed the performance and safety of a hybrid BCI with EMG, EOG or both.

Studies with Stroke Patients (Clinical Group)

A total of 208 stroke patients (with sample size varying 3-74) were involved in the 11 clinical studies. One study (Ang et al., 2014) reported a 3-armed RCT with control groups as device-only and SAT while another study (Frolov et al., 2017) was a multi-centre RCT with sham as the control group. Five studies were uncontrolled – where the aims were either to study classification accuracies during sessions (Barsotti et al., 2015), to monitor clinical outcomes improvement from Day 0 until the end of the programme (Bundy et al., 2017; Carino-Escobar et al., 2019) or both (Norman et al., 2018; Chowdhury, Meena, et al., 2018). Two studies (Wang et al., 2018; Tsuchimoto et al., 2019) were RCTs that compared the effects of the intervention against SHAM feedback. Another study (Chowdhury, Raza, et al., 2018) compared the classification accuracies of healthy and hemiplegic stroke patients against two BCI classifiers, while the remaining study (Ono et al., 2016) compared classification accuracies from stroke patients who receive congruent or incongruent visual and kinaesthetic feedback.

2.3.2. Technology Evaluation

EEG Acquisition

The EEG acquisition systems involved in the studies ranged from low-cost devices having few electrode channels (2-15 gel or saline-soaked silver/silver chloride [Ag/AgCl] electrodes) to standard EEG caps that had higher spatial resolution (16-256 gel or saline-soaked Ag/AgCl electrodes). Studies involving MI accounted for the placement of EEG channels (N=21). This allowed us to determine the usage frequency among electrodes and is presented in Figure 2.3 as a heat map generated in R Studio (using the packages: "akima", "ggplot2" and "reshape2") against the 10-20 international electrode placement system.

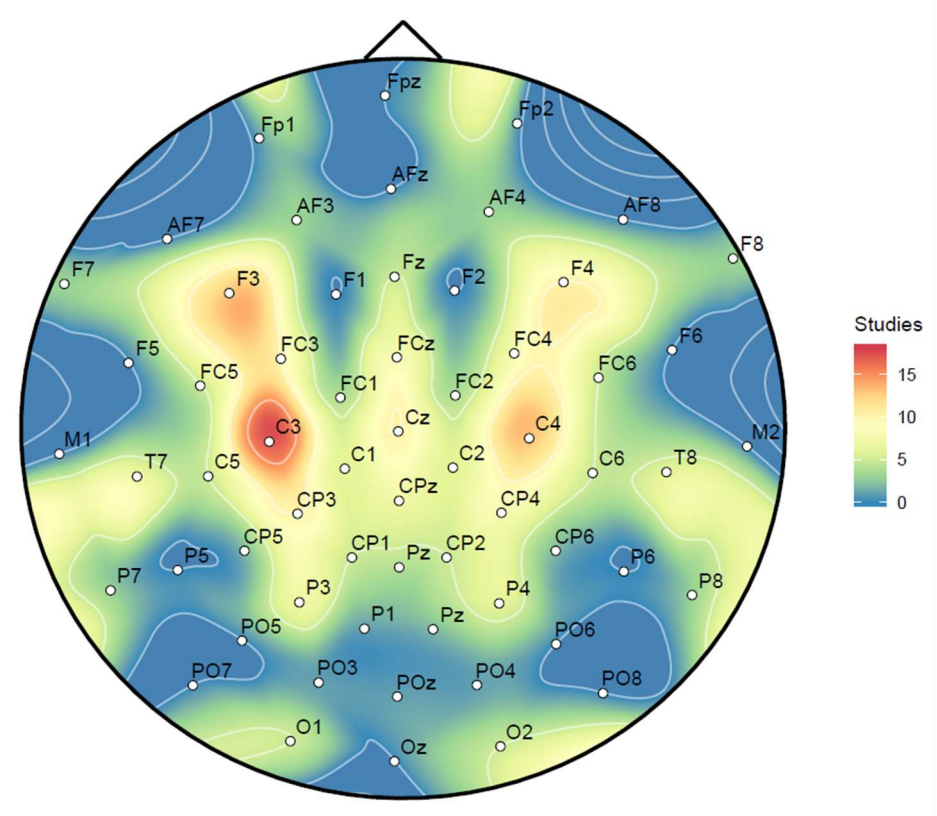

Figure 2.3: EEG channel usage across motor imagery studies (N=21)

It can be seen that the EEG channels used for MI studies are concentrated towards electrodes along the central sulcus (C) region and the frontal lobe (F) region of the placement system where the motor cortex strip lies. Among these, C3 (N=17) and F3 (N=14) were mainly

used, presumably because most of the participants were right-handed. The next most frequent were C4 (N=13) and the electrodes F4, Cz and CP3 (N=10).

Signal Processing: Feature Extraction and Classification

In the EEG-based BCI studies examined, it was found that the feature extraction and classification techniques were variable between systems. Table 2.2 provides a summary of pre-processing, feature extraction and classification techniques across the studies.

Table 2.2: BCI feature extraction and classification strategies

Study	Pre-Processing	Feature Extraction	Classification	Mental Task
(Ang et al., 2014)	Band-pass (0.05-40 Hz)	Filter Bank Common Spatial Pattern (FBCSP) algorithm (Ang et al., 2012)	Naïve Bayesian Parzen Window classifier (Ang et al., 2012)	MI vs rest
(Barsotti et al., 2015)	Band-pass (8-24 Hz)	ERD (β and μ-decrease), CSP	SVM with linear kernel	MI vs rest
(Bauer et al., 2015)	Band-pass (6-16 Hz) using zero-phase lag FIR	ERD (β-decrease)	Linear autoregressive model based on Burg Algorithm	MI vs rest
(Bundy et al., 2017)	Unspecified in the manuscript	ERD (β and μ-decrease)	Linear autoregressive model	MI (affected, unaffected) vs rest
(Chowdhury, Raza, et al., 2018)	Band-pass (0.1 Hz-100 Hz), Notch (50 Hz)	CSP Covariance-based, ERD/ERS (β and μ-change)	SVM with linear kernel, Covariate Shift Detection (CSD)-based Adaptive Classifier	left vs right MI
(Coffey et al., 2014)	Band-pass (0.5 Hz-30 Hz), Notch (50 Hz)	CSP Covariance-based	Linear Discriminant Analysis (LDA) classifier	MI vs rest
(Diab et al., 2016)	Unspecified in the manuscript	Time epochs (unspecified)	Artificial Neural Network (ANN)-based Feed Forward Back Propagation	Non-MI open vs closed
(Frolov et al., 2017)	Band-pass (5-30 Hz), FIR (order 101), IIR notch Chebyshev type I filter (50 Hz)	Time epochs (10 s)	Bayesian-based EEG covariance classifier (Bobrov et al., 2012)	MI (affected, unaffected) vs rest
(Ono et al., 2016)	Band-pass (0.5-30 Hz), notch (50 or 60 Hz)	Time epochs (700 ms), ERD (μ-decrease)	Linear Discriminant Analysis (LDA) classifier	MI vs rest

(Ramos-Murguialday et al., 2012)	Band-pass (8-12 Hz, 12-18 Hz, 18-25 Hz)	Time epochs (5 s), Spatial filter, ERD/ERS (β and μ-change)	Linear autoregressive model	MI vs rest
(Vukelic and Gharabaghi, 2015)	Band-pass (16-22 Hz)	ERD (β-decrease)	Linear autoregressive model based on Burg Algorithm	MI vs rest
(Witkowski et al., 2014)	Band-pass (0.4-70 Hz), Laplacian filter	ERD/ERS (β and μ-change)	Linear autoregressive model based on Yule-Walker algorithm	MI vs rest

SVM = Support Vector Machines, FIR = Finite Impulse Response, IIR = Infinite Impulse Response

There was a wide variation in the implemented signal processing strategies, but a unifying theme across studies was the attempt to: (i) discriminate mental states recorded in EEG across different manual tasks; (ii) classify the different states to produce a viable signal.

While classification accuracy is contingent on the number of mental state classes the system is trying to discriminate, classification accuracies do provide a comparable metric among BCI systems. This review found a high variation in the reported mean classification accuracies among the BCI systems in this study (i.e., 2-class left-hand and right-hand classification)-ranging from 40% (below chance-level) (Ono et al., 2016; Frolov et al., 2017; Norman et al., 2018) up to 95% (King et al., 2011; Holmes et al., 2012; Diab et al., 2016; Li et al., 2019). For reference, two recent reviews on the state-of-the-art classification accuracies for motor imagery BCI find ranges between 63-97% (Gonzalez et al., 2018) and 68-90% (Chaudhari and Galiyawala, 2017).

Robot-Assisted Rehabilitation

Robotic hand rehabilitation systems provide kinaesthetic feedback to the user during BCI trials. Most of these devices are powered by either DC motors, servomotors or pneumatic actuators that transmit energy via rigid links or Bowden cables in a tendon-like fashion. The studies in this review included single-finger (Cantillo-Negrete et al., 2015; Carino-Escobar et al., 2019; Tsuchimoto et al., 2019), multi-finger (Norman et al., 2018) (including EMOHEX (Chowdhury et al., 2015; Chowdhury, Raza, et al., 2018; Chowdhury, Meena, et al., 2018)), full hand gloves

(Li et al., 2019; Zhang et al., 2019) (including mano: Hand Exoskeleton (Randazzo et al., 2018) and Gloreha (Tacchino et al., 2017)) and full arm exoskeletons with isolated finger actuation (BRAVO-Hand (Barsotti et al., 2015)). Nine of the studies (Holmes et al., 2012; Ramos-Murguialday et al., 2012; Coffey et al., 2014; Ramos-Murguialday and Birbaumer, 2015; Chowdhury et al., 2015; Stan et al., 2015; Bundy et al., 2017; Randazzo et al., 2018; Li et al., 2019) presented their novel design of a hand rehabilitation device within the article while some reported on devices reported elsewhere (i.e., in a previous study of the group or a research collaborator). Two commercially-available devices were also used: AMADEO (Tyromotion, Austria) is an end-effector device used in 3 studies (Bauer et al., 2015; Vukelic and Gharabaghi, 2015; Naros et al., 2016), and Gloreha (Idrogenet, Italy) is a full robotic hand glove used by Tacchino et al. (Tacchino et al., 2017). AMADEO and Gloreha are both rehabilitation devices that have passed regulatory standards in their respective regions. AMADEO remains the gold standard for hand rehabilitation devices as it has passed safety and risk assessments and provided favourable rehabilitation outcomes. The International Classification of Functioning, Disability and Health (ICF) provides three specific domains that can be used to assess an intervention of this kind: improving impairments, supporting the performance of activities and promoting participation (Kersten, 2004; Oña et al., 2018). In this case, a gold standard device prioritises user safety (established early in the development process) and delivers favourable outcomes on scales against these domains. Figure 2.4 shows the main types of robotic hand rehabilitation devices.

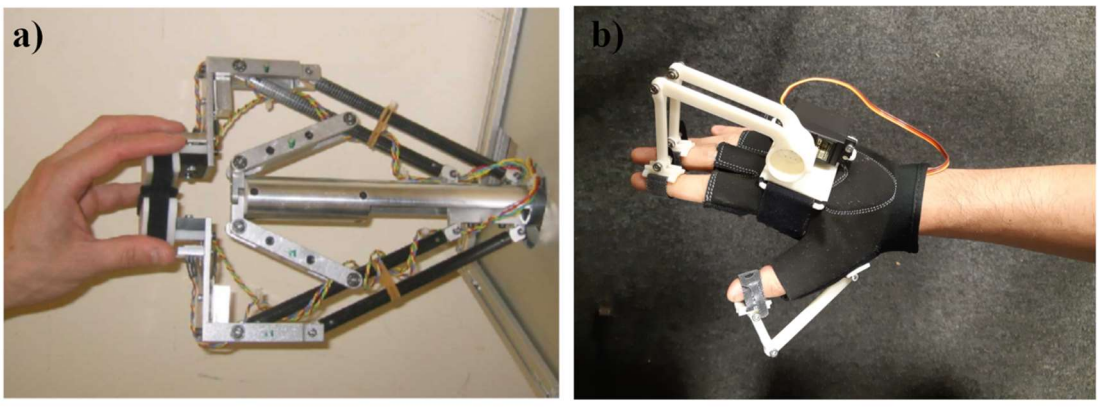

Figure 2.4: Types of robot-assisted hand rehabilitation devices. (a) end-effector devices (Haptic Knob) from (Dovat et al., 2006), (b) wearable hand exoskeletons/orthoses

Technology Readiness Assessment

A Technology Readiness Assessment (Office of the Director of Defense Research and Engineering Washington DC, 2009) was performed for each study and the Technology Readiness Levels (TRL) are presented in Table 2.3. While some of the system components (especially among robotic devices) were commercially available (having TRL 9+), I performed a technology readiness assessment on the whole system to provide an evaluation of its maturity and state-of-the-art development with regard to rehabilitation medicine. I further assessed the TRL of each system at the time of the publication and its subsequent development.

Table 2.3: Technology readiness assessment of the BCI-hand robot systems

Levels	**Description**	**Studies**
TRL 1	Lowest level of technological readiness	
	Literature reviews and initial market surveys	
	Scientific application to defined problems	
TRL 2	Generation of hypotheses	
	Development of research plans and/or protocols	
TRL 3	Testing of hypotheses – basic research, data collection and analysis	Most studies from the prototype group (N=18) (Fok et al., 2011; King et al., 2011; Holmes et al., 2012; Ramos-Murguialday et al., 2012; Coffey et al., 2014; Bauer et al., 2015; Cantillo-Negrete et al., 2015; Vukelic and Gharabaghi, 2015; Ramos-Murguialday and Birbaumer, 2015; Chowdhury et al., 2015; Stan et al., 2015; Naros et al., 2016; Diab et al., 2016; Tacchino et al., 2017; Randazzo et al., 2018; Ono et al., 2018; Li et al., 2019; Zhang et al., 2019)
	Testing of design/prototype – verification and critical component specifications	
	Initial proof-of-concept in limited amount of laboratory/animal models	
TRL 4	Proof-of-concept of device/system in defined laboratory/animal models	(Witkowski et al., 2014)
	Safety testing – problems, adverse events, and potential side effects	
TRL 5	Comparison of device/system to other existing modalities or equivalent devices/systems	(Barsotti et al., 2015), (Ono et al., 2016), (Chowdhury, Raza, et al., 2018), (Tsuchimoto et al., 2019)

TRL 5 (con't)	Further development – testing through simulation (tissue or organ models), animal testing	
	Drafting of Product Development Plan	
TRL 6	Small scale clinical trials (Phase 1) – under carefully controlled and intensely monitored clinical conditions	(Carino-Escobar et al., 2019), (Chowdhury, Meena, et al., 2018), (Norman et al., 2018), (Wang et al., 2018)
TRL 7	Clinical trials (Phase 2) – safety and effectiveness integration in operational environment	(Ang et al., 2014), (Frolov et al., 2017)
TRL 8	Clinical trials (Phase 3) – evaluation of overall risk-benefit of device/system use	
	Confirmation of QSR compliance	
	Awarding of Premarket Approval for device/system by CDRH or equivalent agency	
TRL 9	The device/system may be distributed/marketed	

QSR = Quality System Requirements, CDRH = Center for Devices and Radiological Health

2.3.3. Clinical Use

Clinical Outcomes Measures

Most of the studies adopted FMA-UE, ARAT and GS measurements to assess clinical outcomes. Six studies (Ang et al., 2014; Bundy et al., 2017; Frolov et al., 2017; Wang et al., 2018; Chowdhury, Meena, et al., 2018; Carino-Escobar et al., 2019) reported patient improvement in these measures when subjected to BCI-hand robot interventions; in contrast with their respective controls or as recorded through time in the programme. For Ang et al. (Ang et al., 2014), FMA-UE Distal scores were reported in weeks 3, 6, 12 and 24, and the BCI-device group (N=6) yielded the highest improvement in scores across all time points as compared to the device only (N=8) and SAT (N=7) groups. Bundy et al. (Bundy et al., 2017) reported an average of 6.20±3.81 improvement in the ARAT scores of its participants (N=10) in the span of 12 weeks, while Chowdhury et al. (Chowdhury, Meena, et al., 2018) reported a group mean difference of +6.38 kg ($p=0.06$) and +5.66 ($p<0.05$) in GS and ARAT scores, respectively (N=4). Frolov et al.'s (Frolov et al., 2017) multi-centre RCT reported a higher improvement in the FMA-UE Distal, ARAT Grasp and ARAT Pinch scores of the BCI-device group (N=55) when compared to the

control/SHAM group (N=19), but not in the ARAT Grip scores where the values are both equal to 1.0 with $p<0.01$ for the BCI-device group and $p=0.045$ for the control.

Physiotherapy Evidence Database (PEDro) Scale for Methodological Quality

For the studies that had a clinical testing component, a methodological quality assessment by the PEDro Scale was performed. Two studies which appeared on the PEDro search (Ang et al., 2014; Frolov et al., 2017) had predetermined scores in the scale and were extracted for this part while the rest were manually evaluated by the authors. Table 2.4 shows the results of the methodological quality assessment against the scale. Note that in the PEDro Scale, the presence of an eligibility criteria is not included in the final score.

Table 2.4: Methodological quality of clinical studies based on PEDro scale

	Criteria	**Ang et al.**	**Barsotti et al.**	**Bundy et al.**	**Carino-Escobar et al.**	**Chowdhury-b**	**Chowdhury-c**	**Frolov et al.**	**Norman et al.**	**Ono et al.**	**Tsuchimoto et al.**	**Wang et al.**
1	Eligibility criteria*	1	1	1	1	1	1	1	1	0	1	1
2	Random allocation	1	0	0	0	0	0	1	0	0	1	1
3	Concealed allocation	0	0	0	0	0	0	0	0	0	1	1
4	Baseline comparability	1	0	1	0	1	1	1	0	0	0	0
5	Blind subjects	0	0	0	0	0	0	0	0	0	1	1
6	Blind therapists	0	0	0	0	0	0	0	0	0	1	0
7	Blind assessors	1	0	0	0	0	0	1	0	0	0	1
8	Adequate follow-up	1	1	1	1	1	1	0	1	1	1	1
9	Intention-to-treat analysis	0	0	1	1	1	1	0	1	0	0	0
10	Between-group comparisons	1	0	0	0	1	0	1	0	1	1	1
11	Point estimates and variability	1	1	1	1	1	0	1	1	1	1	1
Total		6	2	4	4	5	3	5	4	3	7	7

*Not included in the final score

2.4. Discussion

2.4.1. General Discussion of Systematic Review Results

This review is the first systematic examination of BCI-driven robotic systems specific for hand rehabilitation to the best of my knowledge. Through this review, I found several limitations present in the studies identified, and I examine these in more detail here and provide recommendations for future work in this area.

To clarify the state of the current development of BCI-hand robot systems, I looked into the maturity of technology used in each study as determined by its readiness level (TRL). All but one in the prototype group was rated as having TRL 3, while the clinical group was more varied in their TRL (ranging from 5 to 7). The system used by Witkowski et al. (Witkowski et al., 2014), a prototype study, was rated TRL 4 due to the study being performed based on improving and assessing its safety features. It is also worth noting that while a formal safety assessment was not performed for the TRL 3 prototypes of Stan et al. (Stan et al., 2015), Randazzo et al. (Randazzo et al., 2018) and Tacchino et al. (Tacchino et al., 2017), safety considerations and implementations were made; a criterion to be satisfied before proceeding to TRL 4. The system used by Chowdhury et al. is an excellent example of improving a TRL from 5 to 6 with a pilot clinical study published within the same year (Chowdhury, Raza, et al., 2018; Chowdhury, Meena, et al., 2018). The two systems used in the RCT studies by Ang et al. (Ang et al., 2014) and Frolov et al. (Frolov et al., 2017) achieved the highest score (TRL 7) among all of the studies, which also meant that no BCI-hand robot system for stroke rehabilitation has ever been registered and commercially-released to date. This suggests that such systems lack solid evidence for propelling commercialisation and technology adoption.

Heterogeneity in the study designs was apparent in both the clinical and prototype groups. The lack of control groups and random allocation in clinical studies (e.g., only 4 out of 11 studies are in the huge sample size RCT stage) made us unable to perform a meta-analysis of effects and continue the study by Cervera et al. (2017) with a focus on BCI-hand robot interventions. Results from the methodological quality assessment showed that only two studies (Wang et al., 2018; Tsuchimoto et al., 2019) scored 7 on the PEDro scale. Although non-

conclusive, these results support the notion that most of the studies are not aligned with the criteria of high-quality, evidence-based interventions.

Almost all the clinical studies (except for Carino-Escobar et al. (Carino-Escobar et al., 2019) and Frolov et al. (Frolov et al., 2017)) limited their recruitment to chronic stroke patients. The reason may be due to the highly variable recovery rates in patients at different stages of their disease (Ballester et al., 2019). Baseline treatments were also not reported in the clinical studies. Instead, the BCI-robot interventions were compared to control groups using standard arm therapy; an example of this was done by Ang et al. (Ang et al., 2014). The heterogeneity of experimental designs reported in this review raises the need to develop clearly defined protocols when conducting BCI-hand robot studies on stroke patients. Until new systems have been assessed on this standard, it will be challenging to generate strong evidence supporting the effectiveness of BCI-robotic devices for hand rehabilitation.

In the development of any BCI-robotic device, several design and feature considerations need to be made to ensure that the systems are both fit for purpose and acceptable to the end-user. These design considerations must go beyond the scope of understanding the anatomy of the hand and the physiology of motor recovery in response to therapy. Feedback from stroke patients should also be an essential part of this design process. Among the extracted studies, I surveyed the extent of end-user involvement in the initial stages of development (i.e., through consultations, interviews, and therapy observations) and found no explicit statements about these in the reports. I recommend, as good practice, for future work in this area to report the type and degree of patient or physician involvement in device development to allow reviewers and readers to gauge the potential usability of the system more readily.

I was able to profile the BCI-hand robot systems regarding their technical specifications and design features. In hardware terms, a BCI-hand robot system involves three major components: (1) An EEG data acquisition system with several electrodes connected to a signal amplifier; (2) A computer where raw EEG data is received then processed by filters and classifiers and where most of the cues and feedback during training is presented via a visual display; (3) a robotic hand rehabilitation system for providing the physical therapy back to the user.

The majority of the studies (N=19) used a BCI solely based on EEG, while the rest were combined with other sensors: EEG with EMG (Ramos-Murguialday et al., 2012; Ang et al., 2014; Bauer et al., 2015; Ramos-Murguialday and Birbaumer, 2015; Chowdhury et al., 2015; Naros et al., 2016; Tacchino et al., 2017; Chowdhury, Raza, et al., 2018), EEG with force sensors (Chowdhury, Meena, et al., 2018) and an EEG-EMG-EOG hybrid system (Witkowski et al., 2014; Zhang et al., 2019). This integration mainly aims to improve signal quality by accounting for the artefact or by providing added modalities. For example, action potentials such as those caused by ocular, muscular and facial movements interfere with nearby electrodes, and the presence of an added electrophysiological sensor accounting for these would enable the technician to perform noise cancellation techniques as the first step in signal processing.

The choice of EEG system and the type of electrodes provides a technical trade-off and affects the session both in terms of subjective experiences (i.e., ease-of-use, preparation time, cleaning, comfortability) and data performance. Due to the presence of a conducting gel/solution, standard "wet" electrodes provide a degree of confidence in preventing signal disruption within a short duration, usually enough for a standard stroke therapy session. However, this also makes the setup, use and cleaning in the experiment more challenging, non-ambulatory and reliant on a specialised laboratory setup (Graimann et al., 2010). Conversely, dry electrodes offer an accessible and portable alternative by using dry metal pins or coatings that comb through hair and contact the scalp directly. The signal fidelity of dry electrodes is still debated in the BCI community. A systematic comparison between dry passively-amplified and wet actively-amplified electrodes reported similar performance in the detection of event-related potentials (ERP) (Kam et al., 2019). However, for a study involving dry active electrodes (Mathewson et al., 2017), high inter-electrode impedance resulted in increased single-trial and average noise levels compared to both active and passive wet electrodes. In classifying MI, movement-related artefacts adversely affect active dry electrodes, but these can be addressed through a hybrid system of other physiological sensors to separate sources (Saab et al., 2011).

Almost all of the studies included used a standard EEG system with "wet" electrodes (e.g., g.USBamp by g.tec medical engineering GmbH and BrainAmp by Brain Products), while three used Emotiv EPOC+, a semi-dry EEG system that uses sponge conductors infused with

saline solution. While the use of dry electrodes has been observed in pilot and prototype studies of BCI-hand robot systems (Norman, 2017; Ushiba et al., 2014; Holmes et al., 2012; Fok et al., 2011) and other motor imagery experiments (Guger et al., 2011; Mladenov et al., 2012; Grummett et al., 2015; Abdalsalam et al., 2017), no dry EEG system was used in the final 30 studies that tested healthy or stroke participants. It is expected that as dry EEG systems continue to improve, their use in clinical studies of BCI will also become increasingly prominent.

The degree of BCI-robotic control for the majority of the studies (N=26) was limited to triggering the device to perform grasping (opening and closing of hand) and pinching (a thumb-index finger pinch or a 3-point thumb-index-middle finger pinch) movements using MI and other techniques. A triggered assistance strategy provides the patient's minimum amount of active participation in a BCI-robot setup (Marchal-Crespo and Reinkensmeyer, 2009). The main advantages of this are that it is easy to implement, requiring less computational complexity in signal processing. However, a higher spatial or temporal volitional control over the therapeutic device increases its functionality and can be used to develop more engaging tasks for stroke therapy. Among the studies, no robotic control setup was able to perform digit-specific MI which corresponds to the spatial aspects of volitional control. This is a limitation caused by the non-invasive setup of EEG and is due to the low spatial resolution brought by the distances between electrodes (Srinivasan, 1999). The homunculus model, a representation of the human body in the motor strip, maps the brain areas where activations have been reported to occur for motor processes. The challenge of decoding each finger digit MI in one hand is that they only tend to occupy a small area in this strip. Hence even the highest resolution electrode placement system (i.e., the five per cent or 10-5 system – up to 345 electrodes) would have difficulties accounting for digit-specific MI for BCI.

In contrast to EEG, electrocorticography (ECoG) have been used to detect digit-specific MI. The electrodes of ECoG come in contact directly with the motor cortex and is an invasive procedure, making it non-ideal for use in BCI therapy (Liao et al., 2014). However, it is worth noting that some studies were successful in implementing continuous control based on ERD/ERS patterns. Bundy et al. (Bundy et al., 2017) and Norman et al. (Norman et al., 2018) were both able to apply continuous control of a 3-DOF pinch-grip exoskeleton based on spectral power

while Bauer et al. (Bauer et al., 2015) provided ERD-dependent control of finger extension for an end-effector robot. These continuous control strategies have been shown to be very useful in BCI-hand robots for assistive applications (i.e., partial or full device dependence for performing ADL tasks (Johnson et al., 2008)). Whether this type of control can significantly improve stroke recovery is still in question as the strategy of robots for stroke rehabilitation can be more classified as a therapeutic "exercise" device.

Signal processing and machine learning play a vital role in developing any EEG-based BCI. The pre-processing techniques (e.g., filtering, artefact removal), types of features computed from EEG, and the classifier used in machine learning can significantly affect the performance of the robotic system in classifying the user's intent via MI (Arvaneh et al., 2011). False classification, especially during feedback, could be detrimental to the therapy regime related to the reward and punishment mechanisms that are important in motor relearning (Quattrocchi et al., 2016). For example, false negatives hinder the reward strategy essential to motivate the patient, while false positives would also reward the action with the wrong intent. In this review, a critical appraisal of the signal processing techniques was done on each system to recognise the best practices involved. The current list of studies has revealed that approaches to developing MI-based EEG signal processing are highly diverse, which makes it difficult to compare across the systems and hinders the development of new BCI systems informed by the strengths and weaknesses of existing state-of-the-art systems. The diversity in the design process can be beneficial to develop complex MI EEG-based BCI systems to achieve high efficiency and efficacy. However, such newly developed systems should be open-sourced and easily reproducible by the research community to provide valid performance comparisons and drive forward the domain of robotic-assisted rehabilitation.

In addition to MI, other strategies for robotic control were reported. Diab et al. (Diab et al., 2016) and King et al. (King et al., 2011) both facilitated the movements of their respective orthoses by physical practice, while Stan et al. (Stan et al., 2015) utilised a P-300 evoked potential speller BCI, where the user visually focused on a single alphanumerical character situated in a grid. The chosen character then corresponded to a command for the hand orthosis, thereby producing the desired stimulus for the patient. While the latter study reported a 100%

accuracy rate in terms of intention and execution, the EEG channels were situated in the visual cortex rather than the motor strip, which deviates from activating the desired brain region for plasticity. This highlights a broader issue on the intent behind a BCI-robotic system. Given that any potential signal that a patient can reliably modulate can be used to trigger a robot and that such an approach would be antithetical to the goal of many MI-based systems, engineers may consider how they can tailor their systems to ensure that a user implements the appropriate control strategy (and corresponding neural networks). For example, this can be implemented by taking a hybrid approach that includes motor-related intent recognition such as EMG and force sensors to recognise residual movement from an impaired limb.

In order to facilitate hand MI and account for significant time points in the EEG data, all the studies employed a cue-feedback strategy during their trials. Nineteen of the studies presented a form of visual cue, while the rest, except for two unspecified (Fok et al., 2011; Tsuchimoto et al., 2019), involved cues in auditory ("bleep") (Ramos-Murguialday et al., 2012; Bauer et al., 2015; Ramos-Murguialday and Birbaumer, 2015; Naros et al., 2016; Tacchino et al., 2017), textual (King et al., 2011; Holmes et al., 2012; Stan et al., 2015) or verbal (Diab et al., 2016) forms. As for the provision of matching sensory feedback, 16 studies presented a combination of kinaesthetic and visual feedback, with some also providing auditory feedback during successful movement attempts. All the studies provided kinaesthetic feedback through their robotic devices. Some systems with visual feedback, such as Wang et al. (Wang et al., 2018), Li et al. (Li et al., 2019), Chowdhury et al. in both their clinical studies (Chowdhury, Raza, et al., 2018; Chowdhury, Meena, et al., 2018) and Ono et al. in their clinical (Ono et al., 2016) and pilot testing experiments (Ono et al., 2018), used a video of an actual hand performing the desired action. Ang et al. (Ang et al., 2014) and Stan et al. (Stan et al., 2015), in a different strategy, provided visual feedback through photo manipulation and textual display, respectively. While these two studies reported promising results, it should also be considered that such cue and feedback types (including Graz visualisations and auditory forms) are non-representative of hand movement and may not provide the same stimuli as an anthropomorphic representation of a hand moving its desired course. This may be essential when we base principles of stroke recovery in alignment with how MI correlates with AO – an underlying theme of the motor simulation theory proposed by Jeannerod (Jeannerod, 2001). Figure 2.5 shows how different

kinds of visual cue and feedback can be presented to participants to help facilitate motor imagery.

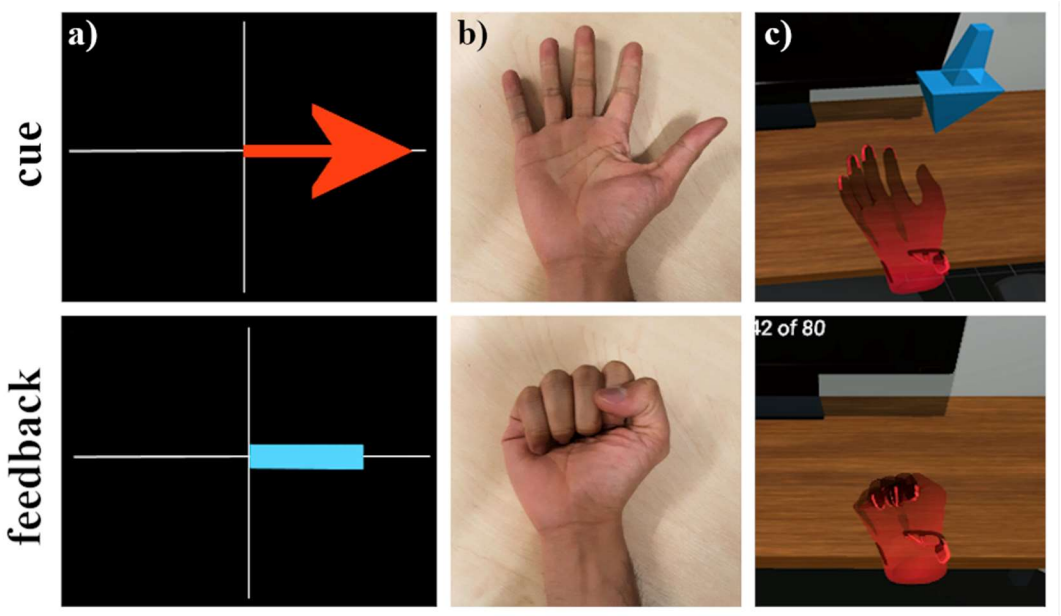

Figure 2.5: Visual cue and feedback during motor imagery trials in different conditions. (a) Graz motor imagery visualisations – the arrow (cue) tells the user which side of the limb (left or right) should be imagined, while the blue bar is the feedback provided after running new motor imagery attempts to a pre-trained classifier model (b) video recordings of hand movement which are played instead of the abstract arrow and bar Graz visualisations (c) proposed animated virtual hand representation of the same motor imagery paradigm through virtual or augmented reality

2.4.2. Future Directions

There is great potential for BCI-hand robots in the rehabilitation of an affected hand following a stroke. Nevertheless, it is important to emphasise that there is currently insufficient evidence to support such systems within clinical settings. Moreover, the purported benefits of these systems rest on conjectures that require empirical evidence. In other words, there are grounds for supposing that MI could be beneficial within these rehabilitation settings but no supporting evidence. This systematic review has also revealed several technological limitations to existing BCI-hand robotic systems. There is an urgent need to address these limitations to ensure that

the systems meet the minimum required product specification levels (in measuring brain activity, processing signals, delivering forces to the hand, and providing rich feedback and motivating settings). The ethics and usefulness of conducting clinical trials with such systems must be thoroughly reviewed until they can demonstrate minimum levels of technological capability. Considerations must be made regarding what standards these systems should obtain before subjecting them to a clinical trial.

2.4.3. Ideal Setup for a BCI-hand Robot

I summarise the information gathered from this review about what constitutes an acceptable setup for a BCI-hand robot for stroke rehabilitation. My focus is on improving individual components in data acquisition, processing, the robotic device, and the stimuli. Table 2.5 presents the features and specifications of an acceptable, fully integrated system.

Table 2.5: Exemplary features and specifications of future BCI-hand robot systems

Component	**Features and Specifications**
Data Acquisition	• Dry EEG system with 8-16 channels, comfortable and easy to use
System and Software	• Inclusion of other bio-signal sensors such as EMG, EOG, force, accelerometers to remove artefacts and improve classification
	• Robust and reliable signal processing software: machine learning-based algorithms that discriminate brain states such as MI or evoked potentials with high classification accuracies (≥95%) and lower calibration times.
	• Low latency in the delivery of the feedback should be considered
Hand Robot	• Safe, comfortable, and aligned with the hand's range of motion
	• Effective in providing kinaesthetic feedback
	• Use of back drivable or soft actuators that effectively assist movement without additional injury
	• Multiple levels of safety and emergency features (mechanical, electronic, software), clear operation

Visual Cue and Feedback	• Provide rich visual cues and feedback to intended tasks taking account of its combination with other sensory modalities (e.g., tactile, auditory) • A geometric representation of the hand (video or simulated environment) which can be in multiple platforms such as display monitors or VR/AR on a head-mounted device • Gamification of therapy exercises to provide an engaging regime to stroke patients

Implementing these features in an ideal BCI-robot setup needs to be weighed against socioeconomic factors in healthcare delivery to be considered market-ready. An ideal BCI system should primarily provide above chance-level classification after the first session on the first day of therapy. Ideally, the classification algorithm should also translate and adapt to following sessions or days, reducing the number of training sessions and focusing on the main therapy tasks. An alternative approach is to focus on making the setup an engaging experience. In other words, the delivery of intervention can be started immediately when the patient wears the EEG cap and runs the BCI system. For the hand robot system, more specific criteria can be followed with the numerous design protocols, regulation standards and assessment matrices mentioned in this review. Nevertheless, end-user involvement in the design with the prioritisation of safety while allowing the most natural hand movement and ROM possible is the recommended goal.

2.4.4. Ideal Setup for Clinical Trials

I also propose a set of specialised criteria for BCI-hand robot systems in addition to the standard motor improvement scores (e.g., ARAT, FMA-UE) evaluated during clinical trials. Firstly, classification accuracies between intended and interpreted actions from the data acquisition and software component should always be accounted to track the effectiveness of BCI in executing the clinical task. In addition to this, system calibration and training procedures, especially in their duration, should be detailed in the protocol to document the reliability of the classification algorithm. There is not much to consider in the use of robotic devices as they are most likely to be mature (if not yet commercially available) before being used as the hardware component in

the study. However, the devices' functionality (i.e., task to be performed, degree of control and motion, actuation, power transmission, etc.) should always be stated as they contribute to evaluating interactions between other components in the system. Lastly, controls for the clinical study must always be included, even with small-scale patient studies. As discussed in this article, these controls may be in the form of sham, standard arm therapy (SAT), standard robotic therapy, congruency feedback and quality of stimuli. Having regarded and implemented these criteria would help homogenise the clinical data for future meta-analyses, strengthen evidence-based results and provide reliable documentation for individual and interacting components.

2.4.5. Proposed Roadmap

I suggest that the immediate focus for BCI-controlled robotic device research should be on the engineering challenges. Only when these challenges have been met that it is valid and ethical to subject the systems to clinical trials. I recommend that the challenges be broken down into the following elements: (1) data acquisition; (2) signal processing and classification; (3) robotic device; (4) priming and feedback environment; (5) integration of these four elements. The nature of these challenges means that a multidisciplinary approach is required (e.g., including psychologists, cognitive neuroscientists, and physiologists to drive the adoption of reliable neural data acquisition). It seems probable that progress will be made by different laboratories tackling some or all of these elements and coordinating information sharing and technology improvements. Once the challenges have been met (i.e., there is a system that can take neural signals and use these to help drive a robotic system capable of providing appropriate forces to the hand within a motivating environment), then robust clinical trials can be conducted to ensure that the promise of this approach does translate into solid empirical evidence supporting the use of these systems within clinical settings.

Chapter 3
Theoretical Framework

3.1. Introduction

This chapter presents the theoretical framework of the thesis. I will first discuss the theory of brain-computer interfaces, including why it is used as a viable signal of intent for active robotic control and then review the basics of electroencephalography-based BCI, focusing on motor imagery as a task paradigm. Continuing from the findings in Chapter 2, I will then lay out a potential solution for improving motor imagery BCI based on two factors: visual stimuli and kinaesthetic stimuli. Finally, I will end the chapter by clearly stating my hypothesis and research aims, providing context to the following chapters of this current work.

3.2. Signals of Intent for Active Robotic Control

Robot-assisted devices for rehabilitation can either be passively or actively controlled (Wu et al., 2018; Marchal-Crespo and Reinkensmeyer, 2009). Both control strategies aim to provide physiotherapy by performing repetitive range-of-motion exercises in a clinical or home setting. The main difference between the two is in the modality of the input signal. Passive robotic devices are controlled by pre-programmed commands to perform a mechanical motion and are similar to a traditional session given by a physiotherapist. On the other hand, active robotic devices depend on the user's intention to move or perform a task. Active participation in such therapy sessions is a crucial factor in increasing the rate of recovery in patients (Wu et al., 2018). Because of this principle, an active control strategy is utilised in robot-assisted rehabilitation (G.Y. Kim et al., 2017) and video game therapy (Vanbellingen et al., 2017).

In order to provide signals for the active control of a robot for rehabilitation, we focus on the physiological signals of intent. A *signal of intent*, which can be external or internal, is acquired when the intention to move or perform a task is recognised and translated into

executable robot commands. Rehabilitative intervention is administered when the robotic device, in the form of an exoskeleton or end-effector, performs the motion aligned with the patient's joints and linkages (G.Y. Kim et al., 2017). When executed successfully, whether as a continuous signal or a trigger, the robot provides the movement needed to close the neural loop between intention and execution. This active control strategy for therapy promotes activity-dependent neuroplasticity in stroke survivors undergoing therapy (Fregni and Pascual-Leone, 2006; Hallett, 2001) and is achieved by the repeated utilisation of cognitive functions and personal experience to a task (Ganguly and Poo, 2013).

External signals of intent refer to voluntary muscle movement and must be evident in musculoskeletal action. Examples of these include finger taps, eye movements, and voice commands. They are based on muscle activation brought upon by the intent signal coming from the brain descending into the motor pathways, which control skeletal muscle movement. For patients who have had a stroke, the intact regions of the brain can still provide such signals, but they are weaker in terms of magnitude (Marchal-Crespo and Reinkensmeyer, 2009). Not all of these external signals are optimal for controlling a robot for rehabilitation. The signal of intent must be closely related to the intended action. In this case, the focus should be on the movement of the upper extremities. In order to minimise the categorical differences between the signal of intent and the intended action, eye movement and voice commands should be ruled out as a viable signals for robotic control in this study.

We now look at two types of external signals of intent that can be easily accessed and interpreted for robotic control. First, we have thin, flexible force sensors which can detect slight contact or pressure (Ashruf, 2002). They are made up of small resistors that record values according to the applied force. A simple and minimal movement such as a finger tap is only needed to recognise an intent with this sensor. This can be used as a trigger for the robot to perform the rest of the movement, thereby delivering the assistive intervention for its user. This technique can be ideal for patients with weak or spastic muscles as it combines both the advantages of an active and passive strategy for motor therapy. Second, we have electromyography (EMG) sensors that record electrical activity from skeletal muscles (Konrad, 2006). An EMG signal is generated when individual muscle fibres exhibit a depolarization-

repolarization process in its membrane during excitation. This creates a difference in electric charge between the two ends. Collectively, this difference can be detected by electrodes and amplified to give the signal; formally called as a motor unit action potential. Among different methods to acquire EMG, we look at non-invasive techniques particularly surface EMG (Konrad, 2006). Unlike intramuscular EMG, which uses needle electrodes, surface EMG is portable and easily accessible as it uses conductive electrodes that record electrical muscle activity above the skin. With the correct placement of skin electrodes, one can extract motor intent from the regions of interest in the musculoskeletal system (Manguerra et al., 2018; Leonardis et al., 2015; Dipietro et al., 2005) are some examples of surface EMG being utilised as an active control method for robot-assisted rehabilitation. Figure 3.1 shows a map of external signals of intent and their usability as a control signal for a robot-assisted rehabilitation setup. The methods I deem to be non-viable and non-optimum for the current rehabilitation setup are greyed out.

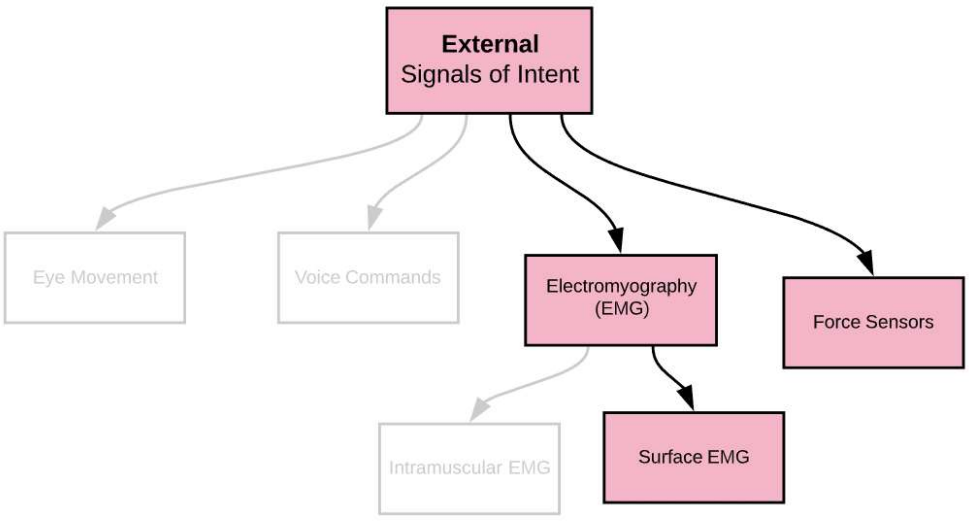

Figure 3.1: External signals of intent

While using force sensors and surface EMG can be easily accessible and direct in acquiring external signals of intent, there are some limitations in using such techniques. For example, the disrupted motor pathways caused by the damaged brain regions after stroke may not be enough to elicit an EMG signal strong enough to be detected by electrodes (Marchal-Crespo and Reinkensmeyer, 2009). This may also be the case for spasticity, where the muscle

tone is excessive, therefore, cannot be sensibly interpreted by the sensing system (Chen et al., 2018). There are also issues involving high signal-to-noise ratios brought upon by subcutaneous fat diminishing the EMG signal (Kuiken et al., 2003). These limitations can make external signals of intent non-optimal as the primary source of the robotic device for rehabilitation. Therefore, as an alternative or complementary approach, we can increase the functionality of such devices by looking into internal signals of intent.

Internal signals of intent originate from inside the central nervous system, particularly along the brain's cortical regions. These processes, when correctly interpreted, can bypass the efferent motor pathways and control a device directly. This is the principal basis for developing the architecture of brain-computer interfaces (BCI) (Wolpaw et al., 2002; Graimann et al., 2010). Brain activity decoding is more expansive in its methods and techniques than those with force sensors or EMG. It also requires more complex processing because its signals have more dimensionality in the spatial and temporal domains. During specific brain processes and states (e.g. cognition, planning and execution of motor-related activity), the brain elicits signature electrical signals brought by the transmission of chemical communicators (neurotransmitters) between individual neurons in specific regions of interest (Lovinger, 2008). These impulses can be recorded, interpreted and imaged by various methods (Lystad and Pollard, 2009). Finding the optimum technique for controlling a BCI requires having the right amount of spatial resolution, temporal resolution and accessibility, among other factors (Lenartowicz and Poldrack, 2010). Spatial resolution in brain imaging refers to how well a technique measures individual neuronal populations during a particular activity. Decoding motor-related brain activity relies mainly on the sensorimotor cortex. A homunculus model (see Figure 3.2), a distorted representation of human body parts, shows how much space in the cortex is occupied by sensory and motor activities (Sinha et al., 2019).

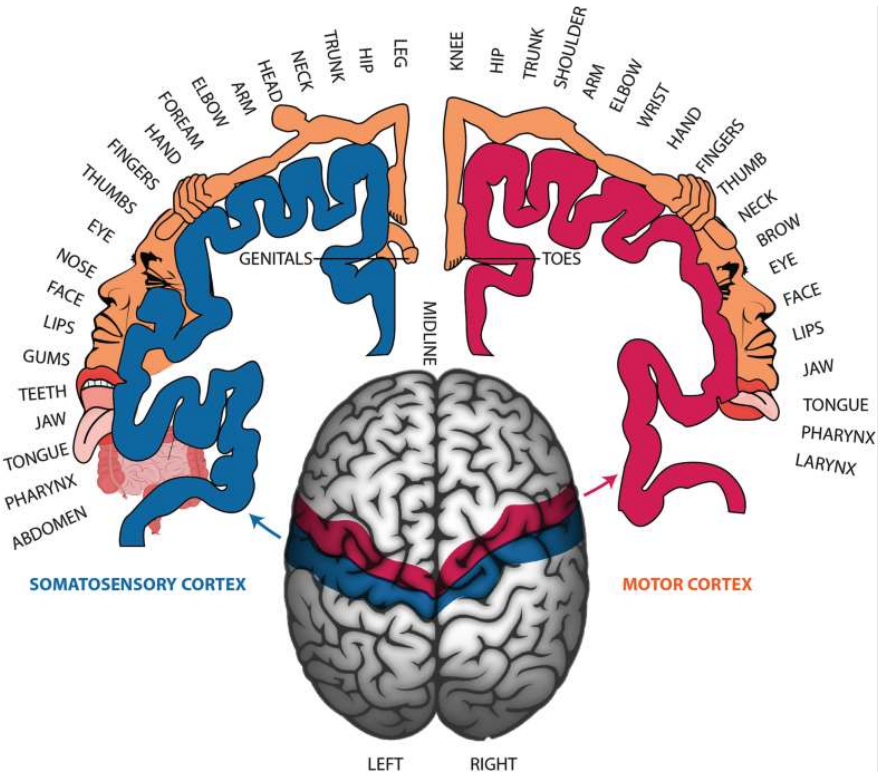

Figure 3.2: Human homunculus of the sensorimotor cortex from (Sinha et al., 2019)

Therefore, a technique with low spatial resolution would give us a "blurry" picture of the brain activity in the exact regions of interest. Likewise, a higher spatial resolution in a technique would resolve more activated brain regions; the more potential it can discriminate motor imagery tasks for BCI control (Chacko et al., 2019; Yong and Menon, 2015). The temporal resolution in brain decoding refers to how well a technique measures a brain activity signal in the time domain. This is usually determined by the frequency of samples recorded per second (unit: Hertz or Hz). Neural signatures for motor processes are quick and hard to find. They can span from milliseconds to seconds, and a good brain activity decoding system must record and process these samples seamlessly.

The third requirement for an ideal brain activity decoding system is its accessibility. An ideal BCI-robot system for rehabilitation is portable/mobile, easy to set up, and user-friendly. This also means that the system should not require a costly laboratory setup nor a tedious and time-consuming patient preparation protocol for each therapy session. With these requirements in place, I can immediately rule out imaging techniques requiring room-scale space, such as

magnetoencephalography (MEG), positron emission tomography (PET) and functional Magnetic Resonance Imaging (fMRI), as these involve a bulky equipment setup (Lenartowicz and Poldrack, 2010; Lystad and Pollard, 2009). Some techniques also require electrodes to be implanted in the cortical or subcortical regions, such as electrocorticography (ECoG) (Hill et al., 2012) and depth electrodes (Viskontas and Fried, 2009), among others. These invasive methods would require at least two surgical procedures: placing the electrodes before enrolling in the therapy programme and removing them. Because the ultimate goal of motor rehabilitation is to get out of the programme as soon as possible and continue doing activities of daily living independently, I also ruled these techniques out of this study. A non-invasive technique called functional near-infrared spectroscopy (fNIRS) measures hemodynamic patterns (i.e., blood oxygen) in the brain via optical absorption (Berger et al., 2019). This technique can provide a high temporal resolution and optimum spatial resolution and is relatively portable than room-scale techniques. However, this technique is currently in its infancy and is less accessible to be adopted by developers of BCI-robot therapy systems.

With all of these in mind, we look at electroencephalography (EEG), an accessible, non-invasive and widely studied brain imaging procedure (Teplan, 2002). With the proper signal processing pipeline, the temporal and spatial resolutions of EEG required for motor activity interpretation can be achieved (Burle et al., 2015). EEG records brain activity from the scalp using conductive silver/silver chloride electrodes in dry, saline-soaked or gel forms (Teplan, 2002). It has been argued that EEG has a relatively high temporal resolution but a sub-optimal spatial resolution (Burle et al., 2015). Furthermore, since EEG is recorded from the scalp, the electric signals get diminished as it passes through layers of anatomical barriers such as the meninges and the bones of the skull before reaching the skin where the electrodes are in contact (Nunez et al., 1994). While these physiological and technical limitations can pose a threat to its usability in BCI control, the growing research and development in signal processing algorithms and hardware implementation make it one of the premier techniques in acquiring motor-related signals of intent (Graimann et al., 2010; Lazarou et al., 2018; Rashid et al., 2020). Figure 3.3 summarises the brain recording and imaging techniques used in decoding internal signals of intent. As with the external signals of intent, the methods I deem to be non-viable and non-optimum for the current rehabilitation setup are greyed-out.

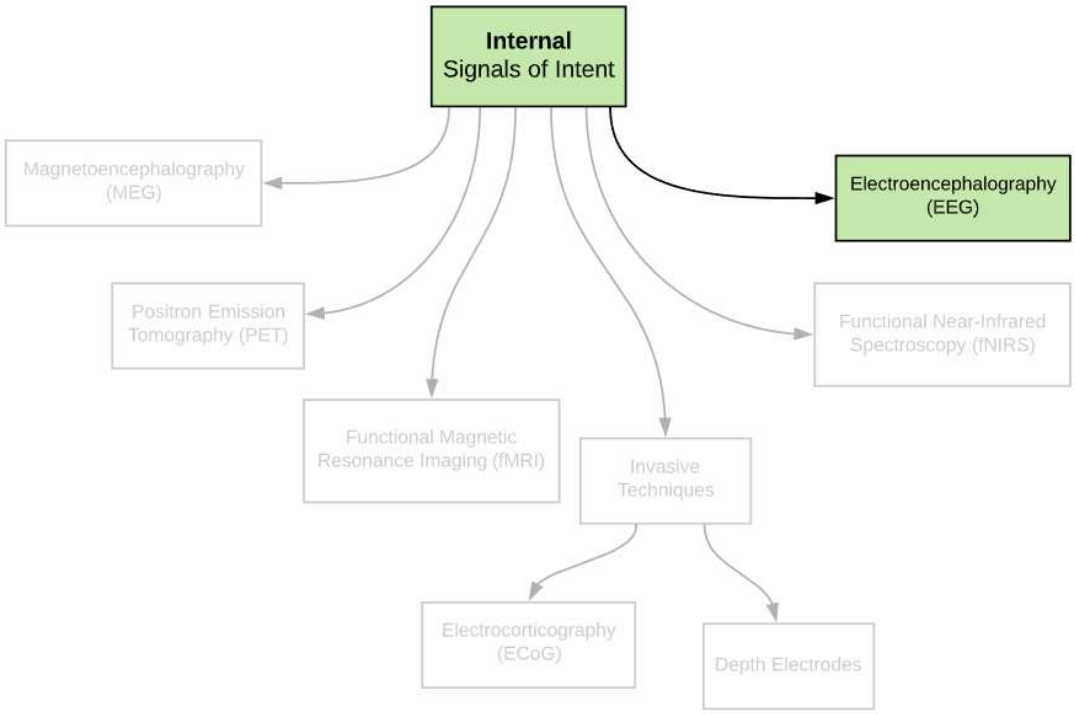

Figure 3.3: Internal signals of intent

3.3. Electroencephalography-based Brain-Computer Interfaces

The types of EEG-based BCI can be categorised based on their application or intended function. Each application has a corresponding decoding technique, electrode montage, and processing pipeline to detect a particular task's neural signatures. Vidal (1973) and Wolpaw et al. (2012) were the first to introduce mental strategies and brain patterns that can be decoded to control an EEG-based BCI. (Graimann et al., 2010) provided a comprehensive introduction to these systems and their applications. In their book, EEG signals for BCI control were categorised into those that use (1) selective attention and (2) motor imagery (Graimann et al., 2010). (Lotte, 2014) provided a different perspective that categorised EEG-based BCI on oscillatory and non-oscillatory activity. Recently, (Lazarou et al., 2018) have provided an in-depth review of these systems applying to motor rehabilitation. Their review categorised EEG-based BCI according to the following neurophysiological input: slow cortical potentials, evoked potentials, and sensorimotor rhythm. For the current study, it is most beneficial for the end-user to use an EEG

method closely related to motor activities in rehabilitation. EEG methods for BCI control can utilise non-motor related intent. Instead, these techniques rely on visual processes (i.e., depend on external visual stimuli) and other mental states such as attention and emotion. While some of these techniques have been implemented in assistive devices, its application for robot-assisted rehabilitation may be less optimal. These systems rely on the visual response of the user rather than the self-induced intent to perform an action (Fazel-Rezai et al., 2012). For the current study, the following techniques have been ruled out:

- **Event-Related Potential (ERP) BCI** – ERPs can be extracted as a direct response to a specific sensory, cognitive, or motor event (Luck, 2005). The P300 Speller BCI is an example of a non-motor related ERP used as a signal to control a BCI. The P300 signal is extracted from electrodes around 250 to 500 milliseconds after a visual cue and is prominent along the parietal lobe region. This signal is often associated as a measure of cognitive function, particularly in decision making (Farwell and Donchin, 1988; Fazel-Rezai et al., 2012). (Stan et al., 2015) have implemented this method to control a robot by spelling various letters from a grid-like pattern.

- **Visual Evoked Potential BCI** – BCI types that are based on the brain's natural response to visual stimuli and are initially characterised by a negative peak at 100 milliseconds post-stimuli (N1) followed by a positive peak at 200 milliseconds (P2) (Vidal, 1973; Vidal, 1977). A variant of this technique uses Steady-State Visual Evoked Potentials (SSVEP), which are responses to visual stimuli at specific frequencies (i.e., 3.5 Hz – 75 Hz) (Morgan et al., 1996; Müller et al., 1998).

I now arrive with two EEG-based signals that are most associated with motor intent:

- The first one is a type of motor-related slow cortical potential called Bereitschaftspotential (BP), also known as pre-motor potential or readiness potential. This signal is measured in the fluctuations of the δ band (0.1-4 Hz) at the primary motor cortex (M1) and supplementary motor area (SM1) about a second before movement onset (Bhagat et al., 2016). It is composed of two distinct components: BP1 (early BP) occurs

at -1.2 to -0.5 seconds, while BP2 (late BP) is at -0.5 seconds before movement onset (Bhagat et al., 2016).

- The second one is based on the modulation of the sensorimotor rhythm (SMR) during action simulation, including motor imagery and action observation. Particularly, the EEG band power in the μ (9-11 Hz) and β (13-24 Hz) frequency bands produce signature patterns of desynchronisation and synchronisation during the execution of these events when compared to EEG band power at the resting state (Neuper and Pfurtscheller, 2001). These event-related spectral perturbations are called event-related desynchronisation (ERD) or synchronisation (ERS). Contrary to BP, ERD/S happens at the onset of motor execution, motor imagery and action observation and can be sustained for more than a few seconds (Pfurtscheller and Lopes da Silva, 1999; Pfurtscheller and Aranibar, 1977).

The nature of the signal determines how the EEG processing pipeline is developed as the stream of data will be eventually used in the active control of a robotic therapy system. While BP is a good predictor of movement onset, it is a hundred times shorter (thus more challenging to extract) than ERD/S. A good artefact rejection strategy and a high number of calibration trials will be required to predict these signals accurately. This also means that the training time for a BCI decoder will take longer, increasing the chances of user fatigue even before the actual therapy starts. ERD/S arising from motor imagery and execution can be much easier to extract, given that the magnitude of the signal is based on relative power changes seconds after the stimulus. For this reason, I selected the use of SMR modulations, particularly an ERD/S signal from motor imagery, as a viable internal signal of intent for robotic control.

It is believed that motor simulation, which includes imagery and action observation, have a shared network of activations with that of motor execution or physical practice (Jeannerod, 2001; Jeannerod, 2006). A recent meta-analysis (Hardwick et al., 2018) provided more insight into this shared network and found that these neural correlations have provided consistent recruitment in the motor cortex, parietal cortex, and subcortical regions. Several research groups have argued that with regards to activity-dependent neuroplasticity and the overall aim of rehabilitation, it is best to tap into nearby and related neural structures for the rewiring process;

given that the region being tapped is still intact and functioning well (Hatem et al., 2016; Hallett, 2001; Zeiler and Krakauer, 2013). In the last two decades, motor imagery for conditioning (Lotze and Halsband, 2006; Cumming and Ramsey, 2009) and rehabilitation (Jackson et al., 2001) have been implemented successfully. However, its true potential in BCI has only been realised due to the rapid advances in brain imaging and signal processing (Chaudhari and Galiyawala, 2017).

In some cases, motor attempt (rather than imagery) is encouraged as it is reported to provide better classification accuracies in BCI (Bai et al., 2020; Chen et al., 2021). This would best suit the clinical population (i.e., patients with hemiplegia or hemiparesis) undergoing therapy or in a clinical trial (Muralidharan et al., 2011). However, early development of novel BCI techniques requires the system to be tested on a healthy population and using attempted movement by a healthy individual to control a BCI would lead to actual movement. In this case, the advantages or disadvantages of using attempted movement over imagery in the early development phase of BCI would now depend on the nature of the study being performed.

Motor imagery can be performed in visual or kinaesthetic forms. Visual imagery refers to the visualisation of action, while kinaesthetic imagery refers to rehearsing the sensation of muscle activation and proprioception (Neuper et al., 2005). The ability to perform each or both types of motor imagery can differ among individuals. Several scales based on subjective ratings or self-report questionnaires have been developed to measure this (McAvinue and Robertson, 2008). Examples of these include the Vividness of Movement Imagery Questionnaire (VMIQ) (Isaac et al., 1986), the Movement Imagery Questionnaire (MIQ) (Hall et al., 1985) with revised versions called MIQ-R (Hall and Martin, 1997) and MIQ-RS (Gregg et al., 2010), and the Florida Praxis Imagery Questionnaire (FPIQ) (Ochipa et al., 1997) among others. (Collet et al., 2011) developed the motor imagery index (MII) as a robust method that includes psychometric, behavioural, and psychophysiological evaluations. However, this method has yet to be tested on a larger scale of participants to confirm its viability.

3.4. Brain-Computer Interfaces based on Motor Imagery

3.4.1. Basic Principles of BCI Use

An EEG-based BCI has three main components: (1) an EEG acquisition system, (2) a computer that functions both as a processor and stimuli presenter, and (3) a device to be controlled (which can be the same computer unit as previously mentioned) (Graimann et al., 2010). The EEG acquisition system sits at the 'brain-end' of this interface. Over the past decades, EEG-based BCI technology has rapidly improved simultaneously with other engineering and scientific fields (Rashid et al., 2020). Table 3.1 presents a list of these fields and their contributions to the development of EEG-based BCI.

Table 3.1: Fields of development in EEG-based BCI

Development Fields		**Contributions**
Hardware	Electronics	Signal amplifiers, wireless transmission of data, batteries, portability, supporting devices
	Materials	Electrode design and conductivity
Software	Computing	Signal processing pipeline, machine learning
Theory	Neuroscience, Psychology	Experimental protocols, stimuli presentation, user experiences, technology adoption
Application	Medicine, Sports, Industry	Stroke rehabilitation, prosthetics, physical and mental wellbeing, athletic conditioning, occupational health

Chapter 4 will discuss the hardware and software aspects as I seek to develop an EEG-based BCI with motor imagery as the primary task paradigm. For this section, I will focus on the theoretical aspects of BCI design, particularly on the experimental nature of BCI use. A BCI is organised as a hierarchy system that includes sessions, phases, and trials, similar to a typical EEG experiment. A session usually starts and ends with the preparation and dismantling of the BCI hardware, respectively. Multiple sessions can be performed in a day. However, this depends on the procedural design for a particular BCI. Figure 3.4a illustrates this hierarchal organisation for one BCI session, while Figure 3.4b shows a classic motor imagery BCI paradigm adapted from (Marchesotti et al., 2016).

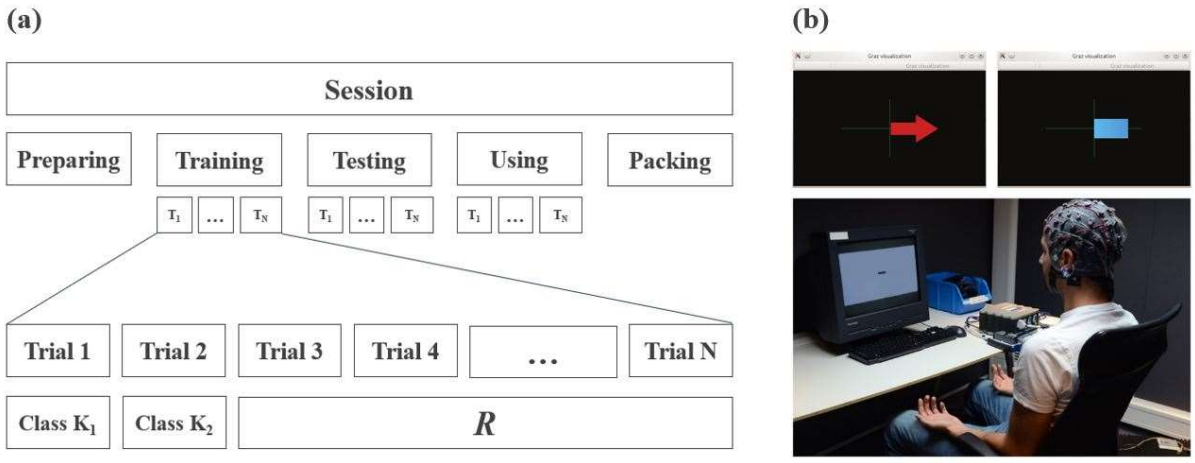

Figure 3.4: Brain-computer interfaces based on motor imagery. (a) Hierarchal structure in BCI, (b) classic motor imagery BCI paradigm from (Marchesotti et al., 2016) – the red arrow provides the directional cue to the user while the blue bar is the feedback arising from the classifier output after processing new motor imagery attempts.

There are phases of BCI use within a session that relate to a specific objective. This may be for training a classifier model (training phase), testing the classifier for its accuracy (testing phase), or using a BCI freely and without any structure (use phase). In each phase, a user performs a number of trials (T) for a specific task (e.g., motor imagery of hand grasping) and these trials can be further categorised into a pre-determined class (K) (e.g., consider left- or right-hand grasping as an example). The classes may dictate the degree of control for a BCI. The trials are arranged in a random order within the training and testing phases to minimise bias for a particular class. The classic motor imagery BCI paradigm, as seen in Figure 3.4b (Müller-Putz et al., 2016; Marchesotti et al., 2016), is the simplest example of this BCI setup. This approach allows a user to control a BCI based on movement position or hand direction (i.e., contralateral left- or right-hand movement) (Müller-Putz et al., 2016; Marchesotti et al., 2016). In the training phase, directional cues in each trial are delivered visually by a display monitor. Once a cue is displayed, the user performs the motor imagery corresponding to the intended class (i.e., left- or right-hand grasping) for a number of N trials evenly divided for each of the two classes. A resting-state interval of a few seconds is applied between trials to signal the user to stop performing the current imagery task and get a baseline of the EEG signals.

After the training phase, a classifier generates a model that can discriminate classes based on sensorimotor rhythm modulations. In the testing phase, a similar process is performed. However, a bar is presented as feedback immediately after the trial cue to reflect the model's predicted class (i.e., whether this new motor imagery attempt falls to the left- or right-hand class based on the classifier model being trained with the data from the training phase). A score is often displayed based on online classification accuracy during this phase – the correctly predicted classes in each trial out of the total trials presented (see Equation 3.1).

$$Online\ Classification\ Accuracy\ (\%) = \left(\frac{\sum K_1 + \sum K_2}{T_N}\right) 100 \qquad \text{(Equation 3.1)}$$

Where ΣK_1 and ΣK_2 are the correctly predicted left- and right-hand motor imagery classes and T_N is the total number of trials in the testing phase. The literature Virgilio Gonzales et al. (2018) reported that the state-of-the-art online classification accuracies for left-hand versus right-hand motor imagery range from 63% - to 97%. This suggests that such accuracies depend on the synergy between the feature extraction and classification methods used within the motor imagery BCI processing pipeline.

The number of classes in a motor imagery paradigm is also an important consideration in the development process as this determines the control resolution of the BCI device. In Section 3.2 – Signals of Intent, I discussed that motor processes correspond to specific neuronal activations within the motor cortex's localities as mapped by the homunculus model (see Figure 3.2). Therefore, the resolution of control in a motor imagery paradigm greatly depends on the spatial resolution of the brain signal acquisition device (i.e., EEG) and the ability of its software to distinguish patterns and localise their source. The most straightforward control resolution would be binary (i.e., comparing the execution of a mental task versus none), which would also be the easiest to decode. Increasing this to one notch gives us bi-directional control of a BCI (e.g., two motor imagery classes from two different mental states; contralateral left- and right-hand imagery or contralateral left- and right-foot imagery). In other cases, the motor imagery of the tongue is also applied (Morash et al., 2008; Giannopulu and Mizutani, 2021). A setup like this would amount to 6 classes (left hand, right hand, left foot, right foot, tongue, none). While

it may seem beneficial for a BCI system to distinguish a higher number of classes, a few important factors should also be considered:

1. A higher number of classes would also need more participant training data, which translates to longer calibration times leading to BCI use fatigue.
2. Increased variability for the outcomes. A 6-class motor imagery setup gives one out of six chances to successfully translate intent into execution.
3. The patient may not need all of these classes during therapy.

On the other hand, implementing a straightforward control strategy (such as those in binary control BCIs, go/no-go) poses many limitations in the type of tasks that are involved in rehabilitation. This could be one of the reasons why a bi-directional control of a motor imagery BCI (i.e., left- and right-hand imagery) might be an optimum setup for BCIs in development.

The total number of trials in the phases dictates the overall duration of the session. An average trial duration, including the rest interval, lasts for about 14-16 seconds (Marchesotti et al., 2016). Therefore, a phase that consists of 20 trials for each class ($T_N = 40$) will span more than 10 minutes. It is important to note that this procedural design for BCI use can be repetitive and tiresome for many individuals. This means that even if a higher number of trials in the training session can lead to higher online accuracy scores, an optimum duration for BCI training must also be considered to prevent fatigue and maintain the user's active participation. When applied to people who have had a stroke or brain injury, careful consideration of this parameter will prevent the patient from being too tired and unmotivated when they get to the use phase of a BCI.

3.4.2. Signal Processing Methods

The goal of processing a signal of intent for BCI use is to convert raw EEG signals acquired from each trial to a categorised and class-labelled prediction of sensorimotor rhythm modulations. In order to do this, we need to treat the EEG signals as multivariate time series data with M dimensions (i.e., electrode channels) and T timesteps. Figure 3.5, adapted from (Ismail Fawaz et al., 2019), provides a visual overview of this process.

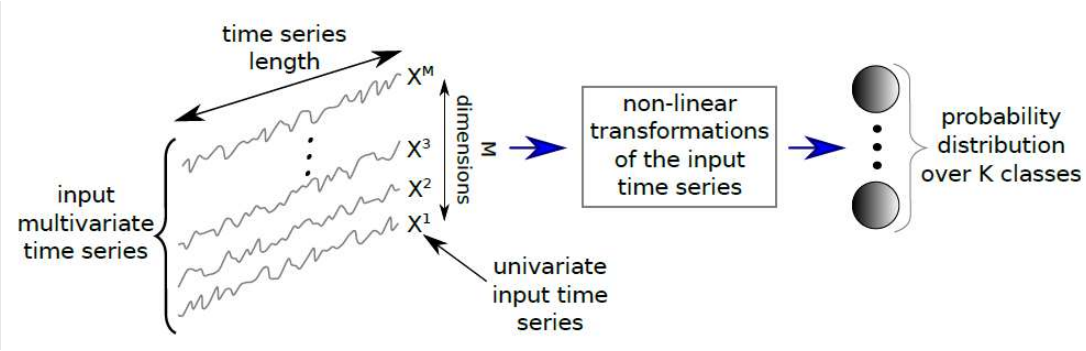

Figure 3.5: Structure and processing overview of raw EEG signals as a multivariate time series from (Ismail Fawaz et al., 2019)

Each time step x_i in a univariate time series $X = [x_1 , x_2 , \dots , x_T]$ is a sample reading of a signal coming from an EEG electrode at a particular time point. The number of samples dictates the length of each trial's time series. All of the trials are then compiled into a tensor, a 3-dimensional array with [N trials, M channels, T timesteps] (see Figure 3.6), and labelled with K classes. During the training of a classifier, the raw EEG tensor undergoes a series of non-linear transformations that extract features from the sensorimotor rhythm modulations (i.e., feature extraction and selection). In the next chapter, I will discuss each of the processing steps involved in a typical BCI pipeline. In the meantime, it is first worth knowing that the feature extraction step, via the data filters and functions, leads to an output of probability values of the distinct K classes. Therefore, the resulting predicted classes can be decided based on various criteria such as the user's sensorimotor rhythm modulations during the training phase, the complexity of the feature extraction method used, and the thresholds applied for each of the pipeline's parameters. After all, the performance of a BCI classifier is predetermined by how well the sensorimotor rhythm modulations between such classes are separated. An exemplary processing pipeline will have to achieve this while maintaining session duration and hardware requirements at the optimum level.

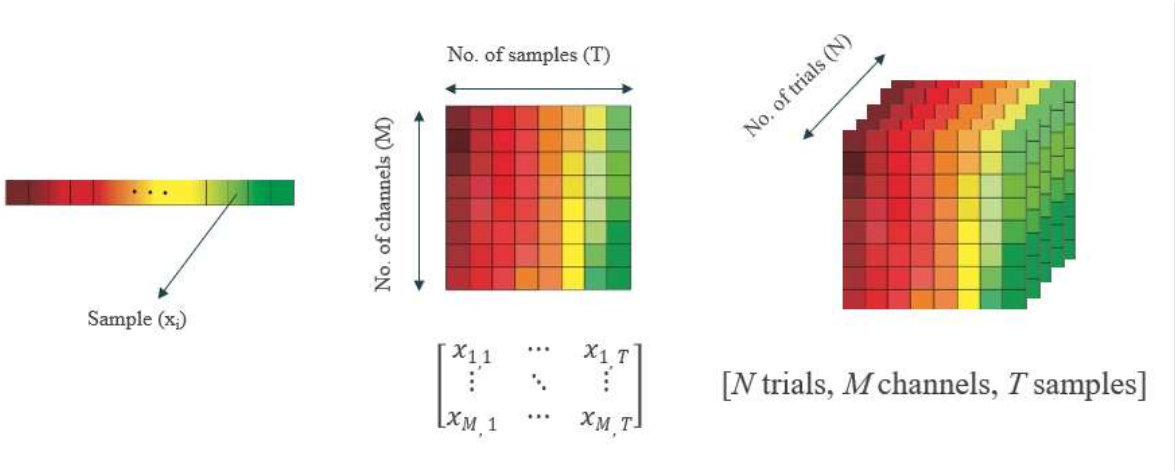

Figure 3.6: Motor imagery EEG tensor. Each trial is labelled with a particular class K_i

In earlier discussions (see Section 3.3), I introduced that spectral band power estimations in the μ and β bands exhibit ERD/S patterns during motor imagery (Pfurtscheller and Lopes da Silva, 1999; Neuper and Pfurtscheller, 2001). The extraction of these neural signatures provides the basis for some of the first motor imagery-based BCI pipelines, especially those that use a Graz (i.e., classic) motor imagery paradigm (Lotte, 2014). ERD/S for each frequency band is calculated by squaring the bandpass-filtered signal leading to the band power samples, averaging across all trials and averaging over the time steps (smoothing). The ERD/S pattern is observed by a power decrease (desynchronisation) and increase (synchronisation) of the frequency band relative to a reference interval (baseline) before the trial. This approach is based on the Power Method (also known as the classical ERD method) (Kalcher and Pfurtscheller, 1995) and can be expressed mathematically as follows (Equations 3.2 – 3.4):

$$A_j = \frac{1}{N}\sum_{i=1}^{N} x^2{}_{f(i,j)} \qquad \text{(Equation 3.2)}$$

Equation 3.2 results in a time course of instantaneous band power (A_j) after averaging over all trials (N). The x^2 with the jth sample of the ith trial is the calculated band power after squaring the bandpass filtered EEG data (x). To calculate the % change in ERD, the average band power of a reference interval (R) must be subtracted and divided from the actual band power:

$$R = \frac{1}{k}\sum_{r_0}^{r_0+k} A_j \qquad \text{(Equation 3.3)}$$

$$ERD\ (\%) = \frac{A_j - R}{R}100 \qquad \text{(Equation 3.4)}$$

within the reference interval, r_o is the starting point (usually set to seconds before stimulus onset), and k is the number of samples used to calculate the average band power. Earlier publications tend to subtract the average band power of the actual samples from the relative interval (R - A_j), resulting in negative values for ERS % and positive values for ERD % (Kalcher and Pfurtscheller, 1995). This was later changed, which I now use in Equation 3.4, to be consistent with the definition of ERD as the power decrease and ERS as the power increase (Pfurtscheller and Lopes da Silva, 1999; Graimann and Pfurtscheller, 2006).

The visualisation of the resulting processed signals can also explain how these pipelines function. Figure 3.7 shows the plots by (Neuper and Pfurtscheller, 2001) as they attempt to extract ERD/S patterns from the C3 electrode (central position, left hemisphere) during the motor imagery of the right foot and hand. When looking at these plots, one must focus on the per cent change of the y-axis after stimulus onset (x = 0). A negative shift in the values depicts ERD patterns, while a positive shift depicts ERS.

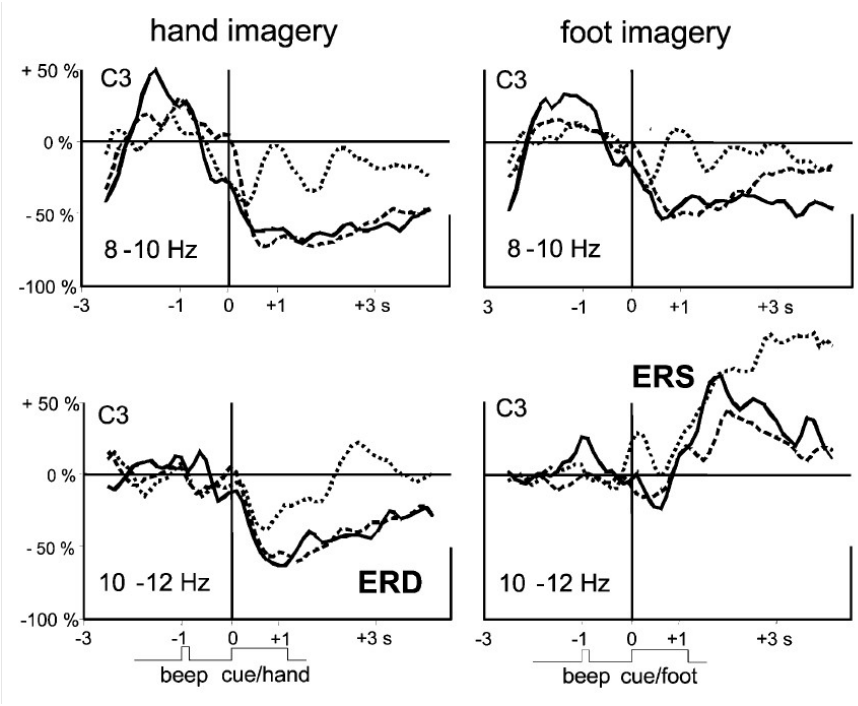

Figure 3.7: Event-related desynchronisation and synchronisation patterns (top two plots: 8-10 Hz, bottom two plots: 10-12 Hz) among three subjects (as depicted by line type – solid, dashed, dotted) relative to rest at the C3 electrode during hand and foot imagery from (Neuper and Pfurtscheller, 2001).

While the processing of ERD/S patterns provides a viable way of calculating and visualising sensorimotor rhythm modulations for BCI control, much information recorded by the electrodes can be lost along the way. Within the ERD/S extraction pipeline, spatial and temporal filtering techniques may be responsible for this loss. With this in mind, a trade-off between the feature extraction methods and the potential information loss during the process should be considered. Several approaches that attempt to extract distinct features from motor imagery-induced classes other than the traditional ERD/S pipeline have been implemented with the rise of the machine and deep learning algorithms (Roy et al., 2019).

Deep learning is a relatively new and powerful approach that provides an alternative to the traditional processing pipeline of EEG-based BCI. The rapid development of this artificial intelligence and machine learning subset may potentially discriminate motor imagery classes with less processing steps. Deep learning approaches use the many layers of artificial neurons

that can be trained to identify one or several distinct features and calculate the probability of a particular class based on the criteria of weights and biases (Ismail Fawaz et al., 2019; Schirrmeister et al., 2017). One example is a deep convolutional neural network (Deep ConvNet) developed by (Schirrmeister et al., 2017), which allows a model to learn local patterns in the raw EEG signal through several connected convolutional layers. Several others have implemented novel architectures that report higher accuracy scores than traditional pipelines (Roy et al., 2019). However, there is still much to discover with deep learning algorithms that the BCI community has not fully adopted its use in clinical settings. I relay most of the concerns on what these convolutional layers perceive during the learning process and the implications of an unsupervised learning approach to the resulting model.

3.4.3. Current Issues and Limitations

With all of these recent developments, motor imagery-based BCIs still have several issues and limitations that need addressing. I summarise these in the following statements:

1. Using motor imagery-based BCI alone is not for a general purpose/'one-size-fits-all' solution to the internal active strategy of robotic control. BCI-illiteracy is currently a major topic of debate in the scientific community as it is reported that around 10%-30% of participants cannot modulate their sensorimotor rhythm – an essential requirement to control a motor imagery BCI (Ahn et al., 2013). Furthermore, this issue is exacerbated when one tries to implement a motor imagery BCI therapy for stroke survivors who have impaired brain substrates where motor imagery is believed to be elicited. BCI researchers have been addressing this by improving sensing capabilities through a hybrid BCI that combines EEG with other sensors such as EMG and/or EOG (Zhang et al., 2019; Witkowski et al., 2014). Furthermore, developing more robust processing algorithms will improve the signal quality and sensitivity of those who find it hard to modulate sensorimotor rhythm during motor imagery based BCI training.

2. Motor imagery BCI's intra- and inter-subject variability makes the training and calibration phase a long and tedious process (Saha and Baumert, 2020). The user's acquired fatigue poses a concern for those wanting to implement such systems for clinical

use. Two of the possible ways to resolve this is to either increase the classifying accuracy after training with better algorithms and processing pipelines ('go better' approach) or to reach an optimum accuracy level with the least number of trials to shorten the duration of the training phase ('go faster' approach).

3. More key information about the neural correlates of motor imagery classes might be lost during the signal processing steps. It is important to know the extent of these and their relevance to the generation of decision boundaries for classification. It might be a case that some unutilised data contain key information that might help improve BCI use. This can be explored further by comparing widely accepted approaches to those using raw or less processed EEG data, such as those in deep learning algorithms. By visualising and analysing both approaches side-by-side, one might extract and study the mechanisms that drive these decision boundaries and increase the overall control resolution of motor imagery BCI.

4. On the other hand, more attention might be placed on the new algorithms and techniques in signal processing but less on the human-facing side of the BCI training, as raised by (Jeunet et al., 2016) and (Lotte et al., 2013). The current protocols for BCI training might not be enough to elicit active participation from the user. Where the user, having an experience of BCI training and use, is overlooked by the delivery of abstract stimuli (i.e., arrows and bars in the Graz paradigm). The proposition is to look into both human and machine learning aspects and improve these with as much concurrency as possible.

These points agree with the key findings reported in the recent systematic review of BCI-robot systems in Chapter 2. In this review, I reported that:

1. There are limitations evident in the resolution of hand motor imagery (i.e., discriminating contralateral hand movement or go/no-go decisions) and the degree of robotic control (i.e., triggering or continuous control)

2. The task design, cues, and matching sensory feedback play an important role in the ability to perform motor imagery

3. There is a degree of inferiority concerning the visual and kinaesthetic stimuli presented in most BCI-robot systems, which may contribute to the lack of adoption of motor imagery BCI for clinical use.

Therefore, it might be worth addressing these limitations with a user-centred design approach, particularly on the visual and kinaesthetic stimuli that facilitate the trials, as a key motivator in improving the technology and making a novel contribution to this field.

3.5. Understanding the Visual and Kinaesthetic Stimuli

3.5.1. The Visual Stimuli

In Section 3.3., I presented Jeannerod's theory on action simulation and the shared network of neuronal structures among processes that involve motor imagery, motor execution, and action observation (Jeannerod, 2001). Prior to this, it is also believed that a network of 'mirror neurons' is activated when an individual observes and recognises a motor task being done by another individual (di Pellegrino et al., 1992). These findings give basis to the use of action observation as a supplementary tool to facilitate motor imagery and execution as described in recent EEG experiments: motor imagery with action observation (Eaves et al., 2016) and motor imagery with action observation and motor execution (Ono et al., 2018; Wang et al., 2018). The use of action observation to facilitate motor imagery and/or motor execution for EEG-based BCI has been limited to presenting a video or animation of hand movements on a flat computer display screen (Ono et al., 2018; Wang et al., 2018). With the emergence of immersive technologies such as VR and AR, one can deliver a novel approach to enhancing the visual stimuli through action observation with the following benefits:

1. Embodiment – a first-person embodied avatar performing a pre-determined action of everyday experiences can provide an enhanced and extended sense of ownership, agency and self-location for the user; based on the principles of the rubber hand illusion and the body transfer illusion (Škola and Liarokapis, 2018). Furthermore, it was reported that a stimulus with more humanlike hands resulted in higher motor imagery performance

among participants than those provided with a stimulus akin to a robotic gripper (Alimardani et al., 2016).

2. Gamification and progressive training – gamification is the provision of objectives, themes, and performance measures for a particular task, while progressive training is the practice of changing the difficulty (i.e., the pace of the task, hurdles to achieve the task, etc.) as the user gets better or worse in the task. These features are said to motivate the user to perform better, improve their attention, and increase their immersion in the game (Škola et al., 2019).

3. Enhanced visual environment – VR provides a new platform for human behavioural experiments by subjecting the participant to an immersive simulated environment. However, this relies on the degree of validity and fidelity of the task and the virtual environment (Harris et al., 2020). It must be noted that the goal of implementing a VR platform for motor imagery based BCI must be on the limitations of enhancing the nature of the task to elicit signals of intent and its capability to promote active participation during the session. Otherwise, elements may distract the user instead, leading to an added noise to the signal being processed.

4. Benefit for the therapist or researcher – the implementation of VR and other immersive technologies in human behaviour experimentation and exploration have been given much attention recently (Harris et al., 2020; Brookes et al., 2019). Currently, tools have been developed to support data collection so that therapists and researchers can get more out of the platform than deliver enhanced visual stimuli (Brookes et al., 2019).

Apart from Skola (2019), a number of efforts have integrated BCIs with AR/VR systems. Tan et al. (2017) provided a general review of these, while Salisbury et al. (2016) and Wen et al. (2021) surveyed studies in the context of neurorehabilitation. Among these is REINVENT which stands for "Rehabilitation Environment using the Integration of Neuromuscular-based Virtual Enhancements for Neural Training" (Spicer et al., 2017). It is a low-cost BCI-VR device targeted to deliver motor rehabilitation of the upper limbs in severe stroke patients. REINVENT was developed on the basis that action observation and BCI-neurofeedback can help with the rehabilitation of the paretic upper limb. This device has since been tested on its feasibility with

a clinical study that involved four chronic stroke patients (Vourvopoulos et al., 2019). Other applications for BCI-VR systems have also been developed. Tremmel et al. (2019) used an EEG-VR system to estimate three varying levels of cognitive workload in an immersive VR environment using low-frequency (θ-β) EEG bands. Coogan and He (2018) integrated BCI2000, a popular software package in early BCI development, with the Unity gaming engine platform. This work also provided a template layer for developers/researchers to utilise in various applications (e.g., gaming, psychology, internet-of-things, etc.) by modifying the current paradigm in Unity. While BCI-VR systems may carry a high potential to improve the current BCI-robot rehabilitation paradigm, there are still challenges that need to be addressed to be fully adopted in a clinical setting. Wen et al. (2021) suggested that the low data transfer rate, EEG signal quality (e.g., movement artefacts, electromagnetic interference), analysis algorithm and familiarity with the virtual environments are some of these challenges. The current work allowed me to encounter most of these problems and I discuss in the succeeding chapters my recommendations on how to address them.

3.5.2. The Kinaesthetic Stimuli

During motor imagery-based BCI training, a preference to perform kinaesthetic imagery rather than visual imagery is observed (Neuper et al., 2005). As discussed in Section 3.2., kinaesthetic motor imagery refers to the sensation of muscle activation and proprioception during the simulation of action, while visual motor imagery more relates to its visualisation. These two modalities have exhibited differences in their neural correlates (Chholak et al., 2019; Stecklow et al., 2010). However, kinaesthetic motor imagery was reported to exhibit more prominence in spatial patterns, particularly around the hand sensorimotor cortex area (Neuper et al., 2005). Several theories agree that the neural mechanisms involved in kinaesthetic motor imagery overlap those involved during motor execution, including the posterior parietal cortex, the cerebellum, the basal ganglia and the premotor cortex (Ridderinkhof and Brass, 2015). Moreover, the accessibility of kinaesthetic motor imagery is attributed to the personal experience of each individual (Stecklow et al., 2010; Ridderinkhof and Brass, 2015).

When combined with physical practice, kinaesthetic motor imagery was reported to improve performance in healthy adults (White et al., 1979) and stroke survivors (Chowdhury, Meena, et al., 2018). Chowdhury et al. (2018) reported improvements in neural activity ($p<0.05$) and rehabilitation outcomes (Action Research Arm Test, ARAT; $p<0.05$) after the intervention. Liu et al. (2014) reported improved hand function scores (ARAT $p=0.04$) in groups that combined physical practice with MI and stronger neural activity in the contralateral somatosensory motor cortex compared to a control group who did physical practice alone. Therefore, it would make sense to investigate how these findings translate into motor imagery based BCI training. Aside from the mechanical feedback delivered after successful motor imagery trials (Ono et al., 2018), an anatomically congruent kinaesthetic stimulation provided by a robotic hand glove or exoskeleton can perform physical practice before kinaesthetic motor imagery.

3.6. Research Aims and Hypotheses

3.6.1. Research Gaps and Questions

The current developments and limitations of motor imagery BCI systems highlighted the importance of the visual and kinaesthetic stimuli in all phases of the intended therapy session. Through the discussions in the previous sections, I found a clear research gap in the enhancement, integration, and alignment of these stimulus modalities with the current motor imagery BCI protocol. The implementation of an enhanced embodiment and visual environment in VR has not been applied to the physical practice brought by a robotic mechanism during motor imagery tasks. Furthermore, the gamification of visual and kinaesthetic motor imagery training, which are potential implementors of a co-adaptive approach in BCI, has not been implemented using these components after a thorough search of the literature. It is possible that a clear understanding of the interactions between the enhanced visual and kinaesthetic implementations with respect to motor imagery BCI systems and with each other must be obtained. Finally, the research community has not addressed how these modalities affect simple hand grasping motor imagery tasks. With these in mind, I propose the design and development of an enhanced visual and kinaesthetic stimuli delivery system and the integration of these

modalities into a unified motor imagery BCI prototype. Figure 3.8 presents the theoretical basis of this work as a graphical summary based on the engineering design process and methodology leading to the proposed prototype components.

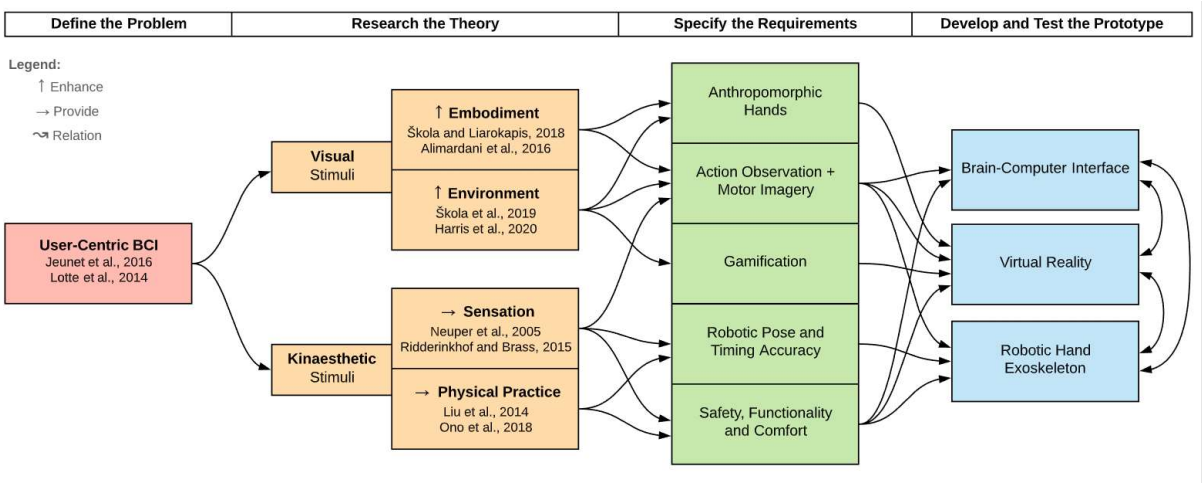

Figure 3.8: Theoretical framework of the study based on the engineering design process. Through a systematic review of existing literature, the need to develop user-centric BCI was defined (problem statement) to improve the visual and kinaesthetic stimuli (theory). The technical requirements to solve this problem are then enumerated, resulting in a BCI-VR-robot prototype's proposed integration. The directional arrows represent the flow of ideas and their relation to each process stage.

The unified motor imagery BCI prototype will be composed of the following components:

- Component 1: A core EEG-based BCI that extracts and processes the spectral band power from the raw EEG signal (feature extraction) during contralateral hand motor imagery tasks. The features are then used to train a logistic regression model (classifier) to discriminate hand movement imagery classes.
- Component 2: A VR platform for a motor imagery BCI paradigm that uses the principles of action observation and the embodiment and animation of anthropomorphic hands as the main source of the participants' cue and feedback stimuli. The enhanced visual

environment and gamification of motor imagery shall also be implemented to improve attention and active participation during the therapy sessions.

- Component 3: A robotic hand exoskeleton for hand grasping to deliver an enhanced kinaesthetic stimulus for motor imagery based BCI therapy. This device, which should be worn by a participant during motor imagery BCI training, can be activated simultaneously during the trial to induce guided proprioception and kinaesthetic sensation to the user and aid in performing kinaesthetic motor imagery.

I ask the following questions in order to test the proposed prototype on its theoretical basis and to give recommendations for future iterations:

a. How does the enhanced visual and kinaesthetic stimuli, individually and combined, through a BCI-VR-robot system affect motor imagery signal strength in measures of online classification accuracy, predicted class probabilities, and EEG signal?

b. Do these changes, if any, progress over time (i.e., learning effects)?

3.6.2. Research Aims

In order to address these research questions, I set the following specific objectives:

1. Develop a core motor imagery based BCI system. The system must input a multivariate time series of raw EEG data and output class predictions based on a pre-trained classifier. The predictions can then be used as a trigger to deliver feedback to the user.

2. Design and implement a VR-based virtual environment and integrate it with the core motor imagery BCI system. The combined BCI-VR component must:

    a. Provide a virtual embodiment of the hands, perform animations of hand grasping, and be able to track the user's hand position and orientation

    b. Provide an enhanced task environment through virtual elements and gamification

3. Design and implement a robotic hand exoskeleton and connect it to the motor imagery BCI and VR systems. The robotic hand exoskeleton must:
    a. Deliver full grasping sensation on both hands through its motors and linkages
    b. Be tested on technical specifications relating to functionality and safety
4. Integrate a full BCI-VR-robot system. The integrated system must be tested on its efficacy in enhancing motor imagery signal strength based on online classification accuracy (scores in the game), predicted class probabilities against the true class, and ERD/S patterns of its EEG signal

3.6.3. Hypotheses

In Table 3.2, I provide the hypotheses for the current study. Note that when I mention BCI performance, I refer to the following three measures: (1) online classification accuracy, (2) class probabilities, and (3) EEG signal.

Table 3.2: Research hypotheses

System and Effects		**Hypothesis**
H1	BCI-VR main effect	The enhanced visual stimuli through the VR component will significantly improve motor imagery BCI performance when compared to a control (without VR)
H2	BCI-robot main effect	The enhanced kinaesthetic stimuli through the robotic hand exoskeleton will significantly improve motor imagery BCI performance when compared to a control (without a robot)
H3	BCI-VR-robot interaction	The combined enhanced visual and kinaesthetic stimuli will significantly improve motor imagery BCI performance when compared to the prior conditions and the control
H4	BCI-VR-robot learning effect	These effects will significantly increase as the number of sessions for each condition increases

Chapter 4

Development of a Motor Imagery based Brain-Computer Interface Paradigm in Virtual Reality

4.1. Introduction

This chapter explains the development of a motor imagery task paradigm using a non-invasive EEG-based BCI system and VR. The imagination of left- and right-hand grasping was utilised to elicit changes in the sensorimotor rhythm, which a pretrained machine learning classifier can then decode. The BCI development section includes discussions on the hardware, software, and signal processing components of the BCI system, serving as the backbone of the prototype. The gamification of an immersive VR environment involving physical hand tracking and embodied hand animations was also integrated into the task paradigm. Finally, a discussion on the implications of the current BCI-VR prototype was done to summarise its contribution to current motor imagery based BCI systems and lay the groundwork for future experiments.

4.2. Brain-Computer Interface Development

4.2.1. Hardware

In this work, an Enobio-8 EEG data acquisition system from Neuroelectrics (Barcelona, Spain) was used. Enobio-8 is a portable and low-cost device that can record and stream EEG from 8 electrode channels with two reference electrodes. The system uses standard 4-mm pellets of silver/silver chloride sintered electrodes with a circular contact area of 1.75 cm^2. Electric signals are recorded from the scalp through a conductive electrolyte gel (Signa Gel) from Parker Laboratories, Inc. (New Jersey, USA). To get a good spatial coverage of the primary motor cortex (M1) and surrounding areas, electrodes were set to the C3, C4, FC5, FC6, C1, C2, CP5,

CP6 locations of a neoprene EEG cap. These locations are based on the 10-10 international electrode placement system for EEG and are based on the most common electrodes used among the 21 motor imagery BCI studies listed in Chapter 2 – Systematic Review. Referencing was made using the Common Mode Sense (CMS) and Driven Right Leg (DRL) electrodes which are set to be attached to the right earlobe of the user. All ten electrodes are connected to a wireless amplifier which transmits the recorded EEG data through a wireless fidelity (Wi-Fi) connection (see Figure 4.1 for the full setup).

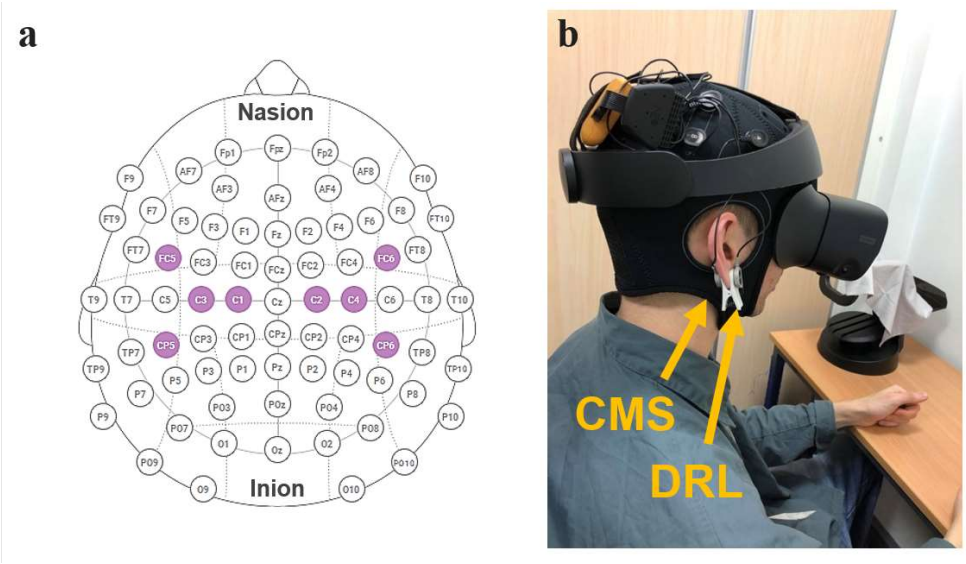

Figure 4.1: EEG and VR hardware setup

A Wi-Fi enabled Hewlett-Packard Omen-17 gaming laptop computer (California, USA) received the transmitted data which are then compiled within the Neuroelectrics Instrument Controller software (NIC2) for further processing. For this setup, the minimum specifications for the personal computer are provided as follows:

- Operating System: 64-bit Windows 10 (Microsoft Corporation, Washington, USA)
- Random Access Memory (RAM): 8 GB
- Graphics Processing Unit (GPU): 6 GB
- Ports and Connectivity: (3) USB, (1) Display Port or HDMI, Wi-Fi capable

4.2.2. Software

The workflow of the BCI software is based on the trial structure previously described in Chapter 3. Several software modules communicate to pass streaming data (i.e., EEG signals, event markers, prediction streams, etc.) around the BCI framework in each trial. These software modules are a combination of applications that are either commercially available, open-sourced, or custom-made. Most custom-made scripts were written using the Python programming language (version 3.7.4). A link to the GitHub repository of these software modules can be accessed here: https://github.com/paulbaniqued/bci-vr-robot-integration. Figure 4.2 presents a schematic of the current BCI-VR-robot system's software applications and hardware components.

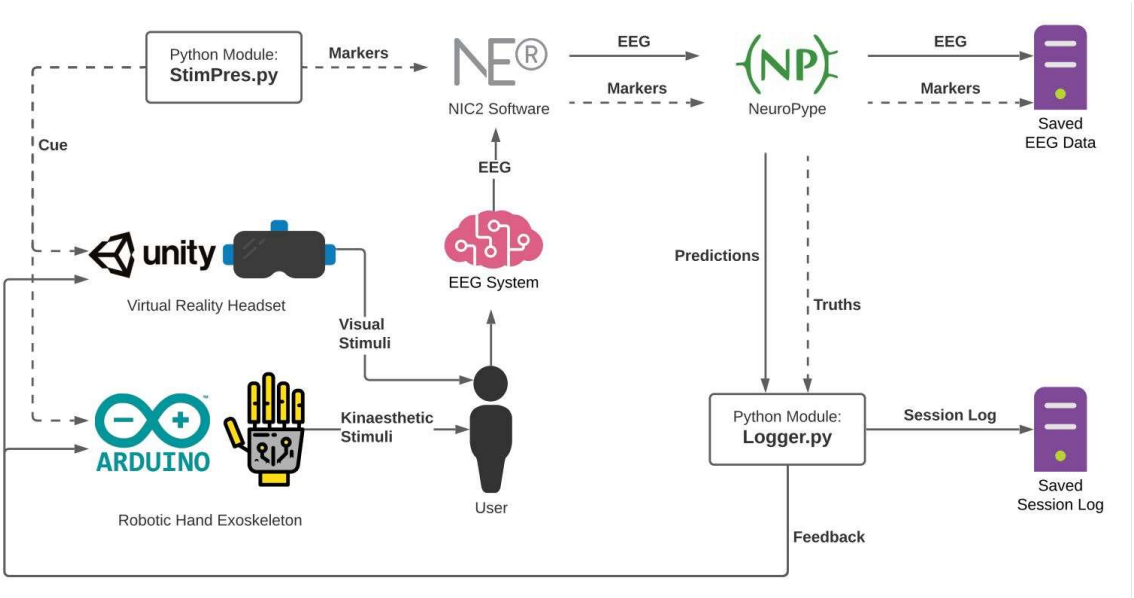

Figure 4.2: System components of the BCI-VR-robot prototype

The first software component is a novel Python module for stimuli presentation called StimPres.py. This module allows the generation of a trial list (default setting: 60 trials, 30 per class), randomized for the two classes, which are then sent out as event markers (a timestamp aligned to the EEG data to mark an event) and cue triggers (a signal to trigger other software modules to present the cue: imagine left-hand, imagine right-hand, rest, etc.) via

Labstreaminglayer or LSL ("pylsl") – both of these are sent out simultaneously. LSL is a streaming protocol that can collect, synchronise, and stream time-series data to the computer's local network. The entire GitHub repository of LSL can be accessed at the following link: https://github.com/sccn/labstreaminglayer. The StimPres.py module provides a uniquely identified outlet data stream to send out integer codes corresponding to the events happening within each trial. Visual and audio stimuli were also generated from the script via the "tkinter" and "playsound (version 1.2.2)" packages, respectively. These packages allowed the presentation of classic motor imagery elements on the personal computer (see Table 4.1 for their full descriptions).

Table 4.1: Event markers and corresponding elements

Marker	Event Description	Visual and Auditory Stimuli
1	Start of the session	■ Blank screen.
2	Get ready for trial. Start of the baseline period.	+ Green fixation cross. Low tone.
3	Start of the trial. Cue is LEFT HAND.	← Red left Arrow. High tone.
4	Start of the trial. Cue is RIGHT HAND.	→ Red right Arrow. High tone.
5	End of the trial. Start of rest period.	■ Blank screen.
6	End of the session.	Window closes. Victory sound.

As the event markers are streamed via LSL, the NIC2 software (see Figure 4.3) receives and synchronises this with the incoming raw EEG signals at a sampling rate of 500 samples/second. The NIC2 module also performs experimental protocol settings such as labelling electrode channels and LSL streaming via an outlet EEG.

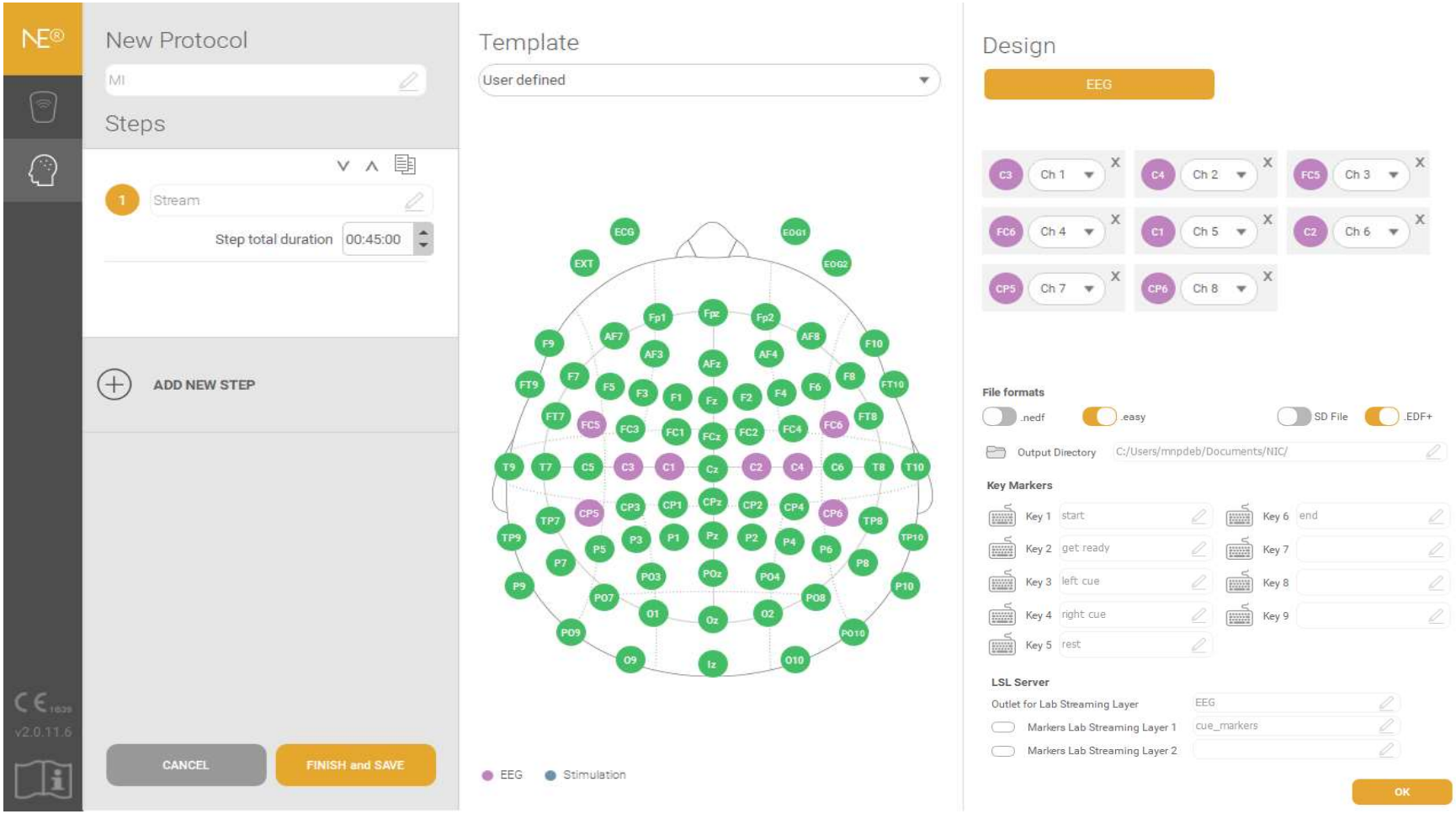

Figure 4.3: NIC2 software interface

Figure 4.4 shows the program flowchart for the StimPres.py module.

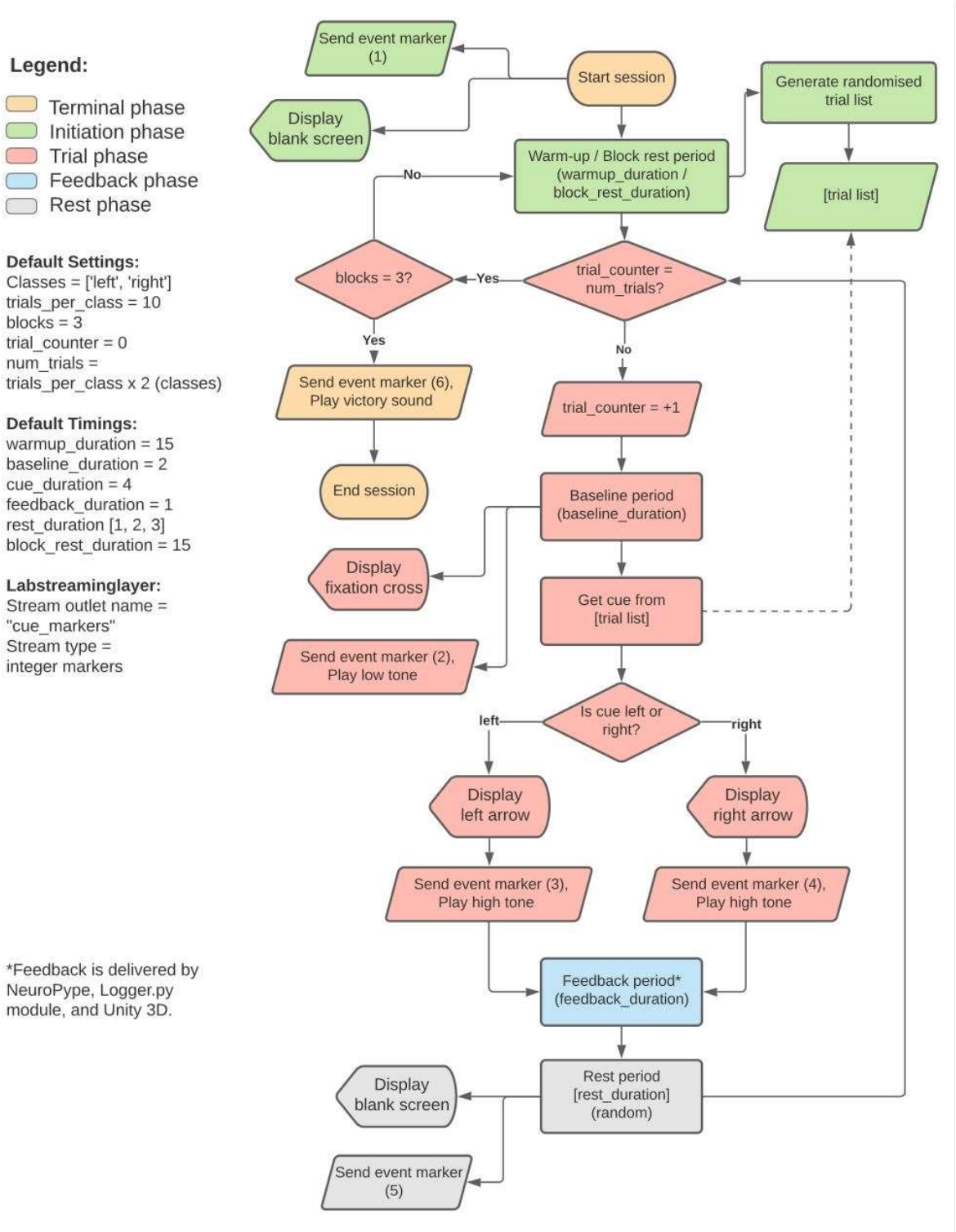

Figure 4.4: Program flowchart of the StimPres.py Python module - the BCI system's backbone experiment controller and stimuli presenter. The default settings and timings are indicated on the left-hand side of the figure.

The combined EEG and marker stream are then received by NeuroPype, a python-based signal processing pipeline from Syntrogi, Inc. Intheon (California, USA). NeuroPype allows the design and implementation of a BCI by converting raw EEG data into class probabilities through a simple machine learning algorithm. Details of this pipeline and algorithm are discussed in Section 4.2.3. Moreover, NeuroPype also saves the raw and bandpass filtered EEG data into an Extensible Data Format for time series (.XDF extension) for offline analysis. Finally, class probabilities from the NeuroPype pipeline ("Prediction" stream) are streamed back to the local computer network via LSL.

A novel Python module for results logging called Logger.py receives the incoming "Prediction" stream and compares it with the event markers from the StimPres.py module (renamed as "Truth" stream to reflect the true class of the trial). A default setting for this script provides a correct prediction if the predicted class (i.e., the class with a probability that is greater than 0.50) matches the true class of the trial. Likewise, if the true class probability falls below 0.50, then the trial is labelled as incorrect. Aside from visually displaying a bar plot of class probabilities, a chime sound was played for the correct trials, while a buzzer sound was played for incorrect trials. To increase confidence for true positive predictions, a 0.60 threshold value for class probabilities was implemented instead of the default >0.50 criterion. This was based on a previous discussion by (Combrisson and Jerbi, 2015). In this iteration, the trials that did not meet the threshold were not presented with a rewarding visual and auditory stimulus. At the end of each trial, a log of the true class, predicted class, left class probability, right class probability, and score are written as one row on a compiled data frame which are then saved as comma-separated values (CSV) file. To enable blinding during BCI experiments, session log filenames were encrypted by generating a unique combination of alphanumeric identifier codes corresponding to that session – encryption keys were stored in a JSON (JavaScript Object Notation) file. Figure 4.5 shows the program flowchart of the Logger.py Python module.

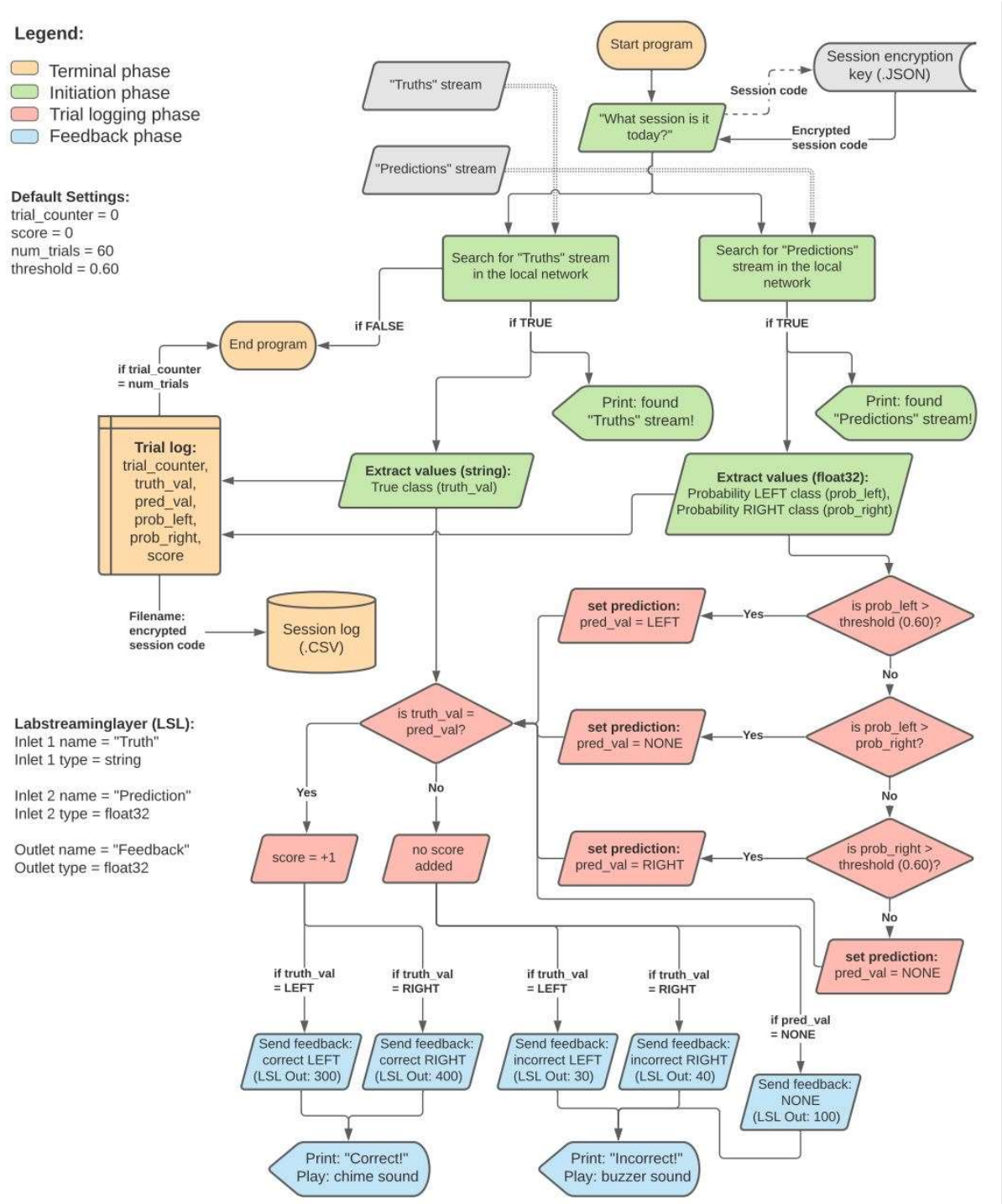

Figure 4.5: Program flowchart of the Logger.py Python module

4.2.3. Signal Processing

The decoding of raw EEG signals into class probabilities were performed in NeuroPype using a simple motor imagery scenario. A notch filter was first used to remove line noise from the raw

EEG signal at 50 Hz using the NIC2 software. The pre-processed EEG data with event markers are then streamed out to the NeuroPype pipeline designer module via LSL. NeuroPype follows a "drag-and-drop" user interface containing nodes and connectors which are saved into a NeuroPype Pipeline Designer file with a .PYP extension. A node corresponds to a particular process or steps in the signal processing pipeline (e.g., feature extraction, classification, file management, etc.). These often contain several input and output slots for various data streams. Some nodes can also display data visualisations such as time series plots, bar charts and spatial heat maps. Nodes are then connected by lines through which an order of steps can be arranged. For this setup, the pipeline begins and ends with an LSL input and output node to allow communication with other modules. This also allows the .PYP file to be running in the background while the StimPres.py module presents its visual stimuli on the display monitor.

In Chapter 3, it was discussed that a typical BCI session follows a training and testing phase structure. These phases are dependent on the trial-based session protocol implemented by the StimPres.py module through its event markers. The event markers generated in this module also determine the timing and length of epochs. Epochs are slices of time series data labelled with a given class for a BCI task in the current BCI system. Two NeuroPype pipeline scenarios were designed for this setup, corresponding to the training (mi-training.pyp) and testing (mi-testing.pyp) phases of the BCI session. These scenarios both depend on the stream of event markers provided by the StimPres.py module and are aligned with the EEG data by the NIC2 software. The training phase scenario involves a simple collect-and-record pipeline that utilises an LSL input node and a 'Record to XDF' node. In addition, two other nodes are attached to the LSL input node: the first is a visualisation node that allows the plotting of the raw EEG and event markers time series for signal quality diagnostics, while the second node is a file writing node that records the bandpass filtered stream in XDF for offline analysis. More details on bandpass filtering will be discussed in the following paragraphs. Upon completing the training phase, the recorded EEG and event marker streams are fed into the testing phase pipeline scenario (mi-testing.pyp) to calibrate machine learning-related nodes such as the spatial filters and classifiers. Figure 4.6 shows the pipeline design of the testing phase pipeline scenario in NeuroPype.

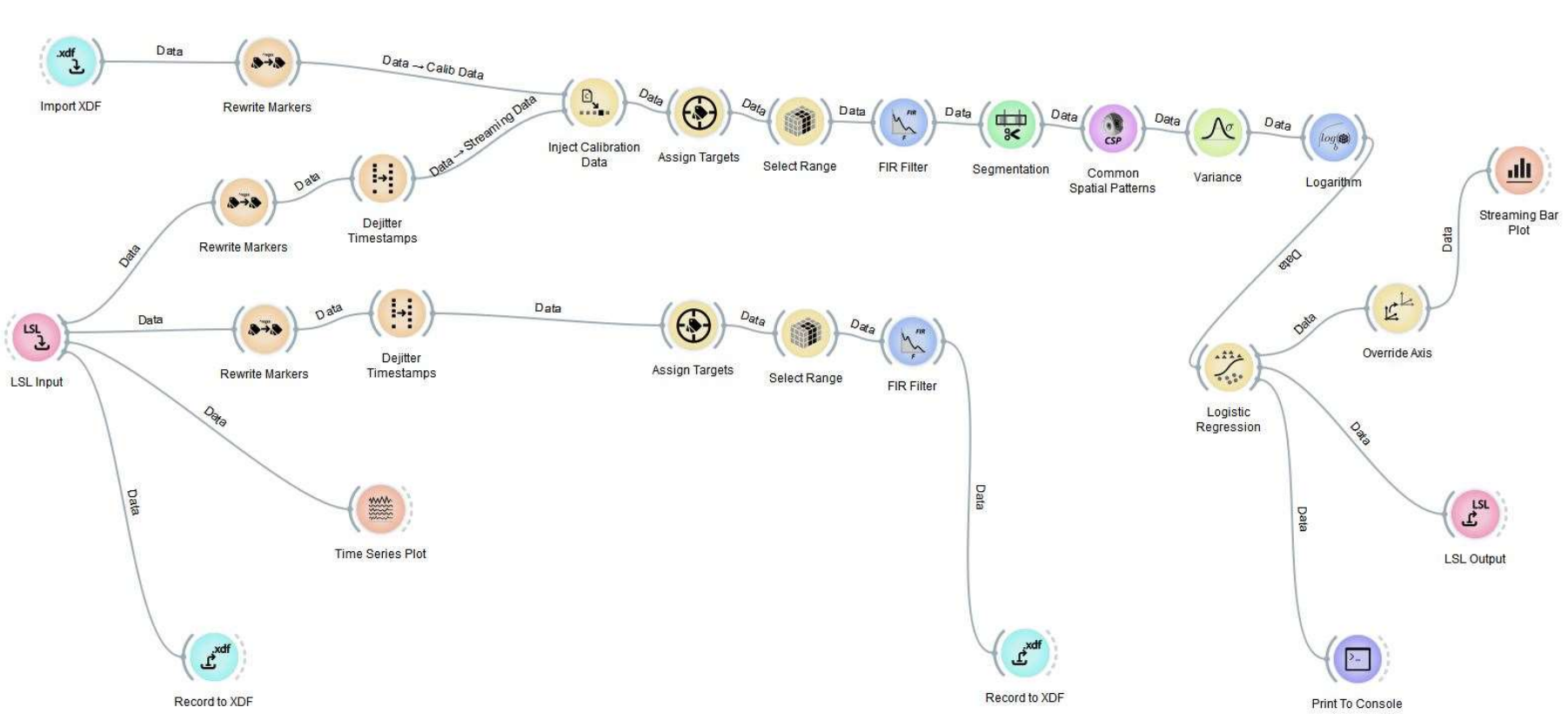

Figure 4.6: Testing phase pipeline design in NeuroPype

The testing phase scenario involves resolving an LSL stream containing the raw EEG signals and event markers using the 'LSL input' node. Aside from the main pipeline, this node is also connected to a file writing node which saves the raw data into an XDF format and a data visualisation node that plots a time-series graph. The next step in the main pipeline is the conversion of event markers which are originally integer64 types, into string types 'left' (0) and 'right' (1) using the 'Rewrite Markers' node. A 'Dejitter Timestamps' node follows this to maintain time synchronisation of the raw EEG data with the event markers. The pre-recorded training data are fed into the pipeline first through an' Inject Calibration Data' node, allowing the machine learning-based nodes (i.e., feature extraction, classification) to be trained for the incoming online stream. The 'Assign Targets' and 'Select Range' nodes are applied to the online stream to allow data reorganisation and labelling.

A bandpass filter between 8-30 Hz is applied to limit the bandwidth of the EEG signal into motor imagery-related frequencies μ and β, as discussed in Section 3.2. A finite impulse response (FIR) filter through an 'FIR filter' node was used in this step and served as the default setting. This node is also connected to a file writing node 'Record to XDF', similar to the one connected to the raw EEG data. Recording a post-filtered signal to XDF allows an additional layer of session recording for offline use. From the bandpass filtered EEG signals, epochs with a length of 4 seconds and labelled by their true class were generated using a segmentation node. This step enables all training and testing trials to be categorised based on their true classes, which is a pre-requisite for training the machine learning-based nodes.

Spatial filters are then generated from the 'Common Spatial Patterns (CSP)' node using the pre-recorded training data. The CSP algorithm allows multi-channel EEG data to be projected into a low-dimensional spatial subspace using its spatial filters (Ramoser et al., 2000; Blankertz et al., 2008). The process starts with input data from the bandpass-filtered and epoched single-trial EEG in the form of an N x T matrix, where N is the number of EEG channels and T is the number of samples per channel. By obtaining a normalised spatial covariance of the data for each class, a projection matrix where each row is a spatial filter containing the weights for each channel is generated. This matrix's top and bottom rows are then selected after being optimised to provide the maximum variance between the two classes. Upon the spatial

decomposition of the signals with the CSP node, the natural logarithm of the variances from the output channels is then calculated. This was done by passing the data to a variance node followed by a logarithm node.

A regularised logistic regression model was trained and used in this scenario to compute for class probabilities. The logistic regression algorithm uses the input variables from the training data with two classes to generate a logistic curve that serves as the classifier for the incoming online trials. The probability that one of the given classes is true is calculated using Equation 4.1.

$$P_{class}(Y = 0 \mid X) = \frac{1}{1 + e^{(w_0 + \sum_i w_i X_i)}} \quad \text{(Equation 4.1)}$$

Where P_{class} is the probability value of the class, e is the base of the natural logarithm, w_0 is the value that yields the probability when X is 0 (intercept), and w_i is the weight factor given a continuous X (slope/coefficient). The hyperplane equation then represents the decision boundary (see Equation 4.2).

$$Y = w_0 + \sum_i w_i X_i \quad \text{(Equation 4.2)}$$

Likewise, the probability of the other (false) class being true is given by Equation 4.3.

$$P_{oth\ \ class}(Y = 1 \mid X) = 1 - P(Y = 0 \mid X) = \frac{e^{(w_0 + \sum_i w_i X_i)}}{1 + e^{(w_0 + \sum_i w_i X_i)}} \quad \text{(Equation 4.3)}$$

The resulting outputs are two class probabilities streams for the given trial's left and right. These values are then displayed to the NeuroPype interface using the ‘Streaming Bar Plot’ and ‘Print to Console’ nodes. As previously mentioned, the testing phase scenario ends with an ‘LSL output’

node where the class probabilities are streamed and named “Predictions”. The stream of event markers that have gone through the pipeline is renamed “Truths”. Both of these streams are then received by the Python Logger.py module for results logging and integration with the VR and robot systems.

4.3. Virtual Reality Game Development

4.3.1. Hardware

An Oculus Rift S head-mounted display (HMD) from Facebook Technologies, LLC./Meta Platforms, Inc. (California, USA) was used as the default VR hardware for the current system. It uses a single fast-switch liquid crystal display (LCD) panel with a total resolution of 2560x1440 pixels (1280x1440 pixels per eye), a refresh rate of 80 Hz, and a field of view of 115°. In addition, the HMD uses a six-degree-of-freedom (6DOF) inside-out rotational and positional tracking with its five built-in cameras, allowing stationary and room-scale experiences. The design of the Oculus Rift S HMD does not interfere with the Enobio-8 EEG system, allowing the placement of its electrodes along the positions described in Section 4.2.1. However, the original attachment of the Enobio-8 amplifier interferes with the Oculus Rift S headband and must be placed just above the adjustable knob and secured using the head strap (see Figure 4.1b).

The position and orientation of the user’s hands were tracked using a Leap Motion controller (Ultraleap, California, USA) mounted to the front of the Oculus Rift S HMD. Leap Motion uses a combination of infrared light-emitting diodes (LED) and depth cameras to recognise hand position and gestures in 3D space. In this current setup, only the position and orientation of the user’s palms were mapped into the 3D space of the virtual environment because the movement of the fingers was triggered by animation to provide the embodied visual cue during trials.

4.3.2. Virtual Environment

A 3D virtual task environment was developed in Unity version 2019.3.6f1 (Unity Technologies, California, USA) based on the classic motor imagery BCI trial structure. The virtual scenario involves the user is situated in a typical task room where a classic motor imagery EEG experiment is performed. A well-lit workspace with a table, chair, and display monitor is imported to the Unity scene from the Google Poly library and other common workplace objects to simulate a realistic room environment. On the virtual display monitor, the usual elements of a classic motor imagery BCI setup (i.e., arrows, bars, trial number, etc.) is arranged. However, the task's centrepieces are the virtual hand models that are tracked using the Leap Motion controller. The virtual hand models and their corresponding assets (i.e., skins, rig, mesh models) were imported from the Leap Motion Hands Module for Unity. A low-polygon hand mesh model was selected and applied with a matte white material to contrast the wood-textured table in the virtual room. A grasping animation for each hand was generated with one movement cycle (i.e., hand open-close-open) corresponding to the trial duration for every cue marker received. Spark particles were generated from the hand for trials involving feedback and set to instantiate if a correct classification was obtained. Figure 4.7 shows the virtual motor imagery task paradigm (training phase) and its various events in Unity.

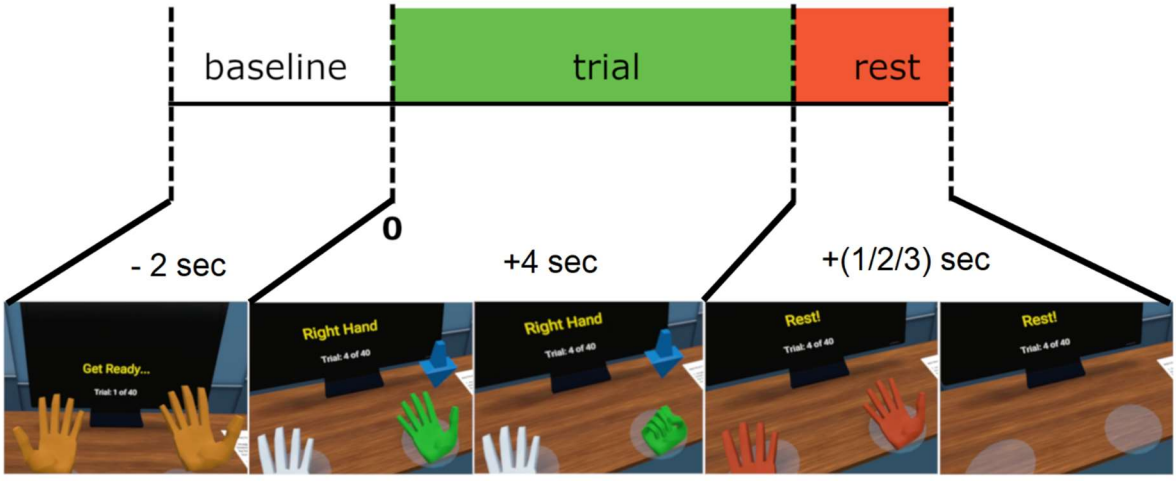

Figure 4.7: Motor imagery task paradigm of the training phase in virtual reality

The cue and feedback elements in the VR scenario were all triggered by LSL using the LSL4Unity and liblsl-Csharp modules from the Labstreaminglayer repository on GitHub. To do this, an empty game object was generated and attached with an LSL prefab containing the LSL Marker Stream script. This script resolved specific streaming data generated from the outlet streams of both the StimPres.py (cue markers) and Logger.py (class predictions) modules every time Unity was switched into game mode.

4.4. Summary

This chapter discusses the development of a BCI-VR prototype focusing on the design and implementation of both its hardware and software components. A backbone BCI system composed of an Enobio-8 EEG system was connected to a series of software modules to process raw EEG data into class probabilities for hand motor imagery. Custom-made modules to present stimuli and log experimental results were also created for this system. An immersive VR environment containing 3D room and game elements was also set up along with a geometric left and right hand that can be animated to provide an embodied visual stimulation for hand grasping. The next chapter (Chapter 5) discusses designing and developing a robotic hand exoskeleton for an enhanced kinaesthetic stimulus for motor imagery BCI.

Chapter 5

Development of a Robotic Hand Exoskeleton for Enhanced Kinaesthetic Stimuli for Motor Imagery Brain-Computer Interface

5.1. Introduction

The functionality and independence after a brain injury such as stroke is greatly improved with the rehabilitation of hand movement (Fregni and Pascual-Leone, 2006). This type of rehabilitation focuses on the dexterous and fine motor movements of the wrist and digits, allowing us humans to perform prehensive actions such as grasping or pinching. The ability to perform prehension is a crucial aspect of daily living as it allows the execution of various tasks such as eating, writing, or grabbing tools. Likewise, the loss or impairment of such abilities results in dependence on an able individual who may not be available at all times. Motor therapy often includes repetitive and goal-oriented exercises to induce use-dependent neuroplasticity (Hallett, 2001). The repeated practice of functional tasks is reported to aid motor recovery by promoting changes in the neural circuitry of the intact regions of the brain after injury (Ganguly and Poo, 2013). The efficacy of this strategy greatly depends on the nature of the task, its intensity, and the time spent in therapy. While increasing the intensity and therapy duration can improve recovery rates, it also comes with additional economical costs which may pose a burden to both the patient and the therapist.

Robotic devices have provided a substantial contribution to the administration of motor therapy to patients in recent years (Chang and Kim, 2013; Wu et al., 2018). Robot-assisted rehabilitation offers a more active approach to therapy than conventional methods (G.Y. Kim et al., 2017; Wu et al., 2018). For hand rehabilitation, I refer to robotic hand exoskeletons

(McConnell et al., 2017), which are a growing development field due to their wearability and biomechanical compatibility (Baniqued et al., 2015). One major advantage of robotic hand exoskeletons is providing an automated kinaesthetic stimulus during therapy. Furthermore, it can support remote therapy sessions (e.g. home use), which prove beneficial by offering the patient a flexible and adaptable working time (Housley et al., 2016). Undergoing treatment at home also gives patients the advantage of practising skills and developing compensation strategies in the context of their home environment.

In Chapter 2, I reviewed BCI-controlled robotic systems for hand rehabilitation and reported a degree of inferiority with respect to the visual and kinaesthetic stimuli presented in most motor imagery-based BCI experiments. These inferiorities may be contributing to the lack of technology adoption of such devices for clinical use. I recommended that enhancing motor imagery stimuli within these strands could improve BCI performance. On the visual aspects, I tapped into immersive technologies such as VR and AR to provide an enhanced virtual embodiment and environment, facilitating the patient during motor imagery BCI training. For the kinaesthetic aspects, I proposed in Chapter 3 the utilisation of wearable robotic devices such as powered exoskeletons. Originally intended to provide mechanical feedback after successful motor imagery trials (Ono et al., 2018), robotic hand exoskeletons can also be programmed to provide a form of kinaesthetic sensation during hand motor imagery tasks. Kinaesthetic motor imagery focuses on reconstructing the sensation of muscle activation and proprioception without execution and is reported to exhibit more prominence in spatial patterns around the sensorimotor hand area (Neuper et al., 2005). When combined with physical practice, kinaesthetic motor imagery was reported to improve performance in healthy adults (White et al., 1979) and stroke survivors (Liu et al., 2014; Chowdhury, Meena, et al., 2018).

This chapter presents a low-cost robotic hand exoskeleton design for immersive BCI-based training and its integration into an enriched motor imagery VR paradigm. The development of the current prototype was maintained at a low cost by three major considerations:

1. Commercially available and easily accessible “do-it-yourself (DIY)” components such as low-cost actuators, microcontroller boards, and other electrical components were used

2. The design was open-sourced and uploaded to the internet, allowing the public to improve, modify, and fabricate using a low-cost 3D printer

3. The assembly and programming were made easy with the eventual goal of being used at home with medical supervision

The next sections will discuss the conceptualisation, development, and implementation stages of the robotic hand exoskeleton prototype. Section 5.2 deals with the design and prototyping stages. Section 5.3 presents the experimental methods used to evaluate and implement the current prototype. Section 5.4 provides the experiments' results and discussion, and Section 5.5 summarises the contribution of the current work.

5.2. Design and Prototyping of a Robotic Hand Exoskeleton

5.2.1. Design Considerations

The functional requirements of the current robotic hand exoskeleton are to provide the kinaesthetic sensation of grasping during motor imagery BCI training in VR. With this in mind, the primary design consideration for the current prototype is its ability to apply sufficient force to move the fingers in its functional range of motion (ROM) from a fully extended pose (i.e., hand open) to a fully flexed pose (i.e., hand closed) (Bain et al., 2014).

Table 5.1 summarises the design criteria of the robotic hand exoskeleton based on its required functionality, wearability, and safety features (Baniqued et al., 2015). I also considered that the current prototype should be cost-effective and accessible to fabricate. To address these requirements, I selected the materials used in the mechanical and electronic components to be commercially available and easily accessible. In the next sections, I describe the design of the robotic hand exoskeleton in terms of its electronic components, mechanical design and assembly, and its integration with the motor imagery BCI-VR paradigm.

Table 5.1: Robotic exoskeleton design criteria

Criteria		Description
1	Wearability	The robotic exoskeleton must account for the dimensions of a medium-sized hand for wearability and comfort.
2	Torque	The robotic exoskeleton must move the hand from fully extended to fully closed using torque requirements
3	Electronics	The robotic exoskeleton's electronic componentry must not interfere with the hand's movement along its joints
4	Hand Tracking	The robotic exoskeleton's hand orientation must be tracked in a 3D virtual environment platform
5	Safety – Mechanical	Safety consideration 1: The robotic exoskeleton must have mechanical stops to avoid exceeding the hand's functional ROM (mechanical level safety)
6	Safety – Electronics	Safety consideration 2: The robotic exoskeleton must have an emergency button that "relaxes" the motors when pressed (electronic level safety)
7	Safety - Software	Safety consideration 3: The robotic exoskeleton's software must account for anomalies in its actuators and "relax" the motors when anomaly is detected

5.2.2. Electronic Components

I first selected the actuation strategy for the current prototype. It is worth noting that while a cable-driven tendon or a soft pneumatic actuation strategy for a hand exoskeleton have been gaining traction in recent years, these strategies would require more complex mechanical components that may not be easily accessible commercially. For example, pneumatic actuators would require the fabrication of soft air-locked chambers and the purchase of bulky air pumps, while a cable-driven tendon requires its cables to have complex assemblies (e.g., Bowden cables and pulleys) to preserve its tension at all times (Heo et al., 2012). I selected a servo motor-driven exoskeleton with rigid links as it is easier to assemble, power, and program than the first two strategies described.

Two LewanSoul LD-20MG full metal gear digital servomotors (Shenzen Hiwonder Technology Co., Ltd., China) with up to 20 kg-cm torque were used to actuate the fingers and thumb using a rigid link mechanism. These servomotors are mounted at the back of the hand between the MCP joint and the wrist, satisfying Criterion 3. A 6V power supply with four AA

batteries was required to operate the actuators, while an Arduino Uno microcontroller board (Arduino LLC, Massachusetts, USA) with a servomotor shield sends the triggers from the computer using pulse width modulation. The servomotors rotate simultaneously from their starting positions at about 90° and 60° for the fingers and thumb, respectively. A red light-emitting diode (LED) acting as a safety indicator was programmed to turn on when the servomotors were in motion. To satisfy criteria 6 and 7, two safety features at the electronic and software levels were included in the prototype. At the electronic component level, an easy-press red emergency button (Gravity: Digital Push Button from DFRobot) was included in the prototype, which enables the servomotors to slowly shift back up until their starting position before temporarily cutting itself from the power supply. At the software level, the servomotors were programmed not to exceed the functional ROM of the fingers and thumb, based on Bain et al. (2014) to avoid hyperflexion and hyperextension of its joints.

5.2.3. Mechanical Design, Fabrication, and Assembly

The human hand can be modelled to have a total of 27 degrees of freedom (DOF), with each of the digits having the following DOF: thumb – 6, index – 4, middle – 4, ring – 4, small – 4 (ElKoura and Singh, 2003). The remaining six DOFs are attributed to the wrist, which is not included in the exoskeleton's mechanism. Each of the finger digits possesses three joints: the metacarpophalangeal (MCP) joint, the proximal interphalangeal joint (PIP), and the distal interphalangeal (DIP) joint. The thumb also has an MCP, but a sole interphalangeal (IP) joint comes afterwards. In current commercially available hand exoskeleton prototypes, the cost increases with the degree of complexity in its mechanism; more complex devices tend to have more specialised components. For the current prototype (see Figure 5.1a), each of the four fingers was simplified to a 3-joint planar mechanism: restricting the movement to the rotational flexion-extension of MCP, PIP, and DIP and removing the abduction-adduction movement of the MCP joints. The finger mechanism follows a serial linkage structure (Heo et al., 2012), where the distal segments of the fingers are in contact with the final link of the exoskeleton. This mechanism allows the exoskeleton to actuate the flexion and extension of the index and middle fingers (pinch-grip mode with the middle and small fingers underactuated) or in unison (full grasp

mode). Due to this strategy, only a single servomotor was required to drive the four fingers at the MCP joint (see Figure 5.1b), while the PIP and DIP joints are underactuated. The thumb mechanism follows a redundant linkage structure (Heo et al., 2012) with two thumb attachments placed at the proximal and distal phalanx. The same strategy was applied to the MCP and IP joints of the thumb to allow a second servomotor to drive it. However, a Cardan joint (see Figure 5.1c) and a flexible servo base made of 3D-printed thermoplastic polyurethane (see Figure 5.1d) was included to allow 2-DOF of additional underactuated thumb movement. Overall, the total DOF that the exoskeleton allows the hand digits to move was reduced from 22 to 16. Appendix B shows the development process of the robotic hand exoskeleton from design to fabrication.

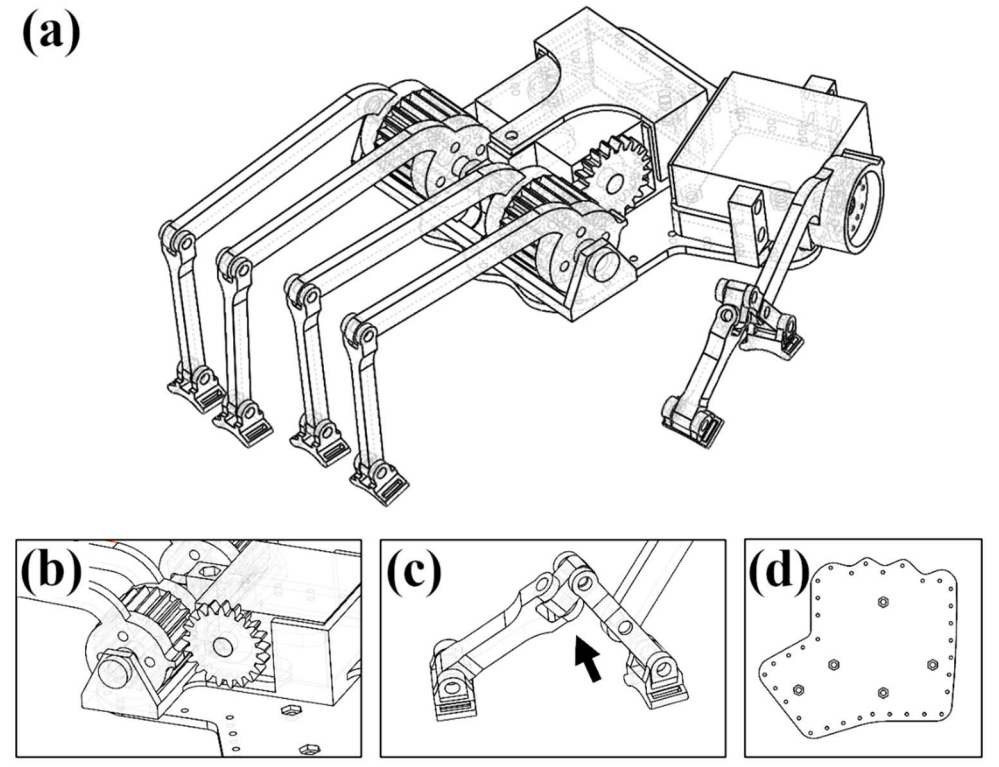

Figure 5.1: (a) Full assembly of the robotic hand exoskeleton (right-hand), (b) gear system and mechanical stops, (c) underactuated Cardan joint for thumb abduction-adduction, (d) flexible base attached to a fabric glove

The robotic hand exoskeleton's individual parts were designed using SolidWorks 2019 (Dassault Systèmes, France). The joints and linkages took account of the measured hand's dimensions to avoid the obstacle (Criterion 2). Mechanical stops were placed along with the first links that connect directly with both the servo gears (Criterion 5). Upon finalising the design, the parts were then printed with an Ender-3 V2 3D Printer (Shenzhen Creality 3D Technology Co., Ltd, China) using a 1.75 mm diameter polylactic acid (PLA) filament with an infill density of 20% and print temperatures of 210°C on the print end and 60°C on the build plate. The flexible servo base was stitched and glued to an elastic fabric glove to maintain rigidity at the back of the hand when the finger servomotor is in operation while maintaining comfort and adaptability to various hand sizes (Criterion 1). Moreover, the flexible servo base also allows compliance with the complex movements of the thumb's carpometacarpal joint. All the attachments for the digit linkages were stitched and glued to the fabric glove at 1 cm beyond the DIP (the two thumb attachments were placed at 1 cm beyond the MCP and IP). Upon completing the assembly of the linkages and electronic components with the fabric glove, the total weight of the device was measured at 280 g per hand. In this work, two exoskeleton systems (i.e. one for each hand) were prototyped and integrated into a BCI-VR system (see Figure 5.2).

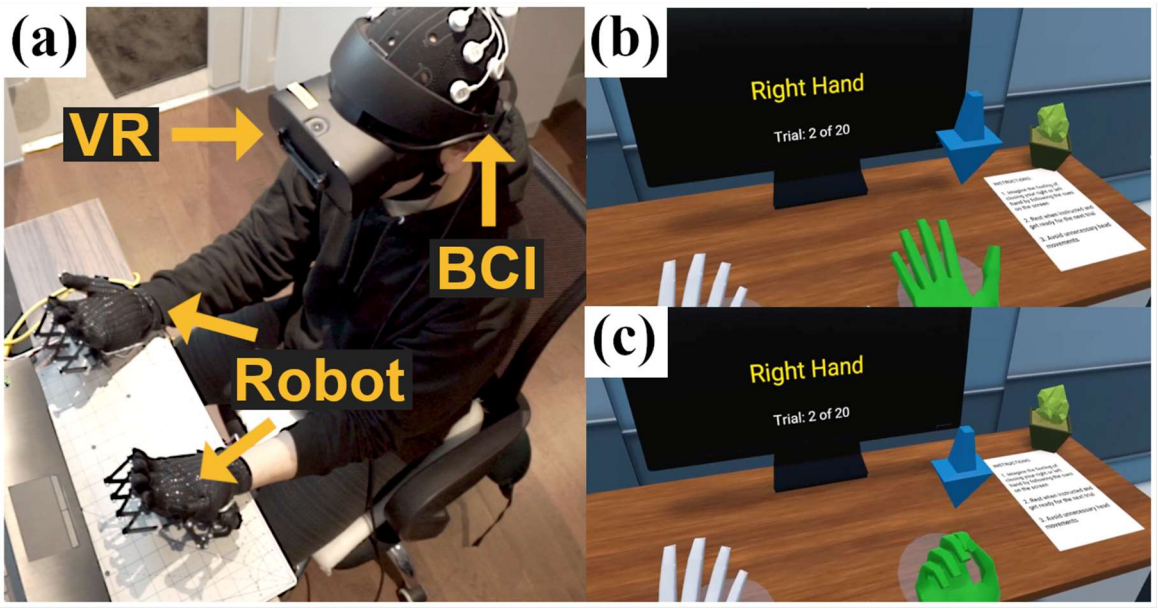

Figure 5.2: (a) Integrated BCI-VR-robot prototype and experimental setup, (b)-(c) hand grasping animation for motor imagery in virtual reality

5.2.4. Systems Integration

The role of the VR and robotic hand exoskeleton systems in the current work is to improve the classic motor imagery paradigm to enhance the delivery of its visual and kinaesthetic stimuli. Chapter 4 described a 3D virtual task environment developed in Unity version 2019.3.6f1 (Unity Technologies, California, USA) following the classic motor imagery BCI structure as presented in Figure 5.2b-c. The virtual scenario represents a typical task room where a classic motor imagery EEG experiment is performed. In addition to the usual abstract cues for motor imagery (i.e. arrows and bars), a virtual hand model is presented to the user during trials. The virtual hand represents the user's robot-wearing physical hand in the virtual environment and was tracked using a Leap Motion controller (Ultraleap, California, USA) mounted to an Oculus Rift S VR headset (Facebook Technologies, LLC./Meta Platforms, Inc., California, USA). In the current work, I used the Leap Motion controller to map the hand's palm position and orientation into the 3D environment through a Unity plugin (Criterion 4). During motor imagery trials, the virtual hand animates a full grasping motion, simultaneous with the robotic hand exoskeleton's actuation and corresponding to the trial's class.

5.3. Joint Angle Profiling

5.3.1. Methodology

A hand model with finger joints (MCP, PIP, DIP), thumb joints (MCP, IP), and anthropometric dimensions was used as a human analogue to evaluate the current robotic hand exoskeleton. The hand model was printed with an Ender-3 V2 3D Printer using PLA filament. With a print density of 20% infill, the total weight of the 3D-printed hand model was measured at 85 g. The assembled hand model was mounted to a tripod with the palm facing directly upward. The robotic hand exoskeleton was then worn on the hand model and placed on a weighted block to provide stability during actuation. The joint angles were tracked and analysed by Kinovea, an open-source video tool for sports analysis. I used a Sony a6000 mirrorless camera to capture the video with a 16-50 mm lens and a capture frame rate of 25 fps. For each hand part (i.e., fingers

and thumb), one movement cycle starts and ends at the position where the hand is fully extended (hand open), with the midpoint being when the hand is fully flexed (full grasp).

Figure 5.3 shows the experimental setup and the Kinovea interface. For this experiment, the duration of one movement cycle was set at 2.24 seconds. The progression of joint angles from 0-100% in the movement cycle was measured and plotted in the R programming language and statistics software. The maximum MCP, PIP, and DIP angles of the hand model were then compared to actual human hands based on the data from existing literature (Bain et al., 2014). This was done to assess if the robotic hand exoskeleton provides functional actuation to the hand without exceeding its safe ROM values.

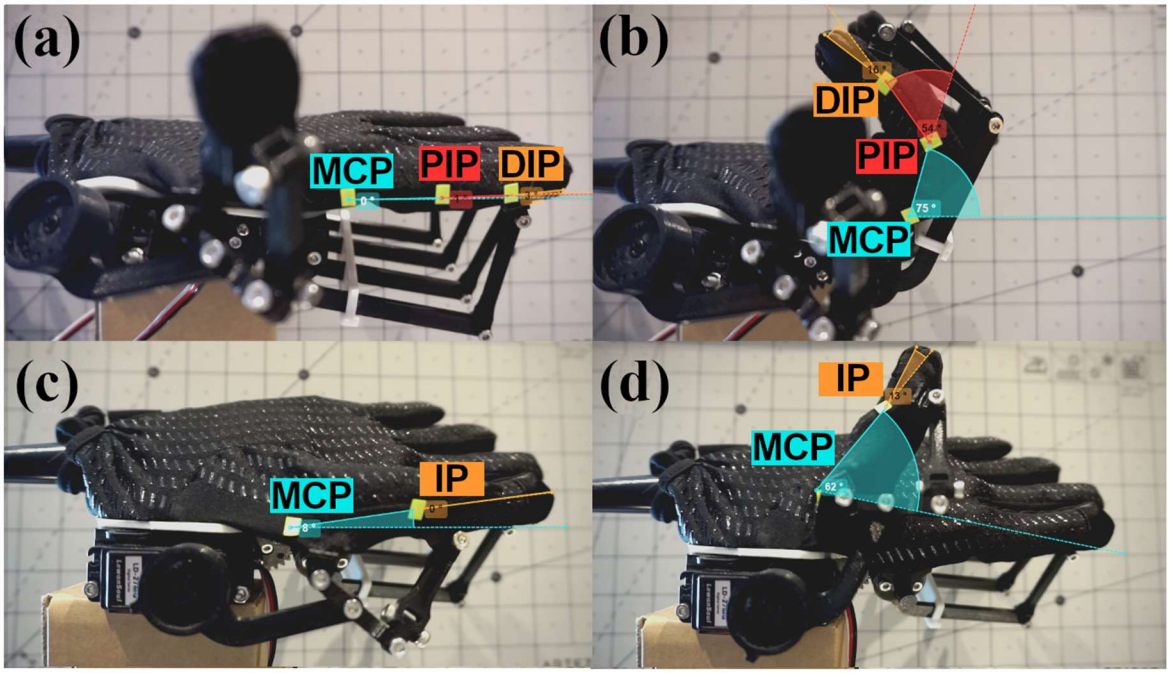

Figure 5.3: Joint angle profiling of the hand digits. (a) finger joints at initial and final states, (b) finger joints at the midpoint state, (c) thumb joints at the initial and final states, (d) thumb joints at the midpoint state

5.3.2. Results and Discussion

The progression of joint angles for one movement cycle (hand open – closed – open) of the fingers and thumb of the hand model were presented on Figures 5.4 and 5.5, respectively.

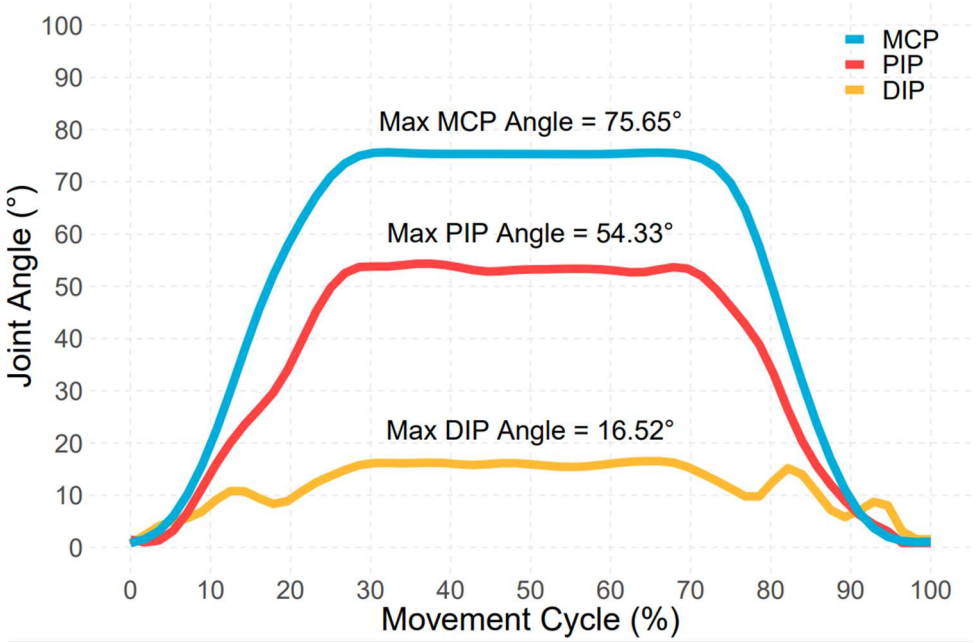

Figure 5.4: Joint angle profile of the fingers for one movement cycle

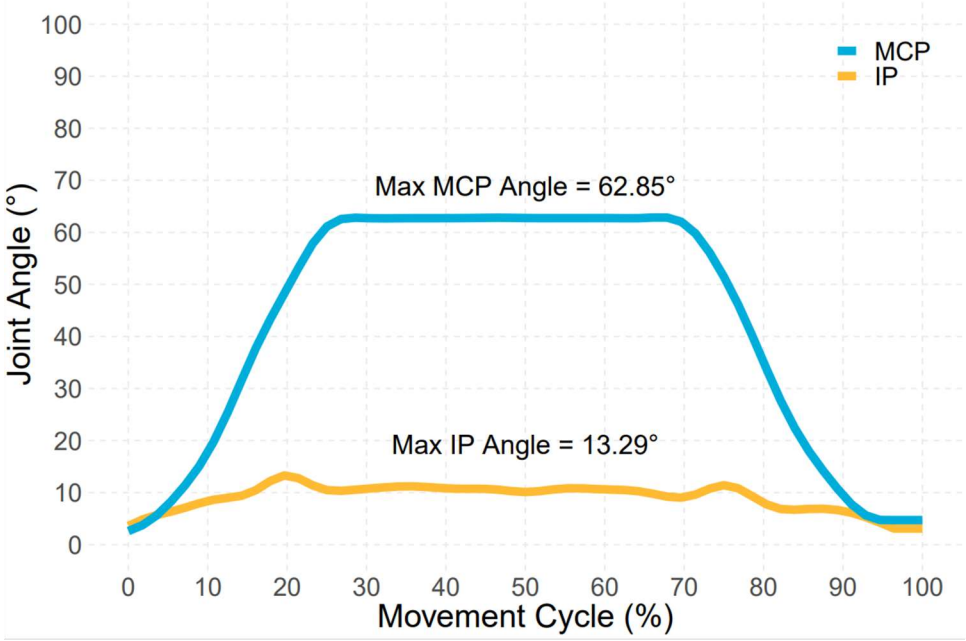

Figure 5.5: Joint angle profile of the thumb for one movement cycle

For the finger mechanism, the maximum angles of the MCP, PIP, and DIP joints of the fingers fall well within the average active ROM of the MCP (90°±9.1), PIP (101°±8.3), and DIP (84°±8.5) joints in literature (Bain et al., 2014). For the thumb mechanism, the maximum IP joint angle was well below the normal IP joint ROM of 73° based on Hume et al. (1990). However, the maximum MCP joint angle exceeded the normal MCP joint ROM of 56° (Hume et al., 1990) by 6.85°. This might be attributed to the flexible servo base accommodating the additional ROM provided by the carpometacarpal joint and offering a degree of compliance to the orientation of the thumb servo at full flexion. I also highlight the slow progression of joint angles for both the fingers and the thumb from their initial positions to their maximum angles, with the servomotors operating at 0-30% and 70-100% of the movement cycle. This was demonstrated by the slopes of the plotted curves and suggests that the current robotic hand exoskeleton can support the actuation of the hand digits in an effective yet safe manner. The measured ROM of the hand model also presents some insights on the degree of kinaesthetic stimuli the robotic hand exoskeleton can provide to its user during motor imagery BCI training.

5.4. Summary

I presented the design of a low-cost robotic hand exoskeleton for an enhanced kinaesthetic stimulus during motor imagery BCI-VR training. I followed the design criteria for functionality, wearability, and safety, resulting in a BCI-VR-robot prototype that can perform hand actuation while being tracked in the physical space and then translated to a virtual environment. In addition, the maximum joint angles of the prototype were measured to be within the normal ROM of hand digits, while a pilot motor imagery experiment of the integrated BCI-VR-robot demonstrated the feasibility of the prototype. Future directions for this device include the integration of better position and orientation sensors and haptic capabilities to increase its functionality in VR while still preserving its accessibility and cost-effectiveness. The next chapter discusses the self-experimentation performed to test the hypotheses of the current work using the integrated BCI-VR-robot prototype.

Chapter 6

Effects of Enhanced Visual and Kinaesthetic Stimuli on Motor Imagery based Brain-Computer Interface: A Self Experiment

6.1. Introduction

This chapter presents a self-experiment performed with an integrated BCI-VR-robot system for hand motor imagery. The experiment tests how the enhanced visual and kinaesthetic stimuli brought by the VR and robotic exoskeleton systems affect motor imagery BCI performance in a single subject. I consider motor imagery BCI performance by looking at three measures: (1) online classification accuracy scores, (2) probability values of the true class being predicted, and (3) event-related desynchronisation and synchronisation (ERD/S) patterns during motor imagery trials in EEG data. This chapter is structured by first presenting the experiment's methodology, followed by the results, and finally, a discussion of my findings and their implications with the aims and objectives of the current study. All the pre-registration documents, protocols, data, and analyses generated from this experiment were uploaded to the Open Science Framework (OSF) and can be accessed via this link: bit.ly/bci-vr-robot-expt

6.2. Methodology

6.2.1. Participant

The sole participant was a healthy 29-year-old adult male with no history of neurological disease or injury. He was classified as right-handed with a score of +60 based on the Edinburgh Handedness Inventory (Oldfield, 1971) and scored an average of 5.14 out of 7.00 on visual

imagery and 5.86 out of 7.00 on kinaesthetic imagery using the Revised-Motor Imagery Questionnaire (MIQ-RS) (Gregg et al., 2010). The participant was familiar with training and operating a classic motor imagery BCI and has previous experience with VR environments.

6.2.2. Study Design

A within-subject 2x2x8 design to investigate the effects of enhanced visual and kinaesthetic stimuli (factors) was done with two levels (visual: VR and no VR; kinaesthetic: robot and no robot). The chosen experimental design resulted in four different conditions: VR only, robot only, combined VR and robot ("both" condition), and control (no VR and no robot condition). The participant performed each condition for eight sessions, having 32 sessions, all within four weeks. Each week was structured by four consecutive experiment days and three rest days. For each experiment day, the participant performed two sessions (one in the morning and one in the afternoon) with different conditions. The morning and afternoon sessions followed the same time of the day and were at least four hours apart. To avoid any order effects across sessions, a counterbalanced schedule was implemented for the conditions (see Table 6.1).

Table 6.1: Counterbalancing conditions for the morning (AM) and afternoon (PM) sessions within the 4-week duration of the experiment

	Day 1		**Day 2**		**Day 3**		**Day 4**		**Days 5-7**
	AM	PM	AM	PM	AM	PM	AM	PM	
Week 1	Control	VR	Robot	Both	VR	Robot	Both	Control	
Week 2	Both	Control	VR	Robot	Control	Both	Robot	VR	REST
Week 3	Control	Both	Robot	VR	Both	Robot	VR	Control	
Week 4	VR	Robot	Both	Control	Robot	VR	Control	Both	

Due to the experimental setup, blinding strategies were also implemented to minimise experimental bias. The levels of blinding were implemented as follows:

1. Blinding of experimental outcomes during the session – the score obtained during the session was hidden from the participant. Only the trial-wise feedback was given to the participant as a form of auditory and visual reward and punishment.

2. Blinding of experimental outcomes after the session – the results log file (comma-separated values or CSV format) saved after every session was encrypted with a randomly generated 10-character unique identifier (e.g., r2gen7xilb, mcz51s28rl, 4oyqqflbey) during the 4-week implementation of the study. After all the sessions had been performed, a JavaScript Object Notation (JSON) key file containing the session names (e.g. “control-1”, “vr-3”, “robot-7”) and their corresponding encryption codes were then used to translate the logged filenames back to its original and unencrypted form.

6.2.3. Experimental Setup

A detailed discussion of the components of a BCI-VR-robot system was done in Chapters 4 and 5. This section briefly reviews these components and their settings for the current experiment. The experimental setup involves three main components: (1) an EEG acquisition system to record brain activity (i.e., BCI system), (2) a visual stimuli presentation system which can either be a VR HMD or a display monitor (for conditions without VR) and (3) a kinaesthetic stimuli presentation system which involves a robotic hand exoskeleton. In addition, all conditions received an auditory stimulus for the “get ready”, cue and feedback (score, error) events.

EEG Acquisition System

In all four conditions, the participant wore an EEG-based BCI system to record motor imagery signals. The EEG acquisition system is an Enobio-8 device by Neuroelectrics. It comprises eight channels with standard silver/silver chloride electrodes placed on a Neoprene head cap and attached to a wireless amplifier transmitting signals via Wi-Fi. A highly conductive electrolyte gel was applied to the participant’s scalp and reference regions to provide continuous conductivity with the electrodes. EEG was recorded with a sampling rate of 500 Hz from the

scalp around the sensorimotor area with electrode locations at C3, C4, FC5, FC6, C1, C2, CP5 and CP6 following the international 10-10 electrode placement system. Referencing was made using Common Mode Sense (CMS) and Driven Right Leg (DRL) electrodes attached to the right earlobe. Data were initially received from the wireless amplifier via Wi-Fi and was streamed to Labstreaminglayer (LSL) through the NIC 2.0 application (Neuroelectrics). Section 4.2 of Chapter 4 presented more details of the development of the EEG-based BCI system.

Visual Stimuli Presentation

The experimental setup's visual stimuli component provided the participant's cue and feedback during motor imagery tasks. For the control and robot conditions, an LCD monitor with a supported refresh rate of 120 Hz and placed at about 60 cm distance from the participant's nasion was used to present directional cues (i.e., red left and right arrows) and feedback (i.e., blue left and right bars) similar to the Graz classic motor imagery paradigm. At 2 seconds before a cue was presented, a green fixation cross was presented to prepare the participant. When feedback was presented (testing phase), a blue bar that corresponded to the predicted class was presented at 500 milliseconds after the cue duration. The length of the blue bar reflected the probability value (range 0-1) of the predicted class. The display monitor was set to blank during rest periods until the next trial came.

For conditions when the participant was required to wear a VR HMD, an Oculus Rift S VR system from Facebook Technologies, LLC/Meta Platforms, Inc. was used. The VR HMD provided a single fast-switch LCD lens with a supported refresh rate of 80 Hz. A virtual environment that resembled a testing room with a desk and a chair was made in Unity 2019.3.6f. The virtual room contained a similar display monitor as the control and robot conditions and presented the same cue and feedback symbols. However, the main difference between VR conditions from non-VR ones, apart from being in a virtual environment, was the presence of a low polygon mesh of a pair of hands. These hands animated a full grasping motion according to the cue of a particular trial. During feedback, if the predicted class matched the true class (correct prediction), a sparkle animation originating from the predicted hand was triggered.

Section 4.3 of Chapter 4 provided a more detailed description of the development and implementation of this virtual environment in the Unity 3D platform.

Kinaesthetic Stimuli Presentation

For robot and combined VR and robot conditions, kinaesthetic stimuli were provided during the trials, which involved wearing a pair of robotic hand exoskeleton devices attached to an Arduino microcontroller unit. The robotic exoskeleton actuated a full hand grasp by powering two 6V servomotors to rotate a rigid link mechanism. The first servomotor actuated all of the fingers at once, while the second servomotor actuated the thumb. These robotic commands were synchronised with the cue duration to enhance the kinaesthetic sensation. During the combined VR and robot condition, the movement of the robotic exoskeleton was programmed to be simultaneous with the movement of the virtual hands through the VR HMD. Chapter 5 provided a detailed description of the design and fabrication of this device.

6.2.4. Motor Imagery Task

In the current experimental setup, a motor imagery BCI session was divided into a training and testing phase, with each phase having 60 trials (i.e., 30 for each class presented randomly). The participant trained the BCI system to decode left- and right-hand motor imagery classes using their EEG signals in the training phase. The participant did not receive any form of feedback during this phase. In the testing phase, the BCI system classified the trials as the participant performed tasks similar to the training phase and received feedback for correct and incorrect classifications. Due to a class probability threshold being applied, the participant did not receive feedback when the resulting probability was below a threshold of 0.6. The trial duration was between 8 to 10 seconds resulting in approximately 10 minutes per phase. With a preparation time of 30 minutes (for equipment setup, application of conductive gel, etc.), 10 minutes for the training phase, 10 minutes for the testing phase, and 10 minutes for post-experiment activities (for cleaning and packing up), the total duration of one session was approximately 60 minutes.

Table 6.2 summarises the conditions and the differences of each in terms of its cue and feedback mechanisms.

Table 6.2: Experimental conditions and their respective stimuli presentation modes

	Ready	**Cue**	**Feedback**	**Rest**
Duration	2 seconds	4 seconds	1 second	1-3 seconds
Control				
Visual: Display	Fixation cross	Left/right arrows	Left/right bars	
Visual: VR HMD*				
Kinaesthetic: Robot*				
Auditory: Speaker	Low tone	High tone	Chime or buzz	
VR				
Visual: Display (VR)	Fixation cross	Left/right arrows	Left/right bars	
Visual: VR HMD		Virtual hands animate	Sparkle (correct)	
Kinaesthetic: Robot*				
Auditory: Speaker	Low tone	High tone	Chime or buzz	
Robot				
Visual: Display (VR)	Fixation cross	Left/right arrows	Left/right bars	
Visual: VR HMD*				
Kinaesthetic: Robot		Robot actuates the hands		
Auditory: Speaker	Low tone	High tone	Chime or buzz	
VR+robot				
Visual: Display (VR)	Fixation cross	Left/right arrows	Left/right bars	
Visual: VR HMD		Virtual hands animate	Sparkle (correct)	
Kinaesthetic: Robot		Robot actuates the hands		
Auditory: Speaker	Low tone	High tone	Chime or buzz	

*The participant was not wearing the device in this condition

6.2.5. Data Analysis

Online Classification Accuracy

Online classification accuracy percentages were calculated based on points earned over the total number of trials in the testing phase. For each trial, a score was earned by satisfying two factors:

(1) if the predicted class matched the true class of the trial and (2) if the predicted class probability exceeded the given threshold of 0.6. Other categories given to the trials in the testing session included correctly classified trials but did not meet the threshold, incorrectly classified trials but did not meet the threshold, and incorrectly classified trials that exceeded the threshold value (i.e., a true mismatch). Pearson correlation and linear regression analyses were performed for overall online classification accuracy scores and conditions to determine what learning effect was achieved. The significance values of the generated linear models were determined by comparing the group slopes of the conditions versus the 50% chance level of a two-class motor imagery BCI task.

To study the main effects and interactions of online accuracy scores among different conditions, a 2x2 factorial analysis of variance (ANOVA) was performed using the programming and statistical package R (version 2019). Factors were determined based on the presence or absence of the enhanced visual and kinaesthetic stimuli. Table 6.3 presents the factors generated from the experimental conditions.

Table 6.3: Experimental conditions in the 2x2 factorial ANOVA

	No VR	**VR**
No Robot	Control Condition	VR Condition
Robot	Robot Condition	VR+robot Condition

The resulting p-values were then subjected to Bonferroni-corrected pairwise comparisons to identify the main effects of the factors. All results were plotted using the ggplot2 library in the R-Studio software.

4x2 confusion matrices were generated using the percentage values categorised into the following groups: the predicted classes (y-axis) and the true classes (x-axis). Due to having a pre-set threshold of 0.6 for the predicted classes, the y-axis of the matrix was further decomposed into four predicted categories instead of two. Each tile in the matrix was filled with ggplot2's default blue colour scale, where the darker tiles have a higher percentage value.

Class Probabilities

For every testing phase in the session, the Python Logger.py module outputs a .CSV file of probability values for the left and right classes of each trial. Data points were first plotted for each day (x-axis) of each condition (facet grid). Violin plots were then generated from these values to visualise the distribution along the y-axis (with a probability scale of 0-1). Box plots were also generated for each day of each condition, where the centre line depicts the median of the data set, the box borders are the lower and upper quartiles, and the whiskers are the minimum and maximum values. All results were plotted using the ggplot2 library in the R-Studio software.

EEG Analysis

EEG data analysis and visualisation were performed in the Python 3.7 language and the Spyder integrated development environment. The following packages were used in this part of the analysis: (1) For EEG analysis: MNE, NumPy, and Pandas, (2) For EEG visualisation: Seaborn and Matplotlib.

Each Extensible Data Format (.XDF) file containing the raw EEG recording, events from markers, and other session information (e.g., channels, time stamps and stream identifiers) were first imported and reconfigured to Python as an MNE object. To represent the hemispherical activity in the left and right regions of the sensorimotor cortex, the C3 and C4 channels were picked for further analysis. The raw EEG data, sampled at 500 Hz, were then epoched (i.e., sliced and labelled) from one second before the event stimuli (-1) and up to four seconds after (+4). With this, one 5-second epoch would contain 2500 timesteps of recorded data per electrode.

The event-related desynchronisation and synchronisation (ERD/S) patterns corresponding to motor imagery (see discussion on Section 3.4.2) were extracted by generating time-frequency representations (TFR) of each electrode (i.e., C3 and C4) for each class (i.e., left

and right). This was based on the method by (Graimann et al., 2002) and was achieved using MNE's "tfr_multitaper" function. This was followed by a cluster-based permutation test to determine significant time-frequency regions (Maris and Oostenveld, 2007). In this series of steps, the epoched data were the first bandpass filtered at a range of 2-36 Hz. As discussed in Section 3.4.2, the ERD/S is determined by the relative power decrease (desynchronisation) and increase (synchronisation) in the spectral band based on a baseline average before the event trigger. For this setup, the baseline was set to -1 to 0 (1 second before the event trigger). The resulting plots are TFRs of left- and right-hand epoched trials per electrode of each session. In addition, averaged TFRs of each phase (i.e., training and testing) per condition were also generated.

To further visualise the separation of left- and right-hand classes, the per-session and per-condition ERD/S values were grouped into the spectral bands of interest for motor imagery: μ (8-12 Hz) and β (13-36 Hz); producing a line plot. Significant time points were calculated by performing a running t-test on each timepoint with an alpha of 0.05. To control the false discovery rates in this calculation, p-values were corrected using the Benjamini-Hochberg method.

Finally, the Common Spatial Patterns (CSP) filters generated from the training phase trials to help decode the testing phase trials were visualised using the CSP module in MNE. As discussed in Section 4.2.3 of Chapter 4, CSP is a supervised signal decomposition technique to estimate spatial filters that can be used to extract discriminant neural sources during the feature extraction step. More details on this technique can be found in this comprehensive tutorial by Blankertz et al. (2008). The resulting scalp topographical maps are the spatial filters based on the four different components set by cross-validation. In this step, all the eight electrode channels in the raw EEG stream were used to visualise the spatial filters.

6.3. Results

The motor imagery BCI performance in VR, robot, and combined VR+robot conditions against a control were measured in three aspects: (1) online classification accuracy scores, which were calculated based on the number of correctly predicted trials over the total number of trials in a

session, (2) probability of the true class being predicted, and (3) the presence and significance of ERD/S patterns in EEG data. In this section, I report the results of the self-experimentation done considering these three BCI performance measures.

6.3.1. Online Classification Accuracy

Figure 6.1 shows a line plot of the online classification accuracy and misclassification percentages per condition across all eight sessions. This was done to easily visualise the percentages (or fractions) taken by the four different classification outcomes during the testing phases of the session and to provide a visualisation of the trials that receive no feedback after decoding ("none" classification).

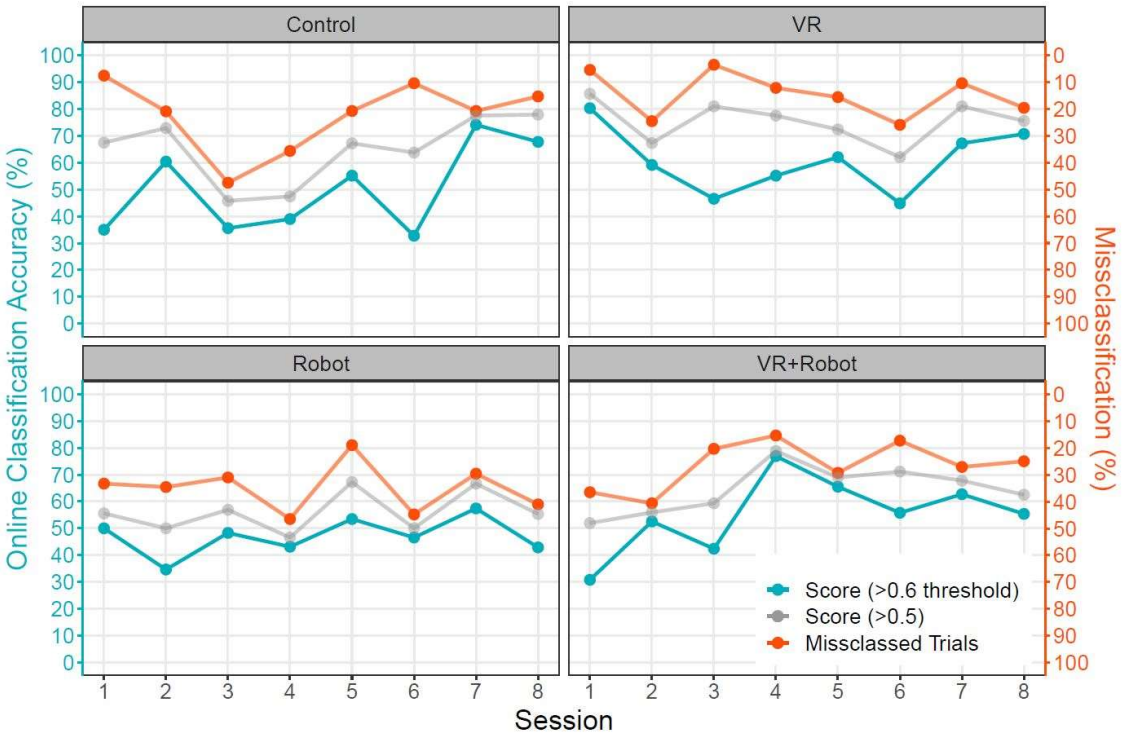

Figure 6.1: Online classification accuracy (left y-axis) and misclassification (right y-axis) percentages. The turquoise plots show the percentage of trials that exceed the pre-set threshold of 0.6 - left y-axis used. Grey plots show the percentage of trials that were correctly classified but did not meet the threshold (anything above 0.5) – left y-axis used. The orange plots show the percentage of misclassified trials – right y-axis used.

Table 6.4 presents the online classification accuracy percentages (score >0.6 threshold) in numeric form (the highest score per condition is italicised and highlighted in bold).

Table 6.4: Online classification accuracy scores (%)

Condition	**1**	**2**	**3**	**4**	**5**	**6**	**7**	**8**	**Mean ± SD**
Control	35.00	60.42	35.59	38.98	55.17	32.76	74.14	67.80	49.98 ± 16.42
VR	80.36	59.18	46.55	55.17	62.07	44.83	67.24	70.73	60.77 ± 12.05
Robot	50.00	34.62	48.28	43.10	53.45	46.55	57.41	42.86	47.03 ± 7.03
VR+robot	30.77	52.54	42.37	76.92	65.52	55.77	62.71	55.36	55.25 ± 14.16

The highest score was the first session in the VR condition (80.36%), followed by the fourth day of the VR+robot condition (76.92%). I report the first session of the VR+robot condition (30.77%) to have the lowest score, followed by the sixth session of the control condition (32.76%). Table 6.4 also presented all sessions' means and standard deviations within a condition. The condition with the highest mean value belonged to the VR condition (60.77% ± 12.05), but its standard deviation would mean that there could be an overlap with the second highest mean value coming from the VR+robot condition (55.25% ± 14.16). I report the robot condition (47.03% ± 7.03) to have the lowest mean value, followed closely by the control condition (49.98% ± 16.42).

The results of the Pearson's correlation analysis on online classification accuracy and the number of sessions reported moderate correlation among control conditions, $r\ (6) = 0.54$, $p = 0.16$, and VR+robot conditions, $r\ (6) = 0.52$, $p = 0.19$, while a weak correlation was reported on robot conditions, $r\ (6) = 0.29$, $p = 0.49$. The VR sessions were the only condition calculated to have a negative r coefficient $r\ (6) = -0.06$, $p = 0.89$; however, the value was small enough to be considered not to correlate. Overall, I calculated a weak correlation, $r\ (30) = 0.31$, $p = 0.08$, among all sessions. In Table 6.5, I summarise the linear regression analysis performed for these percentage values.

Table 6.5: Summary of linear regression analysis of online classification accuracy scores

	Y-Intercept	**p-value (β=0)**	**Slope**	**p-value**
All conditions	45.20	5.09e-10***	1.80	0.08
Control	33.60	0.0274*	3.06	0.16
VR	63.13	0.0009***	-0.30	0.89
Robot	43.33	0.0003***	0.82	0.49
VR+Robot	41.76	0.0064**	3.00	0.19

To visualise this, I generated a trend line depicting the generated linear equation in all sessions regardless of condition (see Figure 6.2a) and all sessions per condition (see Figure 6.2b).

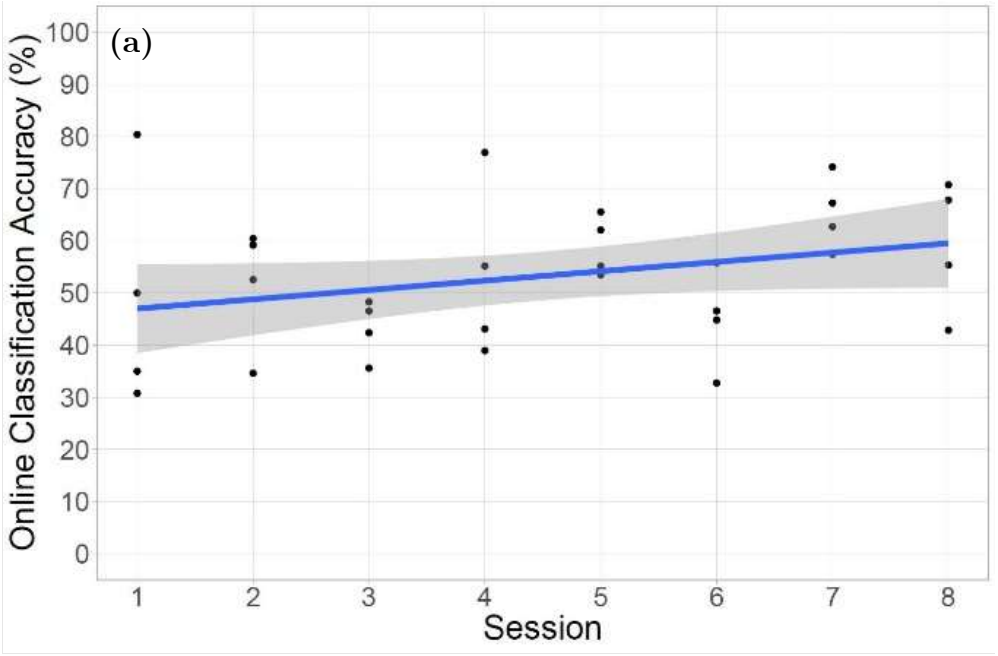

Figure 6.2a: Plot of the linear trend line from the regression analysis of online classification accuracy scores across all sessions

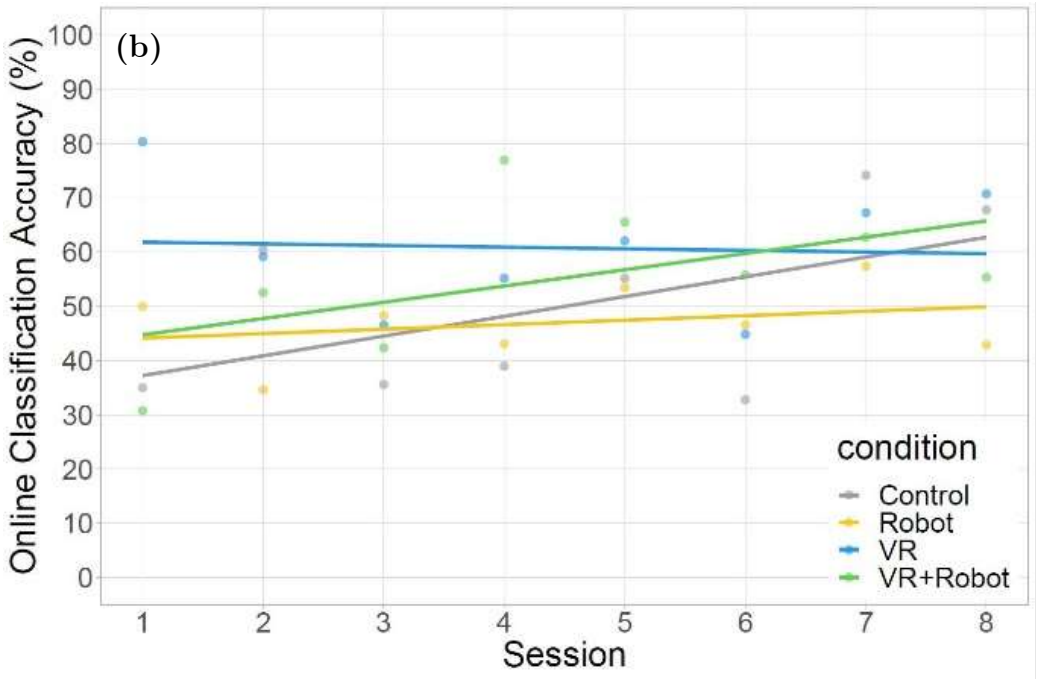

Figure 6.2b: Plot of the linear trend line from the regression analysis of online classification accuracy scores per condition

Among all these groups, only the VR condition has been found to have a negative slope (-0.30), albeit one that is close to zero. Among other conditions, the control condition (3.06) exhibited the highest slope, followed by the VR+robot condition (3.00) and finally the robot condition (0.82). Furthermore, the slope p-values suggested no significant linear incline or decline per condition across all sessions.

A 2x2 factorial ANOVA was conducted to compare the main effects of the visual and kinaesthetic factors on online classification accuracy scores and to check any interaction effects between the two. The visual and kinaesthetic factors included two levels: no VR and VR for the visual factor while no robot and robot for the kinaesthetic factor (see Table 6.3 for the experimental conditions). Shapiro-Wilk tests for normality were applied for all conditions beforehand which yielded the data to have normal distribution: control ($p = 0.17$), VR ($p = 0.91$), robot ($p = 0.97$), and VR+robot ($p = 0.95$).

I observed a main effect in the visual factor which yielded an F ratio of F (1, 28) = 4.34, p = 0.042 Bonferroni-corrected, indicating a significant difference between conditions with VR (M = 58.01, SD = 12.61) and conditions with no VR (M = 48.51, SD = 11.90) in the setup. The main effect for the kinaesthetic factor yielded an F ratio of F (1,28) = 0.863, p = 0.379 Bonferroni-corrected, indicating that the effect was not significant between conditions with robot (M = 51.14, SD = 11.24) and conditions without a robot (M = 55.37, SD = 14.51). Finally, I report no significant interaction between the two factors visual and kinaesthetic, F (1,28) = 0.08, p = 0.78.

Figure 6.3 summarises the results in the form of a box plot. Furthermore, supplementary data and plots for the 2x2 factorial ANOVA, which includes the diagnostic procedures and interaction plot, are made available for reference in Appendix C.

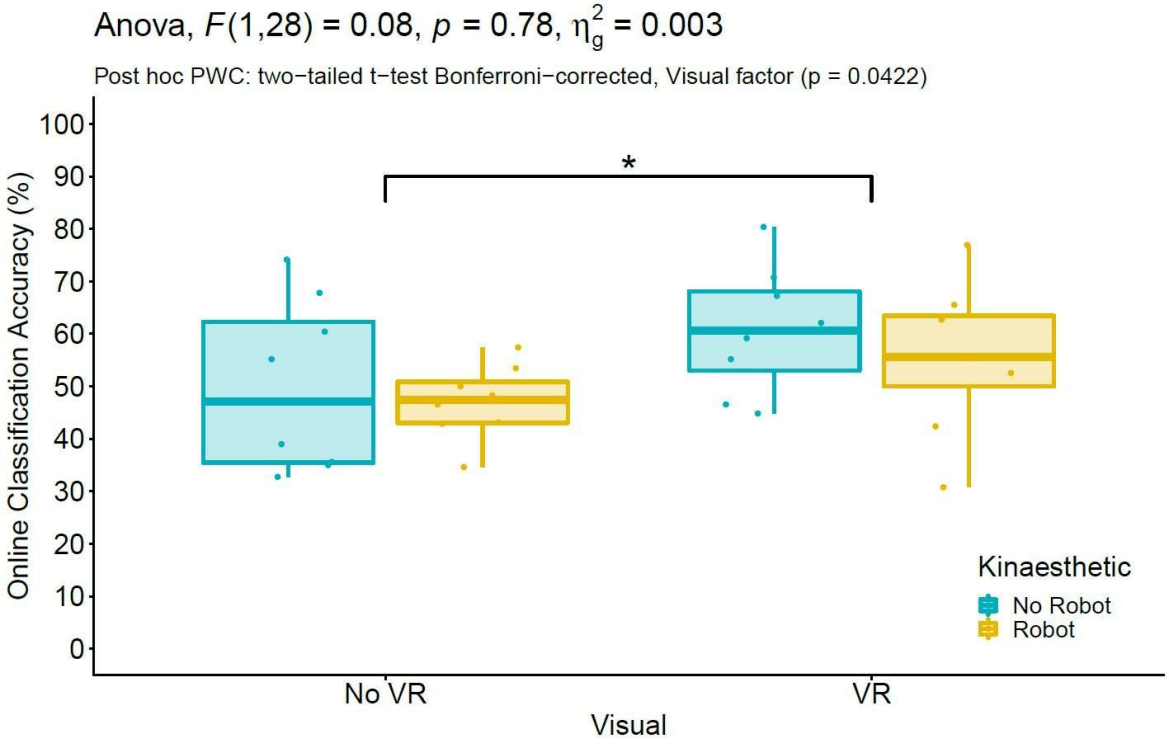

Figure 6.3: Summary of results for the 2x2 factorial ANOVA

Figures 6.4 – 6.7 present all the confusion matrices generated for each session of each condition.

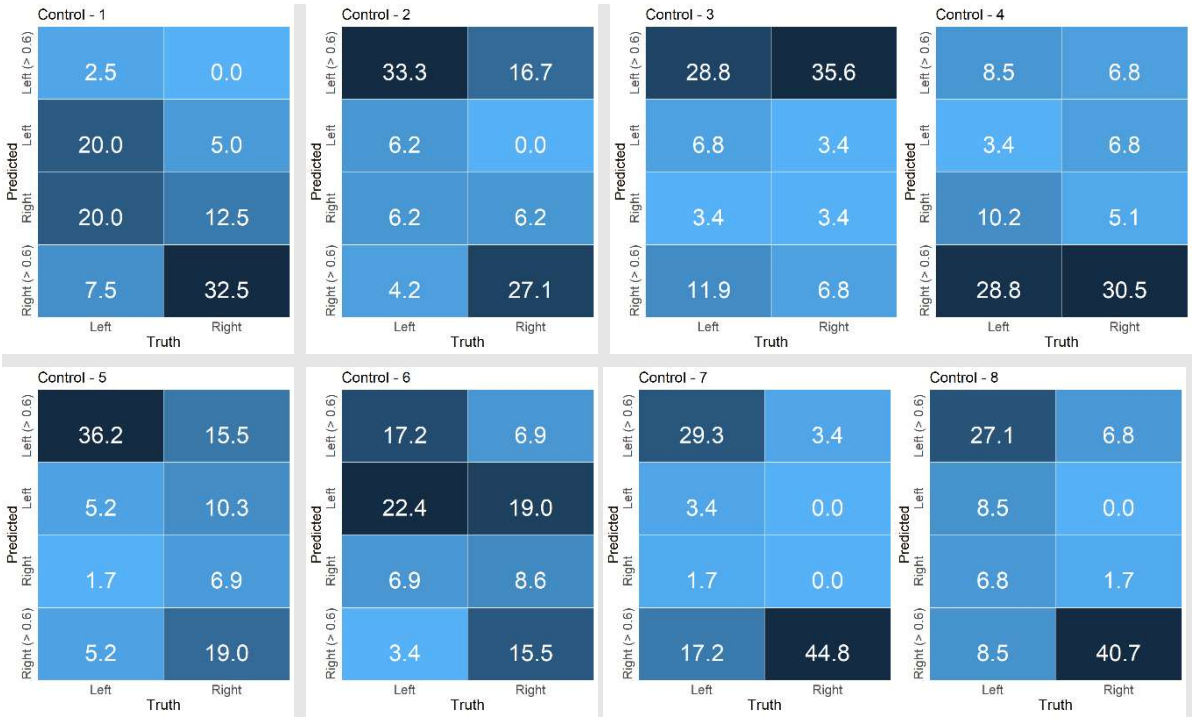

Figure 6.4: Confusion matrices of control sessions

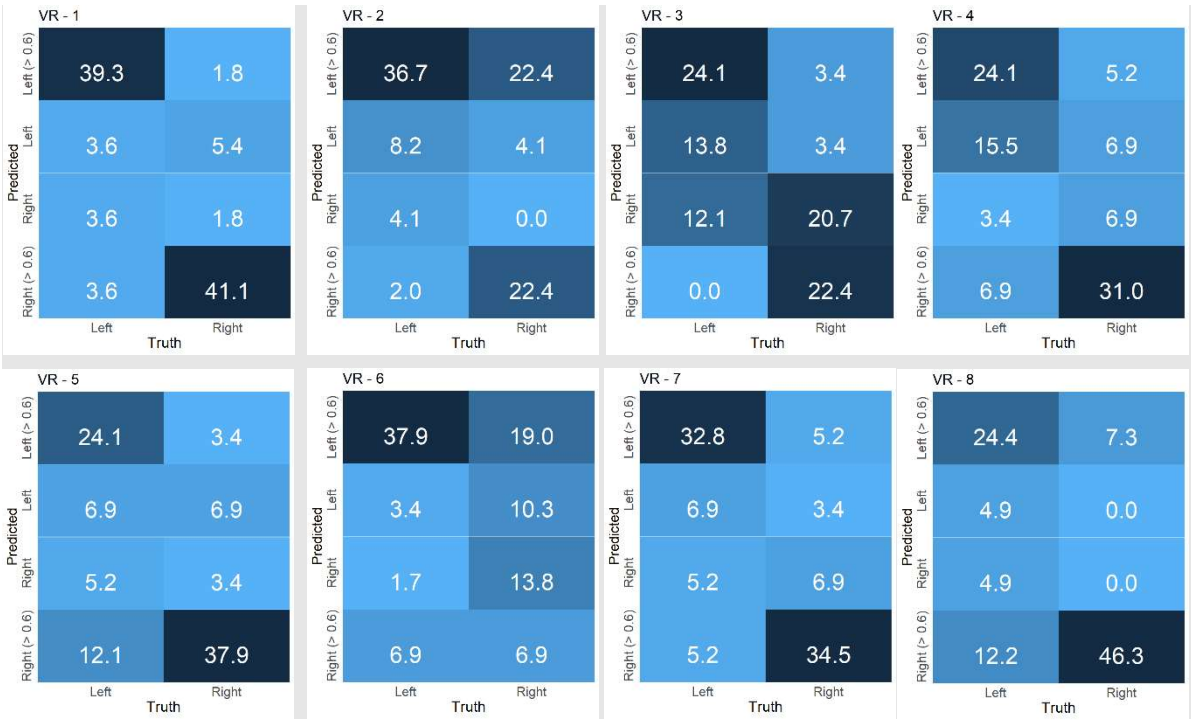

Figure 6.5: Confusion matrices of VR sessions

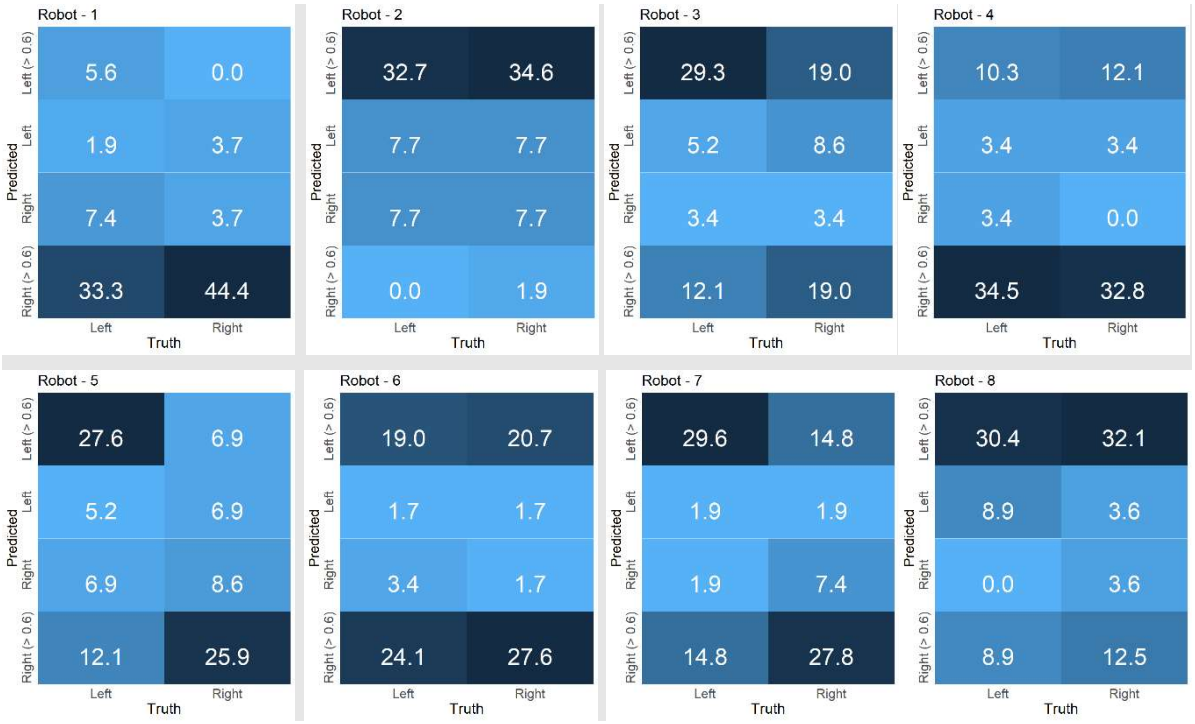

Figure 6.6: Confusion matrices of robot sessions

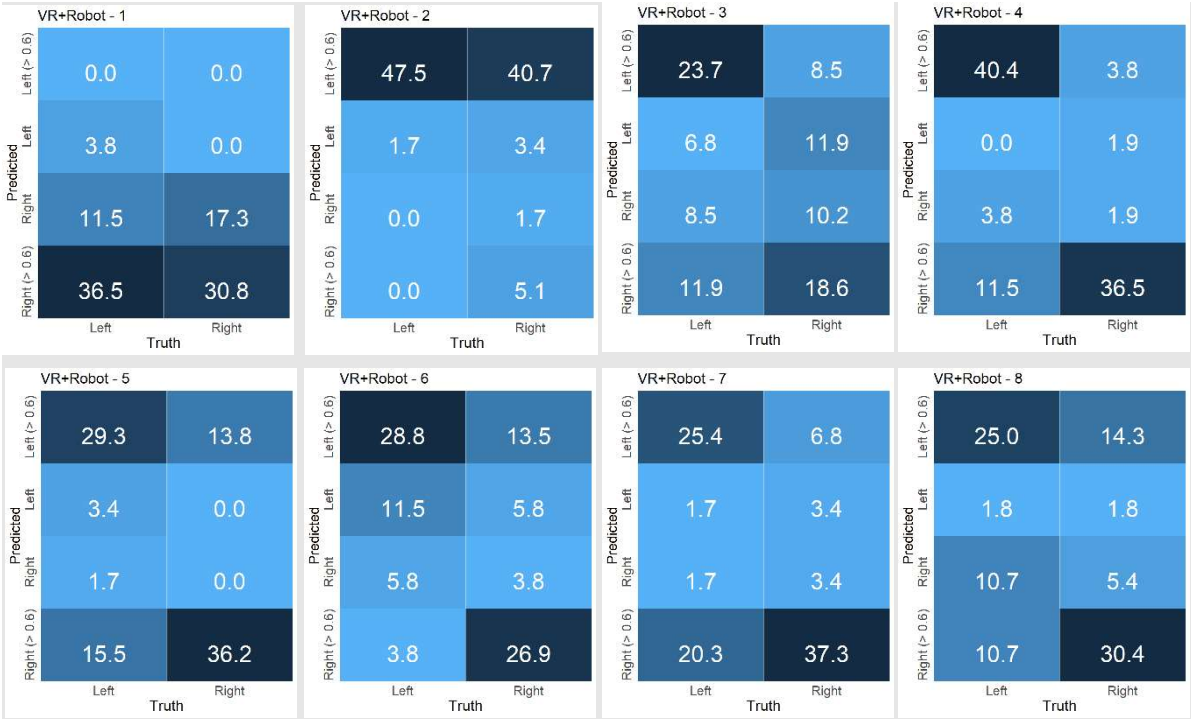

Figure 6.7: Confusion matrices of VR+robot sessions

6.3.2. Class Probabilities

The violin and box plots in Figure 6.8 show the median of the true class probabilities per condition across all sessions. A dashed line was drawn on the 0.6 threshold value for each plot. About 6 out of 8 sessions for both the VR and VR+robot conditions exceeded the threshold line, while the control and robot conditions had 4 and 3 sessions exceeding the threshold line, respectively.

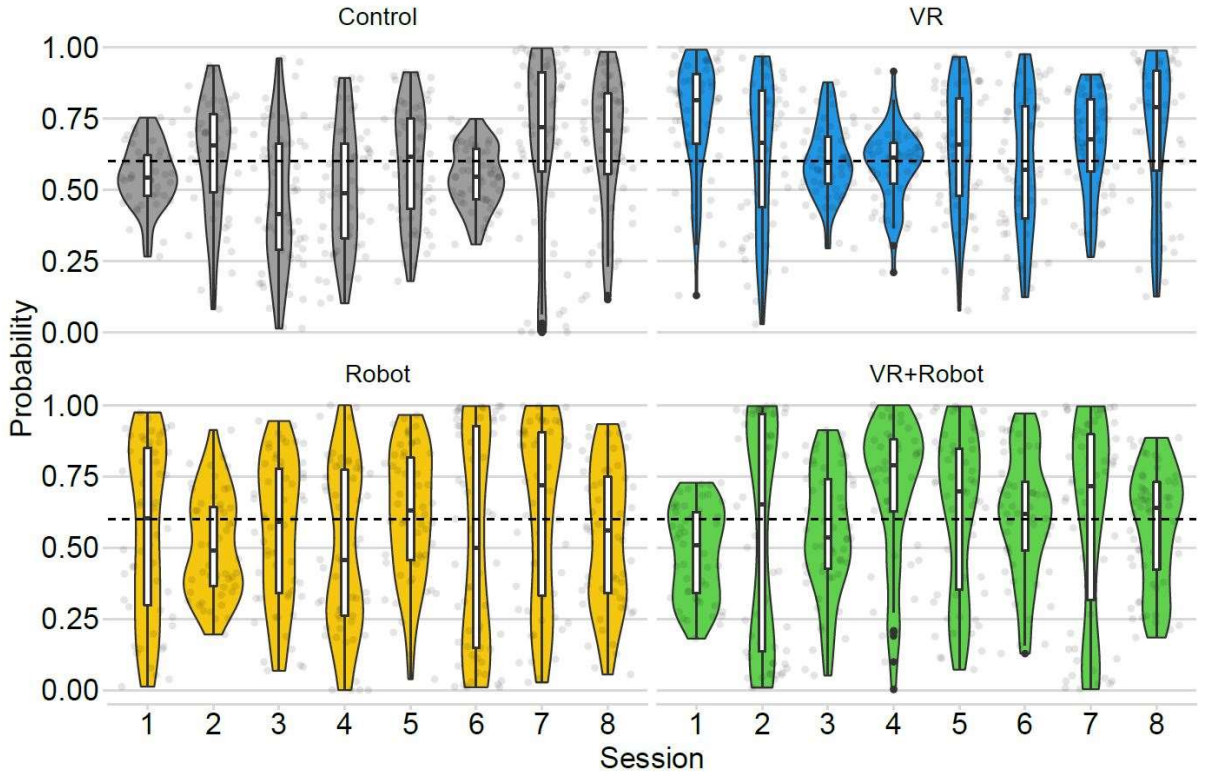

Figure 6.8: Probability values of the true class per condition across all sessions

6.3.3. EEG Analysis

Figures 6.9 – 6.12 show all the session-averaged time-frequency representations (TFRs) of each condition's left- and right-hand classes, while Figures 6.13 – 6.16 show all the session-averaged ERD/S line plots along the μ and β spectral bands. Training and testing phases are presented separately in all plots because the feedback stimuli in the testing phases might present some differences from the data. The colour scale in TFRs and the y-axis in the ERD/S line plots refer to relative event-related spectral perturbations (%). Within TFRs, red-coloured patterns observed across time points (x-axis) depict sensorimotor-related event-related desynchronisation (ERD), while blue-coloured patterns depict event-related synchronisations (ERS). The y-axis in TFRs corresponds to the bandpass frequency range (2-36 Hz). I also extended the plots to a second before the event trigger (-1s) as this was used as the baseline interval to calculate the % ERD/S change. The TFRs and ERD/S line plots generated for the individual sessions of every condition, separated into training and testing phases, can be found in Appendix D, while the topographic visualisations of the CSP spatial filters for the training phase of all sessions are presented in Appendix E.

Due to an overwriting incident within the NeuroPype software, I failed to record the EEG file (.XDF) of the *testing phase* during the 3rd session of the VR condition (*VR-3-Testing*). The online classification accuracy scores and class probabilities were not affected during this incident. However, it is important to consider this when looking at the averaged TFR and ERD/S line plots of the VR condition.

Control - Training

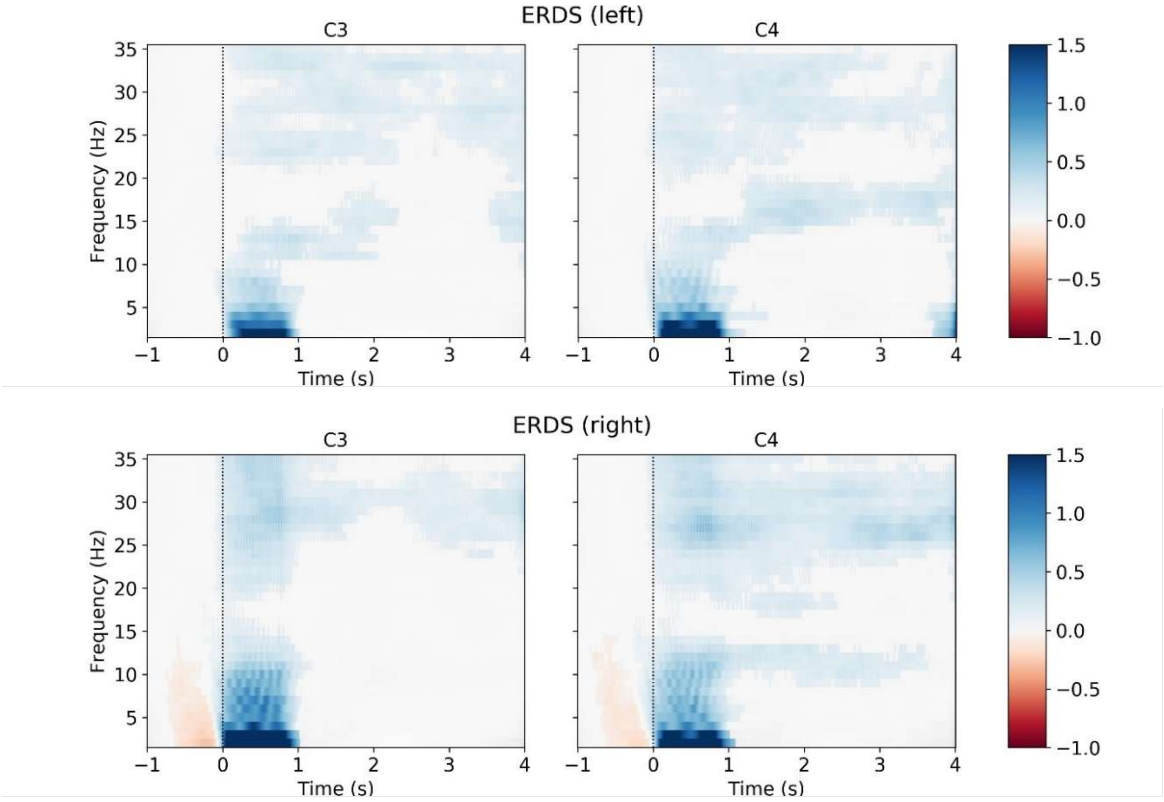

Control - Testing

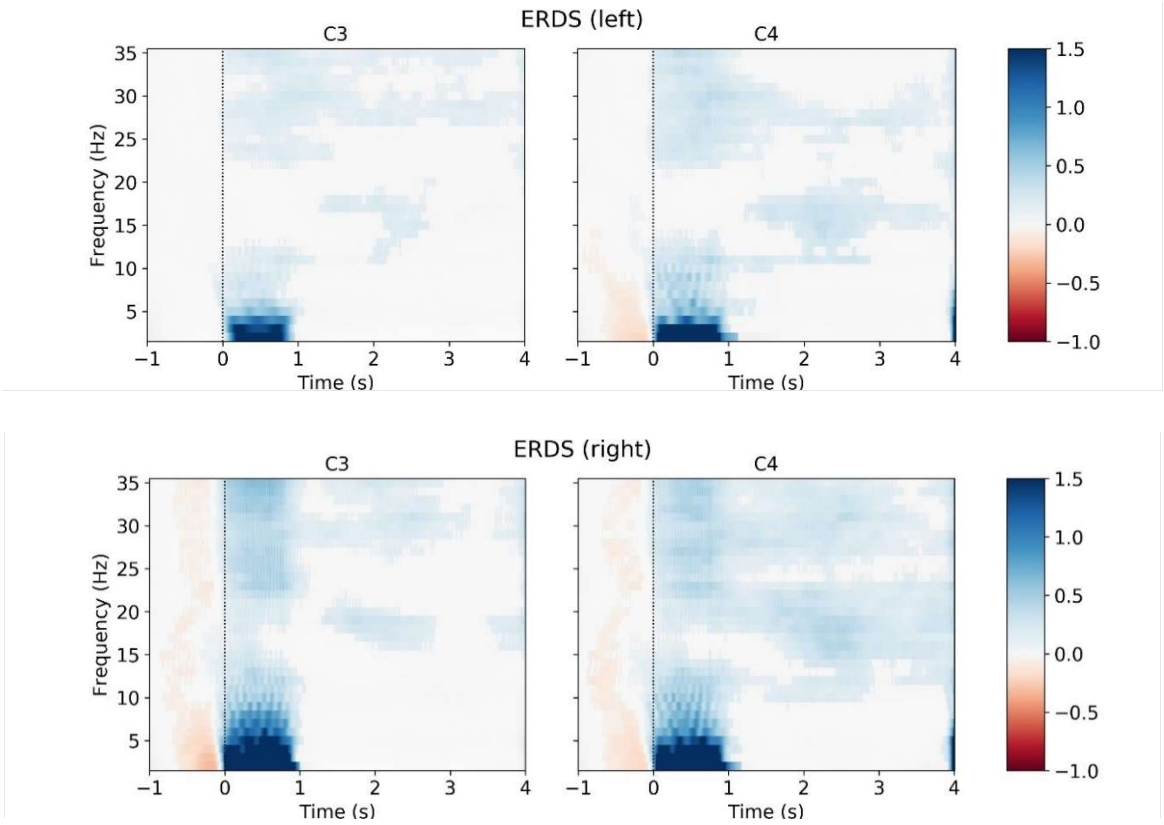

Figure 6.9: Averaged EEG time-frequency representations of the control condition

VR – Training

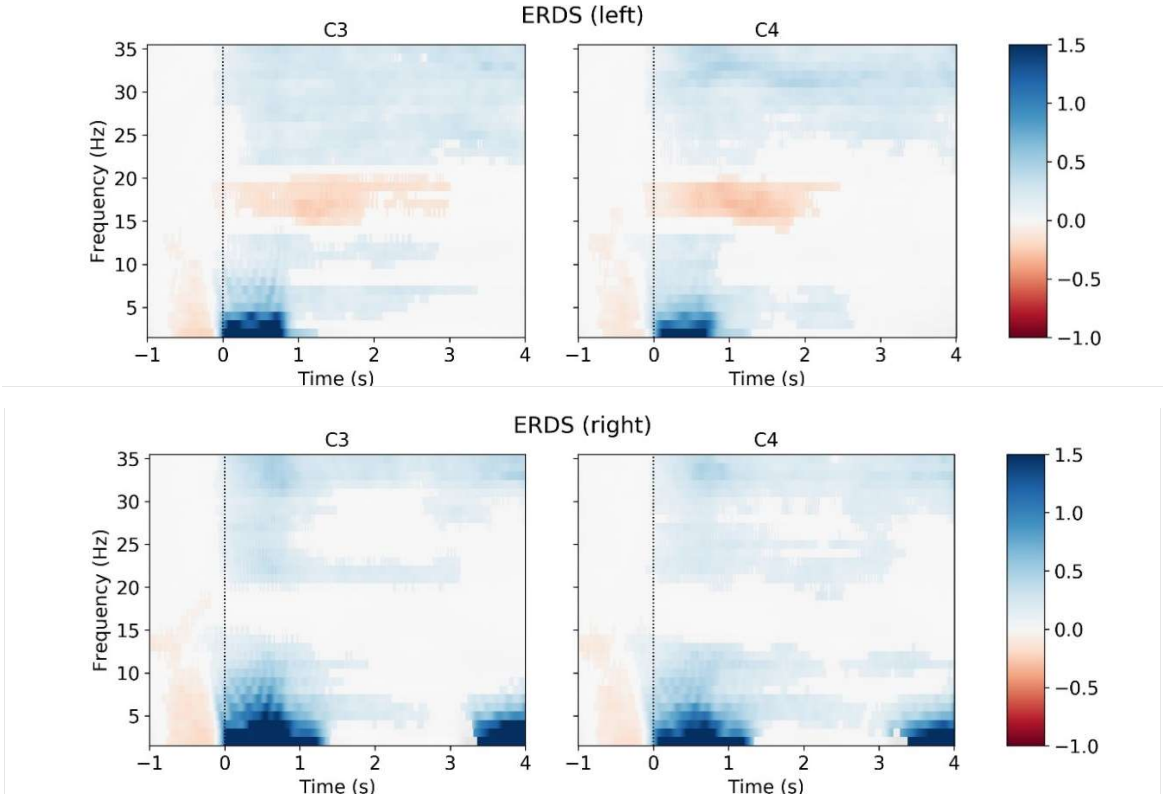

VR – Testing (N = 7)

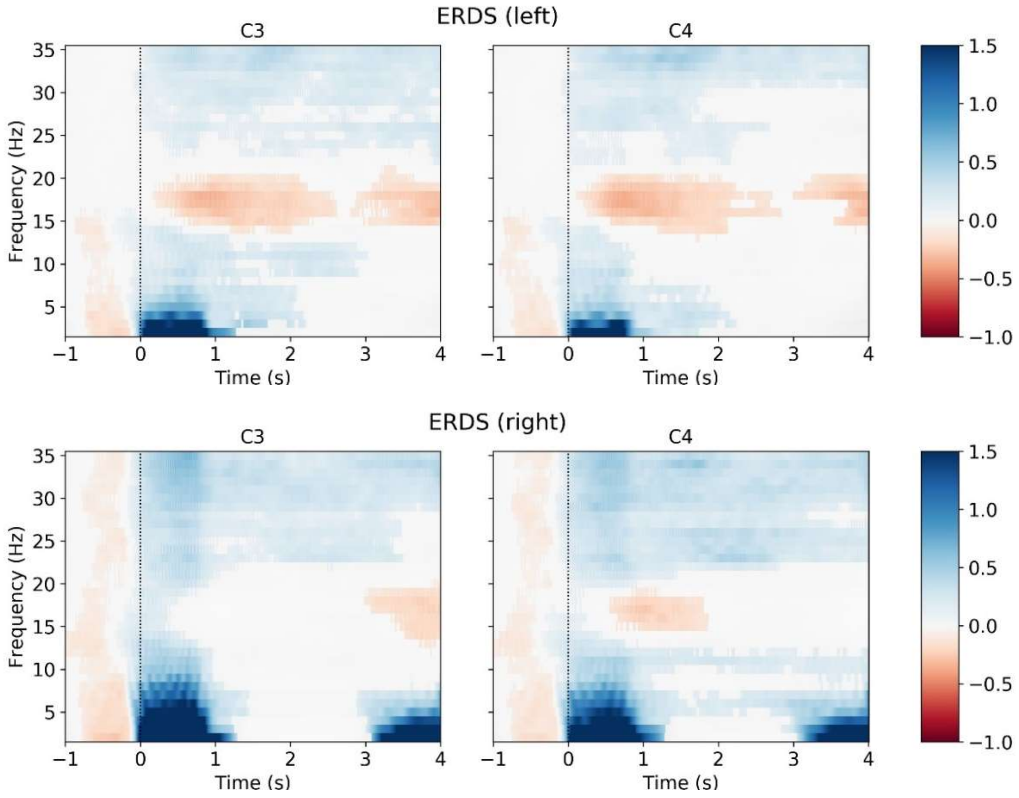

Figure 6.10: Averaged EEG time-frequency representations of the VR condition

Robot - Training

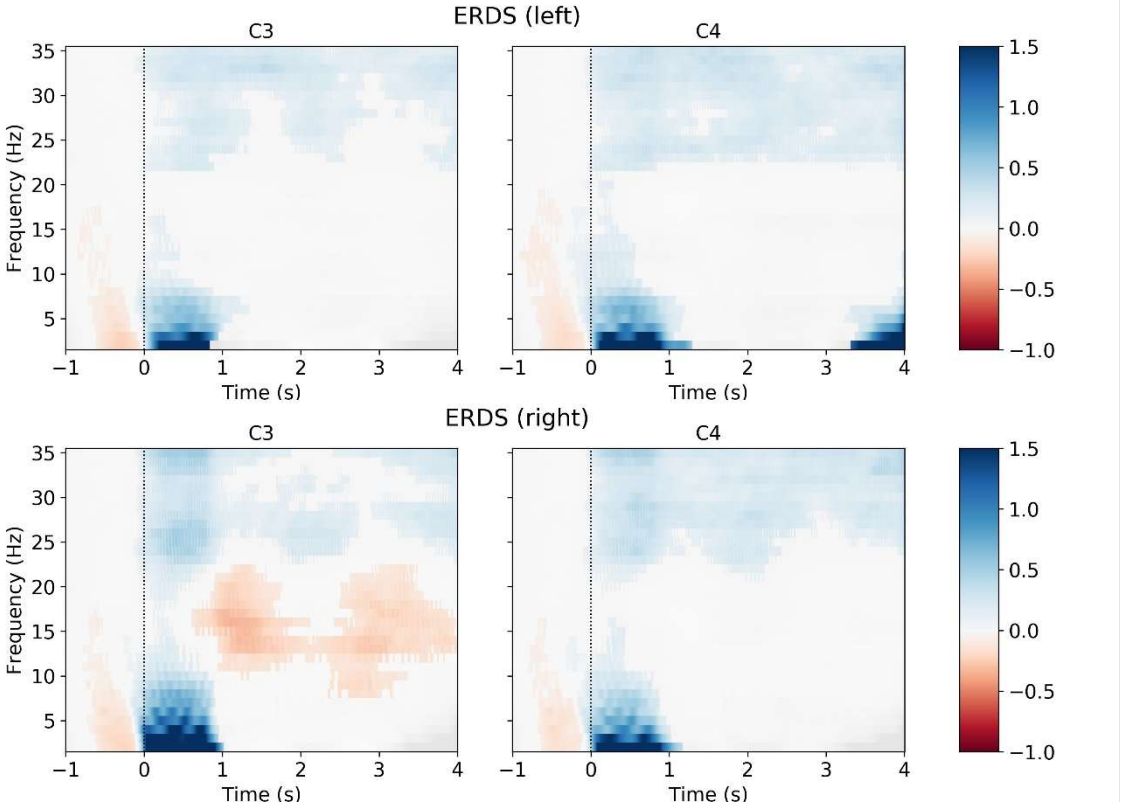

Robot - Testing

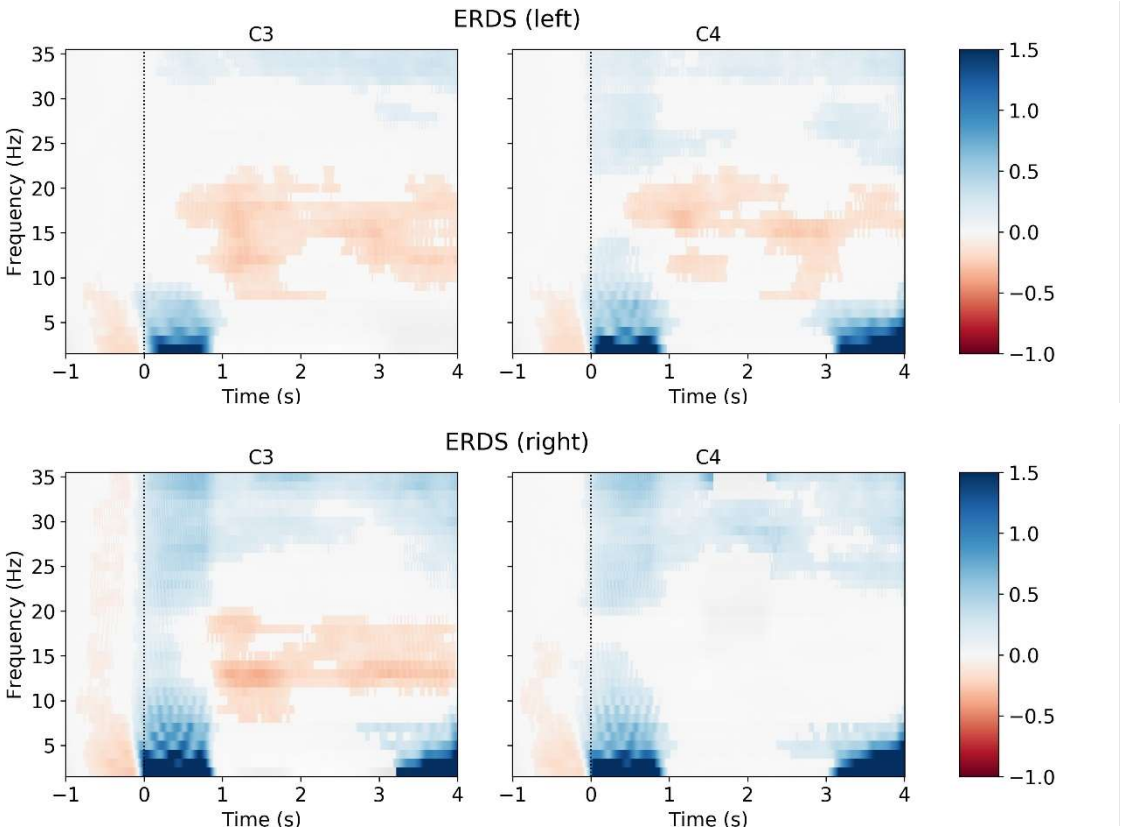

Figure 6.11: Averaged EEG time-frequency representations of the robot condition

VR+robot - Training

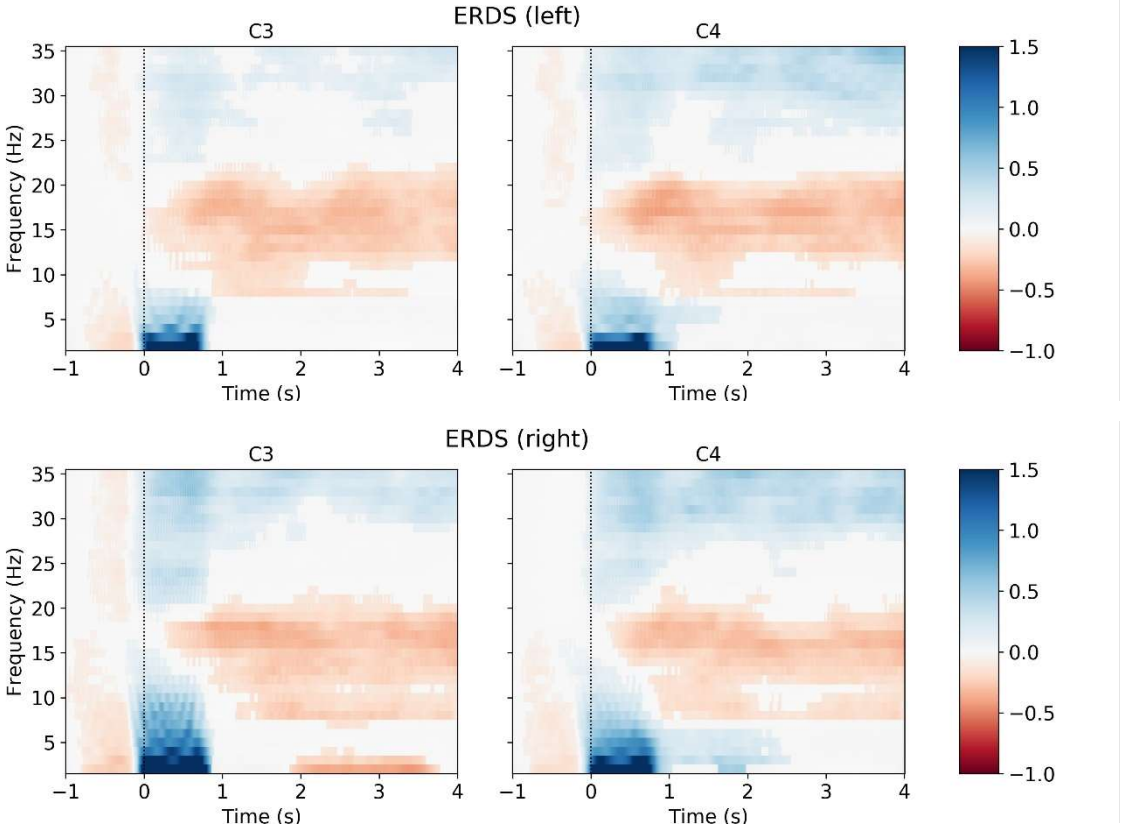

VR+robot - Testing

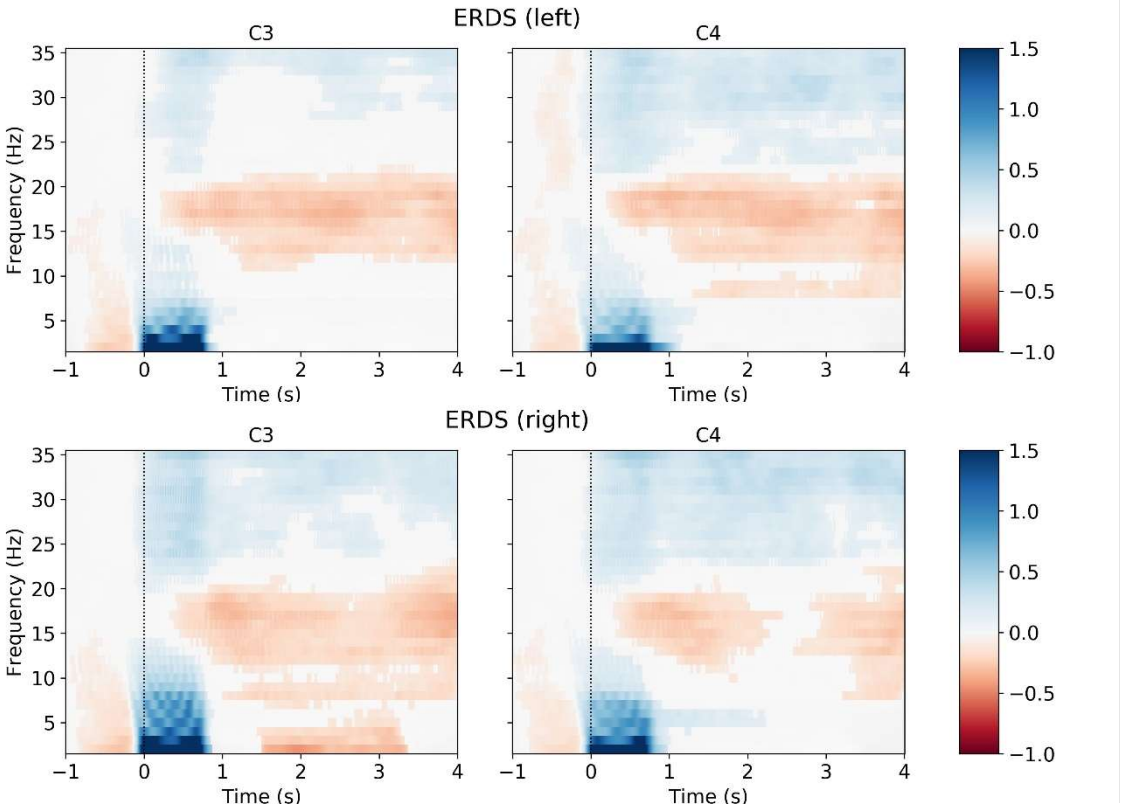

Figure 6.12: Averaged EEG time-frequency representations of the VR+robot condition

Control - Training

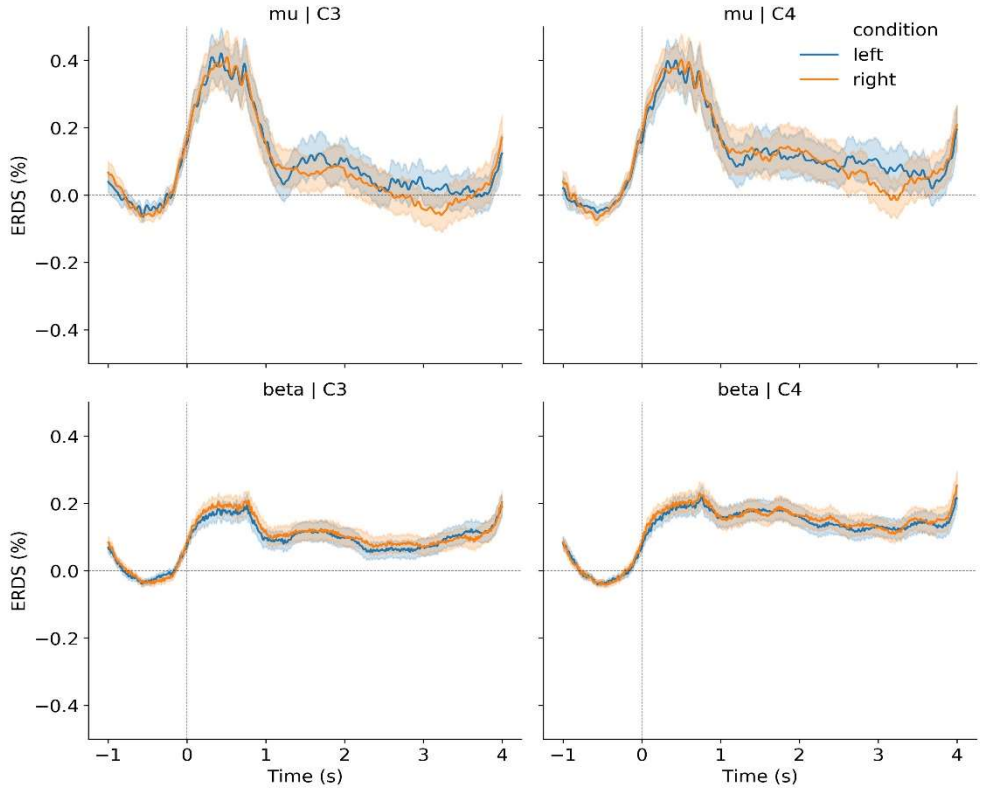

Control - Testing

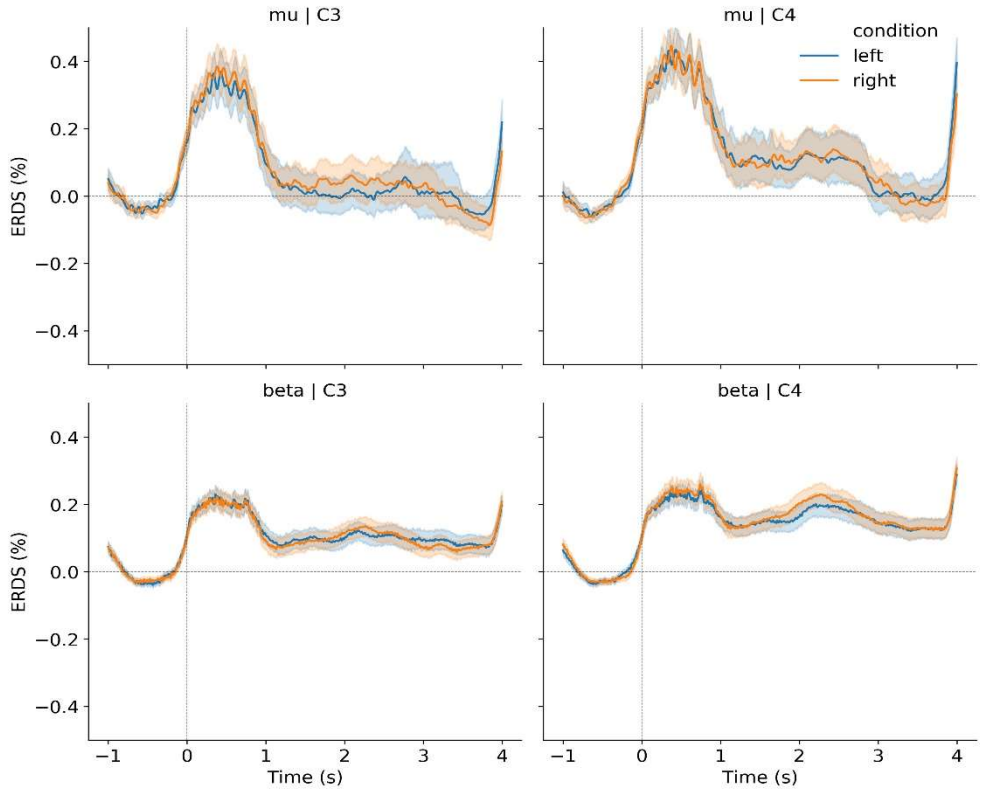

Figure 6.13: Averaged EEG ERD/S line plots of the control condition

VR - Training

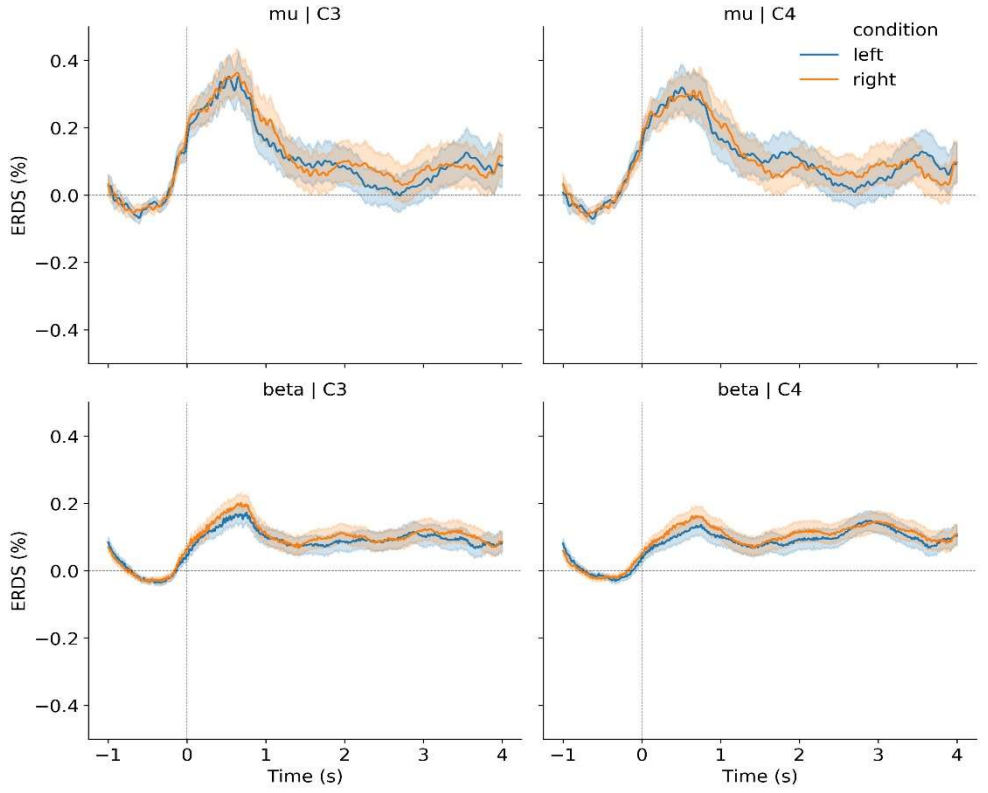

VR – Testing (N = 7)

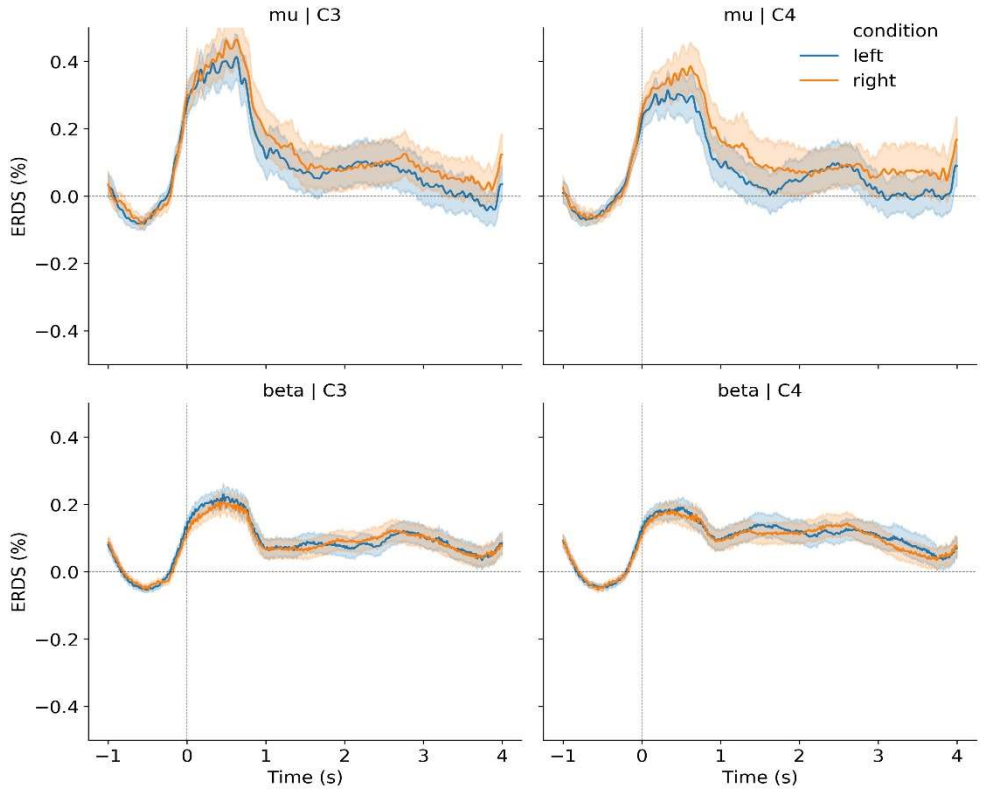

Figure 6.14: Averaged EEG ERD/S line plots of the VR condition

Robot - Training

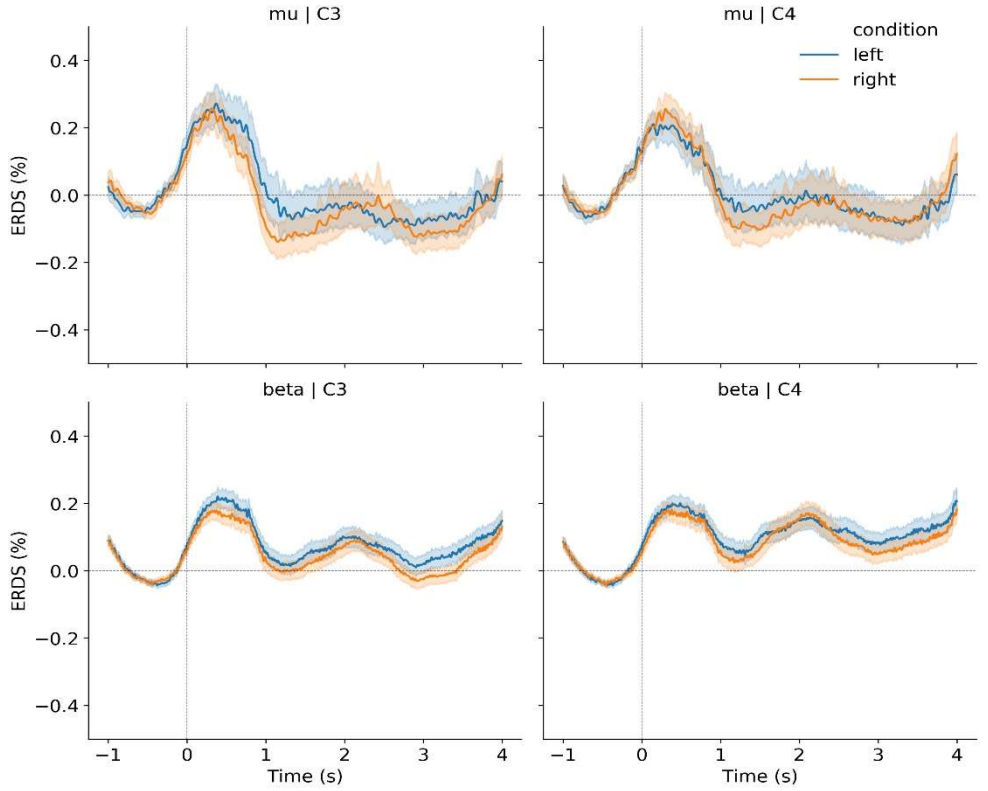

Robot - Testing

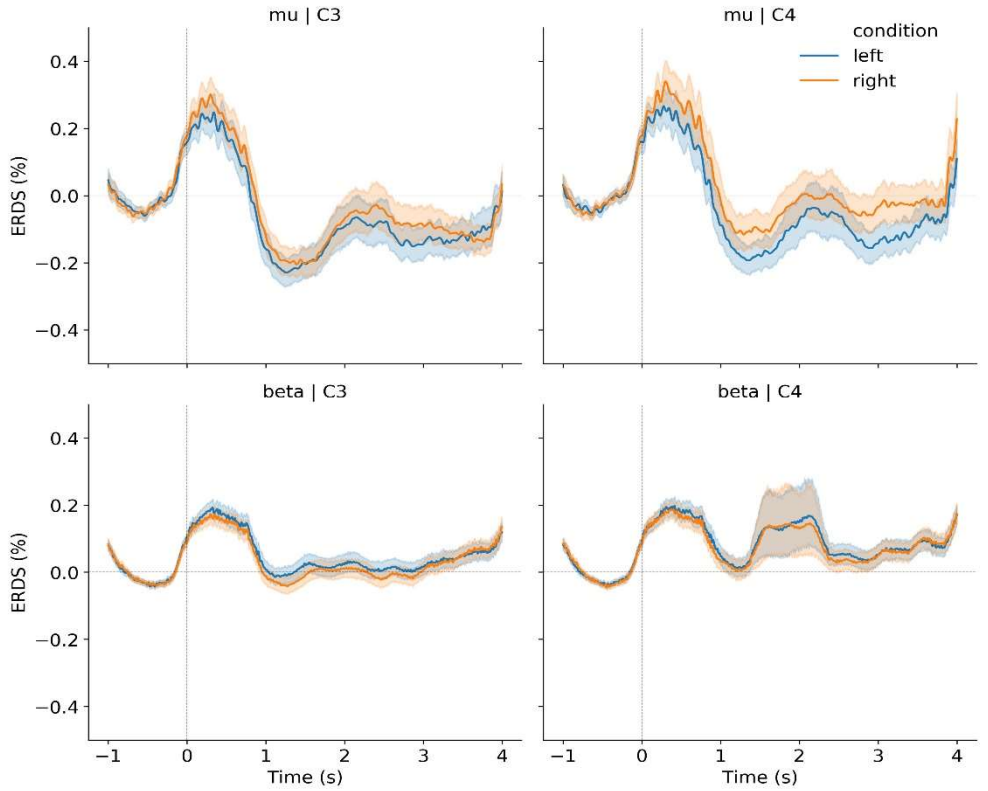

Figure 6.15: Averaged EEG ERD/S line plots of the robot condition

VR+robot - Training

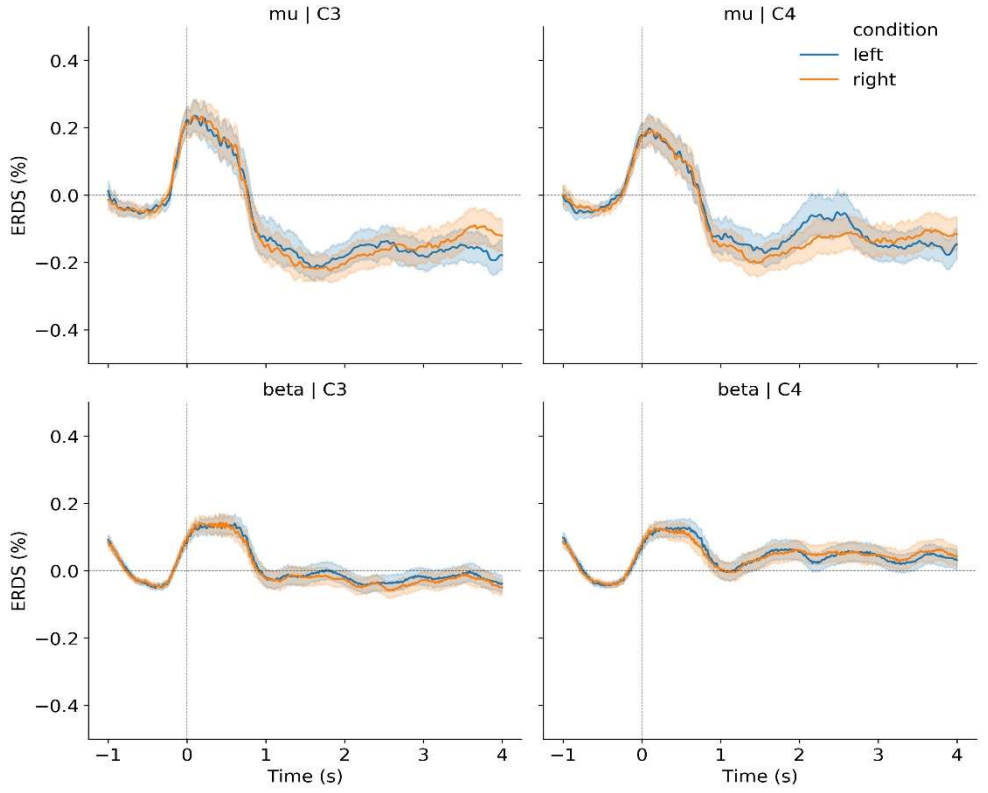

VR+robot - Testing

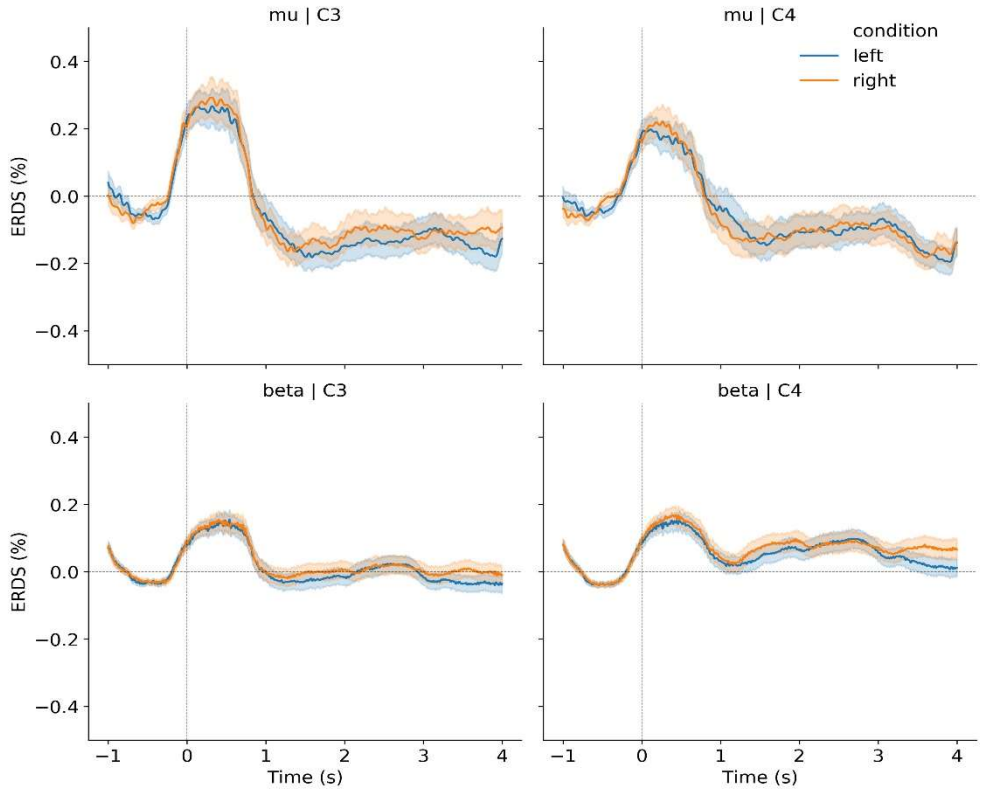

Figure 6.16: Averaged EEG ERD/S line plots of the VR+robot condition

From the averaged TFRs, I immediately observed a strong ERS pattern within one second after the event trigger in the delta (δ) (2–4 Hz) band of the left trials and a strong ERS pattern in the theta (θ) (4–8 Hz) and δ bands of the right trials. For some TFRs (i.e., VR training and testing right trials both channels, robot training and testing left trials C4, and robot testing right trials both channels), a strong ERS pattern in the δ band can also be observed at time 3-4 seconds. No distinguishable ERD patterns were observed in all of the control conditions. For the rest of the conditions, the presence of faint ERD patterns within the μ and β bands were observed except for the VR training right trials of both channels, the robot training left trials of both channels, the robot training right trials of C4, and the robot testing right trials of both channels. Stronger and more vivid ERD patterns can also be observed in all VR+robot TFRs. The running t-test performed on the ERD/S line plots of μ and β bands yielded no significant time points after correcting the p-values based on the Benjamini-Hochberg method.

6.4. Discussion

In this study, I hypothesised that the enhanced visual and kinaesthetic stimuli through an immersive VR environment and a robotic hand exoskeleton, respectively, will increase motor imagery BCI performance. This section provides an in-depth discussion of the results from the previous self-experiment performed using a BCI-VR-robot prototype. I will first look at the three measures of motor imagery BCI performance explained at the beginning of this chapter and then relate my findings to the specific aims and objectives of the study.

6.4.1. Online Classification Accuracy

In the recently performed experiment, both the VR and VR+robot conditions performed better than the control and robot conditions in terms of online classification accuracy scores. Their calculated means were above the 50% mark, which was the chance-level accuracy for a two-class classification setup. However, the high standard deviation calculated in all of these conditions (including the robot and control) suggests a high variability among the scores. It is worth noting

that these scores were also subjected to a >0.6 threshold value to increase confidence in predicting correct trial-wise classifications (Combrisson and Jerbi, 2015). Classifying each trial without a threshold value, as with conventional motor imagery based BCI setups (Lotte, 2014; Virgilio Gonzalez et al., 2018), these sessions would achieve higher classification rates. The grey plots on Figure 6.1 presented how much increase this would make to the current scores. In this no-threshold scenario, all sessions in the VR and VR+robot conditions would score above 50%, while the control and robot conditions would only have two sessions below 50%. Careful consideration of the threshold value is crucial in this experiment. If I prioritise rewarding correctly classified trials with greater confidence (greater account for true positives), then a higher threshold value should be implemented. Practically, this may not be the case for rehabilitation regimens as the motivation to participate actively is given utmost priority during sessions. Physicians and therapists might even want to prescribe an opposite scenario where a patient receives rewarding feedback even if the BCI system has incorrectly classified some of their trials. Nevertheless, I believe a >0.6 threshold provides the optimum level of providing feedback to the user while maintaining confidence for the prediction of trial-wise classes within the motor imagery sessions.

Regarding the progression of scores, no learning effects were observed based on the results from the linear regression analysis. An overall positive trend was calculated as the number of sessions performed increased. A positive trend was also calculated per condition except for VR. However, all calculated slope p-values reported that none of these was significant. This might be due to the participant being an experienced motor imagery BCI user. The case might be different if the experiment was performed with naïve BCI participants.

The results of the 2x2 factorial ANOVA suggested that the enhanced visual stimuli brought by the immersive VR environment could be contributing to the improved motor imagery BCI performance. This agrees with the findings reported from the mean values where the VR and VR+robot conditions performed better. Although I reported significant differences in the enhanced visual factor ($p = 0.0422$), I believe that this value might not be low enough to be considered solid evidence of the actual effect of VR on motor imagery BCI performance. Therefore, I recommend progressing this finding by repeating the experiment within a larger

study population. In this way, I can increase my statistical power and better understand this topic.

6.4.2. Class Probabilities

Analysing the true class probability values allowed me to look at the trial-wise decoding of motor imagery classes using the logistic regression classifier. In this performance measure, the VR and VR+robot conditions also performed better than the control and robot conditions. Both conditions with VR have 6 out of 8 sessions above the threshold line of 0.6. This finding is supported by visualising each session through the confusion matrices presented in Figures 6.4-6.7 of Section 6.3.1. By visual inspection, the sessions that pass the threshold line have more distinct segregation in the true class tiles than lower-scoring sessions where the tiles seem randomly distributed or, in other cases, distinctly misclassified to the wrong class.

6.2.3. EEG Analysis

I first address the presence of strong event-related synchronisation (ERS) patterns in some of the time-frequency (TFR) plots along the δ (1-4 Hz) band for left trials and along the δ and θ (4-7 Hz) bands for right trials. These were either within one second at stimulus onset or within one second before the trial ended. These may be artefacts related to head movement. In the literature, the presence of these artefacts can be manifested in the δ and θ frequencies (Kappel et al., 2017; Britton et al., 2016; Jansen et al., 2012). The current experimental setup performed head movements which might be causing this distinguished artefact. Within one second from when the event trigger was shown, the participant routinely performed a slight and abrupt head movement to focus on the direction of the hand of interest. Likewise, when the trial ended, the participant returned to their initial head position and orientation straight towards the screen and focused on the appearance of the next fixation cross to get ready for the subsequent trial. As this was consistent throughout the sessions, averaging this generated a strong activity in those bands. As a result, this artefact appeared in the EEG data as a strong ERS pattern. To confirm the exact timepoints of head movement, accelerometer and EEG data were acquired

from two healthy adult participants, both male at 20 years of age. These data were obtained from a pilot test performed during the developmental period of the BCI-VR prototype. In this scenario, the participants performed a similar motor imagery BCI task (i.e., a VR condition session) as the current self-experiment. However, accelerometer data were also recorded from the sensors present in the Enobio-8 wireless EEG amplifier (note: no accelerometer data was recorded during the current self-experiment due to computer memory-related limitations). Acceleration data in the x-, y-, and z-axis (mm/s^2) were extracted and processed (i.e., epoched and averaged across all trials) to show head movement occurring within the trial (see Figures 6.17 and 6.18).

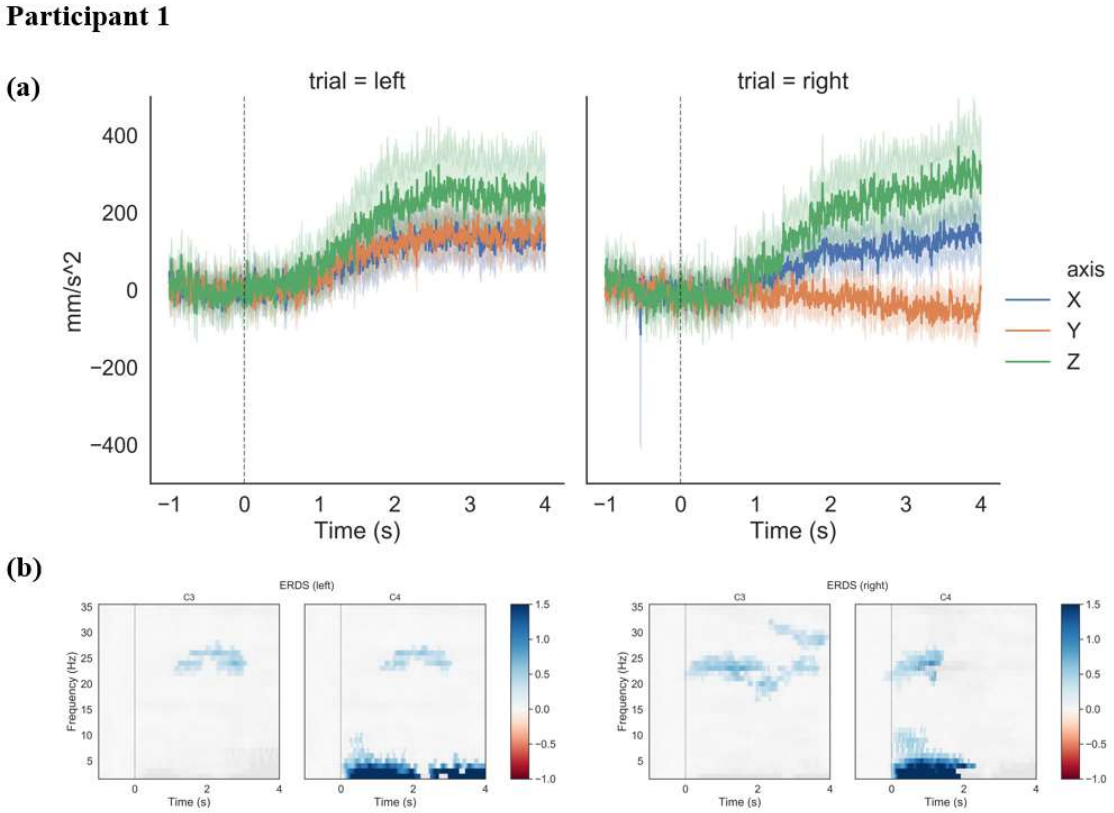

Figure 6.17: Head movement and EEG artefacts in a pilot BCI-VR testing (participant 1)

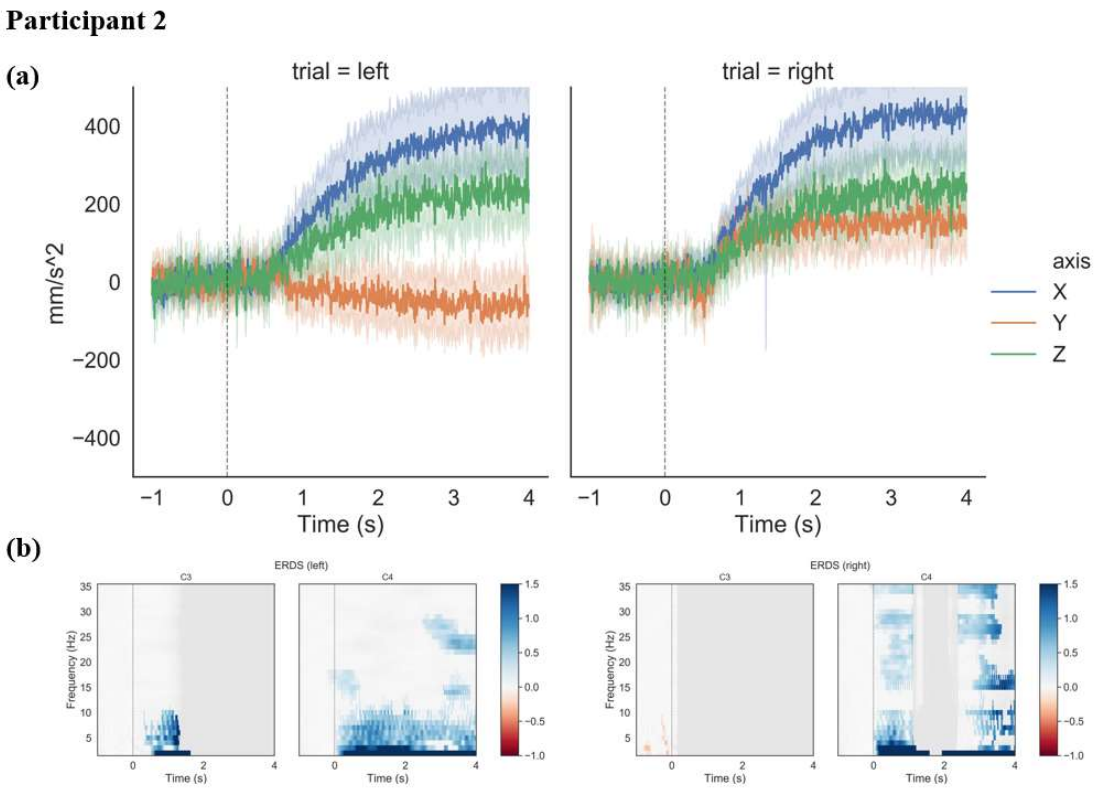

Figure 6.18: Head movement and EEG artefacts in a pilot BCI-VR testing (participant 2)

As presented in the figures, the session-averaged accelerometer data plotted against the EEG TFR of the same session showed both head movements commencing within one second from stimulus onset (time = 0 s). Simultaneously, the presence of similar δ (1-4 Hz) and θ (4-7 Hz) ERS patterns appeared in both their TFR plots. These findings support the assumptions that EEG artefacts caused by head movements may be attributed to the strong ERS patterns observed in the recent self-experiment. Such artefacts might be affecting the decoding process of the classifier during the testing phase. For example, if the artefacts are not equally distributed between the two classes during the training phase, it would favour one class's prediction over the other. However, in the current scenario, the EEG artefacts were evenly distributed across both classes, which can be seen in the averaged TFR plots of each condition (Figures 6.9-6.12). I also think that the presence of these artefacts has not significantly affected the decoding process of the motor imagery classes as the lower cut-off for the bandpass filter in the NeuroPype BCI pipeline was set to 8 Hz. This cut-off frequency excludes most of the δ (1-4 Hz) and θ (4-7 Hz)

bands during the training of the classifier and focuses on the ERD/ERS patterns on the μ (9-11 Hz) and β (13-24 Hz) bands.

Next, I observed the presence of event-related desynchronisation (ERD) patterns in the μ (9-11 Hz) and β (13-24 Hz) bands of some TFR plots. I believe these patterns depict changes in the sensorimotor rhythm during motor imagery trials as it agrees with how ERD patterns should appear based on literature (Maris and Oostenveld, 2007) and as discussed in Section 3.3 of Chapter 3. A few noticeable observations were that I did not see these patterns in the averaged TFR plots of the control condition, while I saw more obvious and vivid patterns as I looked at the averaged TFR plots of the VR+robot condition. While it may seem that the intervention conditions (i.e., VR, robot, VR+robot) were contributing to the enhanced visualisation of ERD patterns in the averaged TFR plots, I cannot directly attribute these differences to the actual decoding process of the motor imagery BCI processing pipeline. One reason is that no distinct ERD/S patterns were observed when I looked at the plots based on hemispherical activity. Based on my discussion in Chapter 3, I should expect the left hemisphere (as represented by the C3 electrode) to have a stronger ERD/S signal in the right-hand trials and vice versa; a contralateral pattern between the hemispheres of the motor cortex and the left and right hands. However, these patterns were not consistently observed in my averaged TFR plots. The second reason is that the intensities of these patterns from the intervention conditions (i.e., VR, robot, and VR+robot) were not significant and therefore cannot be considered as strong evidence that they increase performance at the EEG level. This leads me to suggest that the ERD/S patterns extracted from the TFR plots were only a part of a more prominent feature space that the machine learning-based classifier is using to decode left and right-hand classes.

6.5. Summary

I performed a self-experiment using an integrated BCI-VR-robot prototype to determine the effects of enhanced congruent visual and kinaesthetic stimuli on hand motor imagery based BCI. A 2x2 factorial design allowed me to test three intervention conditions: VR, robot, and combined VR+robot against a control. I hypothesised that an increased motor imagery BCI performance will be observed on the following measures: (1) online classification accuracy scores, (2)

probability values of the true class being predicted, and (3) ERD/S patterns in EEG (refer to Table 3.2 – Research hypotheses). My findings demonstrate a positive effect of the enhanced visual stimuli on online classification accuracy scores and probability values of the true class. Furthermore, I also reported that although faint, ERD/S patterns can be observed in various conditions, excluding the control. In the next chapter, I provide a general discussion on how these findings relate to the overall aims of this thesis and provide a conclusion to summarise my contribution to the scientific field.

Chapter 7
General Discussion and Conclusion

7.1. General Discussion

The overarching hypothesis of this research is that enhanced visual and kinaesthetic stimuli through an immersive virtual reality environment and a robotic hand exoskeleton will improve motor imagery BCI performance. In Chapter 2 (Systematic Review), I reported a list of BCI-hand robot studies and their scarce implementation of a rich and engaging stimulus for their cue and feedback delivery. Chapter 3 (Theoretical Framework) provides a compelling theory on BCI use and enhancing the stimuli presentation processes. In Chapter 4 (BCI-VR Development), I demonstrated an integrated virtual environment and brain-computer interface based on a motor imagery paradigm in VR. While in Chapter 5 (Robotic Hand Exoskeleton Development), I presented a prototype for a robotic hand exoskeleton and its integration with the current BCI-VR system. In Chapter 6 (Experimentation), I presented the methods, results, and discussion of a self-experiment performed to test my hypotheses. A self-experiment, in which I was the researcher and participant, was done to progress this research amid the restrictions to physical research activities brought by the ongoing COVID pandemic. Finally, in this chapter, I provide a general discussion related to my research findings, its contribution to the body of scientific knowledge, and the benefits of an integrated BCI-VR-robot system to the medical community and society as a whole.

The results of my recent experiment showed that enhanced visual stimuli through an immersive VR environment could potentially improve motor imagery BCI performance. Across all the sessions performed, the visually enhanced conditions improved BCI performance in terms of online accuracy scores and true class probabilities. Although I have observed weak and marginal effects, these were deemed significant, nonetheless. However, it is not clear from these findings which factors tap into the internal mechanisms that drive this effect. In the integrated BCI-VR setup, I presented an enhanced visual stimulus to the motor imagery paradigm via two

factors: (1) embodiment and (2) environment. I interpret embodiment as the presence of animating a geometric representation of a five-fingered appendage (a hand) during motor imagery trials.In contrast, the presence of virtual elements brings an enhanced environment (e.g., room setup, lighting, sparkles as rewards, other objects) and other stimuli (i.e., auditory, haptic, etc.) as part of a game.

I now ask the question: "Which among these factors could be driving the neural mechanisms that promote motor imagery performance?". In future experiments, I suggest looking into these factors separately. For example, I envision a similar VR scenario with only the hands presented visually and the remaining elements absent. When looking into the enhanced environment factor, I ask the question: "Does the addition of virtual gamification elements provide motivation or is it a distraction?". It is worth noting that the stimuli presented to a participant, regardless of modality, are reflected in their EEG data (Kaufmann et al., 2013), and I recommend that future BCI-VR developers put importance on this matter. Existing applications in BCI literature implement an immersive paradigm where one can control a spaceship (Škola et al., 2019) or play World of Warcraft (Nijholt et al., 2009) with their brain signals. While these themed scenarios provide us with a good proof of concept for visually-enhanced BCI paradigms, I still believe that their role and mechanism in affecting BCI performance remains unexplored.

In this study, I also introduced a low-cost robotic hand exoskeleton made of 3D-printed materials and high torque servo motors. The current prototype in itself, with further refining, can be used for conventional robot-assisted rehabilitation tasks as they have successfully performed the assistance of simple prehension activities (i.e., full grasping movement and pinch-grip movements). However, for the recent self-experiment, the prototype was utilised as a provider of kinaesthetic stimuli during motor imagery trials. The results presented in Chapter 6 reported that the robot conditions provided no significant difference against the control groups, which suggests that the enhanced kinaesthetic stimulus provided by the robotic hand exoskeleton may not improve motor imagery performance. Therefore, I now ask the question: "Does the robotic exoskeleton increase performance or provide distraction?". Because the current prototype is a low-cost and low-end device, it has many features that can be improved. In the following

list, I enumerate the current limitations of the robotic hand exoskeleton, followed by the recommendations that I made for improving its design:

1. **Actuation** - The choice of actuators influences most of the exoskeleton's mechanical and electronic components and is an essential aspect that needs improvement. I recommend using quieter, more lightweight, and more safety-compliant actuators for the next iteration. The current mechanical design uses rigid linkages that restrict the fingers' movement and a limited range of motion. By using soft pneumatic artificial muscles (Polygerinos et al., 2013; Polygerinos et al., 2015; Coffey et al., 2014) or cable-driven mechanisms (Heo et al., 2012), we can reduce the rigidity of the exoskeleton mechanism while still attaining the required poses for the hand. In addition, we can also move (or alter) the placement of the power driving source away from the hand and into more stable bases, increasing its safety rating and reducing the total weight of the device affecting the hand.

2. **Hand Tracking** – The Leap Motion controller enables static and dynamic hand tracking via infrared sensors and depth cameras. However, the current design of the robotic hand exoskeleton only allows hand tracking with the Leap Motion for a specific pose (i.e., palm facing upwards). This is due to the linkages situated on the other side of the hand (dorsal side) and obstructing the view of the Leap Motion sensors. While this does not affect the current hand grasping motor imagery paradigm, it limits the capability of the BCI-VR-robot prototype to track dynamic hand movements such as pronation and reach-to-grasp. This can be resolved by removing the obstruction (through a change in the actuation strategy and mechanical design) and by using highly reflective gloves and covers, allowing the Leap Motion controller to identify the geometric shape of the hands. As an alternative, one can also use other hand tracking systems, such as motion capture systems that use retroreflective ball markers. In this way, individual markers can be placed on the gloves, captured by an external sensor, and then aligned geometrically using the motion capture software.

3. **Sensors** - The perceptual and sensing capabilities of the robotic hand exoskeleton can be improved by integrating several sensors into the system. My recommendation is to

include accelerometers and gyroscopes in the prototype to measure the hand's linear acceleration and rotation, respectively. By integrating these sensors into the system, we can measure hand movement during tasks (in addition to the hand tracking enabled by the Leap Motion system) and enable more complex tasks and experiments with the device. I also discussed the use of EMG and force sensors in Section 3.2 as a means of acquiring external signals of intent. These were not applied to the current prototype as the main focus of developing a robotic hand exoskeleton was to provide kinaesthetic stimuli during the experiment. However, a device that can acquire signals of intent internally (EEG-BCI) and externally (EMG and force sensor) enables the BCI-VR-robot system to be multimodal.

Providing a seamless, flexible, and quiet experience can also be achieved by more developed and expensive robotic systems. For example, commercial systems such as HaptX (Stamer et al., 2020) and Gloreha (Tacchino et al., 2017) provide the same goals as the current prototype but with higher specifications for their materials.

I also identified some limitations that contributed to my experiment and analysis. First, I look into my BCI system architecture. In this study, I used a basic motor imagery BCI pipeline adapted from (Lotte, 2014). Online and offline (visualisation and analysis) pipelines used a classical feature extraction and classification method based on common spatial patterns and logistic regression. While these processes provide us with a basic but effective classification algorithm (Lotte et al., 2018), I may be missing out on potential information that can improve the online classification accuracy. The advent of deep learning approaches for motor imagery BCI (Schirrmeister et al., 2017; Roy et al., 2019) addresses these limitations with the requirement of using larger datasets (i.e., from similar historical motor imagery EEG data) and fine-tuning hyperparameters with the session's training data. Deep learning might also be a key solution to address inter-session variability (Saha and Baumert, 2020), which is important because training and calibrating an embedded classifier currently takes half of the time allotted for the session. In the future, I see a "wear-and-use" motor imagery BCI setup that eliminates the need for daily session training and calibration. Another limitation of this study is how the experiment was designed and implemented. A self-experiment design based on repeated measures provides

subject-specific data across sessions and conditions. However, I missed out on the statistical power of my perceived effects which can only be obtained by an experiment having a larger sample size. Having said all of this, the current self-experiment design has still provided great contributions to the body of knowledge for future clinical practices. Designing this self-experiment allowed me to devise a novel approach to motor imagery BCI operation. The current method and evaluation presented in these chapters gives a general knowledge or grasp of an idea for a future process flow that may lead to providing us with better home rehabilitation setups.

7.2. Proposed Experimental Design for Human Testing

It would be good to ask what an ideal design would be if the current research questions were to be implemented for a large-scale human experiment involving healthy participants. The first consideration would be to separate the enhanced visual aspects (VR/No VR) from the kinaesthetic ones (Robot/No Robot). As discussed earlier in this chapter, there is a need to dissect and look into the mechanisms that drive enhanced stimuli on motor imagery BCI performance. The visual and kinaesthetic aspects of the current study presented us with their respective fundamental research questions, and I propose that these be addressed as separate experiments before implementing a fully integrated BCI-VR-robot prototype study.

A visual stimuli-focused experiment is similar to the current BCI-VR setup with the VR and control conditions. However, in this scenario, the control condition should involve the participants wearing a VR headset and observing a virtual hand without animation instead of performing the classical motor imagery paradigm without VR. The rationale behind this is that the focus of such an experiment should be to answer whether action observation in the form of a VR animation would improve motor imagery BCI performance. In a similar design, a kinaesthetic stimuli-focused experiment should involve wearing the robot and performing motor imagery with or without actuation in their intervention and control conditions, respectively. The following experimental parameters should then apply to both experiments.

7.2.1. Participants

It would be ideal to recruit at least ten naïve participants for each condition (10 for control and 10 for the intervention), leading to a total of N=20 participants in each experiment. This would allow us to generate the necessary effect size differences among conditions in an optimum time frame. The participants should be randomly assigned to a particular group instead of undergoing multiple conditions to maximise each condition's effect. This would eliminate the need to counterbalance sessions as previously done in the self-experimentation.

7.2.2. Study Design

Each participant would undergo seven consecutive days of motor imagery BCI sessions (1 session per day) in their assigned condition. Using the MIQ-R questionnaire, a measurement of their motor imagery ability should be performed on Day 1 and Day 7 of the study. This design also enables us to perform a double-blind experiment where the participant is not aware of the conditions involved in the study, and the researcher/s (mainly those in charge of data analysis) are blinded from the condition being presented (Note: a technical expert must still be present during the sessions to ensure the safety of the participant and the proper installation of research equipment).

7.2.3. Task Design

I recommend that the nature of the task must still be retained in these scenarios. As discussed in Section 3.4.1 - Basic Principles of BCI Use, the attempt to operate a BCI using contralateral motor imagery of hand grasping allows us to study neural mechanisms optimally. Performing left- and right-hand imagery is a relatively simple task but not elementary. This would allow the participant to quickly familiarise themselves with the nature of the task but still depend on the incoming stimuli during individual trials. However, I would alter some of the elements in the conditions to inform the participants of the task better. For example, I would eliminate the virtual screen presenting the classic motor imagery stimuli elements in the VR condition and incorporate them into the cue and feedback elements happening in the 3D virtual hand. This

would allow them to focus their attention on the hand instead of the other elements in the virtual scenario. Similarly, I would implement a simple tactile cue and feedback system to the robotic hand exoskeleton (i.e., in the form of simple vibrations). In both experiments, I would retain the auditory aspects of the cue-feedback system.

To ensure that the healthy participants perform motor imagery, EMG sensors can be attached over the major muscle groups for grasping (i.e., extrinsic flexors) (Flatt, 2000) to measure muscle activity. In this way, we can detect (subject to a certain threshold) whether motor execution is being performed and reject trials that do so. This can only be applied to healthy participants but not in actual stroke patients where movement attempt is more beneficial (as discussed in Section 3.3 - Electroencephalography-based Brain-Computer Interfaces).

7.2.4. Data Analysis

In the current experiment, I provided three measures of motor imagery performance: (1) online classification accuracy scores, (2) probability values of the true class being predicted, and (3) ERD/S patterns in EEG. In the proposed experiment, I would retain these measures as it excellently captures and evaluates both the human and machine sides of the BCI system. As an added measure, I would like to know if there are learning effects among participants (since the requirement is to recruit naïve subjects and the experimental design allows one participant to focus on a particular condition).

7.3. Conclusion

Integrating brain-computer interfaces, virtual reality, and robotic exoskeletons is a promising area of research and development. One major benefit of such systems is their multimodality and modularity. For the clinical aspects, the multimodality and modularity of a BCI-VR-robot system can provide accessible rehabilitation options and future home use (Vourvopoulos et al., 2015; Zhang et al., 2019; Smith and West, 2008). After all, stroke and other brain and spinal cord injuries are personal diseases that need to be treated on a case-to-case basis (Hui et al., 2021). The modularity feature of this system also allows us to prescribe

various regimens for stroke and injury rehabilitation (i.e., BCI only, VR only, robot only, or a combination of the three). Finally, BCI-VR-robot systems do not thrive on rehabilitation and healthcare applications alone but can also be used in skills learning and education. As discussed in this research, the human brain is capable of neuroplasticity, and the advanced mechanisms involving the brain's visual and kinaesthetic perception are effective factors that should be utilised to their full potential. With these new and emerging technologies, one can provide a holistic and fully immersive experience that allows individuals to learn new skills with excellent efficiency and retention.

References

Abdalsalam, E., Yusoff, M.Z., Kamel, N., Malik, A.S. and Mahmoud, D. 2017. Classification of four class motor imagery for brain computer interface *In*: H. Ibrahim, S. Iqbal, S. S. Teoh and M. T. Mustaffa, eds. *9th International Conference on Robotic, Vision, Signal Processing and Power Applications*. Springer Singapore, pp.297–305.

Ahn, M., Cho, H., Ahn, S. and Jun, S.C. 2013. High theta and low alpha powers may be indicative of BCI-illiteracy in motor imagery. *PLOS ONE*. **8**(11), p.e80886.

Alimardani, M., Nishio, S. and Ishiguro, H. 2016. The importance of visual feedback design in BCIs; from embodiment to motor imagery learning. *PLOS ONE*. **11**(9), p.e0161945.

Ang, K.K., Chin, Z.Y., Wang, C., Guan, C. and Zhang, H. 2012. Filter bank common spatial pattern algorithm on BCI competition IV datasets 2a and 2b. *Frontiers in neuroscience*. **6**, pp.39–39.

Ang, K.K., Guan, C., Phua, K.S., Wang, C., Zhou, L., Tang, K.Y., Ephraim Joseph, G.J., Kuah, C.W.K. and Chua, K.S.G. 2014. Brain-computer interface-based robotic end effector system for wrist and hand rehabilitation: results of a three-armed randomized controlled trial for chronic stroke. *Frontiers in Neuroengineering*. **7**, pp.30–30.

Arvaneh, M., Guan, C., Ang, K. and Quek, C. 2011. Optimizing the channel selection and classification accuracy in EEG-based BCI. *Biomedical Engineering, IEEE Transactions on*. **58**, pp.1865–1873.

Ashruf, C.M.A. 2002. Thin flexible pressure sensors. *Sensor Review*. **22**(4), pp.322–327.

Bai, Z., Fong, K.N.K., Zhang, J.J., Chan, J. and Ting, K.H. 2020. Immediate and long-term effects of BCI-based rehabilitation of the upper extremity after stroke: a systematic review and meta-analysis. *Journal of NeuroEngineering and Rehabilitation*. **17**(1), p.57.

Bain, G.I., Polites, N., Higgs, B.G., Heptinstall, R.J. and McGrath, A.M. 2014. The functional range of motion of the finger joints. *The Journal of Hand Surgery*. **European Volume**.

Ballester, B.R., Maier, M., Duff, A., Cameirao, M., Bermudez, S., Duarte, E., Cuxart, A., Rodriguez, S., Mozo, R.M.S.S. and Verschure, P.F.M.J. 2019. A critical time window for recovery extends beyond one-year post-stroke. *Journal of Neurophysiology*. (122), pp.350–357.

Baniqued, P.D.E., Baldovino, R.G. and Bugtai, N.T. 2015. Design considerations in manufacturing cost-effective robotic exoskeletons for upper extremity rehabilitation *In*: Cebu, Philippines: IEEE.

Barsotti, M., Leonardis, D., Loconsole, C., Solazzi, M., Sotgiu, E., Procopio, C., Chisari, C., Bergamasco, M. and Frisoli, A. 2015. A full upper limb robotic exoskeleton for reaching and grasping rehabilitation triggered by MI-BCI *In*: *2015 IEEE International Conference on Rehabilitation Robotics (ICORR)*., pp.49–54.

Bauer, R., Fels, M., Vukelic, M., Ziemann, U. and Gharabaghi, A. 2015. Bridging the gap between motor imagery and motor execution with a brain-robot interface. *NeuroImage*. **108**, pp.319–327.

Belardinelli, P., Laer, L., Ortiz, E., Braun, C. and Gharabaghi, A. 2017. Plasticity of premotor cortico-muscular coherence in severely impaired stroke patients with hand paralysis. *NeuroImage. Clinical*. **14**, pp.726–733.

Benjamin, E.J., Virani, S.S., Callaway, C.W., Chamberlain, A.M., Chang, A.R., Cheng, S., Chiuve, S.E., Cushman, M., Delling, F.N., Deo, R., de Ferranti, S.D., Ferguson, J.F., Fornage, M., Gillespie, C., Isasi, C.R., Jimenez, M.C., Jordan, L.C., Judd, S.E., Lackland, D., Lichtman, J.H., Lisabeth, L., Liu, S., Longenecker, C.T., Lutsey, P.L., Mackey, J.S., Matchar, D.B., Matsushita, K., Mussolino, M.E., Nasir, K., O'Flaherty, M., Palaniappan, L.P., Pandey, A., Pandey, D.K., Reeves, M.J., Ritchey, M.D., Rodriguez, C.J., Roth, G.A., Rosamond, W.D., Sampson, U.K.A., Satou, G.M., Shah, S.H., Spartano, N.L., Tirschwell, D.L., Tsao, C.W., Voeks, J.H., Willey, J.Z., Wilkins, J.T., Wu, J.H., Alger, H.M., Wong, S.S. and Muntner, P. 2018. Heart disease and stroke statistics-2018 update: a report from the American Heart Association. *Circulation*. **137**(12), pp.e67–e492.

Bergamasco, M., Frisoli, A., Fontana, M., Loconsole, C., Leonardis, D., Troncossi, M., Foumashi, M.M. and Parenti-Castelli, V. 2011. Preliminary results of BRAVO project: brain computer interfaces for robotic enhanced action in visuo-motor tasks. *IEEE ... International Conference on Rehabilitation Robotics : [proceedings]*. **2011**, p.5975377.

Berger, A., Horst, F., Müller, S., Steinberg, F. and Doppelmayr, M. 2019. Current state and future prospects of EEG and fNIRS in robot-assisted gait rehabilitation: a brief review. *Frontiers in Human Neuroscience*. **13**, p.172.

Berger, H. 1929. Über das elektrenkephalogramm des menschen. *Archiv für Psychiatrie und Nervenkrankheiten*. (87), pp.527–570.

Bhagat, N.A., Venkatakrishnan, A., Abibullaev, B., Artz, E.J., Yozbatiran, N., Blank, A.A., French, J., Karmonik, C., Grossman, R.G., O'Malley, M.K., Francisco, G.E. and Contreras-Vidal, J.L. 2016. Design and optimization of an EEG-based brain machine interface (BMI) to an upper-limb exoskeleton for stroke survivors. *Frontiers in Neuroscience*. **10**, p.122.

Birbaumer, N., Ghanayim, N., Hinterberger, T., Iversen, I., Kotchoubey, B., Kubler, A., Perelmouter, J., Taub, E. and Flor, H. 1999. A spelling device for the paralysed. *Nature*. **398**(6725), pp.297–8.

Blankertz, B., Tomioka, R., Lemm, S., Kawanabe, M. and Müller, K.B. 2008. Optimizing spatial filters for robust EEG single-trial analysis. *IEEE Signal Processing Magazine*. **25**(1), pp.41–56.

Bobrov, P.D., Korshakov, A.V., Roshchin, V.I. and Frolov, A.A. 2012. Bayesian classifier for brain-computer interface based on mental representation of movements. *Zhurnal vysshei nervnoi deiatelnosti imeni I P Pavlova*. **62**(1), pp.89–99.

Bousseta, R., El Ouakouak, I., Gharbi, M. and Regragui, F. 2018. EEG based brain computer interface for controlling a robot arm movement through thought. *IRBM*. **39**(2), pp.129–135.

Bozinovski, S. 2013. Controlling robots using EEG signals, since 1988 *In*: S. Markovski and M. Gusev, eds. *ICT Innovations 2012*. Berlin, Heidelberg: Springer Berlin Heidelberg, pp.1–11.

Britton, J.W., Frey, L.C., Hopp, J.L., Korb, P., Koubeissi, M., Lievens, W.E., Pestana-Knight, E.M. and St. Louis, E.K. 2016. The normal EEG *In*: *Electroencephalography (EEG): An introductory text and atlas of normal and abnormal findings in adults, children, and infants*. Chicago: American Epilepsy Society.

Broetz, D., Braun, C., Weber, C., Soekadar, S.R., Caria, A. and Birbaumer, N. 2010. Combination of brain-computer interface training and goal-directed physical therapy in chronic stroke: a case report. *Neurorehabilitation and neural repair*. **24**(7), pp.674–679.

Brookes, J., Mushtaq, F., Jamieson, E., Fath, A.J., Bingham, G., Culmer, P., Wilkie, R.M. and Mon-Williams, M. 2020. Exploring disturbance as a force for good in motor learning. *PLOS ONE*. **15**(5).

Brookes, J., Warburton, M., Alghadier, M., Mon-Williams, M. and Mushtaq, F. 2019. Studying human behavior with virtual reality: the Unity experiment framework. *Behavior Research Methods*.

Bundy, D.T., Souders, L., Baranyai, K., Leonard, L., Schalk, G., Coker, R., Moran, D.W., Huskey, T. and Leuthardt, E.C. 2017. Contralesional brain-computer interface control of a powered exoskeleton for motor recovery in chronic stroke survivors. *Stroke*. **48**(7), pp.1908–1915.

Burle, B., Spieser, L., Roger, C., Casini, L., Hasbroucq, T. and Vidal, F. 2015. Spatial and temporal resolutions of EEG: is it really black and white? A scalp current density view. *International journal of psychophysiology : official journal of the International Organization of Psychophysiology*. **97**(3), pp.210–220.

Cantillo-Negrete, J., Carino-Escobar, R.I., Elias-Vinas, D. and Gutierrez-Martinez, J. 2015. Control signal for a mechatronic hand orthosis aimed for neurorehabilitation *In*: *2015 Pan American Health Care Exchanges (PAHCE)*., pp.1–4.

Carino-Escobar, R.I., Carillo-Mora, P., Valdes-Cristerna, R., Rodriguez-Barragan, M.A., Hernandez-Arenas, C., Quinzaños-Fresnedo, J., Calicia-Alvarado, M.A. and Cantillo-Negrete, J. 2019. Longtitudinal analysis of stroke patient' brain rhythms during an interview with a brain-computer interface. *Neural Plasticity*. **2019**(Article ID 7084618), p.11.

Cervera, M.A., Soekadar, S.R., Ushiba, J., Millan, J. d. R., Liu, M., Birbaumer, N. and Garipelli, G. 2017. Brain-computer interfaces for post-stroke motor rehabilitation: a meta-analysis. *bioRxiv*.

Chacko, S.G., Tayade, P., Kaur, S. and Sharma, R. 2019. Creation of a high resolution EEG based brain computer interface for classifying motor imagery of daily life activities *In*: *2019 7th International Winter Conference on Brain-Computer Interface (BCI)*., pp.1–5.

Chang, W.H. and Kim, Y.H. 2013. Robot-assisted therapy in stroke rehabilitation. *Journal of stroke*. **15**(3), pp.174–181.

Chaudhari, R. and Galiyawala, H.J. 2017. A review on motor imagery signal classification for BCI. *Signal Processing: An International Journal*. **11**(2), pp.16–34.

Chen, S., Shu, X., Wang, H., Ding, L., Fu, J. and Jia, J. 2021. The differences between motor attempt and motor imagery in brain-computer interface accuracy and event-related desynchronization of patients with hemiplegia. *Frontiers in Neurorobotics*. **15**.

Chen, Y.T., Li, S., Magat, E., Zhou, P. and Li, S. 2018. Motor overflow and spasticity in chronic stroke share a common pathophysiological process: Analysis of within-limb and between-limb EMG-EMG coherence. *Frontiers in Neurology*. **9**, p.795.

Chholak, P., Niso, G., Maksimenko, V.A., Kurkin, S.A., Frolov, N.S., Pitsik, E.N., Hramov, A.E. and Pisarchik, A.N. 2019. Visual and kinesthetic modes affect motor imagery classification in untrained subjects. *Scientific Reports*. **9**(1), p.9838.

Chowdhury, A., Meena, Y.K., Raza, H., Bhushan, B., Uttam, A.K., Pandey, N., Hashmi, A.A., Bajpai, A., Dutta, A. and Prasad, G. 2018. Active physical practice followed by mental practice using BCI-driven hand exoskeleton: a pilot trial for clinical effectiveness and usability. *IEEE journal of biomedical and health informatics*. **22**(6), pp.1786–1795.

Chowdhury, A., Raza, H., Dutta, A., Nishad, S.S., Saxena, A. and Prasad, G. 2015. A study on cortico-muscular coupling in finger motions for exoskeleton assisted neuro-rehabilitation. *Conference proceedings : ... Annual International Conference of the IEEE Engineering in Medicine and Biology Society. IEEE Engineering in Medicine and Biology Society. Annual Conference*. **2015**, pp.4610–4614.

Chowdhury, A., Raza, H., Meena, Y.K., Dutta, A. and Prasad, G. 2018. Online covariate shift detection based adaptive brain-computer interface to trigger hand exoskeleton feedback

for neuro-rehabilitation. *IEEE Transactions on Cognitive and Developmental Systems.*, pp.1–1.

Cincotti, F., Pichiorri, F., Arico, P., Aloise, F., Leotta, F., de Vico Fallani, F., Millan, J. d. R., Molinari, M. and Mattia, D. 2012. EEG-based brain-computer interface to support post-stroke motor rehabilitation of the upper limb. *Conference proceedings : ... Annual International Conference of the IEEE Engineering in Medicine and Biology Society. IEEE Engineering in Medicine and Biology Society. Annual Conference*. **2012**, pp.4112–4115.

Coffey, A.L., Leamy, D.J. and Ward, T.E. 2014. A novel BCI-controlled pneumatic glove system for home-based neurorehabilitation. *Conference proceedings : ... Annual International Conference of the IEEE Engineering in Medicine and Biology Society. IEEE Engineering in Medicine and Biology Society. Annual Conference*. **2014**, pp.3622–3625.

Cohen, M.X. 2014. *Analyzing neural time series data: theory and practice* [Online]. Cambridge. Available from: http://lib.ugent.be/catalog/rug01:002161004.

Collet, C., Guillot, A., Lebon, F., MacIntyre, T. and Moran, A. 2011. Measuring motor imagery using psychometric, behavioral, and psychophysiological tools. *Exercise and sport sciences reviews*. **39**(2), pp.85–92.

Combrisson, E. and Jerbi, K. 2015. Exceeding chance level by chance: The caveat of theoretical chance levels in brain signal classification and statistical assessment of decoding accuracy. *Journal of Neuroscience Methods*. **250**, pp.126–136.

Coogan, C.G. and He, B. 2018. Brain-computer interface control in a virtual reality environment and applications for the internet of things. *IEEE Access*. **6**, pp.10840–10849.

Cumming, J. and Ramsey, R. 2009. Imagery interventions in sport *In*:, pp.5–36.

Diab, M.S., Hussain, Z. and Mahmoud, S. 2016. Restoring function in paralyzed limbs using EEG *In*: *2016 IEEE 59th International Midwest Symposium on Circuits and Systems (MWSCAS)*., pp.1–4.

Dipietro, L., Ferraro, M., Palazzolo, J.J., Krebs, H.I., Volpe, B.T. and Hogan, N. 2005. Customized interactive robotic treatment for stroke: EMG-triggered therapy. *IEEE transactions on neural systems and rehabilitation engineering : a publication of the IEEE Engineering in Medicine and Biology Society*. **13**(3), pp.325–334.

Dovat, L., Lambercy, O., Ruffieux, Y., Chapuis, D., Gassert, R., Bleuler, H., Teo, C.I. and Burdet, E. 2006. A haptic knob for rehabilitation after stroke *In*: *2006 IEEE/RSJ International Conference on Intelligent Robots and Systems*. Beijing, China: IEEE.

Eaves, D.L., Riach, M., Holmes, P.S. and Wright, D.J. 2016. Motor imagery during action observation: a brief review of evidence, theory and future research opportunities. *Frontiers in Neuroscience*. **10**, p.514.

ElKoura, G. and Singh, K. 2003. Handrix: animating the human hand *In*: *Proceedings of the 2003 ACM SIGGRAPH/Eurographics Symposium on Computer Animation*. Eurographics Association, pp.110–119.

European Commission 2016. Medical devices: guidance document - classification of medical devices.

Farwell, L.A. and Donchin, E. 1988. Talking off the top of your head: toward a mental prosthesis utilizing event-related brain potentials. *Electroencephalography and clinical neurophysiology*. **70**(6), pp.510–523.

Fazel-Rezai, R., Allison, B., Guger, C., Sellers, E., Kleih, S. and Kübler, A. 2012. P300 brain computer interface: current challenges and emerging trends. *Frontiers in Neuroengineering*. **5**, p.14.

Flatt, A.E. 2000. Grasp. *Proceedings (Baylor University. Medical Center)*. **13**(4), pp.343–348.

Fok, S., Schwartz, R., Wronkiewicz, M., Holmes, C., Zhang, J., Somers, T., Bundy, D. and Leuthardt, E. 2011. An EEG-based brain computer interface for rehabilitation and restoration of hand control following stroke using ipsilateral cortical physiology. *Conference proceedings : ... Annual International Conference of the IEEE Engineering in Medicine and Biology Society. IEEE Engineering in Medicine and Biology Society. Annual Conference*. **2011**, pp.6277–6280.

Formaggio, E., Storti, S.F., Boscolo Galazzo, I., Gandolfi, M., Geroin, C., Smania, N., Spezia, L., Waldner, A., Fiaschi, A. and Manganotti, P. 2013. Modulation of event-related desynchronization in robot-assisted hand performance: brain oscillatory changes in active, passive and imagined movements. *Journal of neuroengineering and rehabilitation*. **10**, p.24.

Fregni, F. and Pascual-Leone, A. 2006. Hand motor recovery after stroke: tuning the orchestra to improve hand motor function. *Cognitive and behavioral neurology : official journal of the Society for Behavioral and Cognitive Neurology*. **19**(1), pp.21–33.

Friesen, C.L., Bardouille, T., Neyedli, H.F. and Boe, S.G. 2017. Combined action observation and motor imagery neurofeedback for modulation of brain activity. *Frontiers in Human Neuroscience*. **10**, p.692.

Frolov, A.A., Mokienko, O., Lyukmanov, R., Biryukova, E., Kotov, S., Turbina, L., Nadareyshvily, G. and Bushkova, Y. 2017. Post-stroke rehabilitation training with a motor-imagery-based brain-computer interface (BCI)-controlled hand exoskeleton: a randomized controlled multicenter trial. *Frontiers in Neuroscience*. **11**, pp.400–400.

Fugl-Meyer, A.R., Jaasko, L., Leyman, I., Olsson, S. and Steglind, S. 1975. The post-stroke hemiplegic patient. 1. a method for evaluation of physical performance. *Scandinavian journal of rehabilitation medicine*. **7**(1), pp.13–31.

Ganguly, K. and Poo, M.M. 2013. Activity-dependent neural plasticity from bench to bedside. *Neuron*. **80**(3), pp.729–741.

George, K., Iniguez, A., Donze, H. and Kizhakkumthala, S. 2014. Design, implementation and evaluation of a brain-computer interface controlled mechanical arm for rehabilitation *In*: *2014 IEEE International Instrumentation and Measurement Technology Conference (I2MTC) Proceedings.*, pp.1326–1328.

Giannopulu, I. and Mizutani, H. 2021. Neural kinesthetic contribution to motor imagery of body parts: tongue, hands, and feet. *Frontiers in Human Neuroscience*. **15**.

Gonzalez, C.D.V., Azuela, J.H.S., Espino, E.R. and Ponce, V.H. 2018. Classification of motor imagery imagery EEG signals with CSP filtering through neural networks models *In*: *Advances in Soft Computing, Lecture Notes in Computer Science*. Springer, Cham, pp.123–135.

Graimann, B., Allison, B. and Pfurtscheller, G. 2010. Brain–computer interfaces: a gentle introduction *In*: B. Graimann, G. Pfurtscheller and B. Allison, eds. *Brain-Computer Interfaces: Revolutionizing Human-Computer Interaction* [Online]. Berlin, Heidelberg: Springer Berlin Heidelberg, pp.1–27. Available from: https://doi.org/10.1007/978-3-642-02091-9_1.

Graimann, B., Huggins, J.E., Levine, S.P. and Pfurtscheller, G. 2002. Visualization of significant ERD/ERS patterns in multichannel EEG and ECoG data. *Clinical neurophysiology : official journal of the International Federation of Clinical Neurophysiology*. (113), pp.43–47.

Graimann, B. and Pfurtscheller, G. 2006. Quantification and visualization of event-related changes in oscillatory brain activity in the time–frequency domain *In*: C. Neuper and W. Klimesch, eds. *Progress in Brain Research* [Online]. Elsevier, pp.79–97. Available from: https://www.sciencedirect.com/science/article/pii/S0079612306590065.

Gregg, M., Hall, C. and Butler, A. 2010. The MIQ-RS: a suitable option for examining movement imagery ability. *Advance Access Publication*. **7**(2), pp.249–257.

Grummett, T.S., Leibbrandt, R.E., Lewis, T.W., De Los Angeles, D., Powers, D.M.W., Willoughby, J.O., Pope, K.J. and Fitzgibbon, S.P. 2015. Measurement of neural signals from inexpensive, wireless and dry EEG systems. *Physiological Measurement*. **36**(7).

Guger, C., Krausz, G. and Edliner, G. 2011. Brain-computer interface control with dry EEG electrodes *In*: *Proceedings of the 5th International Brain-Computer Interface Conference.*, pp.316–319.

Guiochet, J., Hoang, Q.A.D., Kaaniche, M. and Powell, D.J. 2012. Applying existing standards to a medical rehabilitation robot: limits and challenges *In*: *IROS*.

Hall, C., Pongrac, J. and Buckholz, E. 1985. The measurement of imagery ability. *Human Movement Science*. **4**(2), pp.107–118.

Hall, C.R. and Martin, K.A. 1997. Measuring movement imagery abilities: a revision of the movement imagery questionnaire. *Journal of Mental Imagery*. **21**(1–2), pp.143–154.

Hallett, M. 2001. Plasticity of the human motor cortex and recovery from stroke. *Brain research. Brain research reviews*. **36**(2–3), pp.169–174.

Hardwick, R.M., Caspers, S., Eickhoff, S.B. and Swinnen, S.P. 2018. Neural correlates of action: comparing meta-analyses of imagery, observation, and execution. *Neuroscience and Biobehavioral Reviews*. (94), pp.31–44.

Harris, D.J., Bird, J.M., Smart, P.A., Wilson, M.R. and Vine, S.J. 2020. A framework for the testing and validation of simulated environments in experimentation and training. *Frontiers in Psychology*. **11**, p.605.

Hatem, S.M., Saussez, G., Della Faille, M., Prist, V., Zhang, X., Dispa, D. and Bleyenheuft, Y. 2016. Rehabilitation of motor function after stroke: a multiple systematic review focused on techniques to stimulate upper extremity recovery. *Frontiers in human neuroscience*. **10**, pp.442–442.

Heo, P., Gu, G.M., Lee, S.J., Rhee, K. and Kim, J. 2012. Current hand exoskeleton technologies for rehabilitation and assistive engineering. *International Journal of Precision Engineering and Manufacturing*. **13**(5), pp.807–824.

Hill, N.J., Gupta, D., Brunner, P., Gunduz, A., Adamo, M.A., Ritaccio, A. and Schalk, G. 2012. Recording human electrocorticographic (ECoG) signals for neuroscientific research and real-time functional cortical mapping. *Journal of visualized experiments : JoVE*. (64), p.3993.

Hochberg, L.R., Serruya, M.D., Friehs, G.M., Mukand, J.A., Saleh, M., Caplan, A.H., Branner, A., Chen, D., Penn, R.D. and Donoghue, J.P. 2006. Neuronal ensemble control of prosthetic devices by a human with tetraplegia. *Nature*. **442**, p.164.

Holmes, C.D., Wronkiewicz, M., Somers, T., Liu, J., Russell, E., Kim, D., Rhoades, C., Dunkley, J., Bundy, D., Galboa, E. and Leuthardt, E. 2012. IpsiHand Bravo: an improved EEG-based brain-computer interface for hand motor control rehabilitation. *Conference proceedings : ... Annual International Conference of the IEEE Engineering in Medicine and Biology Society. IEEE Engineering in Medicine and Biology Society. Annual Conference*. **2012**, pp.1749–1752.

Housley, S.N., Garlow, A.R., Ducote, K., Howard, A., Thomas, T., Wu, D., Richards, K. and Butler, A.J. 2016. Increasing access to cost effective home-based rehabilitation for rural

veteran stroke survivors. *Austin journal of cerebrovascular disease & stroke*. **3**(2), pp.1–11.

Houwink, A., Nijland, R.H., Geurts, A.C. and Kwakkel, G. 2013. Functional recovery of the paretic upper limb after stroke: Who regains hand capacity? *Archives of physical medicine and rehabilitation*. **94**(5), pp.839–844.

Hui, F.K., Spiotta, A.M., Alexander, M.J., Hanel, R.A. and Baxter, B.W. 2021. *12 Strokes: A case-based guide to acute ischemic stroke management*. Springer, Cham.

Hülsmann, F., Frank, C., Senna, I., Ernst, M.O., Schack, T. and Botsch, M. 2019. Superimposed skilled performance in a virtual mirror improves motor performance and cognitive representation of a full body motor action. *Frontiers in Robotics and AI*. **6**, p.43.

Hume, M.C., Gellman, H., McKellop, H. and Brumfield, R.H. 1990. Functional range of motion of the joints of the hand. *The Journal of Hand Surgery*. **15A**(2), pp.240–243.

Isaac, A., Marks, D.F. and Russell, D.G. 1986. An instrument for assessing imagery of movement: the vividness of movement imagery questionnaire (VMIQ). *Journal of Mental Imagery*. **10**(4), pp.23–30.

Ismail Fawaz, H., Forestier, G., Weber, J., Idoumghar, L. and Muller, P.A. 2019. Deep learning for time series classification: a review. *Data Mining and Knowledge Discovery*. **33**(4), pp.917–963.

Jackson, P.L., Lafleur, M.F., Malouin, F., Richards, C. and Doyon, J. 2001. Potential role of mental practice using motor imagery in neurologic rehabilitation. *Archives of physical medicine and rehabilitation*. **82**(8), pp.1133–1141.

Jansen, M., White, T.P., Mullinger, K.J., Liddle, E.B., Gowland, P.A., Francis, S.T., Bowtell, R. and Liddle, P.F. 2012. Motion-related artefacts in EEG predict neuronally plausible patterns of activation in fMRI data. *NeuroImage*. **59**(1), pp.261–270.

Jeannerod, M. 2006. *Motor cognition: what actions tell the self*.

Jeannerod, M. 2001. Neural simulation of action: a unifying mechanism for motor cognition. *NeuroImage*. **14**(1), pp.S103–S109.

Jeunet, C., Jahanpour, E. and Lotte, F. 2016. Why standard brain-computer interface (BCI) training protocols should be changed: an experimental study. *Journal of Neural Engineering*. **13**(13).

Johnson, M.J., Micera, S., Shibata, T. and Guglielmelli, E. 2008. Rehabilitation and assistive robotics [TC Spotlight]. *IEEE Robotics & Automation Magazine*. **15**(3), pp.16–110.

Johnston, M., Bonetti, D., Joice, S., Pollard, B., Morrison, V., Francis, J.J. and MacWalter, R. 2007. Recovery from disability after stroke as a target for a behavioural intervention: results of a randomized controlled trial. *Disability and Rehabilitation*. **29**(14), pp.1117–1127.

Kalcher, J. and Pfurtscheller, G. 1995. Discrimination between phase-locked and non-phase-locked event-related EEG activity. *Electroencephalography and clinical neurophysiology*. **94**(5), pp.381–384.

Kam, J.W.Y., Griffin, S., Shen, A., Patel, S., Hinrichs, H., Heinze, H.J., Deouell, L.Y. and Knight, R.T. 2019. Systematic comparison between a wireless EEG system with dry electrodes and a wired EEG system with wet electrodes. *NeuroImage*. **184**, pp.119–129.

Kappel, S.L., Looney, D., Mandic, D.P. and Kidmose, P. 2017. Physiological artifacts in scalp EEG and ear-EEG. *BioMedical Engineering OnLine*. **16**(1), p.103.

Kaufmann, T., Holz, E. and Kübler, A. 2013. Comparison of tactile, auditory, and visual modality for brain-computer interface use: a case study with a patient in the locked-in state. *Frontiers in Neuroscience*. **7**, p.129.

Kersten, P. 2004. Principles of physiotherapy assessment and outcome measures *In*: *Physical Management in Neurological Rehabilitation*. 2., pp.29–46.

Kim, G.Y., Lim, S.Y., Kim, H.J., Lee, B.J., Seo, S.C., Cho, K.H. and Lee, W.H. 2017. Is robot-assisted therapy effective in upper extremity recovery in early stage stroke? -a systematic literature review. *Journal of physical therapy science*. **29**(6), pp.1108–1112.

Kim, T., Frank, C. and Schack, T. 2017. A systematic investigation of the effect of action observation training and motor imagery training on the development of mental representation structure and skill performance. *Frontiers in Human Neuroscience*. **11**, p.499.

King, C.E., Wang, P.T., Mizuta, M., Reinkensmeyer, D.J., Do, A.H., Moromugi, S. and Nenadic, Z. 2011. Noninvasive brain-computer interface driven hand orthosis. *Conference proceedings : ... Annual International Conference of the IEEE Engineering in Medicine and Biology Society. IEEE Engineering in Medicine and Biology Society. Annual Conference*. **2011**, pp.5786–5789.

Konrad, P. 2006. *The abc of EMG: a practical introduction to kinesiological electromyography* [Online] Version 1.4. Noraxon USA, Inc. Available from: http://www.noraxon.com/.

Krakauer, J.W. 2005. Arm function after stroke: from physiology to recovery. *Seminars in neurology*. **25**(4), pp.384–395.

Krakauer, J.W. 2006. Motor learning: its relevance to stroke recovery and neurorehabilitation. *Current opinion in neurology*. **19**(1), pp.84–90.

Kuiken, T.A., Lowery, M.M. and Stoykov, N.S. 2003. The effect of subcutaneous fat on myoelectric signal amplitude and cross-talk. *Prosthetics and orthotics international*. **27**(1), pp.48–54.

Laver, K.E., Lange, B., George, S., Deutsch, J.E., Saposnik, G. and Crotty, M. 2017. Virtual reality for stroke rehabilitation. *The Cochrane database of systematic reviews*. **11**(11), pp.CD008349–CD008349.

Lazarou, L., Nikolopoulos, S., Petrantonakis, P.C., Kompatsiaris, L. and Tsolaki, M. 2018. EEG-based brain-computer interfaces for communication and rehabilitation of people with motor impairment: a novel approach of the 21st century. *Frontiers in human neuroscience*. **12**, p.14.

Lenartowicz, A. and Poldrack, R.A. 2010. Brain imaging *In*: G. F. Koob, M. L. Moal and R. F. Thompson, eds. *Encyclopedia of Behavioral Neuroscience* [Online]. Oxford: Academic Press, pp.187–193. Available from: http://www.sciencedirect.com/science/article/pii/B978008045396500052X.

Leonardis, D., Barsotti, M., Loconsole, C., Solazzi, M., Troncossi, M., Mazzotti, C., Castelli, V.P., Procopio, C., Lamola, G., Chisari, C., Bergamasco, M. and Frisoli, A. 2015. An EMG-controlled robotic hand exoskeleton for bilateral rehabilitation. *IEEE transactions on haptics*. **8**(2), pp.140–151.

Li, M., He, B., Liang, Z., Zhao, C.G., Chen, J., Zhuo, Y., Xu, G., Xie, J. and Althoefer, K. 2019. An attention-controlled hand exoskeleton for the rehabilitation of finger extension and flexion using a rigid-soft combined mechanism. *Frontiers in Neurorobotics*. **13**, p.34.

Li, M., Xie, J. and Chen, C. 2018. A review: motor rehabilitation after stroke with control based on human intent. *Proceedings of the Institution of Mechanical Engineers. Part H, Journal of engineering in medicine*. **232**(4), pp.344–360.

Liao, K., Xiao, R., Gonzalez, J. and Ding, L. 2014. Decoding individual finger movements from one hand using human EEG signals. *PLOS ONE*. **9**(1), p.e85192.

Liu, H., Song, L. and Zhang, T. 2014. Mental practice combined with physical practice to enhance hand recovery in stroke patients K. R. Müller-Vahl, ed. *Behavioural Neurology*. **2014**, p.876416.

Lotte, F. 2014. A tutorial on EEG signal-processing techniques for mental-state recognition in brain–computer interfaces *In*: E. R. Miranda and J. Castet, eds. *Guide to Brain-Computer Music Interfacing* [Online]. London: Springer London, pp.133–161. Available from: https://doi.org/10.1007/978-1-4471-6584-2_7.

Lotte, F., Bougrain, L., Cichocki, A., Clerc, M., Congedo, M., Rakotomamonjy, A. and Yger, F. 2018. A review of classification algorithms for EEG-based brain-computer interfaces: a 10 year update. *Journal of Neural Engineering*. **15**(3), p.031005.

Lotte, F. and Guan, C. 2011. Regularizing common spatial patterns to improve BCI designs: unified theory and new algorithms. *IEEE Transactions on Biomedical Engineering*. **58**(2), pp.355–362.

Lotte, F., Larrue, F. and Muhl, C. 2013. Flaws in current human training protocols for spontaneous Brain-Computer Interfaces: lessons from instructional design. *Frontiers in Human Neuroscience*. **7**(568).

Lotze, M. and Halsband, U. 2006. Motor imagery. *Journal of physiology, Paris*. **99**(4–6), pp.386–395.

Lovinger, D.M. 2008. Communication networks in the brain: neurons, receptors, neurotransmitters, and alcohol. *Alcohol research & health : the journal of the National Institute on Alcohol Abuse and Alcoholism*. **31**(3), pp.196–214.

Luck, S.J. 2005. *An introduction to the event-related potential technique*.

Lyle, R.C. 1981. A performance test for assessment of upper limb function in physical rehabilitation treatment and research. *International Journal of Rehabilitation Research*. **4**(4).

Lystad, R.P. and Pollard, H. 2009. Functional neuroimaging: a brief overview and feasibility for use in chiropractic research. *The Journal of the Canadian Chiropractic Association*. **53**(1), pp.59–72.

Maher, C.G., Sherrington, C., Herbert, R.D., Moseley, A.M. and Elkins, M. 2003. Reliability of the PEDro scale for rating quality of randomized controlled trials. *Physical Therapy*. **83**(8), pp.713–721.

Manguerra, M.V., Baniqued, P.D.E., Abad, A.C., Baldovino, R.G., Dungao, J.R. and Bugtai, N.T. 2018. Active motor control for an upper extremity exoskeleton. *Advanced Science Letters*. **24**(11), pp.9937–8840.

Marchal-Crespo, L. and Reinkensmeyer, D.J. 2009. Review of control strategies for robotic movement training after neurologic injury. *Journal of NeuroEngineering and Rehabilitation*. **6**(20).

Marchesotti, S., Bassolino, M., Serino, A., Bleuler, H. and Blanke, O. 2016. Quantifying the role of motor imagery in brain-machine interfaces. *Scientific Reports*. **6**(1), p.24076.

Maris, E. and Oostenveld, R. 2007. Nonparametric statistical testing of EEG- and MEG-data. *Journal of Neuroscience Methods*. (164), pp.177–190.

Mathewson, K.E., Harrison, T.J.L. and Kizuk, S.A.D. 2017. High and dry? Comparing active dry EEG electrodes to active and passive wet electrodes. *Psychophysiology*. **54**(1), pp.74–82.

Matthews, W.B. 1977. Aids to the examination of the peripheral nervous system. *Journal of the Neurological Sciences*. **33**(1), p.299.

Mawase, F., Uehara, S., Bastian, A.J. and Celnik, P. 2017. Motor learning enhances use-dependent plasticity. *The Journal of neuroscience : the official journal of the Society for Neuroscience*. **37**(10), pp.2673–2685.

McAvinue, L.P. and Robertson, I.H. 2008. Measuring motor imagery ability: a review. *European Journal of Cognitive Psychology*. **20**(2), pp.232–251.

McConnell, A.C., Moioli, R.C., Brasil, F.L., Vallejo, M., Corne, D.W., Vargas, P.A. and Stokes, A.A. 2017. Robotic devices and brain-machine interfaces for hand rehabilitation post-stroke. *Journal of Rehabilitation Medicine*. **49**(6), pp.449–460.

McHugh, G. and Swain, I.D. 2014. A comparison between reported therapy staffing levels and the department of health therapy staffing guidelines for stroke rehabilitation: a national survey. *BMC Health Services Research*. **14**(1), p.216.

Mladenov, T., Kim, K. and Nooshabadi, S. 2012. Accurate motor imagery based dry electrode brain-computer interface system for consumer applications *In*: *2012 IEEE 16th International Symposium on Consumer Electronics.*, pp.1–4.

Molteni, F., Gasperini, G., Cannaviello, G. and Guanziroli, E. 2018. Exoskeleton and end-effector robots for upper and lower limbs rehabilitation: narrative review. *Innovations Influencing Physical Medicine and Rehabilitation*. **10**(9, Supplement 2), pp.S174–S188.

Monge-Pereira, E., Ibanez-Pereda, J., Alguacil-Diego, I.M., Serrano, J.I., Spottorno-Rubio, M.P. and Molina-Rueda, F. 2017. Use of electroencephalography brain-computer interface systems as a rehabilitative approach for upper limb function after a stroke: a systematic review. *PM & R : the journal of injury, function, and rehabilitation*. **9**(9), pp.918–932.

Morash, V., Bai, O., Furlani, S., Lin, P. and Hallett, M. 2008. Classifying EEG signals preceding right hand, left hand, tongue, and right foot movements and motor imageries. *Clinical neurophysiology : official journal of the International Federation of Clinical Neurophysiology*. **119**(11), pp.2570–2578.

Morgan, S.T., Hansen, J.C. and Hillyard, S.A. 1996. Selective attention to stimulus location modulates the steady-state visual evoked potential. *Proceedings of the National Academy of Sciences of the United States of America*. **93**(10), pp.4770–4774.

Mukherjee, D. and Patil, C.G. 2011. Epidemiology and the global burden of stroke. *World neurosurgery*. **76**(6 Suppl), pp.S85-90.

Mulder, T. 2007. Motor imagery and action observation: cognitive tools for rehabilitation. *Journal of neural transmission (Vienna, Austria : 1996)*. **114**(10), pp.1265–1278.

Müller, M.M., Picton, T.W., Valdes-Sosa, P., Riera, J., Teder-Sälejärvi, W.A. and Hillyard, S.A. 1998. Effects of spatial selective attention on the steady-state visual evoked potential in the 20-28 Hz range. *Brain research. Cognitive brain research.* **6**(4), pp.249–261.

Müller-Putz, G.R., Schwarz, A., Pereira, J. and Ofner, P. 2016. Chapter 2 - From classic motor imagery to complex movement intention decoding: the noninvasive Graz-BCI approach *In*: D. Coyle, ed. *Progress in Brain Research* [Online]. Elsevier, pp.39–70. Available from: http://www.sciencedirect.com/science/article/pii/S0079612316300437.

Muralidharan, A., Chae, J. and Taylor, D.M. 2011. Extracting attempted hand movements from EEGs in people with complete hand paralysis following stroke. *Frontiers in neuroscience.* **5**, p.39.

Nakano, H. and Kodama, T. 2017. Motor imagery and action observation as effective tools for physical therapy *In*: *Neurological Physical Therapy.* IntechOpen.

Naros, G. and Gharabaghi, A. 2017. Physiological and behavioral effects of beta-tACS on brain self-regulation in chronic stroke. *Brain stimulation.* **10**(2), pp.251–259.

Naros, G., Naros, I., Grimm, F., Ziemann, U. and Gharabaghi, A. 2016. Reinforcement learning of self-regulated sensorimotor beta-oscillations improves motor performance. *NeuroImage.* **134**, pp.142–152.

Neuper, C. and Pfurtscheller, G. 2001. Event-related dynamics of cortical rhythms: frequency-specific features and functional correlates. *Thalamo-Cortical Relationships.* **43**(1), pp.41–58.

Neuper, C., Scherer, R., Reiner, M. and Pfurtscheller, G. 2005. Imagery of motor actions: differential effects of kinesthetic and visual-motor mode of imagery in single-trial EEG. *Brain research. Cognitive brain research.* **25**(3), pp.668–677.

Nijholt, A., Bos, D.P.O. and Reuderink, B. 2009. Turning shortcomings into challenges: Brain–computer interfaces for games. *Intelligent Technologies for Interactive Entertainment.* **1**(2), pp.85–94.

Nojima, I., Mima, T., Koganemaru, S., Thabit, M.N., Fukuyama, H. and Kawamata, T. 2012. Human motor plasticity induced by mirror visual feedback. *The Journal of Neuroscience.* **32**(4), p.1293.

Norman, S. 2017. *Brain computer interface design for robot assisted neurorehabilitation.*[Online] University of California, Irvine. Available from: https://escholarship.org/uc/item/4v18v0d3.

Norman, S.L., McFarland, D.J., Miner, A., Cramer, S.C., Wolbrecht, E.T., Wolpaw, J.R. and Reinkensmeyer, D.J. 2018. Controlling pre-movement sensorimotor rhythm can improve finger extension after stroke. *Journal of Neural Engineering.* **15**(5), p.056026.

Ntsiea, M.V. 2019. Current stroke rehabilitation services and physiotherapy research in South Africa. *The South African journal of physiotherapy*. **75**(1), pp.475–475.

Nunez, P.L., Silberstein, R.B., Cadusch, P.J., Wijesinghe, R.S., Westdorp, A.F. and Srinivasan, R. 1994. A theoretical and experimental study of high resolution EEG based on surface Laplacians and cortical imaging. *Electroencephalography and clinical neurophysiology*. **90**(1), pp.40–57.

Ochipa, C., Rapcsak, S.Z., Maher, L.M., Rothi, L.J., Bowers, D. and Heilman, K.M. 1997. Selective deficit of praxis imagery in ideomotor apraxia. *Neurology*. **49**(2), pp.474–480.

O'Dell, M.W., Lin, C.C.D. and Harrison, V. 2009. Stroke rehabilitation: strategies to enhance motor recovery. *Annual review of medicine*. **60**, pp.55–68.

Office of the Director of Defense Research and Engineering Washington DC 2009. *Technology Readiness Assessment (TRA) deskbook* [Online]. Fort Belvoir, VA, USA: Defense Technical Information Center. Available from: https://apps.dtic.mil/dtic/tr/fulltext/u2/a524200.pdf.

Oldfield, R.C. 1971. The assessment and analysis of handedness: the Edinburgh inventory. *Neuropsychologia*. **9**(1), pp.97–113.

Oña, E.D., Cano-de la Cuerda, R., Sanchez-Herrera, P., Balaguer, C. and Jardon, A. 2018. A review of robotics in neurorehabilitation: towards an automated process for upper limb. *Journal of Healthcare Engineering*.

Ono, T., Mukaino, M. and Ushiba, J. 2013. Functional recovery in upper limb function in stroke survivors by using brain-computer interface: a single case A-B-A-B design. *Conference proceedings : ... Annual International Conference of the IEEE Engineering in Medicine and Biology Society. IEEE Engineering in Medicine and Biology Society. Annual Conference*. **2013**, pp.265–268.

Ono, Y., Tominaga, T. and Murata, T. 2016. Digital mirror box: an interactive hand-motor BMI rehabilitation tool for stroke patients *In*: *2016 Asia-Pacific Signal and Information Processing Association Annual Summit and Conference (APSIPA)*., pp.1–7.

Ono, Y., Wada, K., Kurata, M. and Seki, N. 2018. Enhancement of motor-imagery ability via combined action observation and motor-imagery training with proprioceptive neurofeedback. *Neuropsychologia*. **114**, pp.134–142.

di Pellegrino, G., Fadiga, L., Fogassi, L., Gallese, V. and Rizzolatti, G. 1992. Understanding motor events: a neurophysiological study. *Experimental Brain Research*. **91**(1), pp.176–180.

Pellegrino, G., Tomasevic, L., Tombini, M., Assenza, G., Bravi, M., Sterzi, S., Giacobbe, V., Zollo, L., Guglielmelli, E., Cavallo, G., Vernieri, F. and Tecchio, F. 2012. Inter-

hemispheric coupling changes associate with motor improvements after robotic stroke rehabilitation. *Restorative neurology and neuroscience*. **30**(6), pp.497–510.

Pfurtscheller, G. and Aranibar, A. 1977. Event-related cortical desynchronization detected by power measurements of scalp EEG. *Electroencephalography and clinical neurophysiology*. **42**(6), pp.817–826.

Pfurtscheller, G. and Lopes da Silva, F.H. 1999. Event-related EEG/MEG synchronization and desynchronization: basic principles. *Clinical neurophysiology : official journal of the International Federation of Clinical Neurophysiology*. **110**(11), pp.1842–1857.

Physiotherapy Evidence Database 1999. PEDro Scale.

Polygerinos, P., Lyne, S., Wang, Z., Nicolini, L.F., Mosadegh, B., Whitesides, G.M. and Walsh, C.J. 2013. Towards a soft pneumatic glove for hand rehabilitation *In*: *2013 IEEE/RSJ International Conference on Intelligent Robots and Systems.*, pp.1512–1517.

Polygerinos, P., Wang, Z., Galloway, K.C., Wood, R.J. and Walsh, C.J. 2015. Soft robotic glove for combined assistance and at-home rehabilitation. *Wearable Robotics*. **73**, pp.135–143.

Quattrocchi, G., Greenwood, R., Rothwell, J.C., Galea, J.M. and Bestmann, S. 2016. Reward and punishment enhance motor adaptation in stroke. *Journal of Neurology, Neurosurgery, and Psychiatry*. **88**(9), pp.730–736.

Ramoser, H., Müller-Gerking, J. and Pfurtscheller, G. 2000. Optimal spatial filtering of single trial EEG during imagined hand movement. *IEEE Transactions on Rehabilitation Engineering*. **8**(4), pp.441–446.

Ramos-Murguialday, A. and Birbaumer, N. 2015. Brain oscillatory signatures of motor tasks. *Journal of neurophysiology*. **113**(10), pp.3663–3682.

Ramos-Murguialday, A., Schürholz, M., Caggiano, V., Wildgruber, M., Caria, A., Hammer, E.M., Halder, S. and Birbaumer, N. 2012. Proprioceptive feedback and brain computer interface (BCI) based neuroprostheses. *PLOS ONE*. **7**(10), p.e47048.

Randazzo, L., Iturrate, I., Perdikis, S. and Millán, J. d. R. 2018. mano: a wearable hand exoskeleton for activities of daily living and neurorehabilitation. *IEEE Robotics and Automation Letters*. **3**(1), pp.500–507.

Rashid, M., Sulaiman, N., P P Abdul Majeed, A., Musa, R.M., Ab Nasir, A.F., Bari, B.S. and Khatun, S. 2020. Current status, challenges, and possible solutions of EEG-based brain-computer interface: a comprehensive review. *Frontiers in neurorobotics*. **14**, p.25.

Rathee, D., Chowdhury, A., Meena, Y.K., Dutta, A., McDonough, S. and Prasad, G. 2019. Brain–machine interface-driven post-stroke upper-limb functional recovery correlates

with beta-band mediated cortical networks. *IEEE Transactions on Neural Systems and Rehabilitation Engineering*. **27**(5), pp.1020–1031.

Ridderinkhof, K.R. and Brass, M. 2015. How kinesthetic motor imagery works: a predictive-processing theory of visualization in sports and motor expertise. *Journal of Physiology, Paris*. **109**(1–3), pp.53–63.

Roy, Y., Banville, H., Albuquerque, I., Gramfort, A., Falk, T.H. and Faubert, J. 2019. Deep learning-based electroencephalography analysis: a systematic review. *Journal of Neural Engineering*. **16**(5).

Saab, J., Battes, B. and Grosse-Wentrup, M. 2011. Simultaneous EEG recordings with dry and wet electrodes in motor-imagery *In*: *In proceedings*. Graz, Austria.

Saha, S. and Baumert, M. 2020. Intra- and inter-subject variability in EEG-based sensorimotor brain computer interface: a review. *Frontiers in Computational Neuroscience*. **13**, p.87.

Salisbury, D.B., Dahdah, M., Driver, S., Parsons, T.D. and Richter, K.M. 2016. Virtual reality and brain computer interface in neurorehabilitation. *Proceedings (Baylor University. Medical Center)*. **29**(2), pp.124–127.

Sarasola-Sanz, A., Irastorza-Landa, N., Lopez-Larraz, E., Bibian, C., Helmhold, F., Broetz, D., Birbaumer, N. and Ramos-Murguialday, A. 2017. A hybrid brain-machine interface based on EEG and EMG activity for the motor rehabilitation of stroke patients. *IEEE ... International Conference on Rehabilitation Robotics : [proceedings]*. **2017**, pp.895–900.

Schirrmeister, R.B., Springenberg, J.T., Fiederer, L.D.J., Glasstetter, M., Eggensperger, K., Tangermann, M., Hutter, F., Burgard, W. and Ball, T. 2017. Deep learning with convolutional neural networks for EEG decoding and visualization. *Human Brain Mapping*. **38**(11), pp.5391–5420.

Sharma, N. and Baron, J.C. 2013. Does motor imagery share neural networks with executed movement: a multivariate fMRI analysis. *Frontiers in human neuroscience*. **7**, pp.564–564.

Shiman, F., Irastorza-Landa, N., Sarasola-Sanz, A., Spuler, M., Birbaumer, N. and Ramos-Murguialday, A. 2015. Towards decoding of functional movements from the same limb using EEG. *Conference proceedings : ... Annual International Conference of the IEEE Engineering in Medicine and Biology Society. IEEE Engineering in Medicine and Biology Society. Annual Conference*. **2015**, pp.1922–1925.

Silvoni, S., Ramos-Murguialday, A., Cavinato, M., Volpato, C., Cisotto, G., Turolla, A., Piccione, F. and Birbaumer, N. 2011. Brain-computer interface in stroke: a review of progress. *Clinical EEG and Neuroscience*. **42**(4), pp.245–252.

Sinha, J.K., Aziz, A. and Ghosh, S. 2019. Homunculus *In*: J. Vonk and T. Shackelford, eds. *Encyclopedia of Animal Cognition and Behavior* [Online]. Cham: Springer International Publishing, pp.1–4. Available from: https://doi.org/10.1007/978-3-319-47829-6_1427-1.

Škola, F. and Liarokapis, F. 2018. Embodied VR environment facilitates motor imagery brain–computer interface training. *Computers & Graphics*. **75**, pp.59–71.

Škola, F., Tinková, S. and Liarokapis, F. 2019. Progressive training for motor imagery brain-computer interfaces using gamification and virtual reality embodiment. *Frontiers in human neuroscience*. **13**, pp.329–329.

Smith, J.D. and West, A.A. 2008. A modular rehabilitation system with enhanced functionality and safety to support improved recovery from injury and quality of life. *Proceedings of the Institution of Mechanical Engineers, Part H: Journal of Engineering in Medicine*. **222**(6), pp.947–958.

Spicer, R., Anglin, J., Krum, D.M. and Liew, S.L. 2017. REINVENT: A low-cost, virtual reality brain-computer interface for severe stroke upper limb motor recovery *In*: *2017 IEEE Virtual Reality (VR)*., pp.385–386.

Srinivasan, R. 1999. Methods to improve the spatial resolution of EEG. *International Journal of Bioelectromagnetism*. **1**(1), pp.102–111.

Stamer, M., Michaels, J. and Tümler, J. 2020. Investigating the benefits of haptic feedback during in-car interactions in virtual reality *In*: H. Krömker, ed. *HCI in Mobility, Transport, and Automotive Systems. Automated Driving and In-Vehicle Experience Design*. Cham: Springer International Publishing, pp.404–416.

Stan, A., Irimia, D.C., Botezatu, N.A. and Lupu, R.G. 2015. Controlling a hand orthosis by means of P300-based brain computer interface *In*: *2015 E-Health and Bioengineering Conference (EHB)*., pp.1–4.

Stecklow, M.V., Infantosi, A.F.C. and Cagy, M. 2010. EEG changes during sequences of visual and kinesthetic motor imagery. *Arquivos de neuro-psiquiatria*. **68**(4), pp.556–561.

Tacchino, G., Gandolla, M., Coelli, S., Barbieri, R., Pedrocchi, A. and Bianchi, A.M. 2017. EEG analysis during active and assisted repetitive movements: evidence for differences in neural engagement. *IEEE transactions on neural systems and rehabilitation engineering : a publication of the IEEE Engineering in Medicine and Biology Society*. **25**(6), pp.761–771.

Takahashi, K., Domen, K., Sakamoto, T., Toshima, M., Otaka, Y., Seto, M., Irie, K., Haga, B., Takebayashi, T. and Hachisuka, K. 2016. Efficacy of upper extremity robotic therapy in subacute poststroke hemiplegia: an exploratory randomized trial. *Stroke*. **47**(5), pp.1385–1388.

Tan, X., Li, Y. and Gao, Y. 2017. Combining brain-computer interface with virtual reality: Review and prospect *In*: *2017 3rd IEEE International Conference on Computer and Communications (ICCC)*., pp.514–518.

Taylor, C.L. and Schwarz, R.J. 1955. The anatomy and mechanics of the human hand. *Artificial limbs*. **2**(2), pp.22–35.

Teplan, M. 2002. Fundamentals of EEG measurement. *Measurement Science Review*. **2**.

Tremmel, C., Herff, C., Sato, T., Rechowicz, K., Yamani, Y. and Krusienski, D.J. 2019. Estimating cognitive workload in an interactive virtual reality environment using EEG. *Frontiers in Human Neuroscience*. **13**.

Tsuchimoto, S., Shindo, K., Hotta, F., Hanakawa, T., Liu, M. and Ushiba, J. 2019. Sensorimotor connectivity after motor exercise with neurofeedback in post-stroke patients with hemiplegia. *Neuroscience*. **416**, pp.109–125.

University of Washington Institute for Health Metrics and Evaluation 2021. *Global burden of disease tool* [Online]. [Accessed 27 June 2021]. Available from: http://ghdx.healthdata.org/gbd-results-tool.

Ushiba, J., Morishita, A. and Maeda, T. 2014. A task-oriented brain-computer interface rehabilitation system for patients with stroke hemiplegia *In*: *2014 4th International Conference on Wireless Communications, Vehicular Technology, Information Theory and Aerospace & Electronic Systems (VITAE)*., pp.1–3.

Vanbellingen, T., Filius, S.J., Nyffeler, T. and van Wegen, E.E.H. 2017. Usability of videogame-based dexterity training in the early rehabilitation phase of stroke patients: a pilot study. *Frontiers in Neurology*. **8**, pp.654–654.

Vidal, J.J. 1977. Real-time detection of brain events in EEG. *Proceedings of the IEEE*. **65**(5), pp.633–641.

Vidal, J.J. 1973. Toward direct brain-computer communication. *Annual review of biophysics and bioengineering*. **2**, pp.157–180.

Virgilio Gonzalez, C.D., Sossa Azuela, J.H., Rubio Espino, E. and Ponce Ponce, V.H. 2018. Classification of motor imagery EEG signals with CSP filtering through neural networks models *In*: I. Batyrshin, M. d. L. Martínez-Villaseñor and H. E. Ponce Espinosa, eds. *Advances in Soft Computing*. Cham: Springer International Publishing, pp.123–135.

Viskontas, I.V. and Fried, I. 2009. Human depth electrodes *In*: L. R. Squire, ed. *Encyclopedia of Neuroscience* [Online]. Oxford: Academic Press, pp.1–9. Available from: http://www.sciencedirect.com/science/article/pii/B9780080450469003077.

Vogt, S., Di Rienzo, F., Collet, C., Collins, A. and Guillot, A. 2013. Multiple roles of motor imagery during action observation. *Frontiers in Human Neuroscience*. **7**, p.807.

Vourvopoulos, A., Cardona, J.E.M. and Badia, S.B. i. 2015. Optimizing motor imagery neurofeedback through the use of multimodal immersive virtual reality and motor priming *In*: *2015 International Conference on Virtual Rehabilitation (ICVR)*., pp.228–234.

Vourvopoulos, A., Pardo, O.M., Lefebvre, S., Neureither, M., Saldana, D., Jahng, E. and Liew, S.L. 2019. Effects of a brain-computer interface with virtual reality (VR) neurofeedback: a pilot study in chronic stroke patients. *Frontiers in Human Neuroscience*. **13**, p.210.

Vukelic, M. and Gharabaghi, A. 2015. Oscillatory entrainment of the motor cortical network during motor imagery is modulated by the feedback modality. *NeuroImage*. **111**, pp.1–11.

Wang, X., Wong, W., Sun, R., Chu, W.C. and Tong, K.Y. 2018. Differentiated effects of robot hand training with and without neural guidance on neuroplasticity patterns in chronic stroke. *Frontiers in Neurology*. **9**, p.810.

Wen, D., Fan, Y., Hsu, S.H., Xu, J., Zhou, Y., Tao, J., Lan, X. and Li, F. 2021. Combining brain–computer interface and virtual reality for rehabilitation in neurological diseases: A narrative review. *Annals of Physical and Rehabilitation Medicine*. **64**(1), p.101404.

White, K.D., Ashton, R. and Lewis, S. 1979. Learning a complex skill: effects of mental practice, physical practice, and imagery ability. *International Journal of Sport Psychology*. **10**(2), pp.71–78.

Witkowski, M., Cortese, M., Cempini, M., Mellinger, J., Vitiello, N. and Soekadar, S. 2014. Enhancing brain-machine interface (BMI) control of a hand exoskeleton using electrooculography (EOG). *Journal of NeuroEngineering and Rehabilitation*. **11**(1), p.165.

Wolpaw, J.R., Birbaumer, N., McFarland, D.J., Pfurtscheller, G. and Vaughan, T.M. 2002. Brain-computer interfaces for communication and control. *Clinical neurophysiology : official journal of the International Federation of Clinical Neurophysiology*. **113**(6), pp.767–791.

Wolpaw, J.R. and Wolpaw, E.W. 2012. *Brain-Computer Interfaces, principles and practise*. Oxford University Press USA.

World Health Organization 2011. *World report on disability* [Online]. Malta. [Accessed 10 December 2018]. Available from: https://www.who.int/disabilities/world_report/2011/report.pdf.

Wu, Q., Wang, X., Chen, B. and Wu, H. 2018. Patient-active control of a powered exoskeleton targeting upper limb rehabilitation training. *Frontiers in Neurology*. **9**(654).

Xu, L., Zhang, H., Hui, M., Long, Z., Jin, Z., Liu, Y. and Yao, L. 2014. Motor execution and motor imagery: a comparison of functional connectivity patterns based on graph theory. *Neuroscience*. **261**, pp.184–194.

Yong, X. and Menon, C. 2015. EEG classification of different imaginary movements within the same limb. *PLOS ONE*. **10**(4), p.e0121896.

Yue, Z., Zhang, X. and Wang, J. 2017. Hand rehabilitation robotics on poststroke motor recovery. *Hindawi Behavioural Neurology*.

Zeiler, S.R. and Krakauer, J.W. 2013. The interaction between training and plasticity in the poststroke brain. *Current opinion in neurology*. **26**(6), pp.609–616.

Zhang, J., Wang, B., Zhang, C., Xiao, Y. and Wang, M.Y. 2019. An EEG/EMG/EOG-based multimodal human-machine interface to real-time control of a soft robot hand. *Frontiers in Neurorobotics*. **13**, p.7.

Appendix A

Full Data Extraction Table from the Systematic Review of Wearable Robots and Brain-Computer Interfaces for Hand Rehabilitation After Stroke

This appendix contains the full data extraction table from the systematic review performed on 30 BCI-hand robot studies from January 2010 to October 2019 (see Chapter 2). The data fields include the authors, year published, participant profile, study design, task design, BCI-hand robot specifications, and main outcomes. The table is divided into two sections: (1) studies involving stroke patients and (2) studies involving healthy participants.

Authors	Participants	Study Design	Task Design	BCI-Hand Robot	Main Outcomes
Studies involving stroke patients					
(Ang et al., 2014)	N=21 (7F:14M) Moderate to severe impairment of UE function Mean age: 54.2y Mean stroke duration: 385.1 days	3-armed RCT of motor function with MI-BCI-device as the intervention Control groups: device only (Haptic Knob), SAT	Photo manipulation: hand opening and closing, pronation, and supination Cue: visual (photo) Feedback: visual (photo) and kinaesthetic	EEG: 27 channels to classify ERD/ERS and coupled with EMG to confirm MI Device: Haptic Knob, 2-DOF for hand grasping and knob manipulation Actuation: DC brushed motors with linear belt drive Control: trigger	Clinical outcome measure: FMMA Distal, improvement in weeks 3, 6, 12, 24 BCI-device group = 2.5±2.4, 3.3±2.3, 3.2±2.7, 4.2±3.1 Device only group = 1.6±2.5, 2.9±3.0, 2.5±2.6, 2.5±3.0 SAT group = 0.4±1.1, 1.9±1.9, 1.0±1.3, 0.3±2.1
(Barsotti et al., 2015)	N=3 (1F:2M) Chronic stroke survivors with right arm hemiparesis Mean age: 62±12y	Probing MI classification by BCI training, time-frequency analysis, and robot trajectories Uncontrolled	Reaching-grasping-releasing Cue: visual Feedback: kinaesthetic Minimum time required to perform MI = 2s	EEG: 13 channels to classify ERD Device: BRAVO 2-DOF hand orthosis attached to full UE exoskeleton Actuation: DC motors with rigid links Control: trigger	Mean classification accuracy during BCI training = 82.51±2.04% Average delay from visual cue to robot initiation = 3.45±1.6s Average delay due to patient's ability to start MI = 1.45s
(Bundy et al., 2017)	N=10 Chronic hemiparetic stroke with moderate	Motor function evaluation before and after intervention by	Opening of the affected hand Cue: visual	EEG: 8 channels to classify ERD	Clinical outcome measure: ARAT Score, improvement from baseline to completion (12 weeks)

Bundy et al. (cont'd)	to severe UE hemiparesis Mean age: 58.6±10.3y	MI-BCI from unaffected hemisphere Uncontrolled	Feedback: visual and kinaesthetic	Device: 3-pinch grip, 1-DOF hand exoskeleton Control: continuous depending on the spectral power	Mean ± SD = 6.20±3.81 Note: 5.7 ARAT Score is the minimal clinically important difference in chronic stroke survivors
(Carino-Escobar et al., 2019)	N=9 (4F:5M) Subacute ischaemic stroke Mean age: 59.9±2.8y Mean stroke duration: 158(±74)-185(±73) days	Determine longitudinal ERD/ERS patterns and functional recovery with BCI-robot Uncontrolled	Extension-flexion of hand fingers Cue: visual (Graz MI) Feedback: visual and kinaesthetic	EEG: 11 channels to classify ERD/ERS Device: hand finger orthosis Actuation: DC motor with screw system for linear displacement, flexible links Control: trigger	FMA-UE: N=3 reported equal or higher than 3 score gains, N=3 no score gains, Mean longitudinal ERD/ERS: beta bands have higher association with time since stroke onset than alpha, and strong association with UL motor recovery
(Chowdhury, Raza, et al., 2018)	N=20 10 healthy and 10 hemiplegic stroke patients Mean age (healthy, stroke): 41±9.21y, 47.5±14.23y	Probe non-adaptive classifier (NAC) vs Covariate Shift adaptive classifier (CSAC) of MI in EEG Control group: healthy participants	Extension-flexion of hand fingers Cue: visual Feedback: visual and kinaesthetic	EEG: 12 channels with EMG to classify ERD/ERS Device: EMOHEX 3-finger, 3-DOF each, exoskeleton (thumb, index, middle) Actuation: servomotors with rigid links Control: trigger	Mean classification accuracies during BCI training: Healthy group: calibration = 78.50±9.01%, NAC = 75.25±5.46%, CSAC = 81.50±4.89% Patient group: calibration = 79.63±13.11%, NAC = 70.25±3.43%, CSAC = 75.75±3.92%

(Chowdhury, Meena, et al., 2018)	N=4 (2F:2M) Chronic hemiplegic stroke patients, right-handed, left hand impaired Mean age: 44.75±15.69y Mean stroke duration: 7 ±1.15mo	Motor function evaluation by using active physical practice followed by MI-BCI-controlled device intervention Uncontrolled	Extension-flexion of hand fingers Cue: visual Feedback: visual and kinaesthetic	EEG: 12 channels with force sensors to classify ERD/ERS Device: EMOHEX 3-finger, 3-DOF each, exoskeleton (thumb, index, middle) Actuation: servomotors with rigid links Control: trigger	Classification accuracies of 4 participants: P01 = 81.45±8.12%, P02 = 70.21±4.43%, P03 = 76.88±4.49%, P04 = 74.55±4.35% Clinical outcome measures: GS and ARAT Scores, improvement from baseline to completion (6 weeks) GS scores: group mean difference = +6.38 kg, p=0.06 ARAT scores: group mean difference = +5.66, p<0.05
(Frolov et al., 2017)	N=74 (26F:48M) BCI 55: Control 19 Subacute or chronic stroke with mild to hemiplegic hand paresis, right-handed	Multi-centre RCT of MI-BCI-controlled hand exoskeleton Control group: SHAM	3 Tasks: (1) motor relaxation, (2) imagery of left-hand opening, (3) imagery of right-hand opening Cue: visual Feedback: visual and kinaesthetic	EEG: 30 channels to classify the three mental tasks by Bayesian classifier based on covariance matrices Device: hand exoskeleton by Neurobotics, Russia Actuation: pneumatic motors with spring flexors Control: trigger	Mean classification accuracy during BCI training = 40.6% Clinical outcome measures: FMMA Distal and ARAT Scores, improvement in 10 days of training FMMA Distal = 2.0, p<0.01 (BCI) and 1.0, p=0.046 (control) ARAT Grasp = 3.0, p<0.01 (BCI) and 1.0, p=0.0394 (control) ARAT Grip = 1.0, p<0.01 (BCI) and 1.0, p=0.045 (control) ARAT Pinch = 1.0, p<0.01 (BCI) and 0.0, p=0.675 (control)
(Norman et al., 2018)	N=8 (All male) Chronic cortical and subcortical single	Implementation of sensorimotor rhythm (SMR) control on	Extension of hand finger	EEG: 16 channels mapping SMR changes	Mean classification accuracies:

Norman et al. (cont'd)	haemorrhagic or ischaemic stroke (at least 6 months) Mean age: 59.5±11.8y	robot-assistive movement Uncontrolled	Cue: visual Feedback: visual and kinaesthetic	Device: FINGER robot Actuation: Linear servo-tube actuator with rigid links Control: Visual - continuous (colour change respective to SMR), Robot - trigger	8 participants: 83.1%, 76.3%, 73.3%, 68.2%, 74.5%, 86.5%, 47.9%, 40.0% Box and blocks test (BBT): At screening: mean score = 14.3±10.0, mean change after therapy = 4.3±4.5 (range 0-12). Higher score changes in participants who demonstrated SMR control but not significant (p=0.199)
(Ono et al., 2016)	N=21 (9F:12M) Chronic stroke patients with hemiplegic hands Mean age: 57.9±2.4y	Probe congruent vs. incongruent MI feedback strategies Control groups: congruent (synchronous proprioceptive and visual feedback) and incongruent (proprioceptive feedback given 1s after visual)	Grasping of a tennis ball with a hand Cue: visual (video of hand performing action) Feedback: visual and kinaesthetic	EEG: 9 channels to classify ERD Device: Power Assist Hand - Team ATOM, Atsugi, Japan Actuation: pneumatic motors with rigid links Control: trigger	Mean classification accuracies: Congruent feedback = 56.8±5.2%, chance level=36.4±4.5% Incongruent feedback = 40.0±3.5%, chance level 35.4±4.5%
(Tsuchimoto et al., 2019)	N=18 (3F:14M) Chronic haemorrhagic or ischaemic stroke (from 2mo onwards) Mean age: 58±10y	RCT Implementation of MI-controlled robotic orthosis as neurofeedback Control: SHAM	Extension of hand finger Cue: unspecified Feedback: kinaesthetic and electrical stimulation	EEG: 5 channels to classify MI Device: robotic finger orthosis Actuation: servo motors with rigid links Control: trigger	Significant time-intervention interaction in the ipsilesional sensorimotor cortex. Higher coactivation of sensory and motor cortices for neurofeedback group in the ipsilesional sensorimotor cortices as compared to SHAM

(Wang et al., 2018)	N=24 (4F:20M) Chronic stroke patients with paralysed hands Mean age: 54±9y	RCT Implementation of action observation and motor imagery (AO+MI) with kinaesthetic feedback Control: SHAM	Hand grasping Cue: visual (video of hand action / textual cues in SHAM group) Feedback: visual and kinaesthetic	EEG: 16 channels to classify ERD Device: robot hand Control: Trigger	AO+MI with kinaesthetic feedback group showed significant improvements in FMA-UE across longitudinal evaluation [$\chi 2(2) = 7.659$, $p = 0.022$], no significant difference in SHAM group [$\chi 2(2) = 4.537$, $p = 0.103$]
Authors	**Participants**	**Study Design**	**Task Design**	**BCI-Hand Robot**	**Main Outcomes**
Studies involving healthy participants					
(Bauer et al., 2015)	N=20 (11F:9M) Right-handed Mean age: 28.5±10.5y	Study on MI as compared to motor execution (ME) using BCI-device	Opening of left hand Cue: auditory Feedback: kinaesthetic	EEG: 31 channels to detect ERD, with EMG to classify MI from execution and account for tonic contraction Device: Amadeo, Tyromotion, Austria Control: discontinuation of ERD stops finger extension	Principal component analyses (between MI and execution) generated coefficients for the visual (VIS) and kinaesthetic (KIS) imagery scale, BCI-robot performance (BRI), tonic contraction task (MOC) and visuomotor integration task (VMI). VIS and KIS yielded high coefficients on MI while MOC and VMI yield high coefficients on ME. BRI show high coefficient yields on both MI and ME.
(Cantillo-Negrete et al., 2015)	N=1	Design and implementation of a MI-controlled hand orthosis	Extension-flexion of right-hand finger Cue: visual (modified Graz) Feedback: kinaesthetic	EEG: 11 channels to detect MI Device: 1-DOF hand finger orthosis Actuation: DC motor with screw system for	Classification accuracy = 78%

Cantillo-Negrete et al. (cont'd)				linear displacement, flexible links Control: trigger	
(Chowdhury et al., 2015)	N=6 Age range: 20-30y	Study of cortico-muscular coupling in robotic finger exoskeleton control	Extension-flexion of hand fingers Cue: visual Feedback: kinaesthetic	EEG: 10 channels with EMG to classify MI Device: 3-finger, 3-DOF each, exoskeleton (thumb, index, middle) Actuation: servomotors with rigid links Control: trigger	Mean classification accuracies: passive execution = 69.17%, hand execution = 71.25%, MI = 67.92%
(Coffey et al., 2014)	N=3 (All male) Right-handed Age range: 24-28y	Design and implementation of a MI-controlled hand orthosis	Hand digit and wrist contraction and extension Cue: visual (Graz MI) Feedback: kinaesthetic	EEG: 27 channels to classify MI Device: hand glove controlled by Arduino Actuation: pneumatic Control: trigger	Glove inflation-deflation cycle = 22s Classification accuracies of 3 participants: A = 92.5%, B = 90.0%, C = 80.0%
(Diab et al., 2016)	N=5	Design and implementation of EEG-triggered wrist orthosis with accuracy improvement	Hand opening and closing Cue: verbal instruction Feedback: kinaesthetic	EEG: 14 channels to detect hand movement related EEG Device: actuated Talon wrist orthosis Actuation: linear Control: trigger	Mean classification accuracies: simulation studies = 95%, online BCI training = 86%

(Fok et al., 2011)	N=4	Design and implementation of a MI-controlled hand orthosis	Hand opening and closing Cue: unspecified Feedback: visual (cursor movement) and kinaesthetic	EEG: 14 channels to detect MI-related ERD Device: actuated Talon wrist orthosis Actuation: linear actuator Control: trigger	EEG signals from imagined hand movement was correlated with the contralesional hemisphere and utilised to trigger the actuation of orthosis ERD was detected from 12 Hz bin power of EEG during move condition
(Li et al., 2019)	N=14 (4F:10M) Mean age: 23.8±0.89y	Design and implementation of an attention-controlled hand exoskeleton with rigid-soft mechanism	Hand grasping Cue: visual (video of hand action) Feedback: kinaesthetic	EEG: 3 channels to map signals relative to attention Device: hand exoskeleton Actuation: linear actuator with rigid-soft mechanism Control: Trigger	Mean classification accuracy: 95.54% actuation success rate against the attention threshold
(Holmes et al., 2012)	N=6 (All male, young adults)	Design and implementation of a MI-controlled hand orthosis	Hand opening and closing Cue: textual Feedback: kinaesthetic	EEG: 14 channels to detect hand movement related EEG Device: ExoFlex Hand Exoskeleton controlled by Arduino Actuation: linear actuator connected to chained links that flex Control: trigger	Classification accuracies of 6 participants: T001 = 95%, T002 = 98%, D001 = 91%, U001 = 93%, E001 = 87%, E002 = 86%

(King et al., 2011) King et al. (cont'd)	N=1 (Female) 24y	Contralateral control of hand orthosis using EEG-based BCI	Right hand idling and grasping Cue: textual Feedback: visual and kinaesthetic	EEG: 63 channels to control contralateral hand movement Device: hand orthosis Actuation: servomotors attached to Bowden cables as tendons Control: trigger	Offline classification accuracy = 95.3±0.6%, $p < 3.0866 \times 10^{-25}$ Average lag from voluntary contractions to BCI-robot control = 2.24 ± 0.19s (after 5 sessions)
(Naros et al., 2016)	N=32 (16F:16M) Mean age: 25.9±0.5y	2x2 factorial design with parameters: adaptive classifier threshold and non-adaptive classifier threshold, contingent feedback and non-contingent feedback	Opening of right hand Cue: auditory Feedback: kinaesthetic	EEG: 32 channels to detect ERD, with EMG to classify MI (FC3, C3, CP3 used) Device: Amadeo, Tyromotion, Austria Control: trigger	Significant enhancement in group 1 (adaptive classifier + contingent feedback), p=0.0078 Significant reduction in group 4 (non-adaptive classifier + non-contingent feedback), p=0.0391 Motor performance improvement over baseline from first and last tasks, significant results: Group 1 (adaptive classifier + contingent feedback), p=0.0313 Group 4 = (non-adaptive classifier + non-contingent feedback), p=0.0411
(Ono et al., 2018)	N=28 Right-handed except 1	Implementation of an action observation strategy with visual and proprioceptive, or	Grasping of a tennis ball with a hand Cue: visual (video of hand performing action)	EEG: 9 channels to classify ERD Device: Power Assist Hand - Team ATOM, Atsugi, Japan	AO+MI + proprioceptive and visual feedback: Mean MI-ERD powers of correct feedback vs SHAM provide significant

Ono et al. (cont'd)		auditory feedback to MI Control group: SHAM	Feedback: visual, kinaesthetic and auditory	Actuation: pneumatic motors with rigid links Control: trigger	interaction, $F_{1,17}$=6.618, p=0.020 (6 days) Statistically significant increase in MI-ERD power in correct feedback group over baseline, p=0.012 (6 days)
(Stan et al., 2015)	N=9	Trigger a hand orthosis using a P300 speller BCI	Spell E (enable), A (hand opening) and B (hand closing) in P300 speller BCI to perform hang grasping, moving and releasing objects Cue: textual (spelling) Feedback: visual (textual) and kinaesthetic	EEG: 8 channels focusing on visual cortex Device: hand orthosis Actuation: 2 servomotors and current feedback circuitry Control: trigger	Mean classification accuracies: 100% (on 6th letter flash during calibration)
(Ramos-Murguialday et al., 2012)	N=23 Mean age (contingent positive, contingent negative, SHAM): 26.6±4y, 26.5±5y, 26.2±2y	Probing MI with proprioceptive feedback Experimental groups: contingent positive, contingent negative feedback Control group: SHAM	5 tasks: MI without direct control, MI with direct control, passive, active, rest Cue: auditory Feedback: visual and kinaesthetic	EEG: 61 channels with EMG to classify ERD/ERS Device: hand orthosis Actuation: DC motor M-28 with a worm gearhead and Bowden cables for each finger Control: trigger	Contingent positive feedback provided higher BCI performance during MI without feedback than contingent negative and SHAM; and higher during MI with or without feedback as compared to rest
(Ramos-Murguialday and Birbaumer, 2015)	N=9 Right-handed Mean age: 26.6±4y	Detect oscillatory signatures of motor tasks during EEG	5 tasks: MI without direct control, MI with	EEG: 61 channels with EMG to classify ERD/ERS	Significant change in power in all frequency ranges during MI with direct control before trial initiation

Ramos-Murguialday and Birbaumer (cont'd)			direct control, passive, active, rest Cue: auditory Feedback: visual and kinaesthetic	Device: hand orthosis Actuation: DC motor M-28 with a worm gearhead and Bowden cables for each finger Control: trigger	Kinaesthetic feedback increased significant changes in alpha and beta power; therefore, increasing BCI performance
(Randazzo et al., 2018)	N=9 (2F:7M) Mean age: 23±5y	Design and implementation of a hand orthosis with testing of kinaesthetic effects in EEG	4 tasks: rest (REST), exoskeleton-induced hand motions (EXO), MI of right hand (MI), exoskeleton-induced hand motions plus MI (MIEXO) Cue: visual Feedback: kinaesthetic	EEG: 16 channels to detect MI Device: mano hand exoskeleton Actuation: linear servomotors attached to Bowden cables as tendons Control: passive (exoskeleton not dependent on MI to move during MIEXO task)	Mean classification accuracies among groups: (vs REST) MI = 63.02±5.91%, EXO = 69.64±5.74%, MIEXO = 72.19±6.57% MIEXO vs EXO = 69.91±9.86% Chance level at 95% confidence = 58% (N=50 trials)
(Tacchino et al., 2017)	N=8 (7F:1M) Right-handed Mean age: 26.3±1.9y	2x2 factorial design with parameters: glove, no glove, active movement, passive movement	Opening and closing of hand, 4 tasks: (A) glove with active movement, (B) glove with passive movement, (C) no glove with active movement, (D) no glove and no movement	EEG: 19 channels with EMG to detect ERD/ERS (C3, F3, Cz used) Device: Gloreha hand rehabilitation glove Actuation: electric actuators with	Statistically significant ERD changes in beta and mu bands were observed to initiate earlier in tasks A and C (involves active movement) Stronger and longer ERD was observed in tasks A and B (involves robotic assistance) suggesting reinforced afferent kinaesthetic feedback

Tacchino et al. (cont'd)			Cue: auditory Feedback: kinaesthetic	Bowden cables on each finger Control: passive (glove not dependent on brain-state during tasks)	
(Vukelic and Gharabaghi, 2015)	N=11 (4F:7M) Right-handed Mean age: 25.83±3.1y	Assessment sensorimotor activity during MI with either visual or kinaesthetic feedback	Right hand opening Cue: visual (coloured cursor ball) Feedback: visual and kinaesthetic (separated by experimental groups)	EEG: 128 channels to detect ERD/ERS during MI (F3, CP3, C3 used) Device: Amadeo, Tyromotion, Austria Control: trigger	MI + kinaesthetic feedback group resulted in higher beta ERS (p=0.02) during rest and higher beta ERD (p=0.04) during MI Kinaesthetic feedback provides higher stability and sustained beta ERD activity than visual feedback
(Witkowski et al., 2014)	N=12 (4F:8M) Right-handed Mean age: 28.1±3.63y	Assessment performance and safety of EEG-EOG hybrid BCI	Right hand grasping Cue: visual (coloured squares and arrows) Feedback: kinaesthetic	EEG: 5 channels with EOG and EMG to detect ERD during MI Device: HX hand exoskeleton Actuation: DC motors with Bowden cables for thumb and index fingers Control: trigger	Mean classification accuracies: EEG only = 63.59±10.81% EEG/EOG hybrid = 60.77±9.42% Mean safety criterion violations during rest: EEG only = 45.91±26.8% EEG/EOG hybrid = 10.14±0.3%
(Zhang et al., 2019)	N=6 (2F:4M) Right-handed Age range: 23-26y	Implementation of a multimodal system using EEG, EMG and	Graz visualisation and auditory instructions, eye movements and	EEG with EMG and EOG: 40 channels to analyse ERD/ERS patterns	Mean classification accuracies: EOG = 94.23% EEG = 31.46%

Zhang et al. (cont'd)	EOG to control a soft-robotic hand	physical practice (hand gestures) Cue: visual (Graz MI), auditory Feedback: visual and kinaesthetic	Device: Soft pneumatic finger Actuation: pneumatic actuator with soft structures Control: trigger	EMG = 36.38% Multimodal = 93.83±0.02%

UE = Upper Extremity, MI = Motor Imagery, BCI = Brain-Computer Interface, RCT = Randomised Clinical Trial, SAT = Standard Arm Therapy, EMG = Electromyography, EOG = Electrooculography, ERD/ERS = Event-Related Desynchronisation/Synchronisation, FMMA = Fugl-Meyer Motor Assessment, ARAT = Action Research Arm Test, GS = Grip Strength, DOF = Degrees-of-Freedom

Appendix B

Development of a Low-Cost Robotic Hand Exoskeleton: From Design to Fabrication

This appendix contains the mechanical drawings, illustrations, and images from the low-cost robotic hand exoskeleton fabrication process. All figures in this appendix illustrate the right-hand version of the robotic exoskeleton to represent the device. All distance measurements are in millimetres (mm), while angle measurements are in degrees (°).

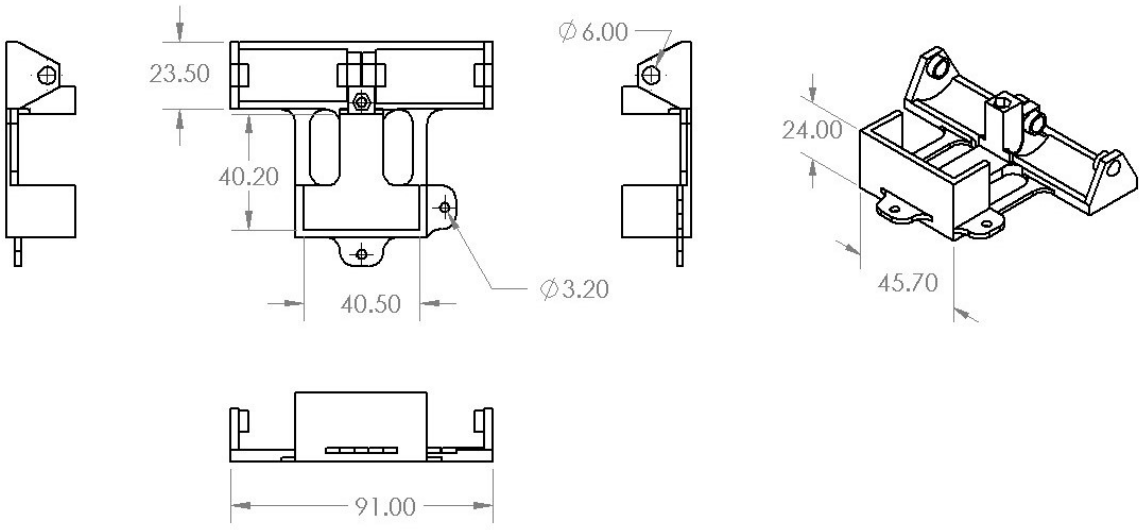

Figure B.1: Main servo base

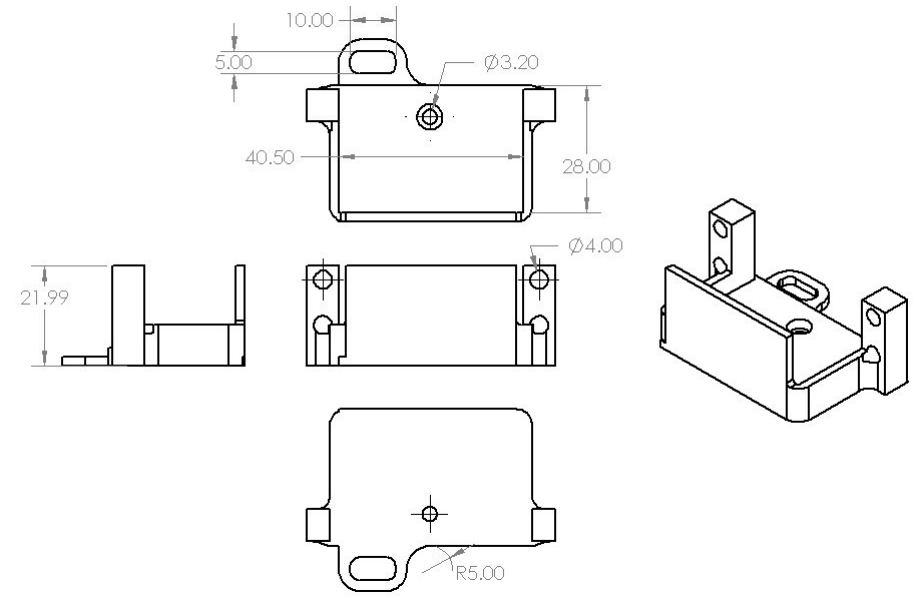

Figure B.2: Thumb servo base

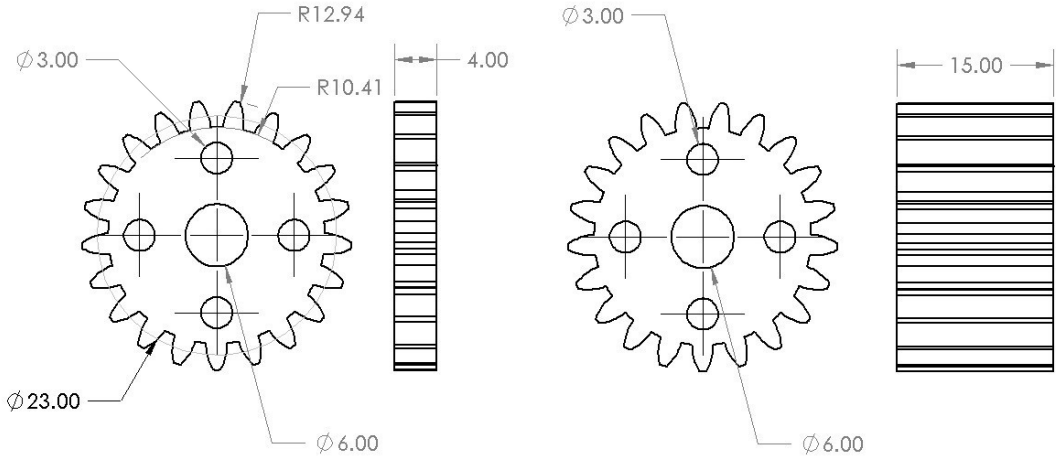

Figure B.3: Main servo gear (left) and finger link 1 gear (right)

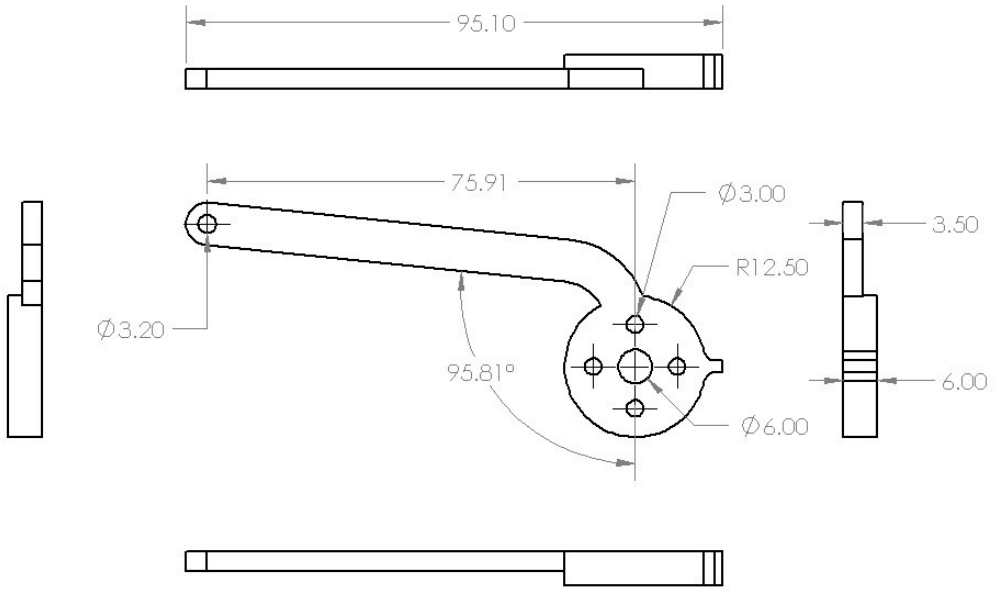

Figure B.4: Finger link 1

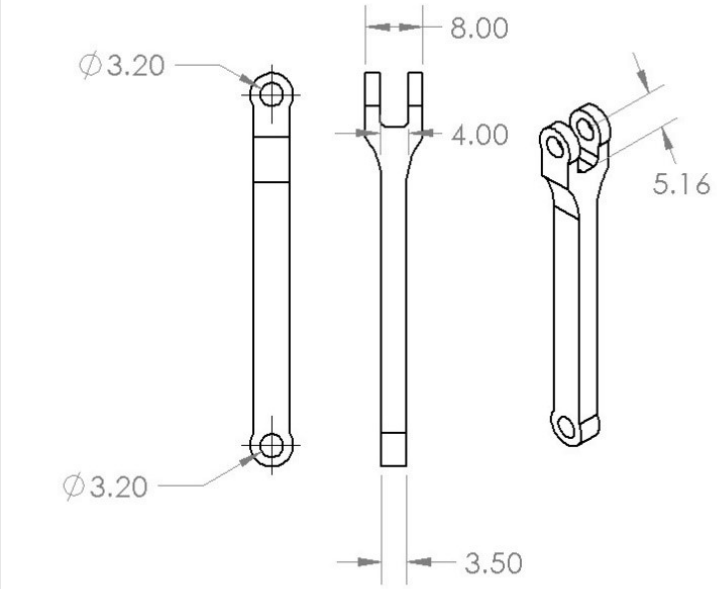

Figure B.5: Finger link 2

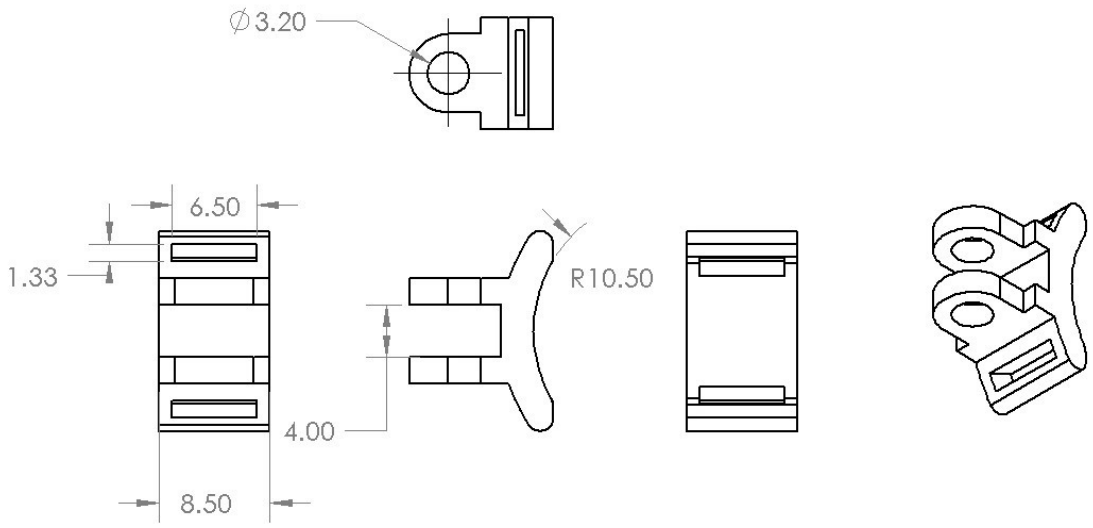

Figure B.6: Finger link attachments

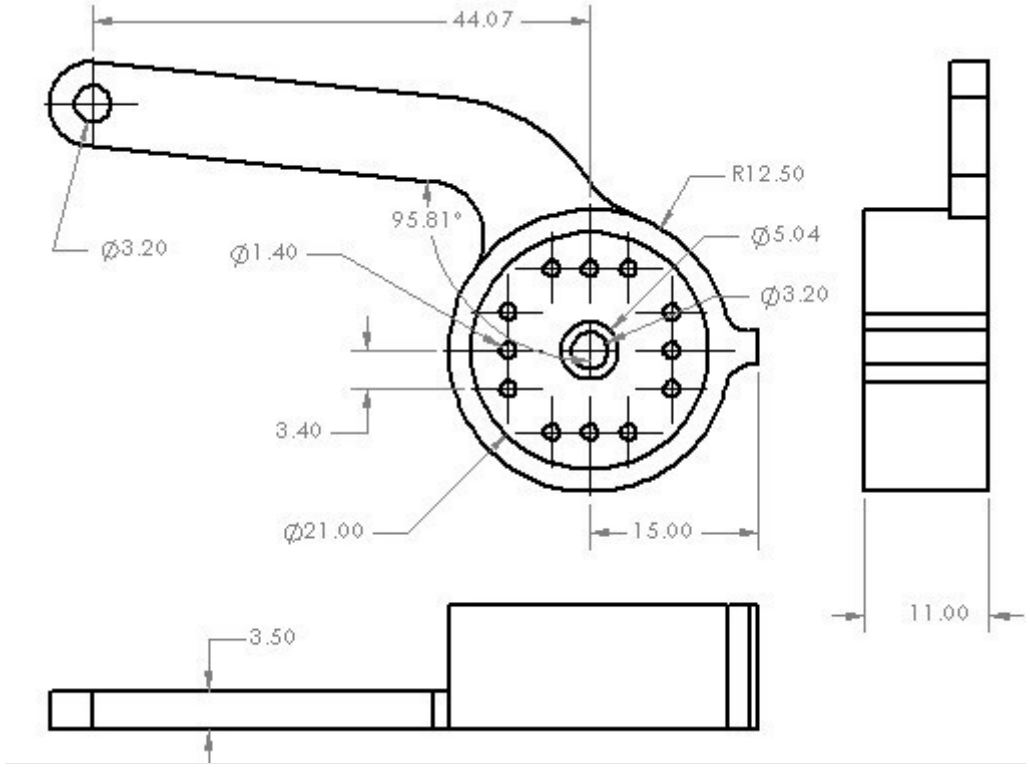

Figure B.7: Thumb link 1

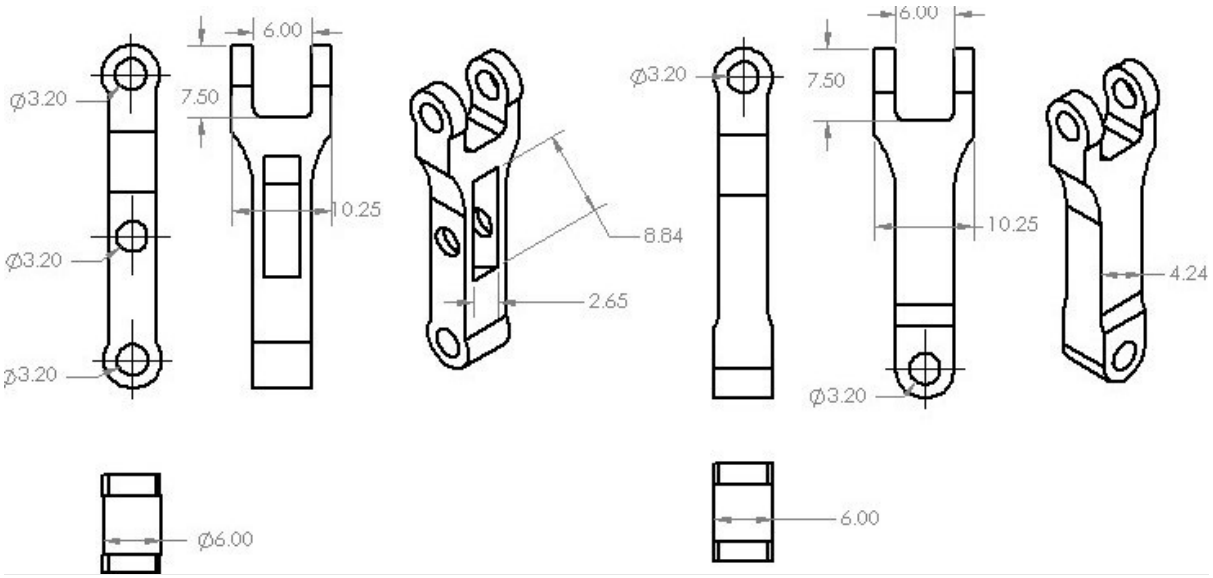

Figure B.8: Thumb link 2a (left) and thumb link 2b (right)

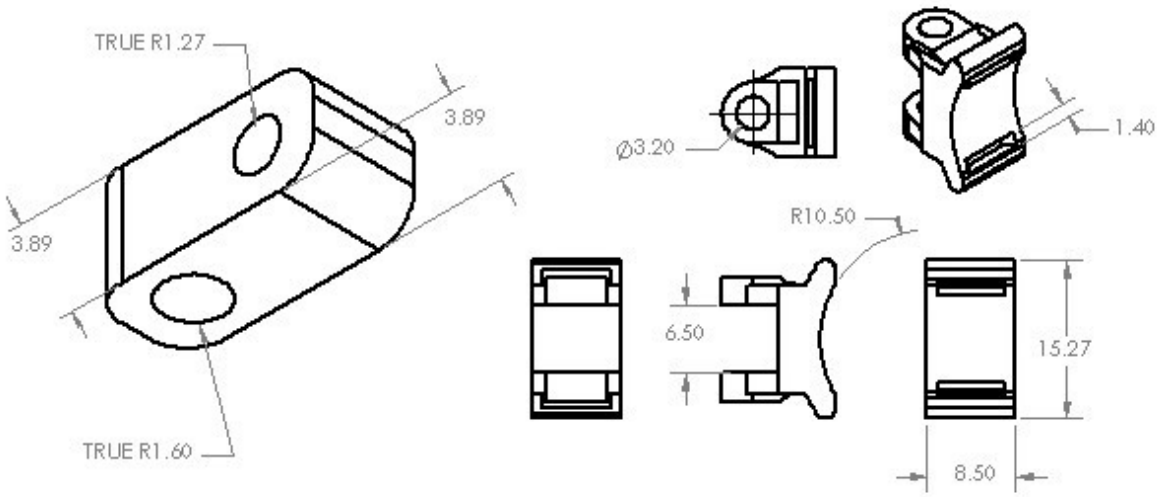

Figure B.9: Cardan joint which connects thumb link 2a and thumb link 2b (left) and thumb link attachments (right)

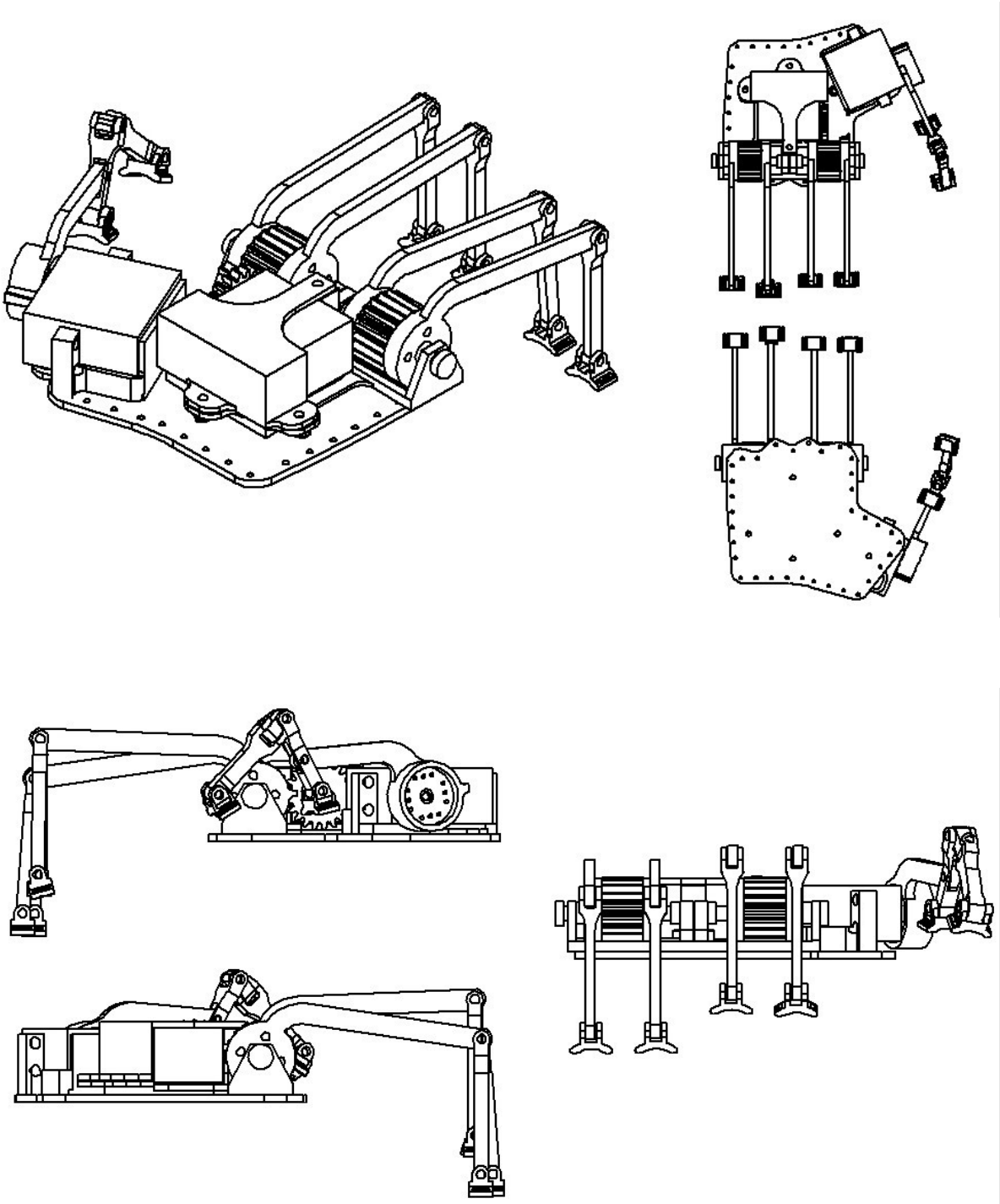

Figure B.10: Full mechanical assembly (right-hand version)

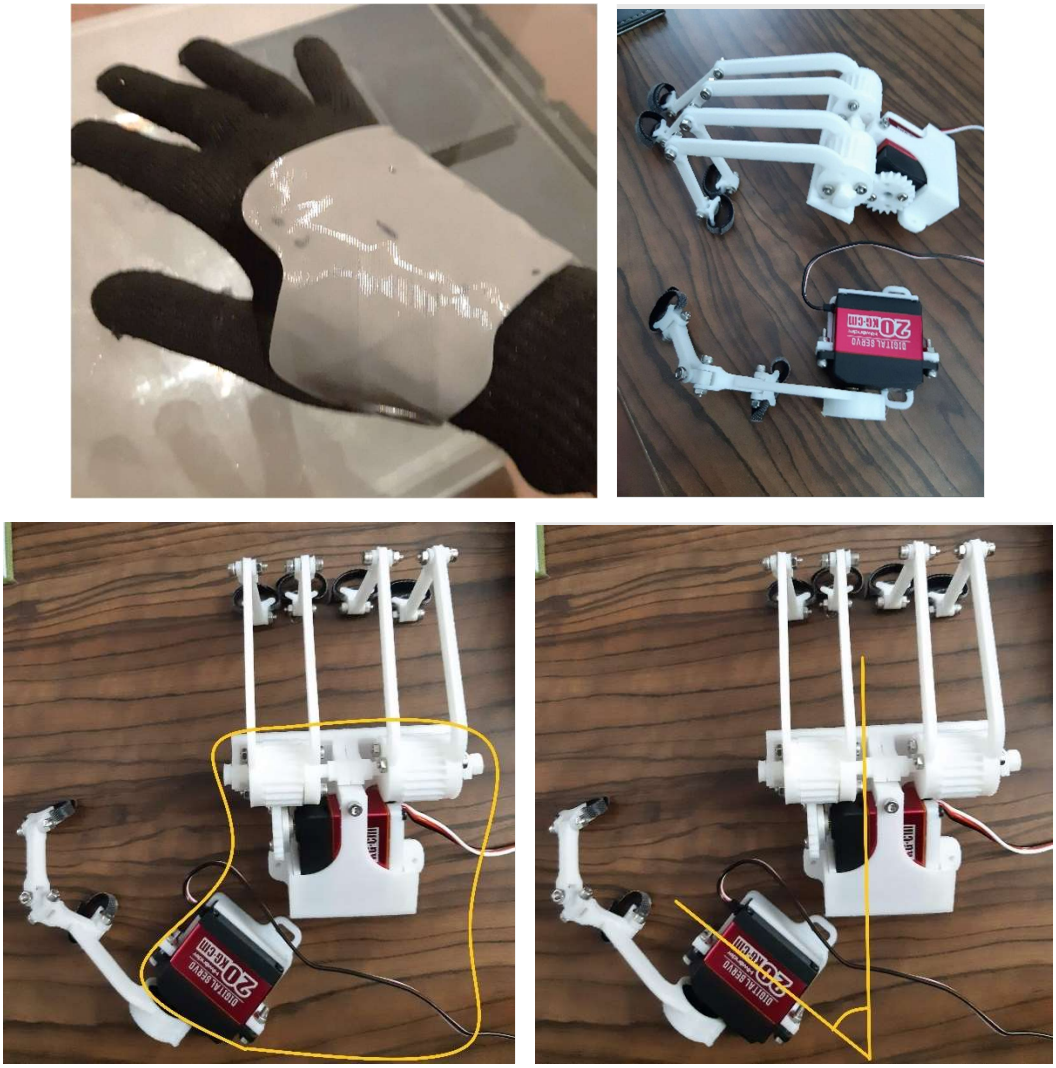

Figure B.11: Fabrication via 3D printing

Figure B.12: Wearing the prototype

Appendix C

2x2 Factorial ANOVA (Additional Details)

This appendix contains supplementary figures and tables from the 2x2 factorial ANOVA performed to treat the experimental data obtained in Chapter 6. All plots and numerical results were obtained from the statistical software R/R-Studio.

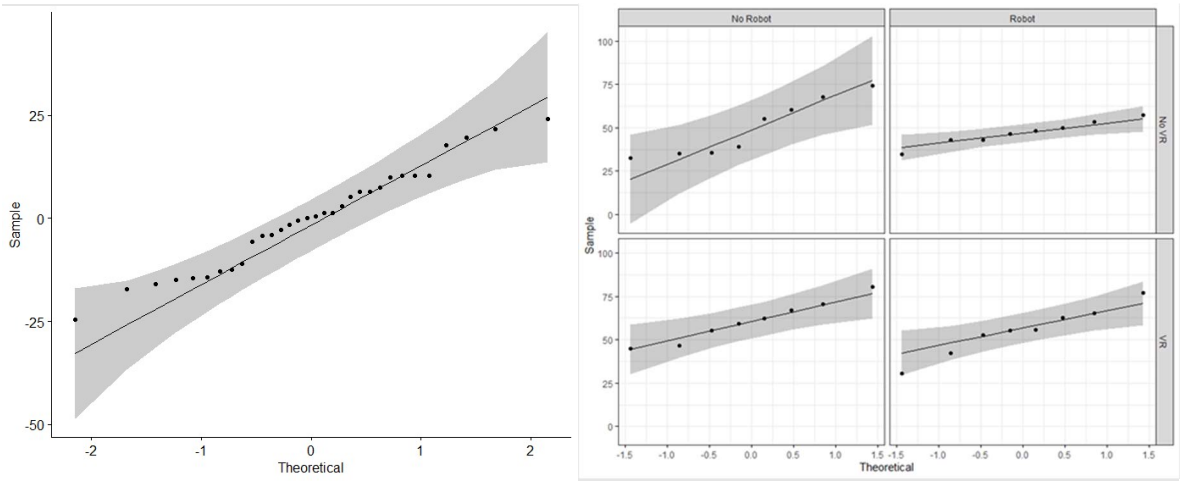

Figure C.1: Shapiro-Wilk Test for Normality: Overall (left) and Per Condition (right)

Table C.1: Shapiro-Wilk Test for Normality: Overall

Variable	Statistic	p-value
Residuals (model)	0.976	0.668

Table C.2: Shapiro-Wilk Test for Normality: Per Condition

Visual	Kinaesthetic	Variable	Statistic	p-value
No VR	No Robot	Score	0.877	0.177
No VR	Robot	Score	0.982	0.177
VR	No Robot	Score	0.971	0.907
VR	Robot	Score	0.978	0.953

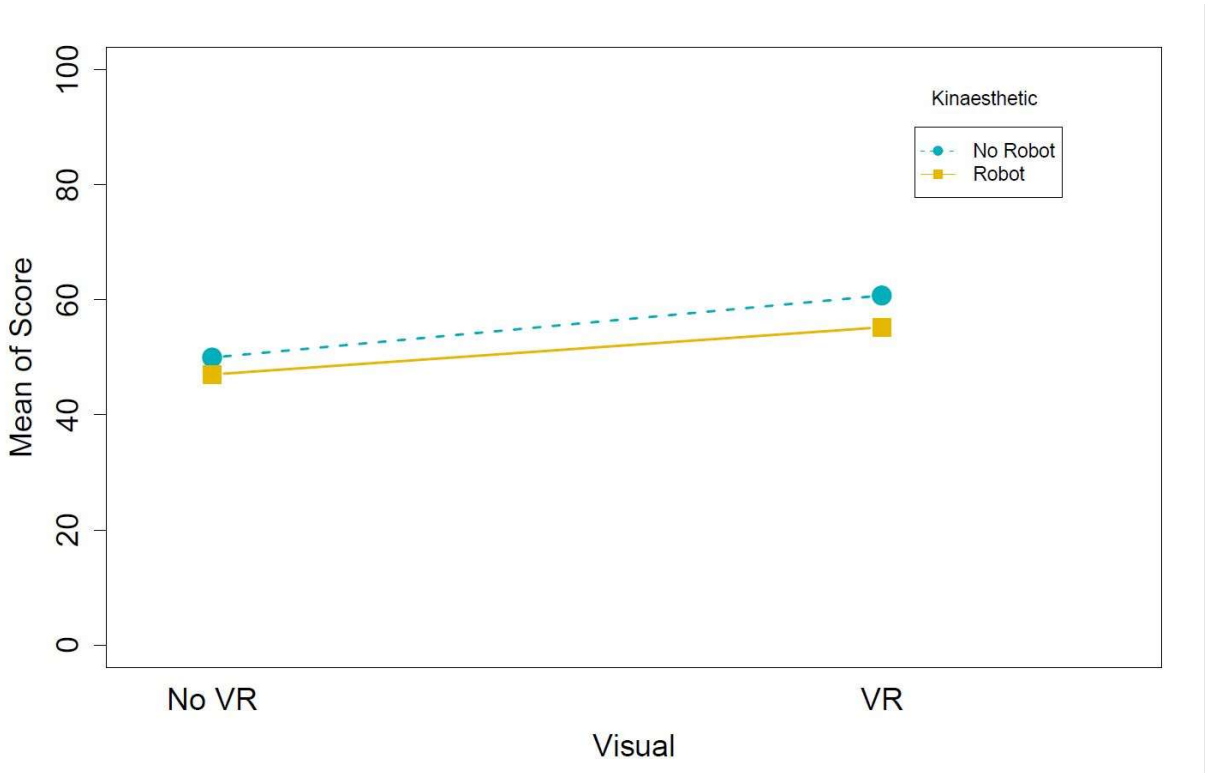

Figure C.2: Interaction plot

Table C.3: Main and interaction effects

Effect	**DFn**	**DFd**	**F**	**p**	**p<.05**	**Ges**
Visual (main)	1	28	4.343	0.046	*	0.134
Kinaesthetic (main)	1	28	0.863	0.361		0.030
Interaction	1	28	0.080	0.780		0.003

Table C.4: Pairwise T-Test and Bonferroni Correction

Y	**Group 1**	**Group 2**	**N1**	**N2**	**p adjusted**	**p<.05**
Score	No VR	VR	16	16	0.0422	*

Appendix D

Individual EEG Time-Frequency Representations and ERD/S Line Plots for All Sessions

This appendix contains the phase EEG time-frequency representations and ERD/S line plots across all sessions and conditions from the experiment in Chapter 6. Conditions that indicate "BOTH" refer to the combined VR+robot condition. The first two plots were generated from the training phase's averaged left and right trials, while the last two plots were generated from the averaged left and right trials of the testing (online) phase. Each page in this appendix shows all the generated EEG time-frequency representations or ERD/S line plots for that particular session (labelled). For the ERD/S line plots, the top quadrants are the mu (μ) spectral band power plots at 8-12 Hz, while the bottom quadrants are the plots for the beta (β) spectral band power at 13-35 Hz.

CONTROL – 1 –TRAINING

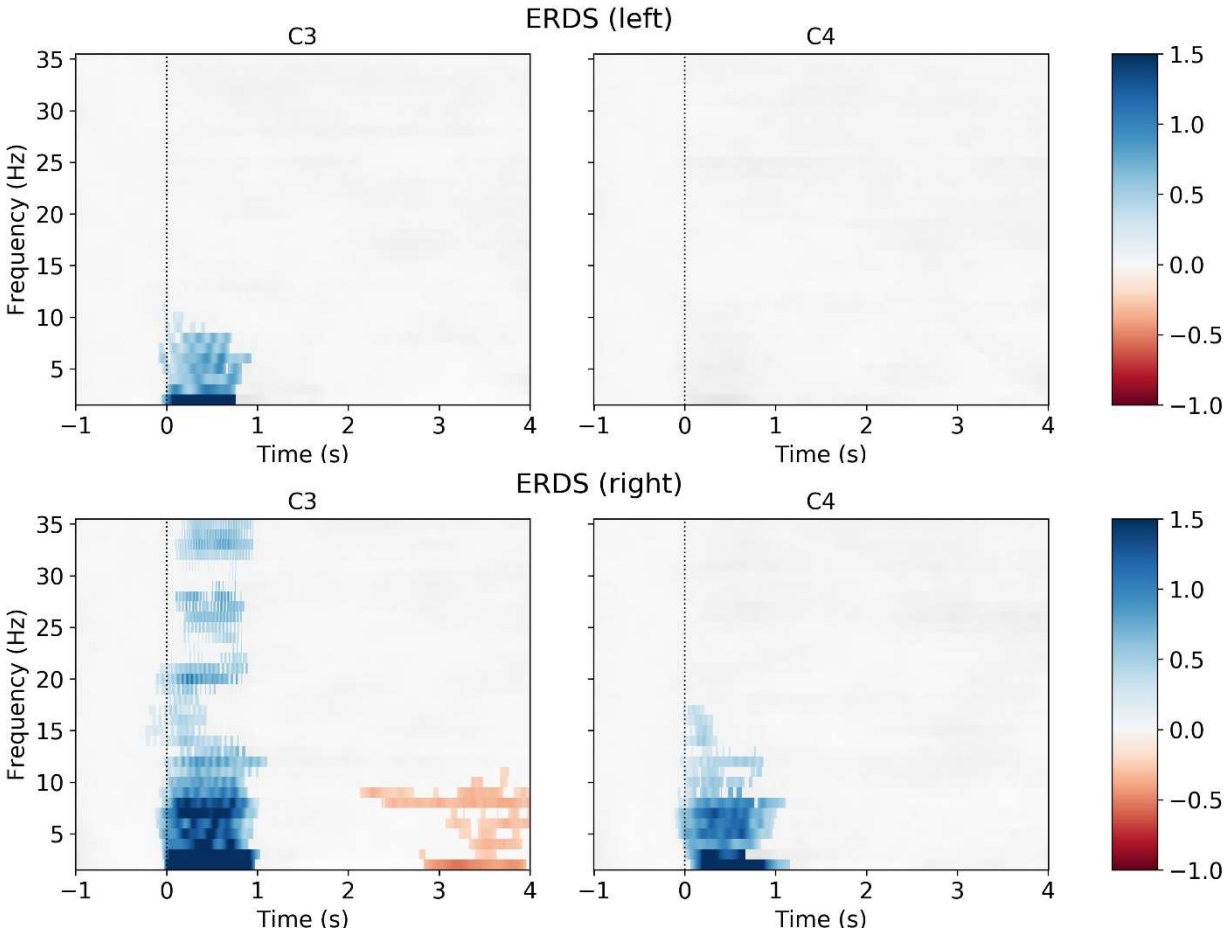

CONTROL – 1 – TESTING

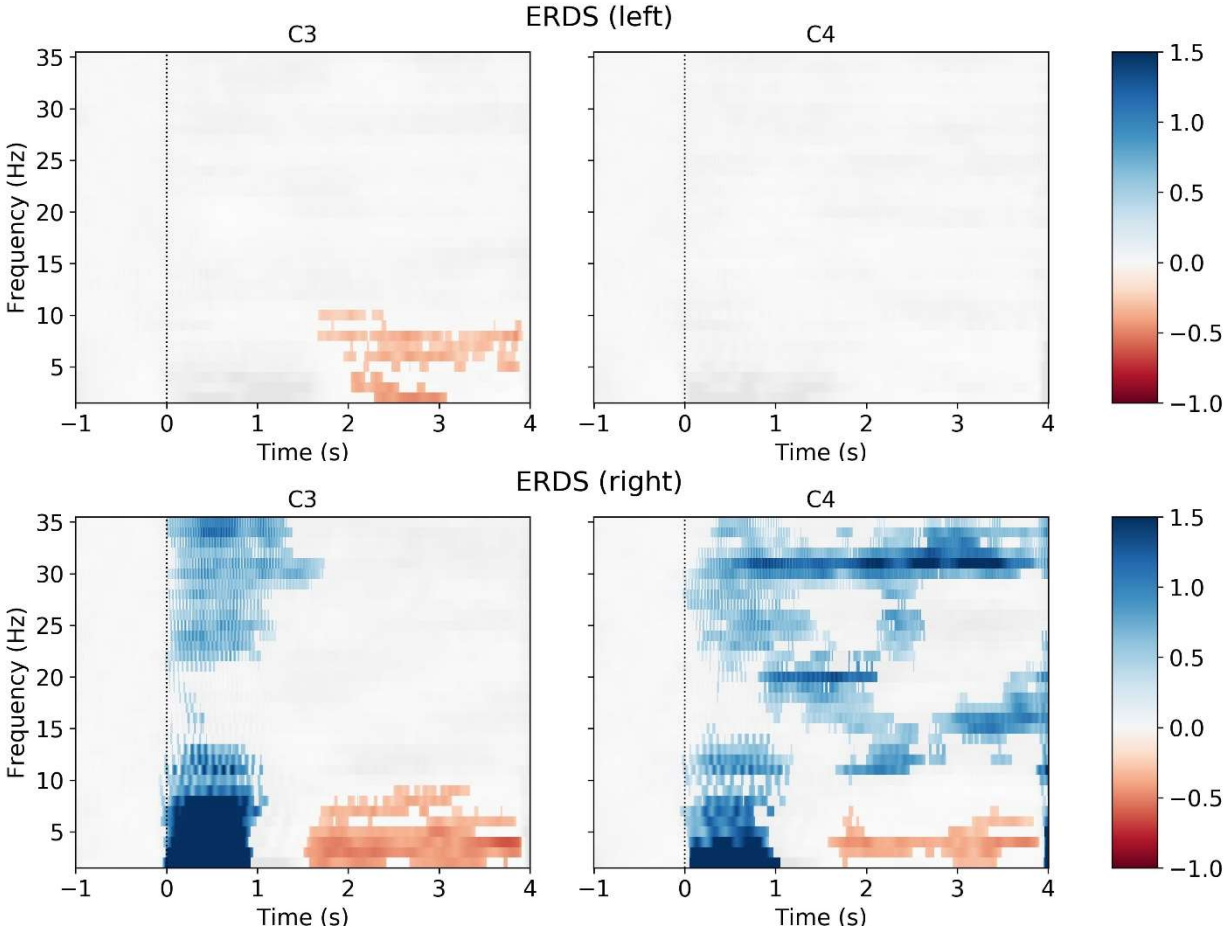

CONTROL – 2 –TRAINING

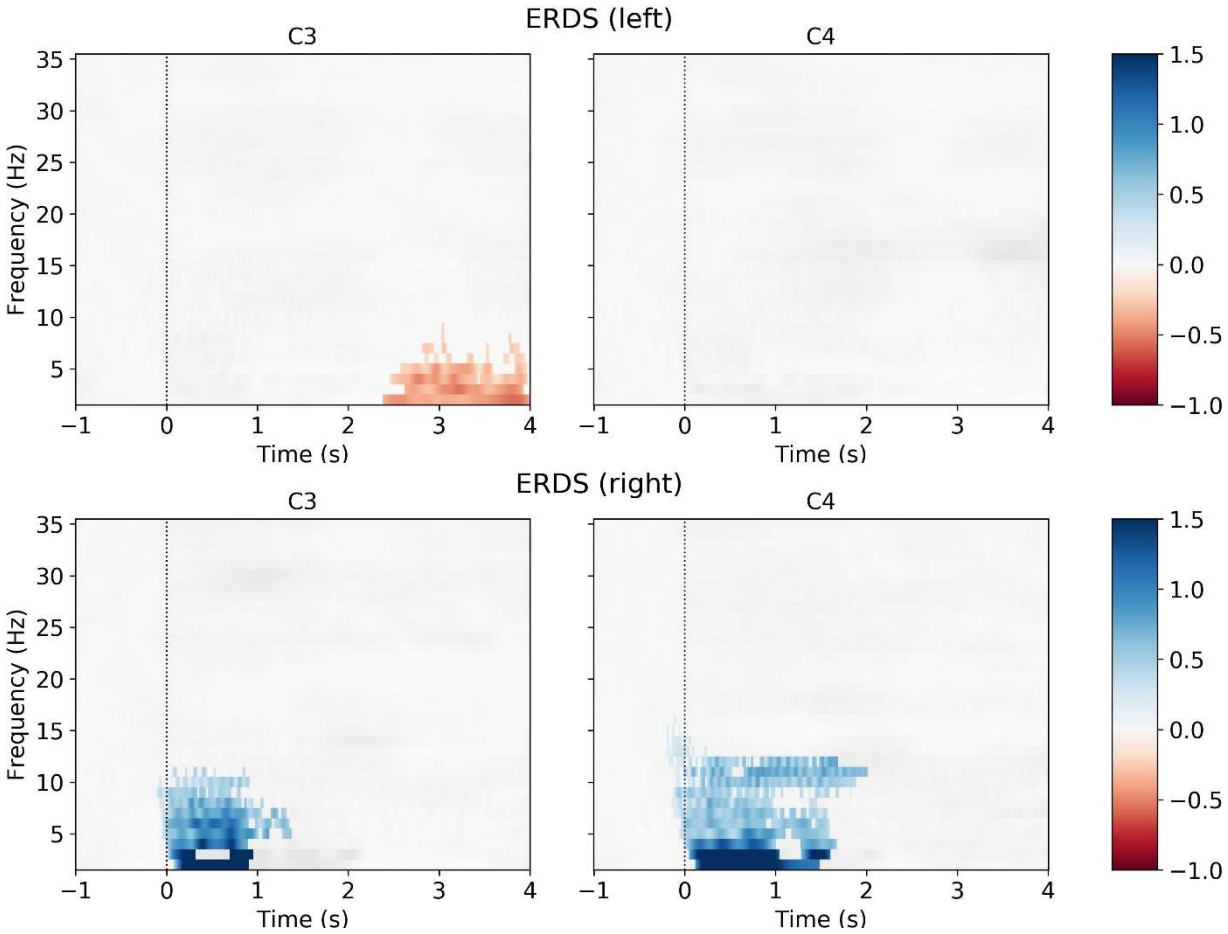

CONTROL – 2 – TESTING

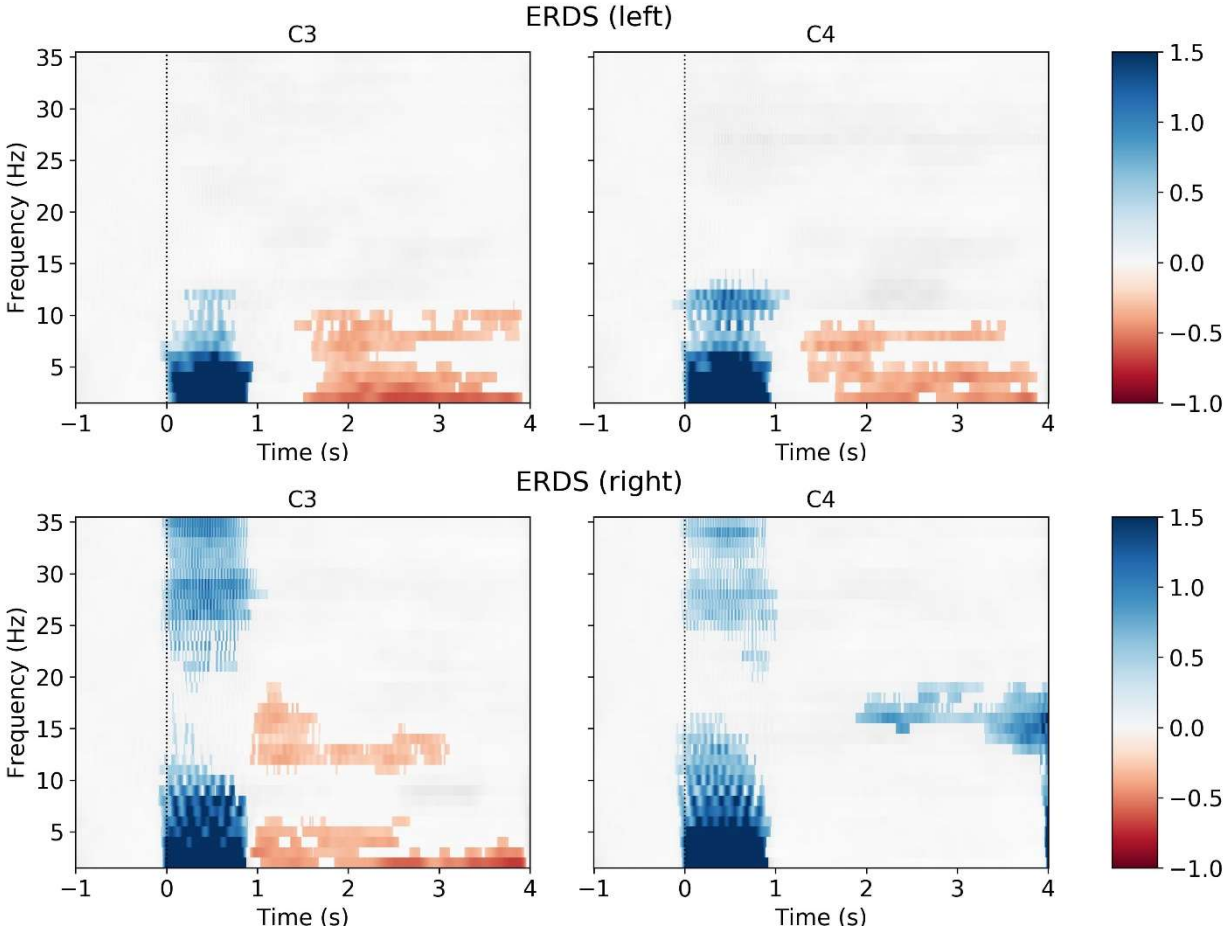

CONTROL – 3 – TRAINING

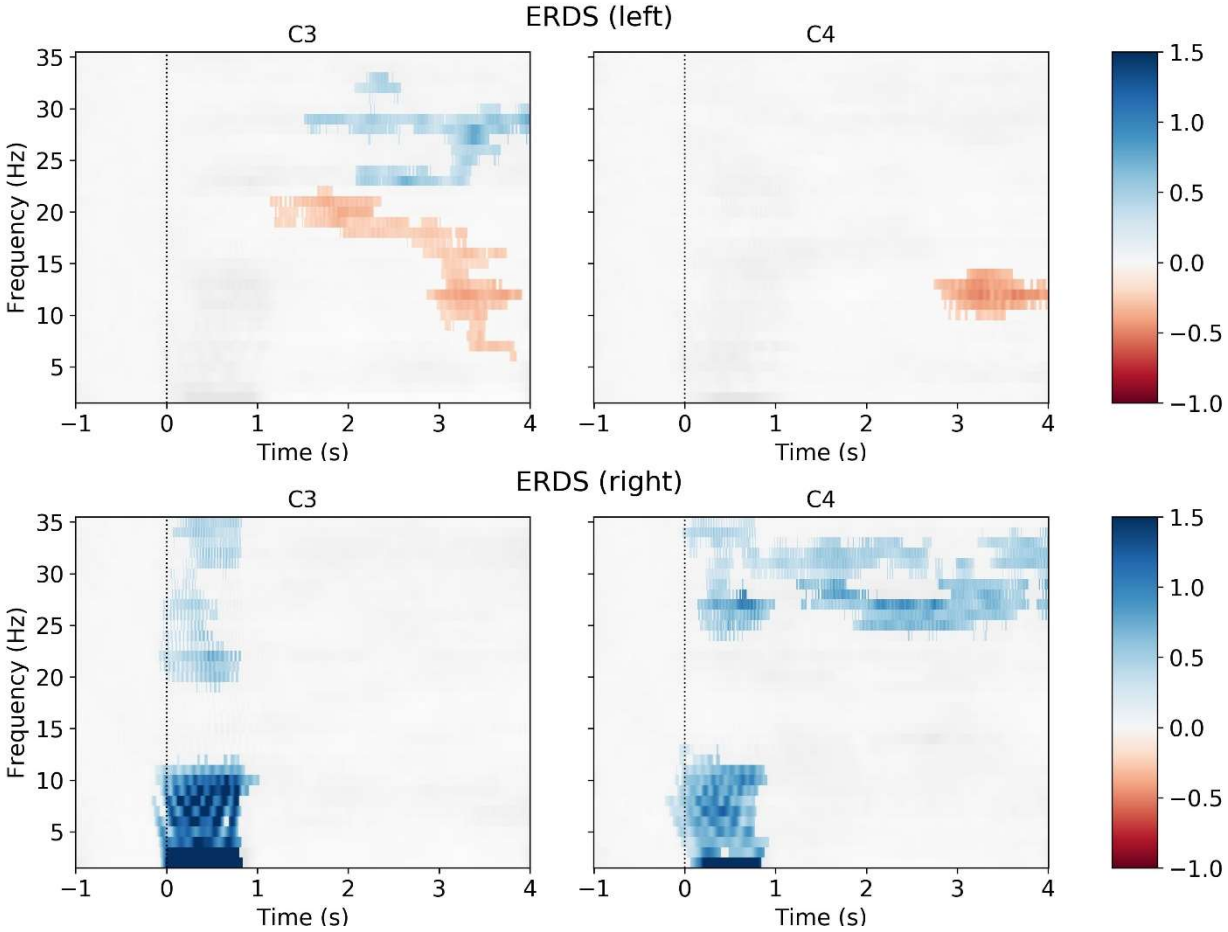

CONTROL – 3 – TESTING

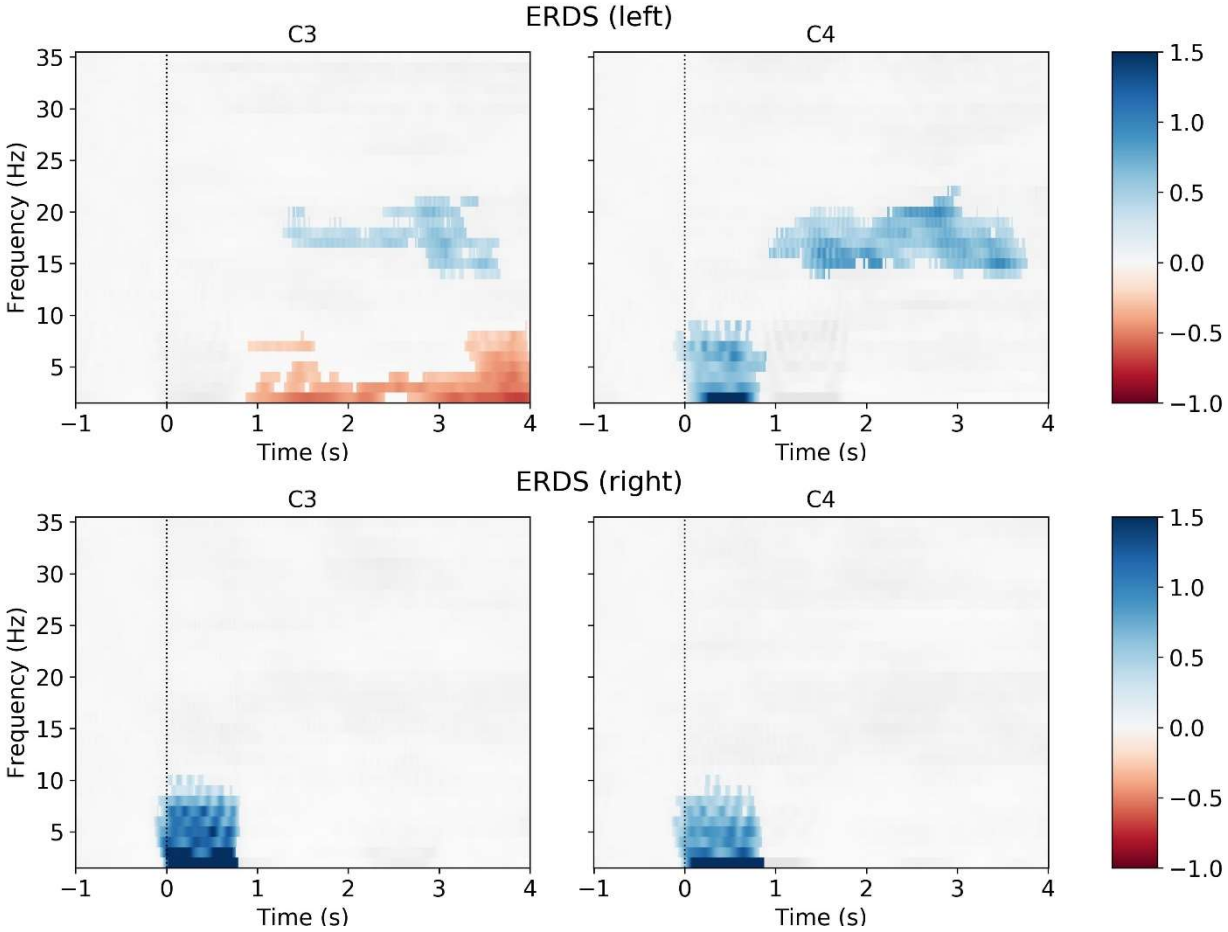

CONTROL – 4 – TRAINING

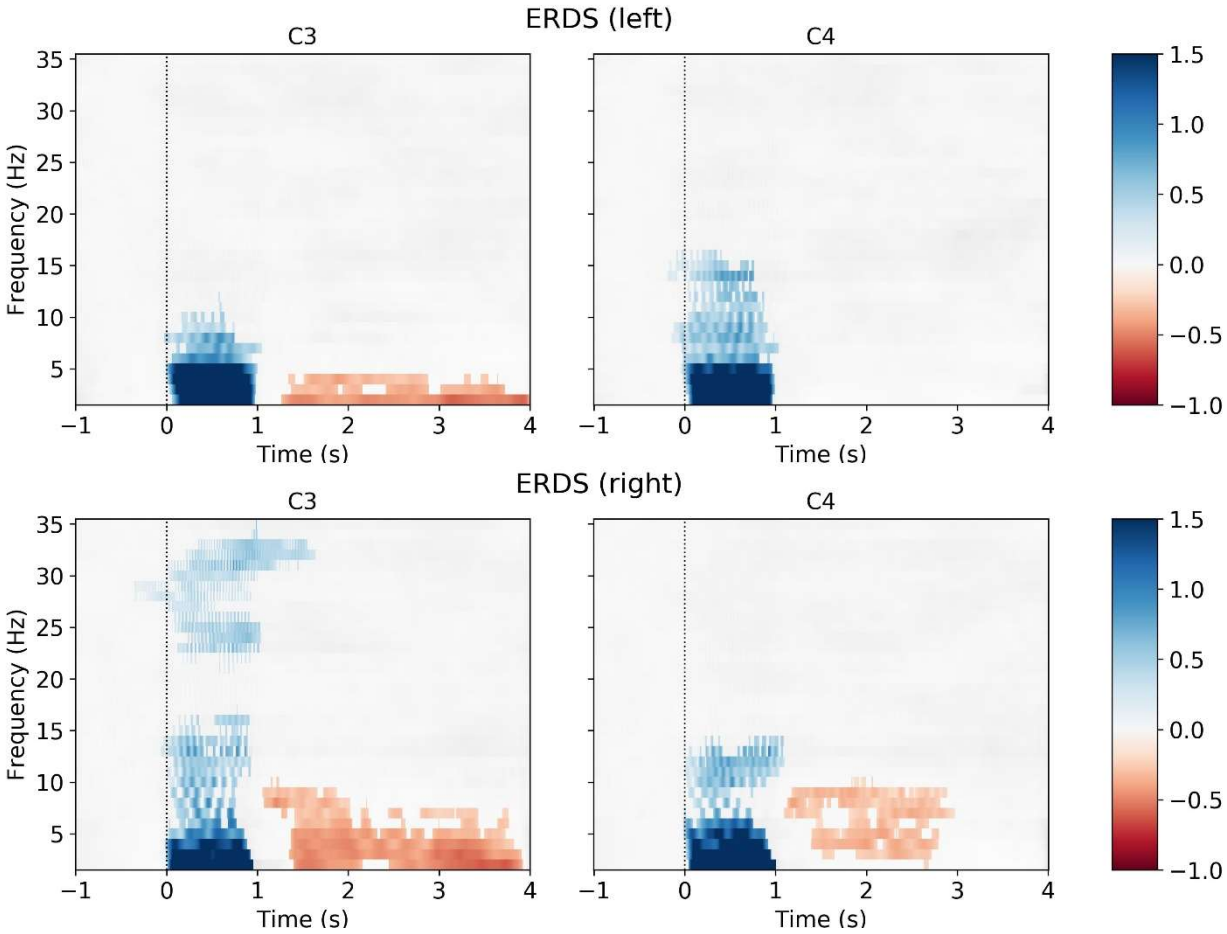

CONTROL – 4 – TESTING

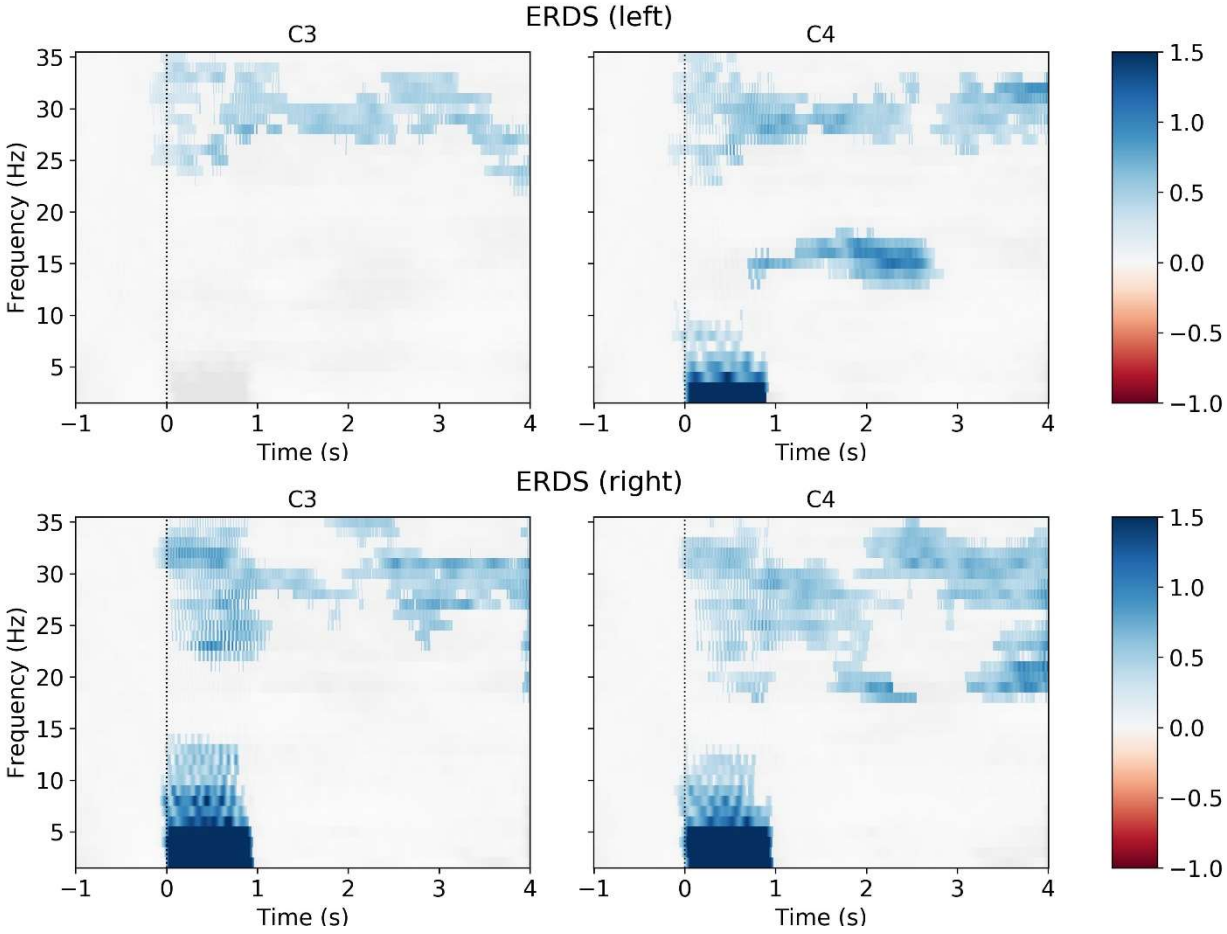

CONTROL –5 – TRAINING

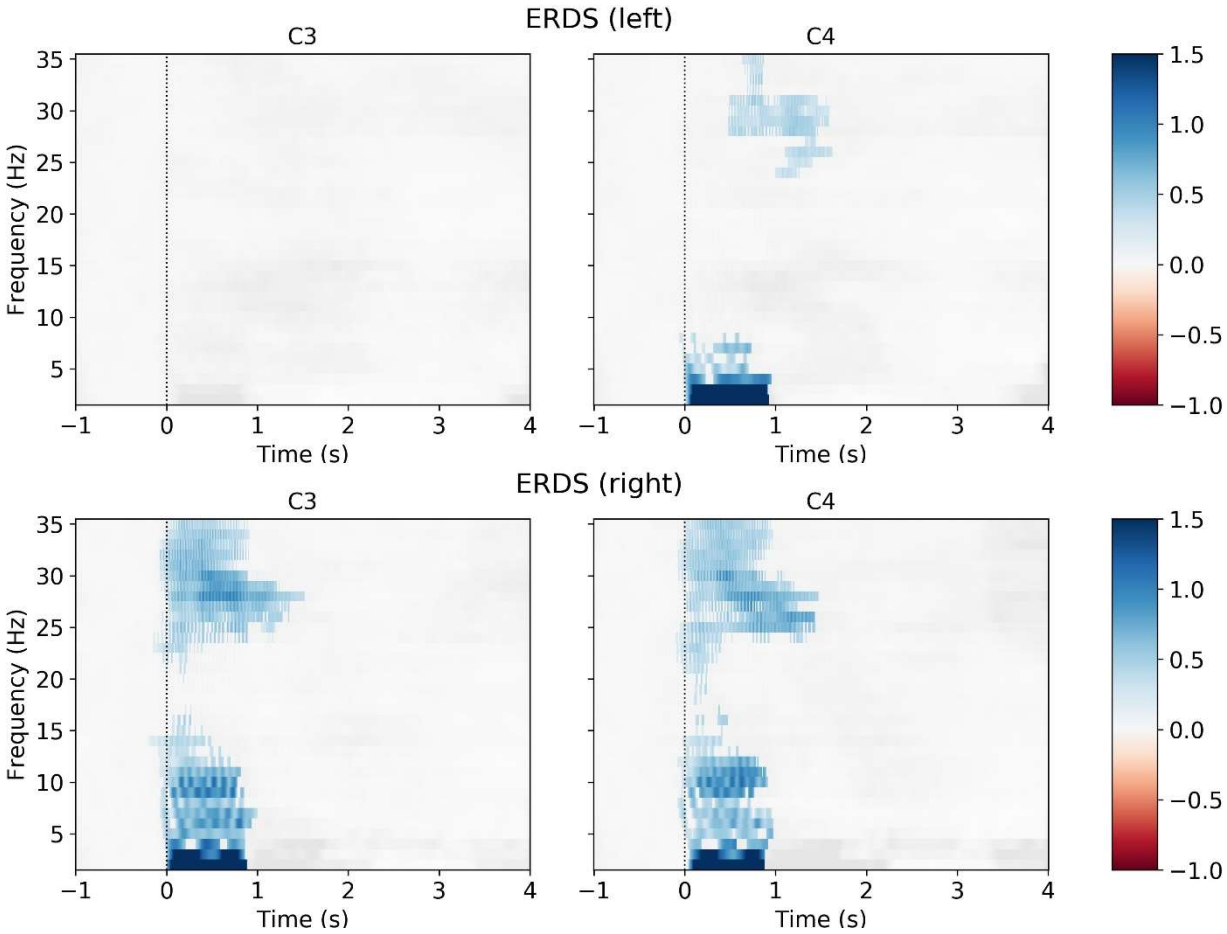

CONTROL – 5 – TESTING

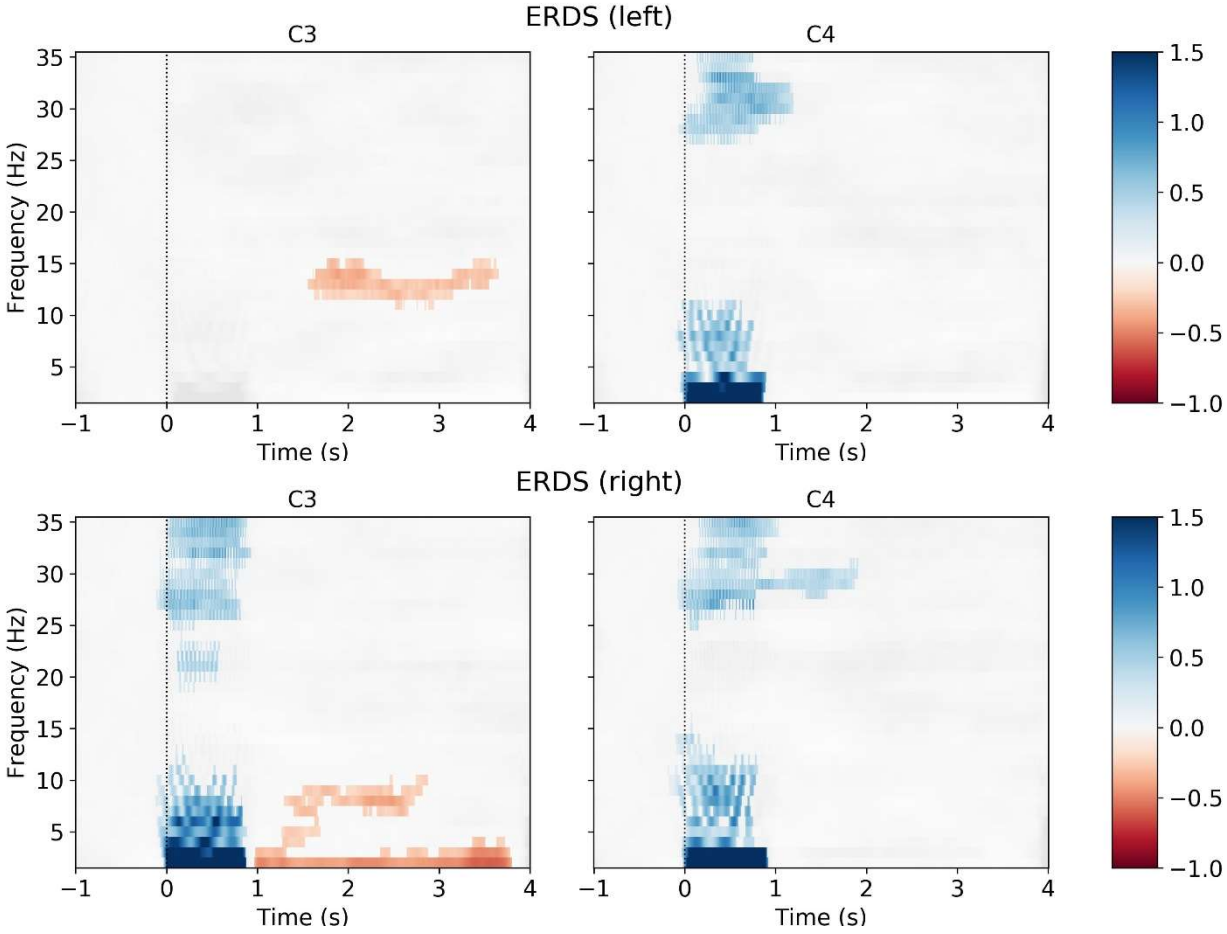

CONTROL – 6 – TRAINING

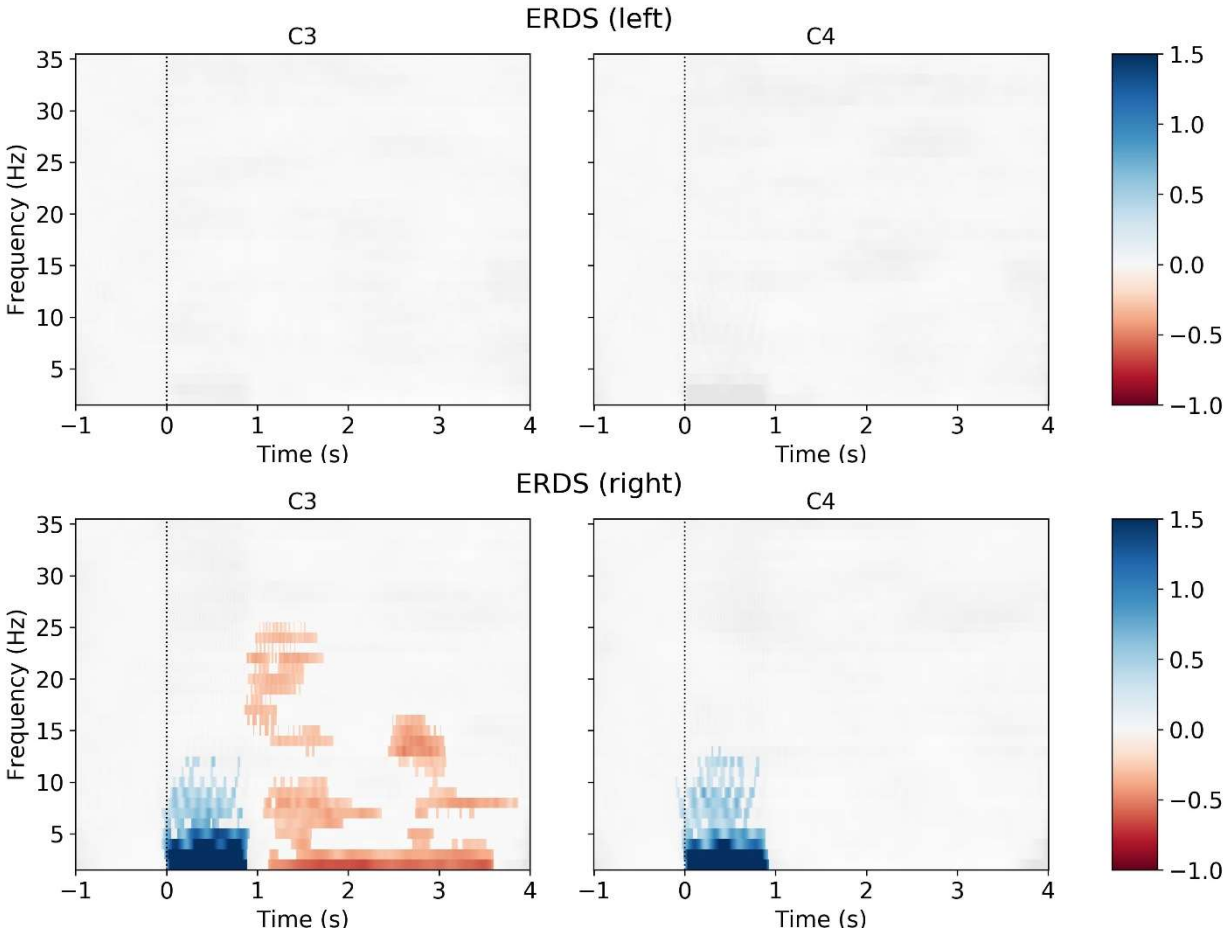

CONTROL – 6 – TESTING

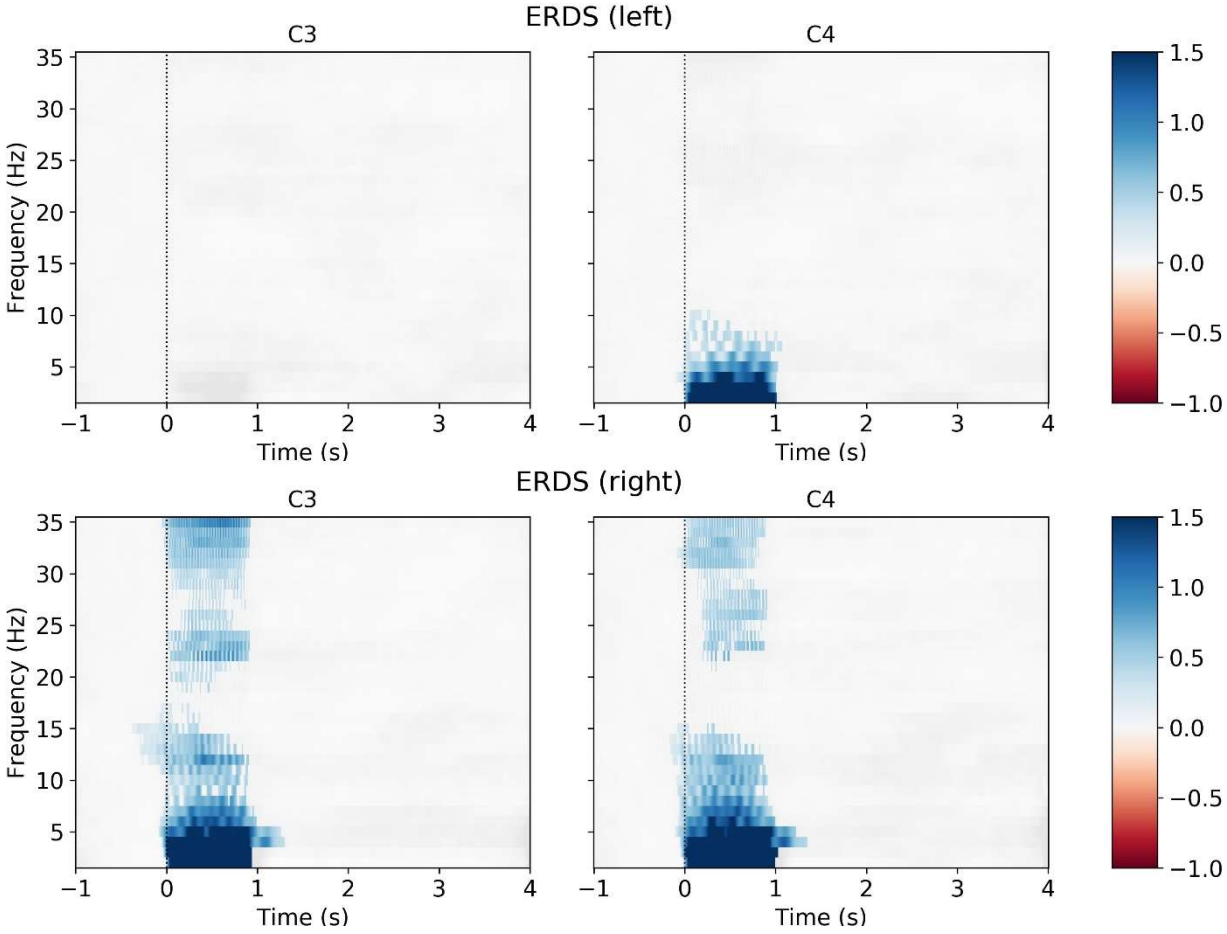

CONTROL – 7 – TRAINING

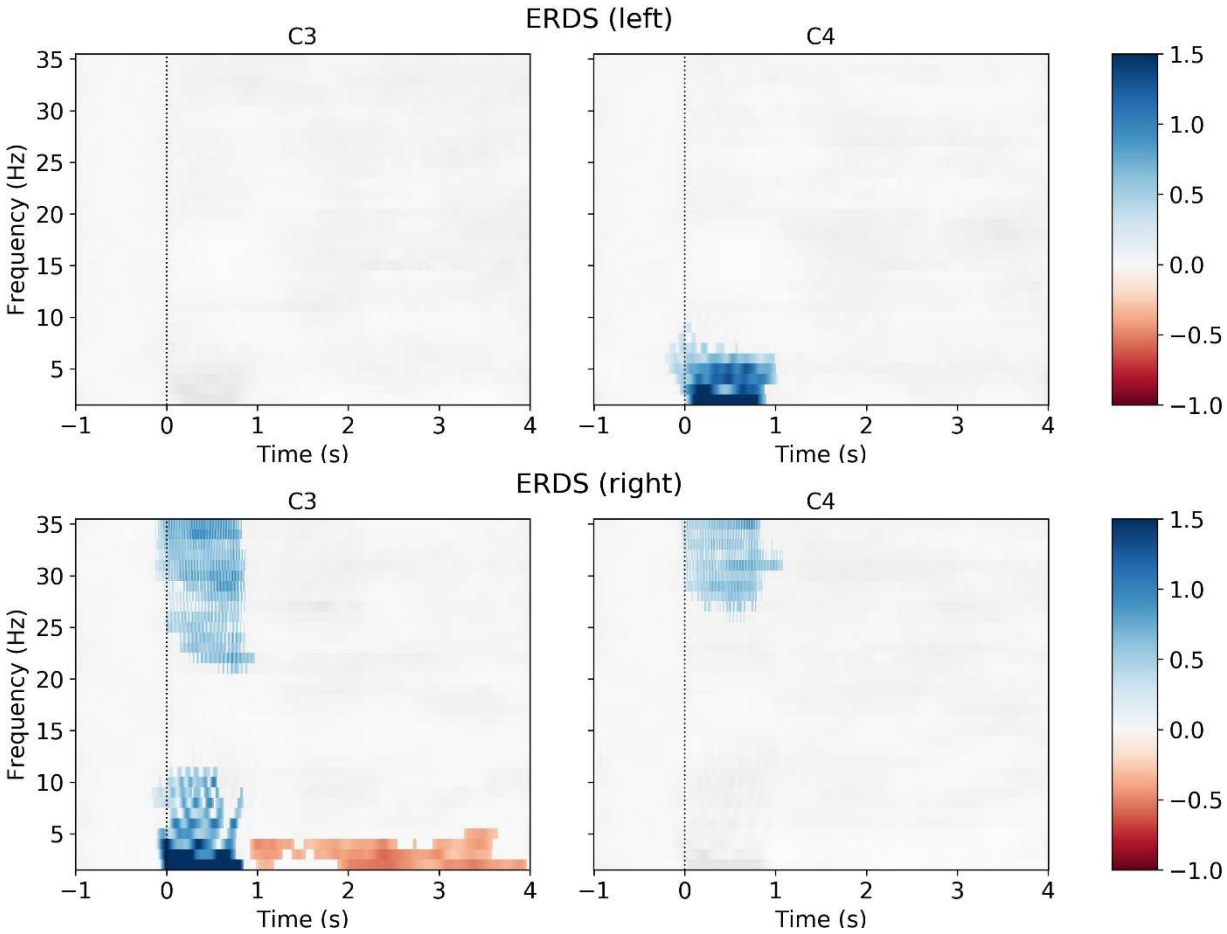

CONTROL – 7 – TESTING

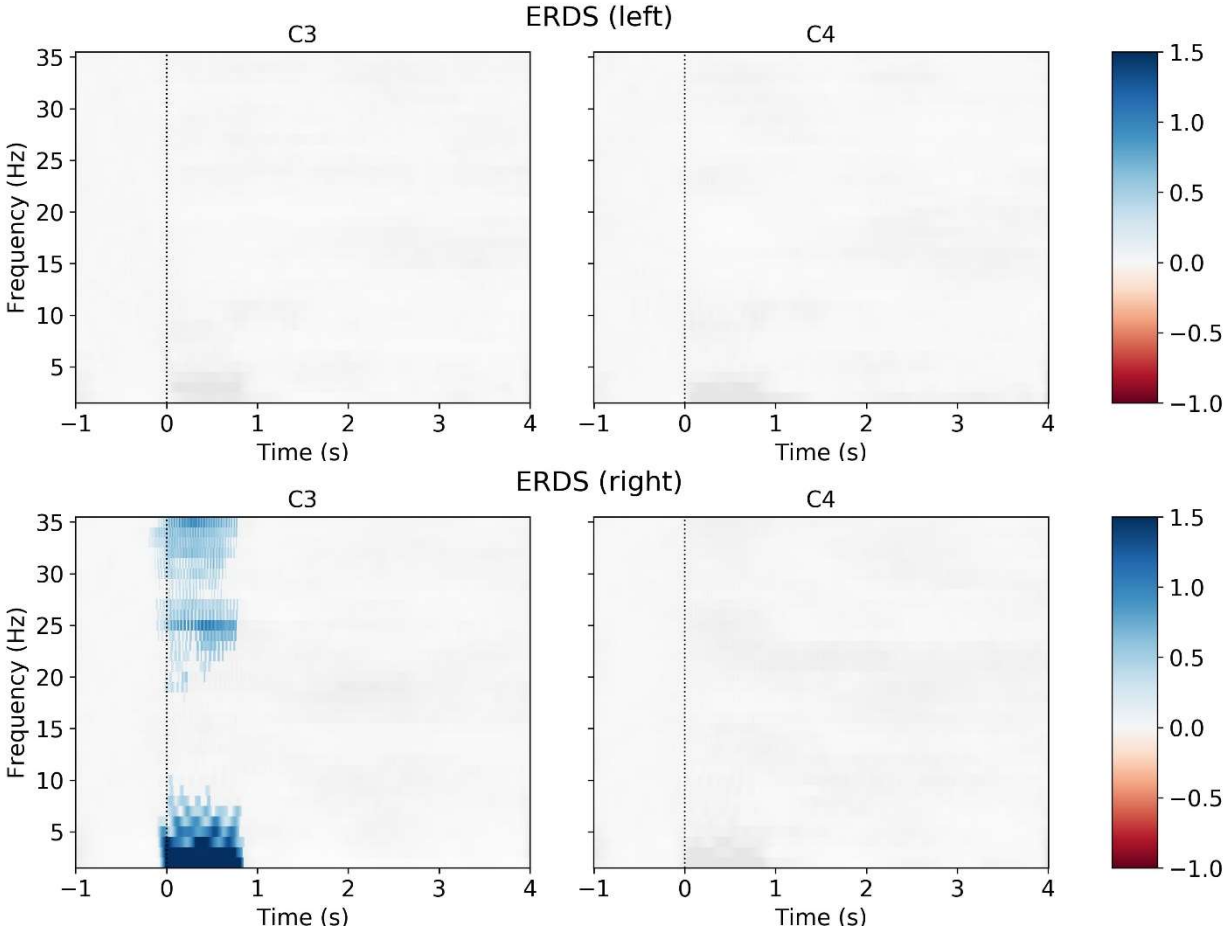

CONTROL – 8 – TRAINING

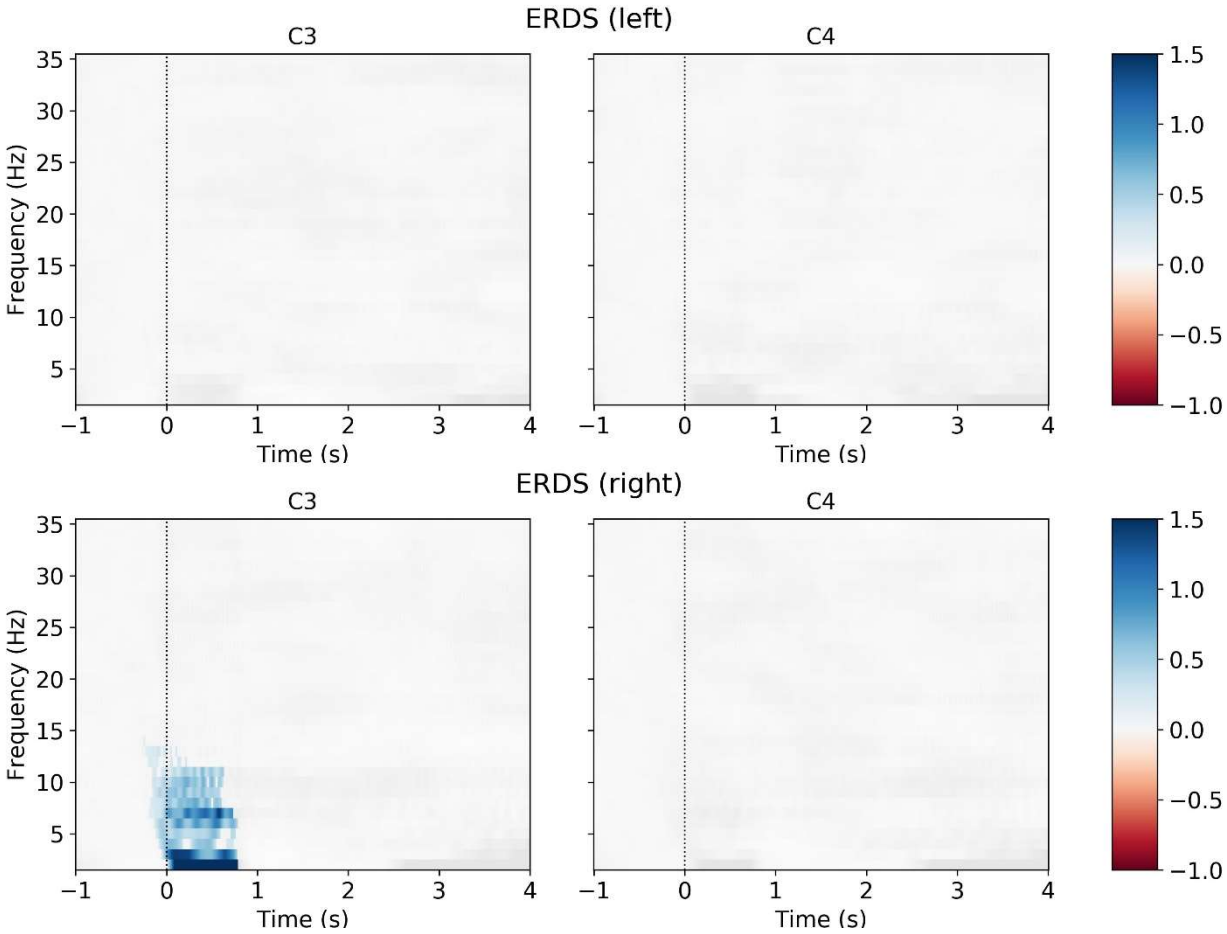

CONTROL – 8 – TESTING

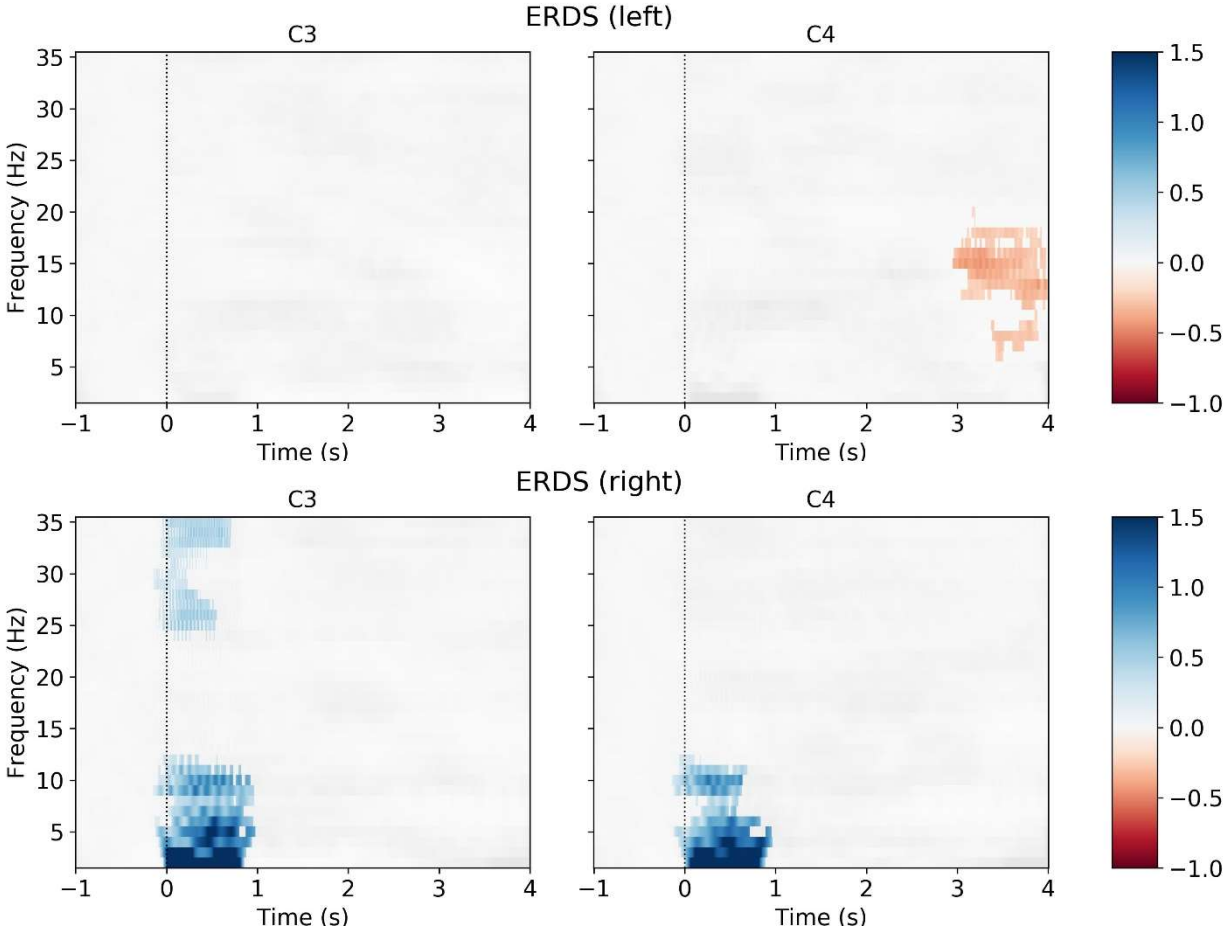

VR – 1 – TRAINING

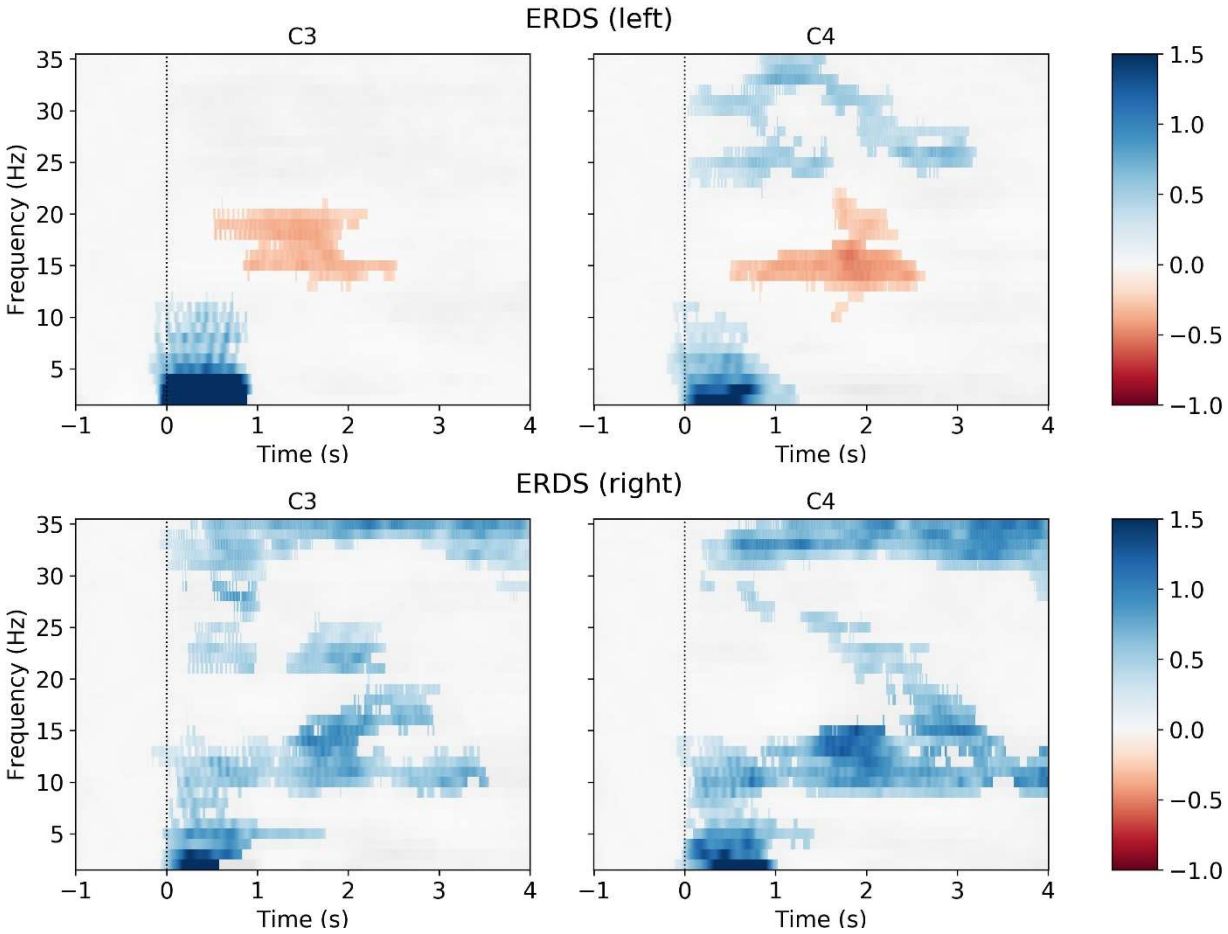

VR – 1 – TESTING

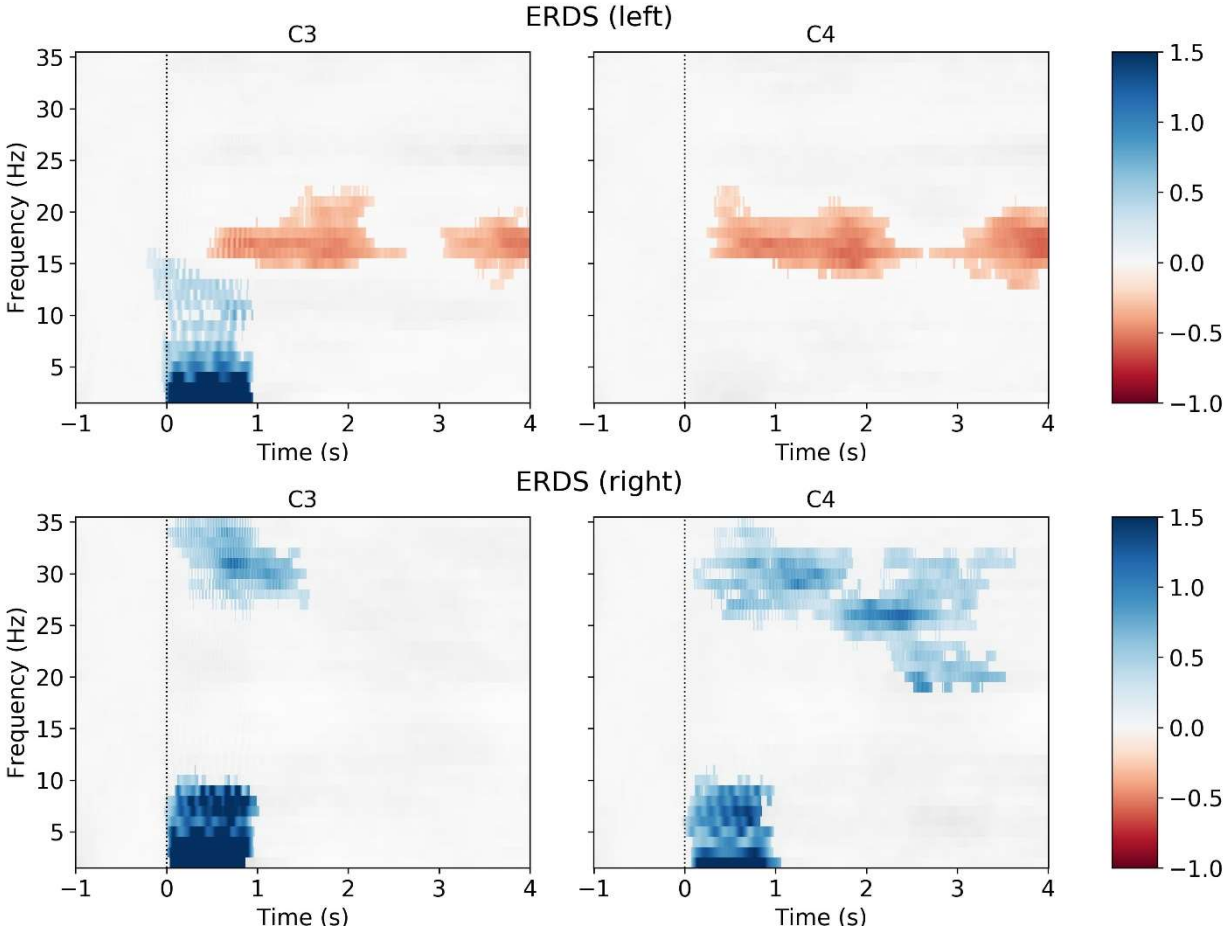

VR – 2 – TRAINING

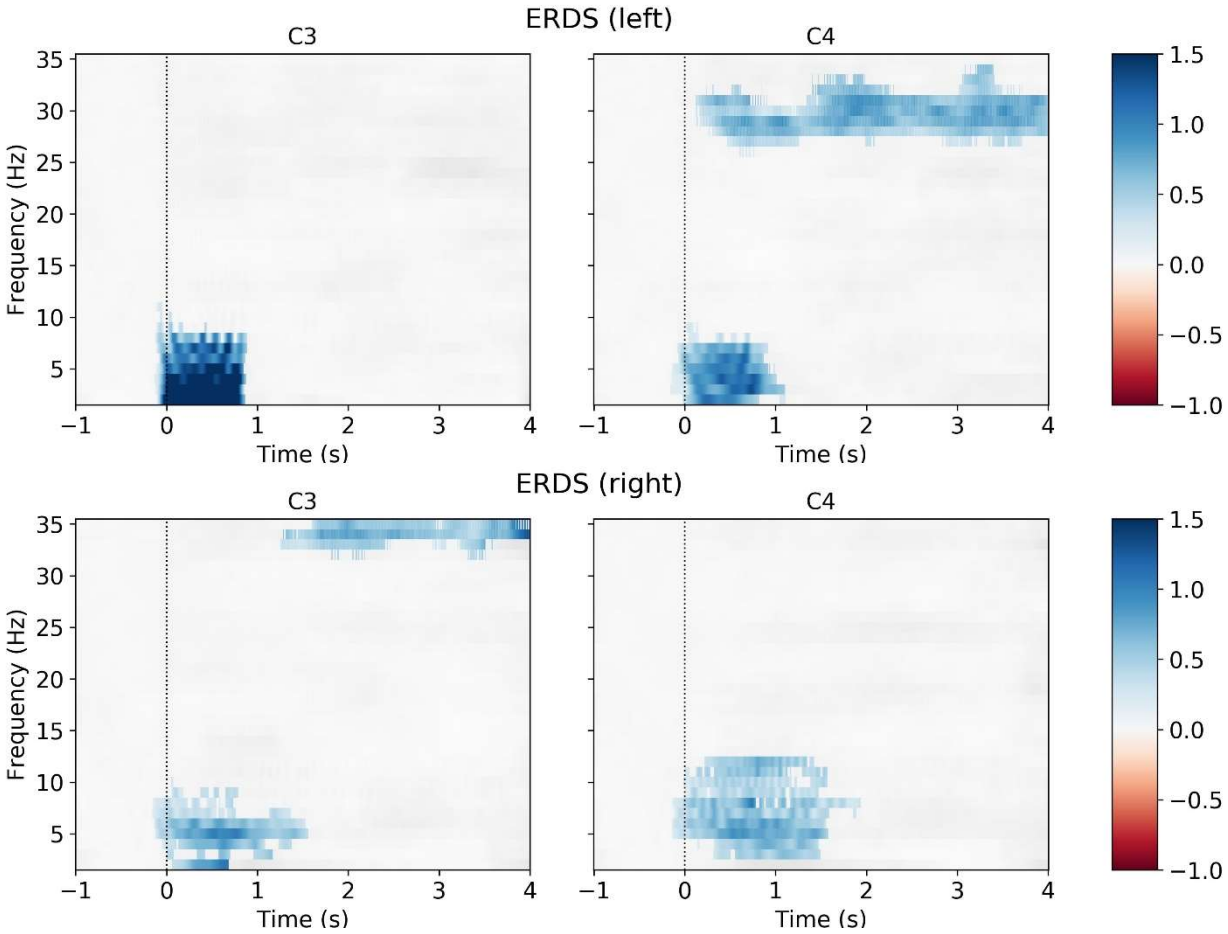

VR – 2 – TESTING

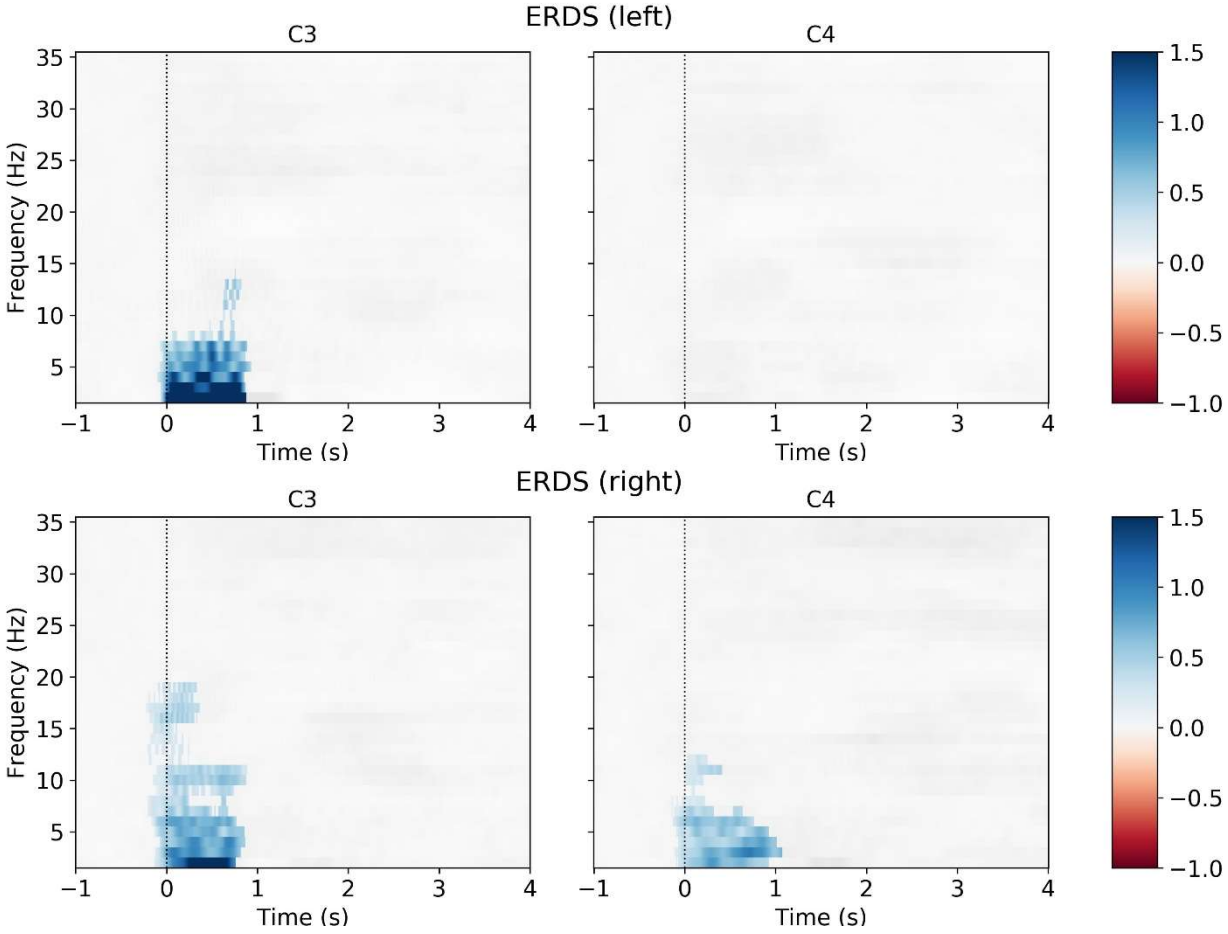

VR – 3 – TRAINING

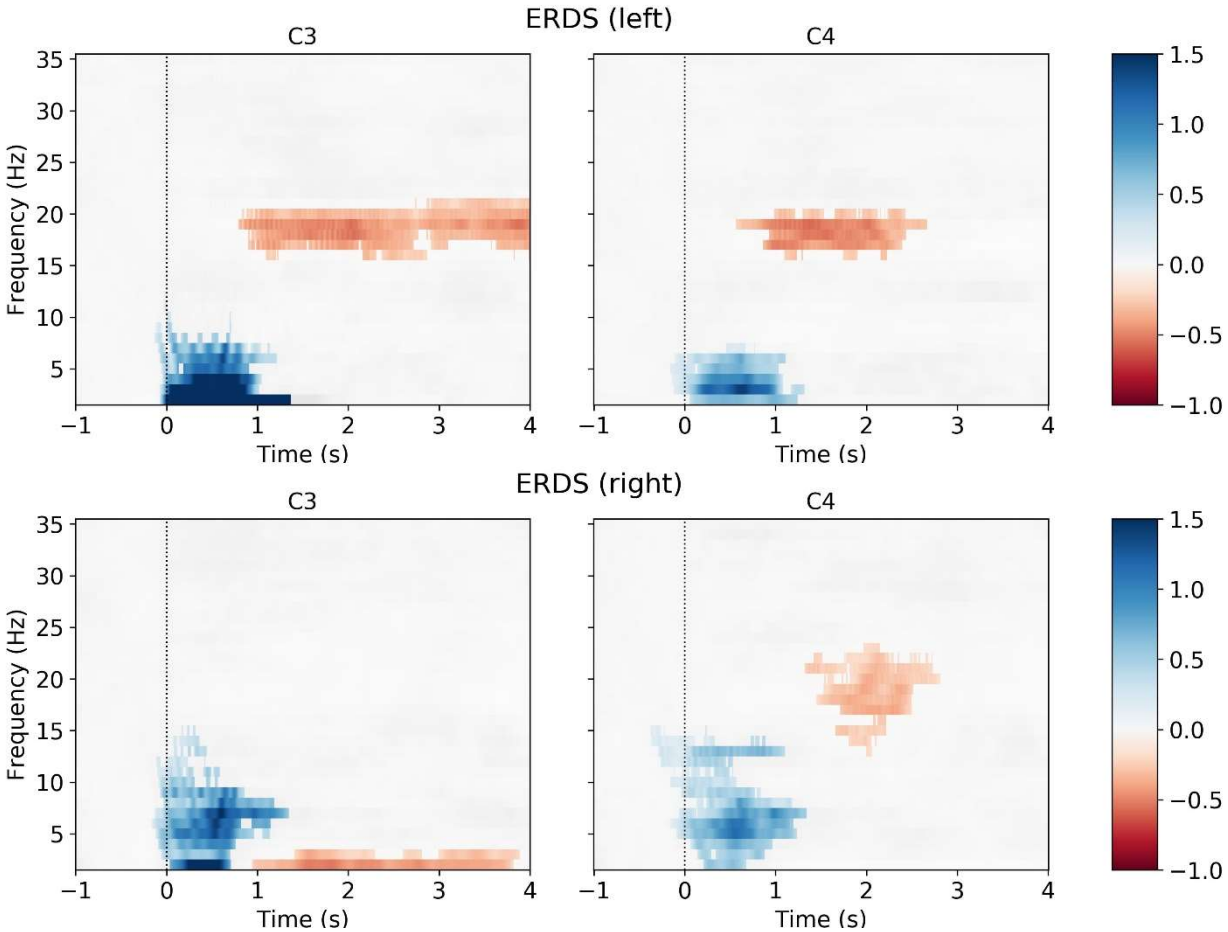

VR – 4 – TRAINING

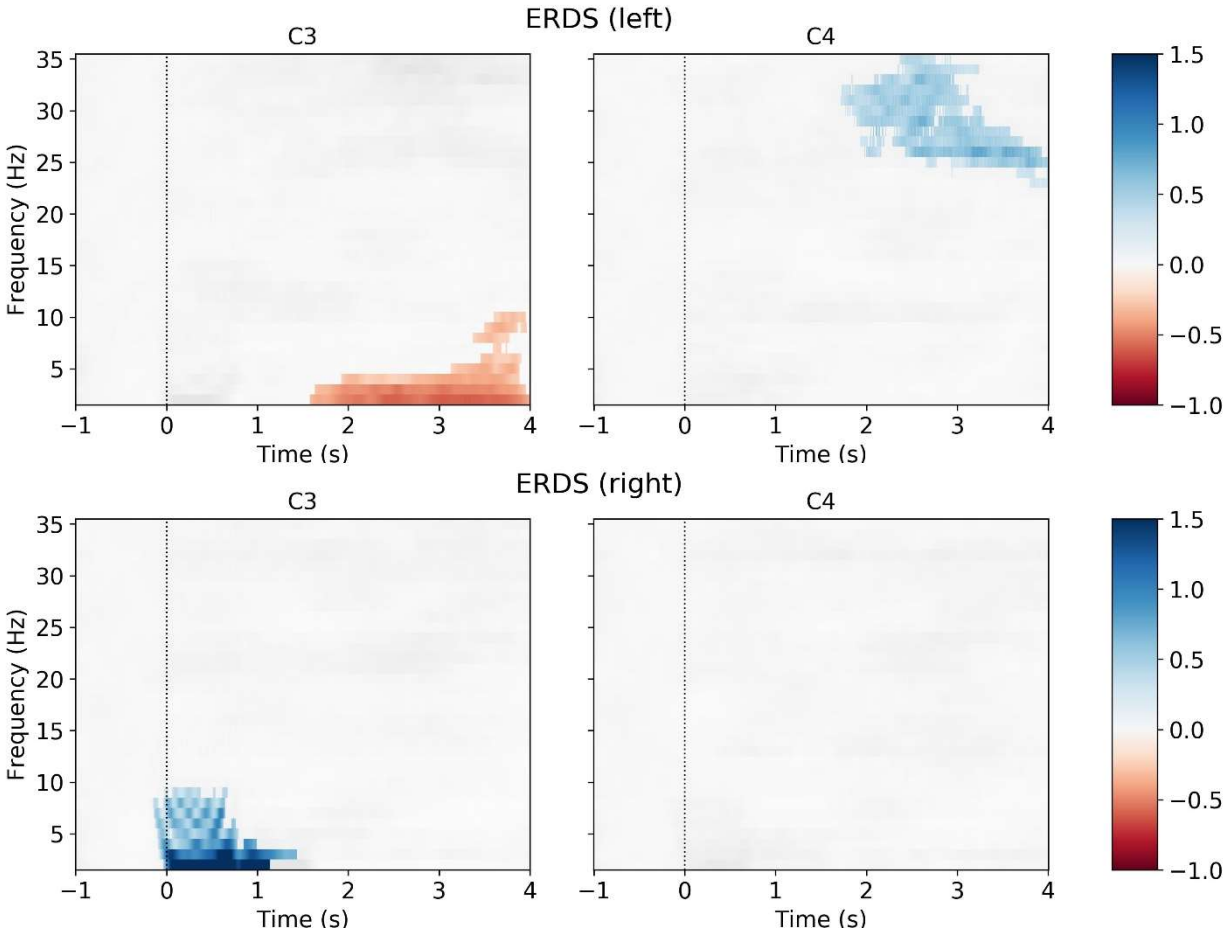

VR – 4 – TESTING

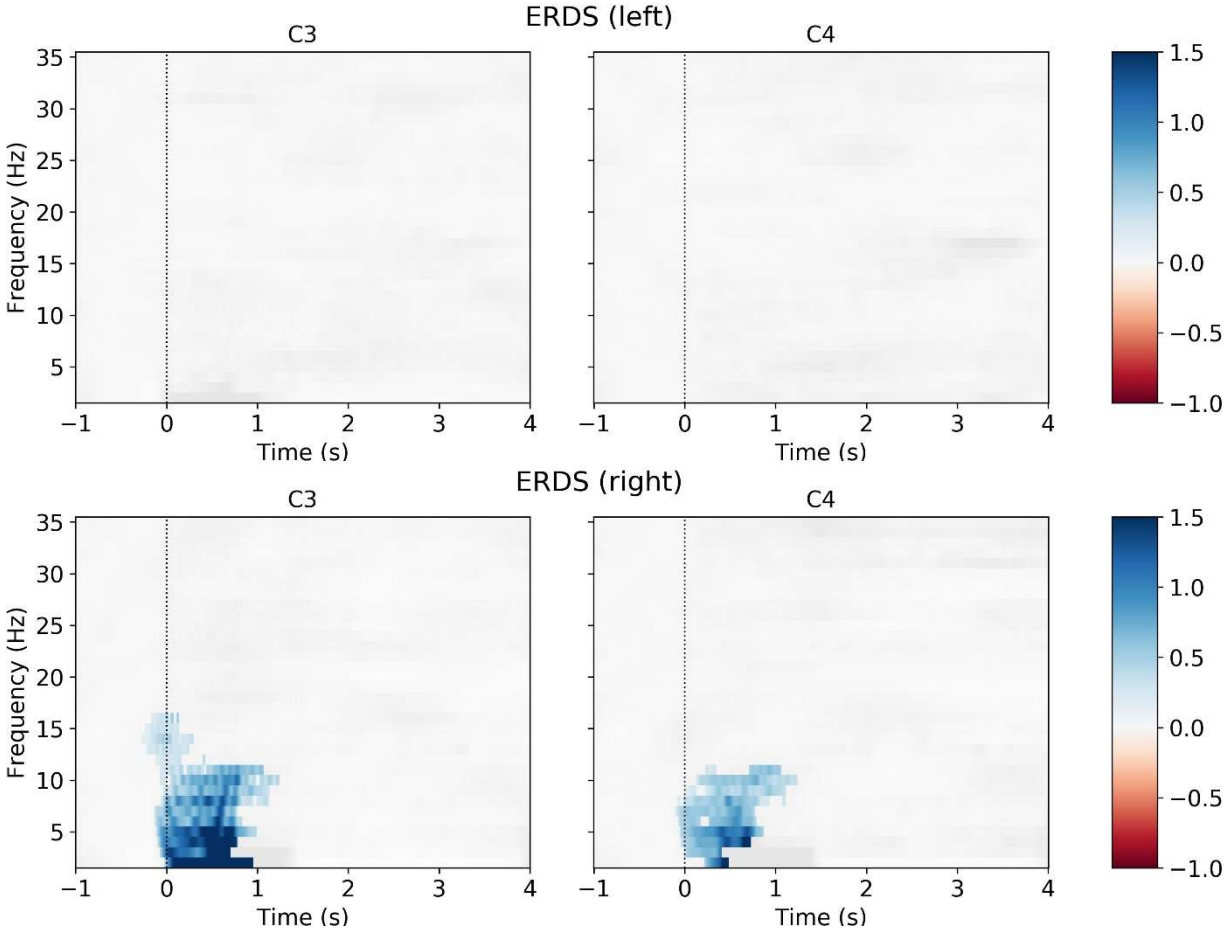

VR – 5 – TRAINING

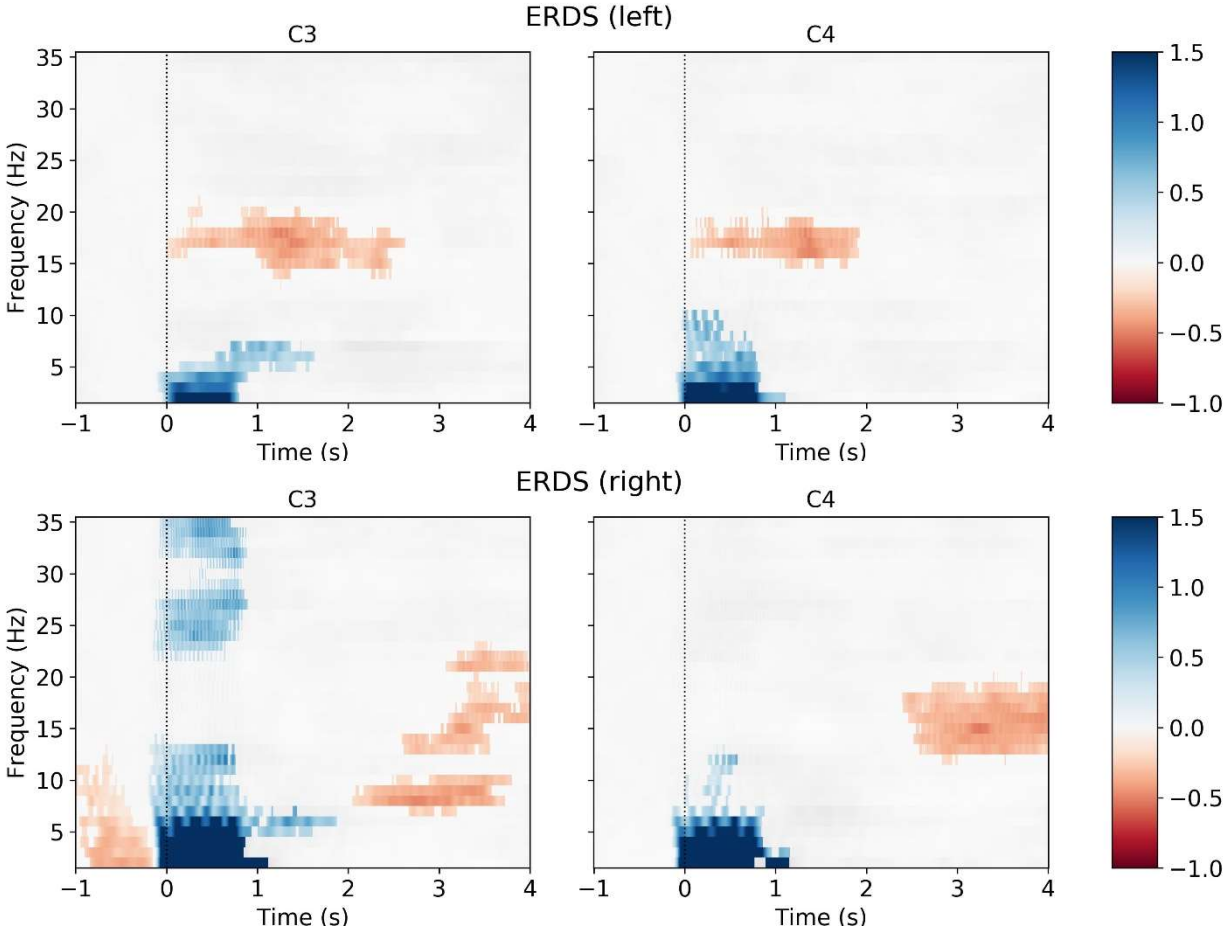

VR – 5 – TESTING

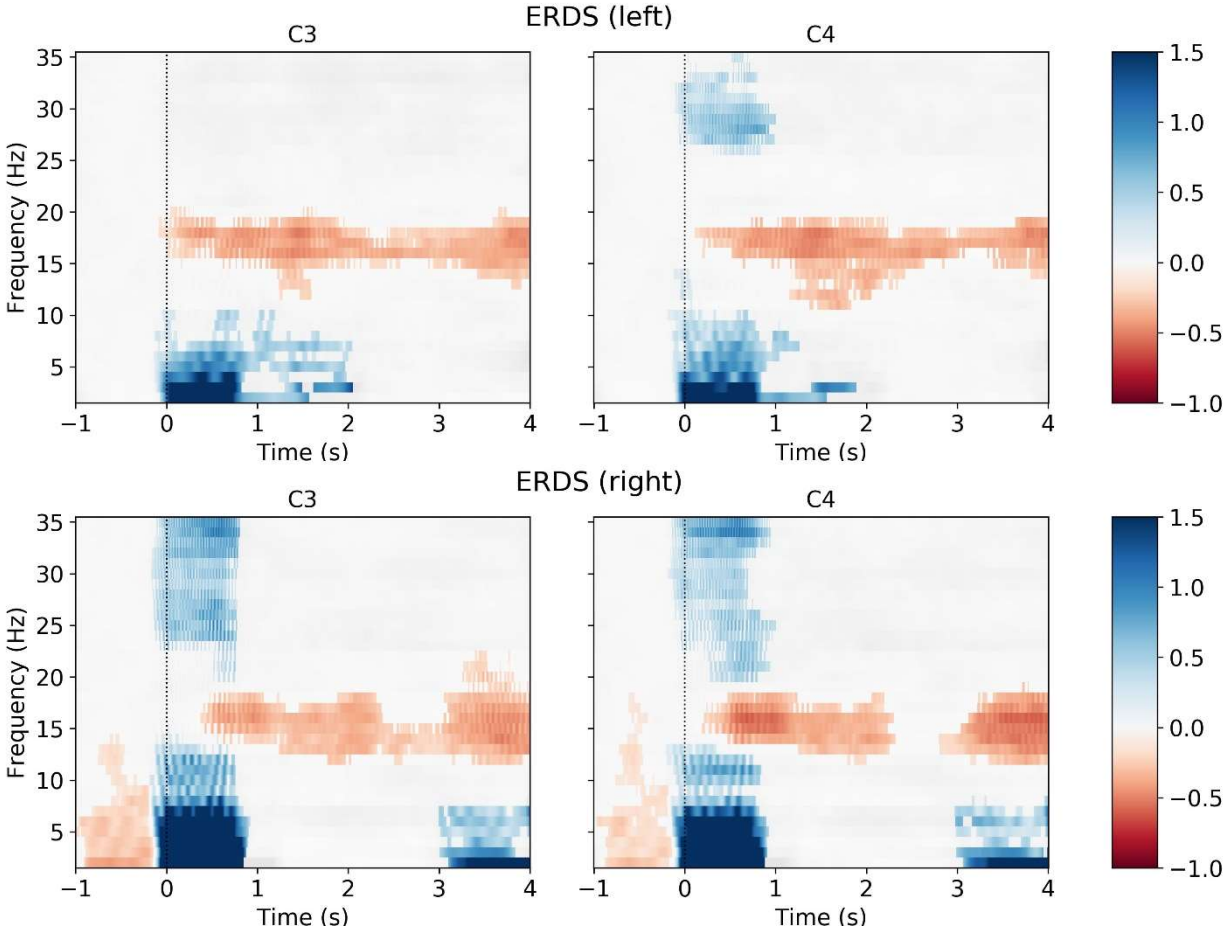

VR – 6 – TRAINING

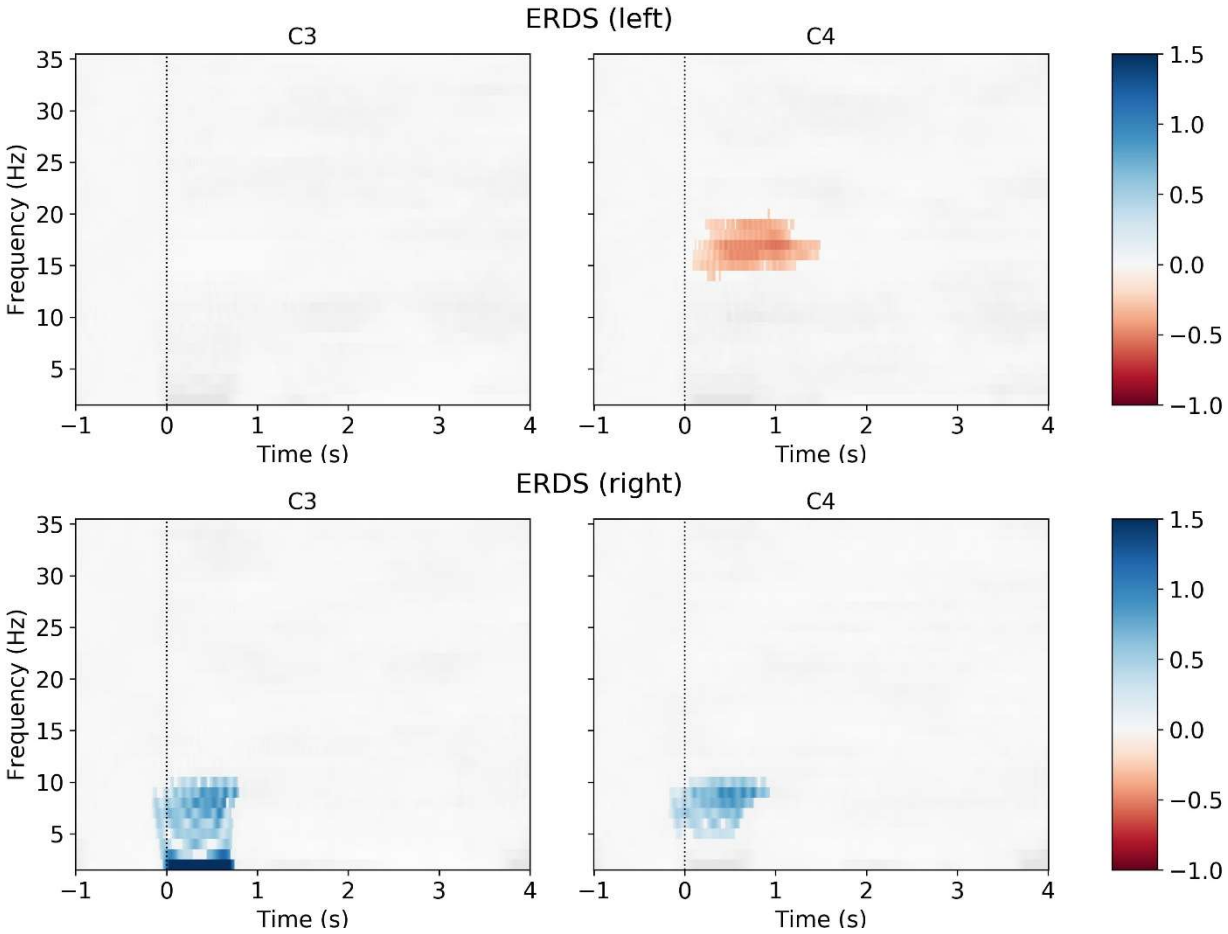

VR – 6 – TESTING

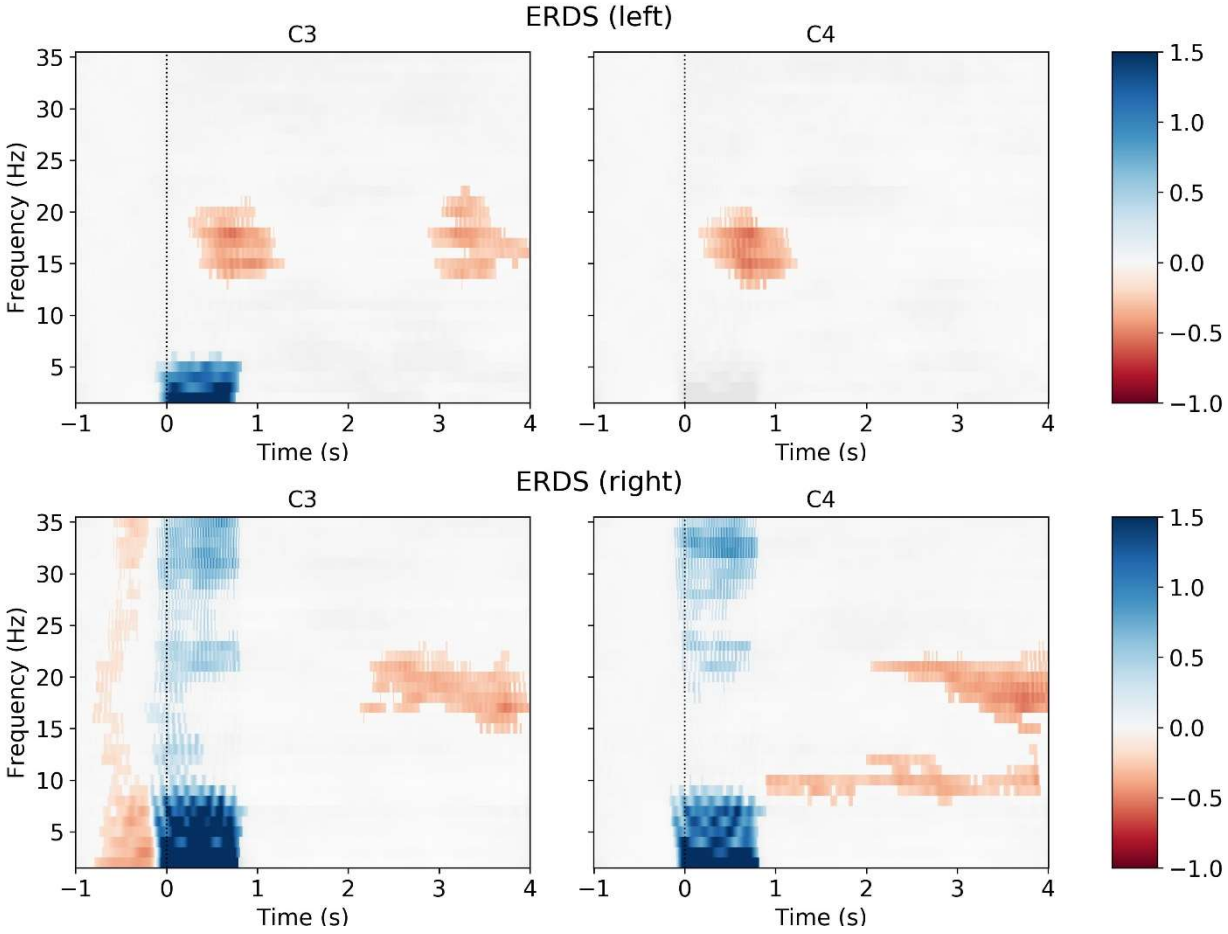

VR – 7 – TRAINING

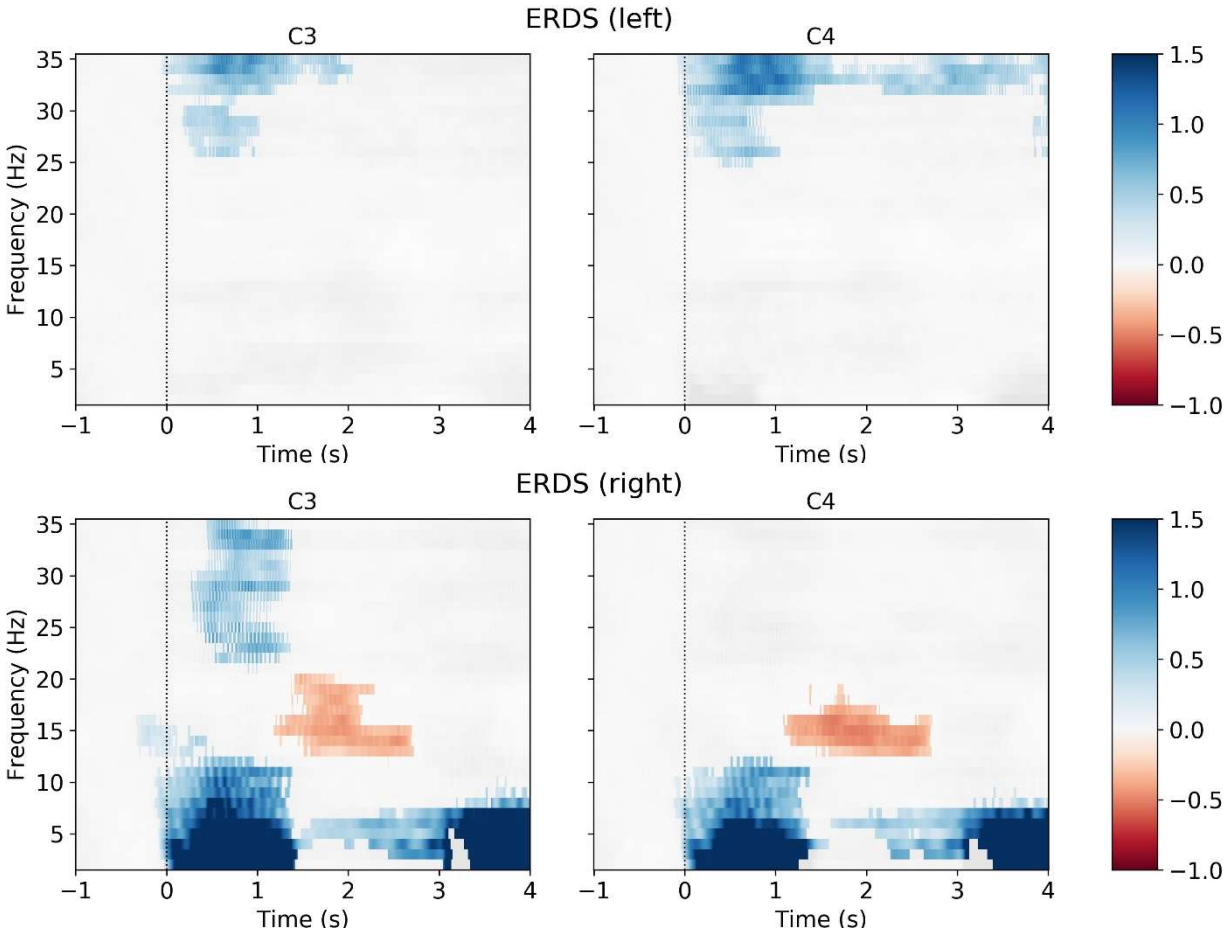

VR – 7 – TESTING

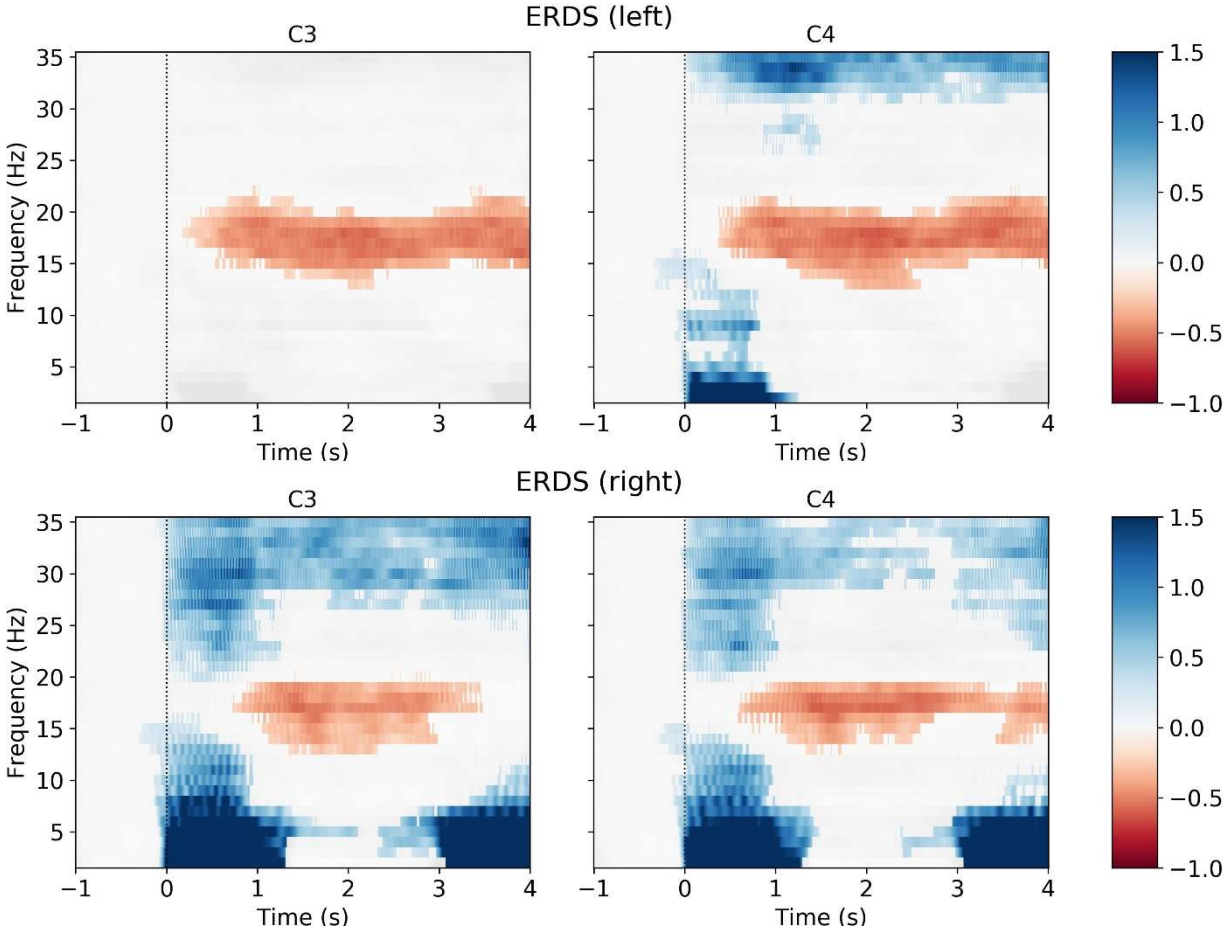

VR – 8 – TRAINING

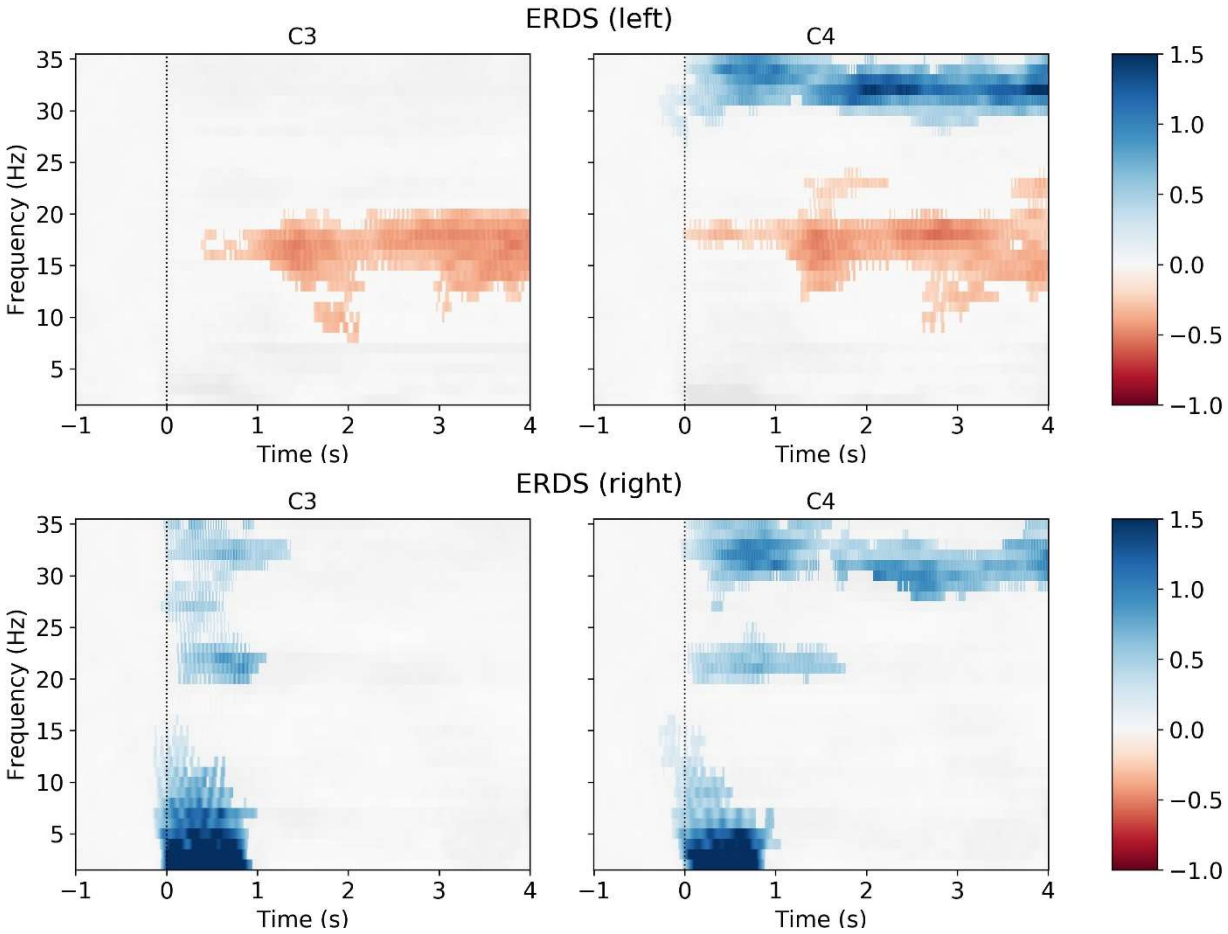

VR – 8 – TESTING

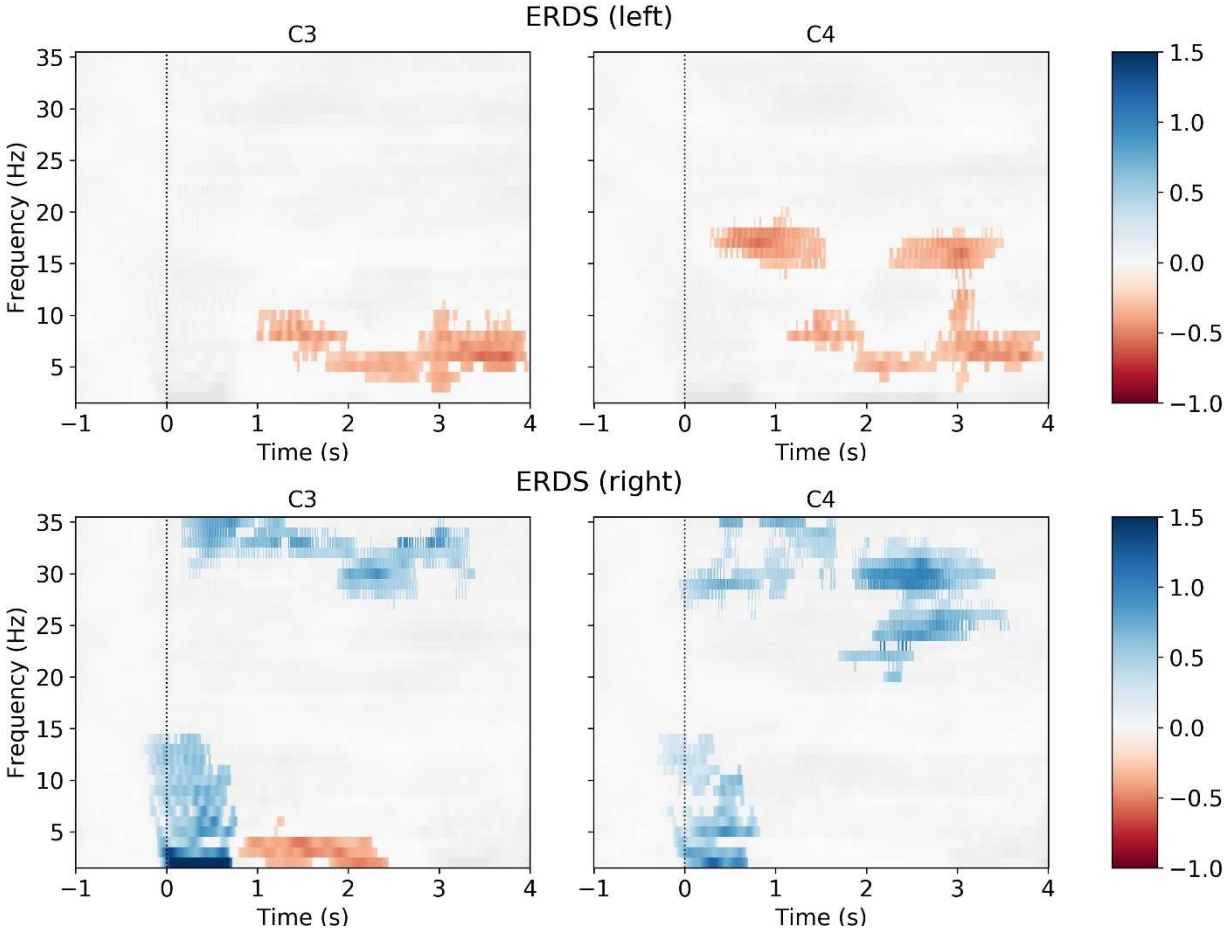

ROBOT – 1 – TRAINING

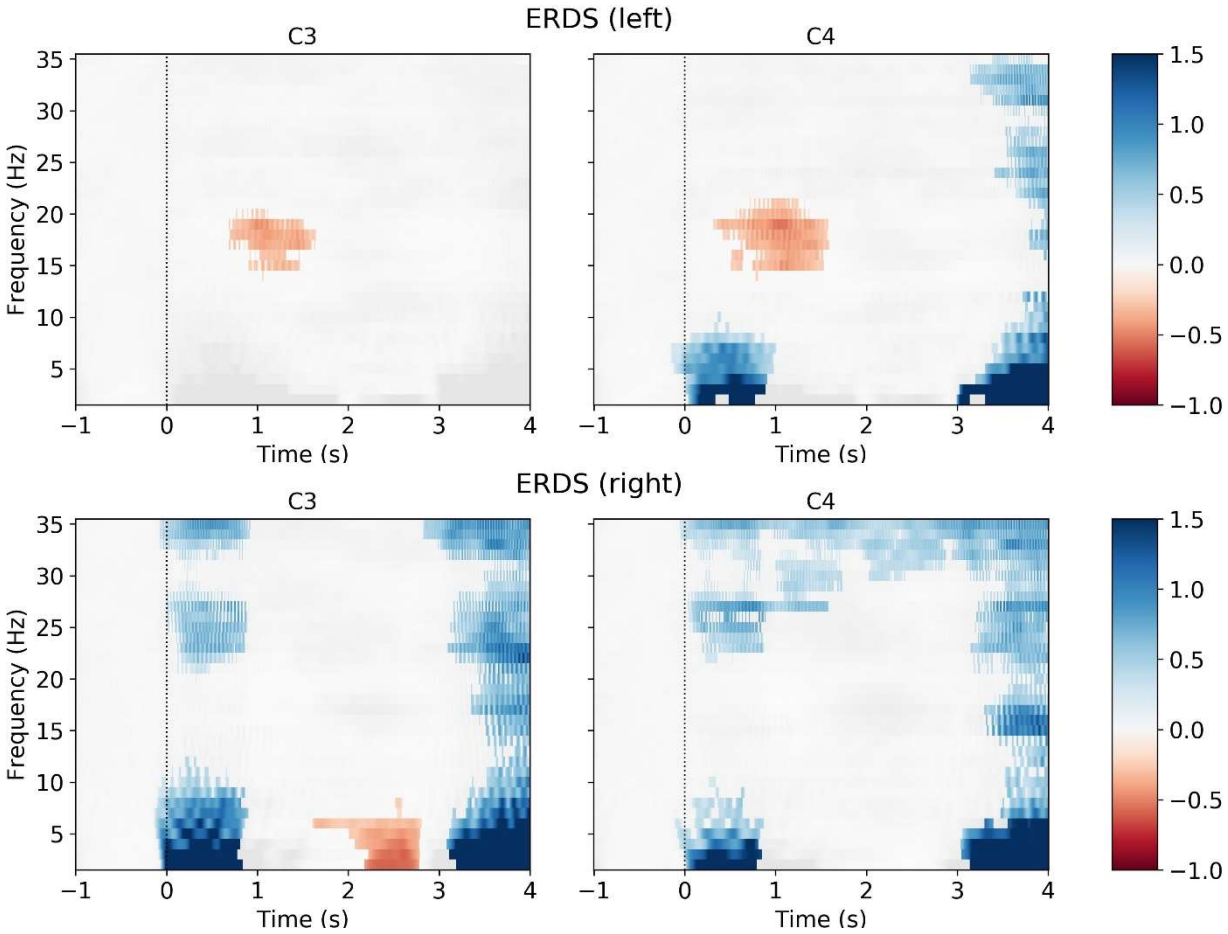

ROBOT – 1 – TESTING

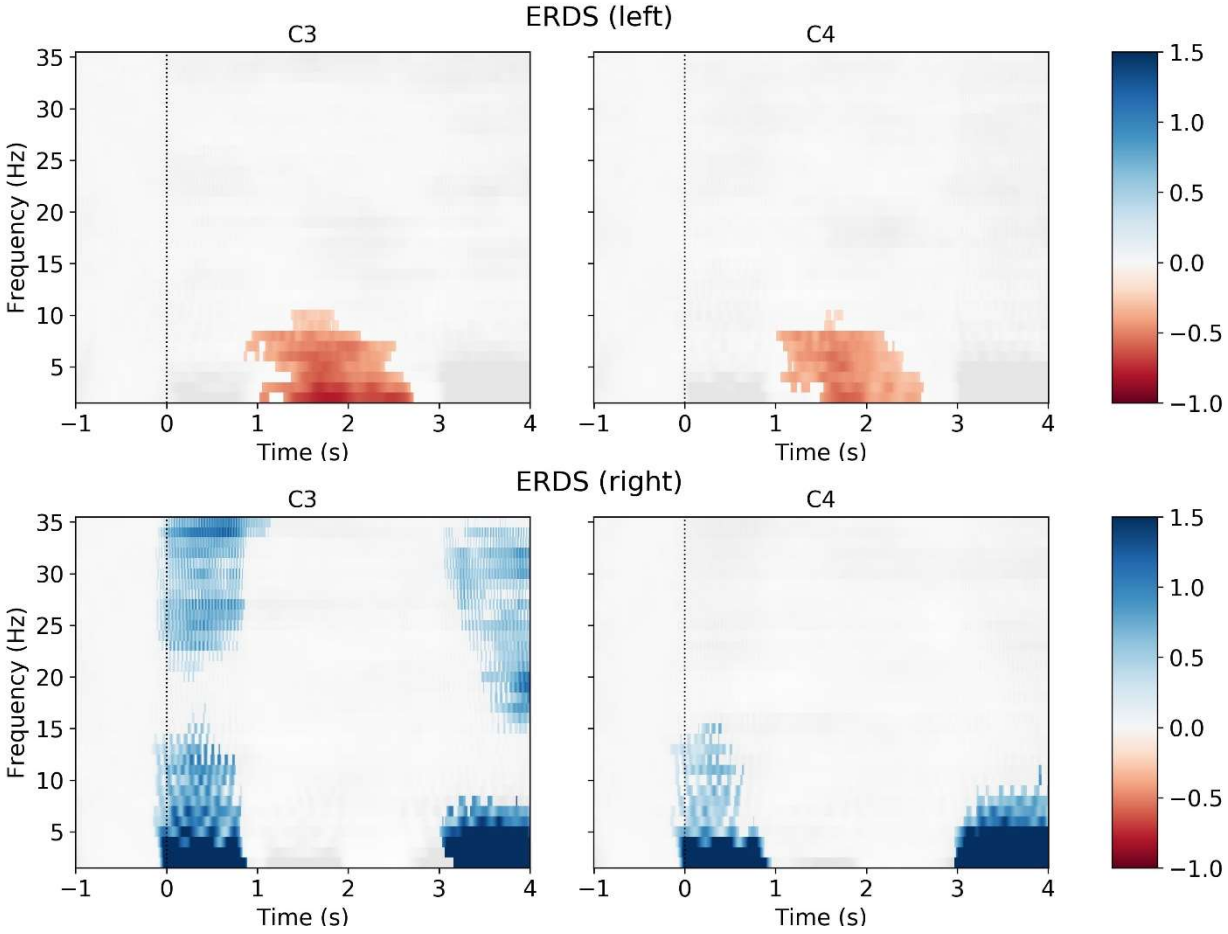

ROBOT – 2 – TRAINING

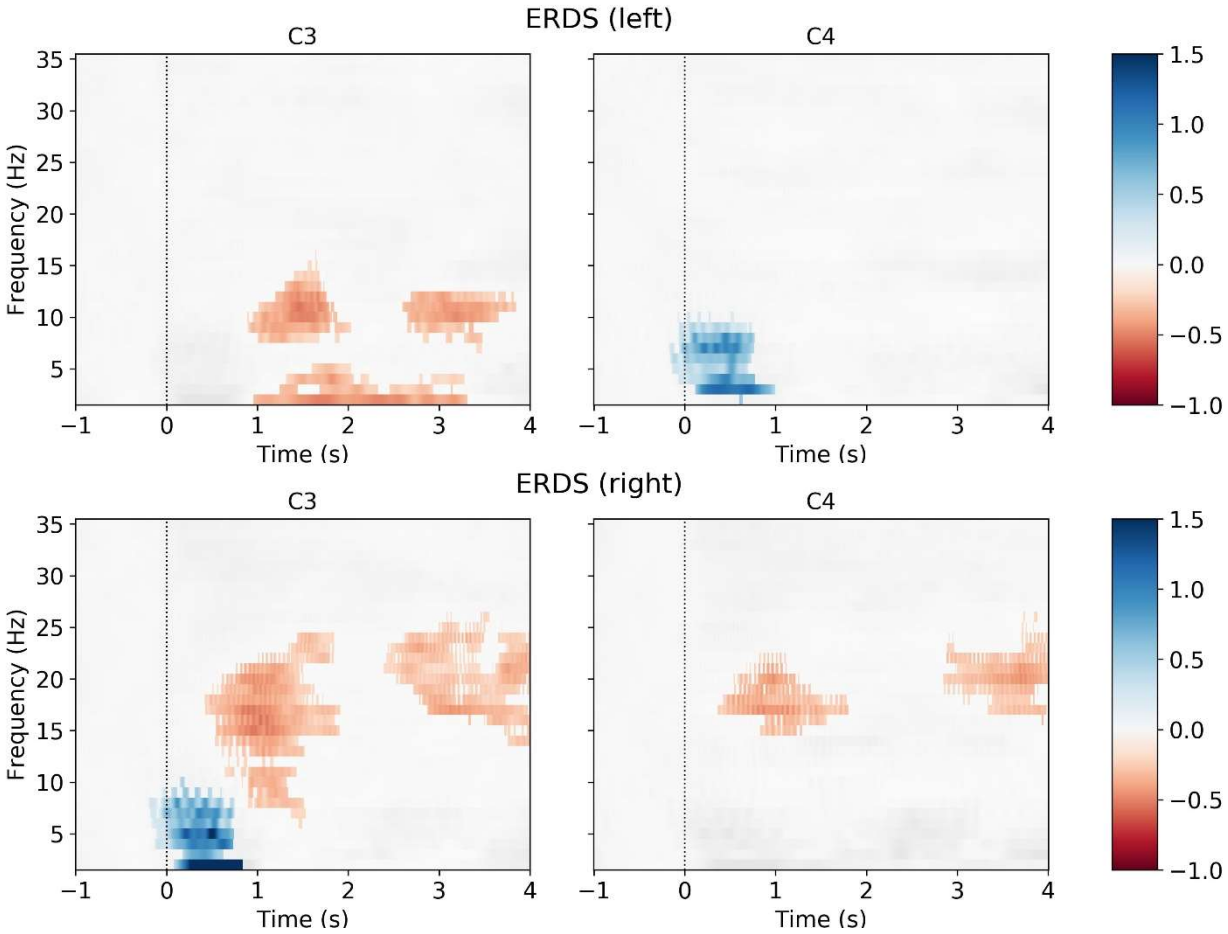

ROBOT – 2 – TESTING

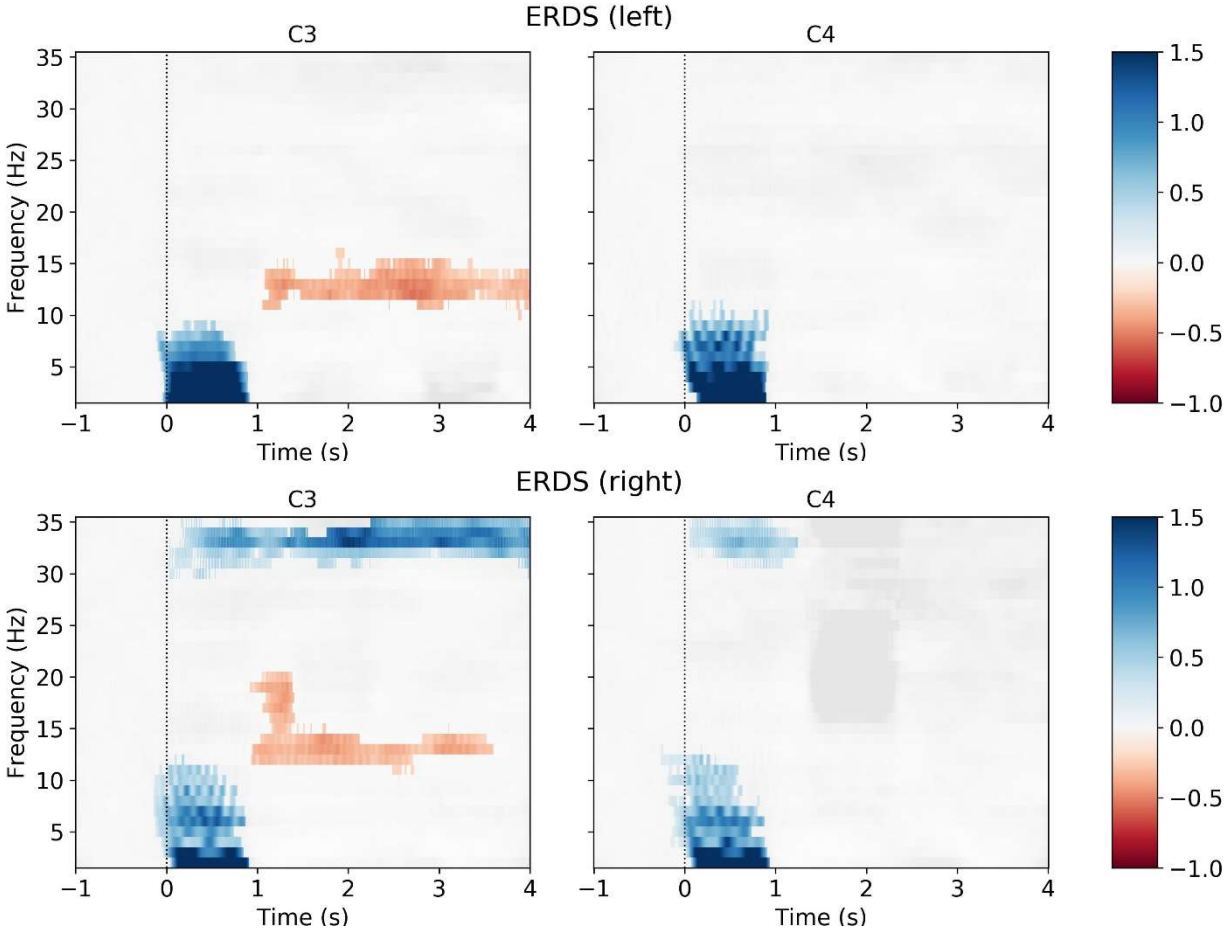

ROBOT – 3 – TRAINING

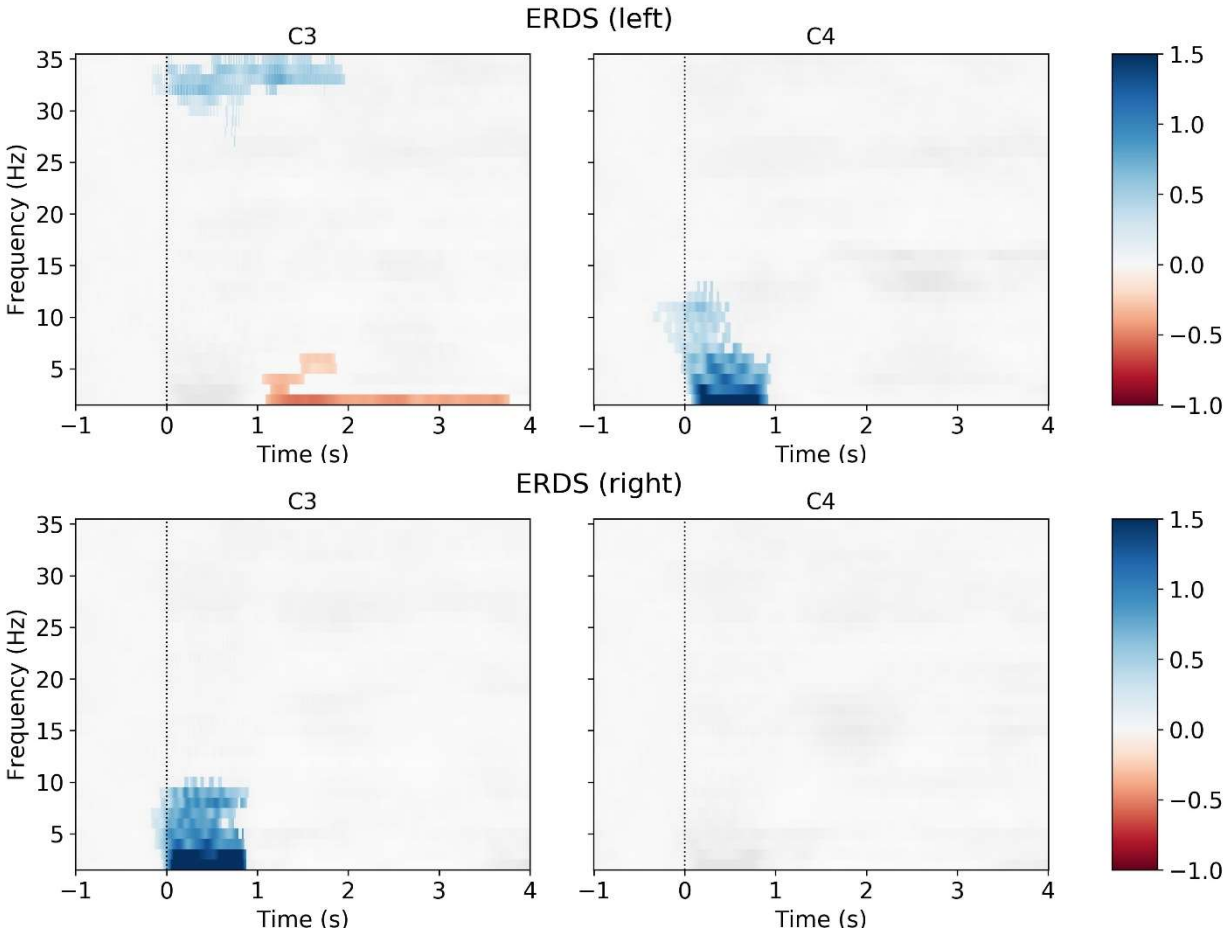

ROBOT – 3 – TESTING

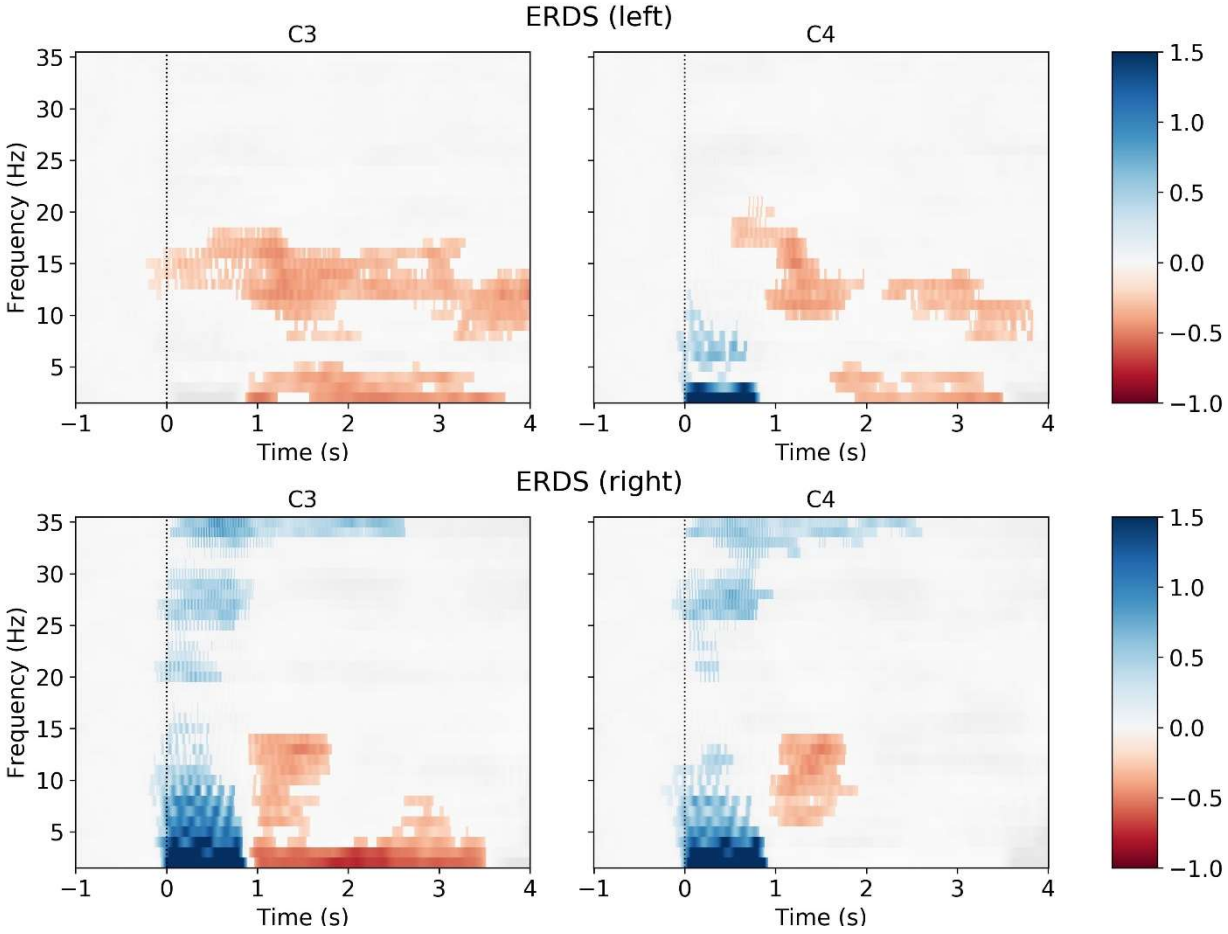

ROBOT – 4 – TRAINING

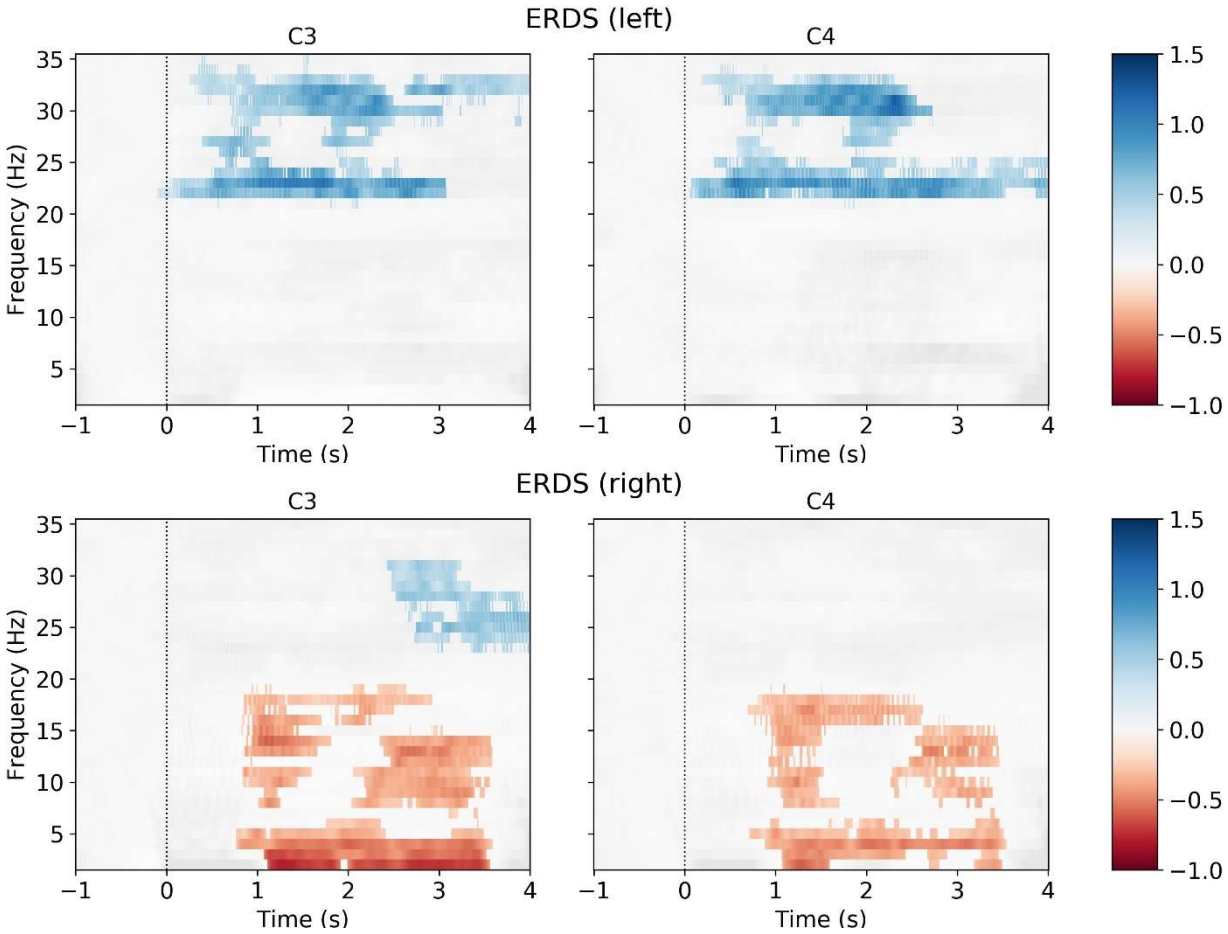

ROBOT – 4 – TESTING

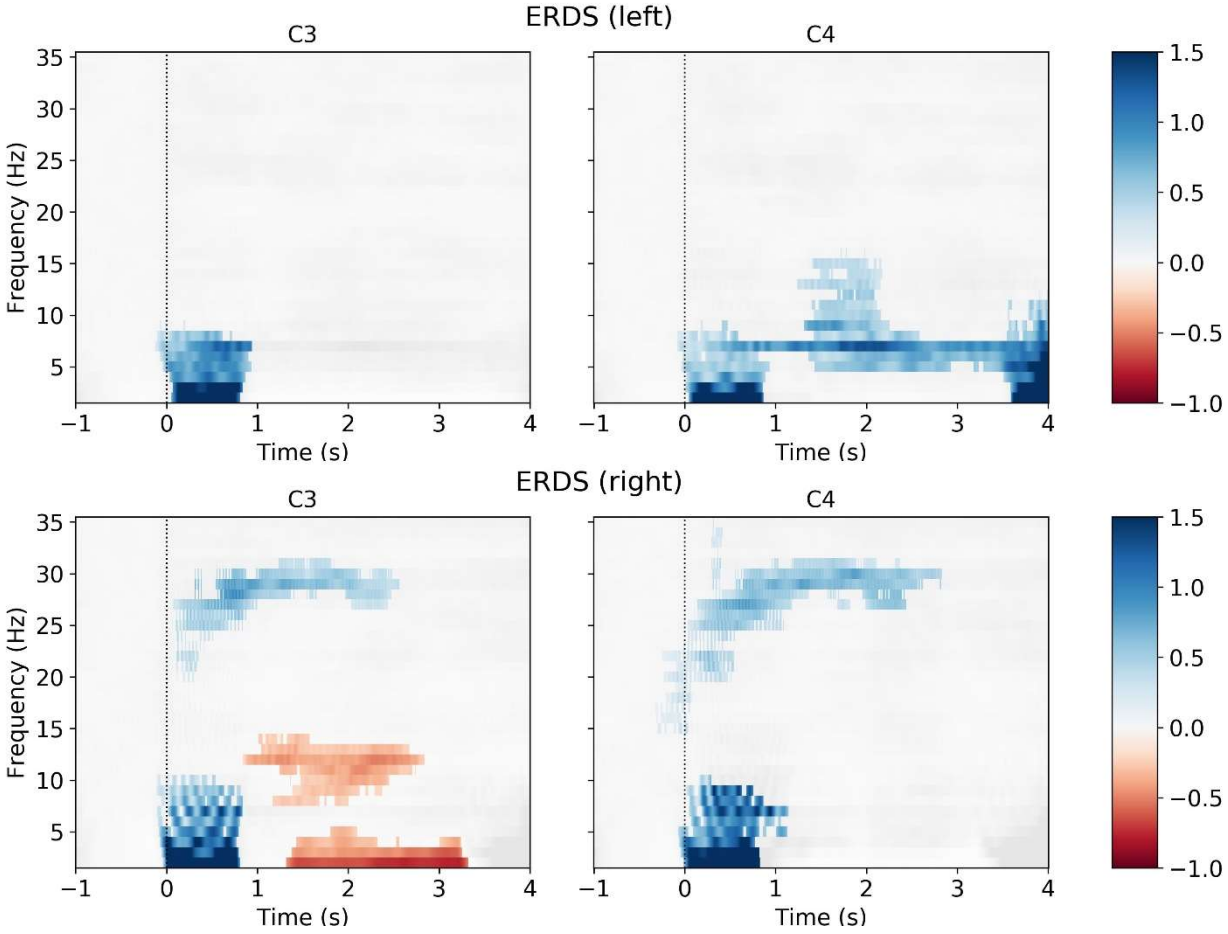

ROBOT – 5 – TRAINING

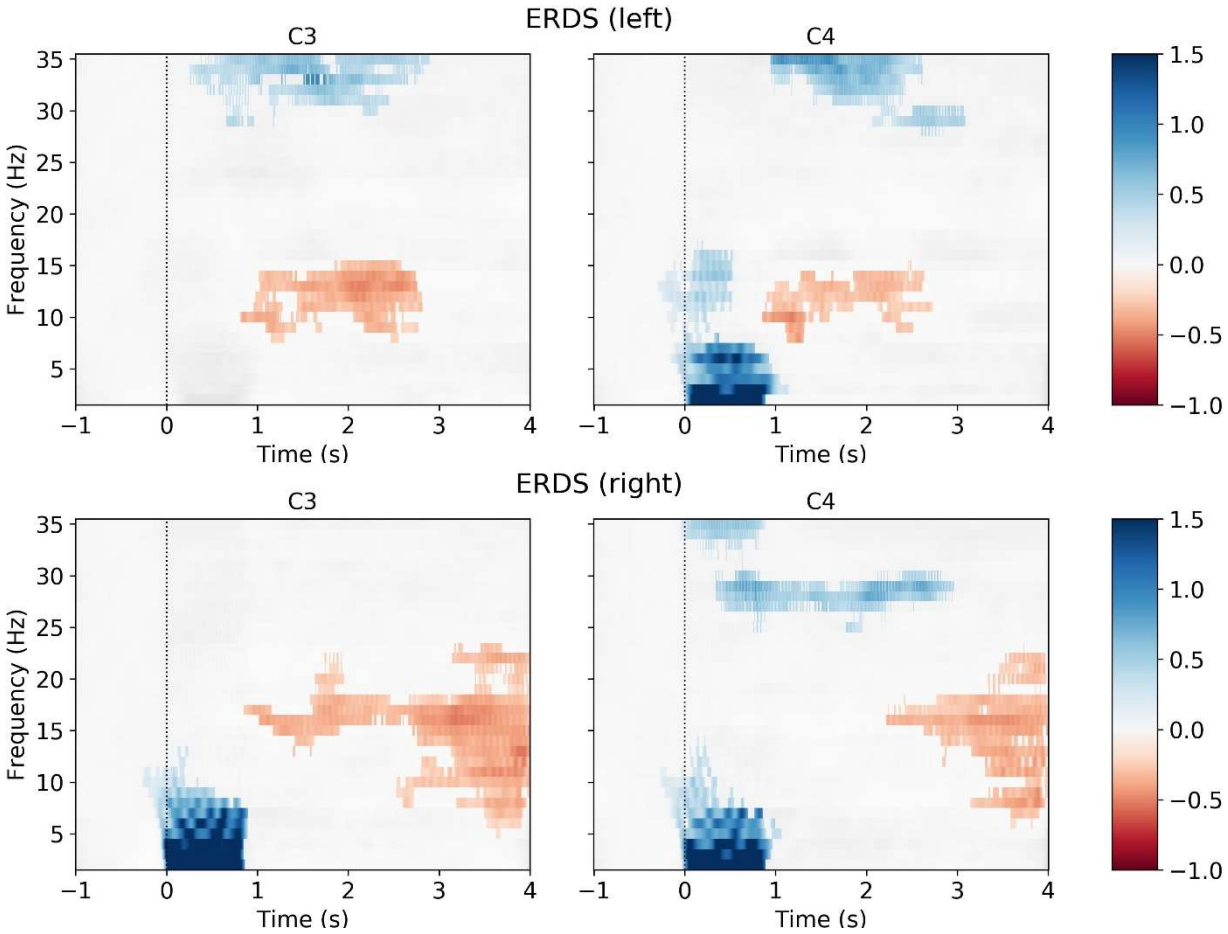

ROBOT – 5 – TESTING

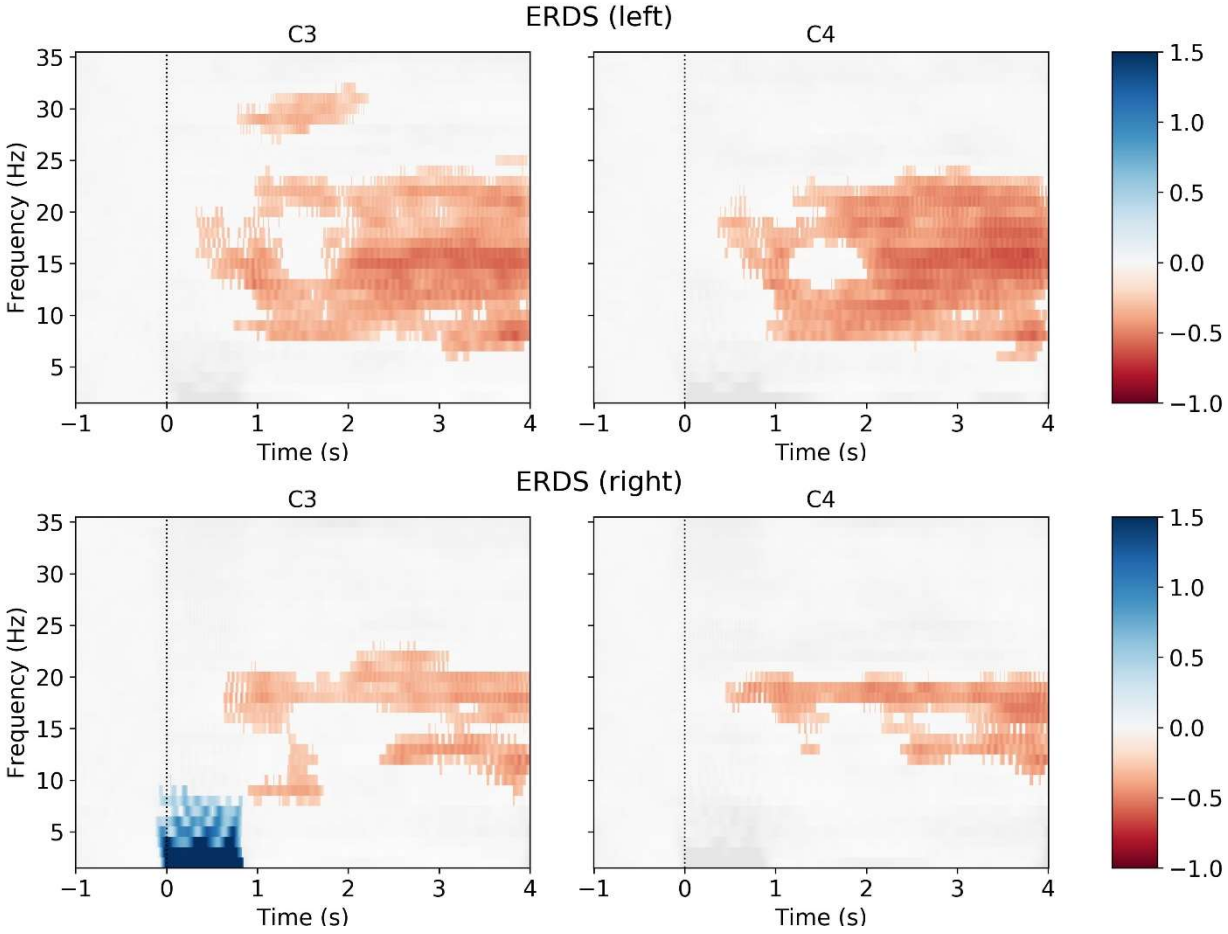

ROBOT – 6 – TRAINING

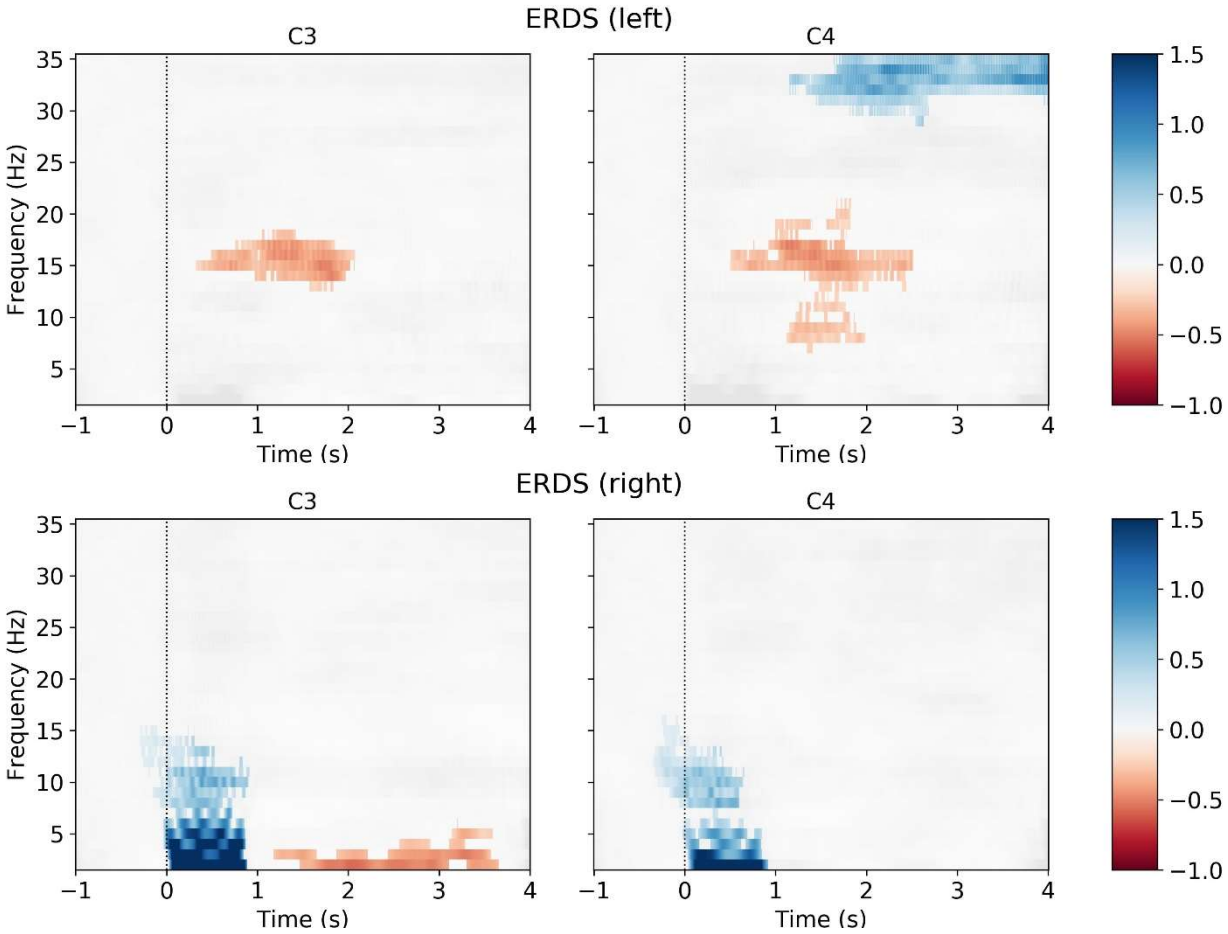

ROBOT – 6 – TESTING

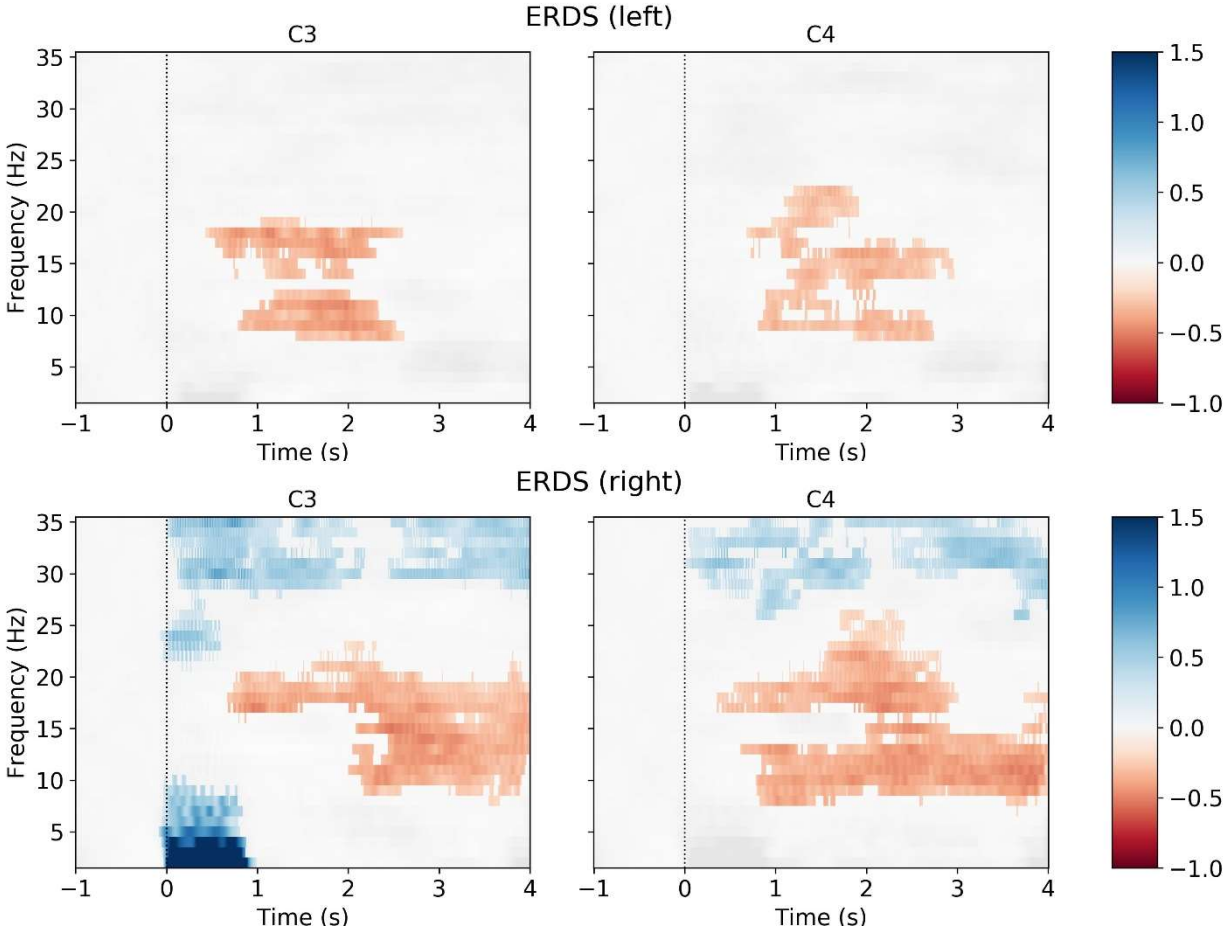

ROBOT – 7 – TRAINING

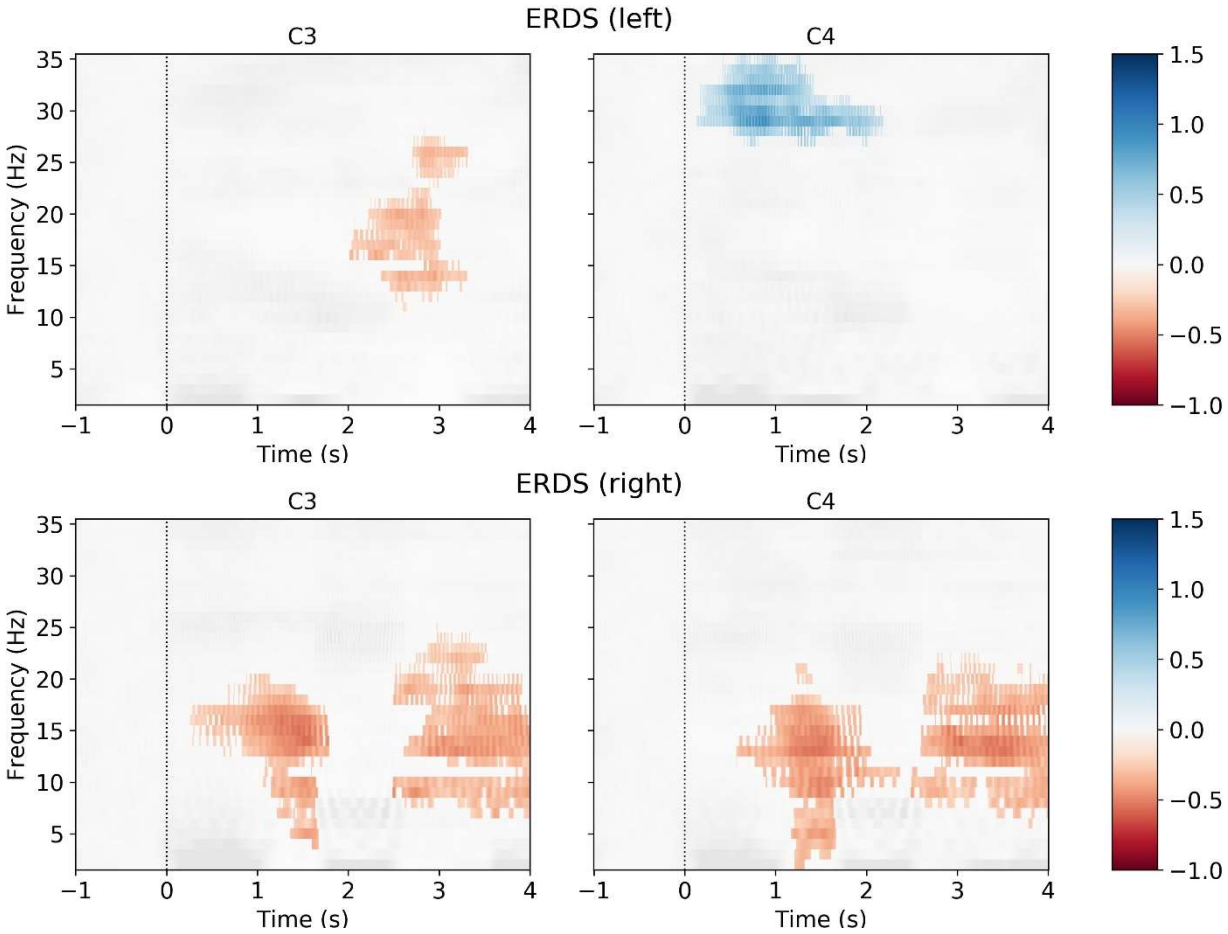

ROBOT – 7 – TESTING

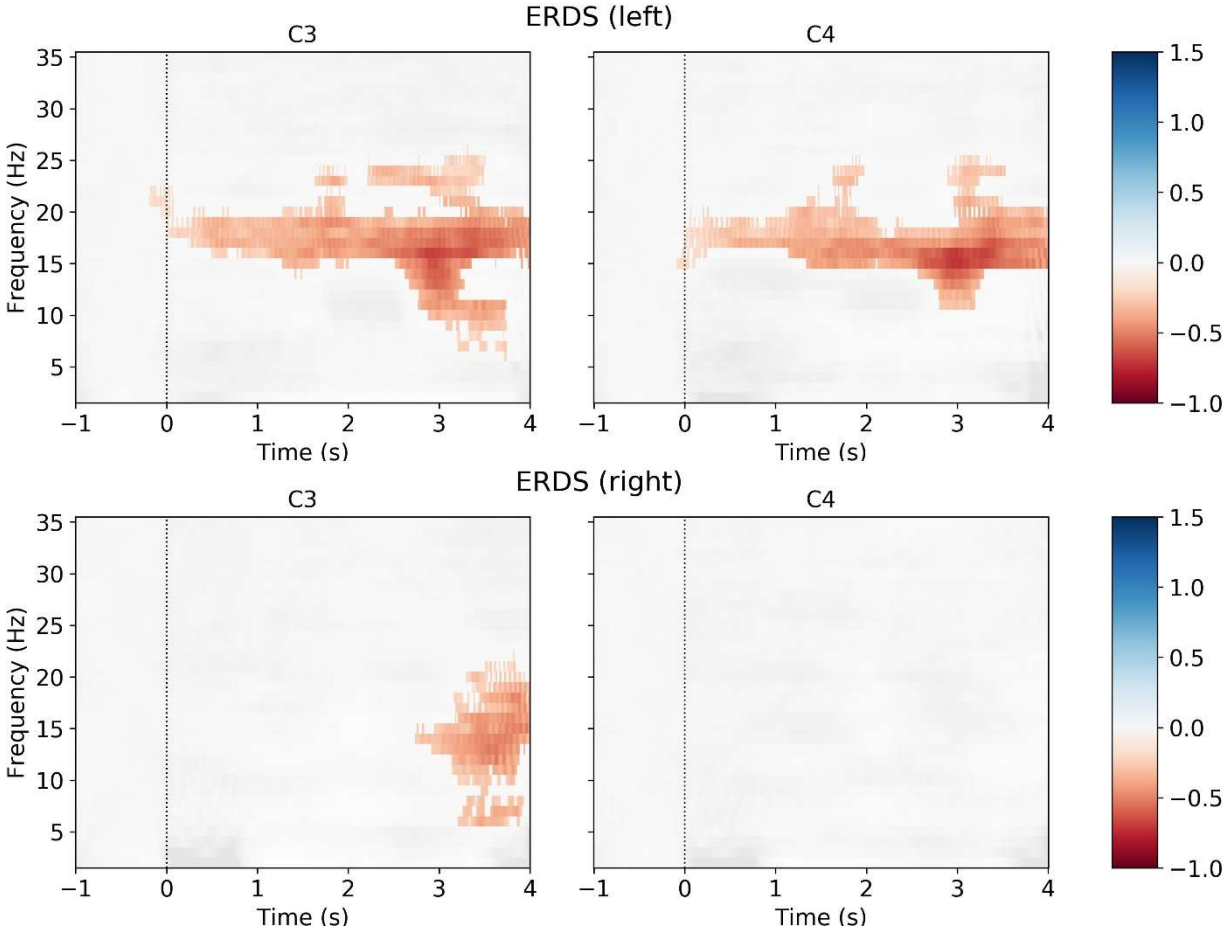

ROBOT – 8 – TRAINING

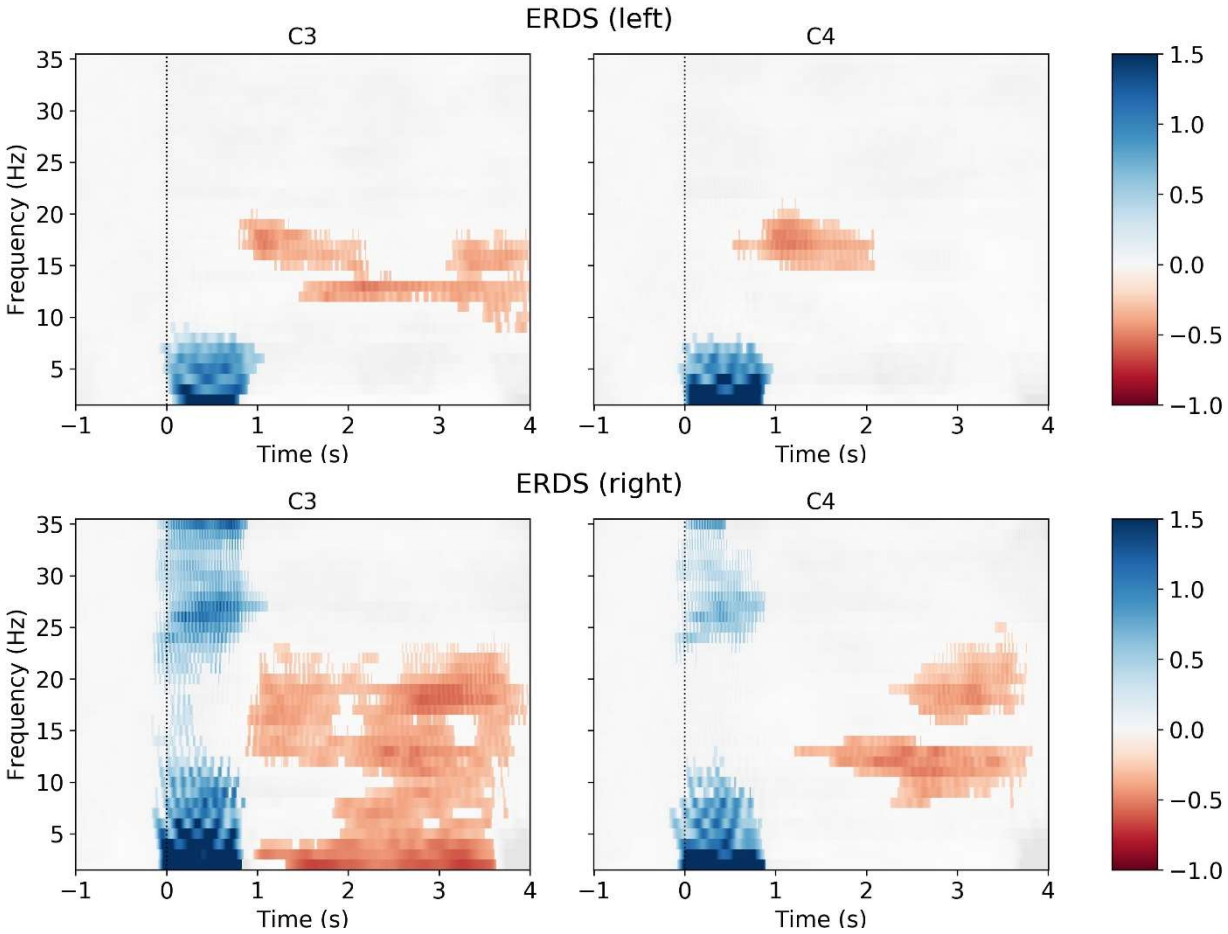

ROBOT – 8 – TESTING

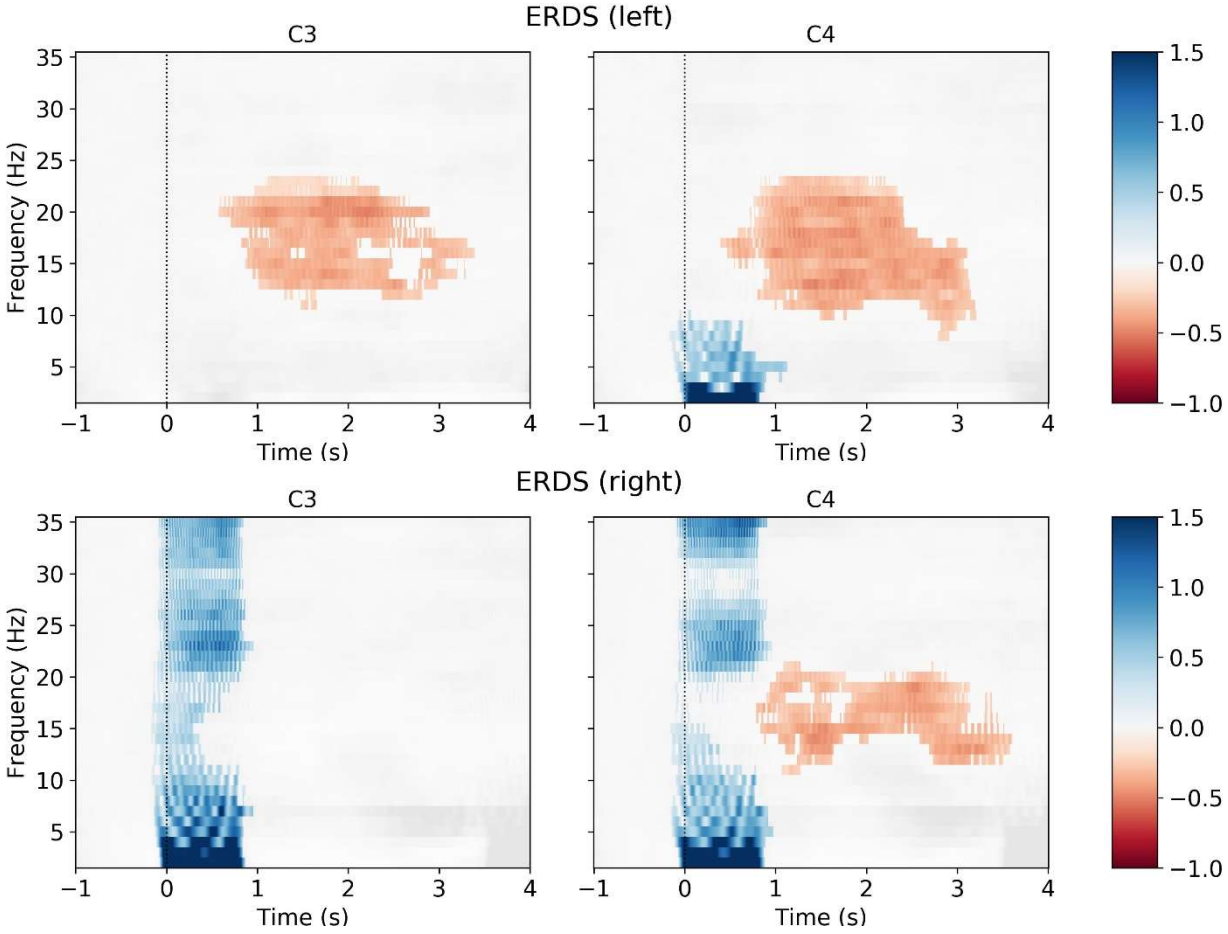

BOTH – 1 – TRAINING

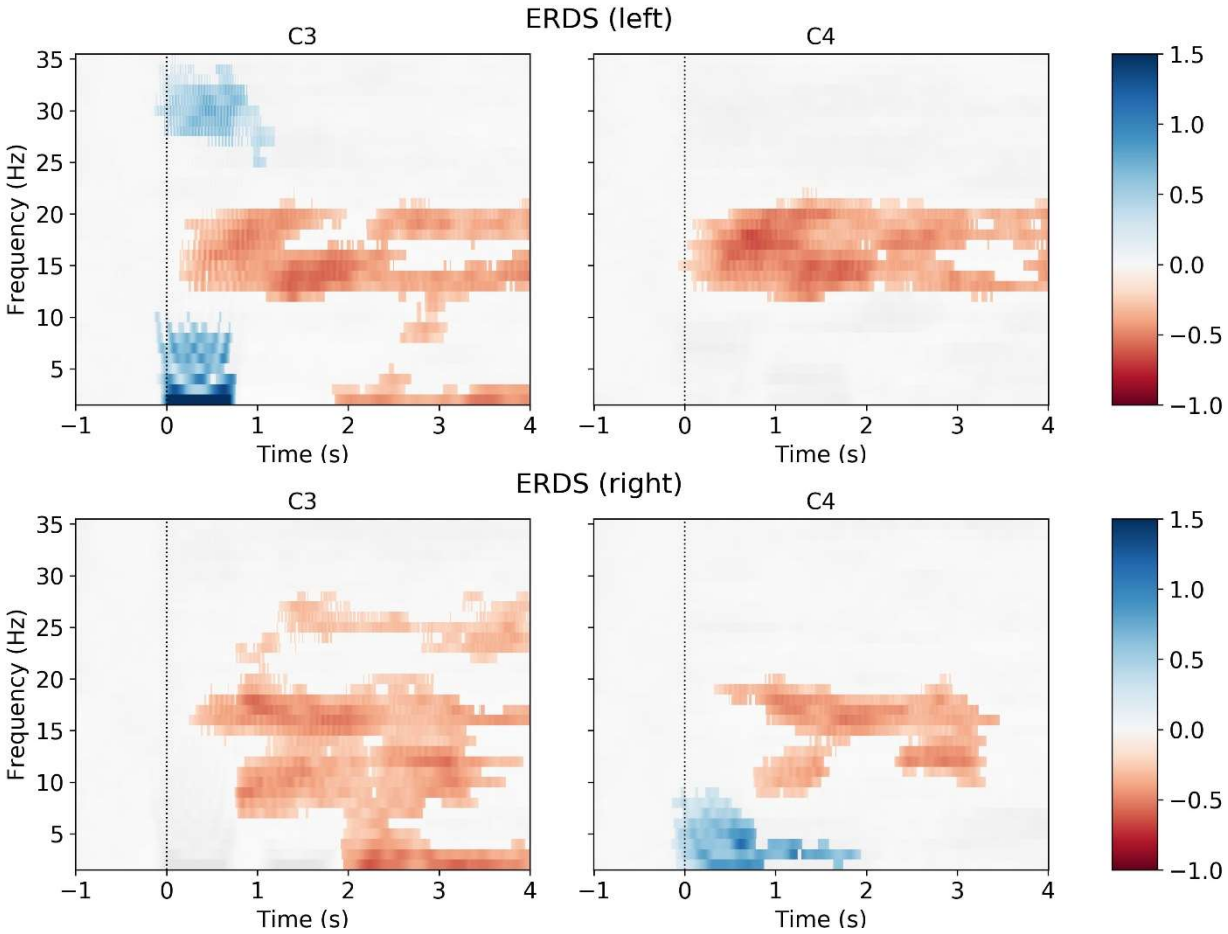

BOTH – 1 – TESTING

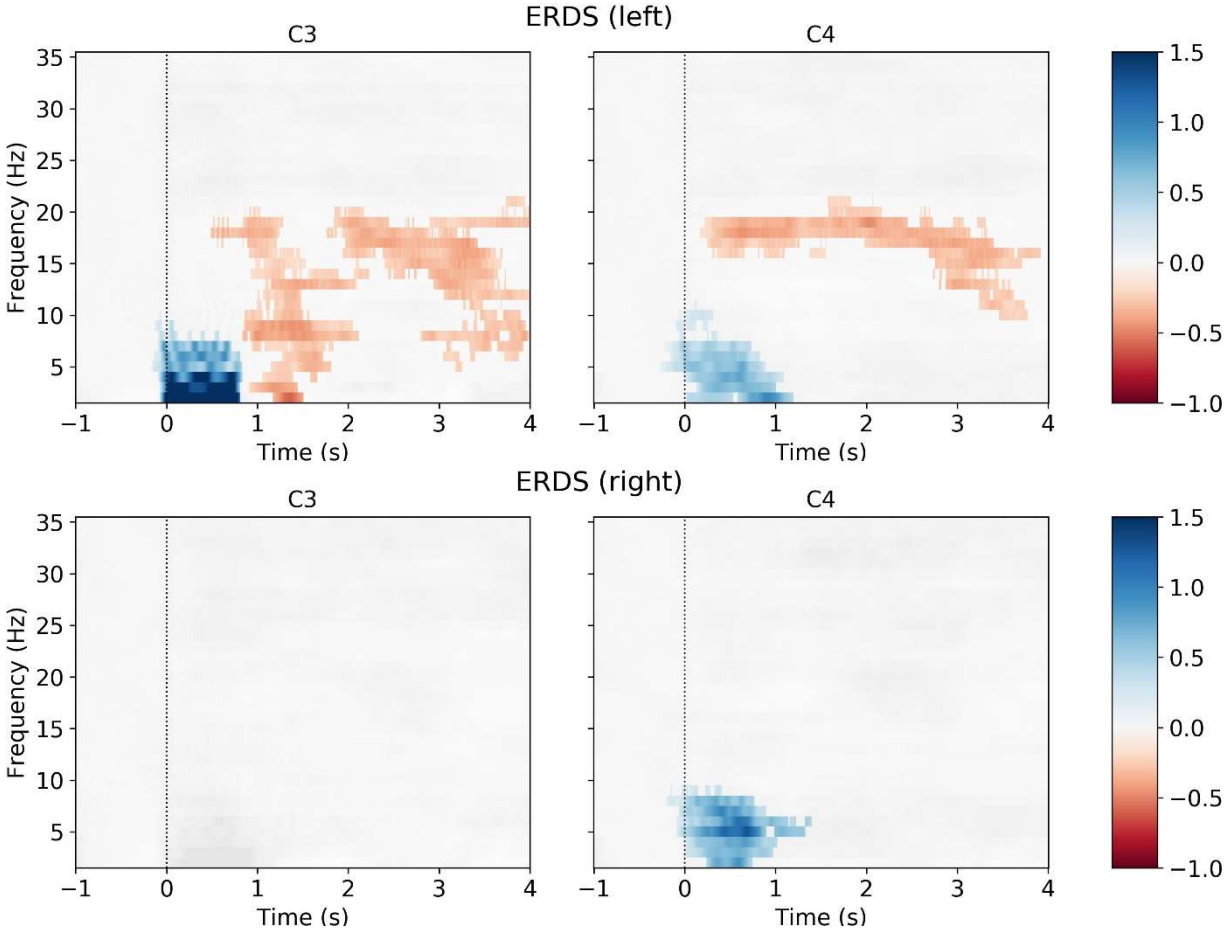

BOTH – 2 – TRAINING

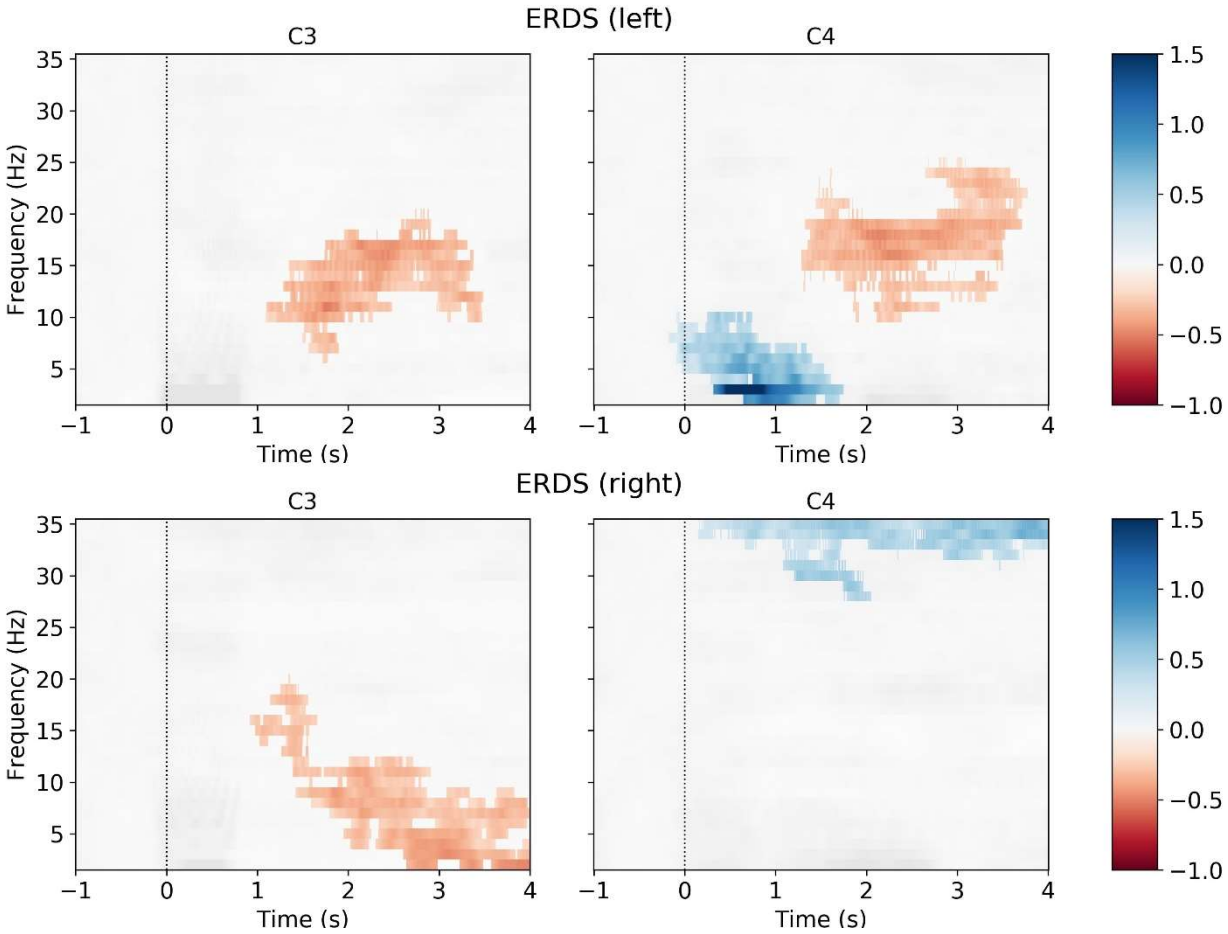

BOTH – 2 – TESTING

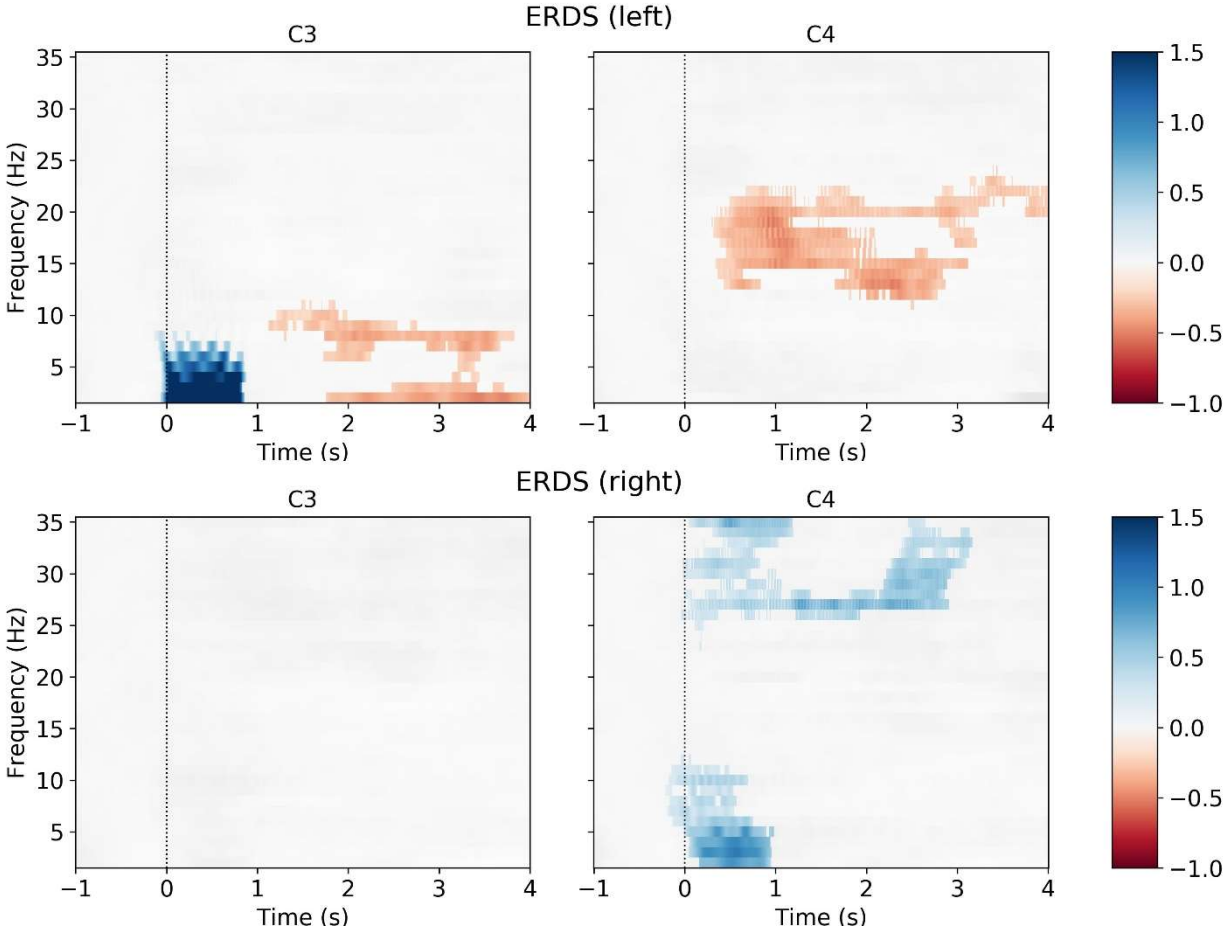

BOTH – 3 – TRAINING

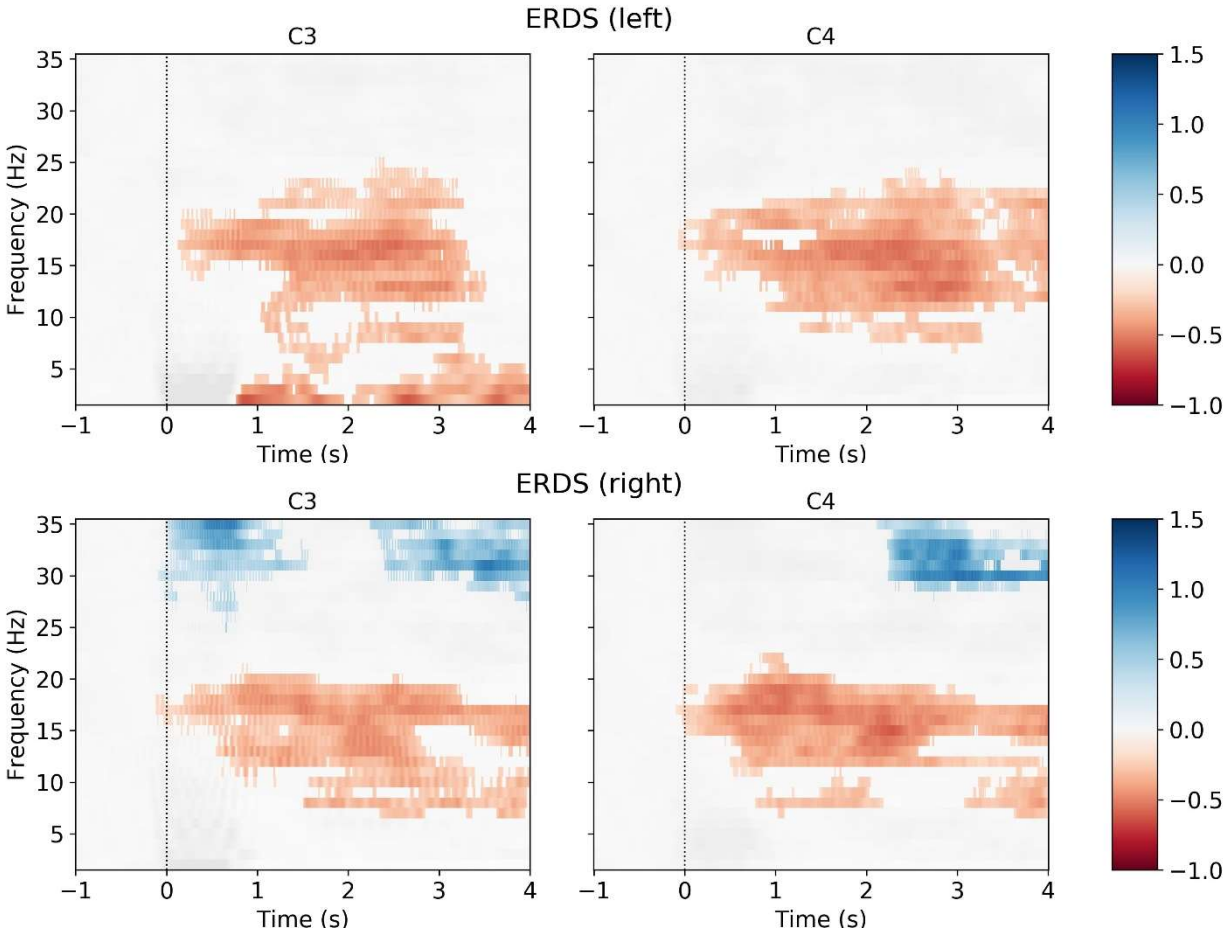

BOTH – 3 – TESTING

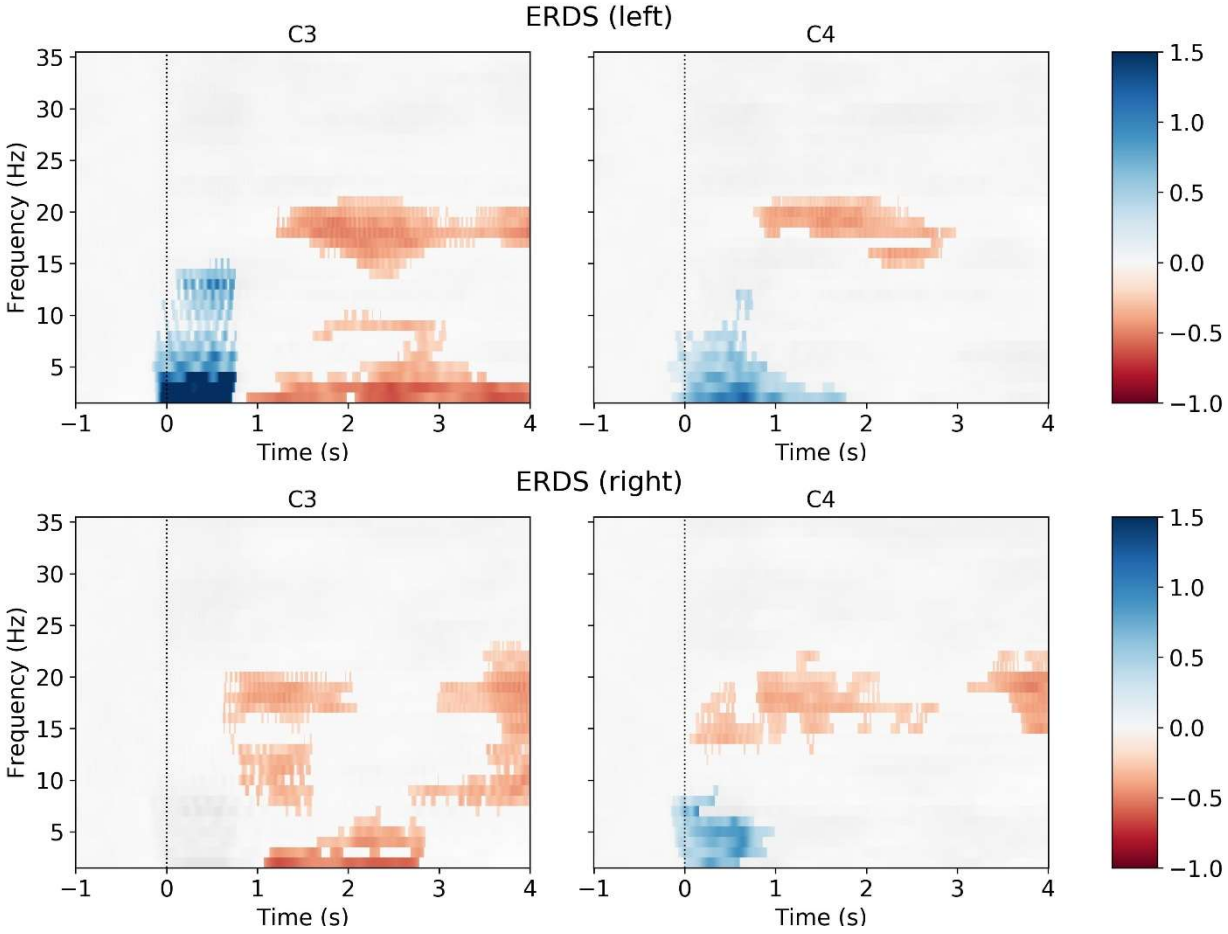

BOTH – 4 – TRAINING

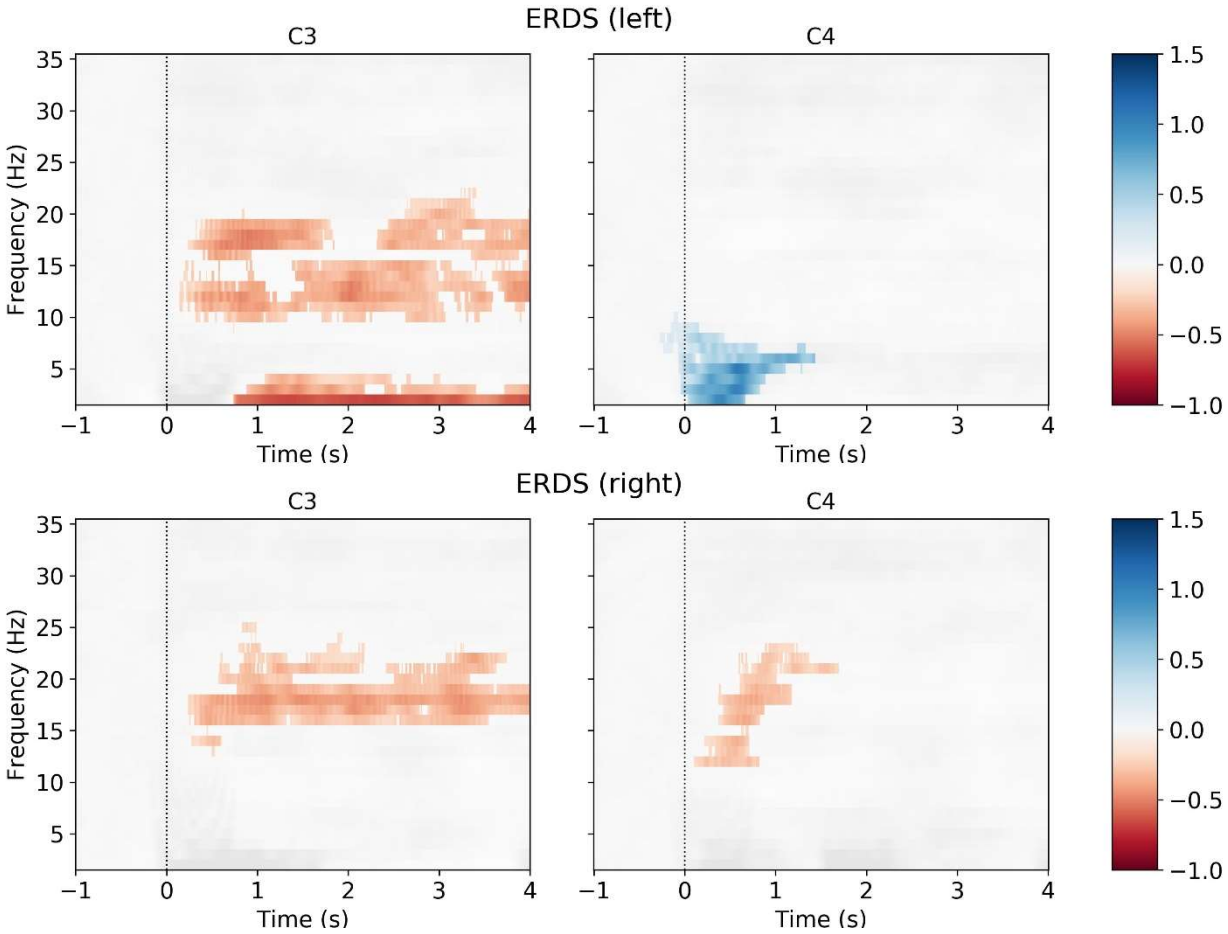

BOTH – 4 – TESTING

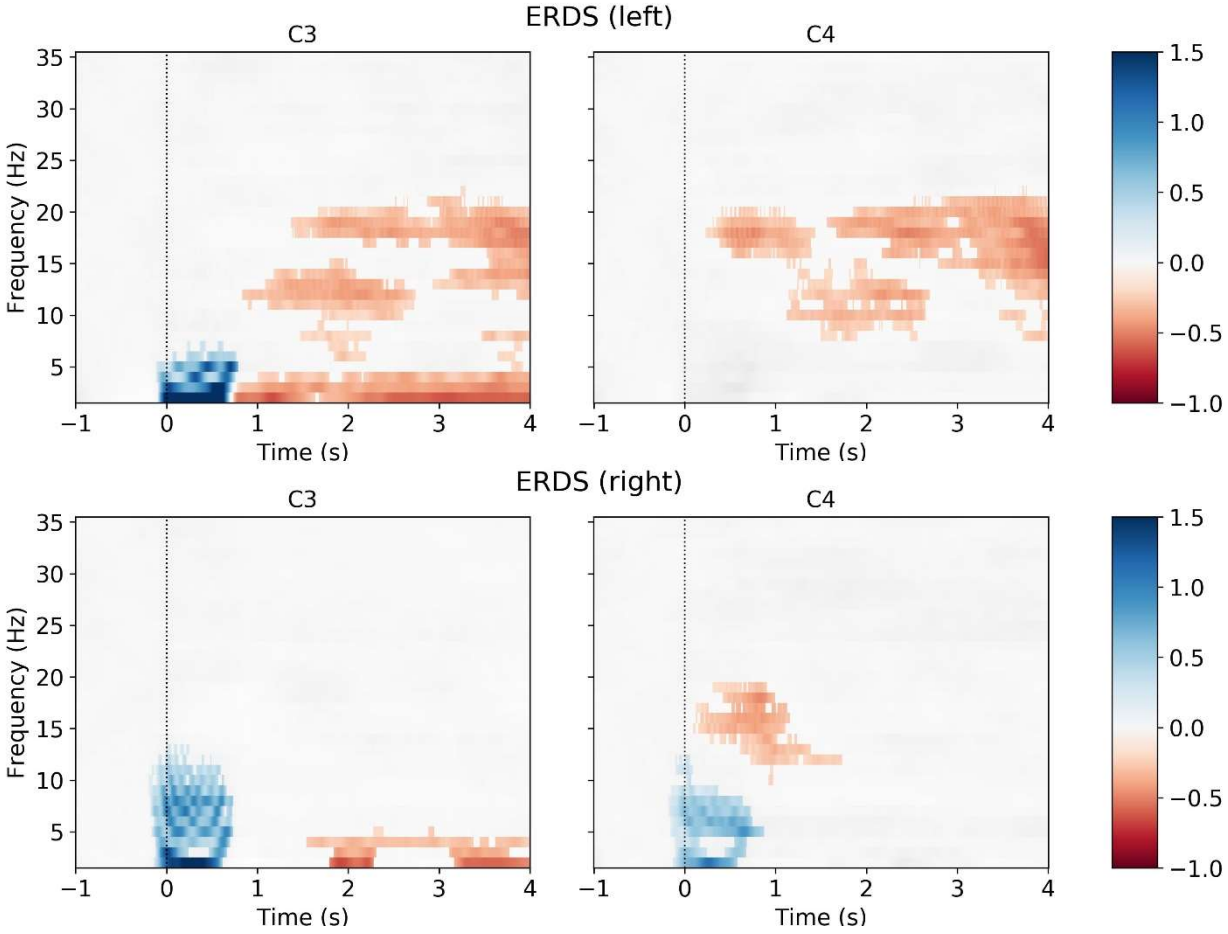

BOTH – 5 – TRAINING

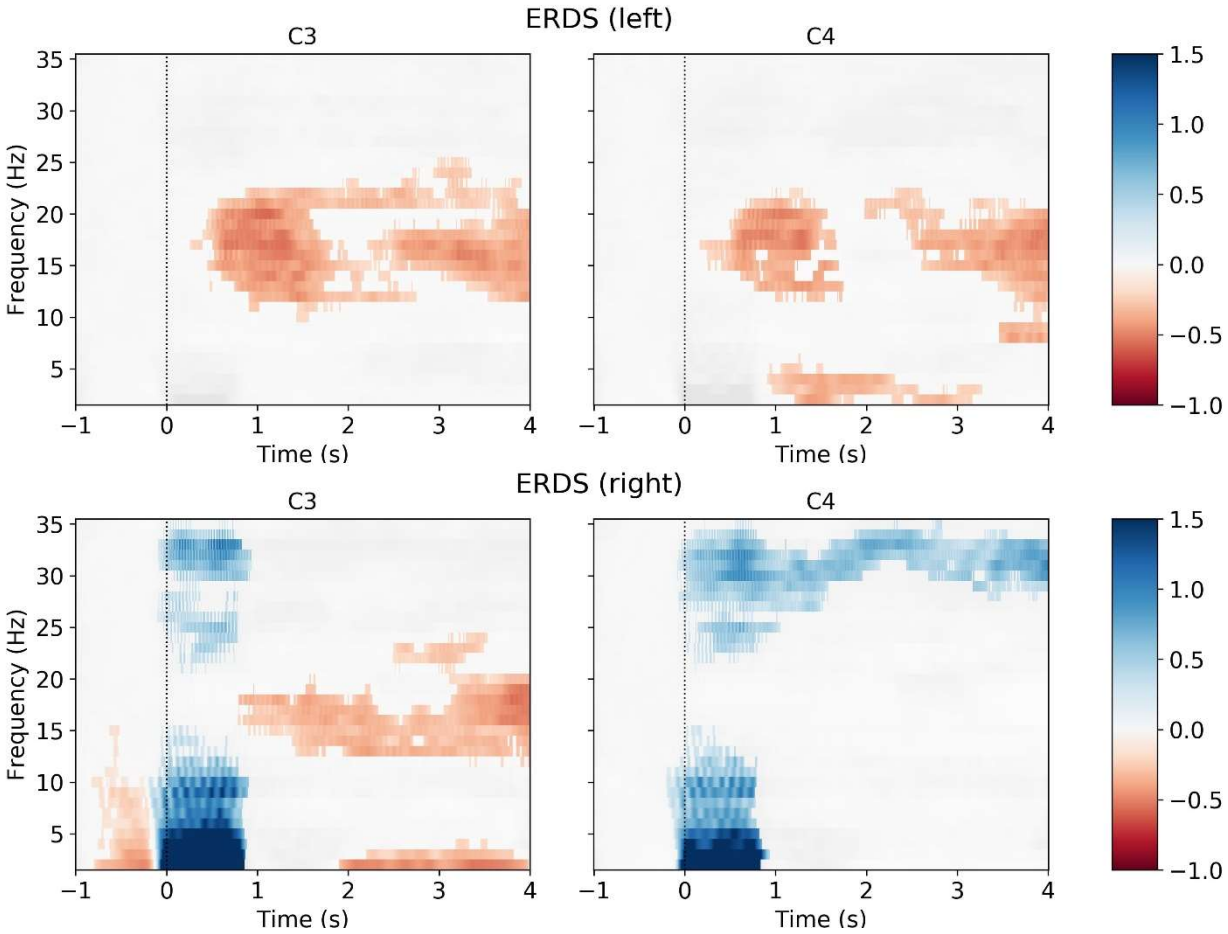

BOTH – 5 – TESTING

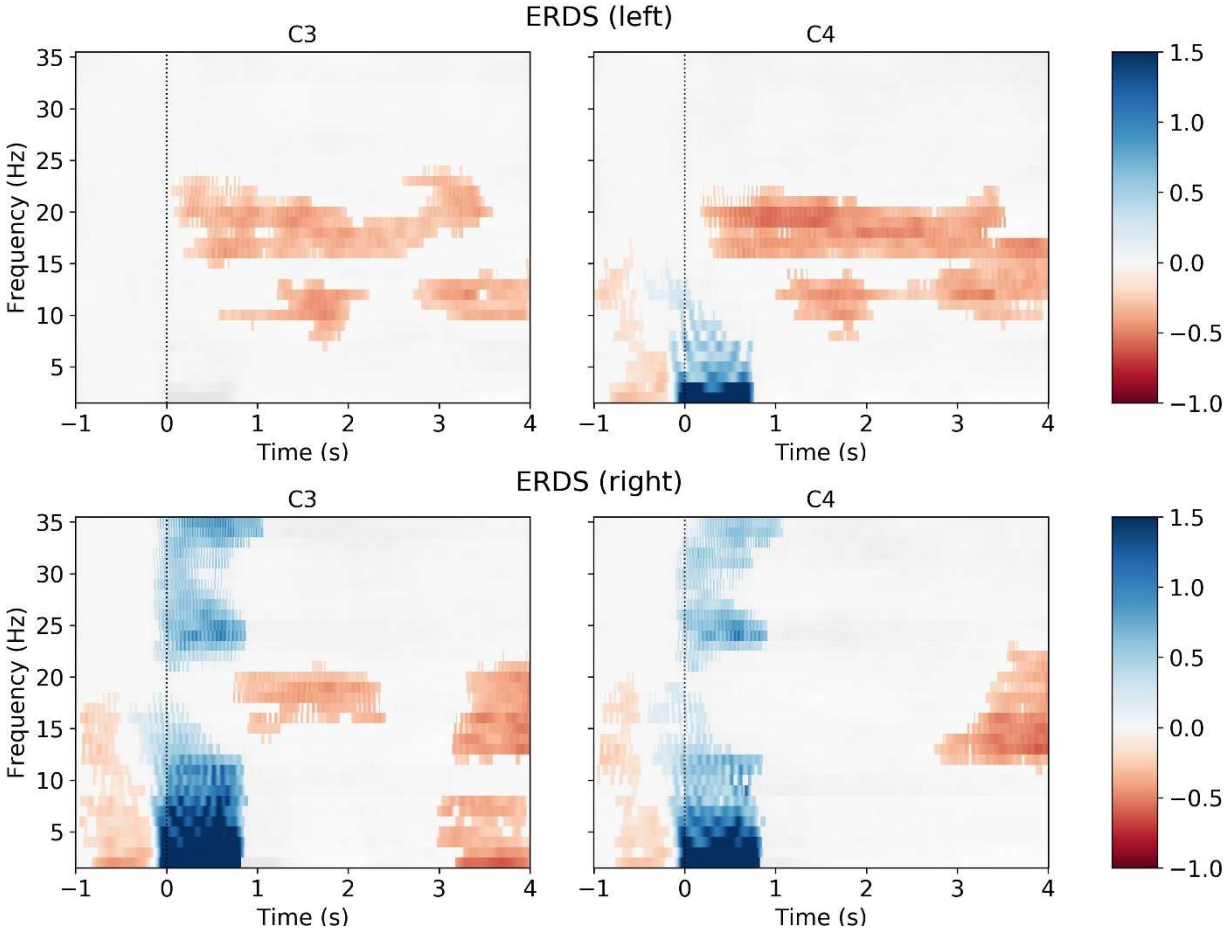

BOTH – 6 – TRAINING

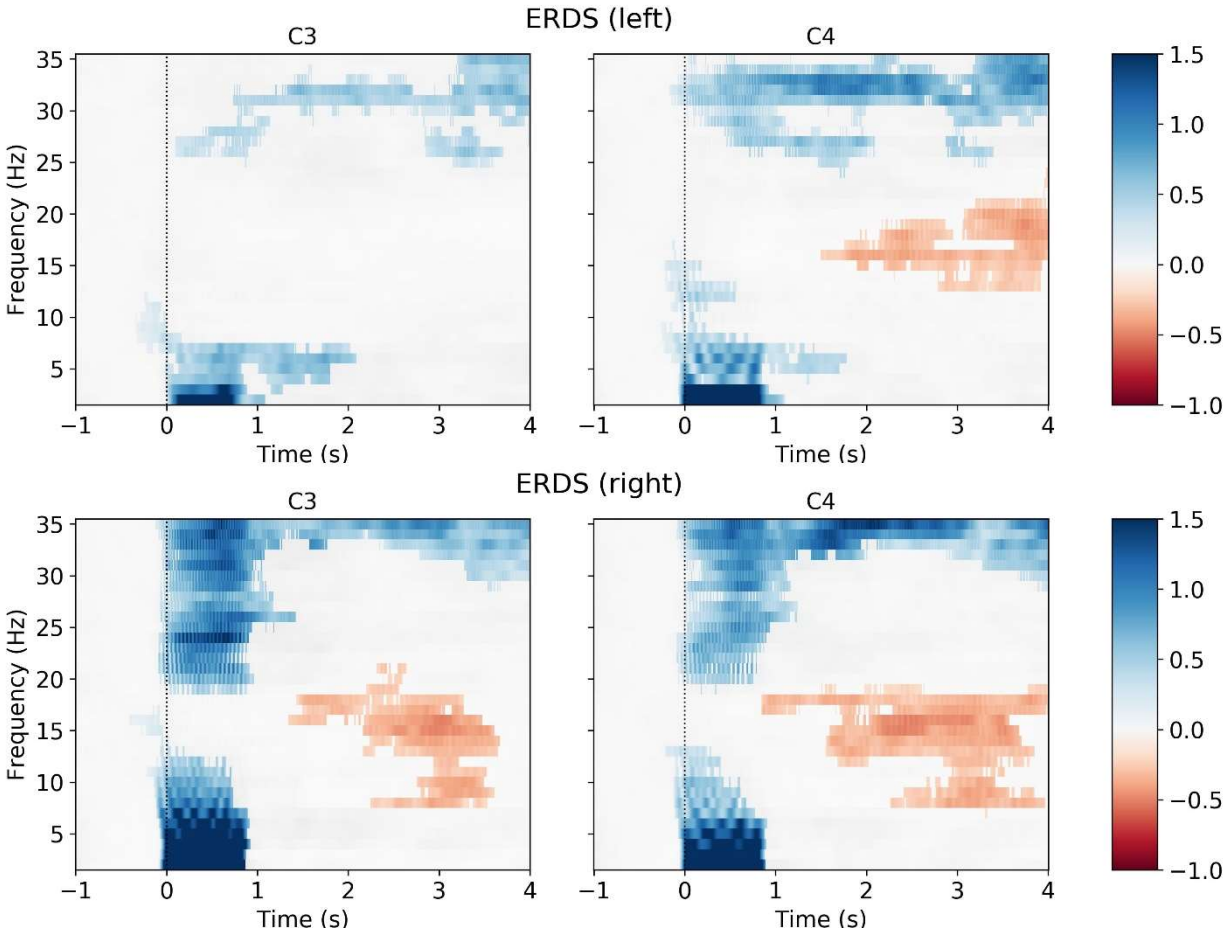

BOTH – 6 – TESTING

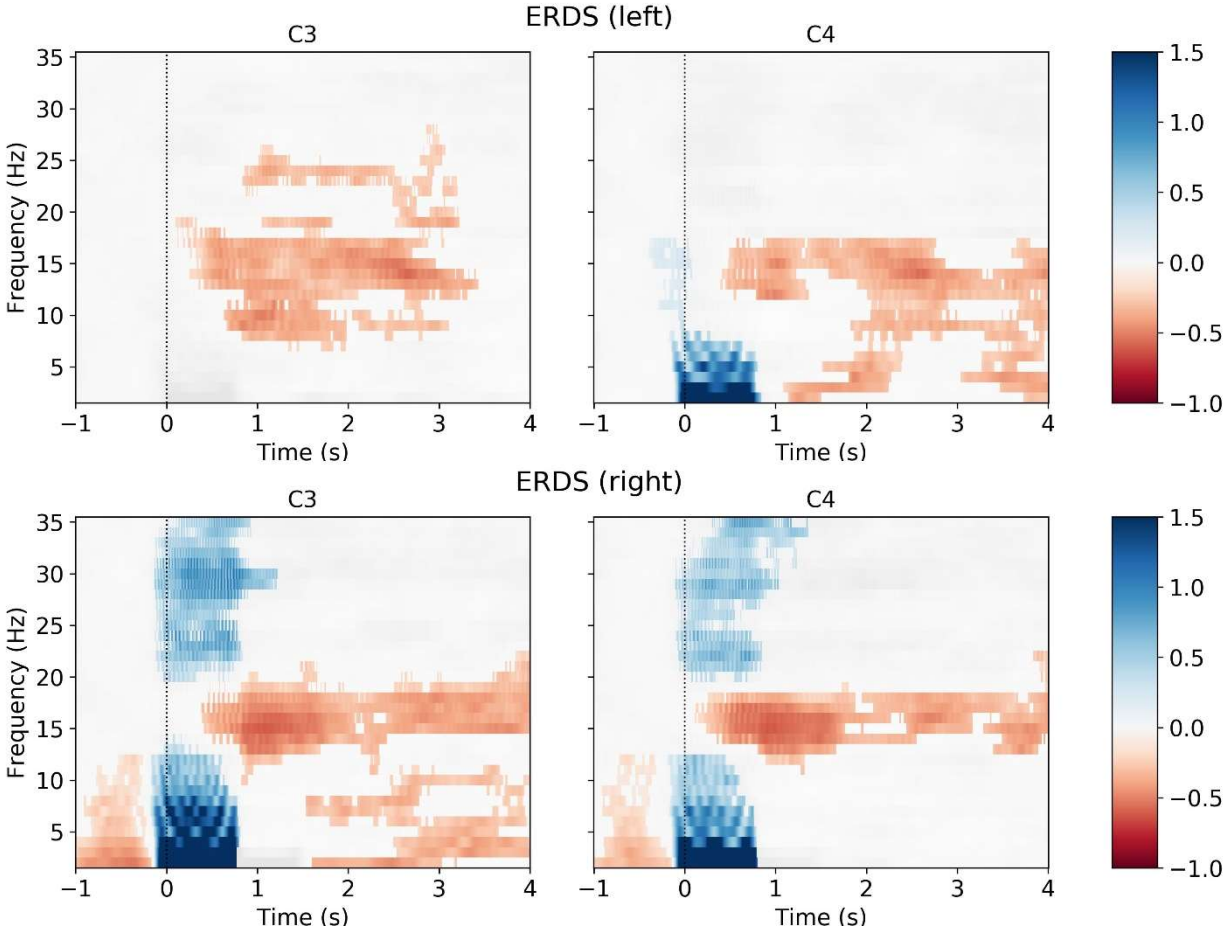

BOTH – 7 – TRAINING

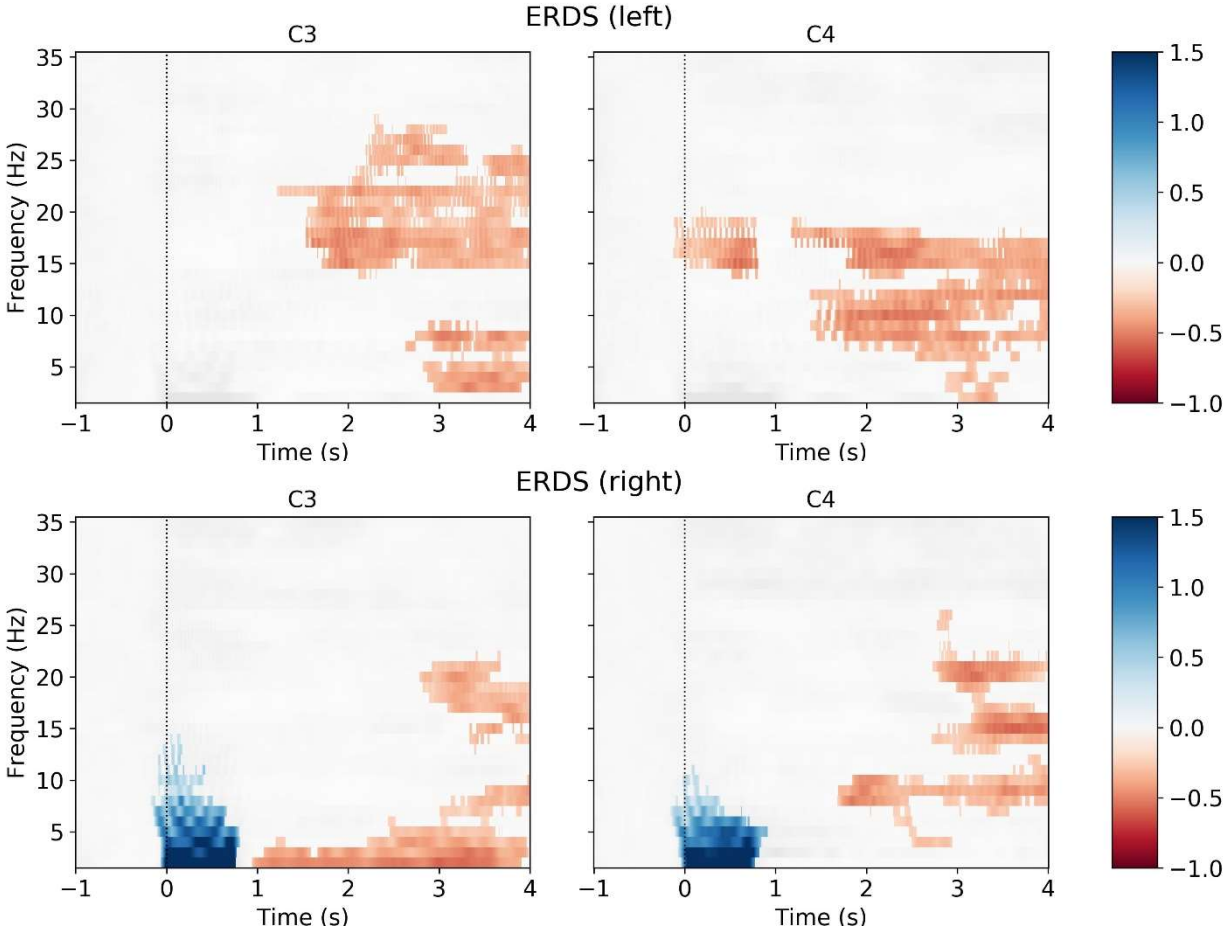

BOTH – 7 – TESTING

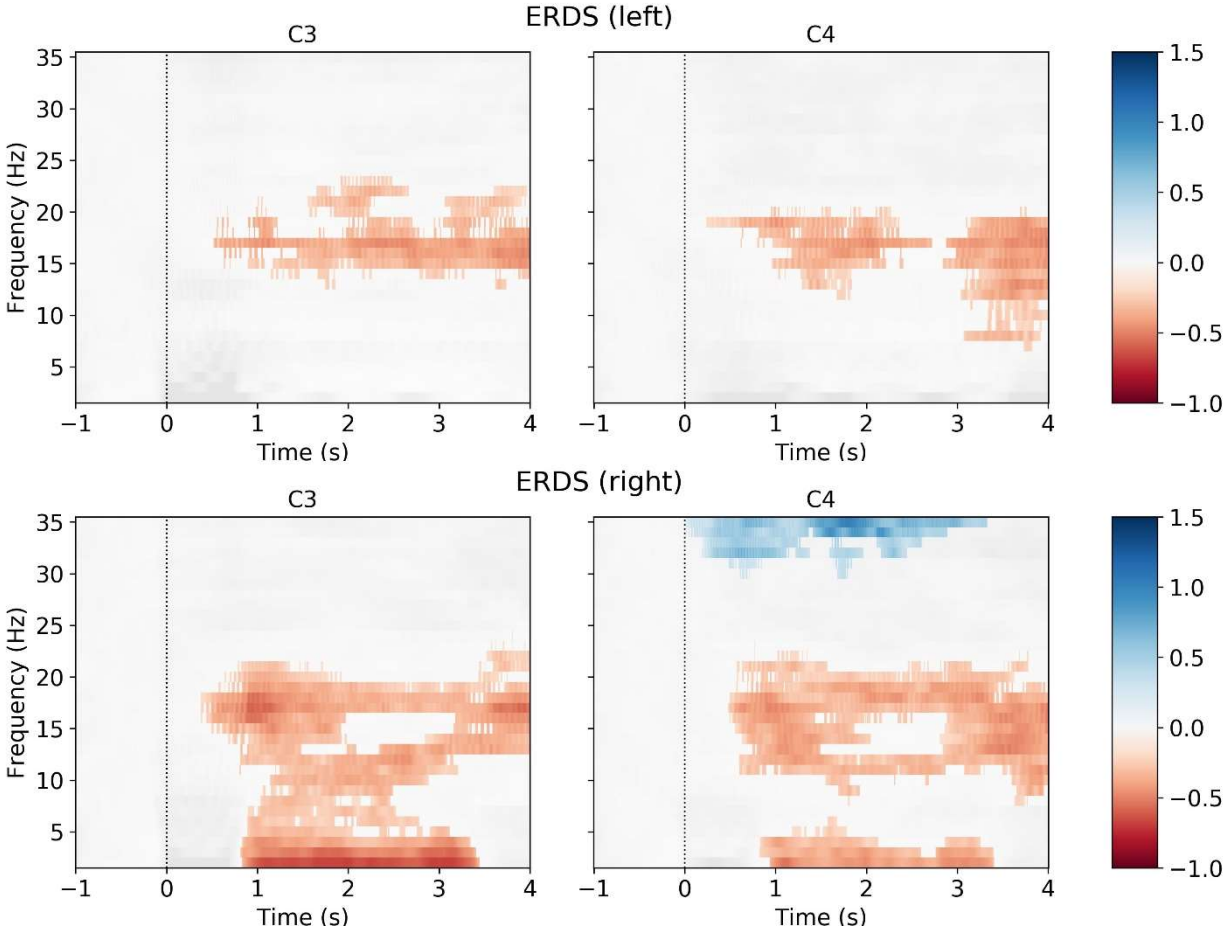

BOTH – 8 – TRAINING

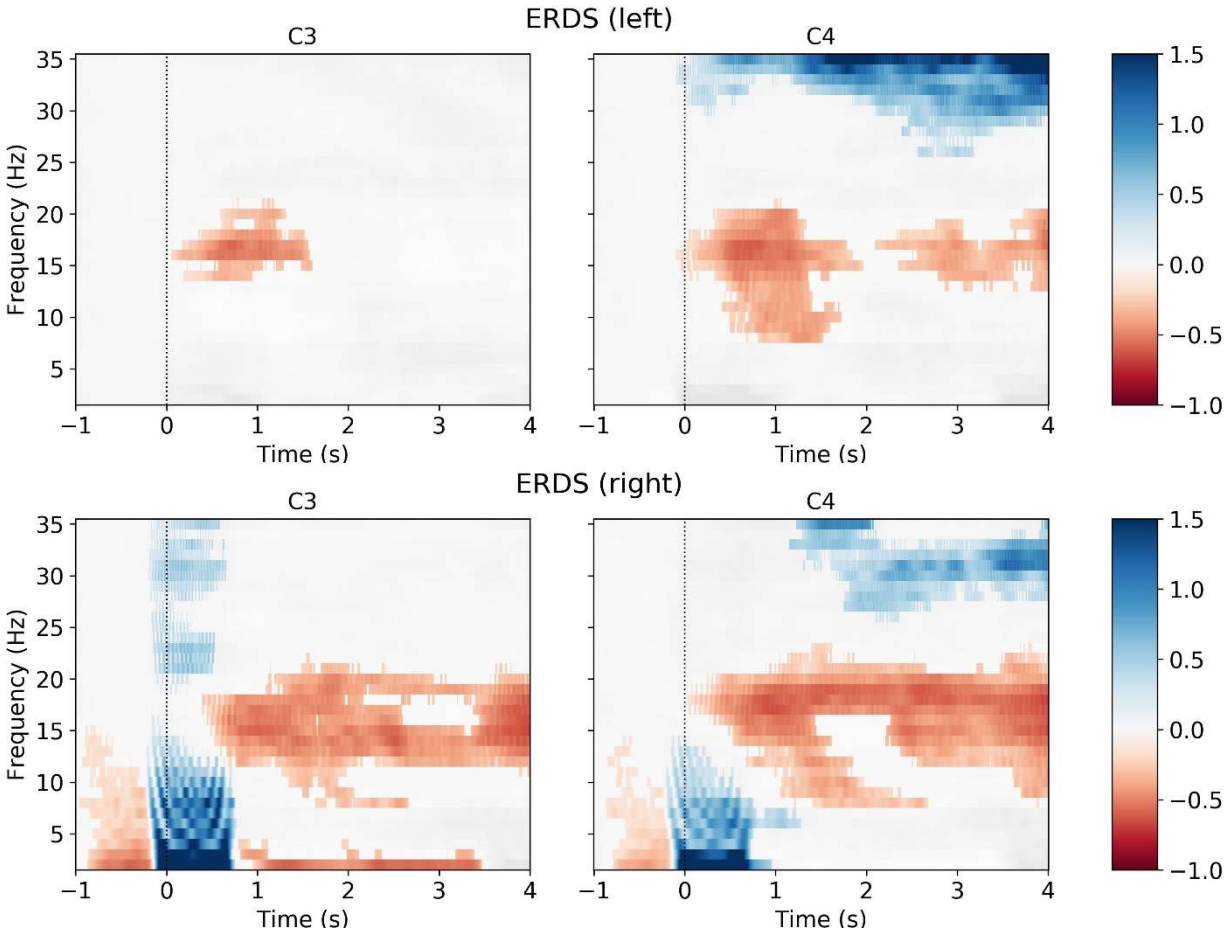

BOTH – 8 – TESTING

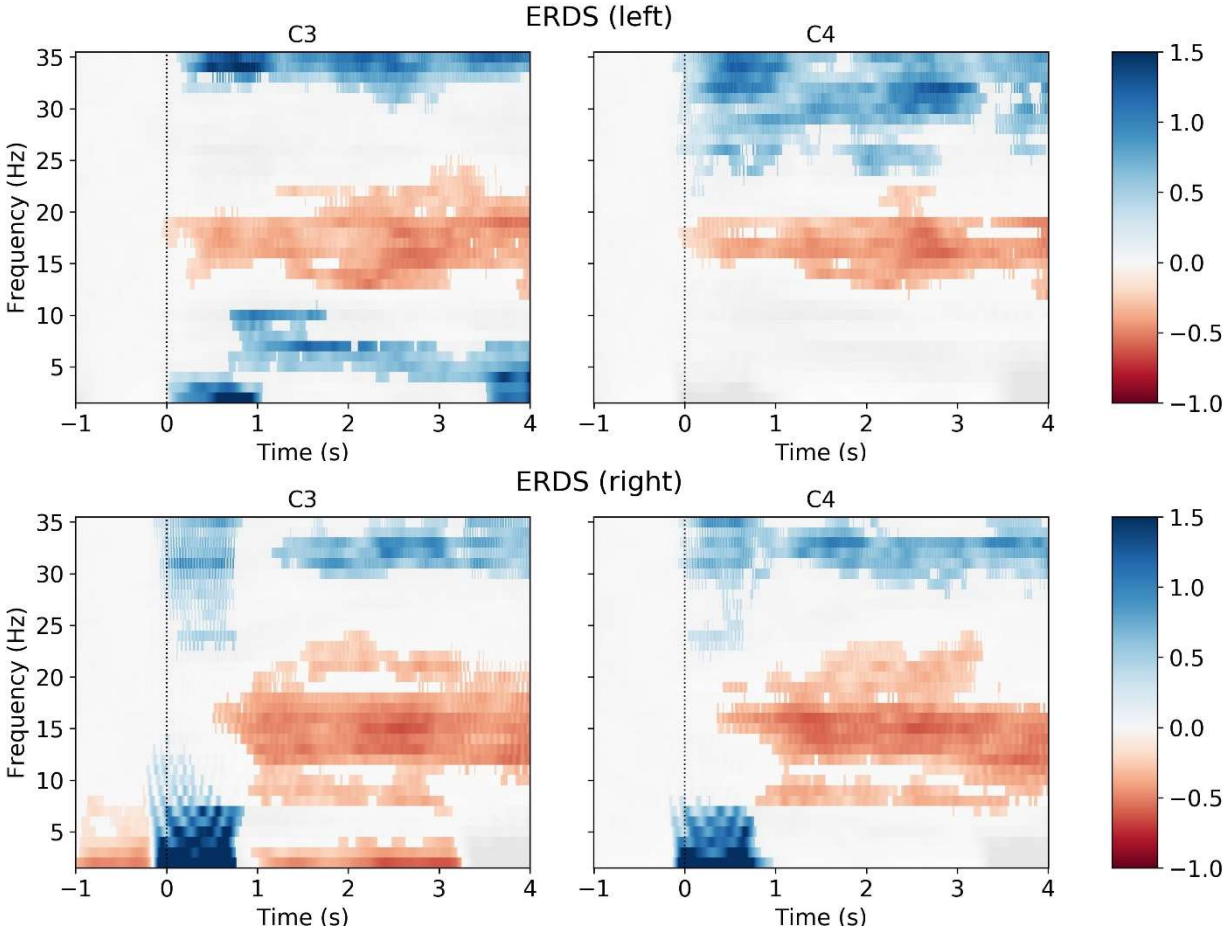

CONTROL – 1 –TRAINING

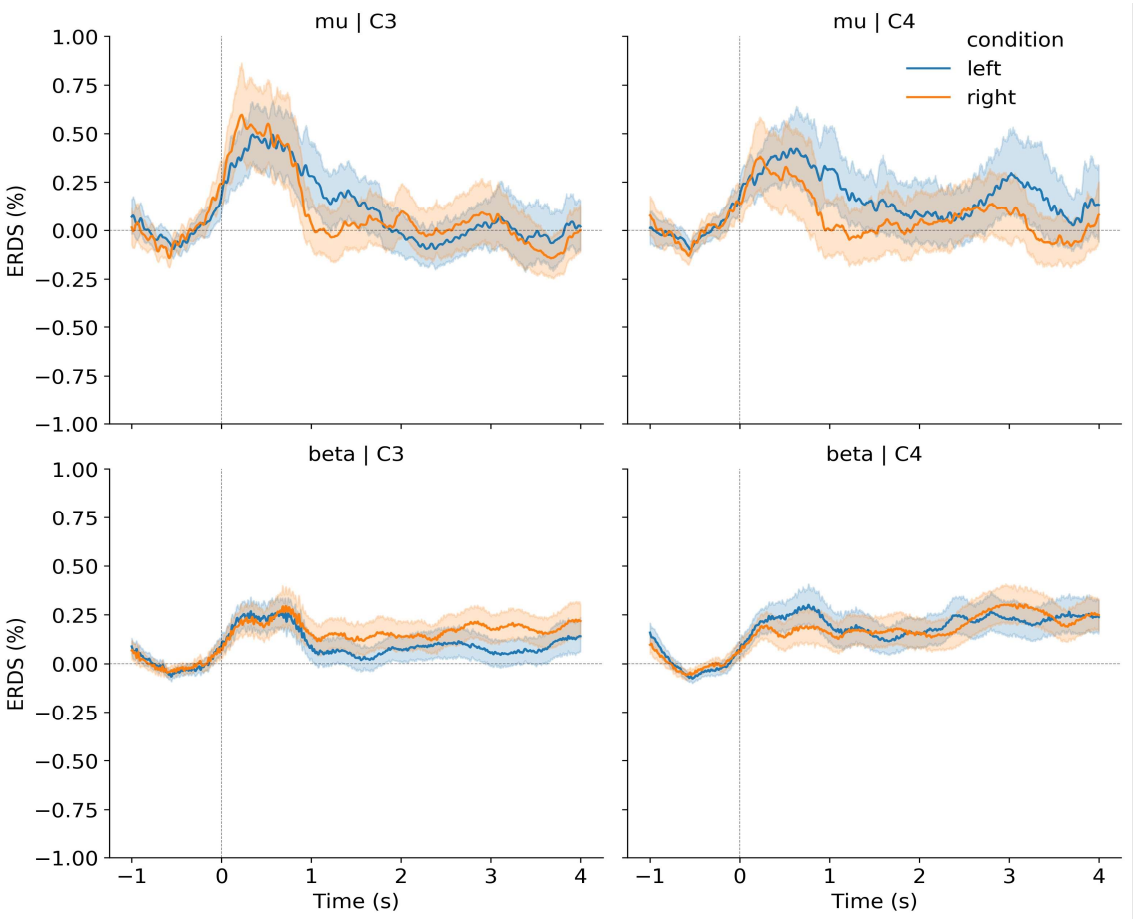

CONTROL – 1 – TESTING

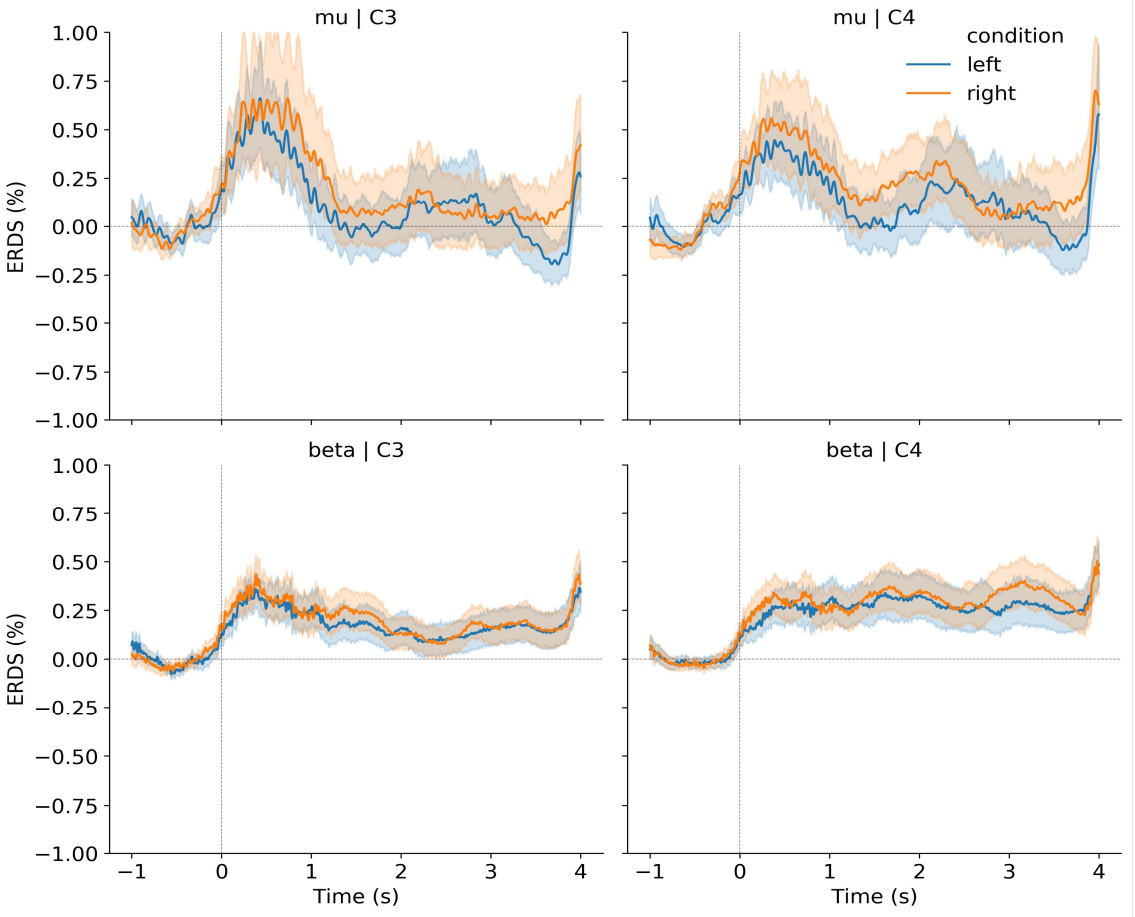

CONTROL – 2 –TRAINING

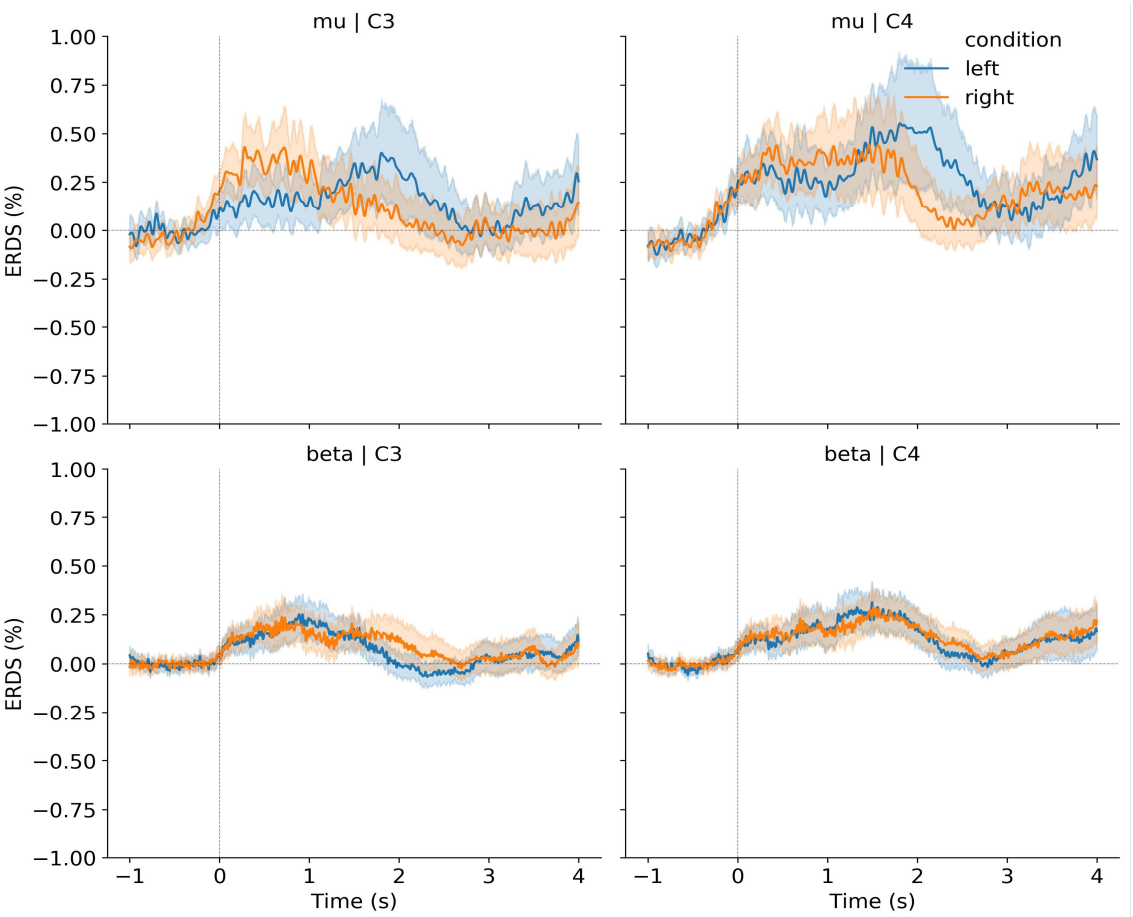

CONTROL – 2 – TESTING

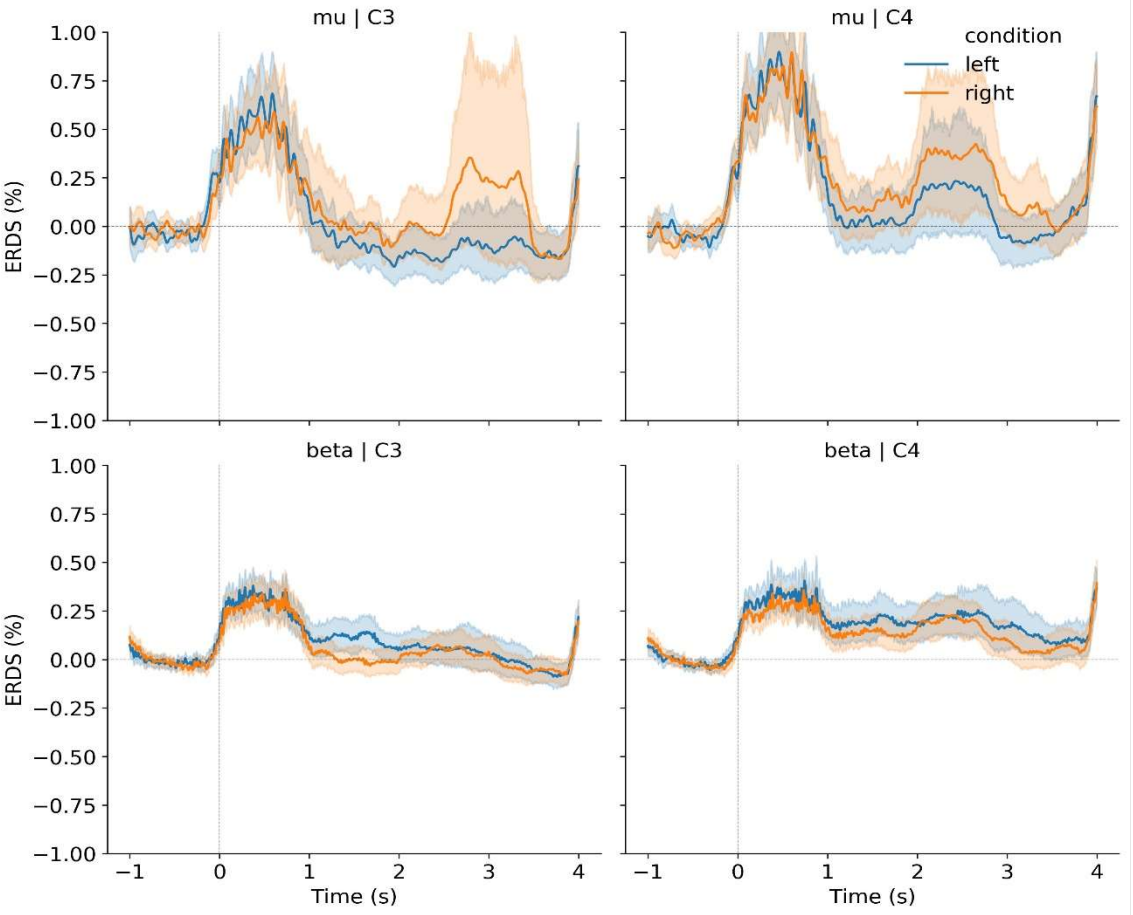

CONTROL – 3 – TRAINING

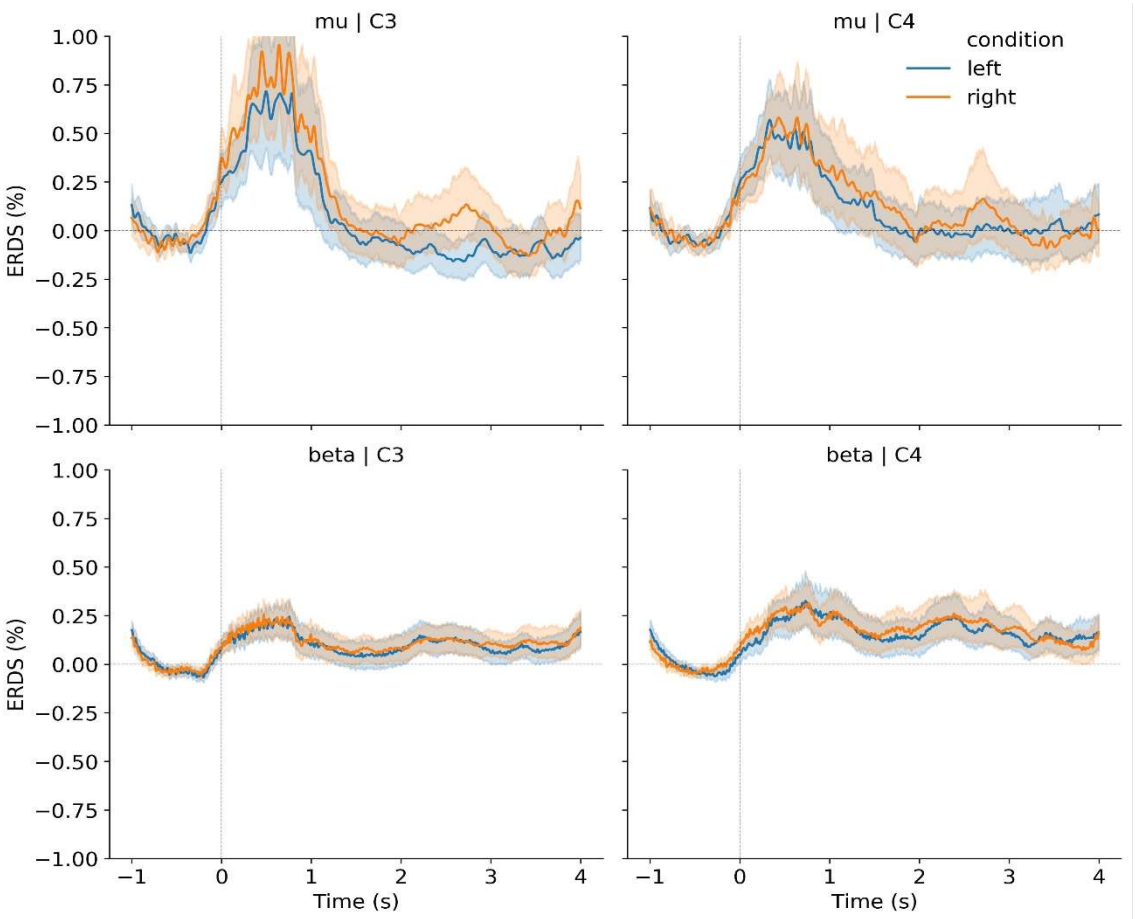

CONTROL – 3 – TESTING

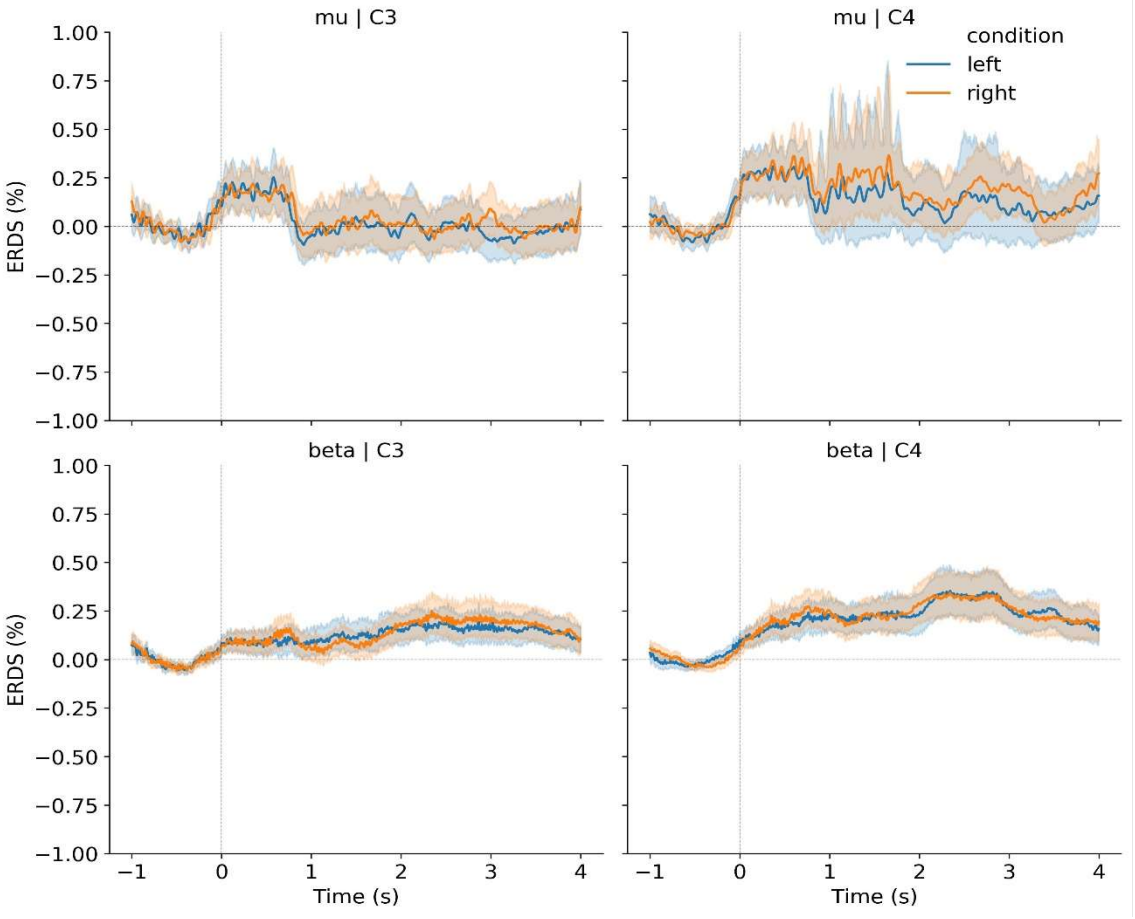

CONTROL – 4 – TRAINING

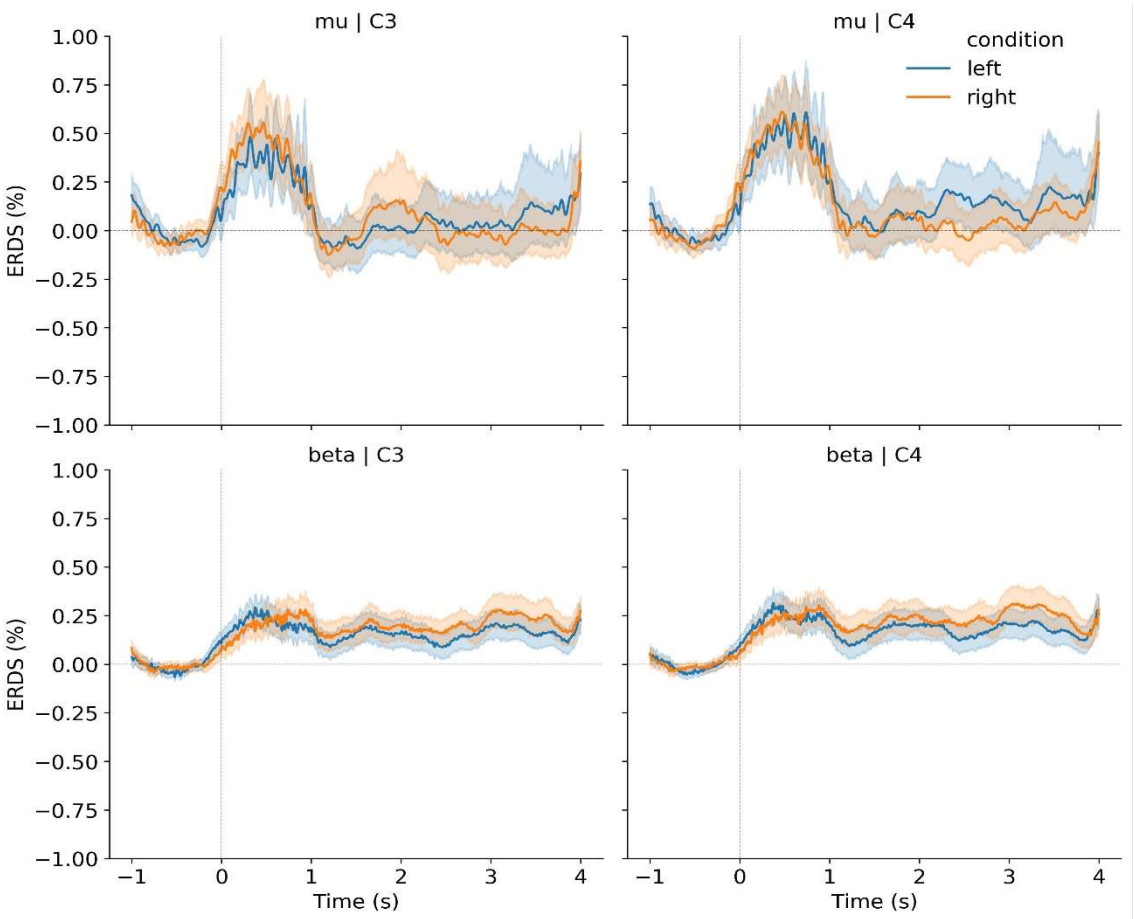

CONTROL – 4 – TESTING

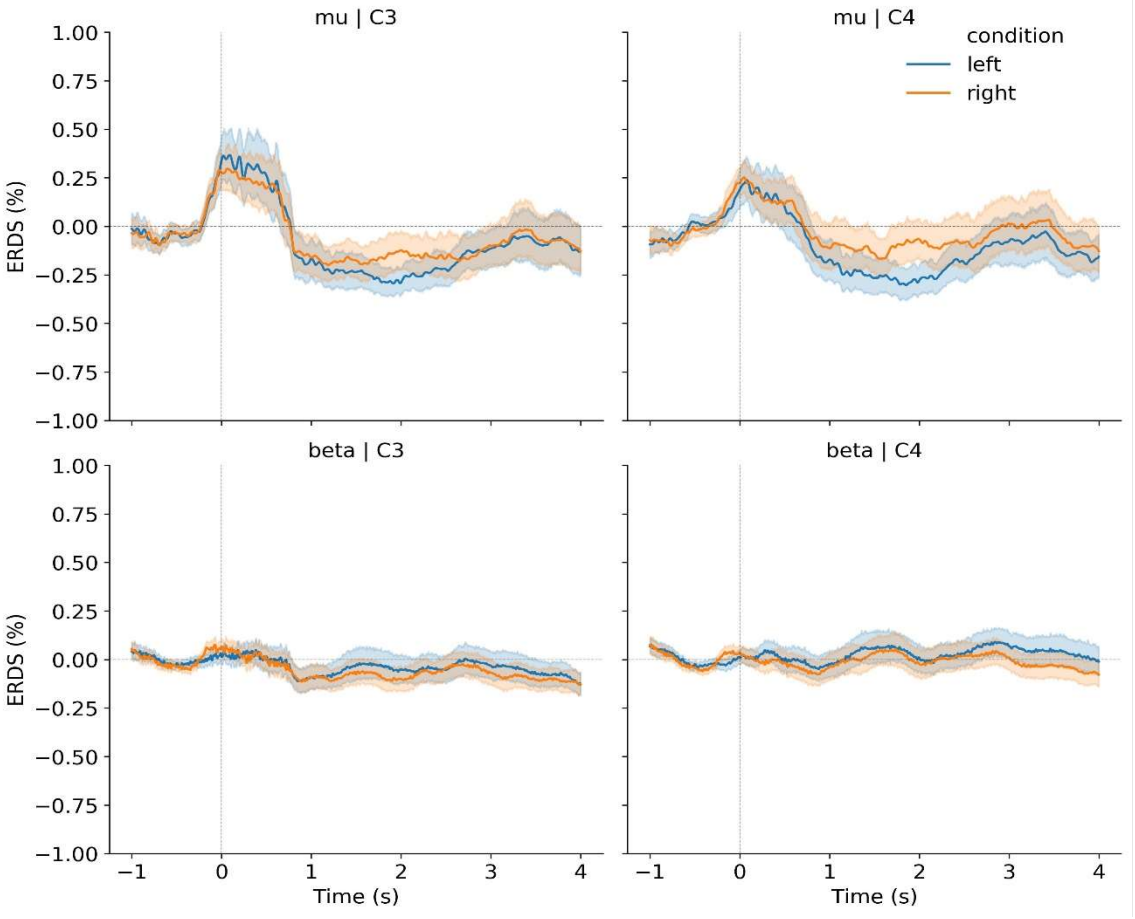

CONTROL –5 – TRAINING

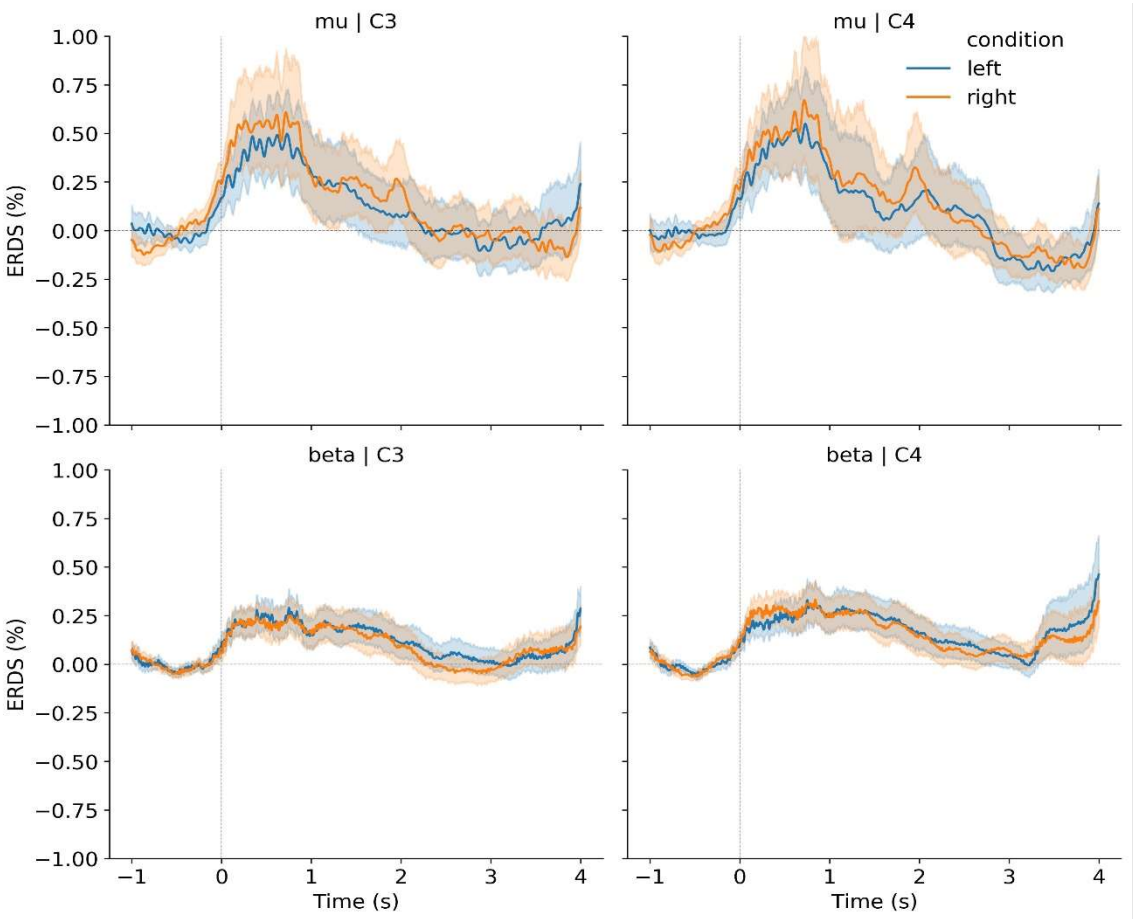

CONTROL – 5 – TESTING

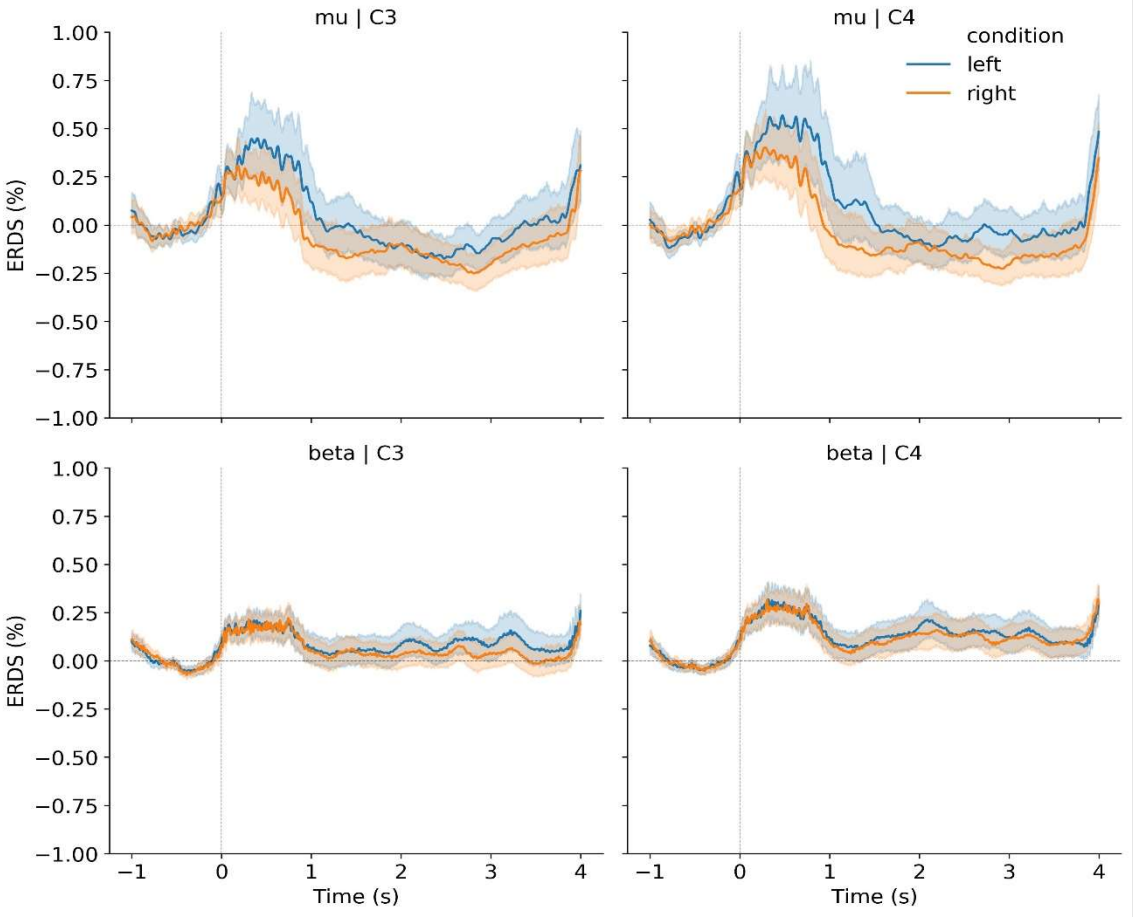

CONTROL – 6 – TRAINING

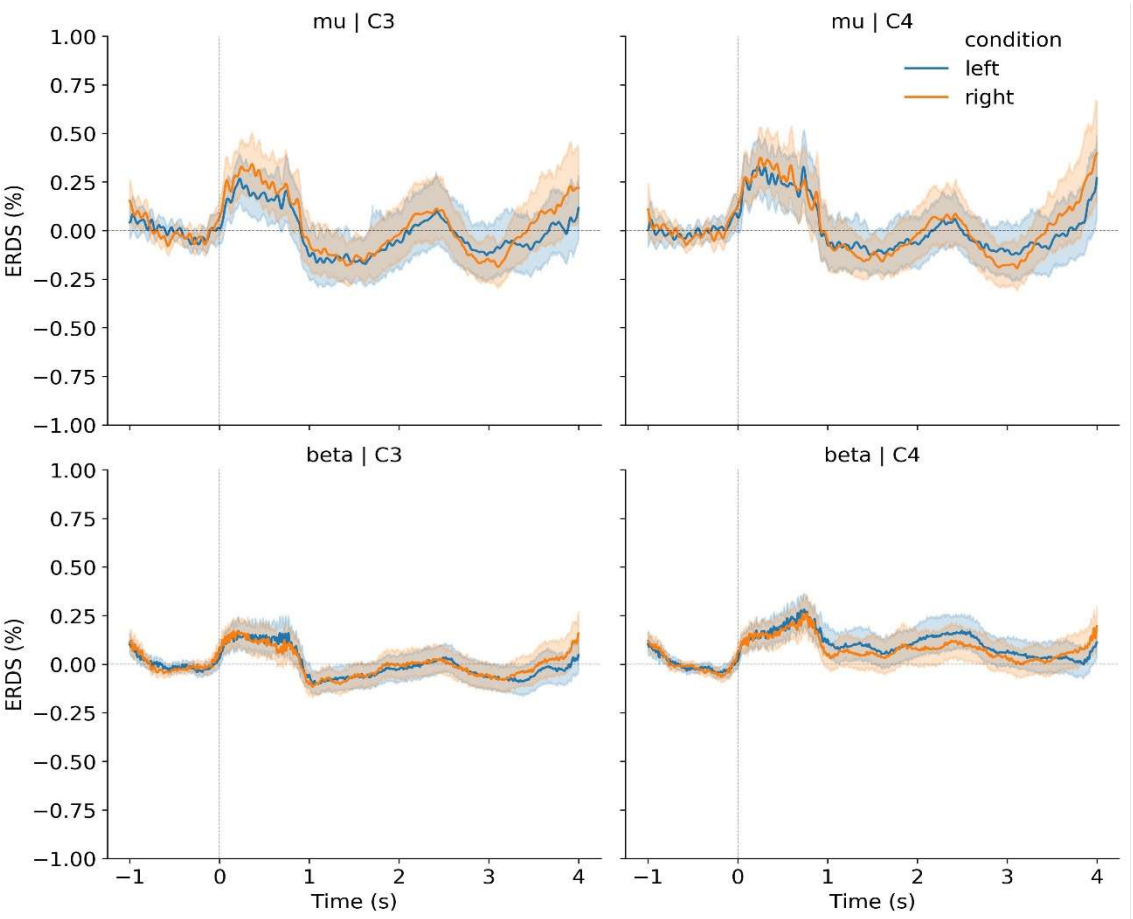

CONTROL – 6 – TESTING

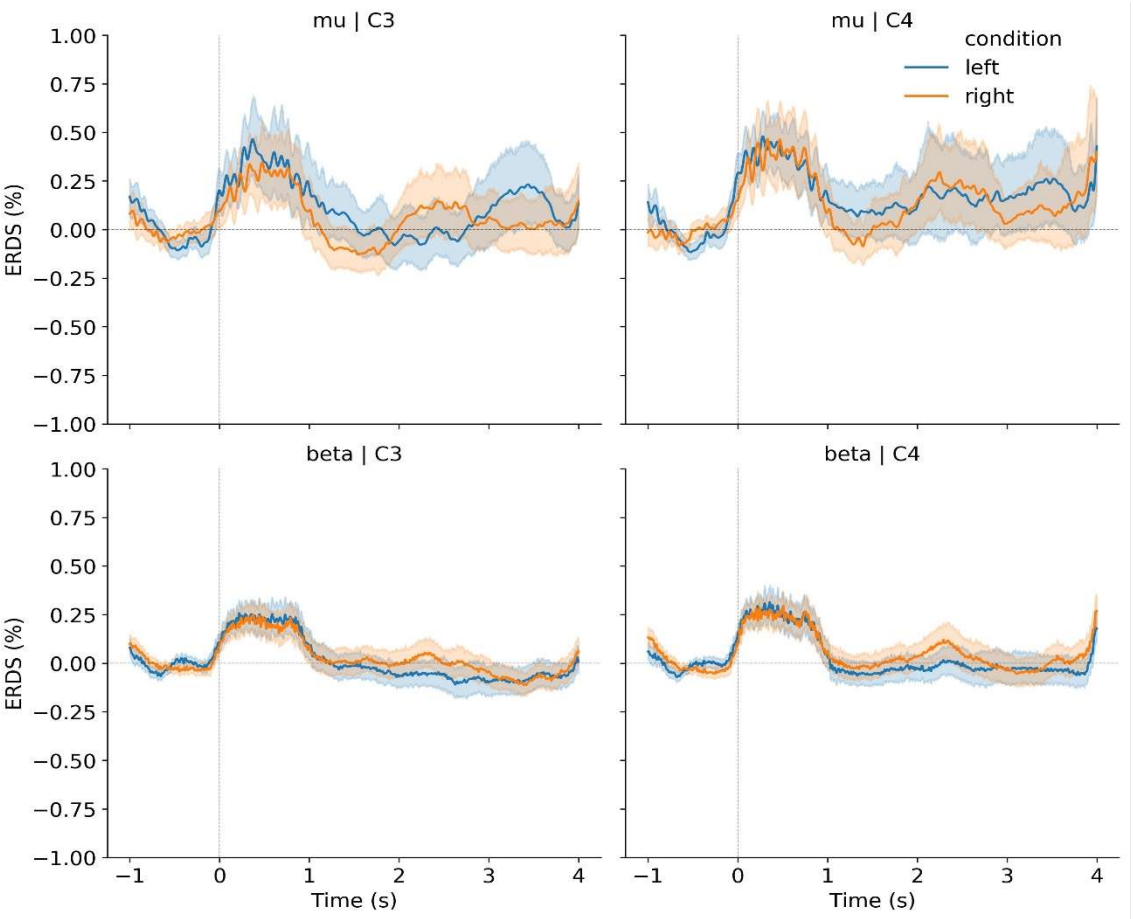

CONTROL – 7 – TRAINING

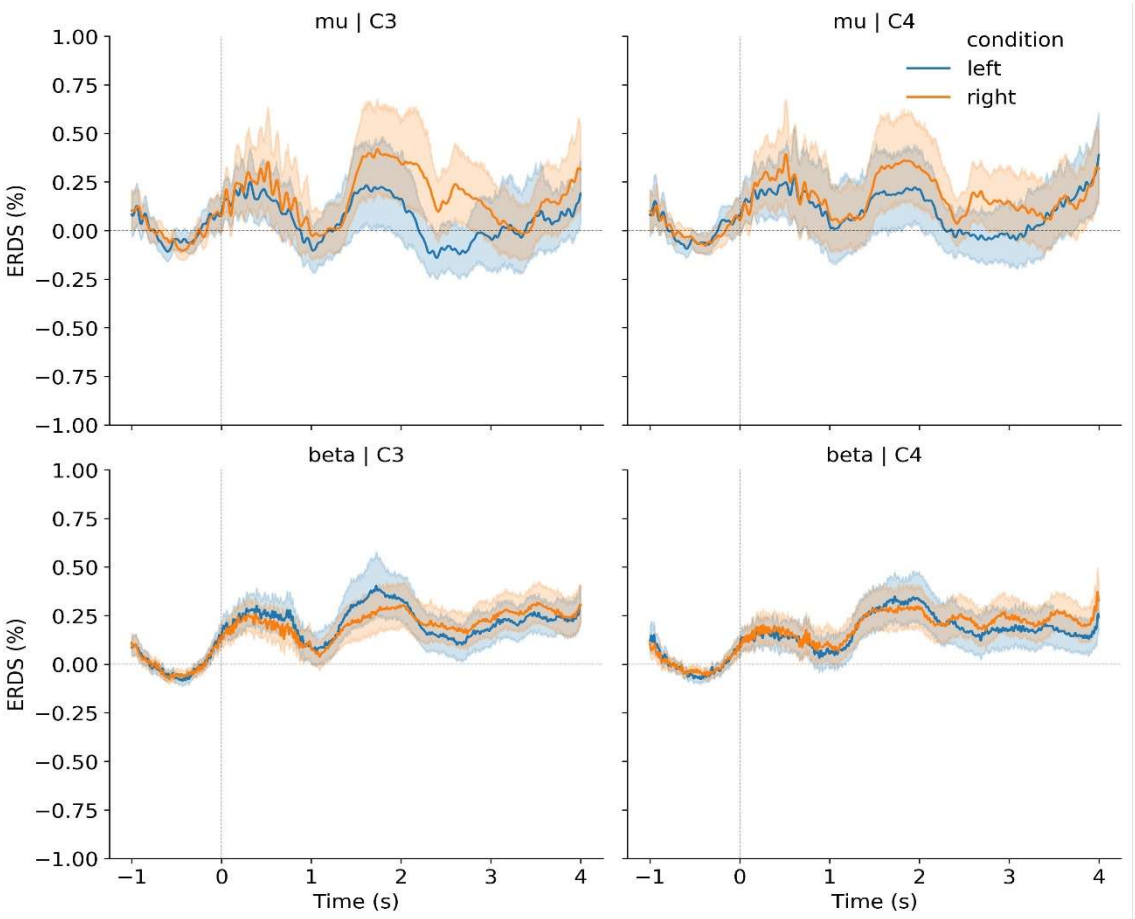

CONTROL – 7 – TESTING

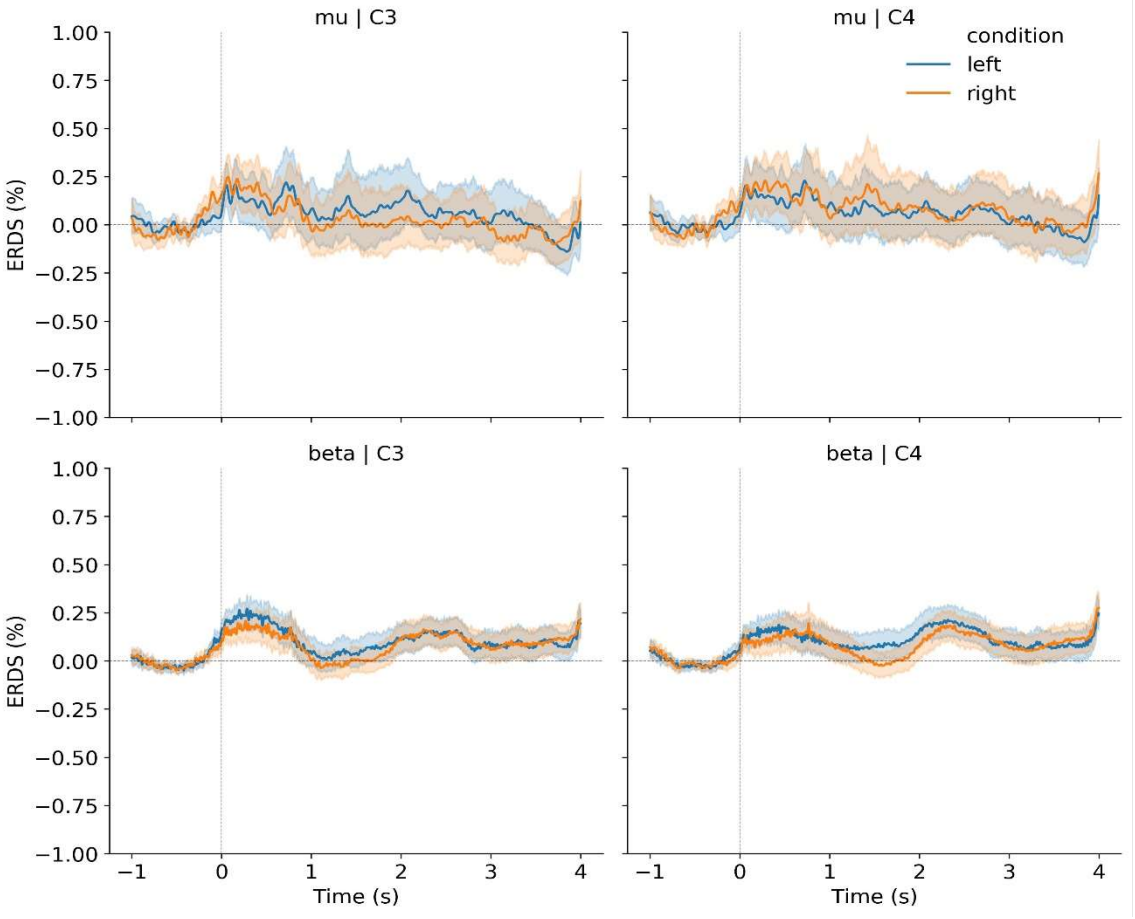

CONTROL – 8 – TRAINING

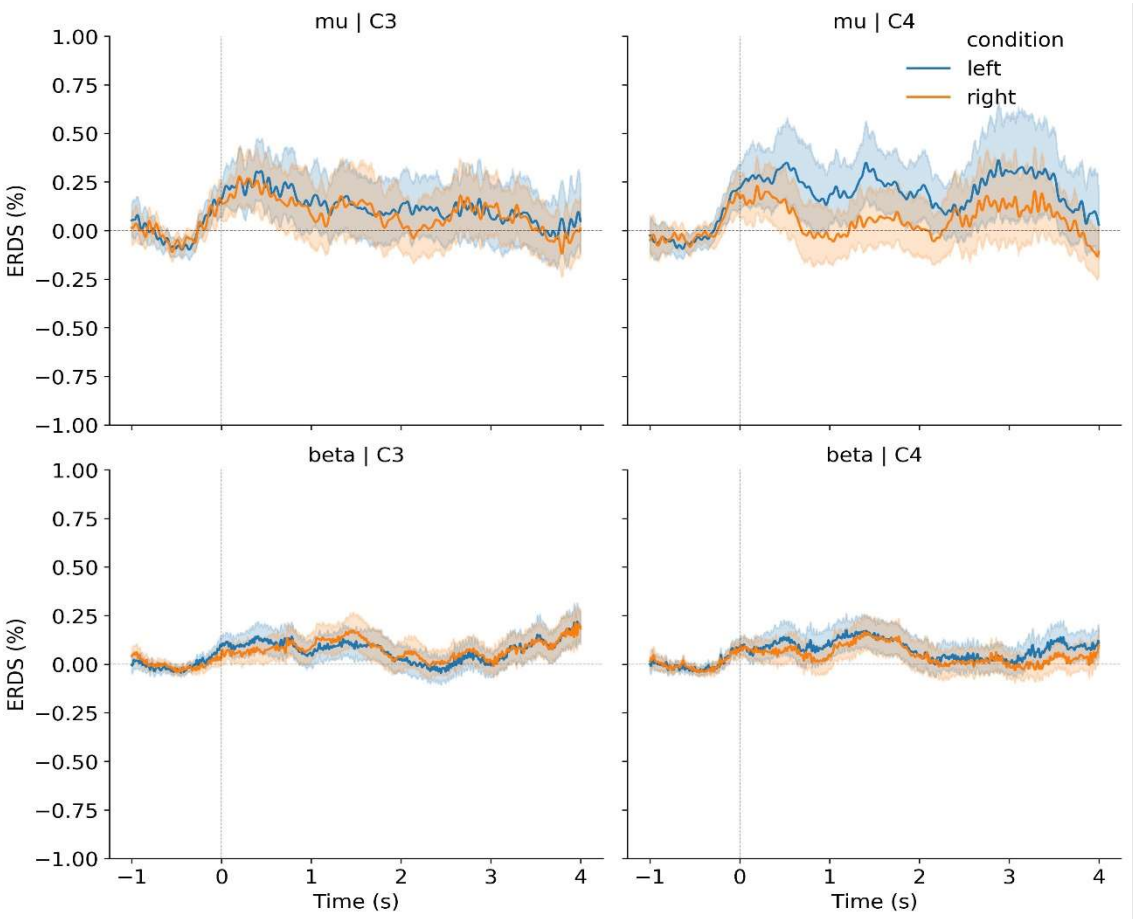

CONTROL – 8 – TESTING

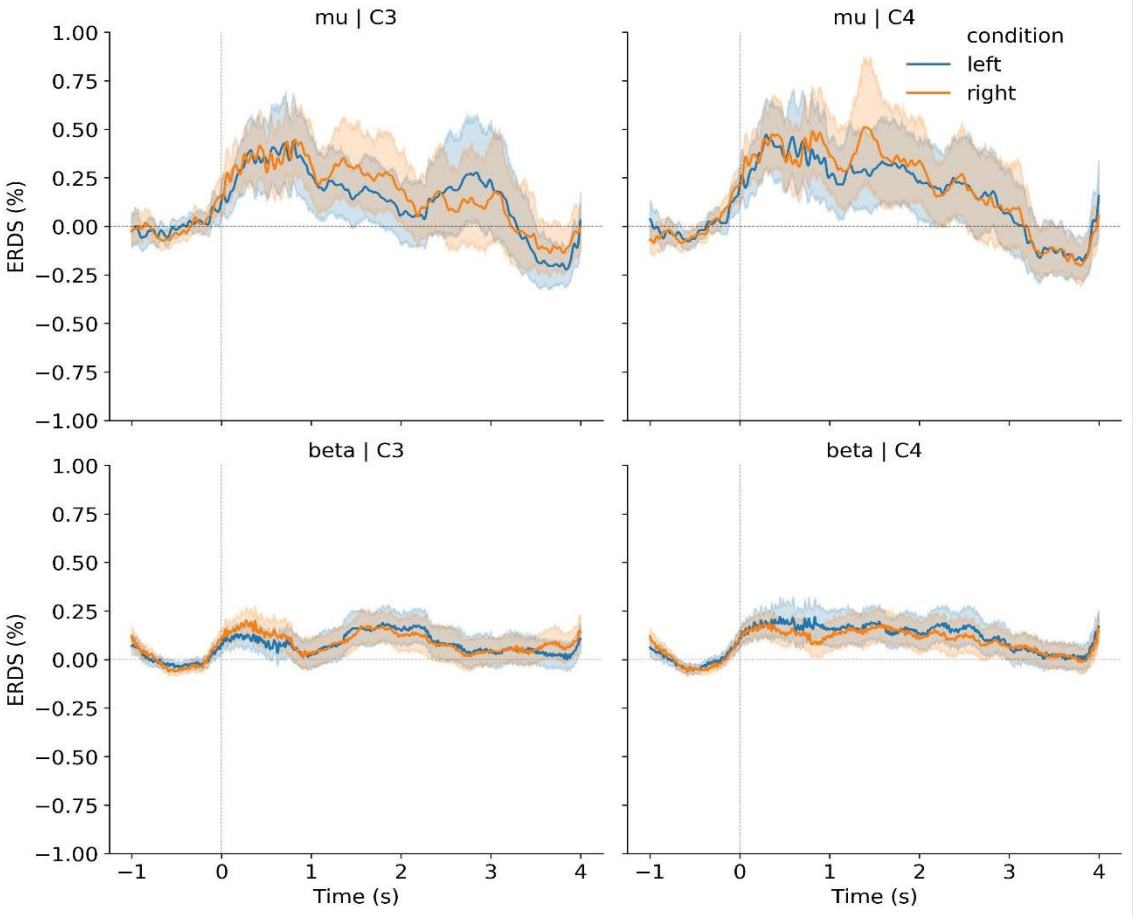

VR – 1 – TRAINING

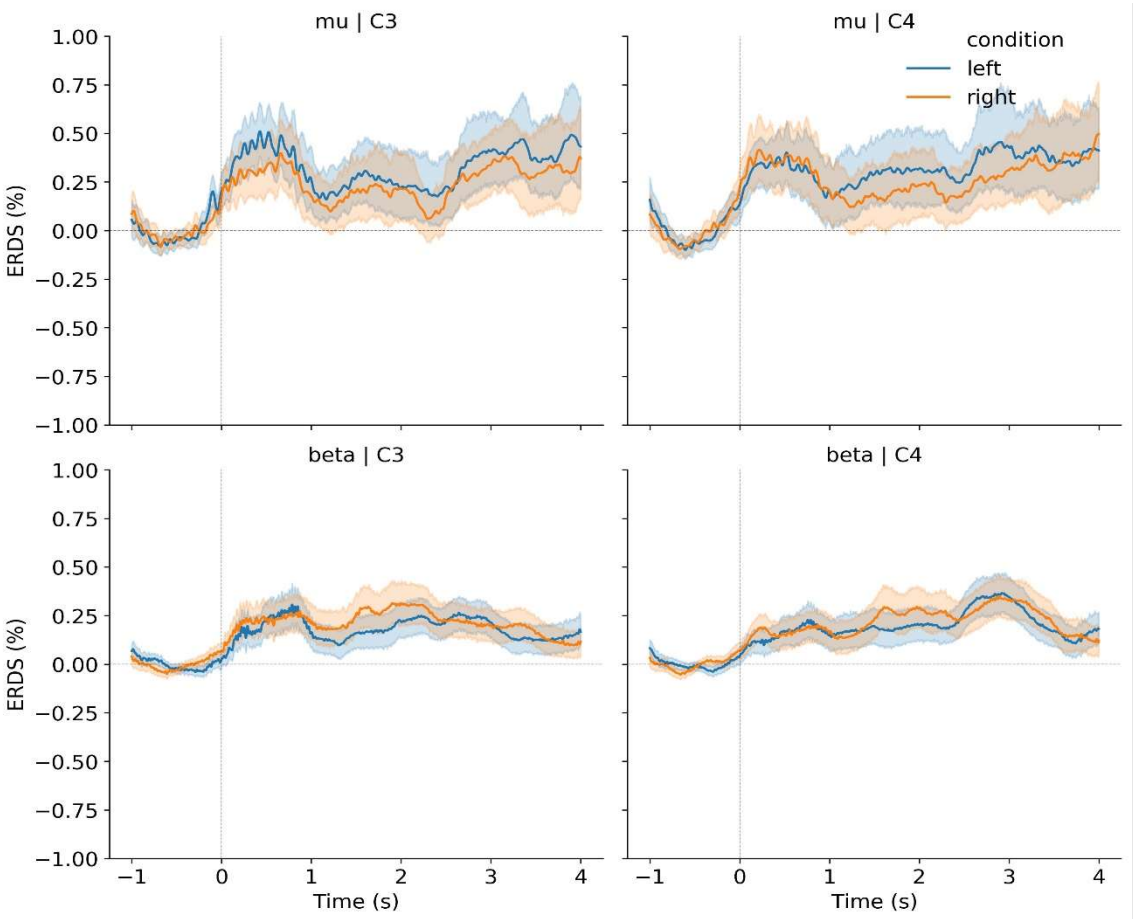

VR – 1 – TESTING

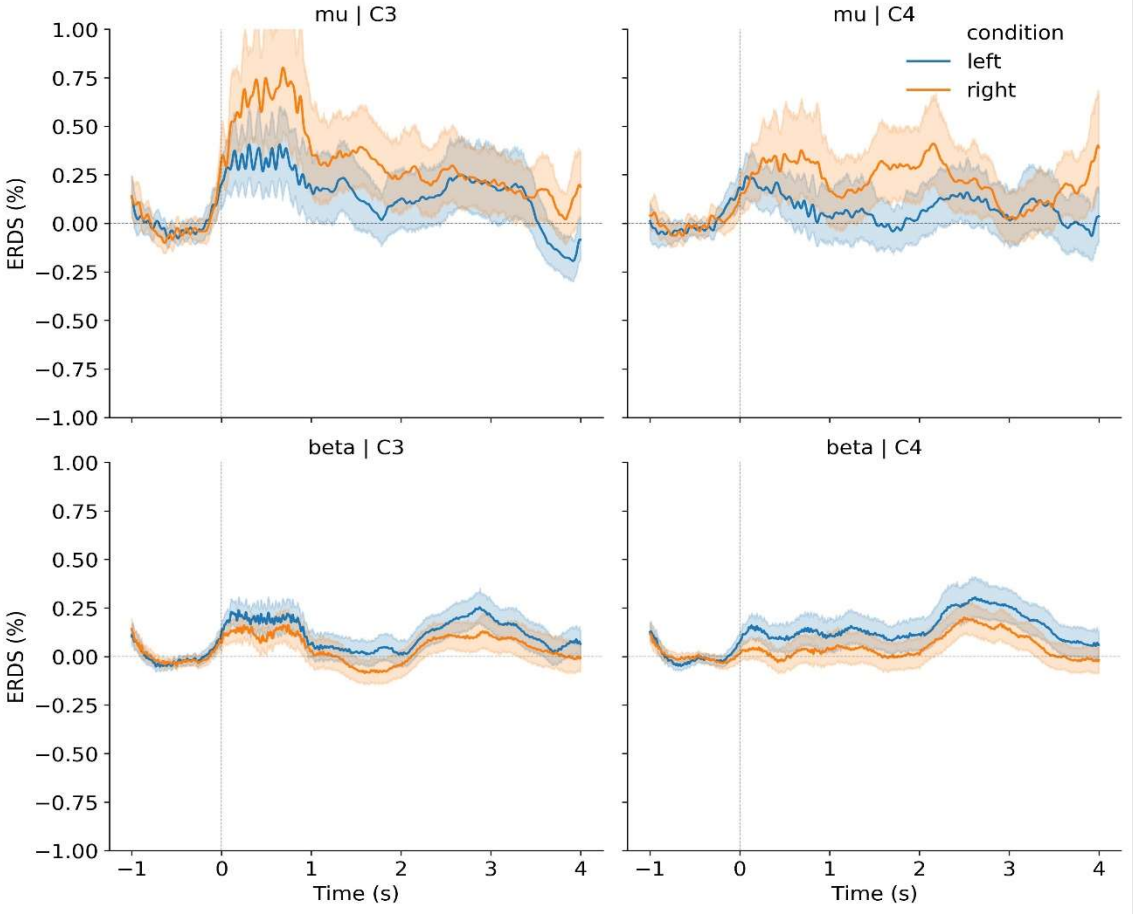

VR – 2 – TRAINING

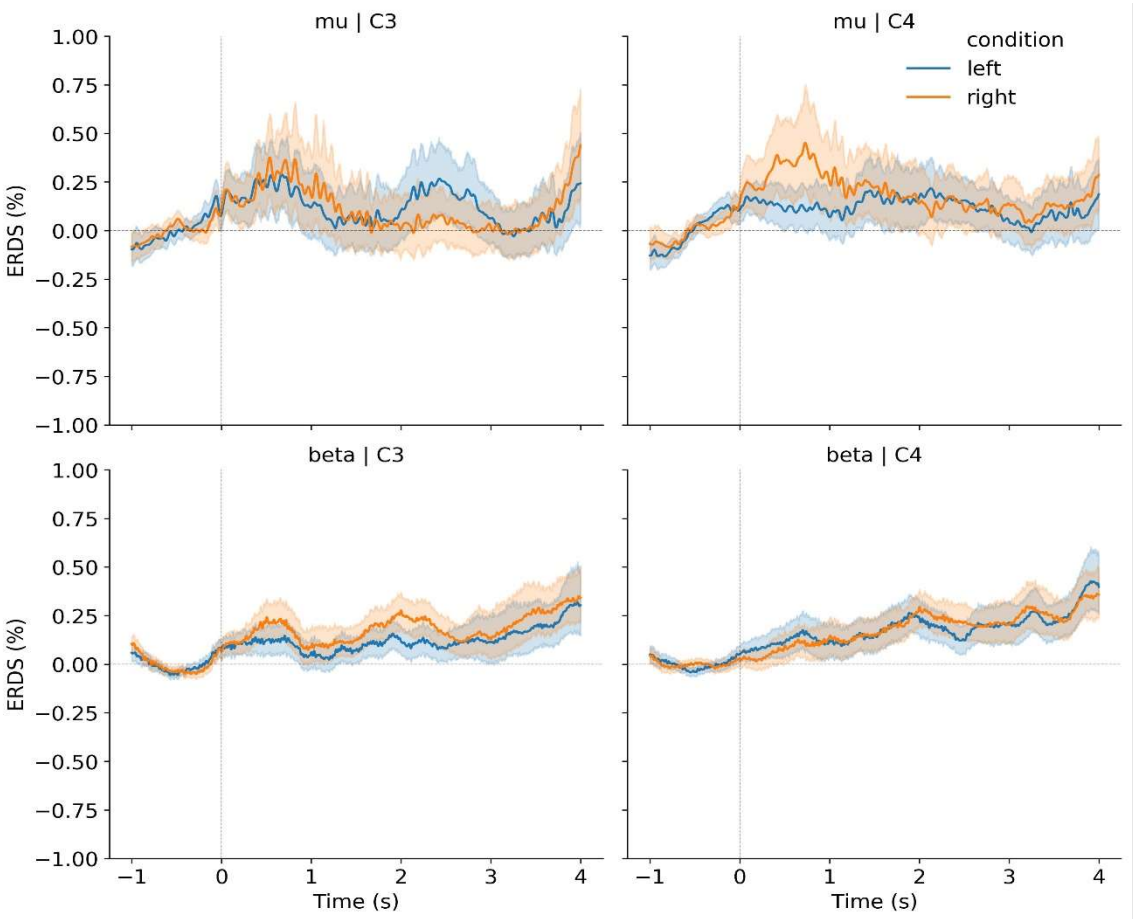

VR – 2 – TESTING

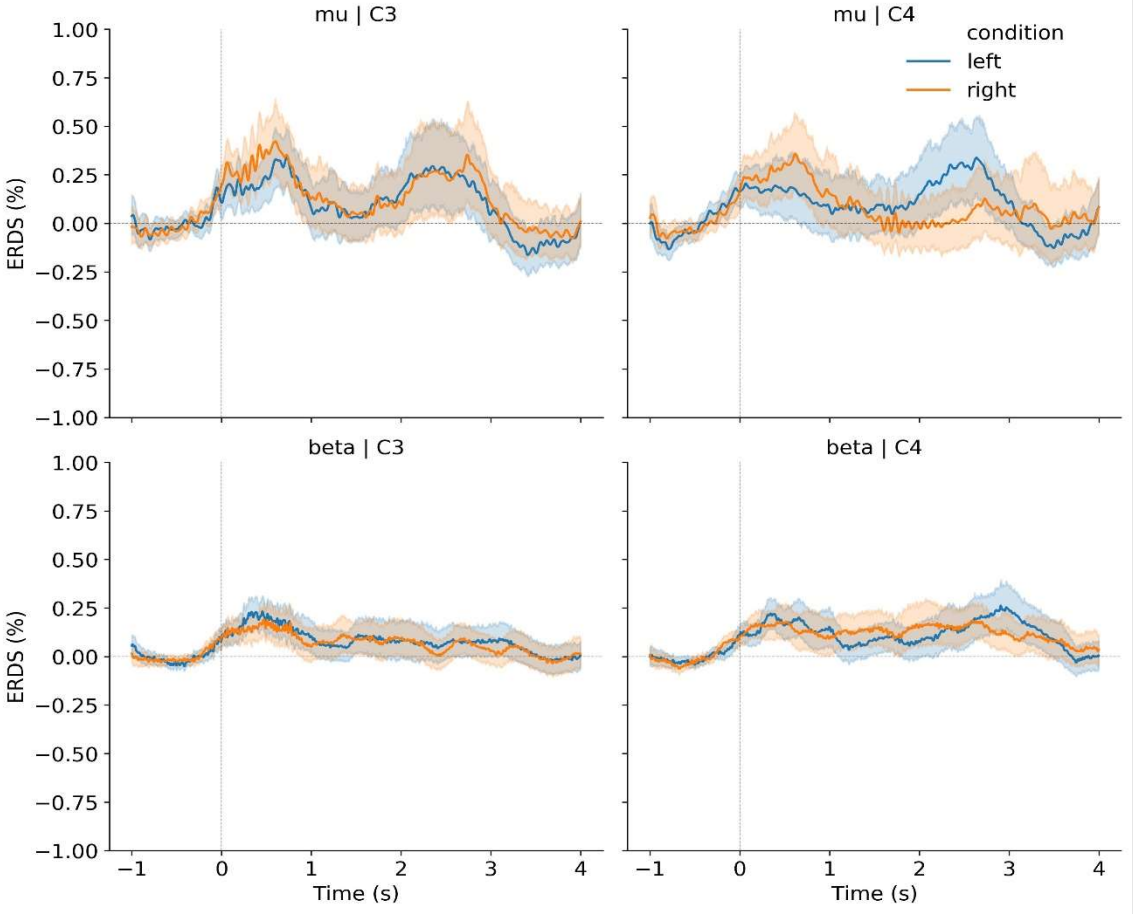

VR – 3 – TRAINING

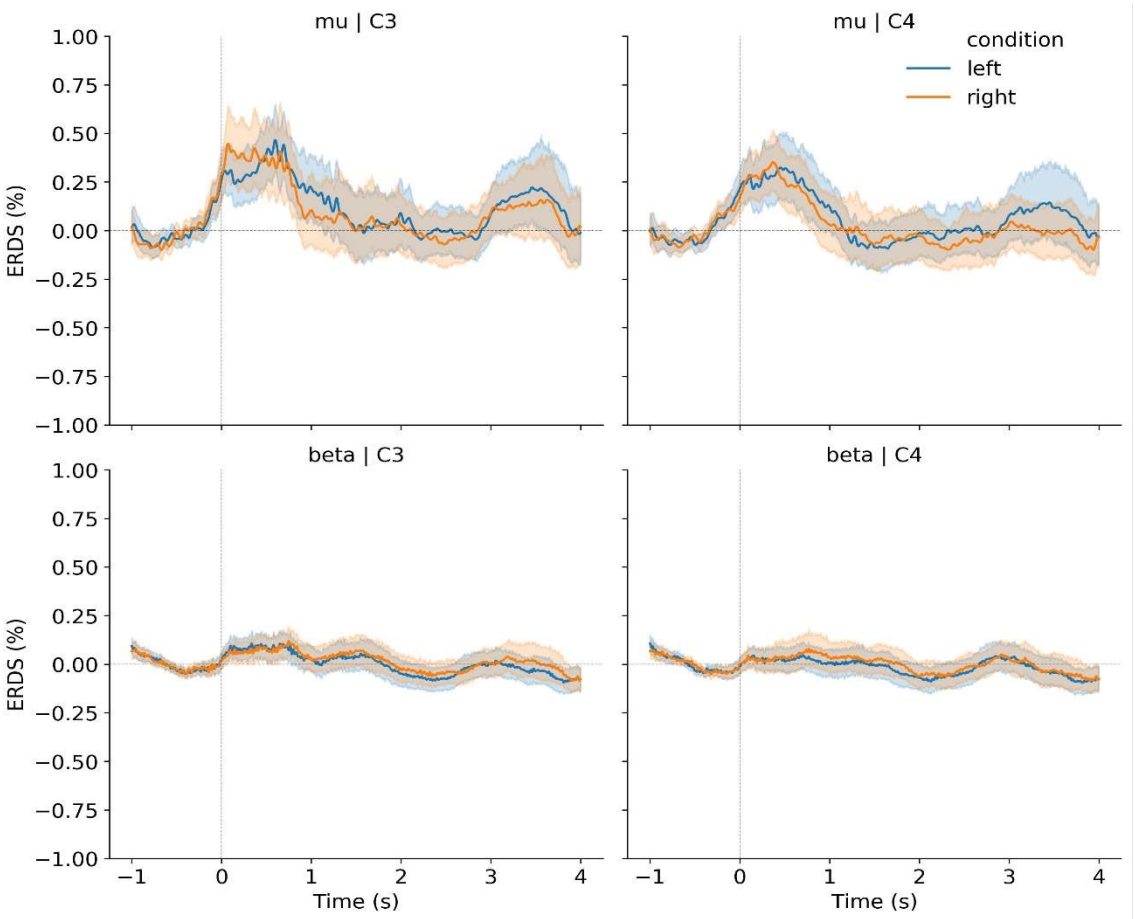

VR – 4 – TRAINING

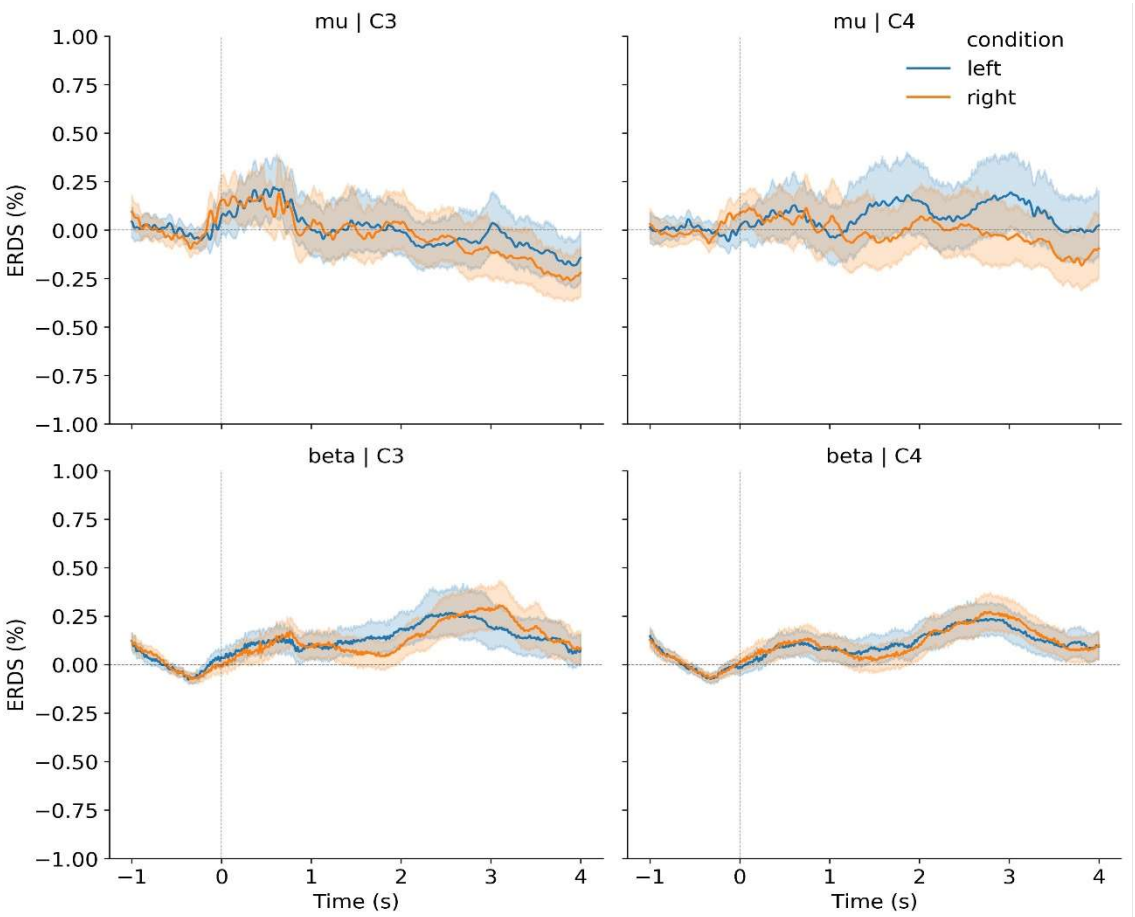

VR – 4 – TESTING

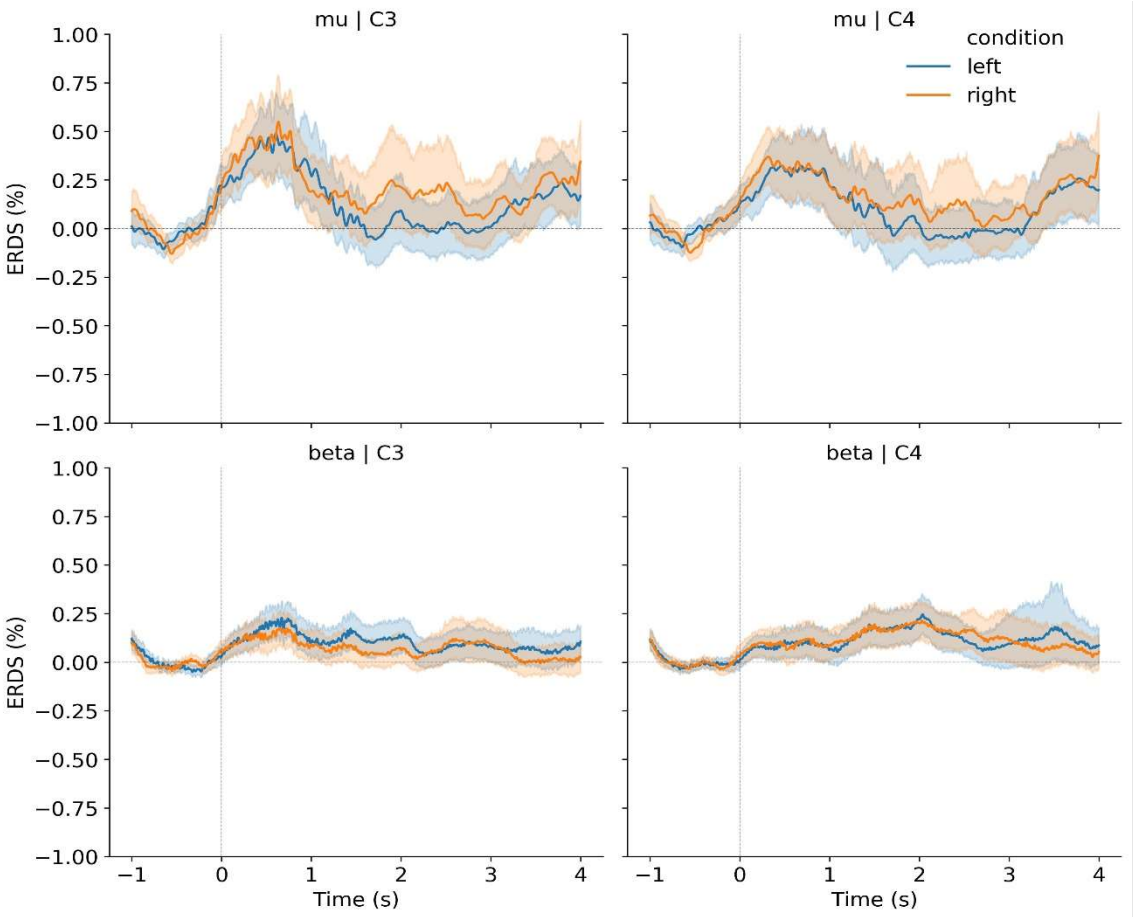

VR – 5 – TRAINING

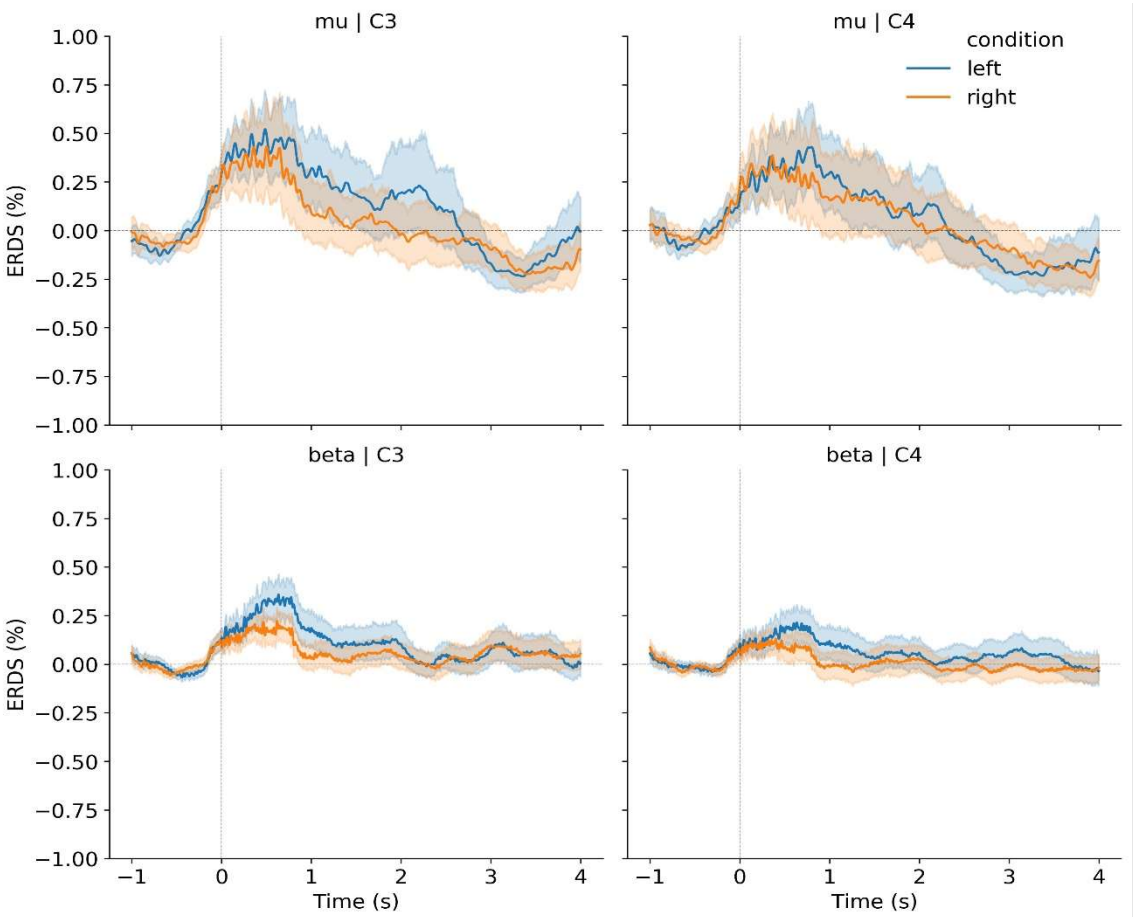

VR – 5 – TESTING

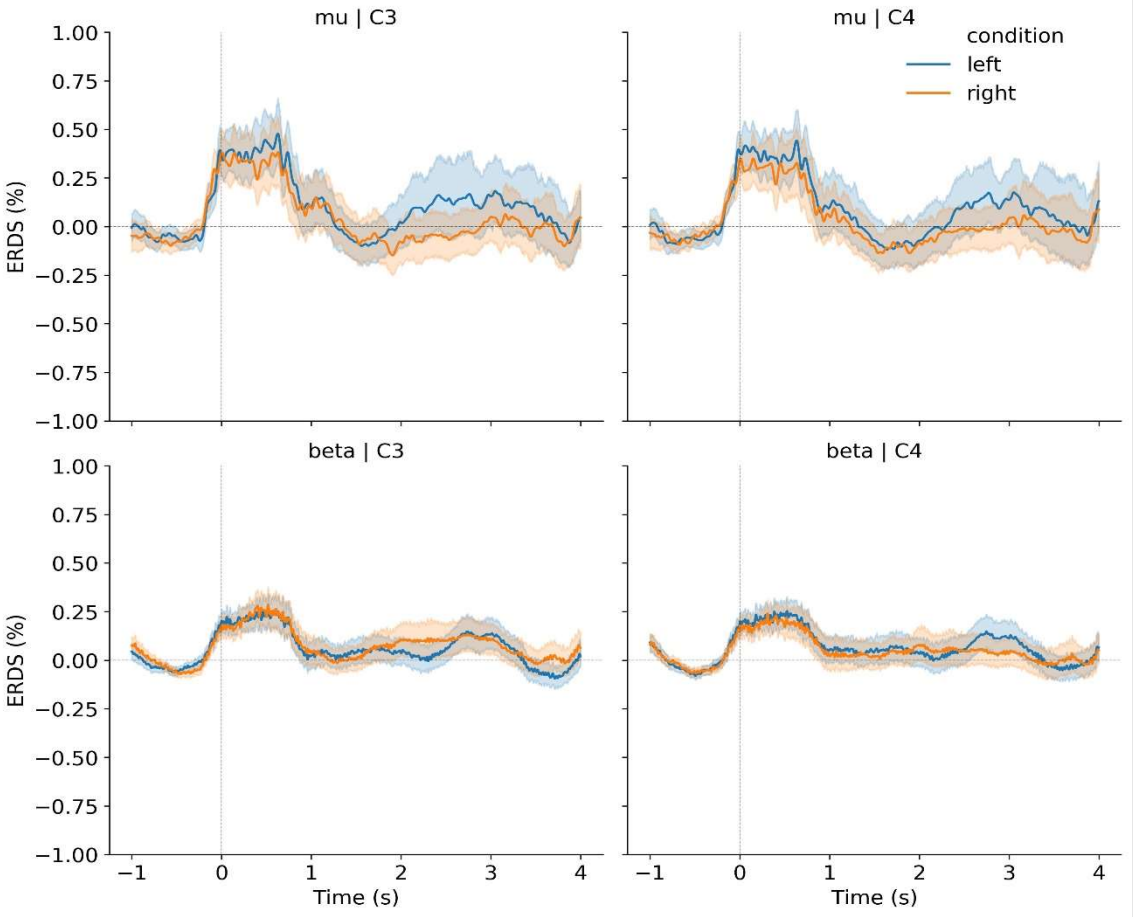

VR – 6 – TRAINING

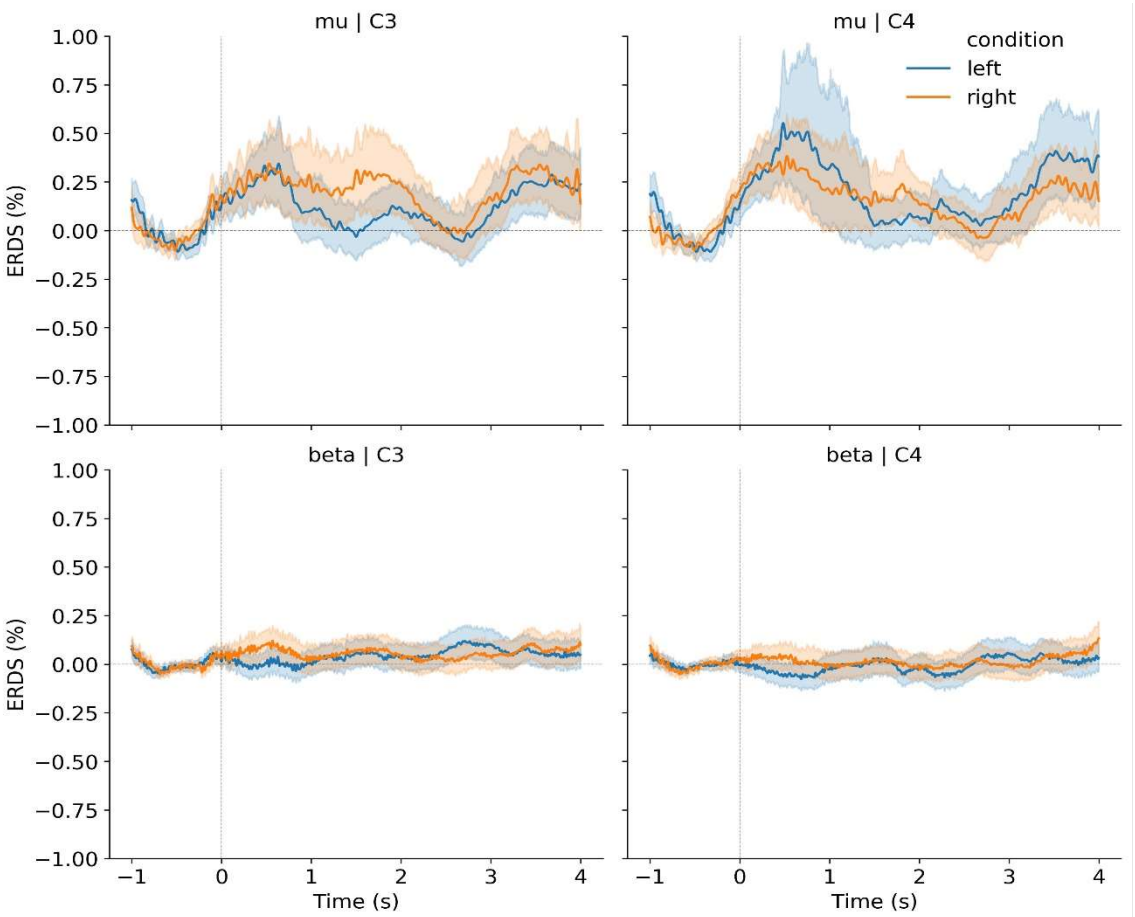

VR – 6 – TESTING

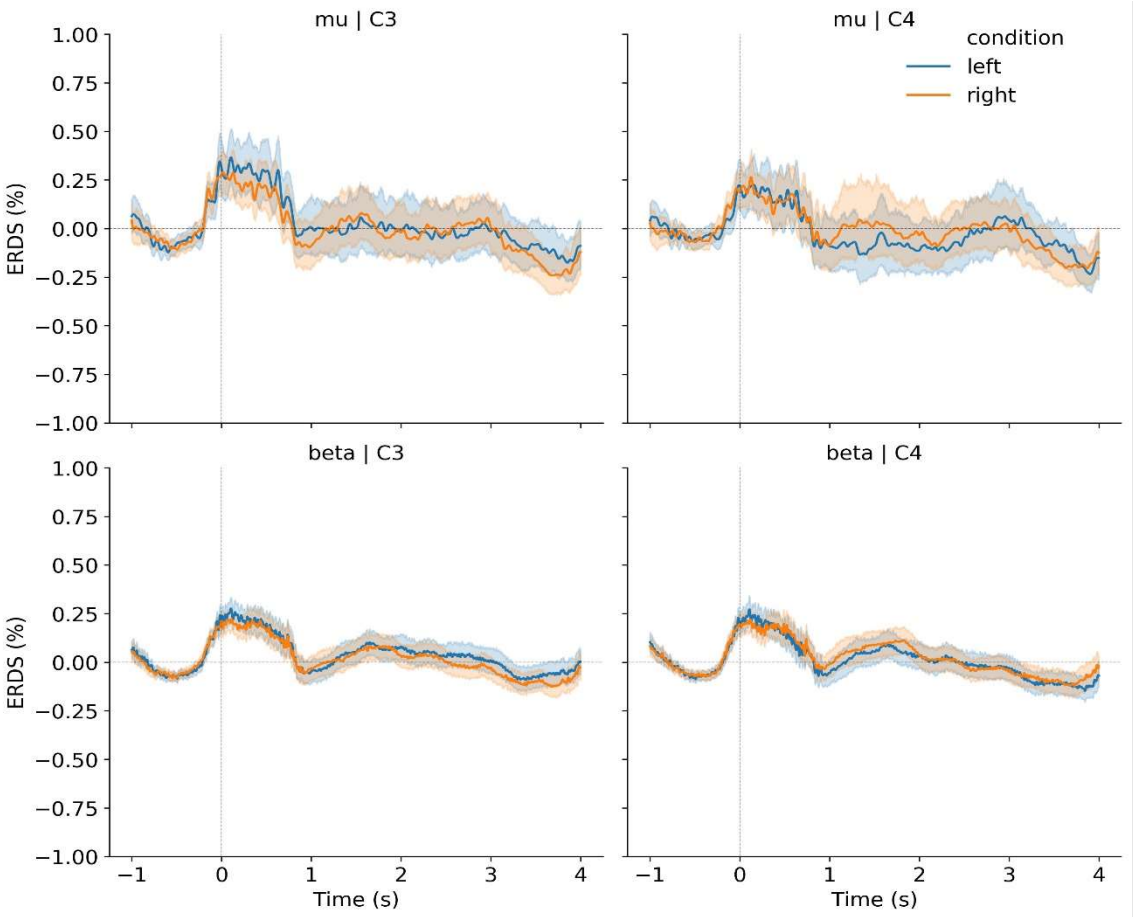

VR – 7 – TRAINING

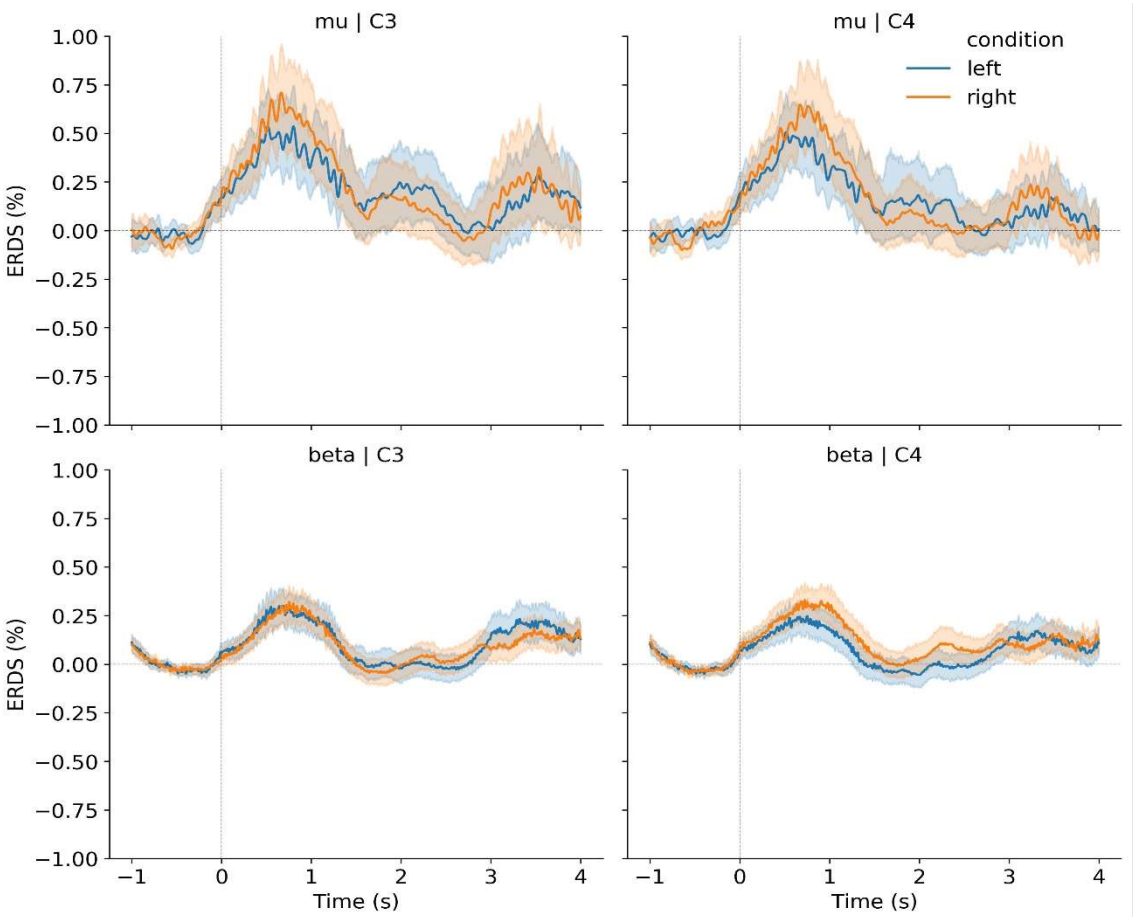

VR – 7 – TESTING

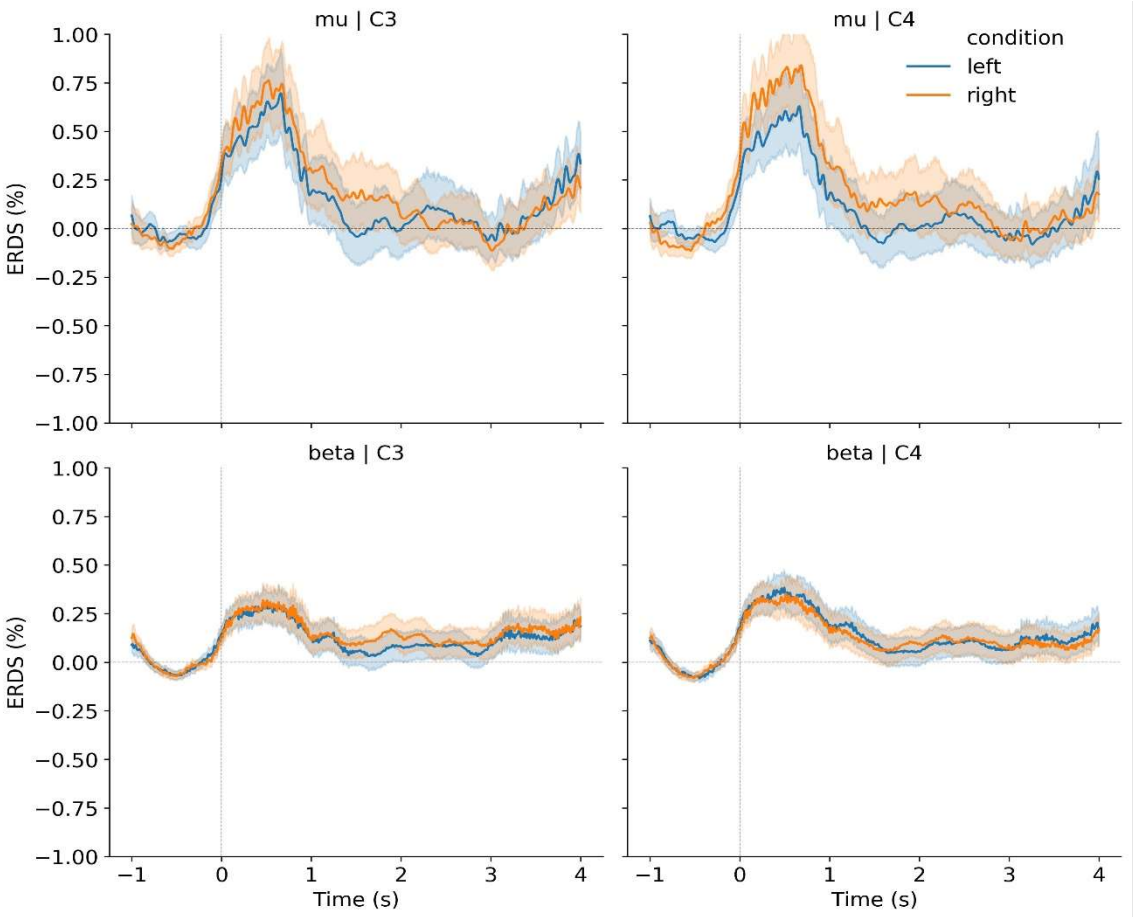

VR – 8 – TRAINING

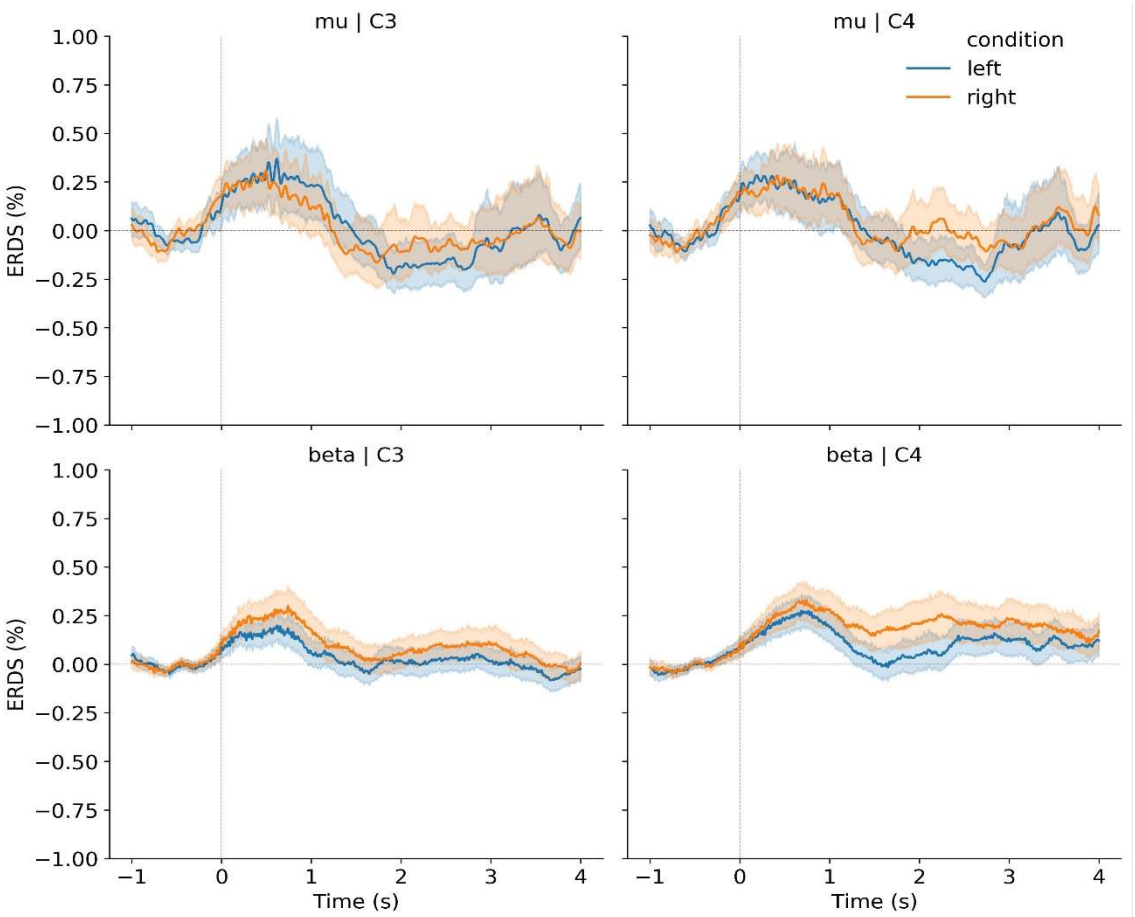

VR – 8 – TESTING

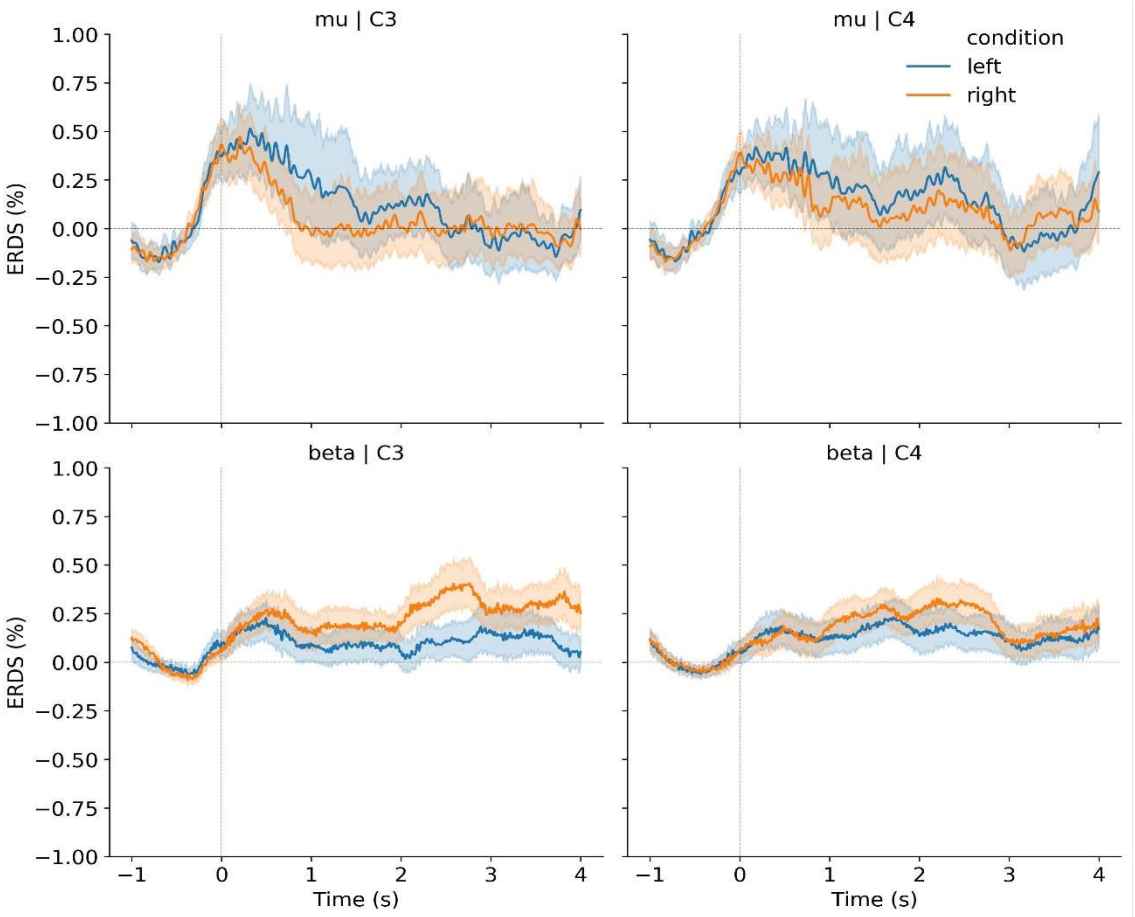

ROBOT – 1 – TRAINING

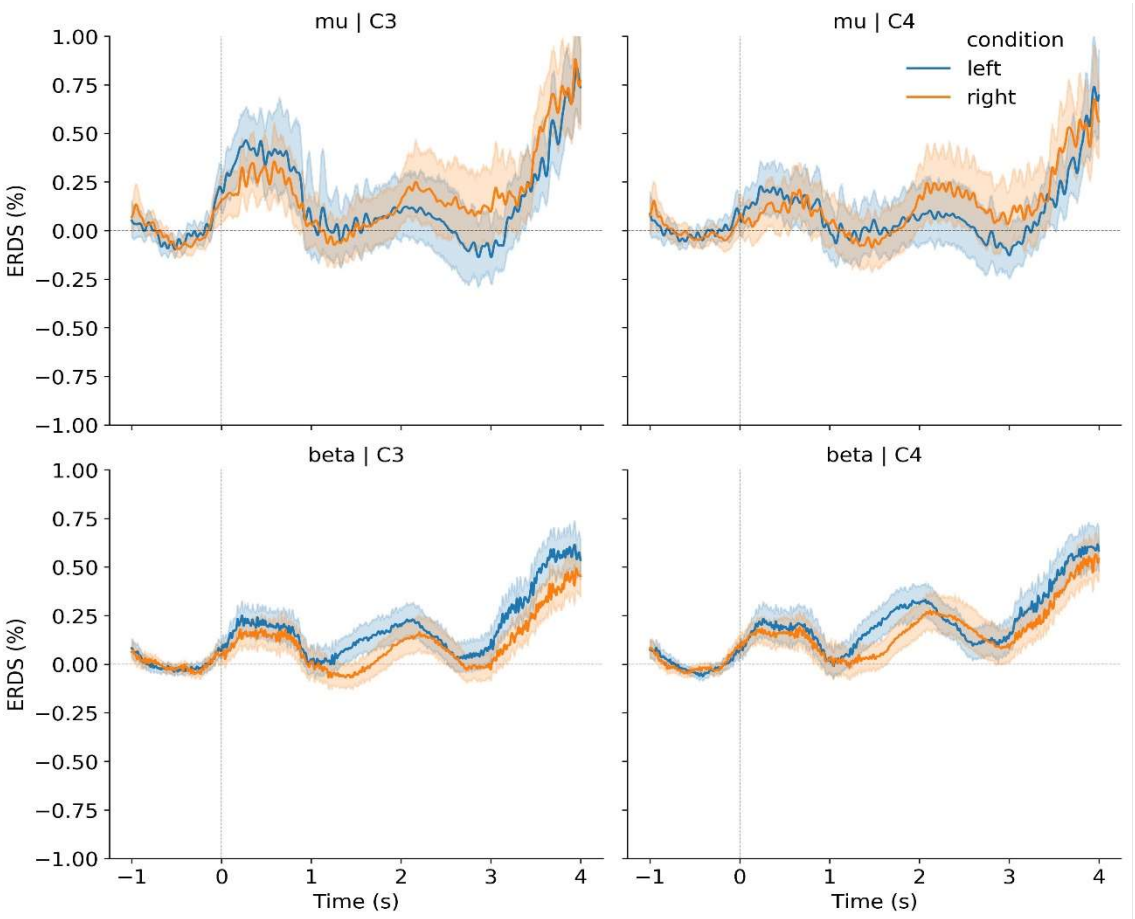

ROBOT – 1 – TESTING

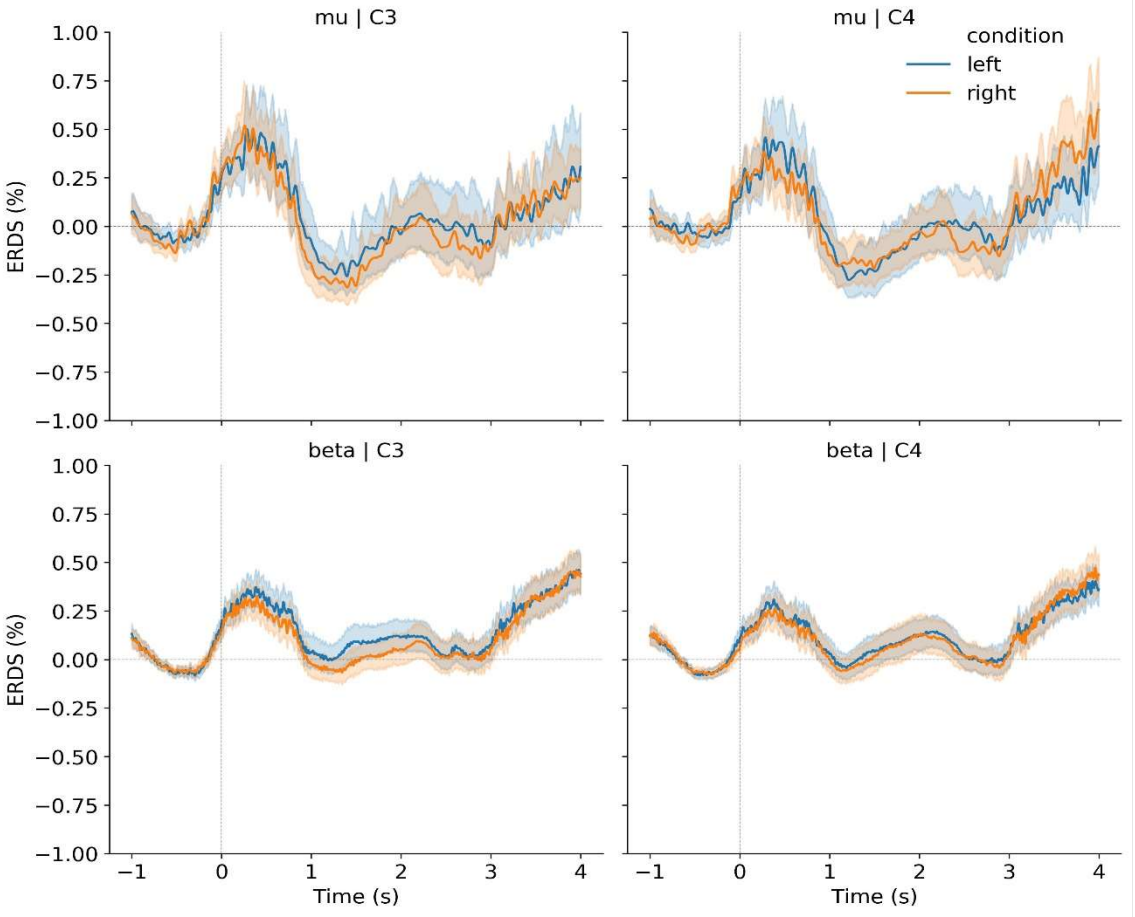

ROBOT – 2 – TRAINING

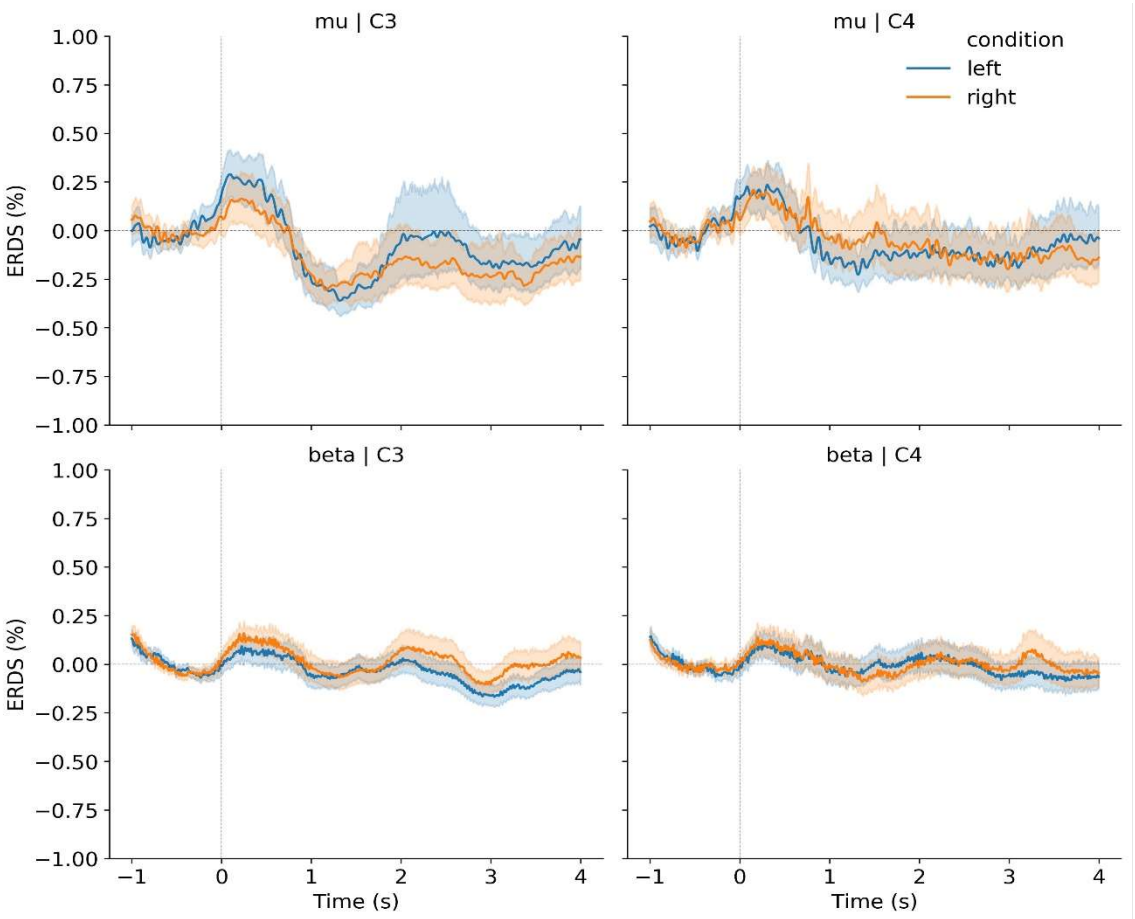

ROBOT – 2 – TESTING

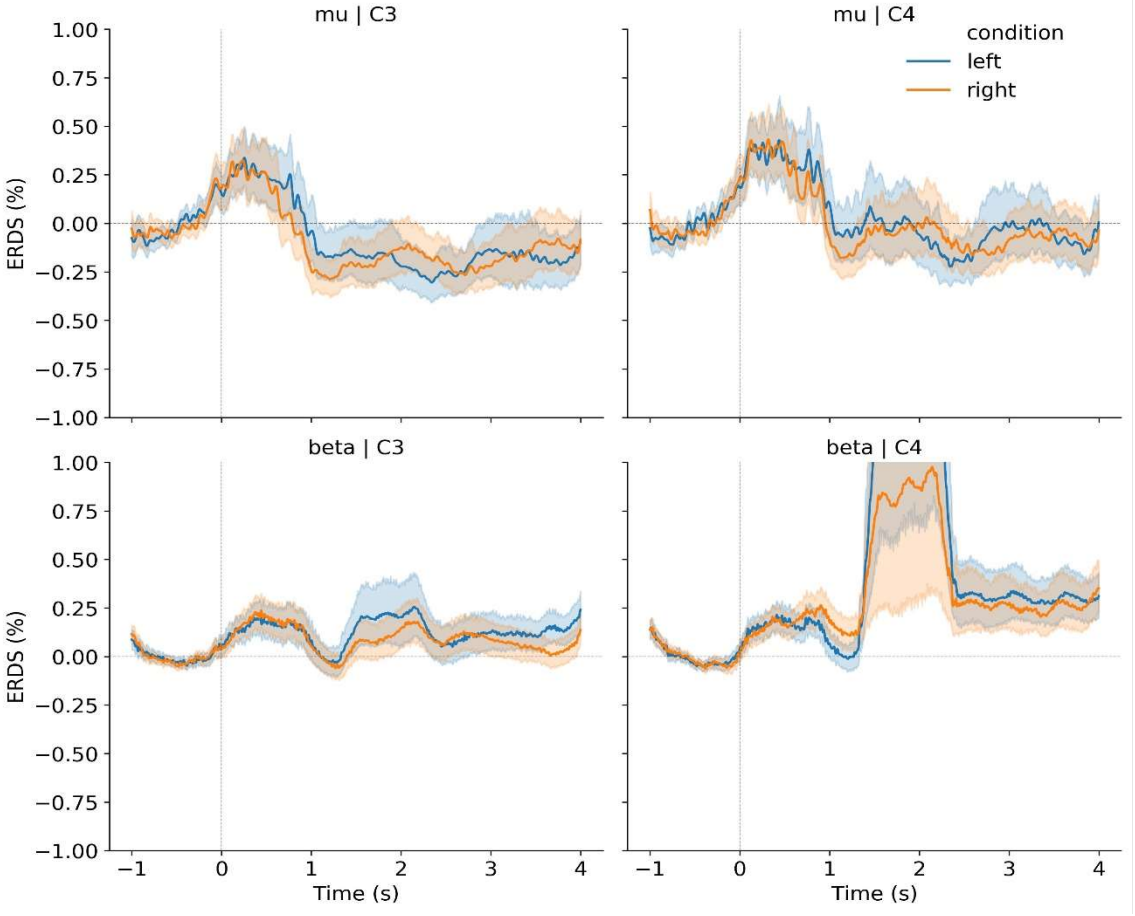

ROBOT – 3 – TRAINING

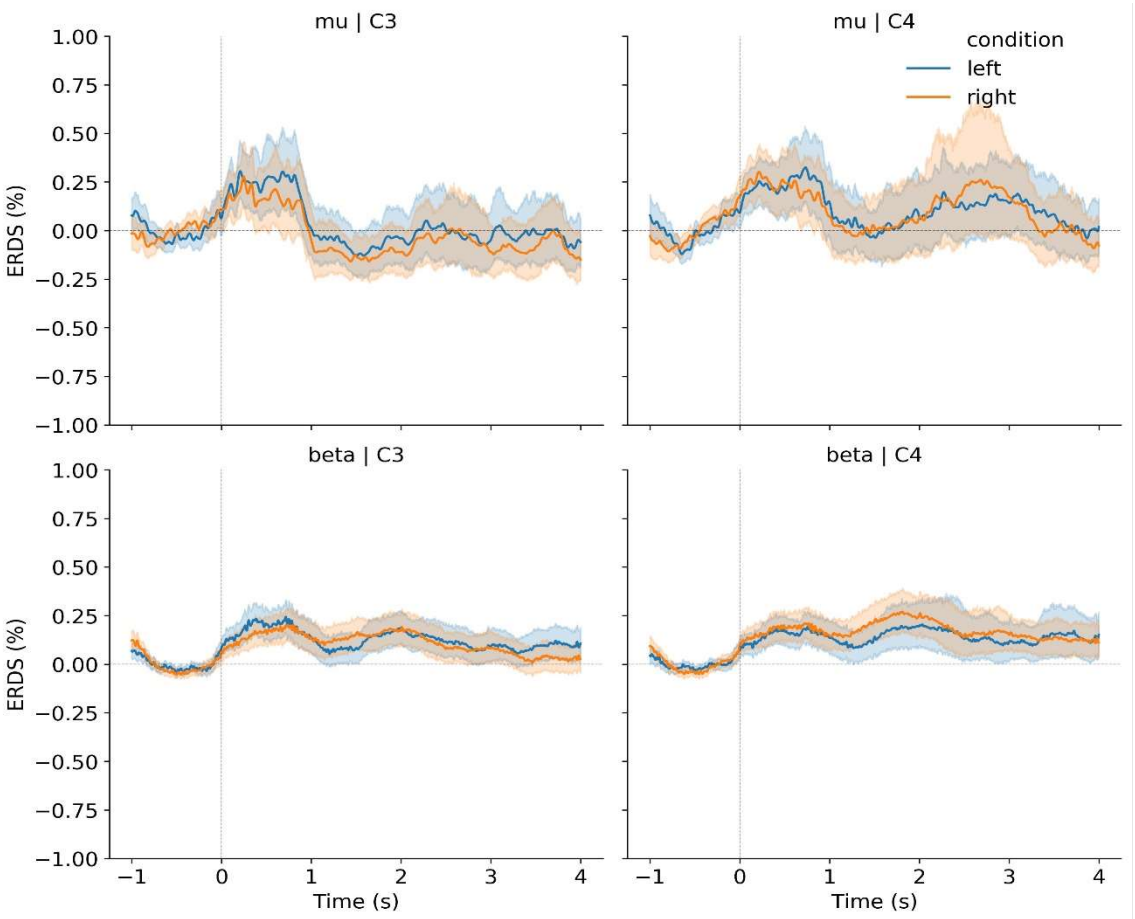

ROBOT – 3 – TESTING

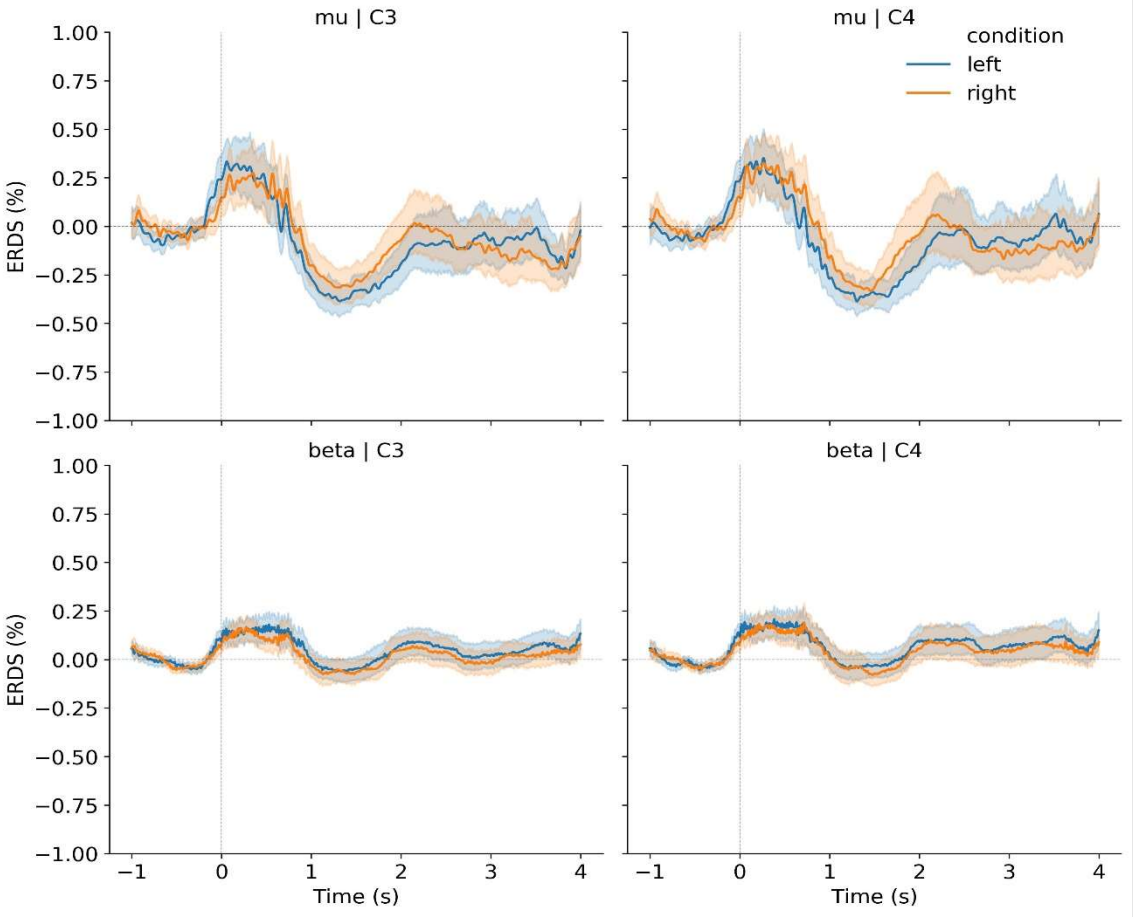

ROBOT – 4 – TRAINING

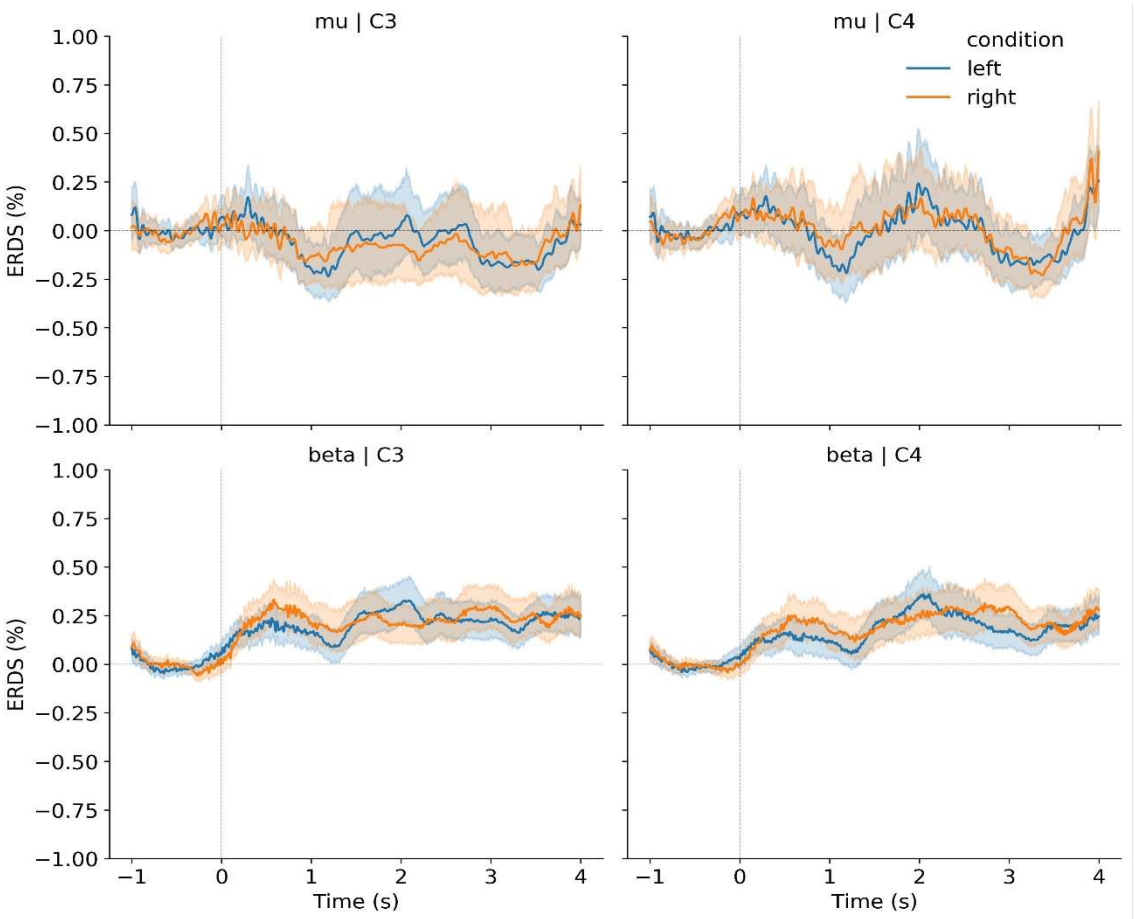

ROBOT – 4 – TESTING

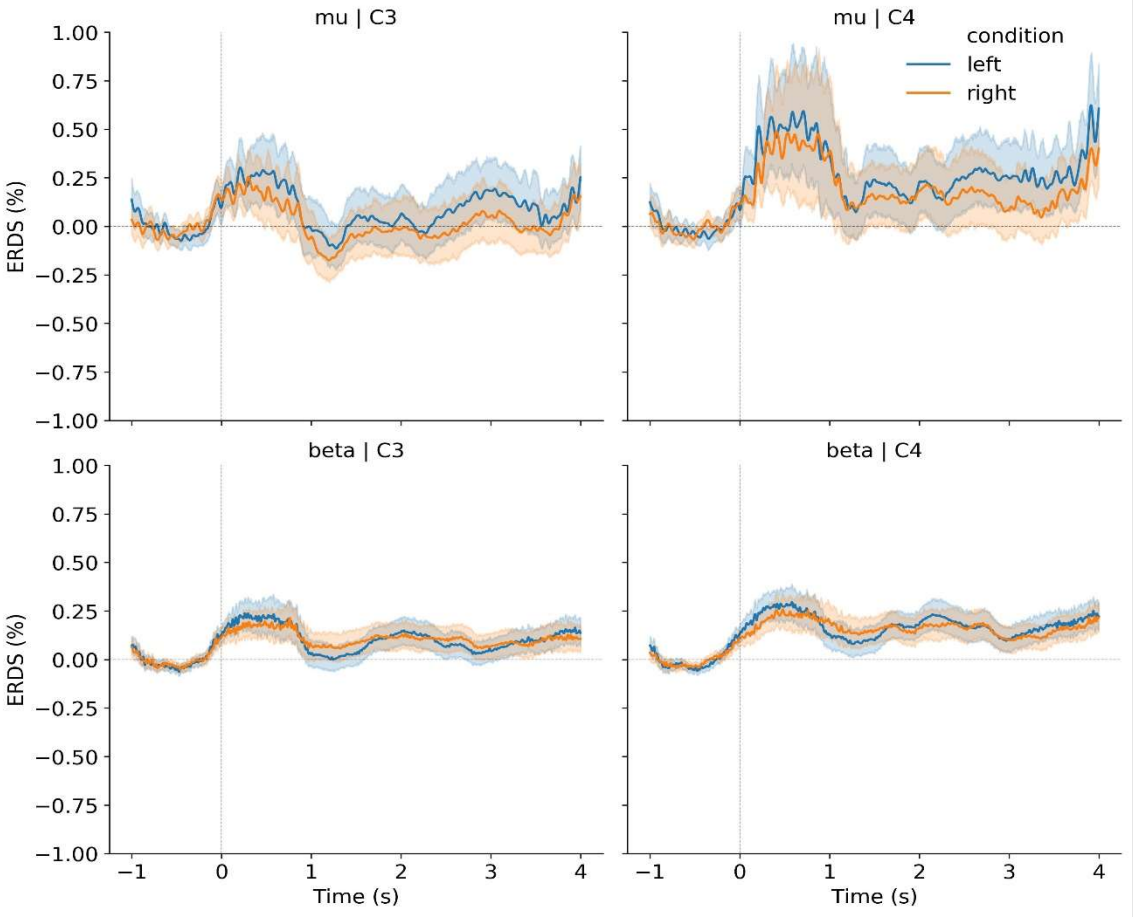

ROBOT – 5 – TRAINING

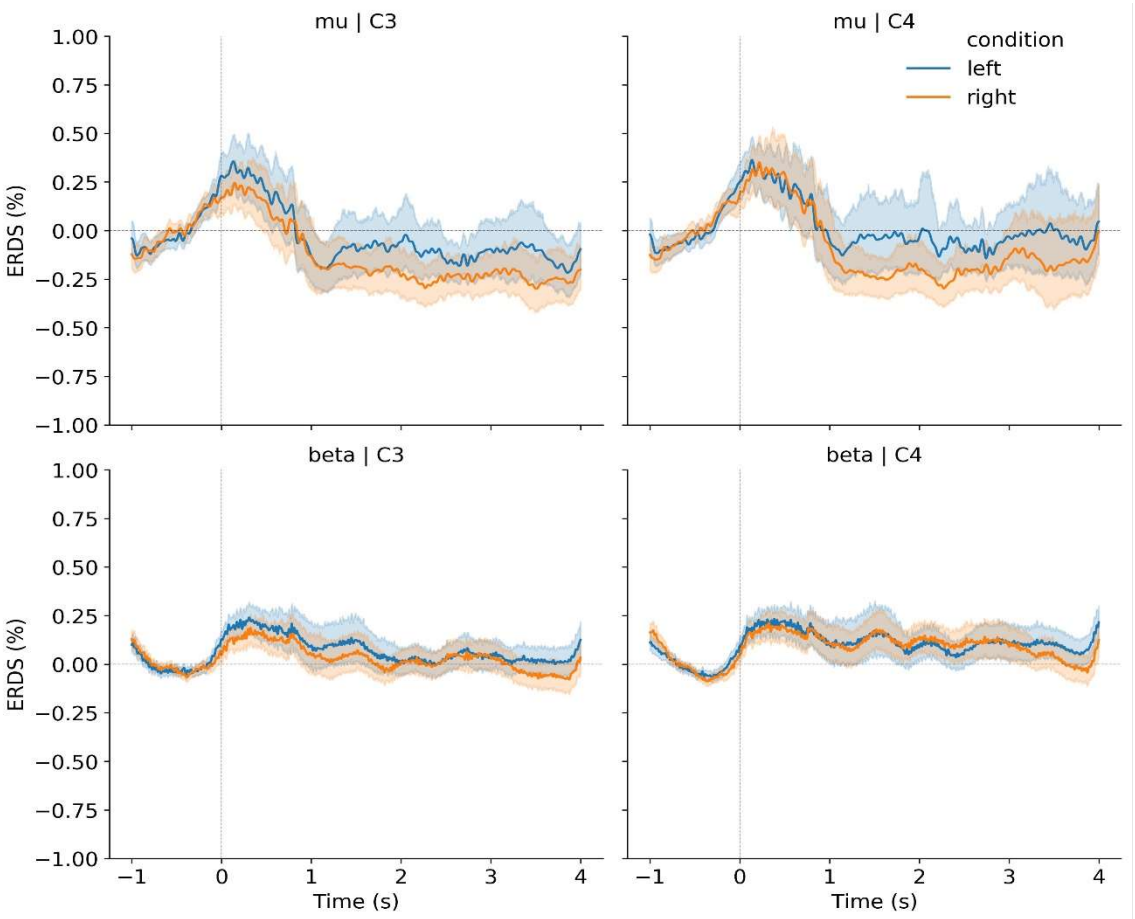

ROBOT – 5 – TESTING

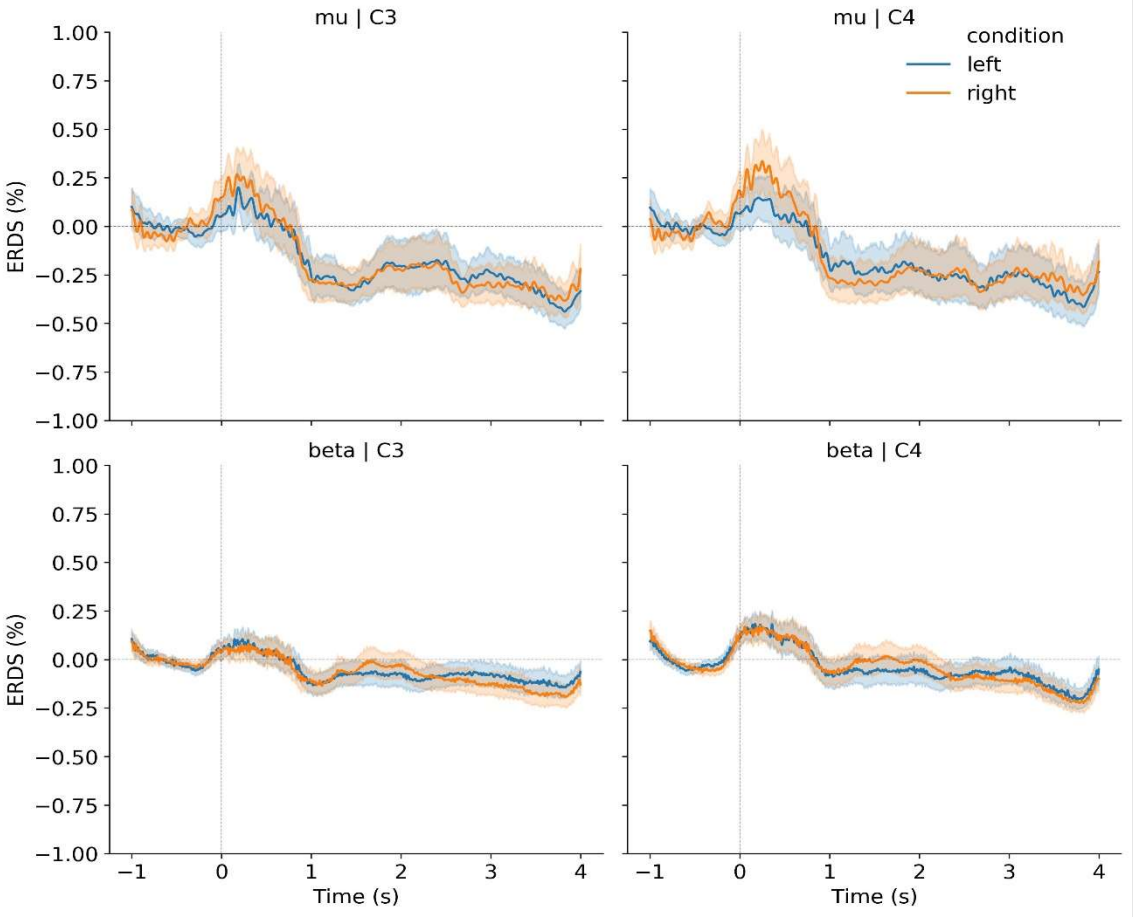

ROBOT – 6 – TRAINING

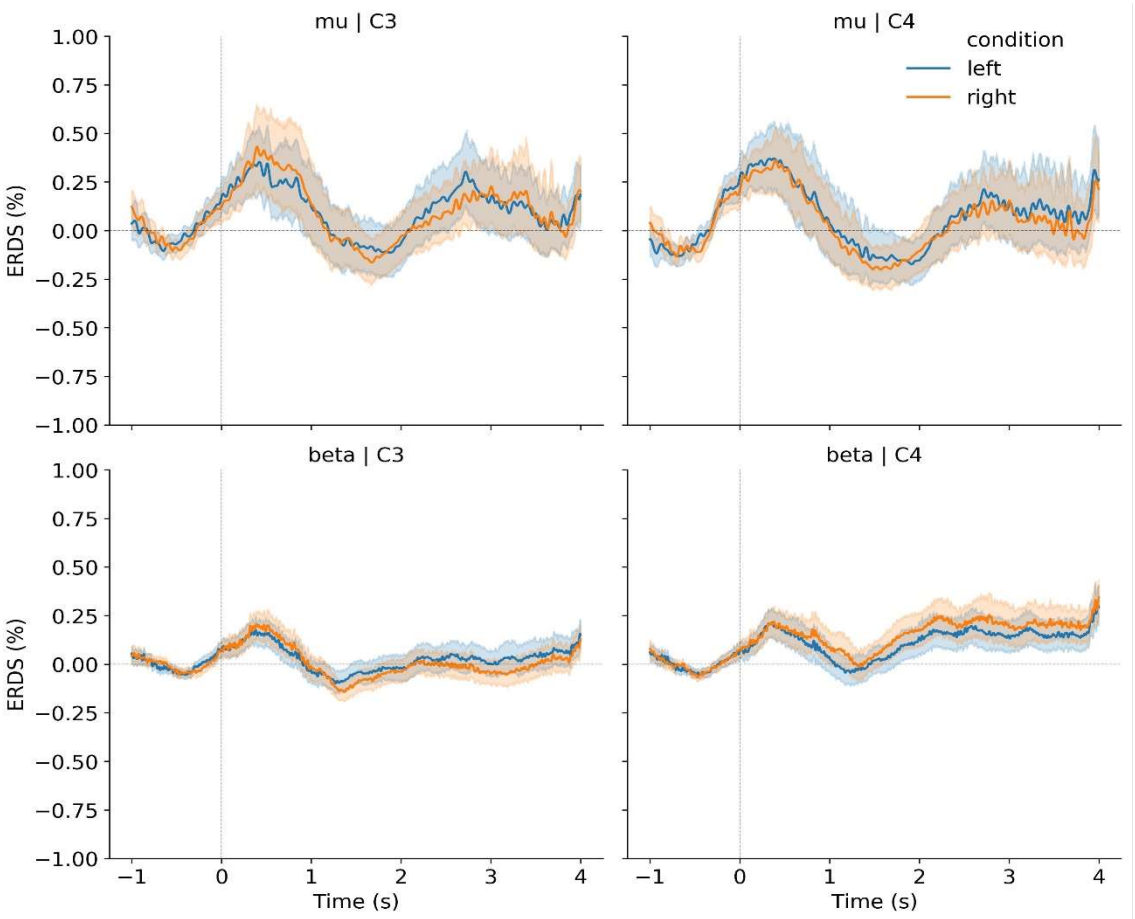

ROBOT – 6 – TESTING

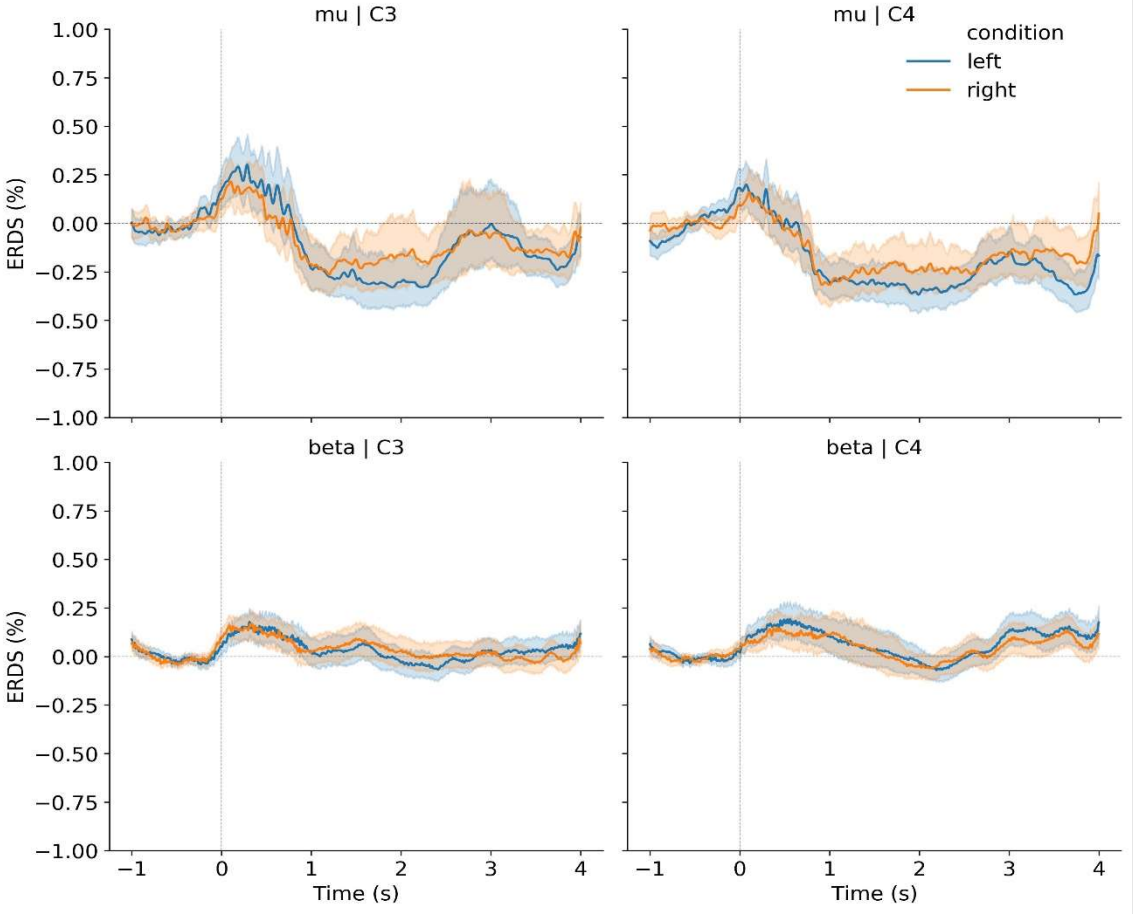

ROBOT – 7 – TRAINING

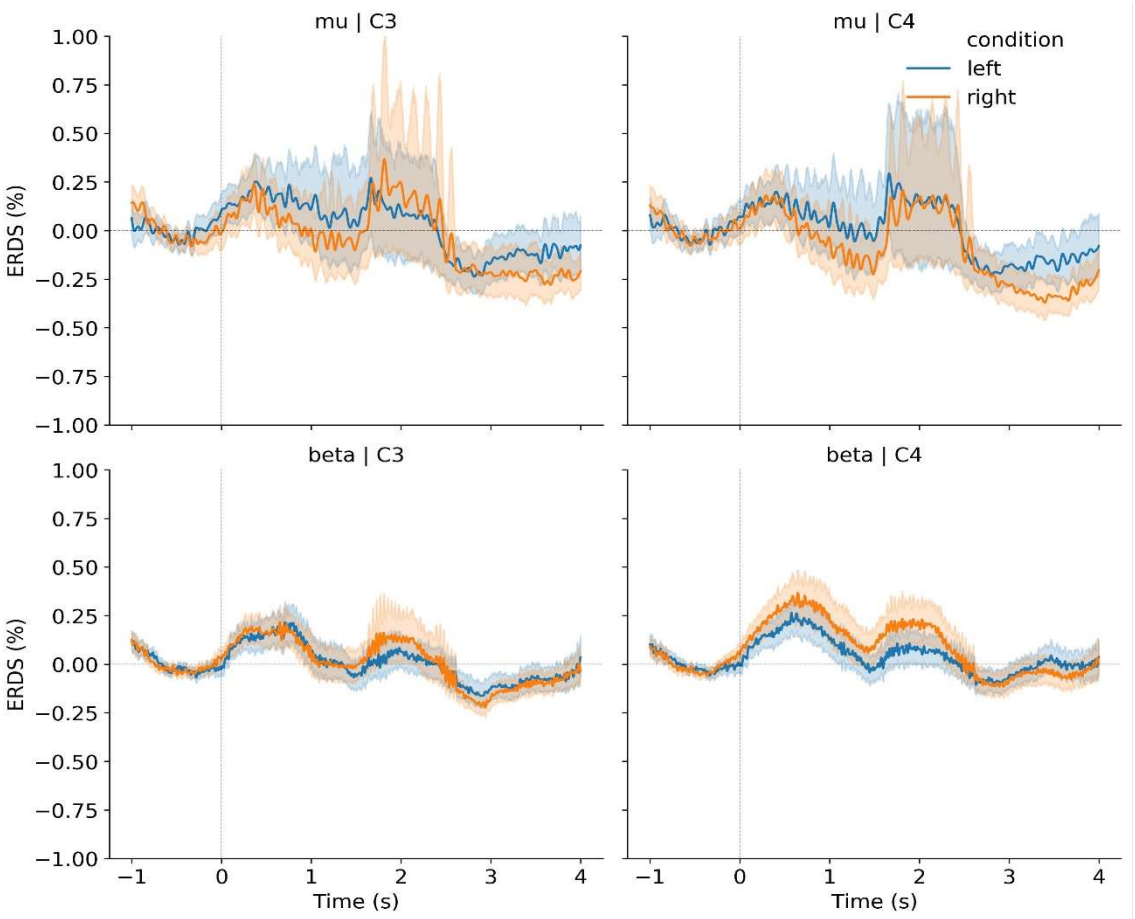

ROBOT – 7 – TESTING

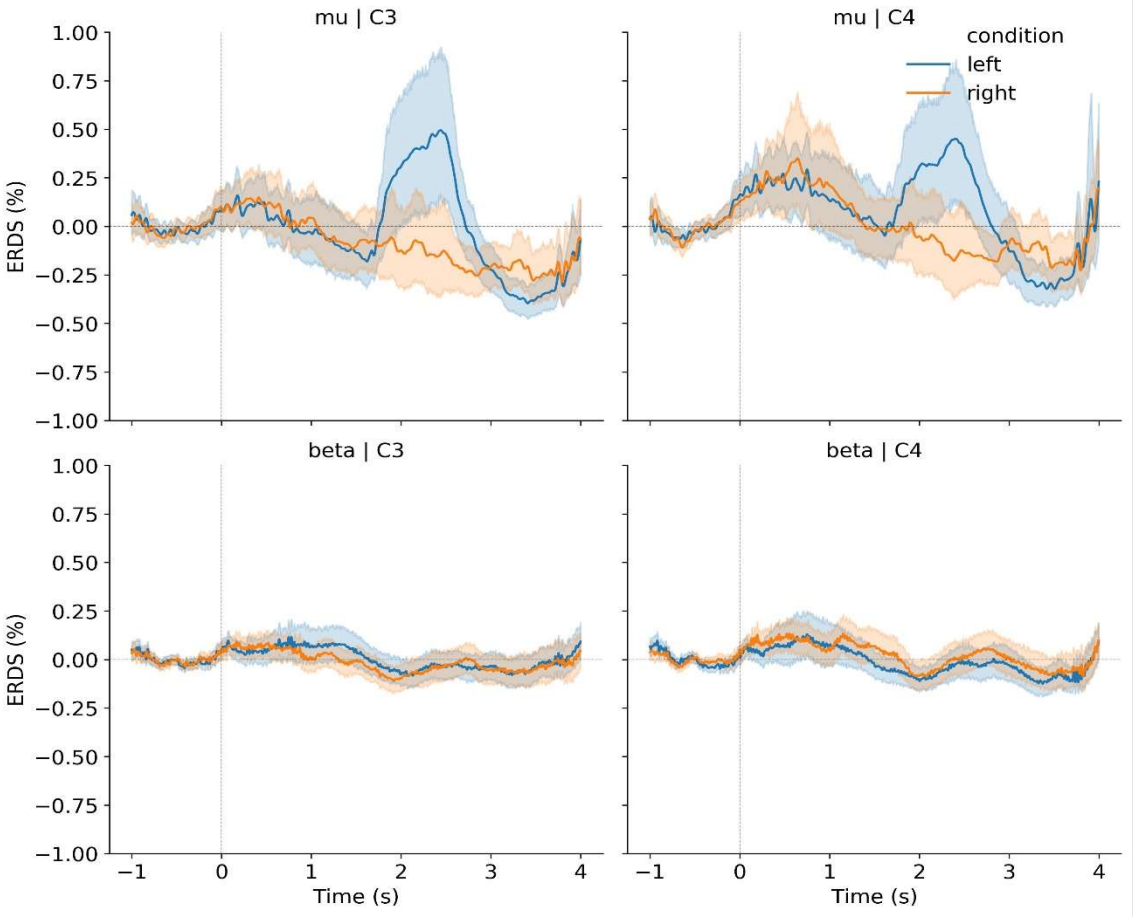

ROBOT – 8 – TRAINING

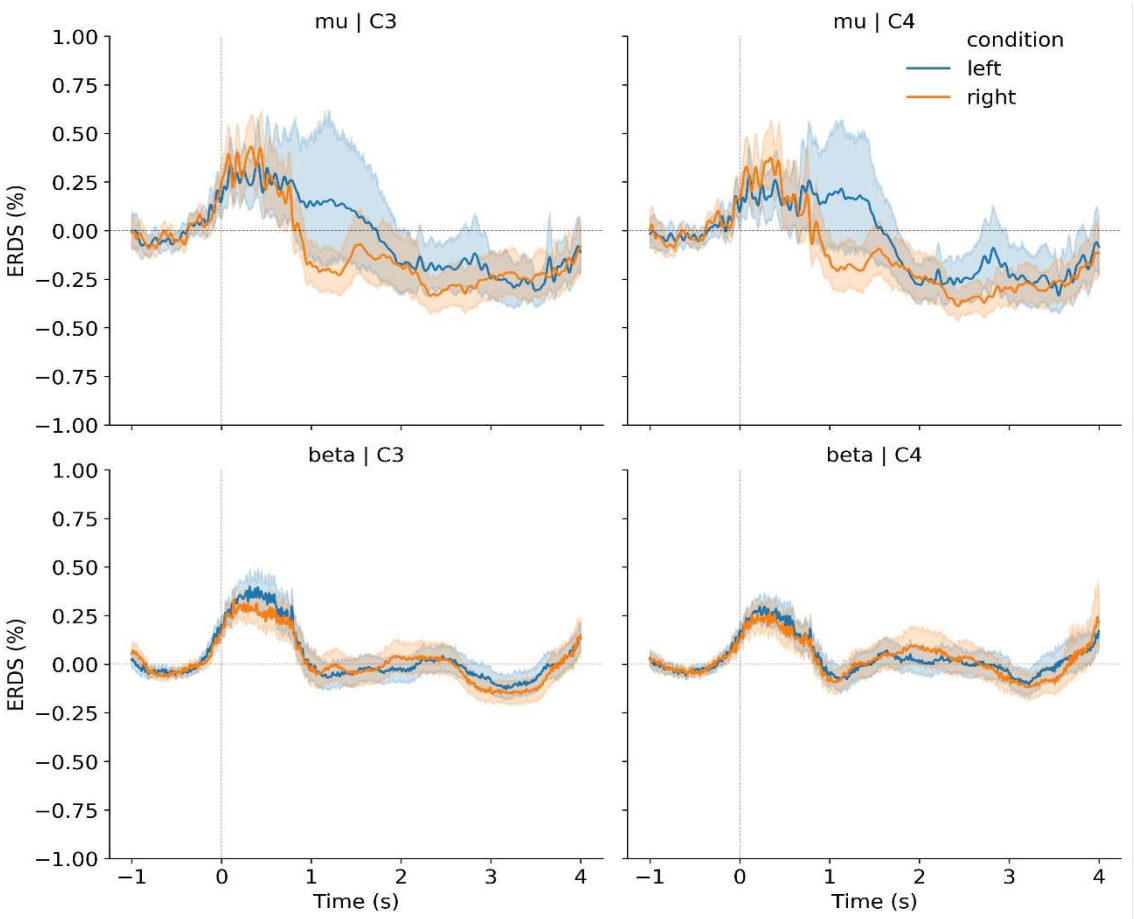

ROBOT – 8 – TESTING

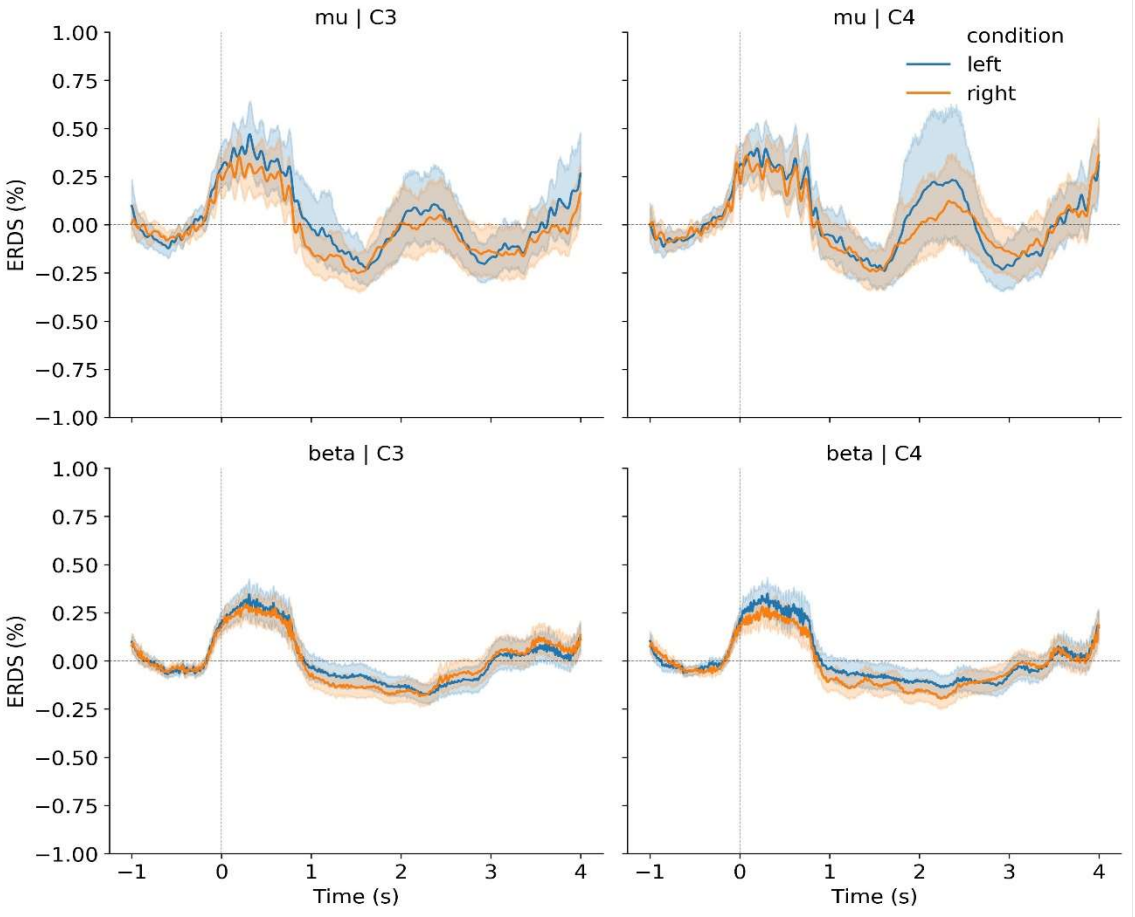

BOTH – 1 – TRAINING

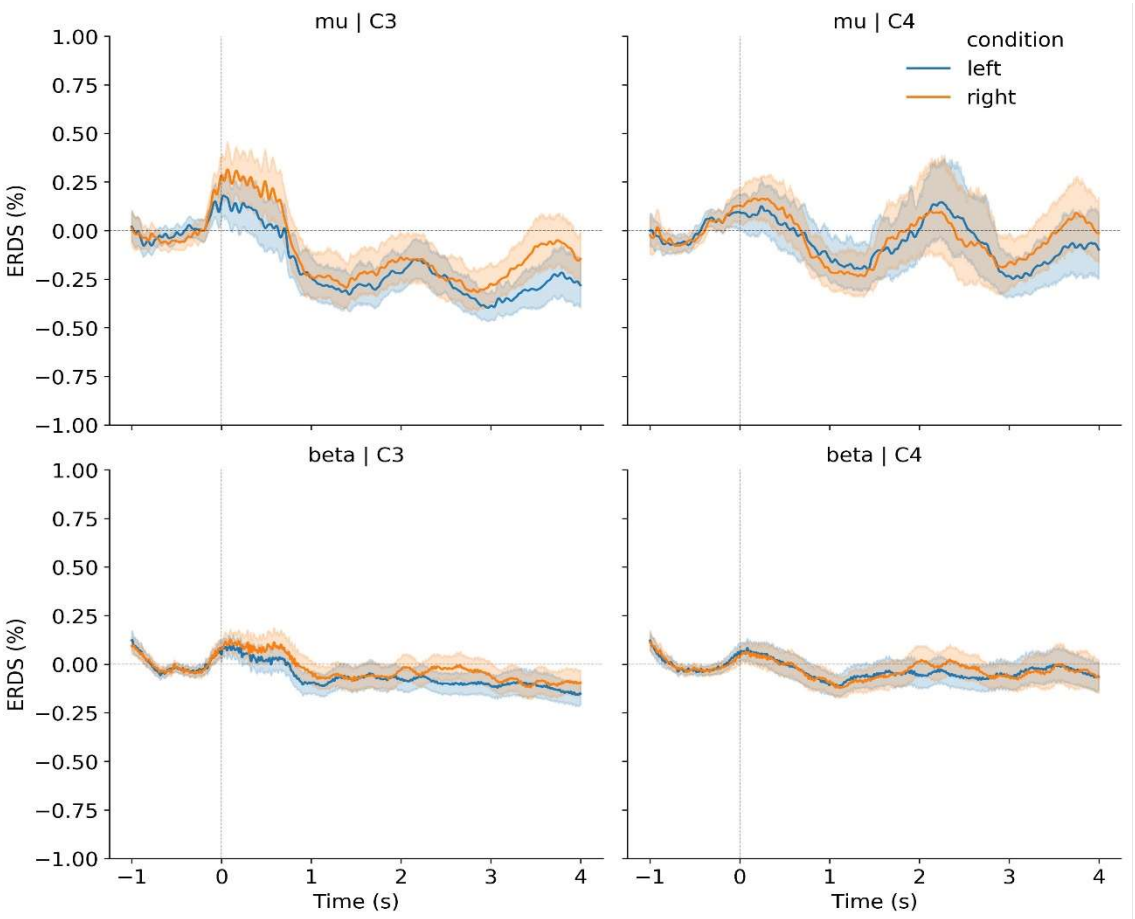

BOTH – 1 – TESTING

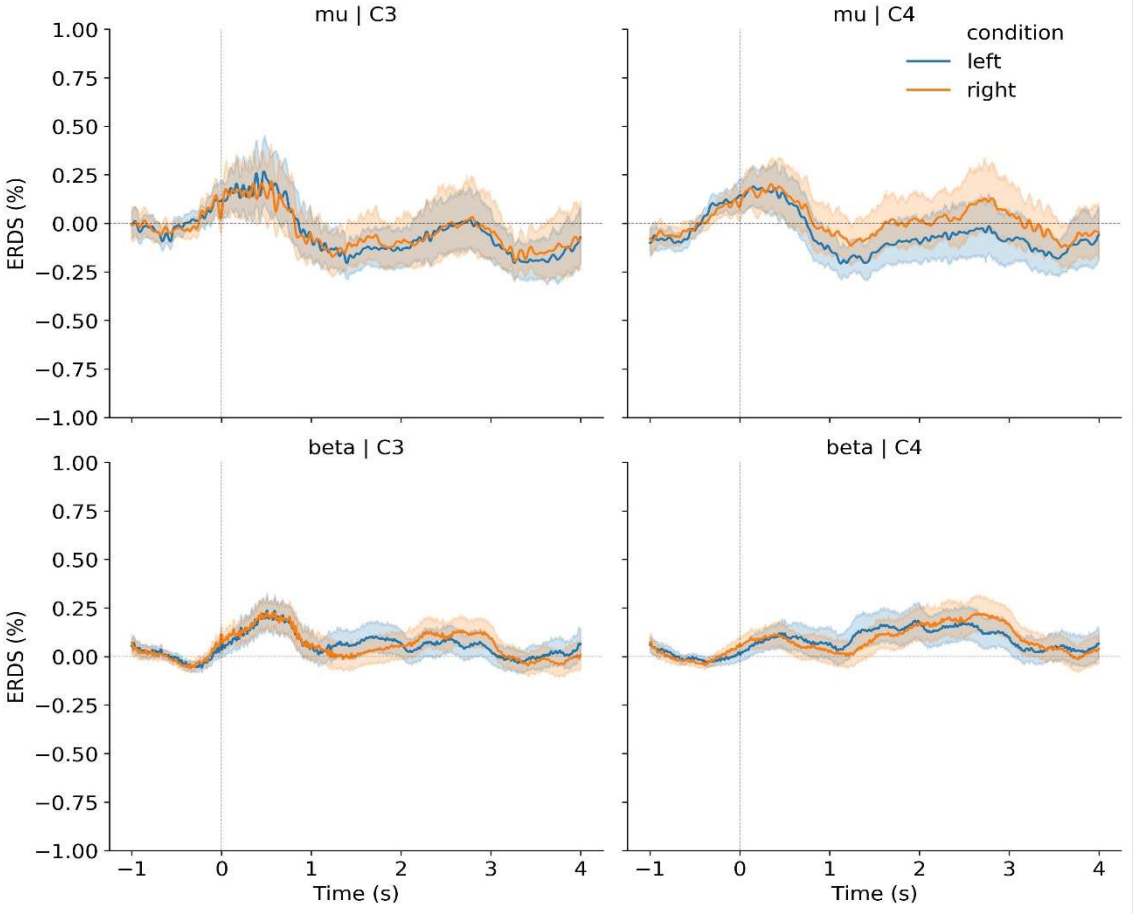

BOTH – 2 – TRAINING

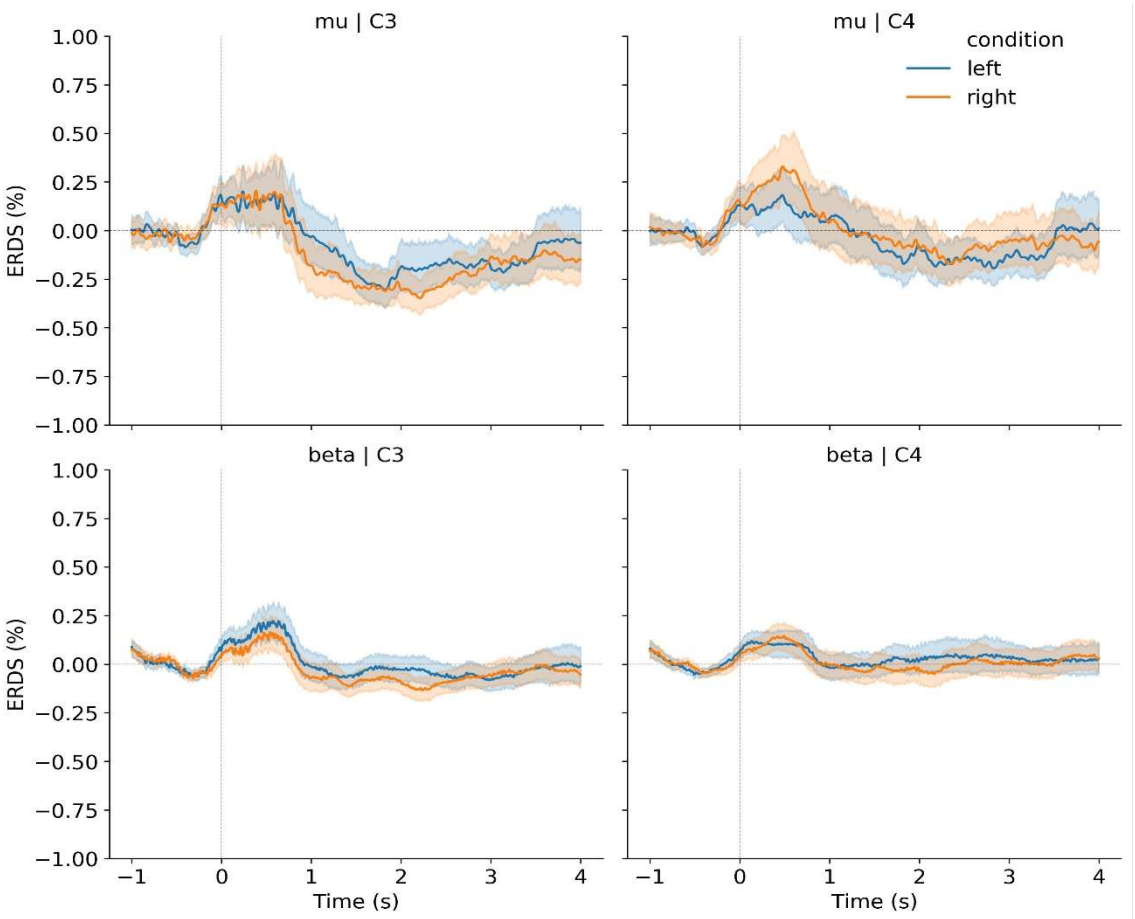

BOTH – 2 – TESTING

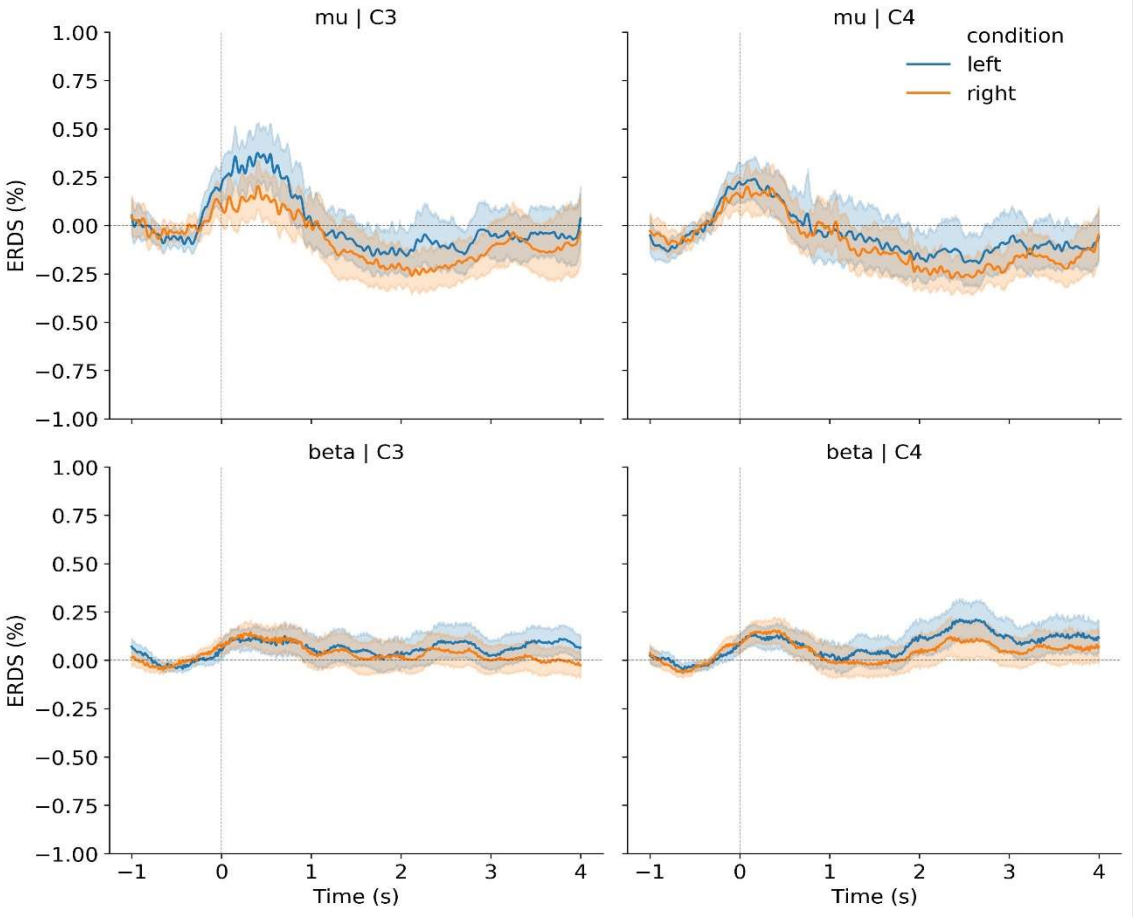

BOTH – 3 – TRAINING

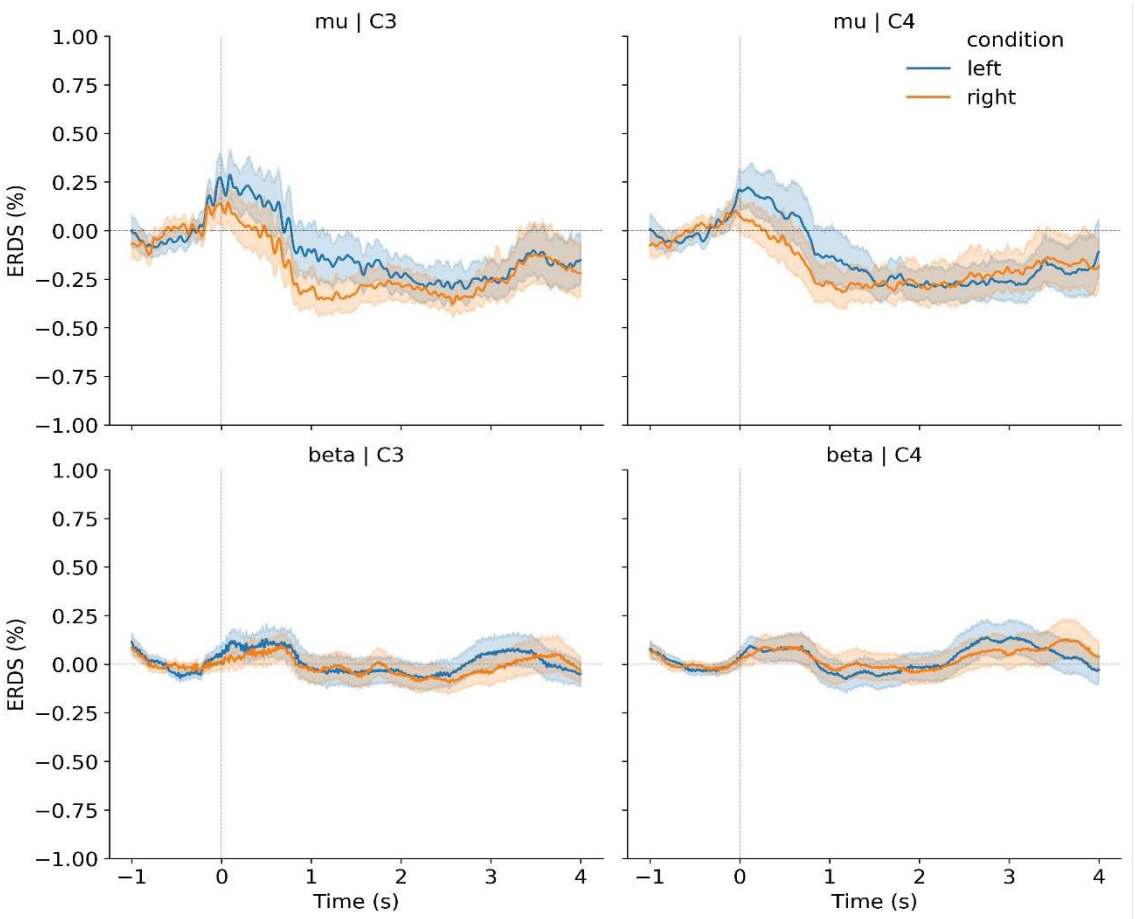

BOTH – 3 – TESTING

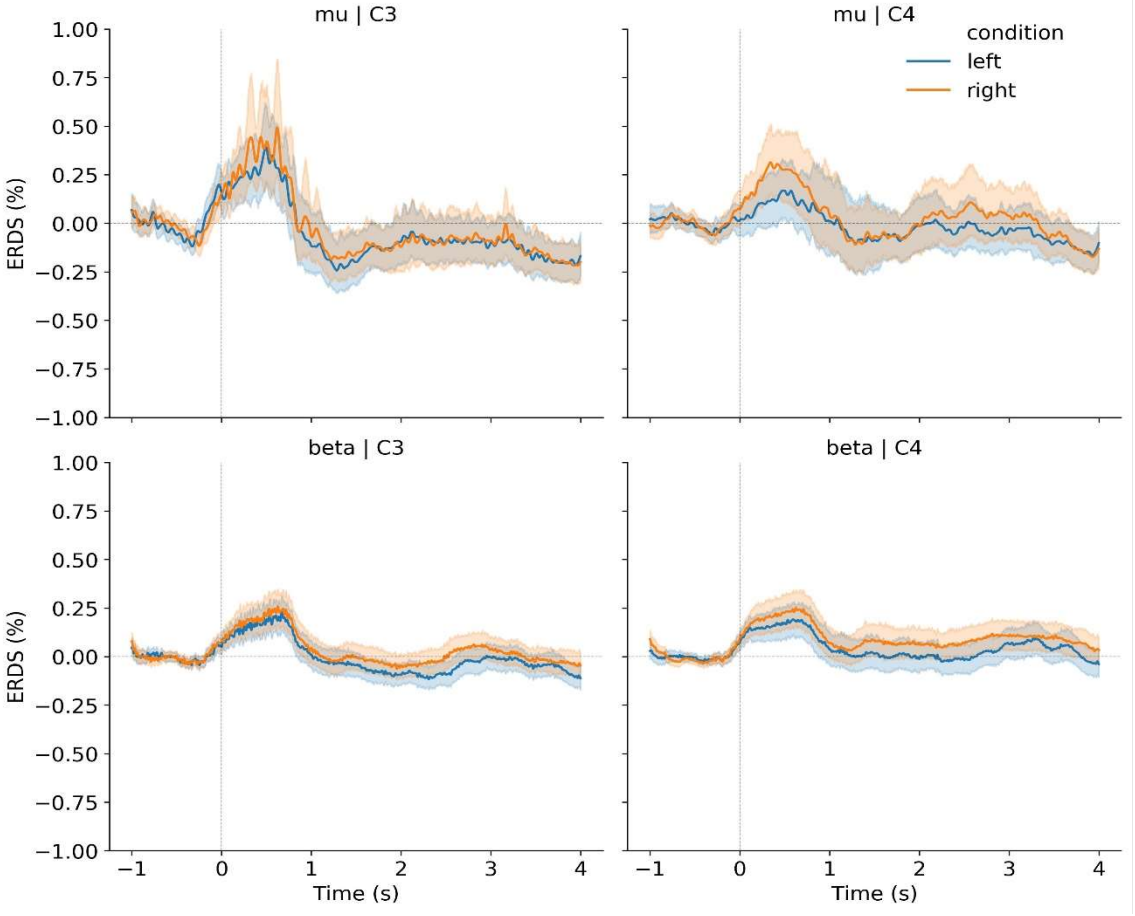

BOTH – 4 – TRAINING

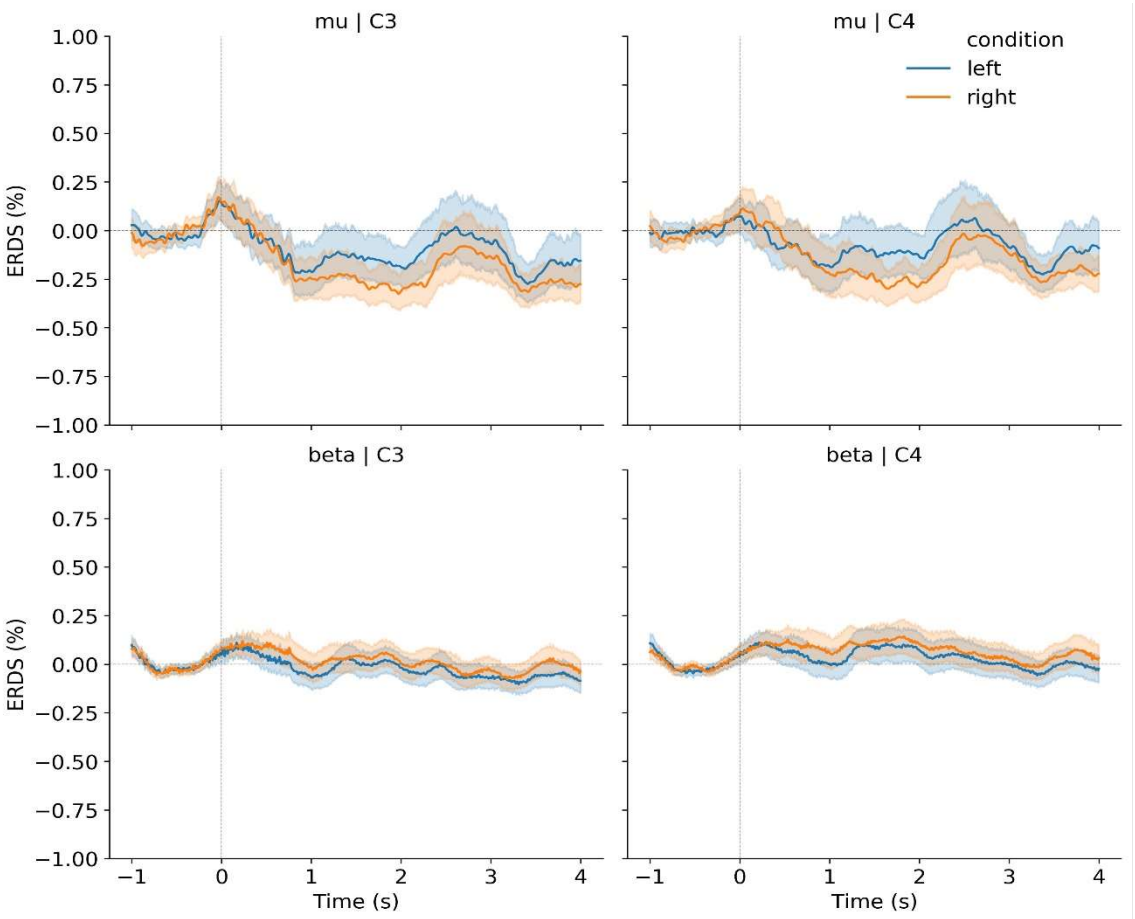

BOTH – 4 – TESTING

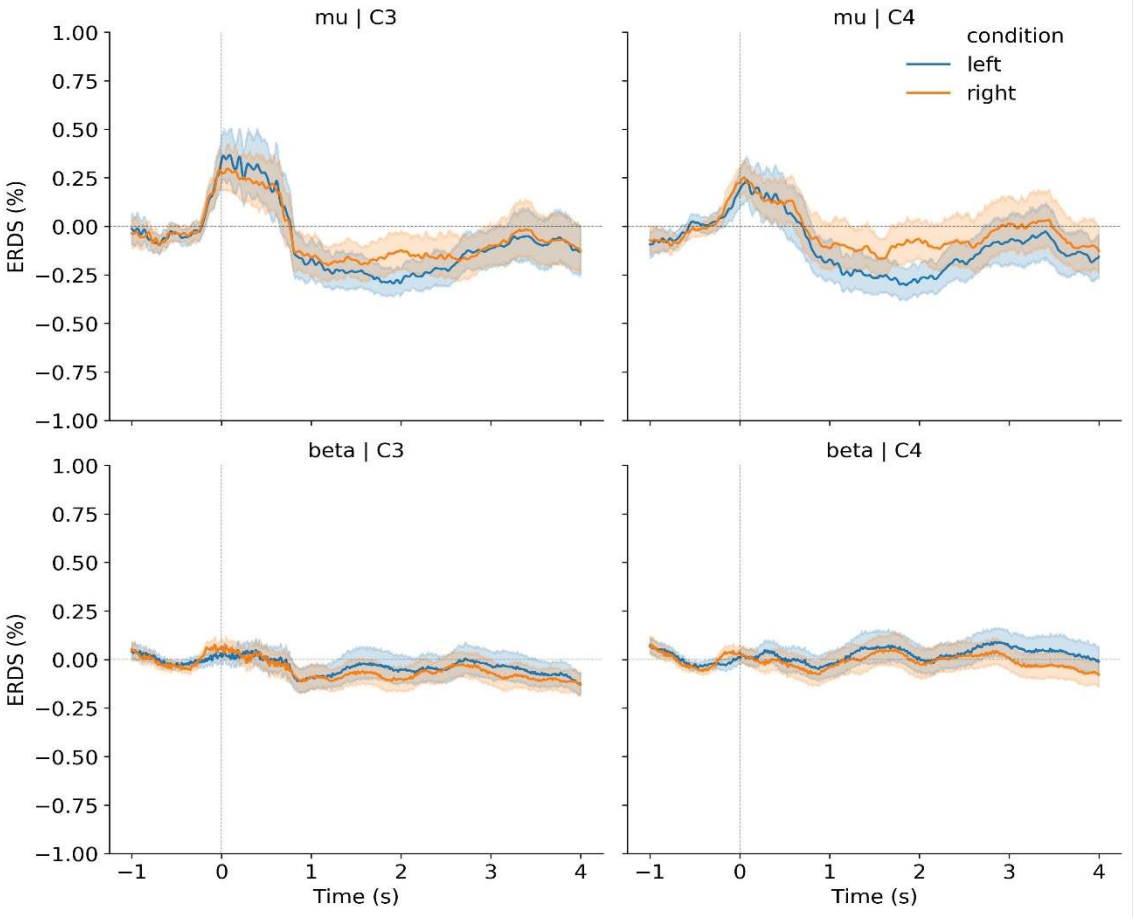

BOTH – 5 – TRAINING

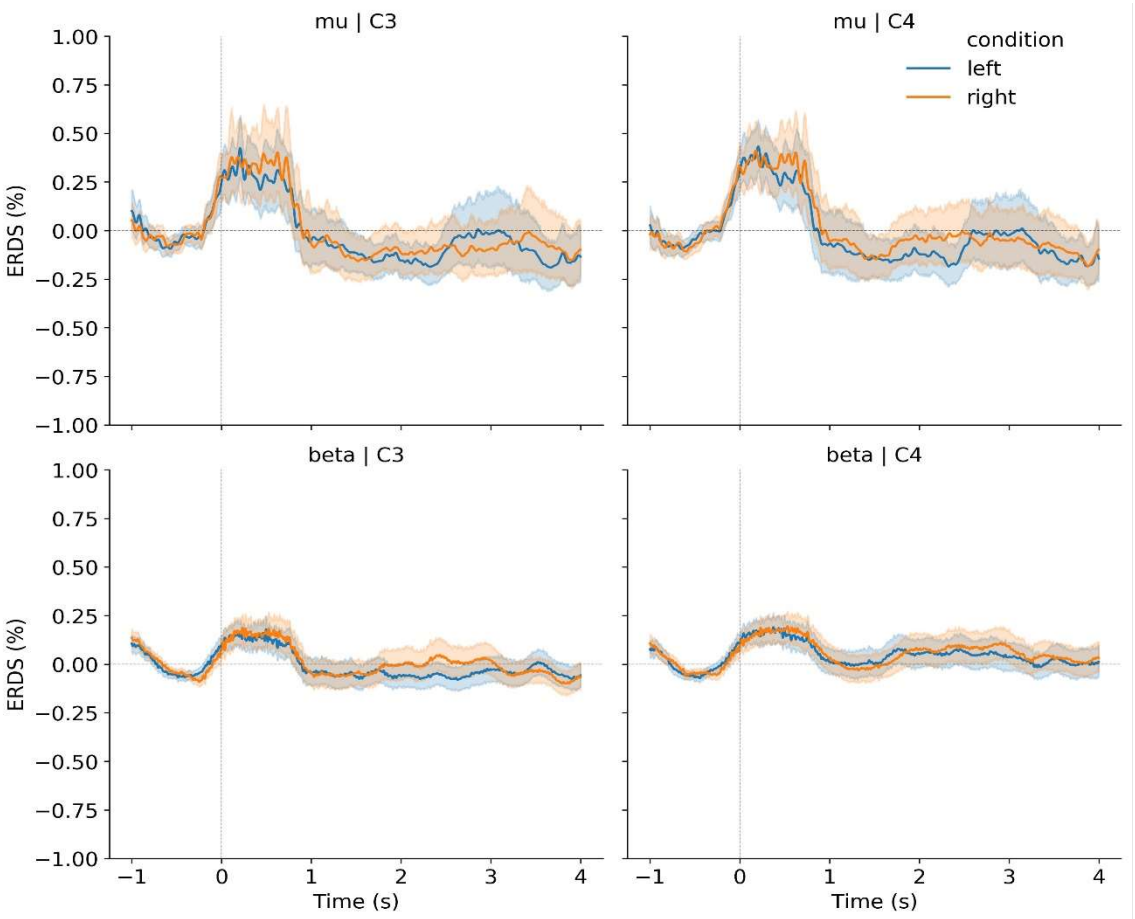

BOTH – 5 – TESTING

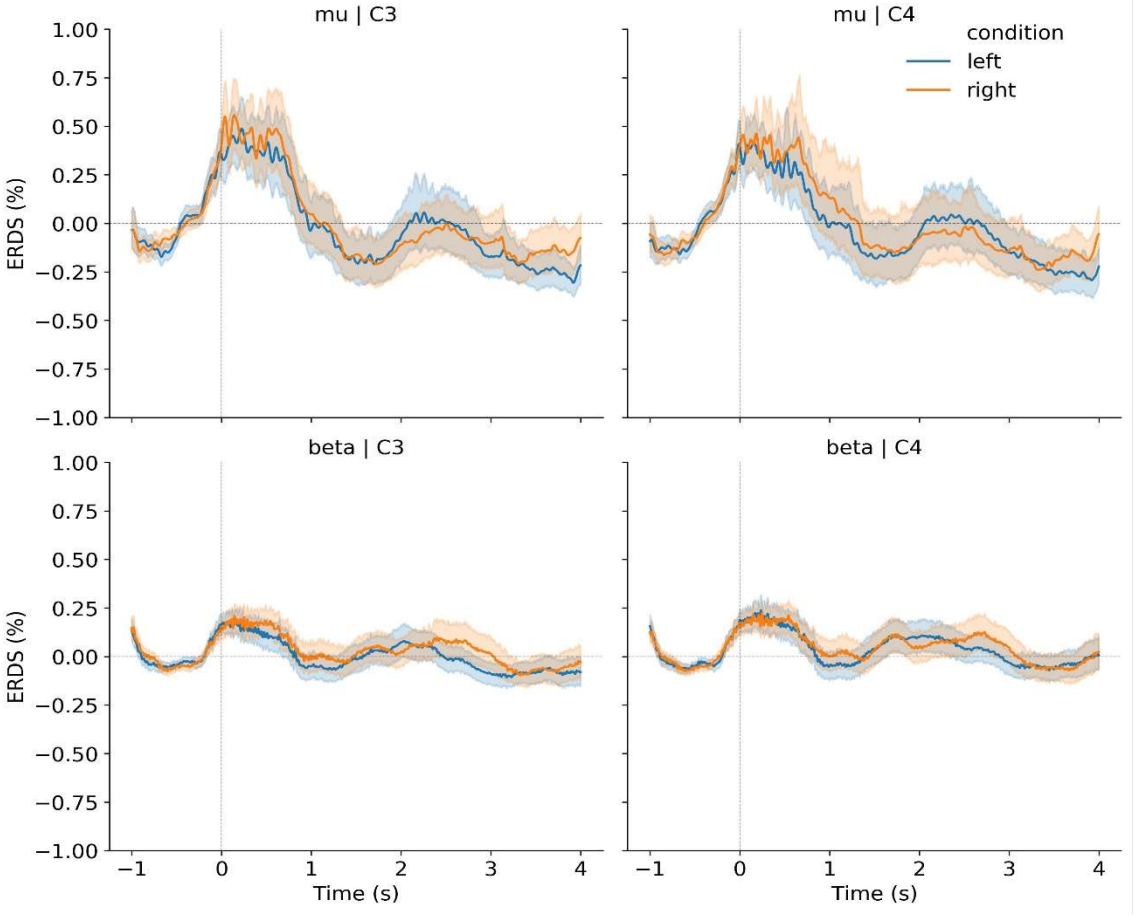

BOTH – 6 – TRAINING

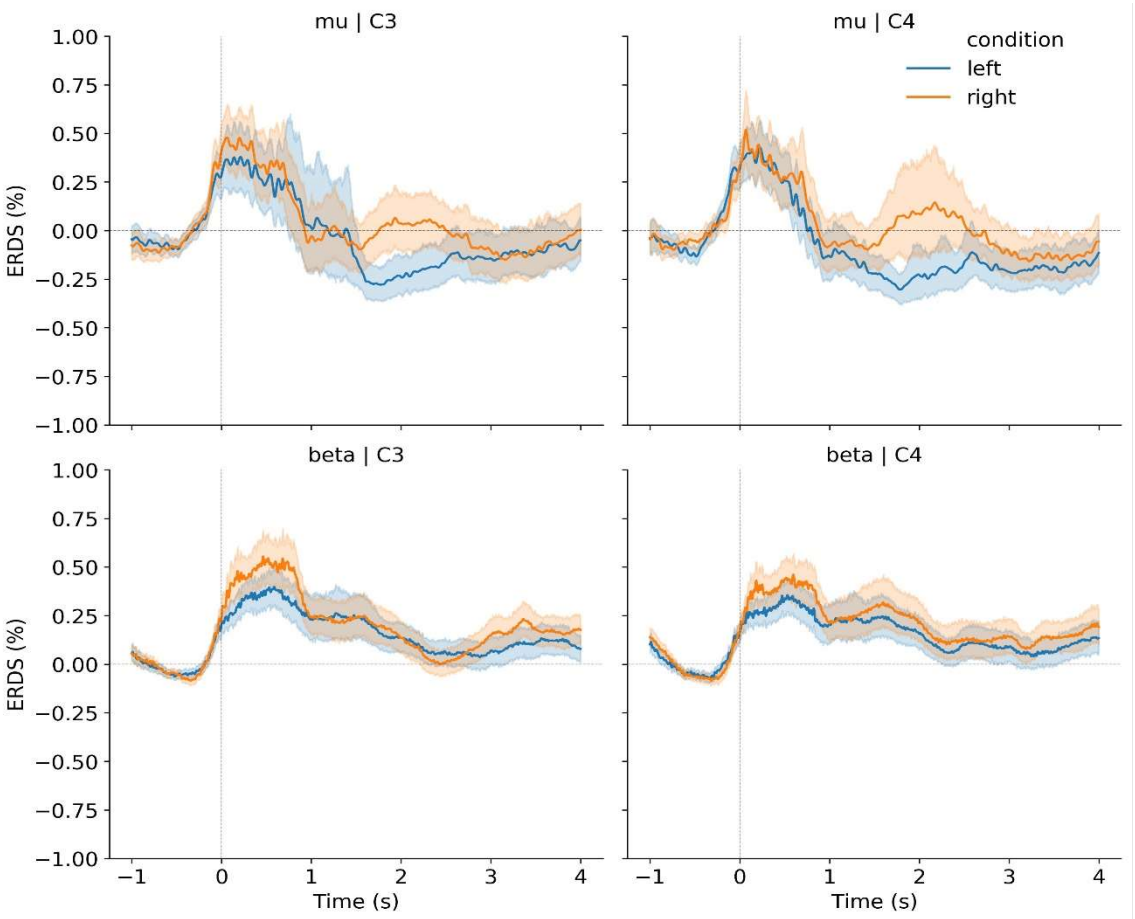

BOTH – 6 – TESTING

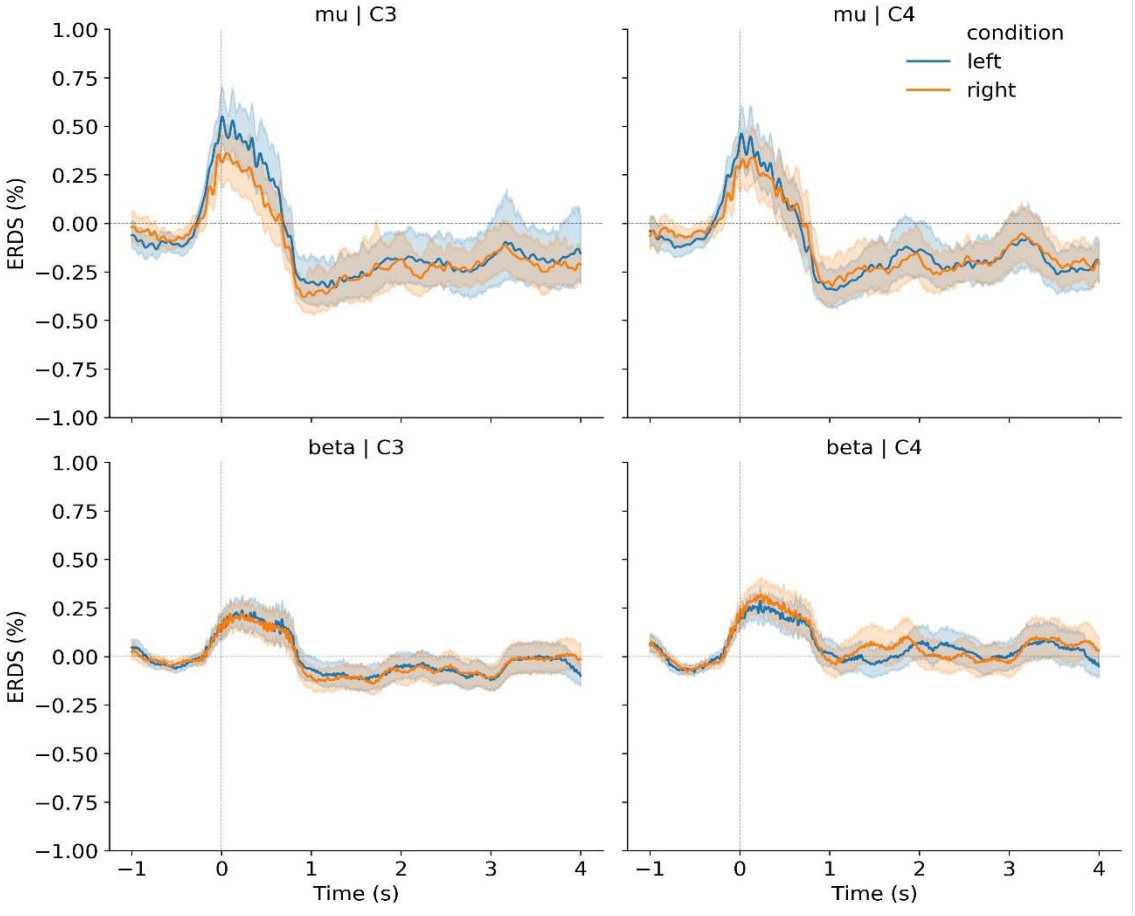

BOTH – 7 – TRAINING

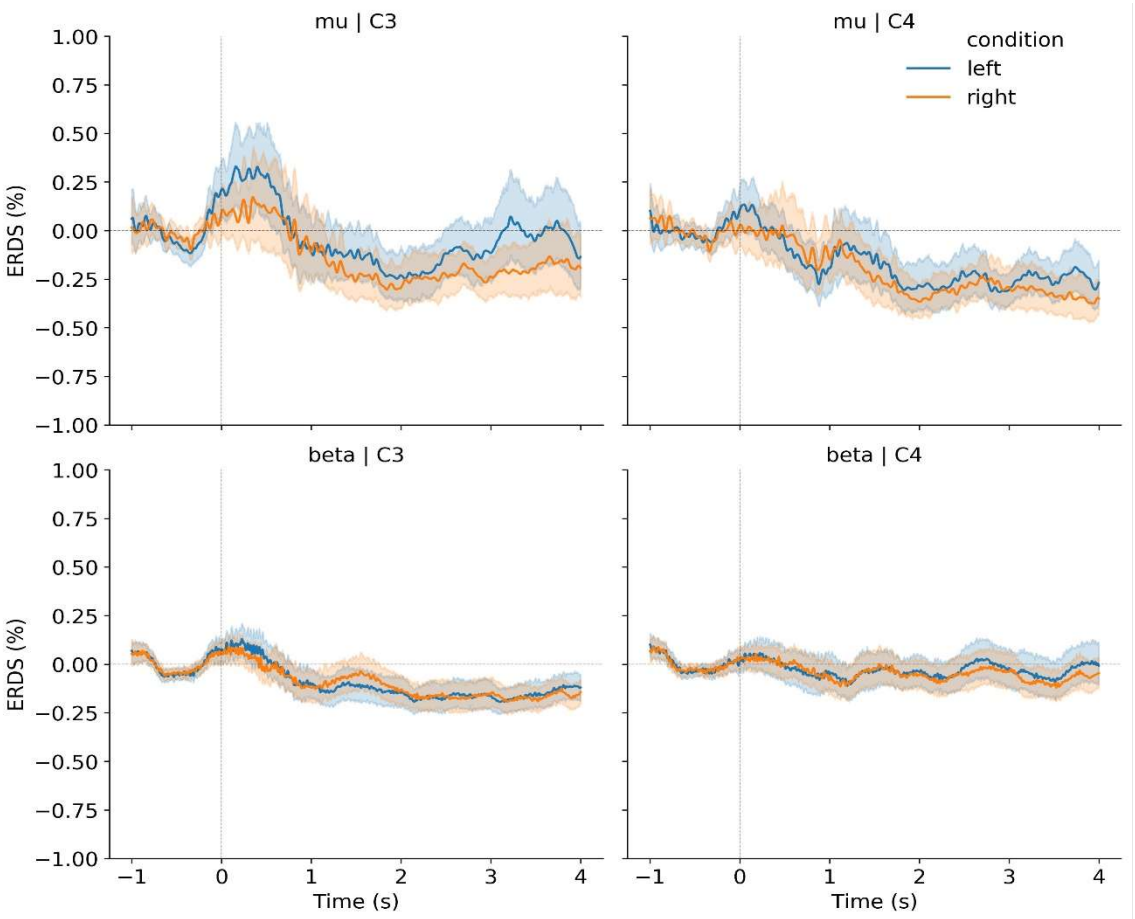

BOTH – 7 – TESTING

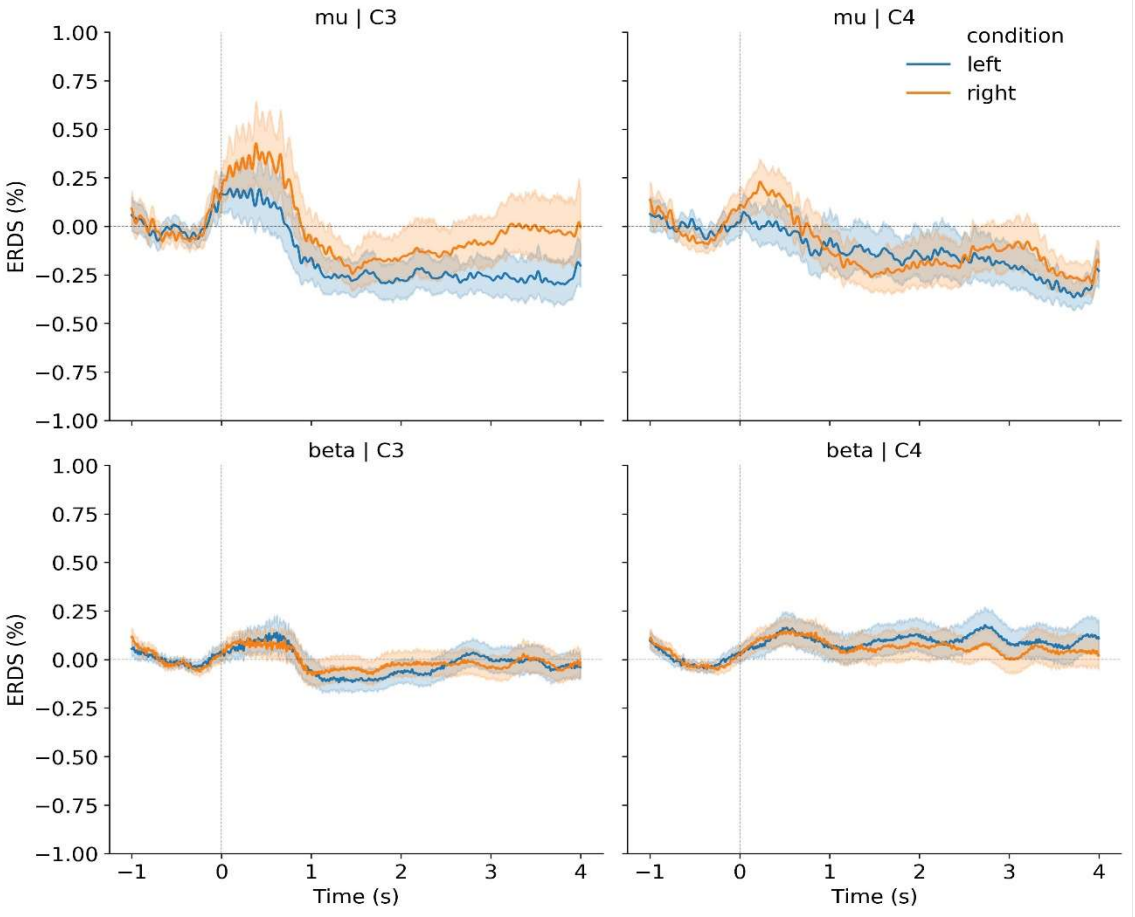

BOTH – 8 – TRAINING

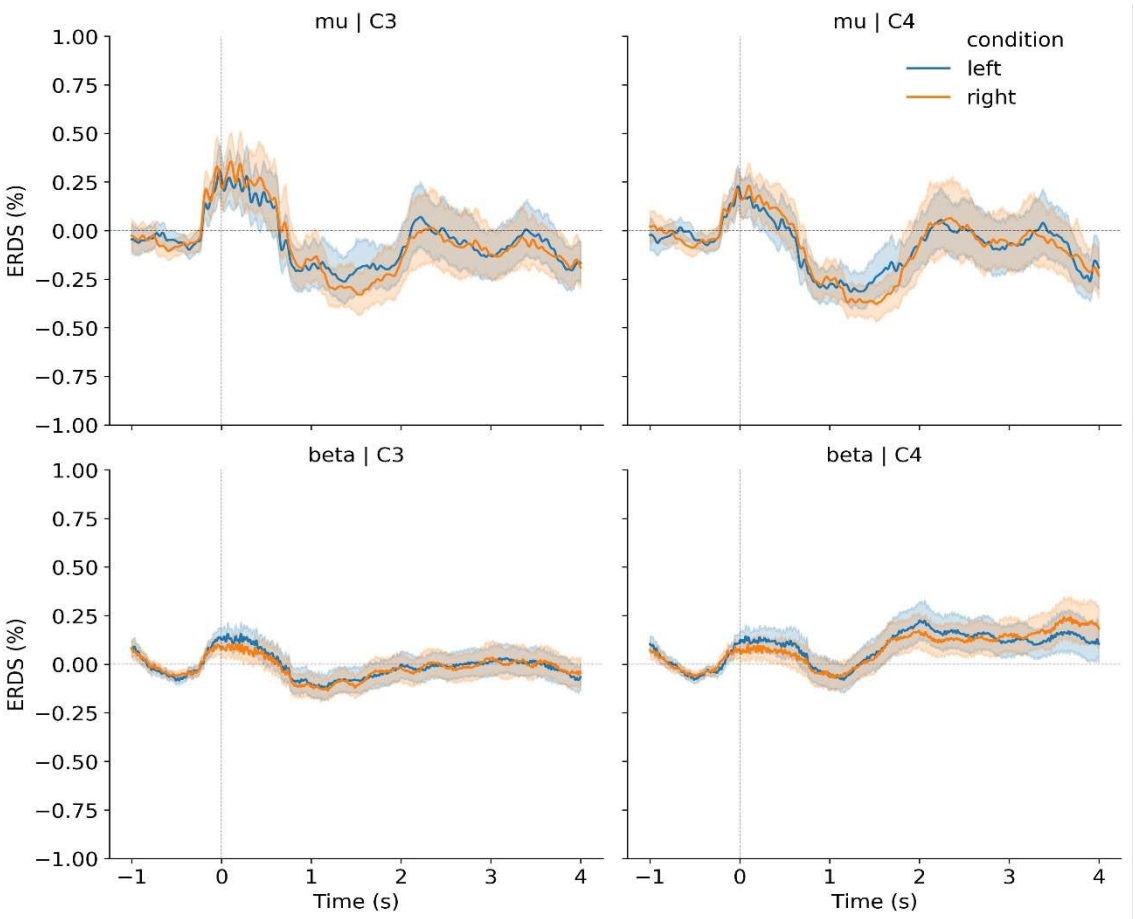

BOTH – 8 – TESTING

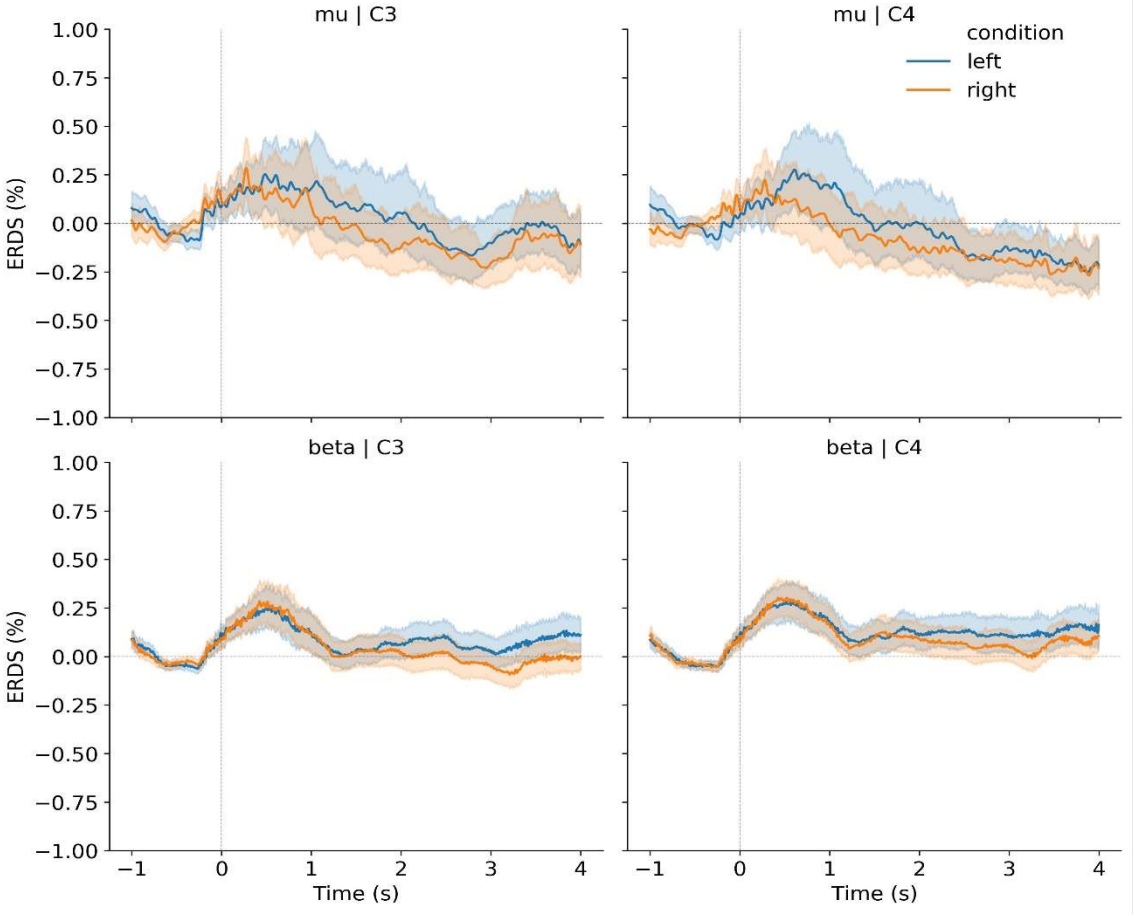

Appendix E

Visualisation of the Spatial Filters based on Common Spatial Patterns for the Training Phase of All Sessions

This appendix contains the visualisation plots of the spatial filters generated from the EEG data of the training phase in each session for each condition using the common spatial patterns module (csp.plot_filters) from the MNE-Python package. Conditions that indicate "BOTH" refer to the combined VR+robot condition. The plots use a spectral colour scale of arbitrary units specific for each session.

CONTROL – 1 –TRAINING

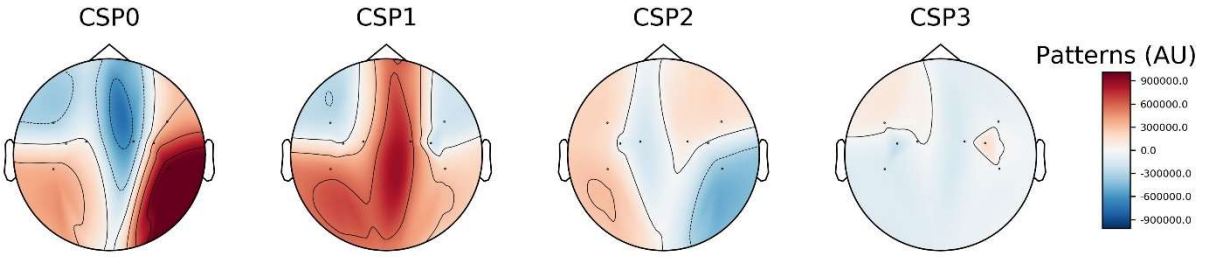

CONTROL – 2 –TRAINING

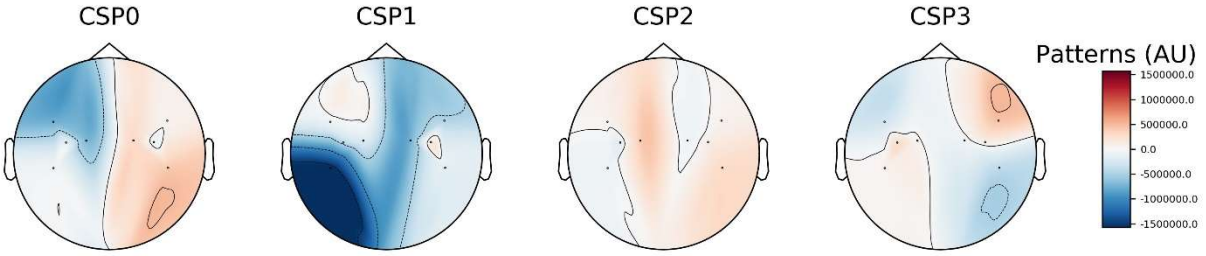

CONTROL – 3 – TRAINING

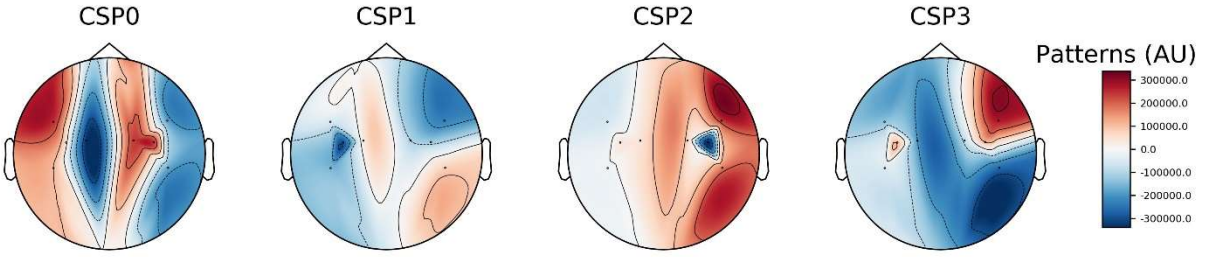

CONTROL – 4 – TRAINING

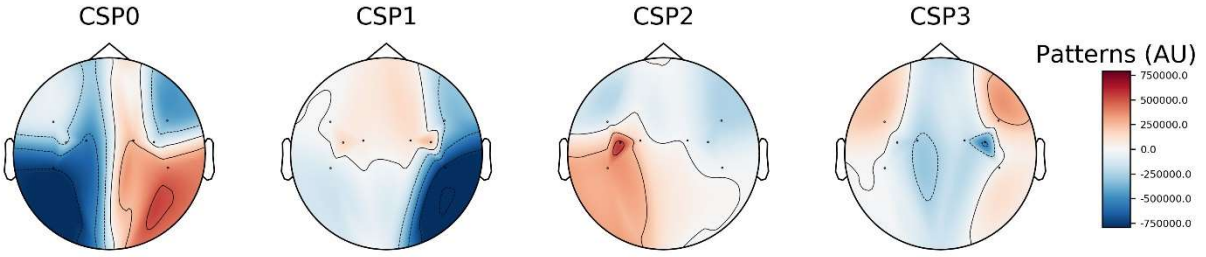

CONTROL –5 – TRAINING

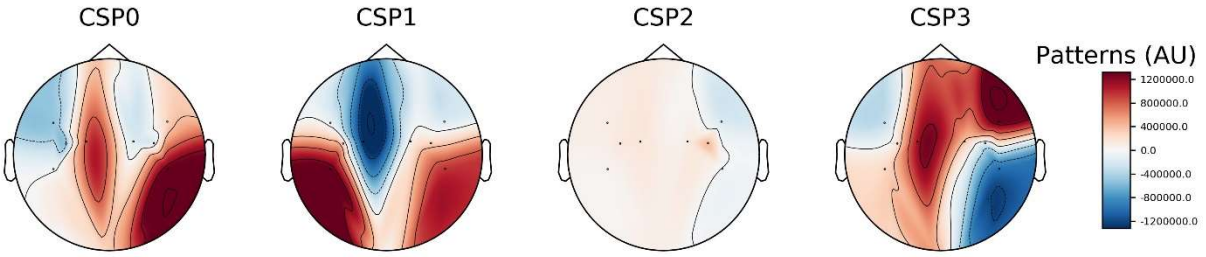

CONTROL – 6 – TRAINING

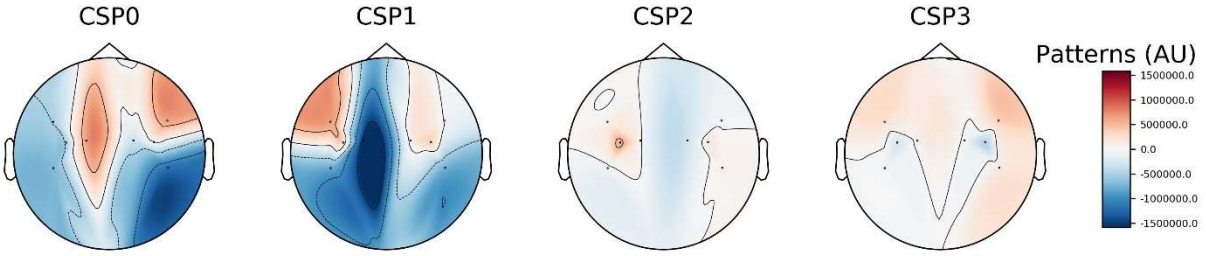

CONTROL – 7 – TRAINING

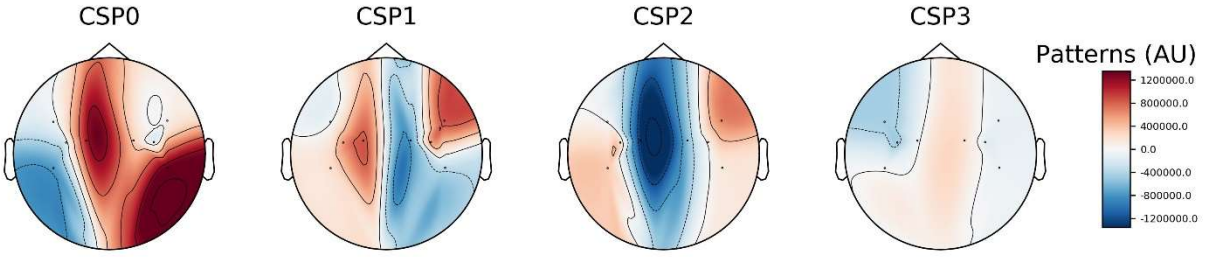

CONTROL – 8 – TRAINING

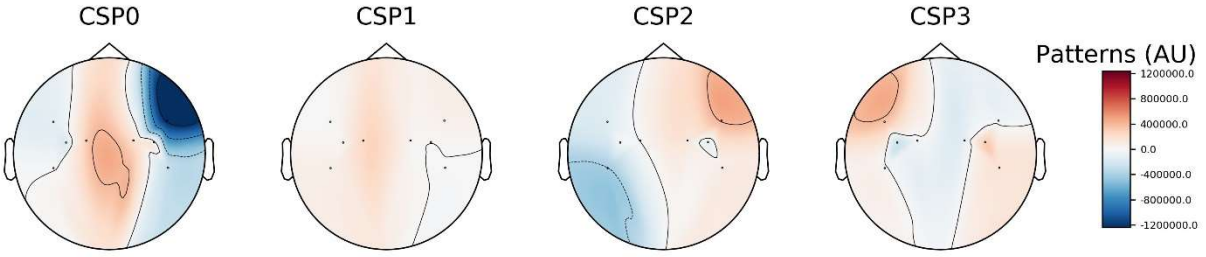

VR – 1 – TRAINING

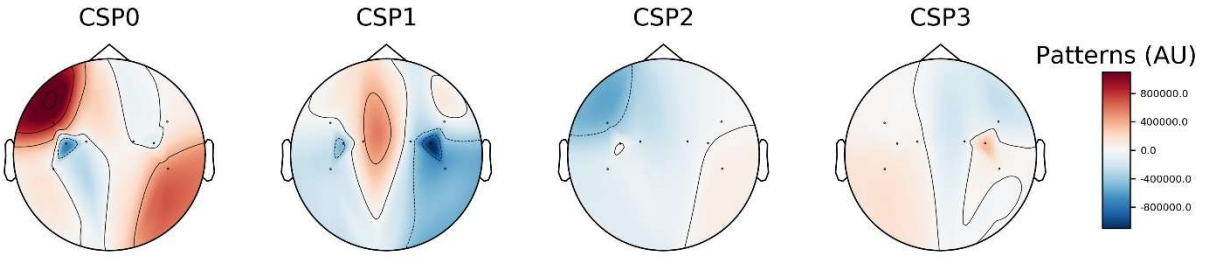

VR – 2 – TRAINING

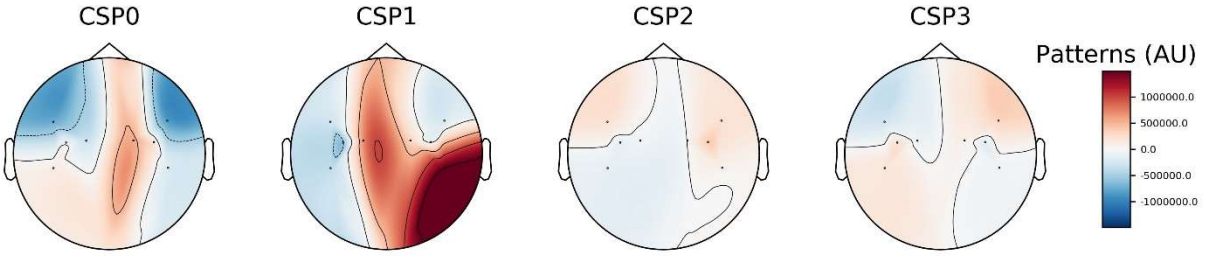

VR – 3 – TRAINING

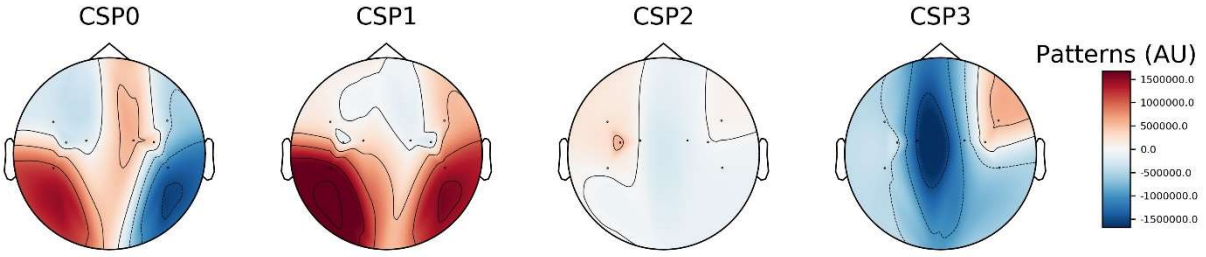

VR – 4 – TRAINING

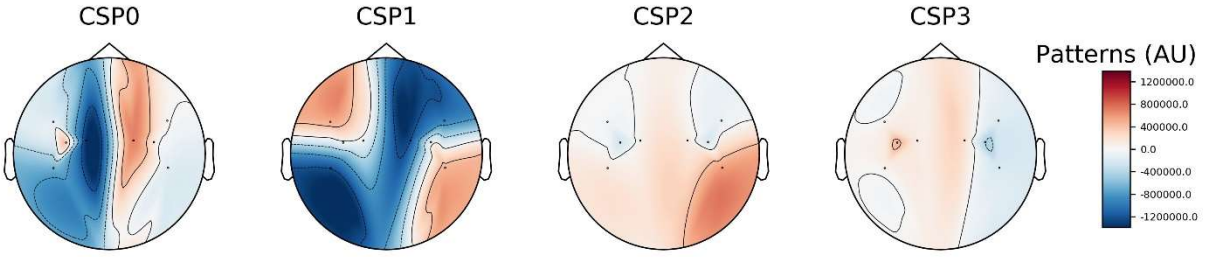

VR – 5 – TRAINING

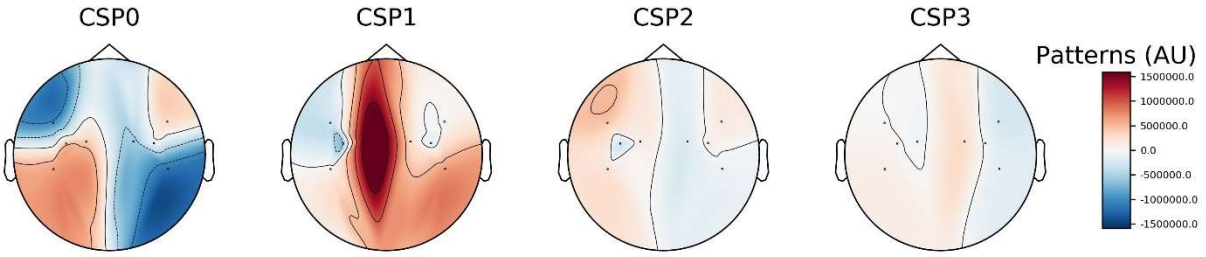

VR – 6 – TRAINING

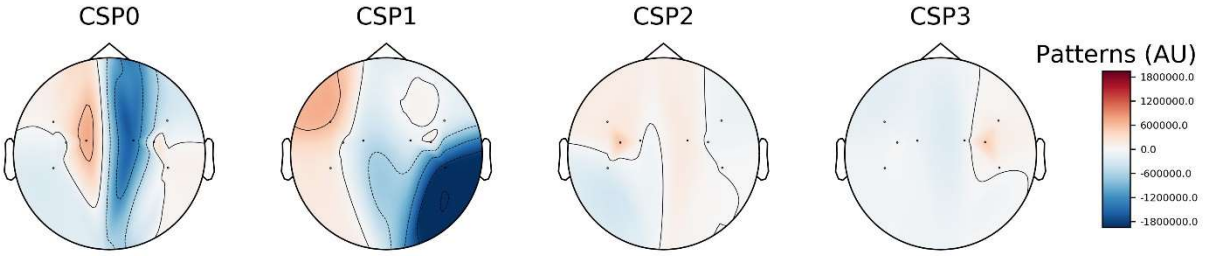

VR – 7 – TRAINING

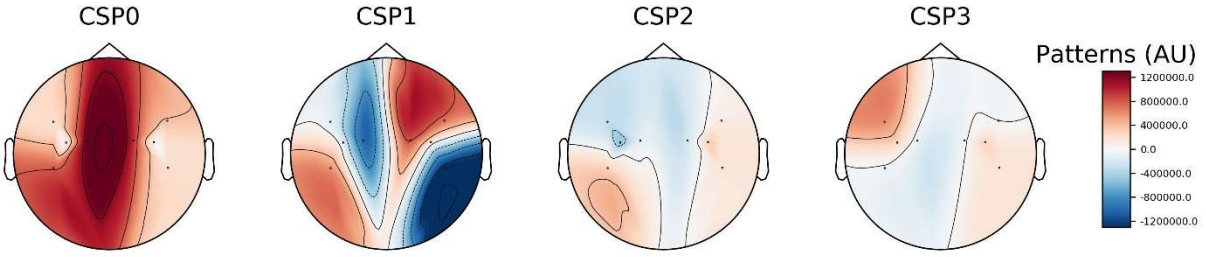

VR – 8 – TRAINING

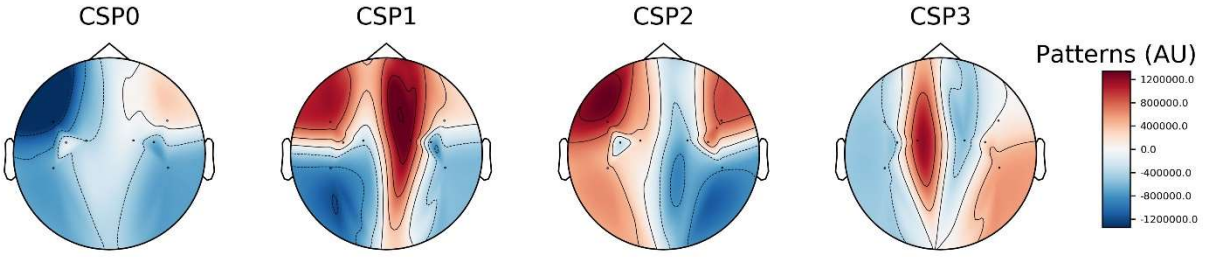

ROBOT – 1 – TRAINING

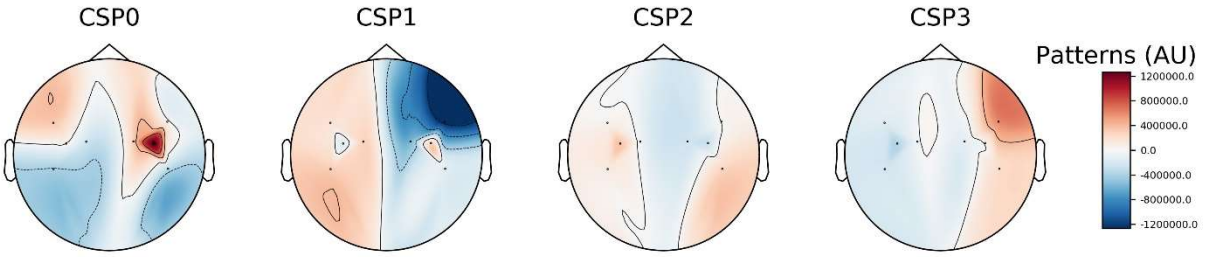

ROBOT – 2 – TRAINING

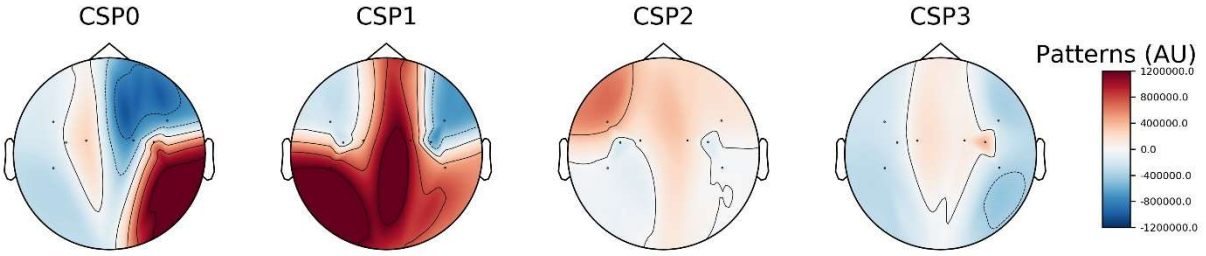

ROBOT –3 – TRAINING

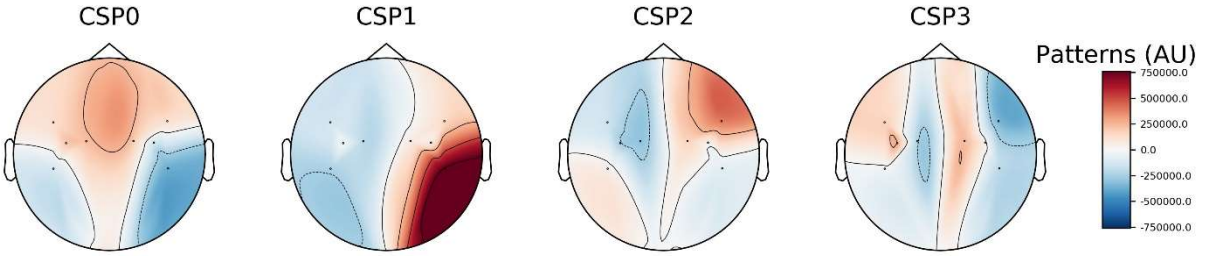

ROBOT – 4 – TRAINING

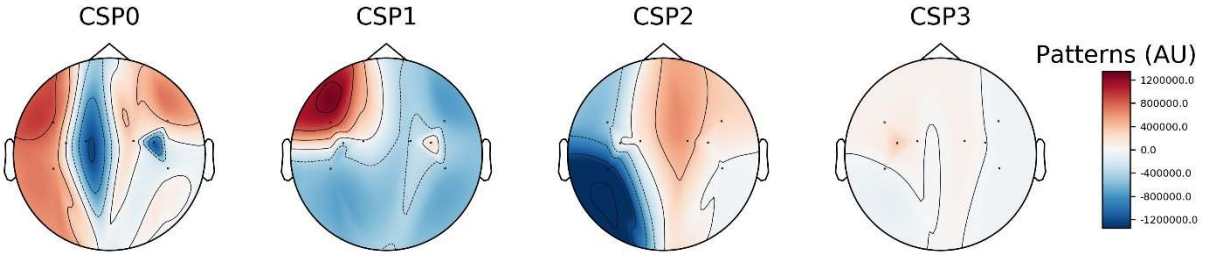

ROBOT – 5 – TRAINING

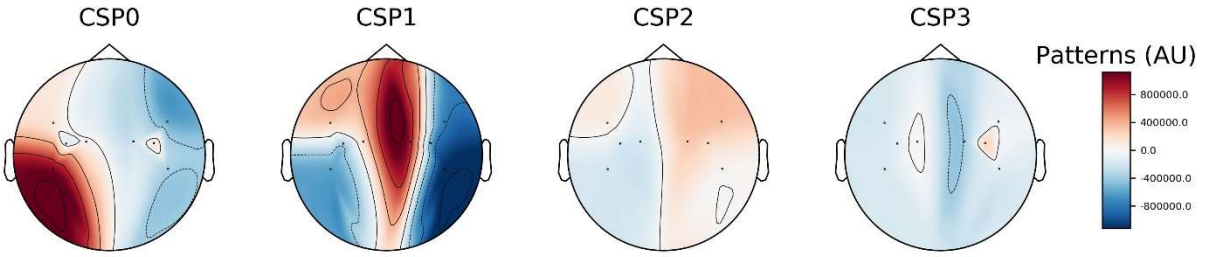

ROBOT – 6 – TRAINING

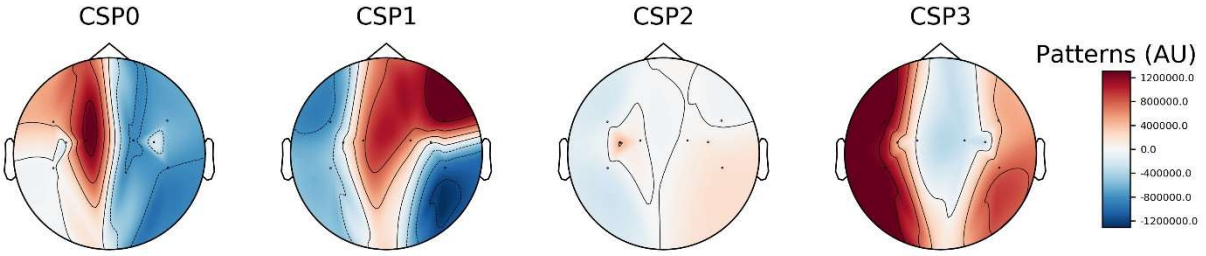

ROBOT – 7 – TRAINING

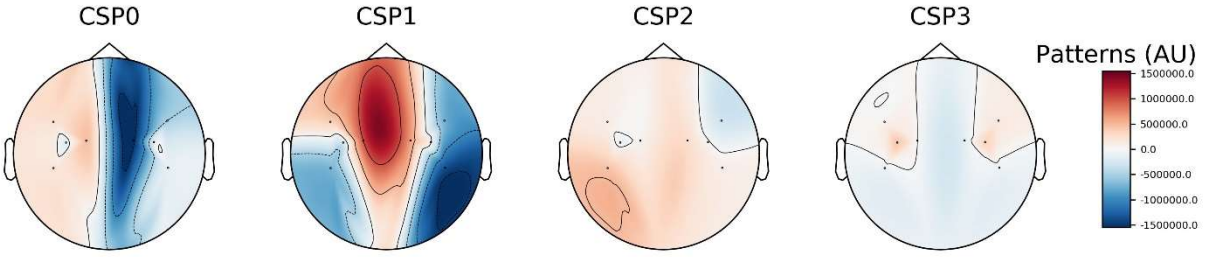

ROBOT – 8 – TRAINING

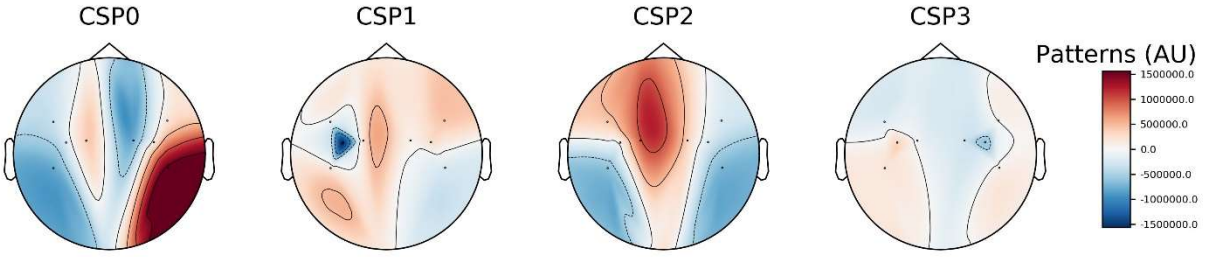

BOTH – 1 – TRAINING

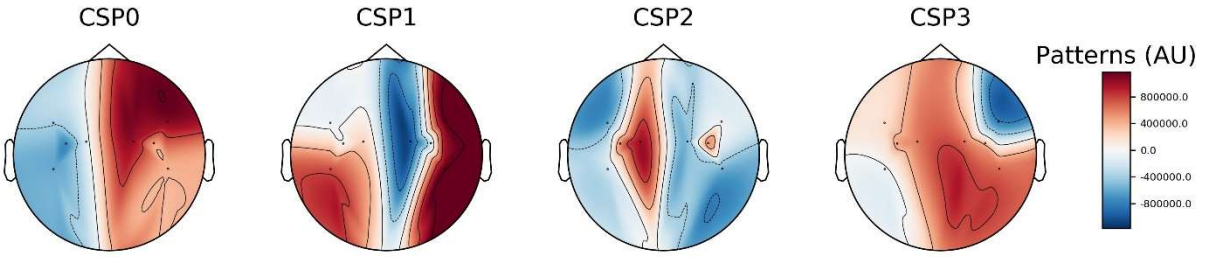

BOTH – 2 – TRAINING

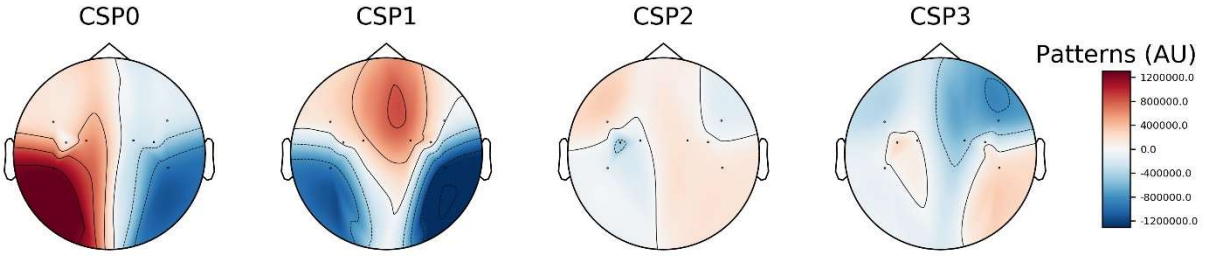

BOTH – 3 – TRAINING

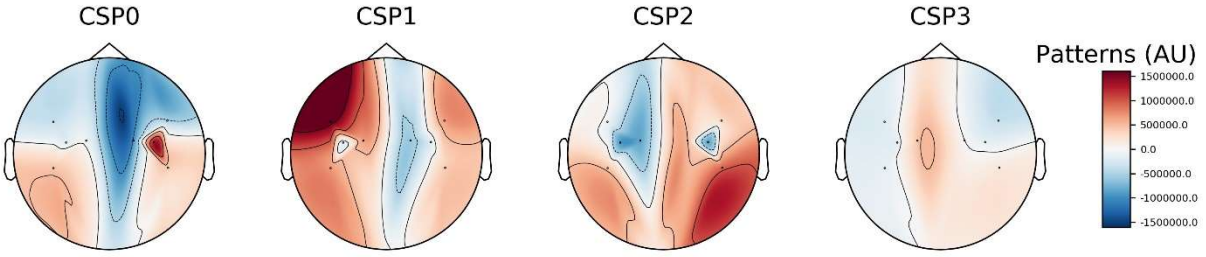

BOTH – 4 – TRAINING

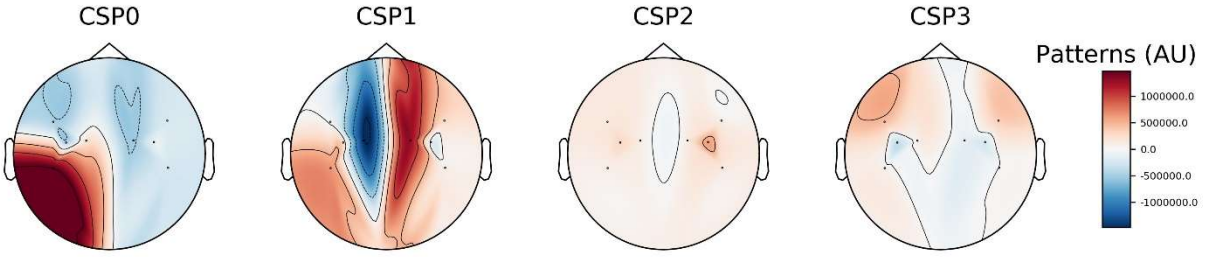

BOTH – 5 – TRAINING

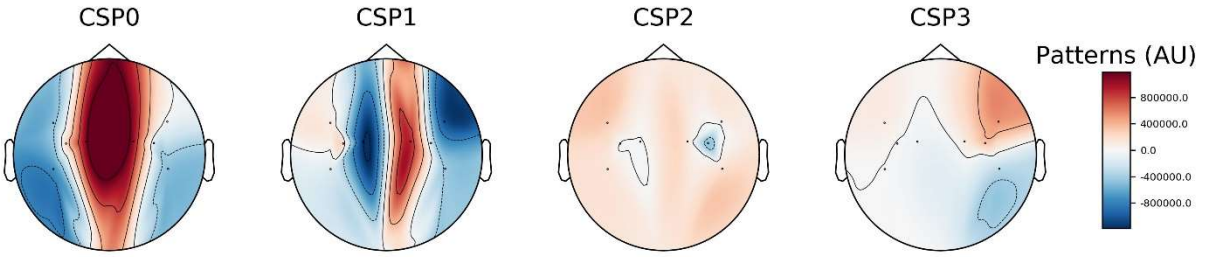

BOTH – 6 – TRAINING

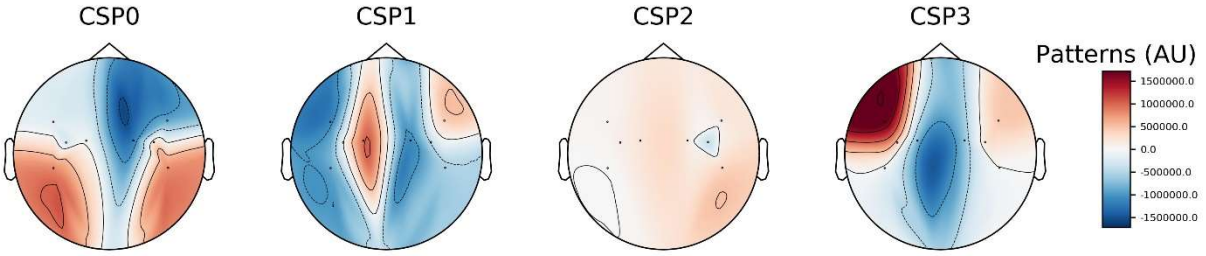

BOTH – 7 – TRAINING

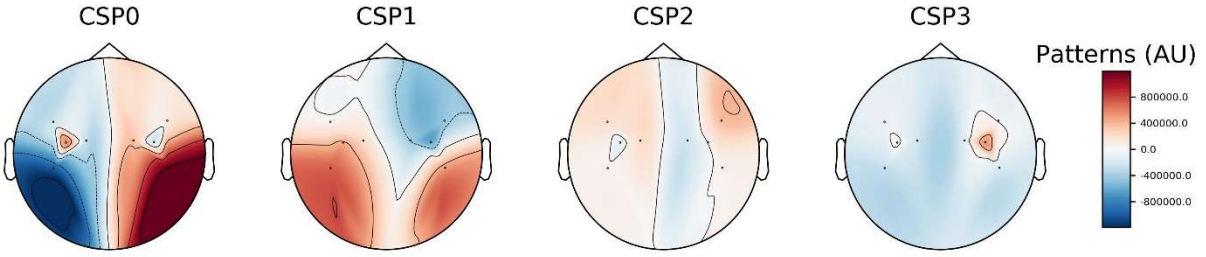

BOTH – 8 – TRAINING